Master thesis

July 2010

Performance evaluation and optimization of the luminosity detector ALFA

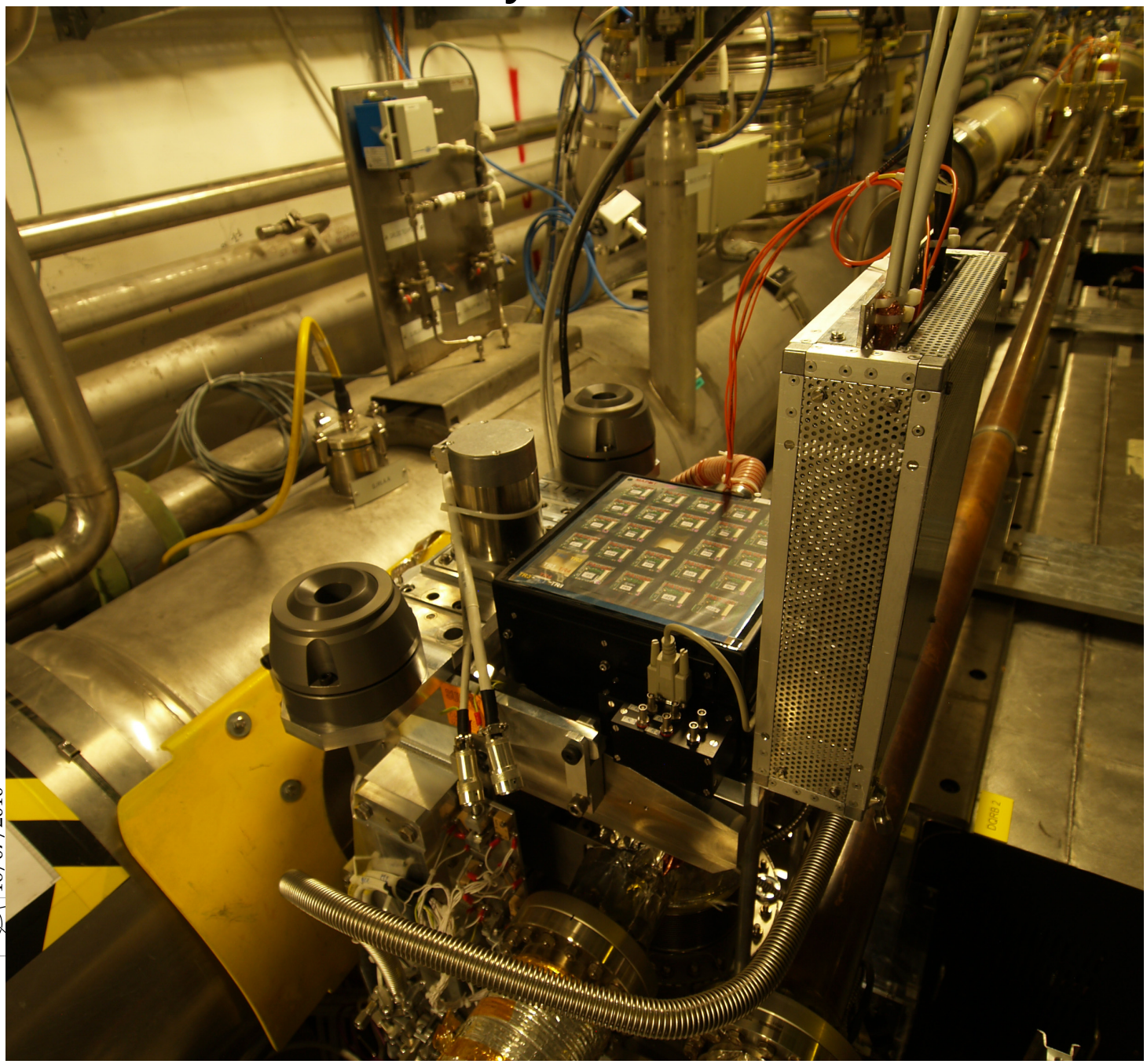

CERN-THESIS-2010-091
16/07/2010

Sune Jakobsen

Supervisors
Per Grafström (ATLAS)
Christian Joram (PH-DT)
CERN

Supervisor
Jørgen Beck Hansen
NIELS BOHR INSTITUTE
UNIVERSITY OF COPENHAGEN


PARS ANCHORAE, ALIQUID SPEI

1. Abstract

The startup of the LHC (Large Hadron Collider) has initialized a new era in particle physics. The standard model of particle physics has for the last 40 years with tremendous success described all measurements with phenomenal precision. The experiments at the LHC will test the standard model in a new energy regime. To normalize the measurements and understand the potential discoveries of the LHC experiments it is often crucial to know the interaction rate - the absolute luminosity.

The ATLAS (A Toroidal LHC ApparatuS) detector will measure luminosity by numerous methods. But for most of the methods only the relative luminosity is measured with good precision. The absolute scale has to be provided from elsewhere. Therefore ATLAS plans to measure the flux of protons scattered under very small angles as this flux relates directly and with good precision to the absolute luminosity. This will be done by the ALFA (Absolute Luminosity For ATLAS) detector.

The detectors will be positioned about 240 m from the interaction point to make it possible to measure sufficiently small scattering angles. To approach close enough to the beam (few millimeters) the detectors will be moved inside the beam pipe contained in Roman Pots with a secondary vacuum. The detector itself is build up from 500 µm squared scintillating fibers. To improve resolution the fibers are staggered. The fibers will be readout by MAPMTs (MultiAnode PhotoMultiplier Tubes). To eliminate background two stations containing an upper and a lower detector will be positioned at each side of the interaction point. The combined tracks for 4 stations will give the flux and angle of the scattered particles, from which the luminosity can be calculated with good precision.

It is essential that each scintillating fiber delivers enough light to make a clear signal. Therefore tests using standard electronics for readout of a MAPMT connected to a prototype detector have been performed. The setup was primarily used to determine the light yield of the scintillating fibers which was measured for both low energy electrons from a source and high energy muons from cosmic rays.

After the method was verified an upgrade was made to custom electronics which allowed readout of a full detector. This made it possible to perform light yield measurements of all fibers by using cosmic muons. As the cosmic test used almost all the parts that eventually will be installed at LHC/ATLAS it thereby also provided a stability test for all components involved.

To verify the performance in conditions as close as possible to the real use in the LHC, two detectors were installed in an ALFA station and tested in a beam. The test beam have the clear advantage that the particle rate is much higher than with cosmic rays and that the particles always comes from the same direction. This makes studies of resolution, cross talk etc feasible. At the test beam a high precision silicon pixel telescope was used to improve the resolution studies and make internal alignment of the detectors.

2. Content

3. Figure list

4. Abbreviation list

ADC	Analog Digital Converter
ALFA	Absolute Luminosity For ATLAS
ALICE	A Large Ion Collider Experiment
ATLAS	A Toroidal LHC ApparatuS
BCM	Beam Conditions Monitor
BR	Branching Ratio
CAN	Controller Area Network
CCC	CERN Control Center
CERN	European Organization for Nuclear Research
CMS	Compact Muon Solenoid
CSC	Cathode Strip Chamber
DAC	Digital Analog Converter
DAQ	Data acquisition
ECL	Emitter-Coupled Logic
ELMB	Embedded Local Monitor Board
FPGA	Field-Programmable Gate Array
HV	High Voltage
ISR	Intersecting Storage Ring
KH	Karl-Heinz Hiller (DESY Zeuthen)
L1	Level 1 trigger
L2	Level 2 trigger
LED	Light Emitting Diode
LHC	Large Hadron Collider
LVDT	Linear Variable Displacement Transducer
MAPMT	MultiAnode PhotoMultiplier Tube
MBTS	Minimum Bios Trigger Scintillator
MDT	Monitored Drift Tubes
MH	Matthieu Heller (PhD student at Laboratoire de l'Accelerateur Lineaire)
MROD	MDT Read Out Driver
NIM	Nuclear Instrumentation Module
OB	Orsay test borads
PCB	Printed Circuit Board
PE	PhotoElectron

PMT	PhotoMultiplier Tube
PSU	Power Supply Unit
QCD	Quantum ChromoDynamics
QED	Quantum ElectroDynamics
QRL	Cryogenic distribution line
RMS	Root Mean Square
ROD	Read Out Driver
RoI	Region of Interest
RPC	Resistive Plate Chambers
SBA	Super BiAlkali
SCT	SemiConductor Tracker
SPS	Super Proton Synchrotron
TAN	Target Absorber for Neutrals
TGC	Thin Gap Chambers
TLD	Thermo Luminescent Dosimeter
TLU	Trigger Logic Unit
TOTEM	TOTal Elastic and diffractive cross section Measurement (Total Cross Section, Elastic Scattering and Diffraction Dissociation at the LHC)
TPC	Time Projection Chamber
TRT	Transition Radiation Tracker
TTC	Timing, Trigger and Control
UBA	Ultra BiAlkali
USB	Universal Serial Bus
vdM	van der Meer
VME	Versa Module Europa
ZDC	Zero Degree Calorimeter

5. Publication list

5.1. First author publications

S. Jakobsen and C. Joram. *Differences in light yield and crosstalk in a scintillating fiber tracker between beam- and cosmic measurements*, Internal ATLAS note: ATL-LUM-INT-2009-004. (14 December 2009). Included as Appendix A.

S. Jakobsen and C. Joram. *Light yield stability over time in bent squared scintillating fibers*, Internal ATLAS note: ATL-LUM-INT-2009-004. (20 May 2010). Included as Appendix B.

5.2. Publications as ATLAS author

ATLAS Collaboration, *Charged-particle multiplicities in pp interactions at sqrt(s) = 900 GeV measured with the ATLAS detector at the LHC*, Phys Lett B 688, Issue 1, 21-42. (15 March 2010).

ATLAS Collaboration, *The ATLAS Inner Detector commissioning and calibration*, EPJC. (26 April 2010).

ATLAS Collaboration, *Readiness of the ATLAS Liquid Argon Calorimeter for LHC Collisions*, EPJC. (14 December 2009).

6. Preface and acknowledgement

Most of the work presented in this thesis was performed in a 14 month employment as technical student at CERN. I would like to thank my direct supervisor at CERN Per Grafström (Head of the ALFA collaboration) for the opportunity, the good advisees and for making me fill very welcome in the ALFA group. I would also like to thank my daily supervisor Christian Joram (Head of the Detector Technology at CERN) for the introduction to the world of instrumentation, the many joint hours in the laboratory, the very wise answers to the many daily questions and for making almost everything possible.

My Danish supervisor at the Niels Bohr Institute Jørgen Beck Hansen also deserves thanks for supporting the decision of my being at CERN for all of thesis work, and advising from home, and keeping me on a track that would lead to a result (this thesis).

Karl-Heinz Hiller (DESY) has oscillated between being a supervisor, a friend and a colleague to me. I have very much enjoined our time together.

I am grateful to Andre Bream (CERN PH-DT) and Thomas Schneider (CERN PH-DT) for having included me in the technical work. I have learned a lot from them. Their professionalism has been a source of inspiration and they have made a really nice work environment.

I have felt welcomed in the ALFA collaboration and have enjoyed working together with many different professionals from technicians reaching over electrical engineers to physicists.

I thank Rolf Kristensen (IT engineer) for being my C++ oracle and always having a fast easy solution of the programming problems I stumbled across.

I would also like to thank my thesis spell correction team: Anne-Mette Thordal-Christensen, Mia Frosch, Joachim Møllesøe Vinther, Jesper Falling Sperling, Rolf Kristensen and Kasper Lincke.

Thanks to all my supervisors (including Karl-Heinz Hiller) for thesis advises.

7. Introduction

This section is a very brief introduction to the European Organization for Nuclear Research (CERN), the Large Hadron Collider (LHC), and A Toroidal LHC ApparatuS (ATLAS).

7.1. CERN

This section is based on [1] and [2]

CERN is the European Organization for Nuclear Research and is located near Geneva on the border between Switzerland and France. It was founded in 1954 by 12 European countries to counteract the dilution of European research to USA after the Second World War. From the very beginning it was clear that CERN was based on openness and fundamental sciences as it is stated here [3]:

"The Organization shall provide for collaboration among European States in nuclear research of a pure scientific and fundamental character (...). The Organization shall have no concern with work for military requirements and the results of its experimental and theoretical work shall be published or otherwise made generally available".

After just a few years the Proton Synchrotron was build and the tradition of CERN making accelerators available for research was started.

CERN have grown much since the start and today it has 20 member states and about 2600 employees + about 8000 users from about 600 universities and institutes. But the goals have basically stayed the same although formulated somewhat differently [3]:

- Research: Seeking and finding answers to questions about the Universe
- Technology: Advancing the frontiers of technology
- Collaborating: Bringing nations together through science
- Education: Training the scientists of tomorrow

The main field of CERN is particles physics, but CERN does also house a number of other fields in need for accelerated particles. The accelerator complex has been expanded over the years and some of the old accelerators are still used as injection to the new accelerators. The accelerator complex and some of the experiments housed by CERN is shown in Figure 7.1.

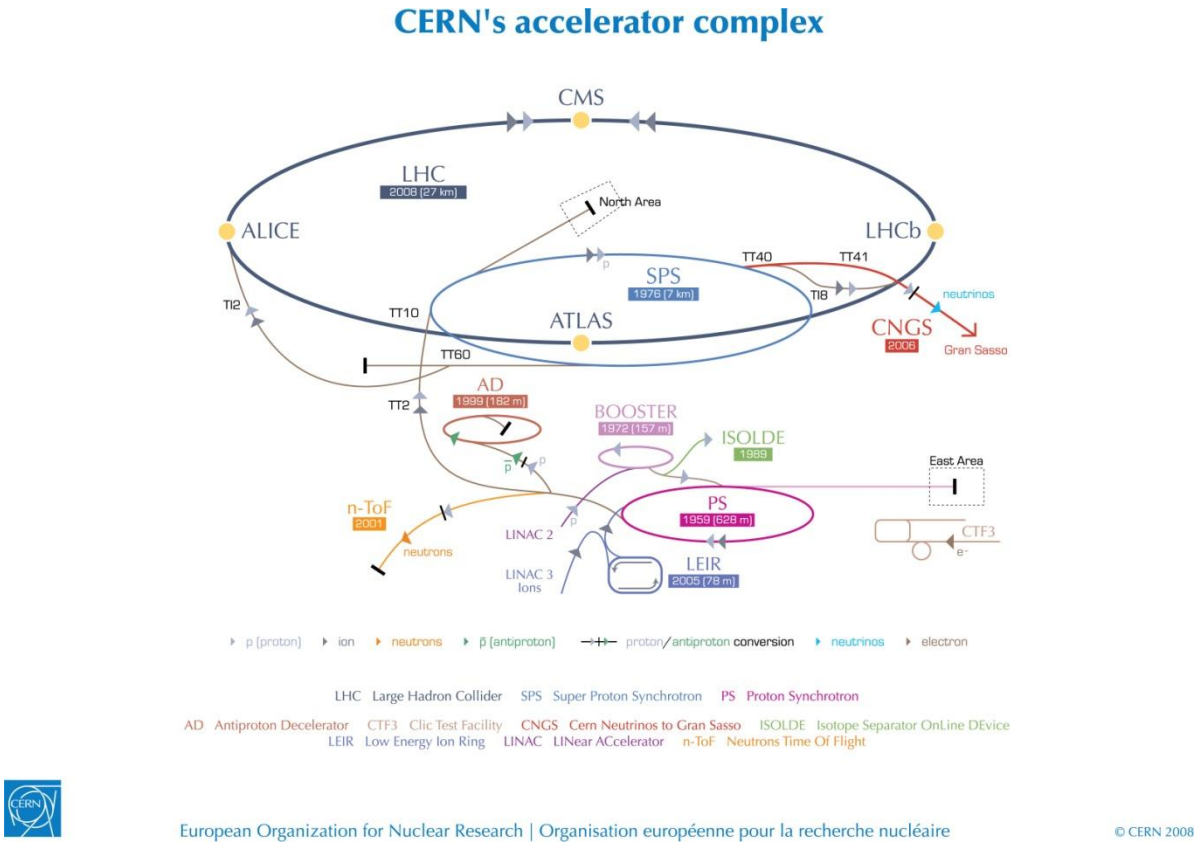

Figure 7.1. The CERN accelerator complex and some of the experiments currently present at CERN. The figure is from [4].

As the size and complexity of the equipment (and thereby the funding needed) for the particle physics seem to be ever growing, the need for an international place like CERN to combine the knowledge and the recourses for Europe (or maybe one day the entire world) becomes more essential in the future.

7.2. LHC

This section is based on [5], [6], [7], [8], [9] and [10].

The Large Hadron Collider (LHC) is mainly a proton-proton collider buried 50 to 175 m underground in a circular tunnel which is 26659 m in circumference. It consists of 9593 magnets and 8 radiofrequency cavities (per beam). For the bending to keep the protons inside the circular trajectory 1232 dipole magnets are used. They are designed to be operated with a current of 11700 A to make a magnetic field of 8.33 T. To make this huge current possible the magnets are superconducting based on niobium-titanium (NbTi), which becomes superconducting at about 10 K. The magnets will be operated at 1.9 K. The magnetic field makes it possible to bend protons with an energy up to 7 TeV. The LHC is also prepared to be operated with heavy ions at 2.76 TeV/u at dedicated runs.

LHC is designed to be feed with protons at 450 GeV from the Super Proton Synchrotron (SPS), see Figure 7.1. At the design luminosity (see Section 8 for definition of luminosity) of $\mathscr{L} = 10^{34} \frac{1}{cm^2 \cdot s}$ there will be 2808 bunches of $1.1 \cdot 10^{11}$ protons each. The speed of the protons at 7 TeV will be $0.999999991 \cdot c$ (c = the speed of light in vacuum) which will give 11245 turn in the LHC every second. This will potentially give bunch collision every 25 ns.

In each of the 4 interaction points there are a detector as shown in Figure 7.2.

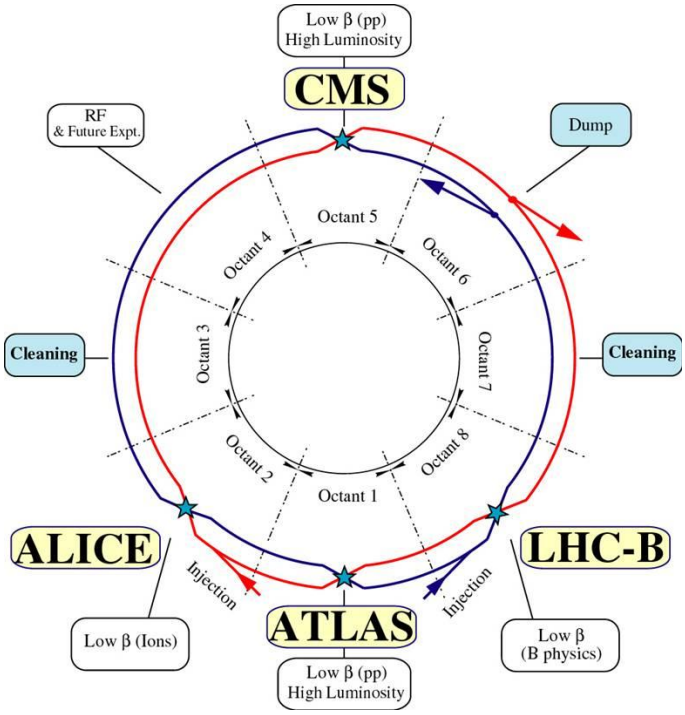

Figure 7.2. The LHC layout with experiments. The figure is from [4].

ATLAS is a general purpose detector and will be discussed further in Section 7.3.

ALICE (A Large Ion Collider Experiment) is optimized for LHC heavy ion runs in which they will study the properties of quark-gluon plasma. It is a classical onion-layer detector which intent to cover close to all angles. ALICE main characteristic is a very large Time Projection Chamber (TPC).

CMS (Compact Muon Solenoid) is a general purpose detector optimized for proton runs. It is a classical onion-layer detector witch intent do cover close to all angles. CMS is 15 m in diameter and 21.5 m long and have a total weight of 12500 t. The magnet is a 4 T superconducting solenoid. The main characteristic of CMS is the very extensive use of silicon detectors.

The very forward regions of CMS are covered by the (independent) detector TOTEM (TOTal Elastic and diffractive cross section Measurement, later referred to as Total Cross Section, Elastic Scattering and Diffraction Dissociation at the LHC). The purpose is given directly by the name. It has a silicon telescope surrounding the beam pipe and 24 Roman Pots (see Section 13.3 for Roman Pot definition) with silicon strip detectors inside. The Roman Pots are located ± 147 m and ± 220 m from the interaction point.

LHCb is specialized for b-physics and the study of CP violations. It is a single arm forward spectrometer.

7.3. ATLAS

This section is based on [11] and [12].

A Toroidal LHC ApparatuS (ATLAS) is a general purpose detector. As shown in Figure 7.3 it is a classical onion-layer detector which intent to cover close to all angles.

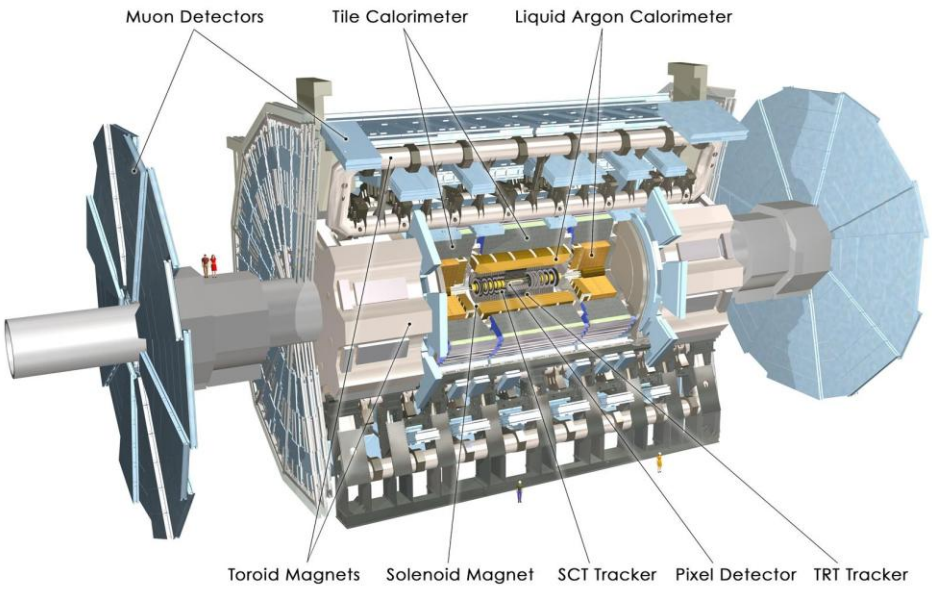

Figure 7.3. The ATLAS detector. The detector has a diameter of 25 m and a length of 46 m. The overall weight is about 7000 t. The figure is from [4].

The detector has a diameter of 25 m and a length of 46 m. The overall weight is about 7000 t. ATLAS has about 100 million electronic channels.

As a general purpose detector ATLAS aims at discovering any yet unseen particles in a new energy range. By investigating this new energy regime ATLAS will test a number of different theories and ideas such as Higgs mechanism, supersymmetry, extra dimensions, dark matter etc.

The potentially new particles will have a very short lifetime and will not be seen directly. Instead the decays from the particle will be seen. These secondary particles have to be identified to make it possible to identify the original particles. The identification of the secondary particles is done (simplified) by looking at the signals (or missing signals) from the layers of the detector system as illustrated in Figure 7.4.

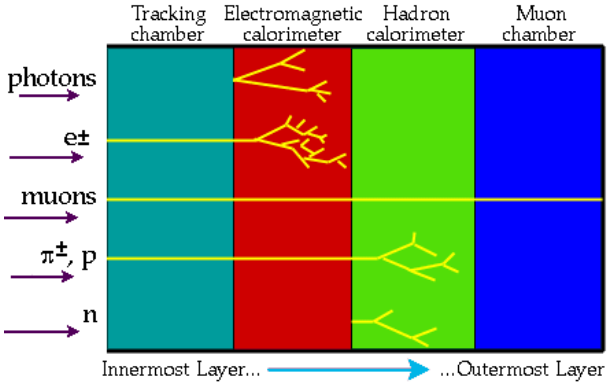

Figure 7.4. Identification of particles in a general detector system. The figure is from [13].

ATLAS is cylindrical around the beam pipe and has magnetic fields to bend the tracks of charge particles. The identification of particles is illustrated in Figure 7.5.

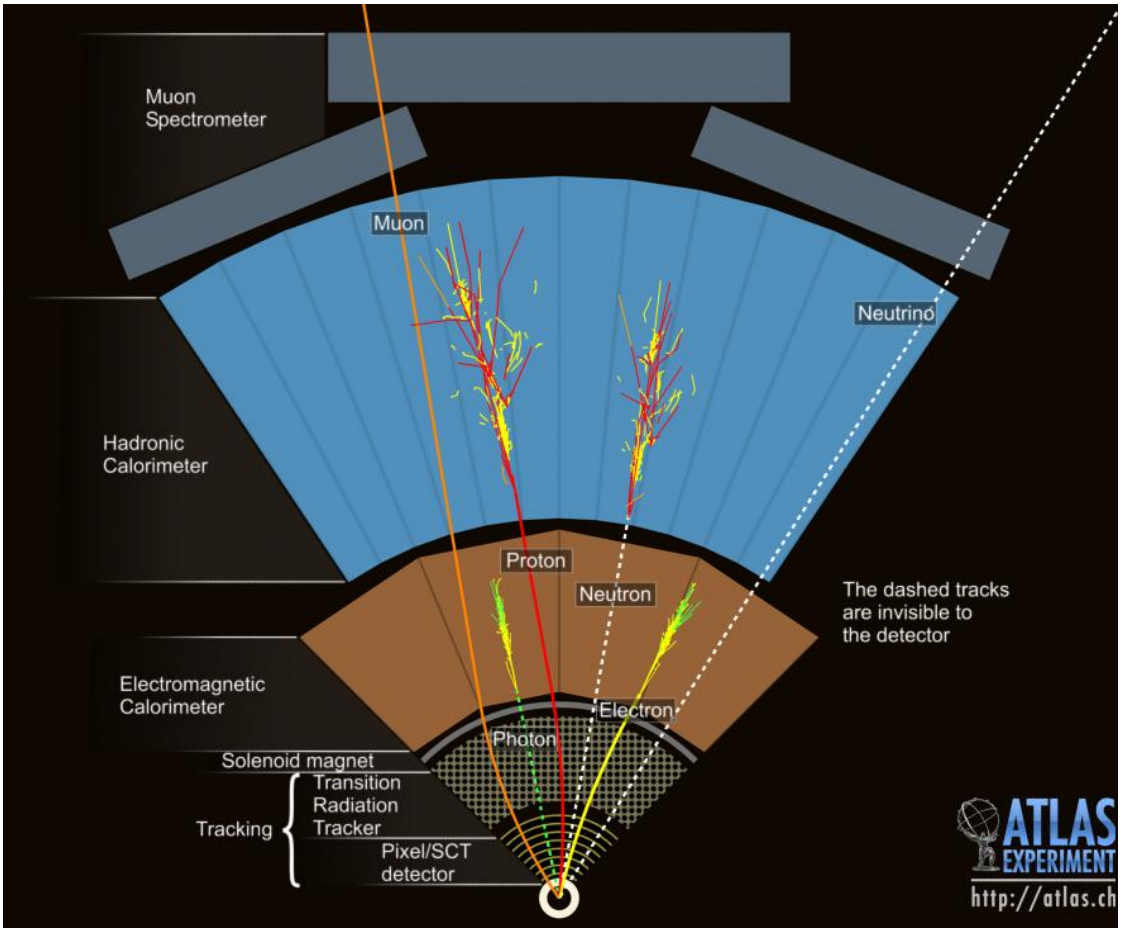

Figure 7.5. Identification of particles in ATLAS. The figure is from [4].

Some details of each layer are described in the following sections.

7.3.1. Magnet system

ATLAS magnet system is divided into two parts as shown in Figure 7.6.

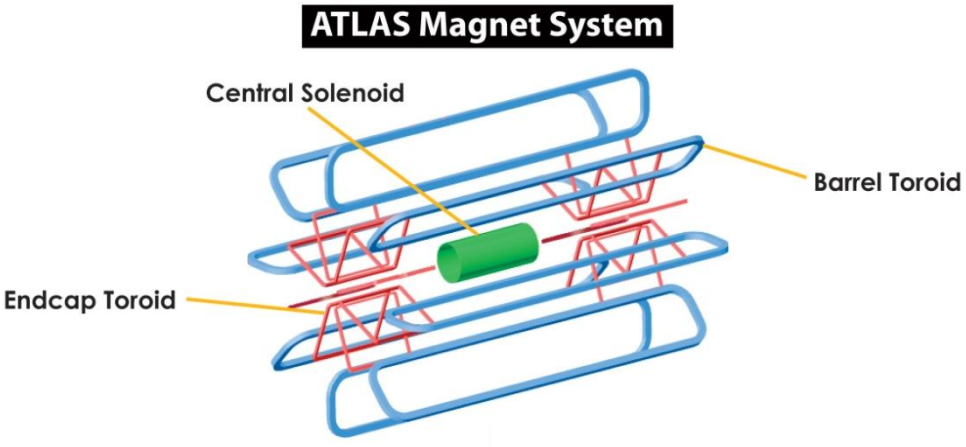

Figure 7.6. The magnet systems of ATLAS. The figure is from [12].

7.3.1.1. The Solenoid

The smallest magnet is the central solenoid that surrounds the tracking detectors. It is 5.3 m long and has a diameter of 2.4 m. The nominal current is 7730 A which provide a magnetic field of 2 T. The magnetic field is used to bend trajectories of charged particles and hence measure the momentum of the particles and thereby provided input for particle identification.

The solenoid is located inside the calorimeters. To keep a reliable energy measurement it is therefore important that not too much energy is absorbed in the solenoid. Therefore the magnet itself is only 4.5 cm thick, but the total weight is still about 5.7 t.

7.3.1.2. The Toroid

As shown in Figure 7.6 the toroid is divided into a barrel section and an end-cap section. Both are located outside the calorimeter but inside the muon system. They are used to bend muons for momentum measurements.

The barrel consists of 8 coils positioned symmetrically around the beam axis. The barrel is 25.3 m long and has an outer diameter of 20.1 m. This gives it a weight of 830 t. The barrel toroid is superconducting and have nominal current of 20500 A. This gives a peak magnetic field of 4 T.

Each end-cap toroid also consists of 8 coils. The end-cap toroid has an inner diameter of 3.3 m and outer diameter of 21.4 m. This gives it a weight of 239 t. The end-cap toroids are superconducting and have a nominal current of 20500 A. This gives a peak magnetic field of 4.1 T.

7.3.2. Inner detectors

The inner detectors are contained inside the solenoid magnet. It has a total diameter of 2.1 m and a length of 6.2 m. The inner detector consists of a silicon pixel detector, a silicon strip detector and a transition radiation tracker as shown in Figure 7.7.

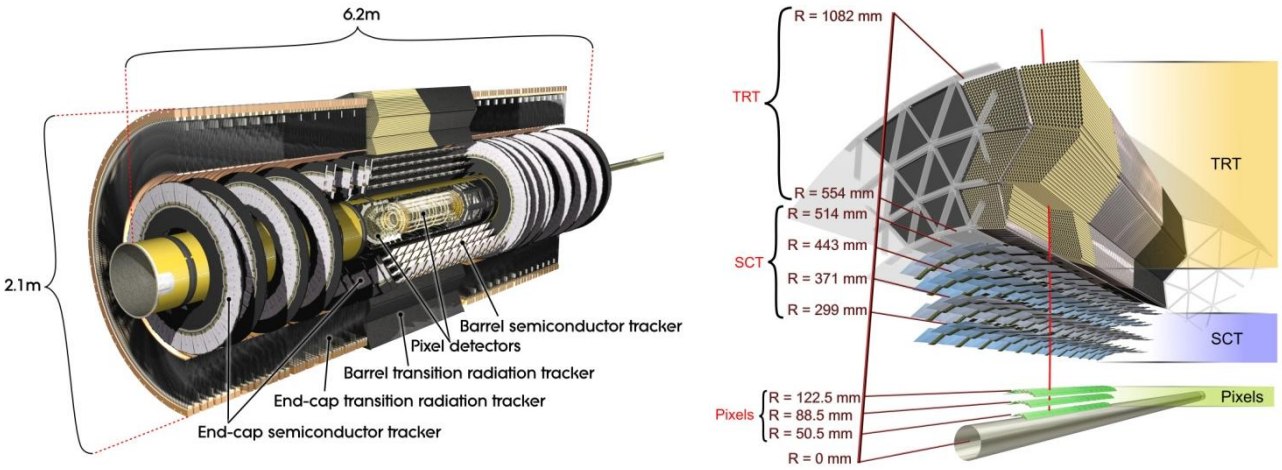

Figure 7.7. *LEFT*: Layout of the ATLAS inner detectors with barrels and end-caps. *RIGHT*: Zoom on the central part of the inner detector. The figures are from [4].

7.3.2.1. The pixel detector

The pixel detector has 3 layers at 50.5 mm, 88.5 mm and 122.5 mm from the center of the beam pipe. Each module of the pixel detector is 62.4 mm long and 21.4 mm wide and has 46080 pixels. This gives a pixel size

of 50·400 μm^2. Each module is read out by 16 chips. The modules are overlapping to give a hermetic coverage. Typically 3 layers are crossed by each track and give the first 3 points for the track reconstruction.

Each layer has a thickness of about 2.5 % radiation length at normal incidence.

The total area of the pixel detector is 1.7 m^2 which is covered by 80 million pixels. The total power consumption is 15 kW.

7.3.2.2. The Semiconductor Tracker

The SemiConductor Tracker (SCT) is a silicon strip detector. The SCT barrel has 4 layers of two-sided modules positioned 299 mm, 371 mm, 443 mm and 514 mm from the center of the beam pipe. There are 18 planar end-caps. Each module is 636·640 mm^2 and has 780 readout strips of 80 µm pitch. The total area covered is 60 m^2 over the barrel and the end-caps.

7.3.2.3. The Transition Radiation Tracker

The transition Radiation Tracker (TRT) is a straw detector. It is build up of 4 mm straws with 30 µm gold-plated tungsten wire in the center. The straws contains a gas mixture of Xe(70%)CO2(27%)O2(3%). The drift time in the gas is measured and gives a resolution of 170 µm per straw. The readout uses a two threshold system, which allows the detector to distinguish between tracking hits and transition radiation hits. This information is used for particle identification.

The barrel section is position between 554 mm and 1082 mm from the center of the beam pipe and has a maximum straw length of 144 cm. There are about 50000 straws in the barrel and each is read out in both ends to reduce occupancy.

Each end-cap consists of 18 wheels and totally there are 320000 radial straws in the end-caps.

7.3.3. Calorimeters

ATLAS calorimeters are separated into an electromagnetic and a hadronic calorimeter and are used to measure the energy of the particles. The electromagnetic calorimeter is based on liquid argon. The barrel of the hadronic calorimeter is based on plastic scintillator tiles, but the end-caps are based on liquid argon.

7.3.3.1. The Liquid Argon Calorimeter

This section is based on [14] and [15].

The Liquid Argon Calorimeter (LAr) is composed of a presampler, a barrel and two end-caps as shown in Figure 7.8.

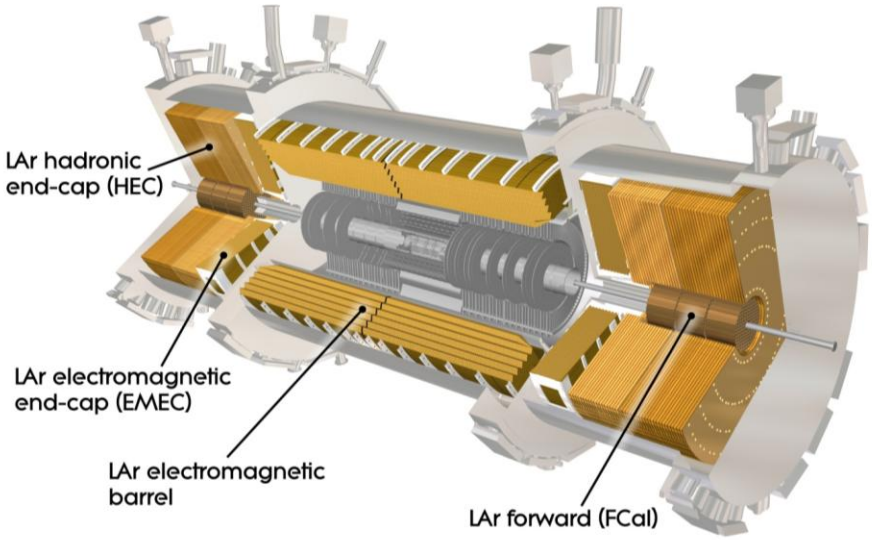

Figure 7.8. The liquid Argon Calorimeter. The figure is from [4].

LAr is a sampling calorimeter and the working principle is as follows: A particle hits the absorber made of lead + stainless steel for support (for the hadronic part the absorber is made of copper). Secondary particles (a shower) are thereby produced. The secondary particles ionize the liquid argon. The ionization is proportional to the energy loss of the particle and is read out. A particle making a shower in the LAr is shown in Figure 7.9.

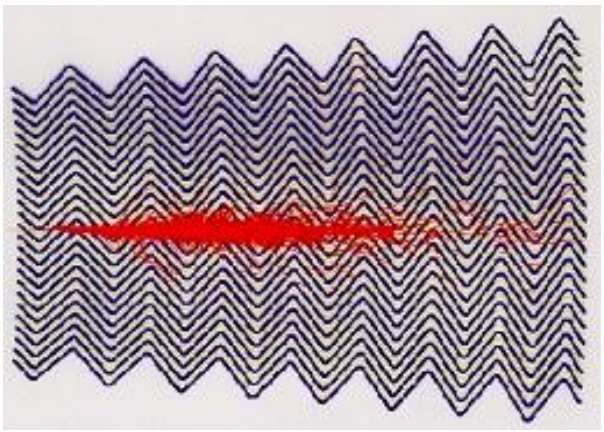

Figure 7.9. Shower in LAr. The figure is from [16].

The absorber layout constitutes a zigzag pattern (as shown in Figure 7.9) to make a homogenous angular coverage.

The inner most part of the calorimeter is a presampler, that is indented to correct for the energy lost before the calorimeter.

The barrel is 6.8 m long, have an inner diameter of 2.3 m and an outer diameter of 4.5 m and have 110000 channels.

The end-caps contain an electromagnetic wheel (EMEC), which has a diameter of 4.5 m and a thickness of 0.632 m, two hadronic wheels (HEC), which has a diameter of 4.5 m and a thickness of 0.8 m and 1.0 m, and a forward calorimeter (FCal) in 3 parts, which has a diameter of 0.91 m and a thickness of $3 \cdot 0.45$ m.

7.3.3.2. The Tile Calorimeter

This section is based on [17].

The Tile Calorimeter is a pure hadronic colorimeter and it surrounds the LAr as shown in Figure 7.10.

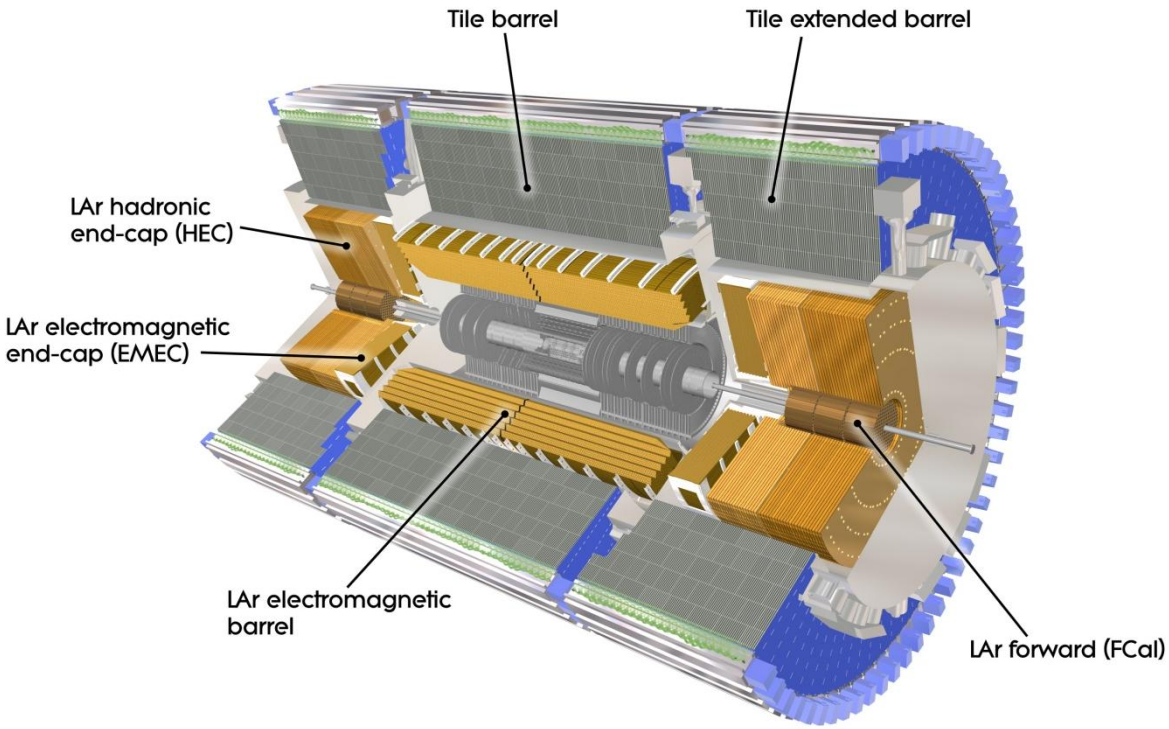

Figure 7.10. The Tile calorimeter. The figure is from [4].

Like the LAr it is a sampling calorimeter using iron as absorbers. The active material is plastic scintillator tiles coupled to wavelength-shifting optical fibers. The readout is done with PhotoMultiplier Tubes (PMTs). Totally the tile calorimeter has 500000 plastic sintillator tiles.

The inner diameter of the tile calorimeter is 4.6 m and the outer diameter is 8.5 m.

The main barrel of the tile calorimeter is made from 64 wedges that each is 5.6 m long and weights 20 t.

The extended barrel is made of 64 wedges that each is 2.6 m long.

7.3.4. Muon spectrometer

This section is based on [18].

The ATLAS muon system has been designed to be a stand-alone muon measurement with both triggering and measuring. The muon spectrometer is divided into a barrel and two end-caps and is shown in Figure 7.11.

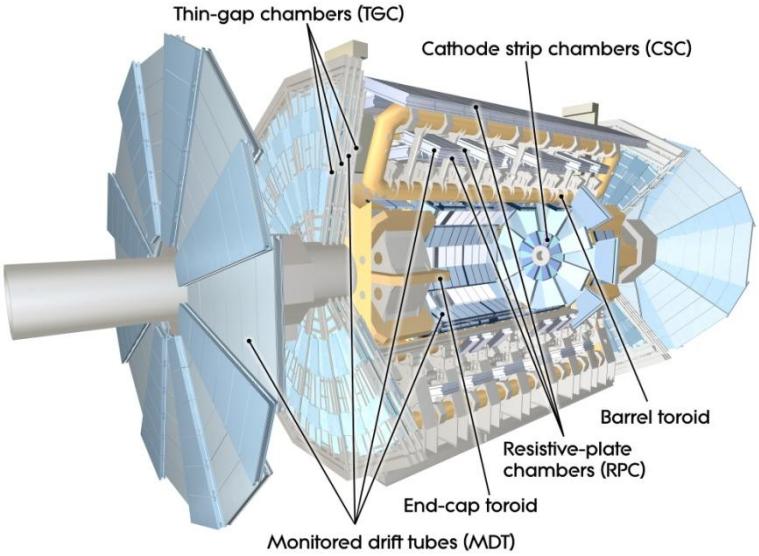

Figure 7.11. Muon system on ATLAS. The figure is from [4].

The barrel is surrounding and inside the toroid (see Section 7.3.1.2) which makes it possible to measure the momentum of the muons. The position is measured with Monitored Drift Tubes (MDT) with a position about 50 µm. The triggering is done with Resistive Plate Chambers (RPC).

The inner station has a Cathode Strip Chambers (CSC), which is multiwire proportional chamber with cathode strip read-out.

In the end-cap the triggering is done with Thin Gap Chambers (TGC), which are multiwire proportional chambers with a smaller distance between the cathode and the wire plane compared with the distance between wires. The position is measured with Monitored Drift Tubes (MDT).

7.3.5. Luminosity and forward detectors

7.3.5.1. Beam Condition Monitors

This section is based on [19] and [20].

The Beam Condition Monitors (BCMs) are first and foremost in place to prevent beam accidents. They are positioned at ± 1.84 m of the interaction point in a radius of 55 mm and therefore have to be very radiation hard (500 kGy over life time). The position and layout is shown in Figure 7.12.

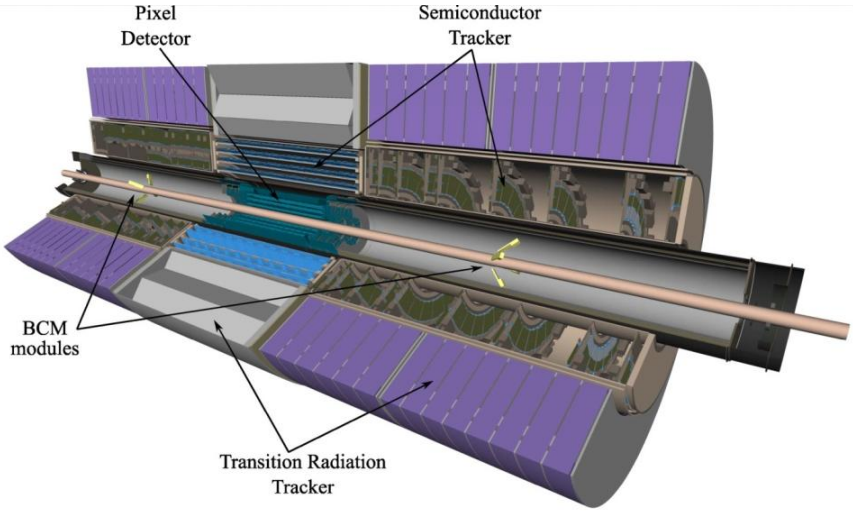

Figure 7.12. BCM in ATLAS. The figure is from page 5 in [19].

In addition they have to be very fast to be able to act in only ~2 turns of the beam (~150 μs). Therefore diamond sensors are used with a rise time shorter than 1 ns. The sensors are shown in Figure 7.13.

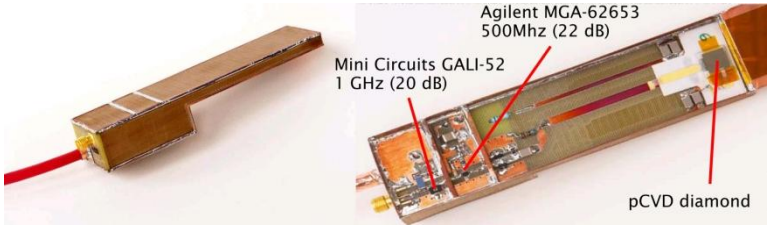

Figure 7.13. The BCM diamond sensor. The figure is from page 6 in [19].

Time-of Flight and pulse height can be measured on a bunch to bunch basis.

The BCM can be used as additional trigger in minimum bias triggering (see Section 7.3.6. about the trigger system).

7.3.5.2. MBTS

This section is based on [21].

The Minimum Bias Trigger Scintillator, MBTS, system is indented to be used only for the first running period with luminosity lower than $10^{33}\frac{1}{cm^2 \cdot s}$. Scintillators are not very radiation hard, so at higher luminosity the MBTS is expected to suffer from radiation damage and become ineffective. At high luminosity it would anyway have too high occupancy to be useful.

The MBTS consist of two detectors. They are located ± 3.56 m from the interaction point on the inner face of the end-cap calorimeter cryostat. Each detector consists of 2 rings of each 8 subsection. The inner ring covers the radial region 153-426 mm and the outer ring covers the radial region 426-890 mm. A disk of the MBTS is shown in Figure 7.14.

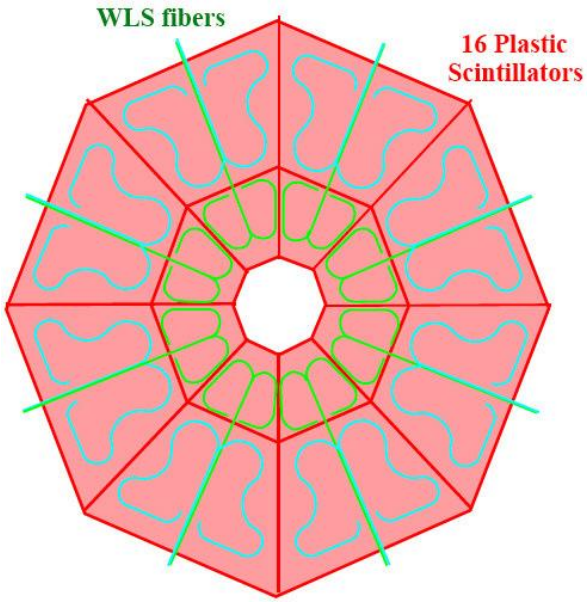

Figure 7.14. A disk of the MBTS consisting of 16 scintillator tiles. The figure is figure 1 in [21].

Each subsection is made of a 2 cm thick scintillator tile coupled to a wave-length shifter. The light from the wave length shifter is converted to an electrical signal in PhotoMultiplier Tubes (PMTs). The readout is done by electronics adapted from the Tile Calorimeter. At normal setting the counters are read out every 10 s.

7.3.5.3. LUCID

This section is based on [22] and [23].

The LUminosity Cherenkov Integrating Detector, LUCID, is a dedicated relative luminosity detector. It is positioned at ± 17 m from the interaction point and closely surrounds the beam pipe. Each LUCID detector consists of 20 aluminum tubes that contains C_4F_{10} (g) at about 1.1 bar. Each tube is 1.5 m long and has a diameter of 15 mm. The tubes are positioned in two circles of radius 96 mm and 115 mm from the beam line. The LUCID detector is shown in Figure 7.15.

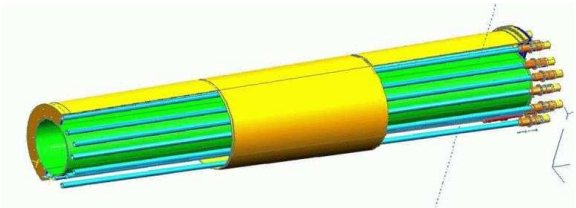

Figure 7.15. The LUCID detector. The beam pipe is green, the aluminum tubes turquoise and the vessel yellow. The figure is figure 1 in [22].

When a charged high energy particle (10 MeV threshold for electrons, 2.8 GeV threshold for charged pions) crosses the gas, Cherenkov light will be emitted. The light is reflected on the inside of the aluminum tube. The principal is shown in Figure 7.16.

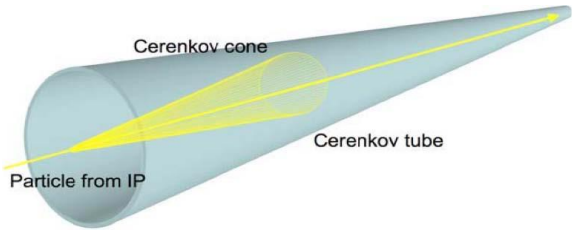

Figure 7.16. Principal of the Cherenkov light in LUCID. The figure is from [24].

16 of the tubes have PhotoMultiplier tubes (PMTs) directly mounted on the end of the aluminum tube. These PMTs are of a radiation hard type. The 4 last tubes are connected to 5 m long fiber bundles that transport the light to a non radiation hard 4 channeled multianode PMT. These multianode PMTs can be used at higher luminosity then the directly coupled, but at the cost of having a less direct measurement.

The design makes the LUCID detector light, radiation hard and with a response time of 10-15 ns, which ensures bunch crossing separation.

The methods LUCID used to determined luminosity is discussed in Section 10.2.

7.3.5.4. ZDC

This section is based on [23] and [25].

The Zero Degree Calorimeter, ZDC, is installed inside the Target Absorber for Neutrals, TAN. The TAN is required to absorb the flux of forward high energy neutral particles so they do not impinge the superconducting beam separation dipoles. Inside the TAN the beam pipe splits from one to two pipes as illustrated in Figure 7.17.

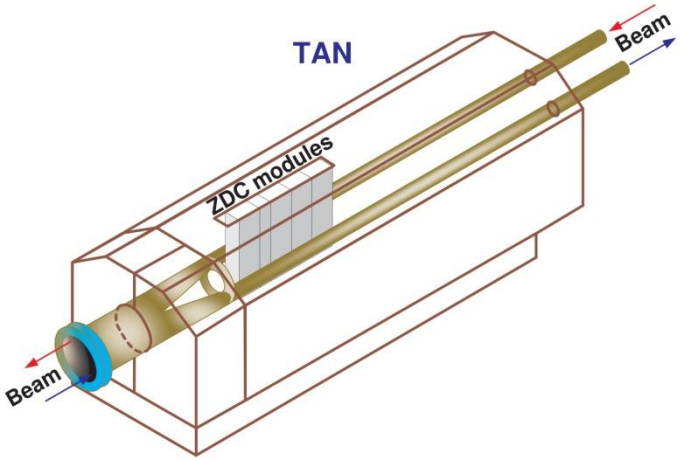

Figure 7.17. The TAN with the ZDC inside. The ZDC is located right after the beam pipe splits into tow pipes. The figure is figure 3.1 in [25].

The TAN (and therefore the ZDC) is located at ± 140 m from the interaction point.

Each ZDC detector has one electromagnetic module and 3 hadronic modules. It is a sampling calorimeter using tungsten as absorber. The active material is quartz rod. Passing particles induce showers in the tungsten and the showers induce Cherenkov light in the quartz rods. The light is readout by multianode PMTs.

The primary purpose of the ZDC is to determine the centrality of heavy-ion collisions. But at the startup phase of LHC with proton-proton collisions, the ZDC will be used to enhance the acceptance of ATLAS and provide additional minimum-bios triggering for ATLAS.

7.3.5.5. ALFA

The Absolute Luminosity For ATLAS, ALFA, is described in detail in Section 13.

7.3.6. Trigger system

This section is based on [26] and [27].

The frequency of bunch crosses at LHC is 40 MHz. The data for a readout of 1 event is about 1-1.5 MB. To store all events is therefore not possible or practical as only a low fraction of the events are interesting for finding new physics. Therefore ATLAS uses a trigger system to bring down the event rate for storage without (hopefully) losing any interesting events. The trigger system is illustrated in Figure 7.18.

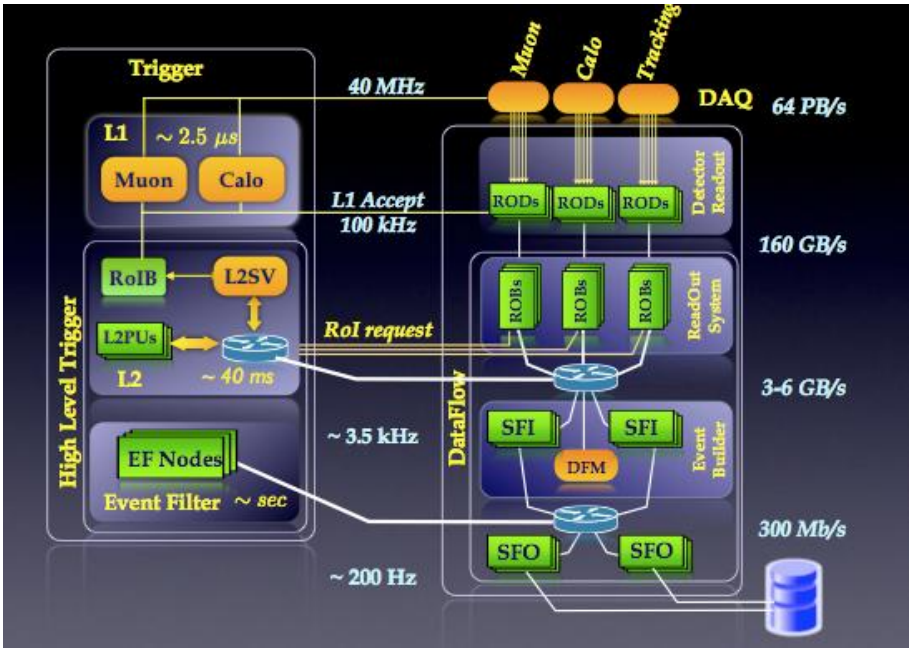

Figure 7.18. ATLAS trigger system. RoI = Region of Interest, RoIB = Region of Interest Builder, L2SV Level 2 SuperVisor, EF = Event Filter, L2PU = Level 2 Processing Unit, ROD = ReadOut Driver, ROB = ReadOut Buffer, SFI = SubFarm Input, SFO = SubFarmOutput, DFM = DataFlow Manager. The figure is from [27].

The level 1 trigger (L1) is based on information from the muon system and the calorimeter only, as it need to be very fast. L1 is therefore also hardware based and makes a decision on whether or not to keep the event in about 2.5 μs. Until this decision has been made all the data of the event have to be kept in pipelines (memory). Pending the L1 decision the event is either thrown away or sent to the level 2 trigger (L2). The rate is here reduced to about 100 kHz.

The level 2 trigger is based on a computer farm and can look more detailed on each event. It uses about 40 μs. To not having to look at all the channels in ATLAS the L1 provides a Region of Interest (RoI) that the L2 should look at. This reduced the channels L2 looks at with about a factor of 10 and thereby makes it faster. L2 reduced the rate to about 3.5 kHz.

The event filter is based on a larger computer farm and makes a full build of the event. It uses the same algorithms as is used offline. This is done on a time scale of seconds and reduced the event rate stored to about 200 Hz.

In the startup face the MBTS can be used with level 1 trigger to get minimum bias triggering. See Section 7.3.5.2 for a description of the MBTS.

8. Definition of luminosity

This section is based on [28](section 25, page 261) and [29].

The probability of a process with cross section σ occurring for a probe particle which sees an oncoming beam (one bunch) with N_1 particles is [29](page 162):

$$P = \frac{N_1}{A}\sigma \tag{8.1}$$

For this artificial case with only one probe particle the "luminosity" is:

$$l = \frac{N_1}{A} \tag{8.2}$$

where A is the cross section area of the beam (one bunch) with N_1 particles. This is illustrated in Figure 8.1.

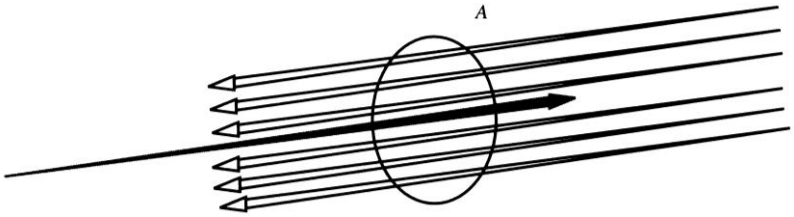

Figure 8.1. A probe particle encounters an oncoming beam with cross section area A. The figure is figure 11.3 in [29].

l is independent for the studied cross section. It is the probability of producing an event normalized to interaction cross section.

If now the probe particle is replaced with a beam (one bunch) of N_2 particles and the beams are circulating with a frequency of f and the cross section area is $A = 4 \cdot \pi \cdot \sigma_{Gauss\ x} \cdot \sigma_{Gauss\ y}$ (beam profile simplified to Gaussian) then equation (8.2) becomes [28](equation 25.2):

$$\mathscr{L} = f\frac{N_1 \cdot N_2}{A} = f\frac{N_1 \cdot N_2}{4 \cdot \pi \cdot \sigma_{Gauss\ x} \cdot \sigma_{Gauss\ y}} \tag{8.3}$$

This is illustrated in Figure 8.2 which replaced Figure 8.1 when the probe particle is replaced with a beam (one bunch) of N_2 particles.

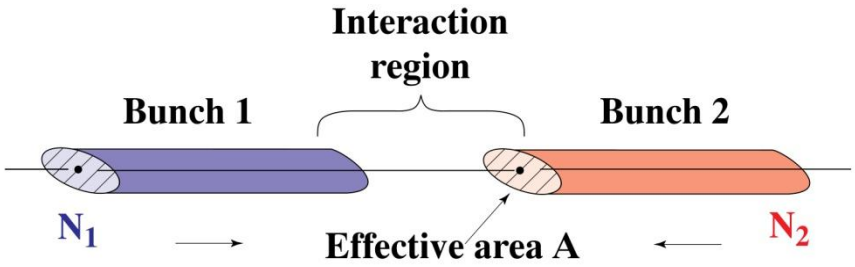

Figure 8.2. Two beams encounters each other with an effective are A. The figure is figure 1 in [30].

As the frequency of the beams now is included, equation (8.1) now becomes the rate of the event with cross section σ [28](equation 25.1):

$$R = \mathscr{L} \cdot \sigma \tag{8.4}$$

The cross section area of the beam is often given as a function of the transverse emittance, ε, and the amplitude function, β. The transverse emittance is a quality concept reflecting the bunch preparation. The amplitude function is a quantity of beam optics and is determined by the magnet configuration of the

accelerator. The transverse emittance and amplitude function relates to the width of the beam, σ_{Gauss}, as [28](equation 25.3):

$$\varepsilon \cdot \beta = \pi \cdot \sigma_{Gauss}^2 \tag{8.5}$$

At the interaction point beam quantities are traditionally quoted with a "*". For example the amplitude function at the interaction point is β*.

The luminosity at the interaction point for two beams of each one bunch can now be written by inserting equation (8.5) into equation (8.3) [28](equation 25.4):

$$\mathscr{L} = f \frac{N_1 \cdot N_2}{4 \cdot \sqrt{\varepsilon_x \cdot \beta_x^* \cdot \varepsilon_y \cdot \beta_y^*}} \tag{8.6}$$

At the LHC there will be up to 2808 bunches. The luminosity will then be given as:

$$\mathscr{L} = f \cdot n_b \cdot \frac{N_1 \cdot N_2}{4 \cdot \sqrt{\varepsilon_x \cdot \beta_x^* \cdot \varepsilon_y \cdot \beta_y^*}} \tag{8.7}$$

where n_b is the number of bunches in the beam.

As the transverse emittance is dictated by the accelerator and cannot be adjusted, the way to achieve high luminosity is to have beams with many particles at a high frequency and adjust the beam optics to have a low amplitude function at the interaction point.

9. Motivation for precise luminosity determination

This section is based on [31].

At the ATLAS experiment a lot of theories will be tested to come closer to the true physics of nature. The theories will be tested by their predictions of the likelihood that some events occur. Therefore ATLAS will look in detail after the interesting events. In some cases it takes a lot of effort to ensure that all interesting events are counted or to even find any of the events. However since the predictions are on the likelihood, the number of events found always has to be normalized to the number of interactions in the sample, the absolute luminosity. Therefore if the absolute luminosity is not determined precisely, all other measurements will suffer and it will be harder or impossible to establish confidence for one theory over another. This can also be seen directly from equation (8.4). If the cross section is determined using the rate and the luminosity, the errors on the luminosity will propagate to the cross section.

An example of the importance of precise absolute luminosity determination is shown in Figure 9.1.

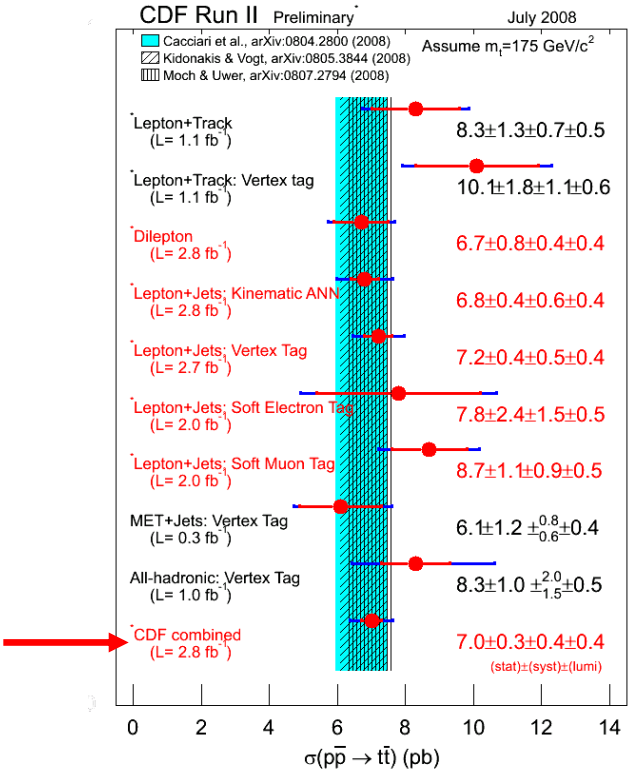

Figure 9.1. Cross section of $p\bar{p} \to t\bar{t}$ measured at CDF at the Tevatron. The uncertainty from luminosity of each channel is not dominating, but no relative improvement is gained on the luminosity uncertainty by combining many channels. The figure is from [32].

The uncertainty from the absolute luminosity is not dominating for a single channel, but no improvement is gained by combining different channels. Because the uncertainty of the absolute luminosity does not become smaller, the uncertainty from luminosity becomes the main contribution to the combined uncertainty. This effect would be even more pronounced for processes with better statistic.

In ATLAS the uncertainty of the absolute luminosity is expected to be dominating for some processes as stated in the ATLAS Detector and Physics Performance [31]:

Section 15.7.3.1 (W production, Cross-section) page 517:

"*The dominant systematic uncertainty for the cross-section measurement is expected due to the determination of the absolute luminosity*".

Section 15.8.4.1 (Top production, Total cross-section) page 534:

"*The precision on the measurement of the total cross-section is expected to be dominated by the knowledge of the absolute scale of the luminosity*".

Section 19.2.12.3 (Determination of the SM Higgs-boson parameters, Measurement of the Higgs-boson rate) page 732:

"*The main systematic error comes from the knowledge of the luminosity*".

The rate of the Higgs-bosons in a given decay channel gives the product of the cross-section and the Branching Ratio (BR) for the channel. This could help to distinguish between a Standard Model Higgs and a Supersymetric Higgs as the rate of the supersymetric Higgs would be strongly suppressed because of the suppression of the HZZ coupling. Therefore it is very important to know the rate with small uncertainties, and as the uncertainty primarily comes from the luminosity, it is very important to minimize the uncertainty of the luminosity. The difference of a luminosity uncertainty of 5 % and 10 % is shown in Figure 9.2.

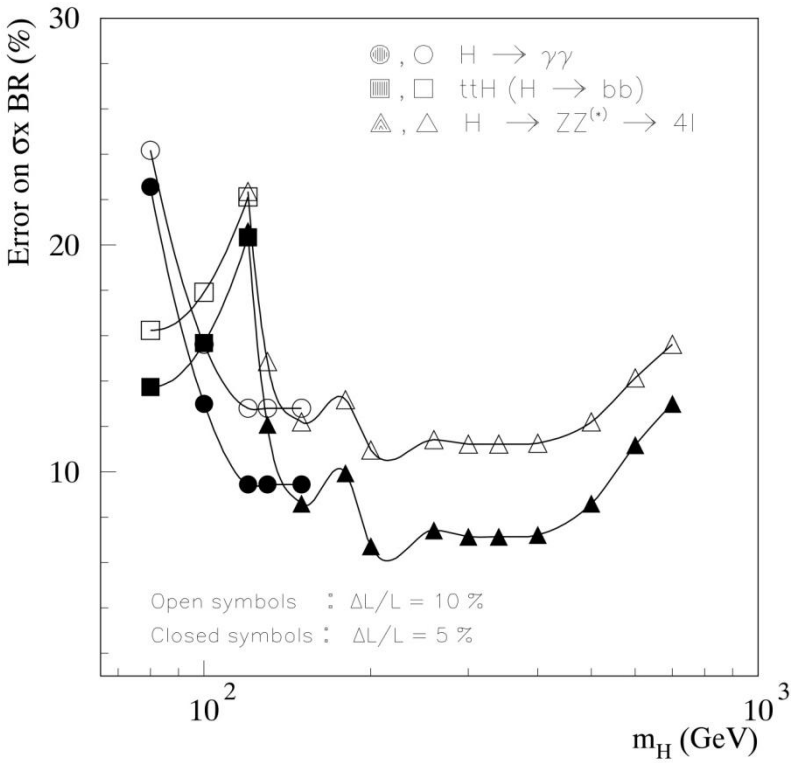

Figure 9.2. Relative precision on the rate (cross-section times the Branching Ratio) for production of Higgs-bosons with an integrated luminosity of 300 fb^{-1}. The figure is figure 19-47 in [31].

In the region 120-600 GeV the precision of the Higgs-boson rate will fall from 12 % to 7 % if the uncertainty of the luminosity is reduced from 10 % to 5 %.

These are examples of the importance of precise luminosity measurements and stress that any improvement in the precision of the luminosity determination will improve the collective outcome.

10. Luminosity determination in ATLAS

The luminosity can be determined in many ways, but most will have very high uncertainty. This section will discuss the luminosity determination methods actually being used at ATLAS.

10.1. Luminosity measurement with the MBTS

This section is based on [21].

The MBTS is described in Section 7.3.5.2. Besides triggering it will also be used for early luminosity measurements. The idea is to use equation (8.4).

As long as the number of interacting protons in each bunch is lower than one, the rate in equation (8.4) scales with the fraction of bunch crossings with an interaction.

The cross section in equation (8.4) can be estimated from simulation.

This method was used to estimate the luminosity in *[33]*. The energy used here was 900 GeV and the cross sections could therefore be simulated with smaller uncertainties than when the LHC is operating at uncharted energies. The cross section was calculated with simulations (PYTHIA) to 52.2 mb (sum of the diffractive and non-diffractive cross sections for inclusive pp collisions). The average number of collisions per bunch crossing was of the order of 10^{-4} and the method therefore valid. The result had a 17 % total systematic uncertainty.

10.2. Luminosity measurement with LUCID

This section is based on [22].

LUCID is described Section 7.3.5.3. LUCID will use inelastic events to measure the instantaneous luminosity. LUCID is even fast enough to measure the instantaneous luminosity on a bunch to bunch basis.

By multiplying equation (8.4) with the time between bunch crossings, Δt, the average number of interactions, μ_{pp}, can be calculated as [22]:

$$\mu_{pp} = \mathscr{L} \cdot \sigma_{pp}^{tot} \cdot \Delta t \tag{10.1}$$

μ_{pp} will not be measured directly, but with a proportional quantity; the mean number of interactions detected by LUCID, μ_{LUCID} [22]:

$$\mu_{LUCID} = k \cdot \mu_{pp} \cdot \varepsilon \tag{10.2}$$

where ε is an acceptance and efficiency factor and k is a calibration factor.

There are a number of methods to evaluate the luminosity from μ_{LUCID}. Here the direct, the zero counting and the proportional methods will be discussed in the following sections.

10.2.1. Luminosity from direct measurement

This method relies on having only one hit or less in the LUCID detector per bunch crossing and can therefore only be used at low luminosities (lower than lower than $10^{32} \frac{1}{cm^2 \cdot s}$) where $\mu_{pp} < 0.01$. The number of hits in the LUCID detector will be proportional to the luminosity by normalizing to the number of bunch crossings. Background events might undermine the method if the background is not well understood.

The method is the same as used for the MBTS discussed in Section 10.1.

10.2.2. Luminosity from zero counting

At higher luminosities (higher than $10^{31}\frac{1}{cm^2 \cdot s}$) where the probability of having more than one interaction per bunch crossing is not negligible, LUCID will shift to count bunch crossings without interactions. The probability of having zero interactions does not relate to μ_{LUCID} linearly, but the relation is known. The sensitivity to background is smaller compared to the direct measurement.

The method has a usable range of $0.01 < \mu_{LUCID} < 4.6$, which covers 99 % - 1 % empty events. Outsides this range the statistical uncertainty becomes dominating.

10.2.3. Luminosity from proportionality

The proportionality method is a common name for all the methods that relies on quantities roughly proportional to the luminosity. This could for example be the total number of hit tubes. Most often for these quantities there are non-linearity problems (that may be overcome with specific corrections). The methods often have advantages in limiting background, but are less direct than the methods described above.

10.2.4. From relative to absolute luminosity in LUCID

The relative scale of luminosity measured with LUCID have a precision of a few percent. But the absolute scale is unreliable until LUCID is calibrated with other luminosity measurements. This is clear from equation (10.2) combined with equation (10.1) as the acceptance and efficiency factor, ε, and the calibration factor, k, have to be determined with high precision from outside sources. Also the cross section is not well known at high energies and will add uncertainties until determined elsewhere.

10.3. Luminosity measurement with the Liquid Argon Calorimeter

This section is based on [34] and [35].

LAr is described in Section 7.3.3.1. In the LAr the luminosity can be measured relatively by monitoring the high voltage current or by measuring the rate of particles. Each method will be described in the following sections.

10.3.1. Relative luminosity from the LAr high voltage current

This section is based on [35].

It has been suggested in [35] to use LAr for relative luminosity measurement. This could also be used in online software and the precision is estimated to be 1 %. The method is based on monitoring the high voltage current and is illustrated in Figure 10.1.

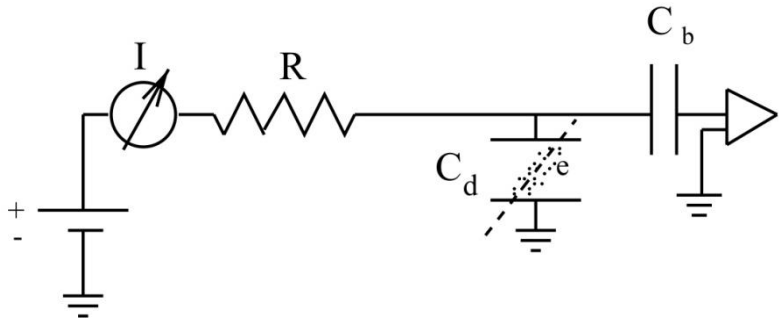

Figure 10.1. A schematic for the useing the current in LAr for relative luminosity measurements. The figure is figure 1 in [35].

The detector is represented by the capacitor called C_d. A particle passes the detector and ionizes the liquid argon. The ionization electrons and ions drift the electric field and induce a current on the anode. The current is measured in the high voltage power supply. The current is therefore proportional to the number of incoming particles, which is proportional to the luminosity.

10.3.2. Absolute luminosity from particles rate

This section is based on [34].

Like for the MBTS (Section 10.1) and the direct method of LUCID (Section 10.2.1) LAr can also measure the rate and equation (8.4) can be used to calculate the luminosity.

This is discussed in [34] for the 2009 data. Most of the background is eliminated by applying trimming cuts: A signal in both + and – direction is required within 5 ns. The cross section is simulated. The errors from the simulation dominate the uncertainty of 21 %.

10.4. Luminosity measurement with BCM

This section is based on [19].

The BCM is described in Section 7.3.5.1 and can be used as a relative luminosity detector. It provides a relative rate and using equation (8.4) with a cross section from simulation or other measurements, the luminosity can measured. Due to the very fast sensors this can be done on a bunch to bunch basis. BCM can also be used for online monitoring of the luminosity.

10.5. Luminosity measurement with the inner detector

This section is based on [36].

The inner detector is discussed in Section 7.3.2. By determining the rate of charged particles and making a correction of the detector efficiency the inner detector of ATLAS (Section 7.3.2) can be used to measure luminosity with equation (8.4). The cross section for equation (8.4) has to come from simulation or other measurements.

For ATLAS, CMS and ALICE (*Rate Normalization Task Force*) it has been agreed to apply the same cuts and use the same software for simulations of this method. Additional the time of the instantaneous luminosity is saved. This should insure directly comparable luminosities for the experiments.

10.6. Luminosity measurement with van der Meer scan

This section is based on [30], [37], [38] and firsthand experience from the ATLAS Control Room.

Equation (8.3) states that the luminosity can be determined if the beam frequency, the number of particles in each beam and the cross section area of the beam is known. The frequency of the beam is very well known (nominal 11245 Hz). The number of particles circulating will be continuously measured with beam current transformers. The accuracy should be 5 % or better. To have a complete luminosity measurement only the area of the beam is missing.

10.6.1. Van Der Meer scan at ISR

Back in the late 1960s S. van der Meer published a method to measure the beam size in the Intersecting Storage Ring, ISR. The idea of this method is so elementally that van der Meer explained it in one sentence:

"*One of the two beams is displaced vertically with respect to the other one, and the counting rate in the monitor is plotted versus displacement".* [38](page 2).

In other words: By adjusting the current and thereby the magnetic field beam 1 was moved. Starting with non-colliding beams no interactions was observed (beside noise and interaction with beam-gas). Moving beam 1 into beam 2 interactions starts to occur and the rate was measured. By scanning beam 1 over beam 2 the beam size could thereby be determined and used to calculate the luminosity.

10.6.2. Van Der Meer scan at LHC/ATLAS

The basic method of the van der Meer, vdM, scan is used at LHC. But because the transverse displacement of the beam at the interaction point is generated with a closed orbit, the beam will also be displaced at the (tertiary) collimator. For the machine protection system to remain efficient the orbit displacement at the (tertiary) collimators has to be kept within a certain range. The displacement at interaction point therefore has to stay within a range that is insufficient to perform vdM scans. Therefore both beams are moved simultaneously in opposite directions. This allowed for a scan range of ± 6σ.

At present a typical scan has 25 points at ATLAS. The movement of the beam is done in 1-2 s, but after the movement a 5 s waiting period is maintained to insure stability. The measuring time at each point is 30 s. The rate is measured in all available detectors, but online the BCM, MBTS, LUCID and ZDC is used to measure the instantaneous luminosity.

A scan is first made in the horizontal direction using the last known optimal value for the vertical direction. An example of the online feedback is shown in the left side of Figure 10.2.

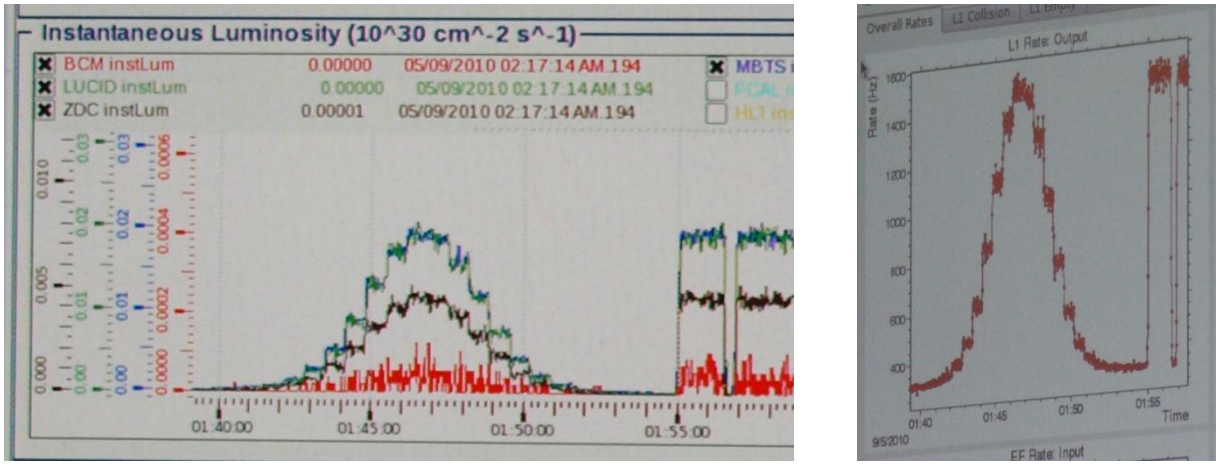

Figure 10.2. ***LEFT*****: Online view of the Instantaneous Luminosity for a horizontal vdM scan. The x-axis is time. The y-axis is instantaneous luminosity in $10^{30}\frac{1}{cm^2 \cdot s}$. MBTS (blue) and LUCID (green) is co-calibrated (From Monte Carlo simulations). The BCM (red) and ZDC (brown) is yet not co-calibrated.** ***RIGHT*****: Online view of the Level 1 trigger rate of ATLAS. The x-axis is time. The y-axis is level 1 trigger rate. Both figures are photographs of the online software taken by the author in the ATLAS Control Room on 09-05-2010 between 01.00 and 3.30 (used with permission).**

The steps are clearly shown in the Gaussian shape. The vdM scan could also clearly be followed in the level 1 trigger rate of ATLAS (see Section 7.3.6 about the ATLAS trigger system) as shown in the right side of Figure 10.2.

Next the horizontal direction is locked to the optimal value and the vertical direction scanned.

In the later analysis the beam position in each step will replace the time in Figure 10.2 and the combined sizes of the beams fitted. The mean value will give the optimal settings for colliding the beams head on (this will differ in each fill and therefore a “small vdM scan” (optimization) is made after each fill).

10.7. Luminosity determination from well-known processes

This section is based on [31].

Using equation (8.4) for a well-known process will give the luminosity. So if the rate can be measured with a high accuracy and the cross section is well known this could be a method for luminosity determination.

10.7.1. Luminosity measurement from Z production

This section is based on [31](section 13.3.4).

The properties of the Z boson is very well known from the LEP experiment [28](page 393). At nominal luminosity the production of Z bosons will have a rate of about 10 Hz in LHC, which should give a statistical uncertainty of 1 % in about 20 min. However the cross section for Z production at LHC energies has significant uncertainties in QCD. The cross section therefore needs to be determined elsewhere for Z production to be used for absolute luminosity determination. However Z production could be used for relative luminosity determination.

10.7.2. Luminosity measurement from two-photon production of e^+e^- pairs

This section is based on [31](section 13.3.3.1).

The cross section for very forward two-photon production of e^+e^- pairs can be calculated at LHC energies within QED to an accuracy better than 1 %. A Feynman diagram of the process is depicted in Figure 10.3.

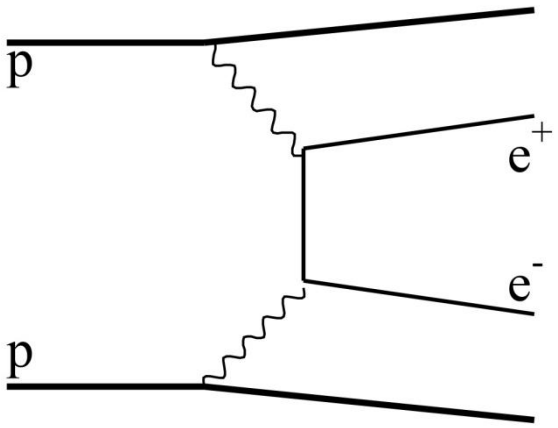

Figure 10.3. Feynman diagram for two-photon production of e^+e^- pairs. The figure is figure 13-4 in [31].

The cross section for the process should give a relative high rate. But the background rate is even larger than the signal. By applying the following cuts it should be possible to eliminate most of the background.

Cuts:

1. Electron energies: 5-20 GeV
2. Electron polar angles $\theta < 0.8$ mrad
3. e^+e^- pair invariant mass < 10 MeV
4. e^+e^- pair transversal momentum < 10 MeV
5. Veto on charged particles with $|\eta| < 7.6$

By applying cut 1-4 the background rate is 139 % of the signal rate. By adding cut 5 the background rate is reduced to about 1 % of the signal rate. The rate estimations are from simulations.

10.7.3. Luminosity measurement from two-photon production of $\mu^+\mu^-$

This section is based on [31](section 13.3.3.2).

Similar to the two-photon production of e^+e^- pairs discussed in Section 10.7.2, the two-photon production of $\mu^+\mu^-$ pairs is well described in QED and the cross section can be calculated with high accuracy. The Feynman diagram of the process is similar to Figure 10.3. The electrons are just replaced with muons. The production rate of muons is lower than for electrons, but the background is also lower. Like for the electrons a number of cuts are applied:

1. Two muon tracks with opposite charges (Trigger criteria)
2. $\mu^+\mu^-$ pair invariant mass < 60 GeV (Suppresses background from Z decays)
3. Transversal momentum of the muons equal (within 2.5 σ)
4. Muons back to back (within 1 degree)
5. Good muon fit (χ^2 probability > 1%)
6. No other reconstructed charged tracks originating from the $\mu^+\mu^-$ vertex (suppress background with high multiplicity)

For an integrated luminosity of 10 fb^{-1} the statistical accuracy should be about 2 %. However even though the cross section for the two-photon production of $\mu^+\mu^-$ pairs can be determined with good accuracy within QED, the background that have to be subtracted still relays on QCD in a yet unknown energy domain (with larger uncertainties), and the final luminosity determination therefore suffers.

10.8. Luminosity determination with the Optical theorem

This section is based on [39](section 2.1).

The cross section of elastic scattering relates to the total interaction cross section through the optical theorem [40](equation 1.10):

$$\sigma_{tot} = 4 \cdot \pi \, \mathrm{Im}[A_{el}(t=0)] \tag{10.3}$$

σ_{tot} Total cross section
A_{el} Forward elastic scattering amplitude
t Transferred four momentum

For small forward scattering angles, θ, the transferred four momentum, *t*, can be found as [39](equation 2-2):

$$-t = (p \cdot \theta)^2 \tag{10.4}$$

p beam momentum
θ forward scatter angle

Equation (10.3) and (10.4) implies that knowledge about the scattering in the forward direction will lead to the total cross section.

10.8.1. Luminosity determination by the elastic scattering and the inelastic rate

By simultaneously measuring the total interaction rate, R_{tot}, and the elastic rate $\left.\frac{dR_{el}}{dt}\right|_{t=0}$ in the forward direction, the luminosity can be determined using the equation (8.4) and the optical theorem equation (10.3) [39](equation 2-3):

$$\mathscr{L} = \frac{1}{16 \cdot \pi} \frac{R_{tot}^2 (1+\rho^2)}{\left.\frac{dR_{el}}{dt}\right|_{t=0}} \tag{10.5}$$

where ρ is defined as:

$$\rho \equiv \left.\frac{\mathrm{Re}\left[A_{el}(t)\right]}{\mathrm{Im}\left[A_{el}(t)\right]}\right|_{t=0} \tag{10.6}$$

The parameter ρ is known sufficiently precisely to not contribute significantly to the systematic error.

The determination of the luminosity from equation (10.5) relies on the total rate being measured. This requires a detector that measures all angles (all range of η). As this is not possible, the very forward part (high η) has to be simulated. The uncertainty of this simulation dominates the uncertainty of the method.

10.8.2. Luminosity determination by the elastic scattering and total cross section from TOTEM

One of the main purposes of the TOTEM (Section 7.2) detector at the LHC is to determine the total cross section at LCH energies with high accuracy. If they succeed this information could be used to determine the luminosity at the ATLAS interaction point. This could be done by inserting equation (8.4) into equation (10.5) to eliminate the total rate, R_{tot} [39](equation 2-6):

$$\frac{1}{\mathscr{L}} = \frac{1}{16 \cdot \pi} \frac{\sigma_{tot}^2 (1+\rho^2)}{\left.\frac{dR_{el}}{dt}\right|_{t=0}} \tag{10.7}$$

The uncertainties of this method would depend on the accuracy of the total cross section achieved by TOTEM.

10.8.3. Luminosity determination from Coulomb scattering

This section is based on [31](section 2) and [41].

A different approach can be used which does not depend on the total rate or other experiments: Measure elastic scattering down to such small t-values that the total cross section becomes sensitive to the electromagnetic amplitude. This will allow determination of both the luminosity and the total cross section.

Back at the UA4 experiment at the CERN SPS proton-antiproton collider the luminosity was determined with this method to a precision of 3 % [41].

For small transferred four momentum values the rate of elastic scattering can be simplified to [39](equation 2-7):

$$\frac{dN}{dt} = \mathscr{L} \cdot \pi \cdot \left|A_C + A_N\right|^2 \approx \mathscr{L} \cdot \pi \cdot \left| -\frac{2 \cdot \alpha_{EM}}{|t|} + \frac{\sigma_{tot}}{4 \cdot \pi} (i+\rho) \cdot e^{\frac{-b \cdot |t|}{2}} \right|^2 \tag{10.8}$$

A_C Coulomb interaction amplitude

A_N Strong interaction amplitude

α_{EM} Electrometric coupling constant

b Slope parameter

At low transferred four momentum the Coulomb term becomes dominating. This is illustrated in Figure 10.4.

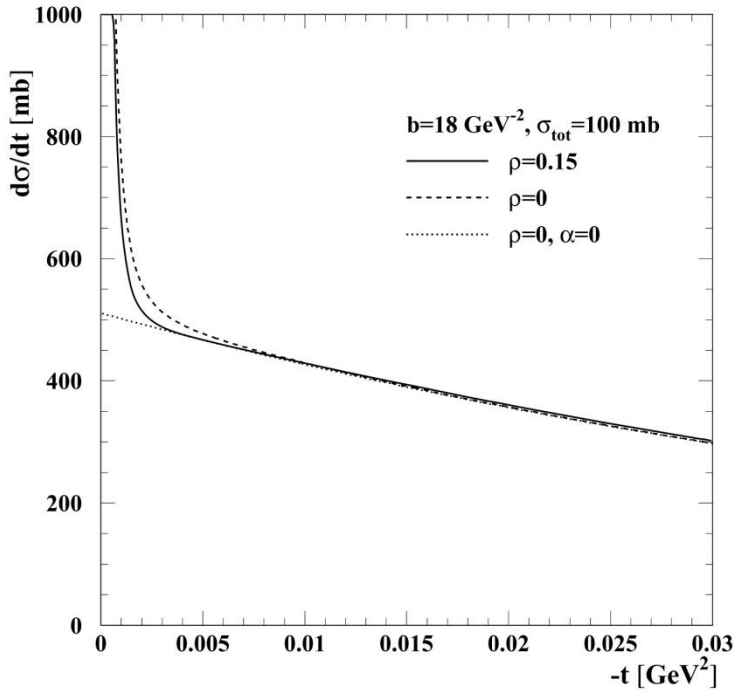

Figure 10.4. Elastic cross section as a function of *t*. The difference between $\rho = 0$ and $\rho = 0.15$ illustrates the Coulomb interference region. The $\alpha = 0$ illustrates the strong interaction contribution. The figure is figure 2.1 in [39].

At nominal LHC energy (7 TeV per beam) the strong amplitude is expected to be equal to the electromagnetic amplitude for $|t| = 0.00065$ GeV^2 which corresponds to a scattering angle of 3.5 µrad. At the SPS the Coulomb region was reached at a scattering angle of 120 µrad. This underlines the challenge of the method at the LHC.

10.8.4. Methods used by ALFA

This section is based on [39](section 2).

The ALFA detector aims at using Coulomb scattering as discussed in Section 10.8.3 and aims for an absolute luminosity determination with a precision of 3 %. This will be done by fitting equation (10.8) and thereby determine the luminosity, the parameter ρ, the total cross section and the slope parameter b.

However reaching the Coulomb region is very challenging and some of the conditions needed for a satisfactory measurement are expected to be close to the limits in performance of the LHC. So if it is not possible to reach the Coulomb region, the methods discussed in Section 10.8.1 and 10.8.2 will be used.

11. Beam properties

This section is based on [39](section 2.2 and 3).

As discussed in Section 10.8 ALFA will determined the absolute luminosity by measuring the transferred four momentum (via the scatter angle) and rate of very forward scatted protons. For this to be possible special beam optics are needed and therefore dedicated runs. At the interaction point the beams needs to be quasi-parallel and must have a divergence significantly smaller than the smallest scattering angles that needs to be observed. This section describes the optical setup for the dedicated ALFA runs.

11.1. Optics for the use of the ALFA detector

This section is based on [39](section 3.1 and 3.6).

LHC has two beam pipes separated by 194 mm. This makes constrains on access to the beam pipes from one side and makes it considerably easier to approach the beam from above and below the beam axis. Therefore the ALFA detectors will approach the beam vertical and the optics will be optimized for a 90 degree phase advance in the vertical plan. The displacement in the y direction is then given by [39](equation 3-6):

$$y = \sqrt{\beta\beta^*}\,\theta_y^* \tag{11.1}$$

From equation (8.5) the distance from the beam center can be expressed as a multiple, n_d, of the beam spot size (about 130 µm) [39](equation 3-9):

$$y = n_d \cdot \sqrt{\varepsilon \cdot \beta} \tag{11.2}$$

By combining equation (10.4), (11.1) and (11.2) the minimum transferred four momentum can now be written as [39](equation 3-10):

$$-t_{\min} = p^2 \cdot n_d^2 \cdot \frac{\varepsilon}{\beta^*} \tag{11.3}$$

where emitance is given by the normalized emitance and the Lorentz factor[39](equation 3-11):

$$\varepsilon = \frac{\varepsilon_N}{\gamma} \tag{11.4}$$

Equation (11.3) can be used to evaluate the minimum transferred four momentum which will be possible to measure. The momentum of the beam, p, has to be kept at the momentum on which the luminosity should be determined (7 GeV/c for nominal LHC energy). The minimum distance from the beam (in beam widths, σ), n_d, will be found during the runs. If the distance gets too small the detector will get radiated very fast and the beam might be lost. A first estimate would be a value of 15 σ. The normalized emitance should be of the order of 1 µm rad and the Lorentz factor is given directly from the beam energy (value about 7500). The betatron-function (amplitude function) at the interaction point, β^*, should be maximized. Around ATLAS this means a value of about 2600 m.

For the values mentioned above the minimum transferred momentum is 0.0006 GeV^2. In Figure 10.4 page 47 this is just inside the Coulomb region.

A concrete optic solution with $\beta^* = 2625$ m has been found to be used for ALFA runs. The solution also includes the position of the detectors 240 m on each side of the interaction point. The optical layout is shown in Figure 11.1.

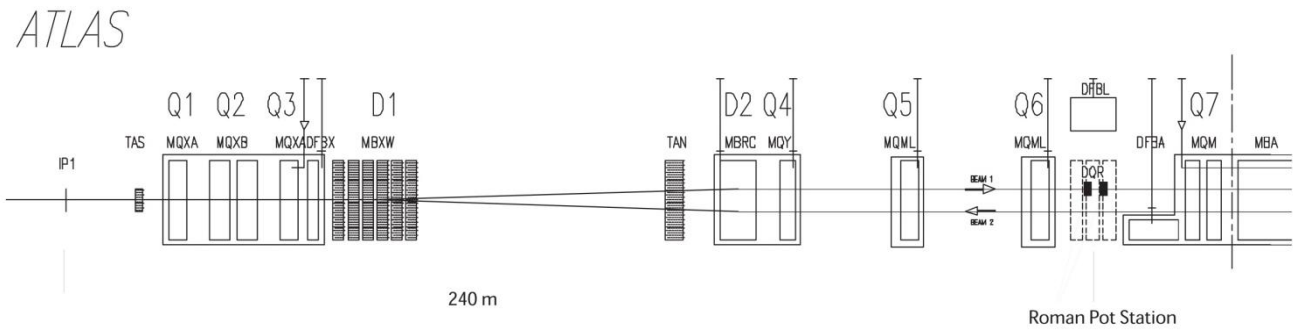

Figure 11.1. Optical layout and position of the ALFA detectors seen from inside the LHC. The figure is figure 3-1 in [39].

The optical solution does not require any additional hardware. However quadruole 4 (Q4) needs reversed polarity compared to standard optic.

The optics are compatible with the optics prepared by the TOTEM collaboration for special runs with $\beta^* = 1540$ m. Therefore TOTEM and ATLAS can have high beta optics at the same time and share the dedicated runs.

In the special runs the luminosity will be $10^{27}\frac{1}{cm^2 \cdot s}$ rather than the nominal $10^{34}\frac{1}{cm^2 \cdot s}$. A factor ~1000 lower luminosities comes directly from the high betatron-function value. Another factor of about 100 is achieved by operating with only 43 bunches rater than 2808 bunches. The lowered number of bunches makes a very good separation between each bunch (2.1 μs or 630 m) and eliminates the need for a crossing angle at the interaction point (normally used to avoid interaction of bunches away from interaction point). Each bunch will have 10^{10} protons rather than the nominal 10^{11} protons. All the changes reduced the luminosity be a factor of 10^7. This makes it much safer to operate the Roman Pots very close to the beam.

11.2. Collimation and beam halo

This section is based on [39](section 3.5).

The LHC has a powerful collimation system for protection and to avoid quenches. The collimation system is based on adjustable primary and secondary collimators. When the beam is collimated a halo is created. This halo can be split into secondary and tertiary parts. An example is given in Figure 11.2.

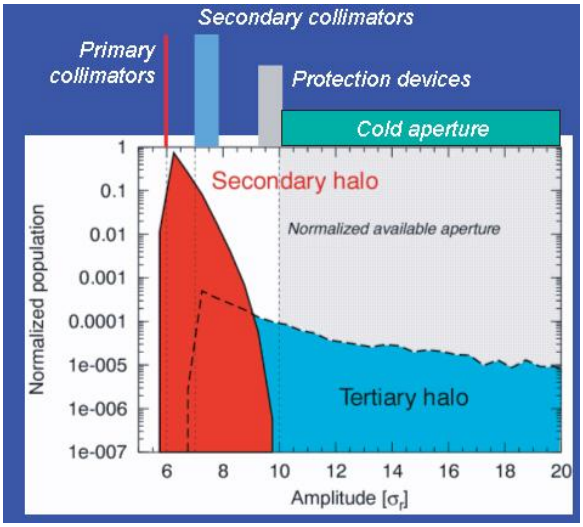

Figure 11.2. Normalized secondary and tertiary halo as a function of the distance from the beam center (in multiple of the beam size, σ). The primary collimators are set at 6 σ. The secondary collimators are set at 7 σ. The figure is figure 3-7 in [39].

Figure 11.2 shows that with the primary collimators set at 6 σ and the secondary collimators set at 7 σ a Roman Pot (see Section 13.3) at 10 σ would be in the shadow of the primary collimator. Unfortunately Figure 11.2 is not based on the special runs for ALFA, but on the standard runs. Also the halo does not only originate from the collimators. Therefore a dedicated simulation study was carried out to estimate the halo in the dedicated runs [39](section 3.5.2). Three sources were considered:

1. Halo particles originating from inefficiencies of the betatron collimation system (BC)
2. Halo particles originating from inefficiencies of the momentum collimation system (MC)
3. Halo particles originating from elastic and quasi elastic scattering of the beam protons on the nuclei of the residual gas (beam-gas).

The results are shown in Figure 11.3.

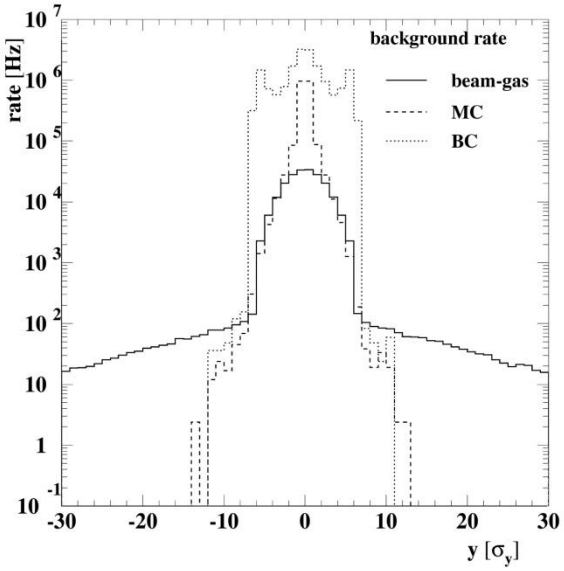

Figure 11.3. The halo in dedicated ALFA runs. The figure is figure 3-9 in [39].

Over 10 σ only the halo originating from the beam-gas is significant.

The integrated rate from the halo above 10 σ is 2000 particles/s. This will be the background for the measurements. However most of this background will be eliminated by demanding coincidence to the opposite (below to above, above to below) detector on the other side of the interaction point.

12. Requirements for the ALFA detector system

This section is based on [39](section 5.1) and [42].

The methods for luminosity determination discussed in Section 10.8 dictates the main requirements for the detector:

1. Spatial resolution (vertical and horizontal) about 30 µm
2. Negligible inactive edge zone (< 100 µm)
3. Uniform trigger and detection efficiency (~100 % trigger efficiency)
4. Precise relative positioning of the detectors (<10 µm)

Beside the directly dictated requirements some additional secondary requirements have to be fulfilled:

5. Operational in vacuum (mbar range)
6. Immunity to RF pick-up from the proton beam
7. Capable to cope with different beam positions
8. Moderate radiation hardness (kGy range)
9. Easy and quick to install and remove
10. Readout speed fast enough to identify each bunch crossing uniquely

Requirement number 1 comes from the resolution in transferred four momentum. With a beam size of about 130 µm a resolution of 30 µm is considered adequate. A high resolution can also be used to reject background. The angle is measured between the two stations 4.14 m apart on one side. The same is done on the other side of the interaction point. If the timing and angles do not agree the event is marked as background.

Requirement number 2 comes directly from equation (10.8). Any inactive zone close to the beam will significantly move the sensitivity in transferred four momentum to a higher value and potentially out of the Coulomb region as shown in Figure 10.4 page 47.

Requirement number 3 also comes directly from equation (10.8). If the trigger or detection efficiency is not well-known the rate cannot be determined correctly. To have uniform triggering ALFA therefore aim at ~100 % trigger efficiency and high detector efficiency.

Requirement number 4 also relates to equation (10.8). The transferred four momentum will be measured by combining events from each side of the interaction point. For this to be possible the position needs to be well-known. If the detectors approach the beam to a distance of 1.5 mm then a systematic shift of $\Delta y = 15\ \mu m$ represents a positioning error of $\frac{\Delta y}{y} = 1\ \%$, which consequently represents a angular error of $\frac{\Delta \theta}{\theta} = 1\ \%$, which implies a 2 % luminosity error [39](section 5.2.3). The relative alignment will be done using beam halo (see Section 13.1.3). For the error of the relative detector position not to become dominating it needs to be known to a precision of 10 µm.

Requirement number 5 relates to the Roman Pot technology (Section 13.3). A secondary vacuum around the detector is necessary to approach the beam.

Requirement number 6 comes from the environment around the detector. The beam will be very close to the detector and could potentially induce noise in any electronic part.

Requirement number 7 originates from the filling of LHC. Each fill might have a different height in the beam pipe. The differences could be of the order of millimeters. The mechanics for the detector have to be able to counteract this.

Requirement number 8 and 9 relates to the limited use of the absolute luminosity detector system. The detector will only be used in dedicated runs. It is planned to remove the detectors and readout system (but leave the stations and Roman Pots) between each dedicated run to avoid radiation damage when the LHC is running at high luminosity. Therefore the detectors have to be easy and fast to removed and install. On the other hand this means that the detector, electronic etc only have to be moderate radiation hard.

Requirement number 10 comes from the desire to identify each bunch individually to potentially make a bunch to bunch luminosity measurement.

13. The ALFA detector

The Absolute Luminosity For ATLAS, ALFA, detector is a tracking detector dedicated for measuring absolute luminosity. This section describes the detector in detail.

13.1. The detector

This section is based on [39](section 5).

The detector is build up of scintillating fibers. The part of the fibers intended to be active are inside a Roman Pot (see Section 13.3) in a vacuum, but the fibers ends are outside. This way the MultiAnode PhotoMultiplier Tubes, MAPMTs, (see Section 13.1.4) used to read out the fibers are outside the Roman Pot. This has the advantage that no electrical part is inside the Roman Pot and therefore there is no risk of RF pick up from the beam. The detector thereby satisfies requirement number 6 in Section 12. The other advantage of the fibers ending outside the Roman Pot is that the MAPMTs do not have to be inside the vacuum which might cause discharge of the MAPMT and trigger PhotoMultiplier Tubes, PMTs. Only the fibers are in the vacuum and they do not harm in any way from the vacuum. The detector therefore satisfies requirement number 5 in Section 12.

The detector consists of a main part used for tracking particles and an overlap part used for alignment. The fibers for the main detector and the overlap detector are read out by MAPMTs. The main detector and the overlap detector have dedicated trigger tiles read out by PMTs. A full detector is shown in Figure 13.1.

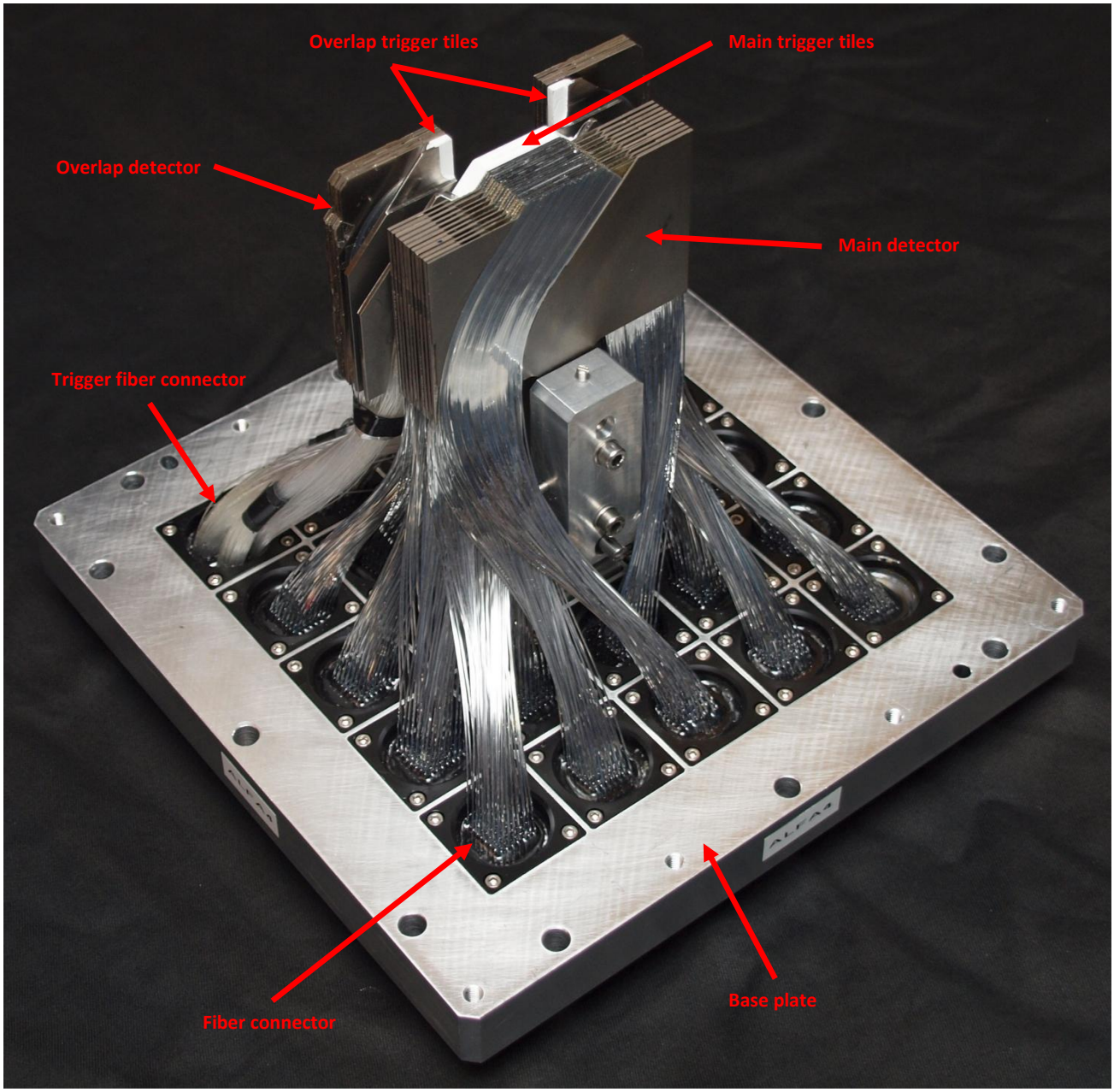

Figure 13.1. An ALFA detector (ALFA4). The detector fit inside the ALFA Roman Pot shown in Figure 13.37 page 79.

The following sections describe each part in detail.

13.1.1. Scintillating fibers

This section is based on [43] and [39](section 5.2).

The scintillating fibers used in the ALFA detectors are made by Kuraray Co LTD (Tokyo, Japan). They are of type SCSF-78, S-type, 0.5 x 0.5 mm^2 and have peak emission at 450 nm. These are squared single cladding fibers as shown in Figure 13.2.

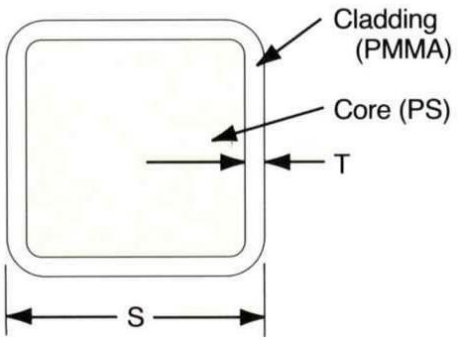

Figure 13.2. Squared scintillating fiber with single cladding. The figure is from [43] page 2.

Squared fibers have a higher trapping efficiency (4.2 % for single cladding) than round fibers (3.1 % for single cladding). This is explained by the total refection needed to trap the light inside the fiber. For a round fiber this is shown in Figure 13.3.

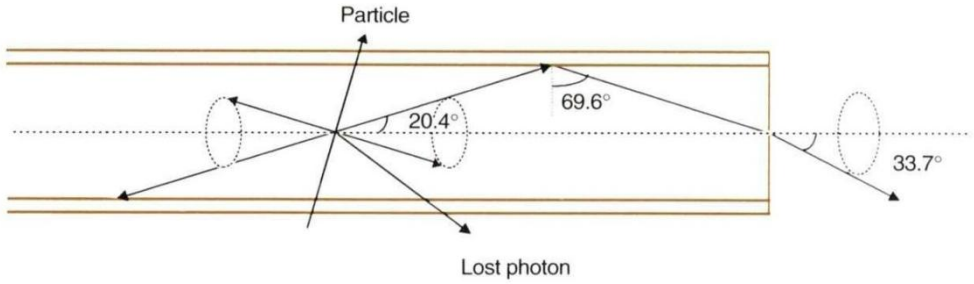

Figure 13.3. Total refection and light trapping in a round fiber with single cladding. The figure is from [43] page 3.

For square fibers trapping angle will be larger for the light reflecting near the corners of the fiber than for the light reflecting in the center of the fiber (which is comparable to all reflections in a round fiber). An additional layer of cladding would also increase the trapping angle as shown in Figure 13.4.

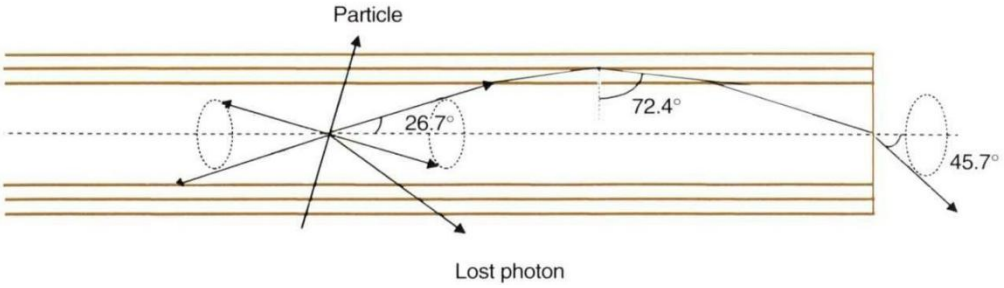

Figure 13.4. Total refection and light trapping in a round fiber with multi cladding. The figure is from [43] page 3.

The total reflection in the fibers with multi cladding allows for a larger trapping angle and thereby increases the light yield. Kuraray claims a 50 % higher light yield. But the additional cladding also means less cross section active material. When the fibers a stacked side by side this becomes significant. The cladding is made of Plexiglas (PMMA) and has a thickness of 2 % (10 µm) of the squared fibers with single cladding. For the round fibers the cladding is 3 % of the fiber per layer cladding. Therefore squared fibers with single cladding have been chosen for the ALFA detectors.

The “S” in the fiber name specifies that the polystyrene is orientated along the length direction of the fiber. This makes the fiber mechanically stronger, but the attenuation length is about 10 % shorter. As the fibers in the ALFA detector are relatively short the difference in attenuation is of only little importance, but the mechanical properties is imported as the fibers needs to be bent. Especially the fibers in the overlap

detectors need a significant bent. This is described in Section 13.1.3 and the long term effects of the bending are tested in Section 15.6.

The fibers are coated with a thin layer of aluminum. This is done to avoid optical cross talk where light propagates from one fiber to the neighbor fiber as illustrated in Figure 13.5.

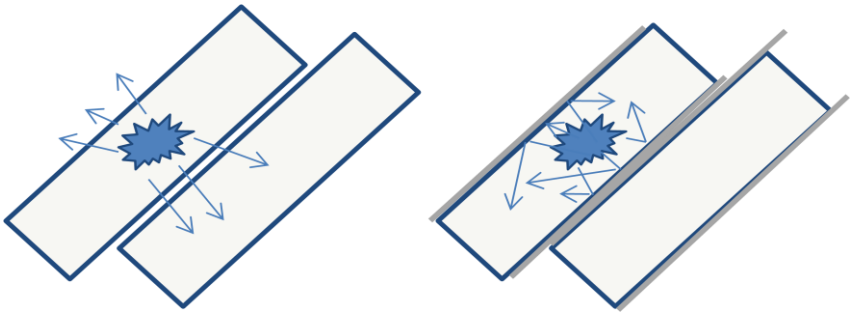

Figure 13.5. *LEFT*: Fibers without an aluminum coating. Light propagate from the hit fiber to the neighbor fiber. *RIGHT*: Fibers with an aluminum coating. Light is reflected back into the hit fiber. The figures are from [42] (Design criteria and performances, C. Joram).

The aluminum coating is applied onto the fibers by evaporation using facilities at CERN.

One end of the fibers is machined and aluminum coated by sputtering at LIP, Lisbon. This is done to make a mirror on the fiber end not intended to be connected to a MAPMT. This increases the light yield. A photo of an uncoated and a coated fiber is shown in Figure 13.6.

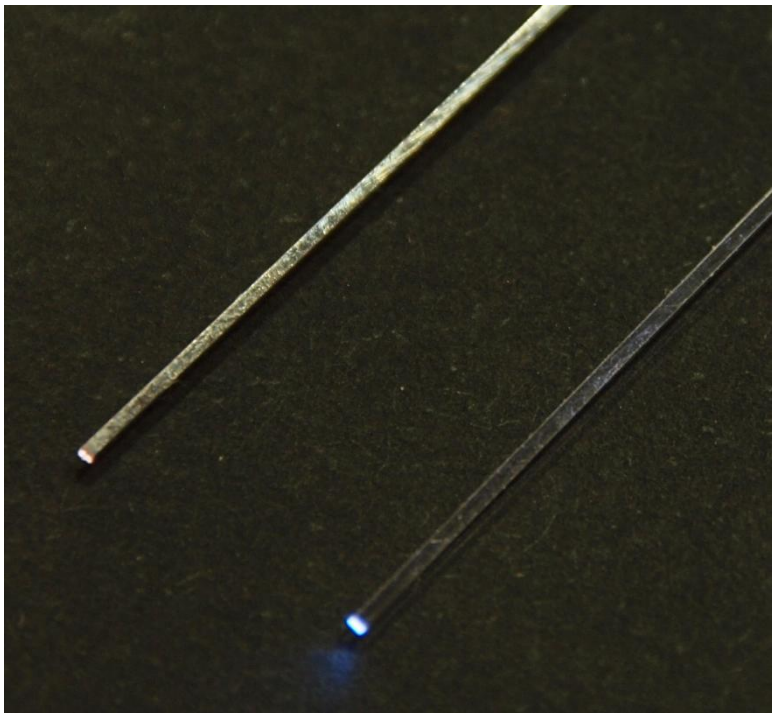

Figure 13.6. *LEFT/TOP*: Aluminum coated fiber. *RIGHT/BOTTOM*: Uncoated fiber.

The fibers in Figure 13.6 are illuminated with white light from the side. The wavelength shifting properties of the scintillating fiber gives the blue color observed.

Requirement number 8 in Section 12 states that the detector and electronic etc need to be moderate radiation hard. The fibers will by far receive the most radiation as they will be very close to the beam and inside the beam halo. Radiation damage on the Kuraray SCSF 78 fibers has been studied by the HERA-B collaboration [44]. For a dose of about 1 kGy the light yield was found to decrease about 10 % and for a dose

of about 10 kGy the light yield was down by 30 %. The ALFA collaboration also made their own study of the radiation damage [45]. The result is shown in Figure 13.7.

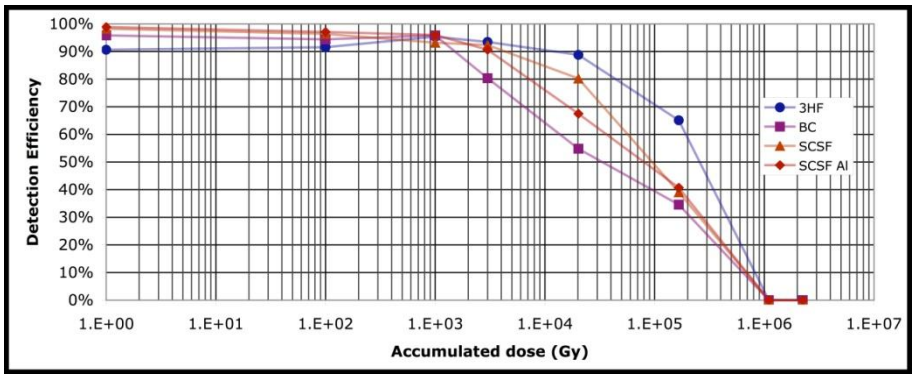

Figure 13.7. Detection efficiency as a function of accumulated dose in the scintillating fibers. The results are included for both the fiber without aluminum cladding (SCSF) and with the aluminum cladding (SCSF Al). Two other competing fibers are also included. The figure is from [45].

For an accumulated dose of about 3 kGy the detection efficiency is still over 90 %, which would be acceptable. Both the HERA-B study and the ALFA study showed that the fibers recovered fully in a few weeks after the test if the accumulated dose was less than 10 kGy.

The studies discussed above shown that the fibers meet with the requirement for radiation hardness.

13.1.2. Main detector

The main detector is build up of layer with 64 fibers in each. Each plane has two perpendicular layers (U and V) glued to a titanium substrate. The pieces to make up a plane are shown in Figure 13.8.

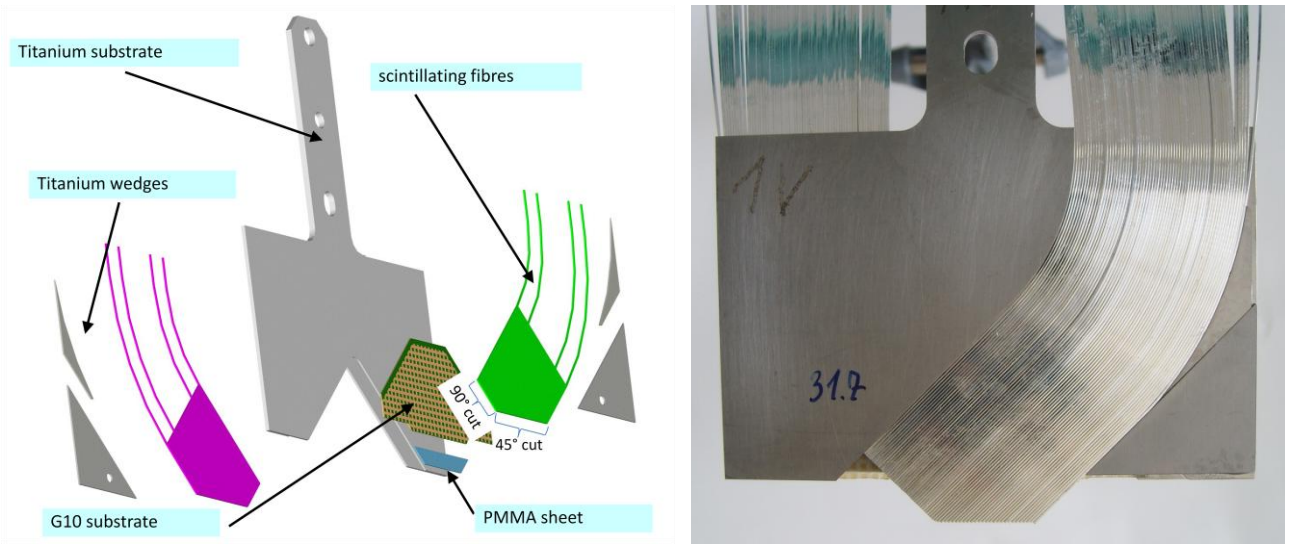

Figure 13.8. *LEFT*: The pieces to make a detector plan. The green fibers make up a V layer. The purple fibers make up a U layer. The figure is from [42](Design criteria and performances slide 4, C. Joram,). *RIGHT*: Photo of detector plane. The fibers for the V layer are shown. The fibers for the U layer are on the back of the titanium substrate. The 45 degree fibers are not cut yet. The figure is from [42](Detector production slide 4, H. Stenzel).

24 of the fibers have a 90 degree cut at the end. The other 40 fibers are cut at 45 degrees. This is done to get the fiber as close as possible to the Roman Pot windows (see Section 13.3) and thereby to the beam as suggested by requirement number 2 in Section 12. As discussed in Section 13.1.1 the fibers are coated with aluminum at the end to make a mirror. When the fibers are machined at 45 degrees the mirror is lost. The ALFA collaboration has therefore made a dedicated study [39](section 5.2.2) of the reflectivity for 90 and 45

degree cut fibers with and without aluminum coating at the end. An external mirror was also included in the study. The results are shown in Figure 13.9.

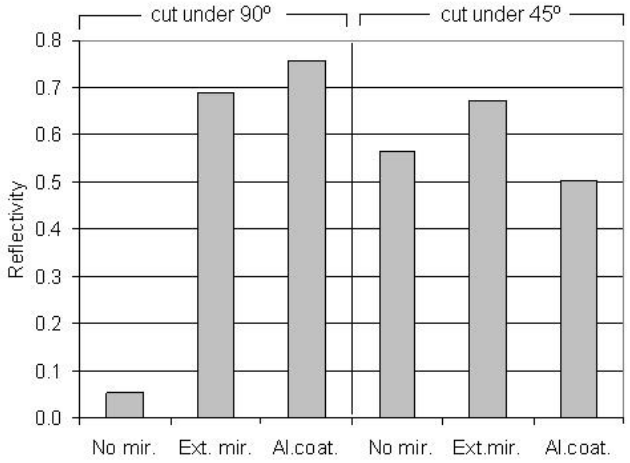

Figure 13.9. Reflectivity with and without aluminum coating at the fiber end for 90 and 45 degree cut fibers. An external mirror was also included in the study. The figure is figure 5-4 in [39].

The results show that for the 90 degree cut fibers a mirror is essential. But for the 45 degree cut fibers the reflectivity is almost independent of the presence of a mirror on the fiber end. This is due to the angle of the light relative to the fiber end as illustrated in Figure 13.10.

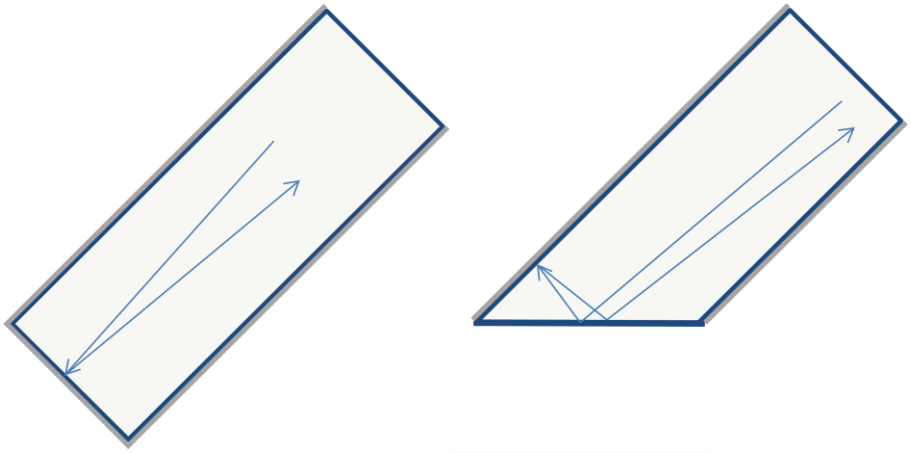

Figure 13.10. *LEFT*: 90 cut fiber. A mirror is needed at the fiber end to reflect the light back into the fiber. *RIGHT*: 45 degree cut fiber. The light is trapped inside the fiber because of total internal reflections. The figures are from [42](Design criteria and performances slide 6, C. Joram). Minor details have been changed in the figure.

For the 90 degree cut fibers the light hits the end at almost 90 degrees. A mirror is needed to reflect the light back into the fiber. For the 45 degree cut fibers the light hits the fiber end at about 45 degrees and most of the light is trapped inside the fiber because of total internal reflections.

Requirement number 1 in Section 12 stats that the resolution of the detector should be about 30 µm. For one plan with an U and a V layer with perpendicular fibers the "pixel" has a width d = 500 µm which give a width in the x-y plane of $\sqrt{2} \cdot 500\ \mu m \approx 707\ \mu m$ as shown in Figure 13.11.

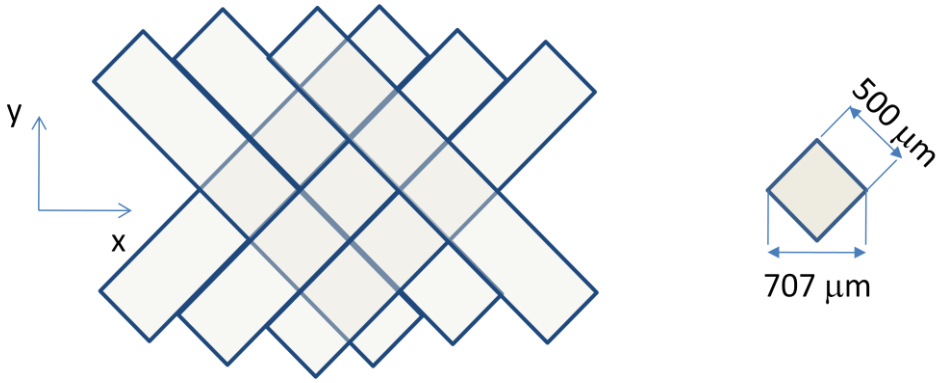

Figure 13.11. ***LEFT*****: Fibers from U and V plan crossing making "pixels".** ***RIGHT*****: Size of one "pixel". The figures are from [42](Design criteria and performances slide 3, C. Joram).**

The resolution of one plan can be calculated as the Root Mean Square, RMS [42](Design criteria and performances slide 3, C. Joram). Explained with more details:

$$RMS = \sqrt{\int_{-\frac{d}{2}}^{\frac{d}{2}} \frac{(x - x_0)^2}{d} dx} \tag{13.1}$$

x_0 is chosen to be 0:

$$RMS = \sqrt{\int_{-\frac{d}{2}}^{\frac{d}{2}} \frac{x^2}{d} dx} = \sqrt{\frac{\frac{1}{3}x^2 \Big|_{-\frac{d}{2}}^{\frac{d}{2}}}{d}} = \frac{d}{\sqrt{12}} \tag{13.2}$$

Equation (13.2) is made in the UV coordinate system, but from geometry it can be seen also to be valid in x-y. For the pixel size of one layer with d = 500 µm the resolution is therefore about 144 µm. Requirement number 1 in Section 12 demanded a resolution of about 30 µm. The resolution of one plan is therefore insufficient. An ALFA detector is therefore using 10 plans. Each plan is shifted by $\frac{1}{10}$ of the fiber diameter. The staggering is shown in Figure 13.12.

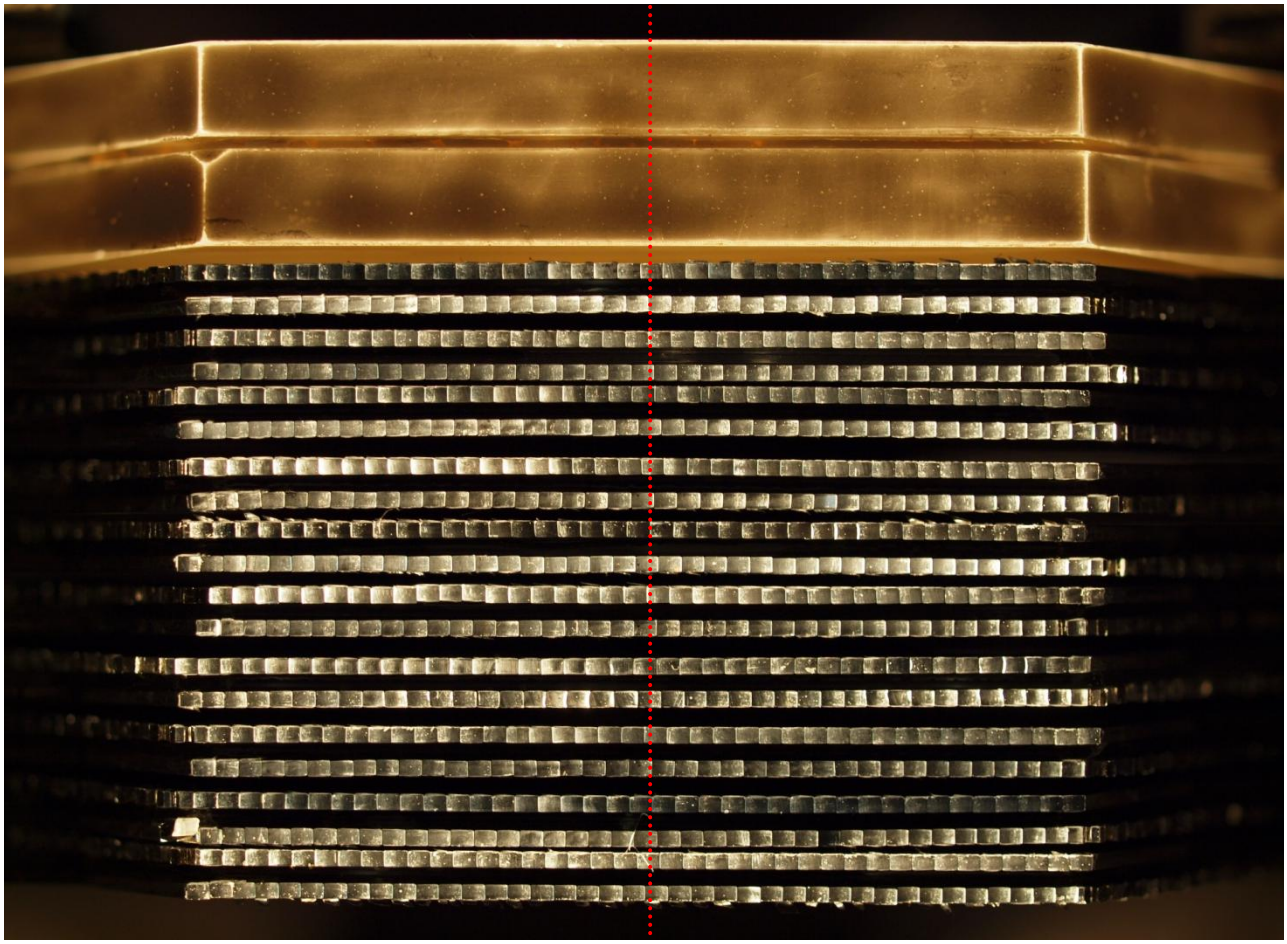

Figure 13.12. Photo of the 10 planes and two main triggers tiles (see Section 13.1.5) in an ALFA detector (ALFA5). The red line represents a particle crossing the detector and illustrates the better resolution determination possible with staggered plans. The fiber ends of the 45 degree cut fibers are made visible by illuminating the fiber connections to the MAPMTs (see Section 13.1.4) with white light.

The staggering does effectively make the pixel size 10 times smaller. Using equation (13.2) the resolution can therefore be calculated to 14.4 µm, which easily satisfy requirement number 1 in Section 12. This is however assuming perfect staggering and 100 % fiber efficiency. The claddings of the fibers are inactive and occupy 2·2 % of the layer width as the fibers are packed side by side. Even with perfect packing of the fibers the fiber efficiency will therefore not exceed 96 %. From the test beam in 2008 [46] the layer efficiency was determined to about 90 %. The position of the fibers on each plan has been measured and a simulation made to determine the resolution. The simulation show a resolution of 25-29 µm for the detectors expected to be installed [47]. This more realistic resolution result still satisfies requirement number 1 in Section 12.

13.1.3. Overlap detector

The overlap detector has a left and a right side. Each side has 30 fibers. These a separated into 15 glued to each side of a titanium substrate. The overlap detector is shown in Figure 13.13.

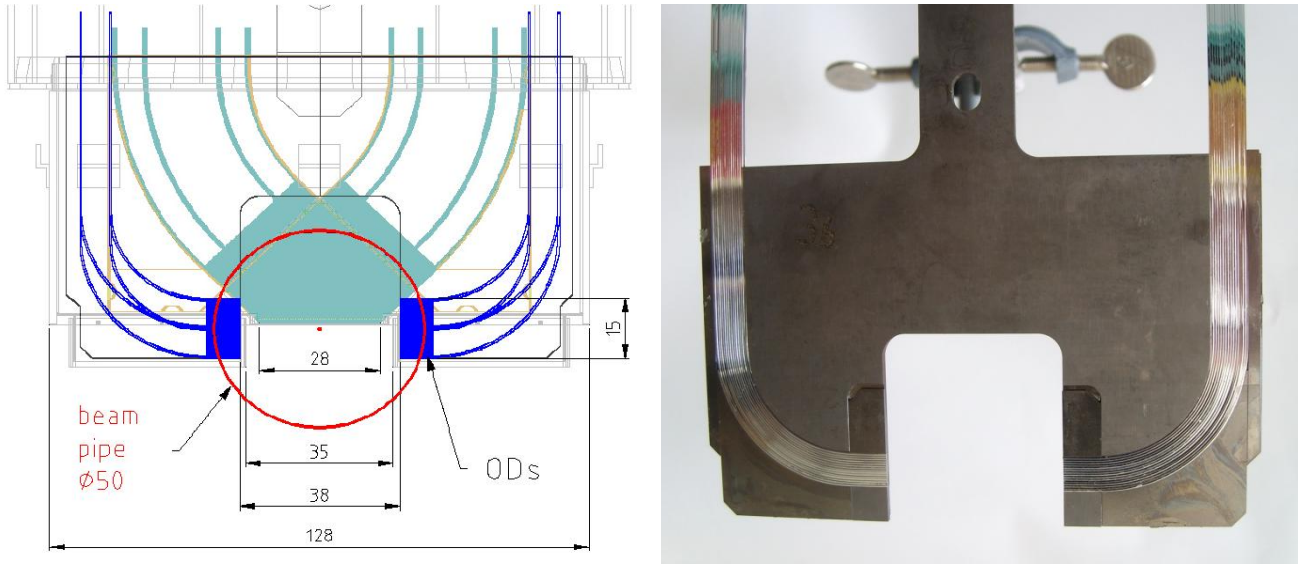

Figure 13.13. *LEFT*: The overlap detector integrated with the rest of the detector. The overlap detector fibers are blue, the main detectors fibers are green. The figure is figure 5-5 in [39]. *RIGHT*: Photo of an overlap plan. One layer of fibers is shown. The other layer is on the back of the titanium substrate and has fibers next to the titanium edge. The figure is from [42](Detector production slide 4, H. Stenzel).

The part of the fiber indented to be active is mounted horizontally and have a 90 degree cut with an aluminum coating as a mirror at the end. To make the horizontal mounting possible and comply with the spacious constrains of the Roman Pot (see Section 13.3) the fibers has to be bent at a smaller radius than the manufacture recurrent (see Section 13.1.1). The recommendations for the minimum bending radius were for round fibers. A larger minimum bending radius is to be expected on square fibers as the outer corners will have more stress than the outside center of a round fiber. Studies on fiber bending [48] and [49] were made and it was concluded that the fibers could be bent to the needed radius at an elevated temperature of about 85 ˚C. The long term stability of the fiber performers for the bent fibers is discussed in Section 15.6 and published as *[50]*.

The purpose of the overlap detector is to align the upper and the lower detector in an ALFA station. Requirement number 4 in Section 12 states that the position needs to be known to a precision of 10 µm. The relative position of the upper and lower detector will be determined by using particles from the beam halo that passes both the upper and the lower overlap detector. The principle is illustrated in Figure 13.14.

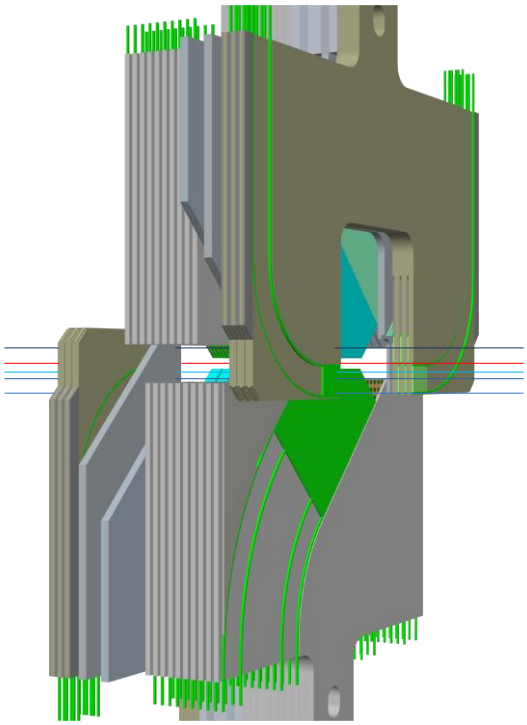

Figure 13.14. The principle of using the overlap detectors to determine the relative upper and lower ALFA detector. The aluminized scintillating fibers are here light green and the trigger scintillator tiles are turquoise. The center of the beam is marked with a red trajectory. The 3 trajectories for halo particles hitting the overlap detectors are deference shades of blue. The figure is a modified version of the original AutoCAD drawings made by A. Bream (CERN PH-DT). The figure is also used as figure 1 in *[50]*.

There are 3 planes of overlap and they a staggered by 166 µm and 333 µm to increase the resolution similar to the staggering of the main detectors (see Section 13.1.2). The resolution on a event by event basis will however not be on the 10 µm from requirement number 4 in Section 12 as is clear from equation (13.2) with d = 166 µm for the staggering. The distance between the detectors can be calculated as [51](equation 1):

$$\text{distance} = \sum_{i=1}^{N} (y_i^1 - y_i^2) \tag{13.3}$$

where y_i^1 is the y-coordinate of the upper overlap detector, y_i^2 is the y-corrdinate of the lower overlap detector, *i* is particle index and *N* is the total number of particles that have hit both overlap detectors.

By using the pitch, *p*, and the number of particles going through one fiber, *n*, and the fractions of the *n* particles going through each fiber in the next plane the resolution can be improved significantly. The principle is illustrated in Figure 13.15.

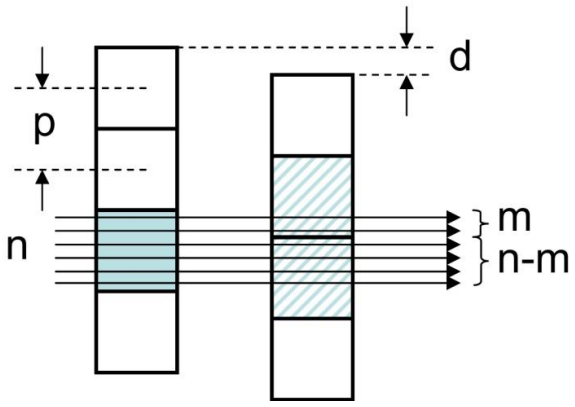

Figure 13.15. Principle of the use of large samples of hits to improve the resolution of the overlap detectors. The figure is figure 8 in [51].

The resolution as a function of the total number of hits has been calculated for different values of the staggering d. The results are shown in Figure 13.16.

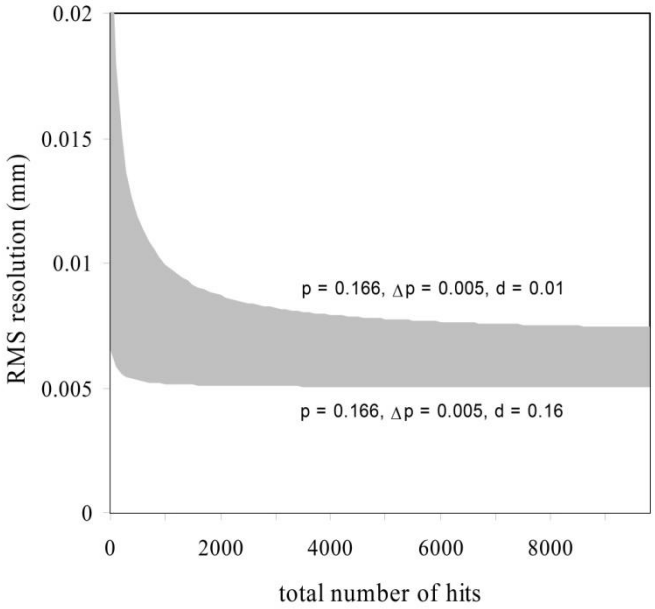

Figure 13.16. The resolution of the overlap detectors as a function of the number of hits. The figure is figure 9 in [51].

Figure 13.16 shown that a resolution better than 8 µm can be expected. This satisfy requirement number 4 in Section 12.

However it is not the overlap detectors themselves that needs to be aligned to very high precision, but the main detectors. Therefore the relative position of the overlap detectors to the main detector needs to be known to a precision better than the relative position of the overlaps on the upper and lower detector. To measure the relative overlap – main detector position is not possible with high enough accuracy with any standard metrology technology. Therefore the relative overlap – main detector position will be determine in a test beam by installing a high resolution telescope in front (or around) an ALFA detector and then have particles going though the telescope and the main ALFA detector or the telescope and the overlap ALFA detector. This is illustrated in Figure 13.17.

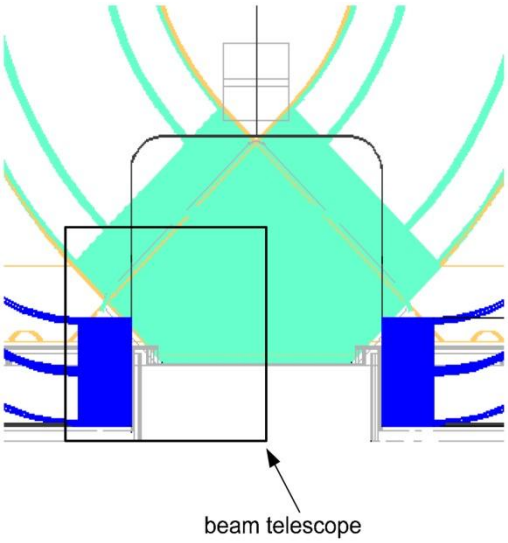

Figure 13.17. Position of a beam telescope to align the main- and the overlap detector. The figure is figure 10 in [51].

If the resolution of the telescope is sufficiently high the relative position of the main- and overlap detector can be determine with high accuracy by accumulating many hits. The alignment of the main- and the overlap detector is one of the mean purposes of the ALFA test beam in the fall of 2010.

13.1.4. MAPMTs

This section is based on [52] and [39](section 5.2.1).

The light from the scintillating fibers has to be converted to an electrical signal. In [39](section 5.2.1) the requirements to the photo detectors are listed:

1. High quantum efficiency at the wavelength of maximum scintillation
2. Capability to detect single photons
3. Fast signal characteristics to allow unambiguous identification of LHC bunches
4. High gain in order to allow the use of simple read-out electronics
5. Relatively low cost per read-out channel
6. Robustness and reliability
7. Moderate radiation hardness

Requirement number 3 is directly adapted from the overall requirement 10 in Section 12. All the listed requirements are achieved by Hamamatsu R7600-00-M64 MultiAnode PhotoMultiplier Types, MAPMTs, which will be used for the ALFA detectors. A Hamamatsu R7600-00-M64 is squared with a side length of 26 mm. A R7600-00-M64 MAPMT is shown in Figure 13.18.

Figure 13.18. LEFT: The MAPMT from the front. The windows of each channel are shown. RIGHT: The MAPMT from the back. The vacuum pin (white) and the pins are shown. The center 64 pins are for each MAPMT channel. The outer pins are the voltage for each dynode.

The MAPMTs has 64 channels each. This corresponds to one layer of the main detector. Each channel is 2·2 mm^2 and is separated by 0.3 mm. The channels are visible in Figure 13.18 but better shown in Figure 17.1 page 232. The fibers from the ALFA detector (main layers and overlap layers) are glued into fiber connectors that separate the fibers by 2.3 mm to correspond to the MAPMTs channels. An ALFA fiber connectors are shown in Figure 13.19.

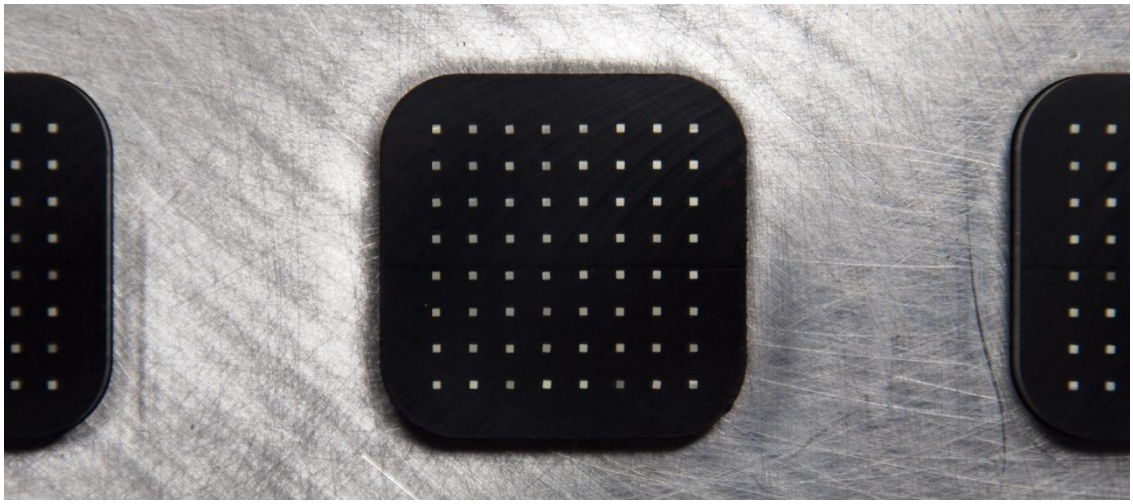

Figure 13.19. Fiber connectors on an ALFA detector. The relative fiber position corresponded to the MAPMT channel position.

Unfortunately the channels positions on the MAPMT are not well defined relative to the sides of the MAPMT and differences are observed from piece to piece. In order to align the MAPMT channels to the fibers custom shims has to be made for each MAPMT. This is described in detail in Section 17. If the MAPMT channels are not be well aligned more cross talk would be observed (see Section 14.7). This is true even though the MAPMT channel is 2·2 mm^2 and the fiber only 0.5·0.5 mm^2 because the light comes out in a cone from the fiber as illustrated in Figure 13.3 page 55. With the unavoidable distance from the fiber end to the photo-cathode in the MAPMT the width of the light becomes significantly larger.

To eliminate the significance of optical cross talk between the fibers as much as possible the mapping in the fiber connectors is made so no neighbor fibers are neighbors on the fiber connector. In this way the optical cross talk between the fibers does not stagger with the cross talk of the MAPMT, which is of the order of 2 % for direct neighbors.

The quantum efficiency is of the order of 26 % in the peak. Hamamatsu has made a new “Ultra BiAlkali”, UBA, version of the MAPMT with higher quantum efficiency. A test of these as discussed in Section 14.5.

The rise time of the MAPMT is about 1 ns and does therefore not make any limitations for the readout speed requirement number 10 in Section 12.

The gain of the MAPMT is of the order 10^6 with a BIAS voltage of -1000 V. But the gain varies from channel to channel with a factor of about 2-3. Moreover the overall gain of the MAPMT also varies about a factor 2-3 from piece to piece. The counteraction of this is discussed in Section 16.3.1.

The MAPMT has 12 dynodes. Each dynode needs a fraction of the high voltage. For this ALFA has developed a one-board voltage divider that will be discussed in Section 13.2.1. The MAPMT are expected to be used with a high voltage of -900 V.

The MAPMT are sensible to magnetic fields because of the dynode structure. They will therefore be housed in a grid made of mu-metal when installed in the LHC tunnel.

13.1.5. Trigger tiles

This section is based on [39](section 5.2.4), [53] and [54].

Requirement number 3 in Section 12 states that the trigger efficiency needs to be well known over the full detecting surface. The approach from the ALFA group is to aim at a ~100 % trigger efficiency over the full surface. This would ensure uniformity and the highest possible use-efficiency of the useful events.

To obtain a ~100 % trigger efficiency a dedicated part of the detector is used for triggering and not the scintillating fibers themselves. The active material is a 3 mm thick plastic scintillator tile. The chosen scintillator tile is produced by Eljen and has the model name EJ-200. It has a rise time of 0.9 ns and a decay time of 2.1 ns and is therefore fast enough to satisfy requirement number 10 in Section 12. The emission spectrum is shown in Figure 13.20.

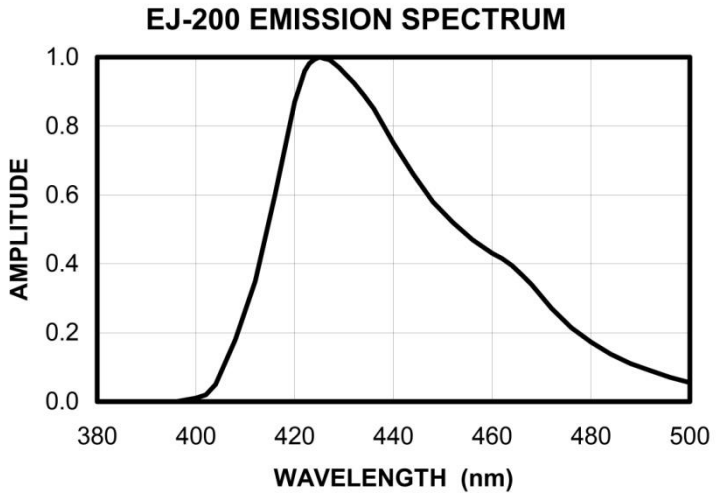

Figure 13.20. Emission spectrum of the EJ-200 scintillator tile. The figure is from [54].

The peak of the emission of about 425 nm is well suited to many PhotoMultiplier Tubes, PMTs. The scintillator tiles are painted with white reflective paint made by Bicron with modelname BC-620. This was chosen after a dedicated study [53] which showed the highest light yield with the white paint. The light yield was above ~40 photo electrons over the whole surface. This should insure a ~100 % efficiency over the whole surface and thereby compile with requirement 3 in Section 12.

The main detector has two separate scintillator tiles mounted on a titanium substrate as shown in Figure 13.21.

Figure 13.21. Titanium substrates with two main trigger scintillator tiles. These scintillator tiles each has two bundles of clear fibers connected to the two largest surfaces. The clear fibers for the bottom scintillator tiles are on the back of the titanium substrate. The figures is from [42](Detector production slide 17, H. Stenzel).

The two separate scintillator tiles are used for the main trigger to make it possible to make a local coincidence.

The main trigger scintillator tiles has a diamond shape (in Figure 13.21 upside down) which correspond to the overlapping of a U and V layer of scintillating fibers in the main detector. On the two longest sides of the

trigger tiles there are glued clear fibers, which act as a light guide and transported the light from the scintillating tile outside the Roman Pot (see Section 13.3) to a fiber connector. The clear fiber bundles are better visible at Figure 14.41 page 128. The clear fibers are 0.5 mm diameter round fibers with multicladding made by Kuraray (Model name: Clear-PSM). A fiber connector for the triggers is shown Figure 13.22. The two bundles with most fibers are from the main triggers.

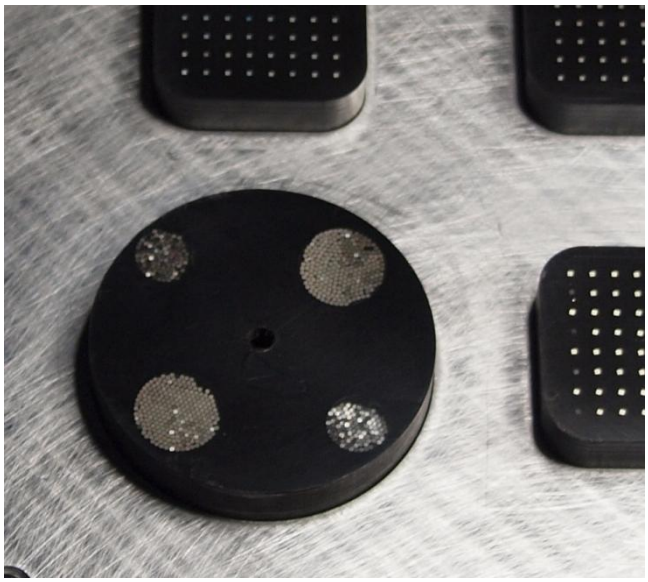

Figure 13.22. Fiber connector for the clear fibers. The two bundles with most fibers are from the main triggers. The two bundles with fewer fibers are from the overlap triggers.

Outside the Roman Pot there are PMTs connected to the fiber connectors. These are discussed in Section 13.1.6.

The overlap trigger consists of a left and a right scintillator tile mounted on a titanium substrate as shown in Figure 13.23.

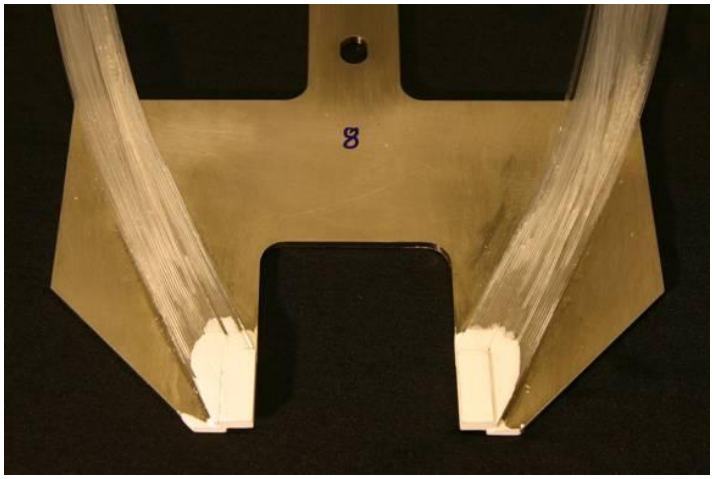

Figure 13.23. Titanium substrates with two overlap trigger scintillator tiles. These scintillator tiles have a bundle of clear fibers connected. The figure is from [42](Detector production Slide 17, H. Stenzel).

Each tile is 15·6 mm^2 and defines the intended active part of the fibers in the overlap detectors. To two of the sides of the scintillator tiles there are glued clear fibers which connect to the same fiber connector (but different positions) as the fibers from the main trigger. The two bundles with fewest fibers on the fiber connector in Figure 13.22 page 67 are from the overlap triggers.

It is not a design requirement that the overlap triggers has a ~100 % efficiency, as they only will be use for alignment and not for the luminosity measurement itself.

The design of the triggers with only plastic scintillator tiles and clear fibers inside the Roman Pot also complies with requirement number 5 and 6 in Section 12.

13.1.6. Trigger PMTs

This section is based on [55], [56] and [53].

The PhotoMultiplier Tupes, PMTs, used the ALFA trigger studies [53] were Hamamatsu R7400P. These are photon counting PMTs with a gain of ~10^6 for an applied voltage of -800 V over the 8 dynodes. The window of the PMT is circular with a diameter of 8 mm and the PMT itself round with a diameter of 16 mm. A photo of the Hamamatsu R7400P is shown in Figure 13.24.

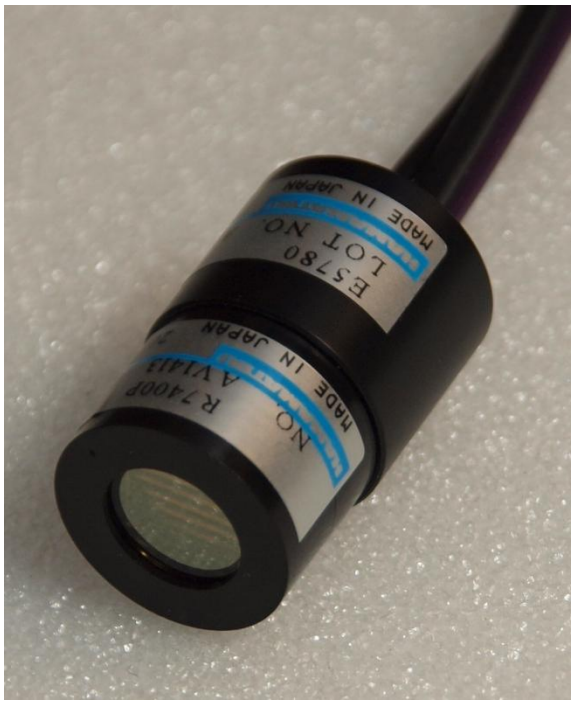

Figure 13.24. Hamamatsu R7400P PMT with voltage divider.

The quantum efficiency is 26 % and peaks at 420 nm. From the emission spectrum of the scinttillator of the trigger tile shown in Figure 13.20, which peaks at 425 nm it is clear the Hamamatsu R7400P and the scintillator tile is well suited for each other. The rise time of the Hamamatsu R7400P is 0.78 ns and thereby meets the requirement number 10 in section 12.

It is expected to be operated at -950 V were the current is about 345 µA.

At a later stage it was decided only to use the Hamamatsu R7400P for the overlap triggers where a ~100 % trigger efficiency not is a requirement. For the main triggers it was decided to use Hamamatsu R9880U-110 which is the next generation of PMTs from Hamamatsu with a quantum efficiency of 35 % at the peak at 350 nm. The quantum efficiency spectrum is shown in Figure 13.25.

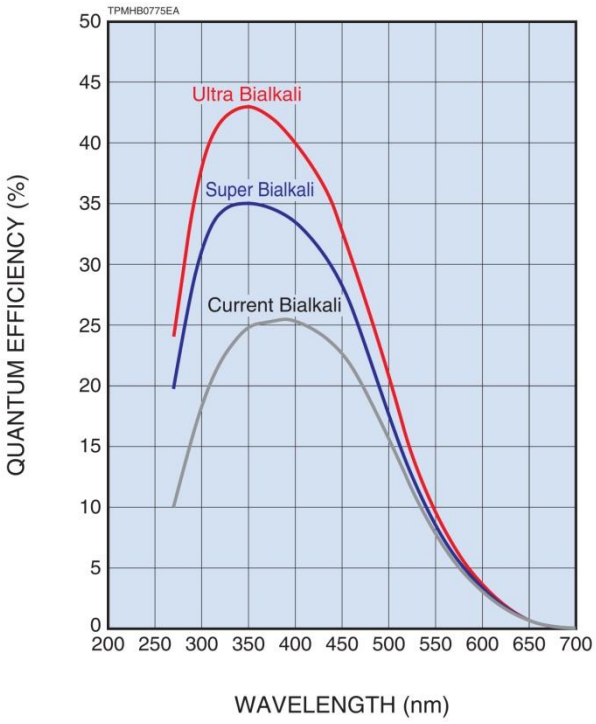

Figure 13.25. Quantum efficiency for 3 generation of PMTs from Hamamatsu. The Hamamatsu R7400P is of type "Current Bialkali" The Hamamatsu R9880U-110 is of type "Super Bialkali". The figure is from [57](page 11).

The peak value of the quantum efficiency is not at well suited for the emission spectrum of the scintillator tile shown in Figure 13.20, which peaks at 425 nm. But at 425 nm the "Super Bialkali" PMT still has significant higher quantum efficiency than the "Current Bialkali". A photo of the Hamamatsu R9880U-110 is shown in Figure 13.26.

Figure 13.26. Hamamatsu R9880U-110 with voltage divider.

The Hamamatsu R9880U-110 is not a photon counting PMT. It has a gain of about $4 \cdot 10^6$ at an applied voltage of -1000 V over the 10 dynodes.

It is expected to be operated at -1100 V were the current is 323 μA.

The R9880U-110 has the same dimensions as the Hamamatsu R7400P PMT, but the voltage divider is a bit longer (probably because of the two additional dynodes). The rise time is 0.57 ns and thereby meets the requirement number 10 in Section 12.

13.2. Electronics

This section is based on [39](section 6), [42](Electronics: Front end PMF, P. Barrillon et al.).

To readout and control the ALFA detector system a number of electronic components is needed. The main requirements are defined in [39](section 6.1):

1. Channel-by-channel adjustable amplifier gain to compensate for the MAPMT gain spread.
2. High speed: it must be possible to associate signals unambiguously with a LHC bunch crossing.
3. Adjustable threshold with a minimum setting of < 0.5 p.e. in order to guarantee high detection efficiency. A common threshold for 64 channels is acceptable if the gains can be adjusted.
4. Negligible cross-talk between channels: < 3%.
5. Compliance with standard ATLAS read-out scheme.
6. Integration and Compactness: the restricted space in the Roman Pot environment requires to design a front-end electronics which is highly integrated, i.e. which deals with the 64 channels of one MAPMT, and which can be mounted directly on the back of the MAPMT, respecting the 40 mm grid of the MAPMT arrangement on the pot.
7. Reliability and robustness: the Roman Pot detectors are located in the LHC tunnel, about 240 m from the ATLAS cavern, making interventions extremely difficult. The electronics moves together with the Roman Pots between beam and 'garage' position. Although these motions are foreseen to be smooth and slow, the mechanics and connectivity of the read-out system must be designed such that a reliable and robust operation can be guaranteed over extended periods.
8. Radiation tolerance: the radiation environment during the specific luminosity runs is not expected to pose serious problems for the electronics. In normal physics runs, once the LHC machine is operated at close to nominal luminosity, the scintillating fibers would soon suffer from radiation damage, and, at a lower degree, the electronics could be degraded as well. It is therefore foreseen to dismantle and remove the detectors and the electronics parts from the pots. The connectivity of the system must allow for a rapid removal/installation of the system.

Requirement number 2 is directly adopted from the overall requirement number 10 in Section 12 and requirement number 8 is directly adopted from the overall requirement number 8 in Section 12.

13.2.1. PMFs

The PhotoMultiplier Frontend, PMF, is mounted directly on the MAPMTs. They are buildup from spacers/isolators and 3 pieces of $30 \cdot 30$ mm^2 Printed Circuit Boards, PCB: A Voltage divider, a passive board and an active board. Each board is discussed in the following sections in the order they are mounted to the MAPMT. The MAPMT and the first isolator are shown in Figure 13.27.

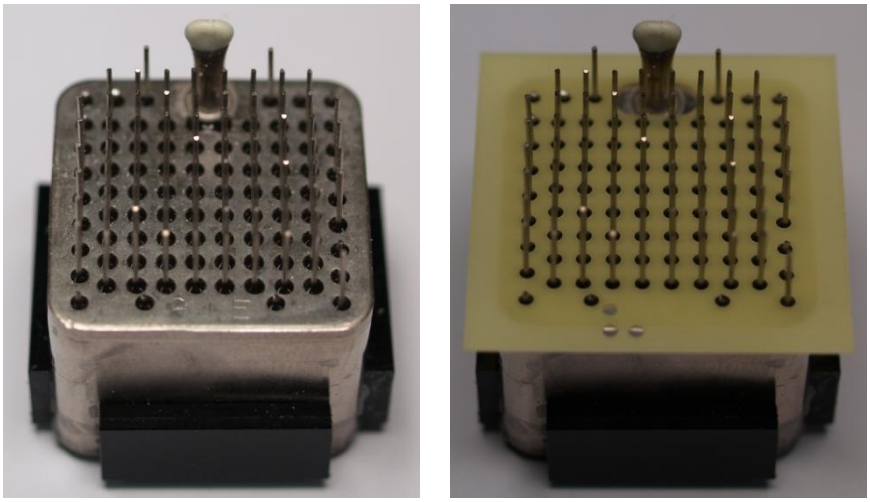

Figure 13.27. *LEFT*: MAPMT. RIGHT: MAPMT + isolator.

13.2.1.1. The Voltage divider

Hamamatsu produces a voltage divider for the MAPMTs, but it did not meet with requirement number 6 as they would take up too much space. Instead ALFA designed a one-board voltage divider on a 2 layer PCB. The overall resistance of the voltage divider is 2.5 MΩ. The MAPMTs are expected to be operated at -900 V. This will give a current of:

$$I = \frac{U}{R} = \frac{900\ V}{2.5\ M\Omega} = 360\ \mu\text{A} \tag{13.4}$$

This is well within the current limit of the high voltage power supply unit of 500 μA (see Section 13.2.5).

The voltage divider and the spacers used to keep forces away from the components on the voltage divider are shown in Figure 13.28 mounted on a MAPMT.

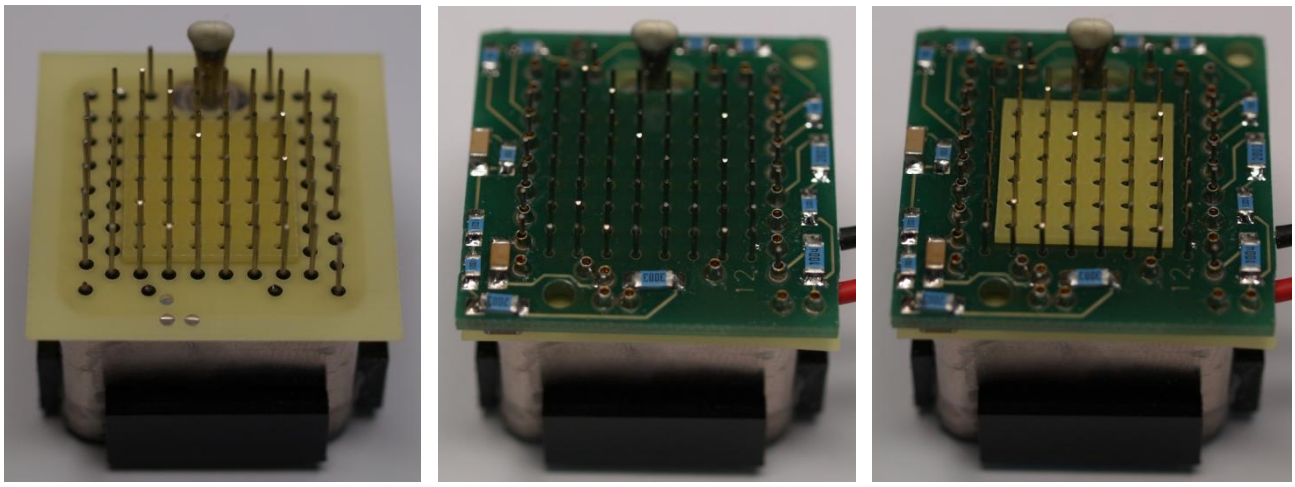

Figure 13.28. *LEFT*: MAPMT + isolator + spacer. MIDDEL: MAPMT + isolator + spacer + voltage divider. RIGHT: MAPMT + isolator + spacer + voltage divider + spacer.

13.2.1.2. The passive board

The passive board is a 4 layer PCB with no active components on it. It is only used to route the signals from the central pins of the MAPMT to connectors on the edge PCB. The routing is optimized to reduce cross talk

to meet requirement number 4. The passive board and isolator to separate the voltage divider and the passive board are shown in Figure 13.29.

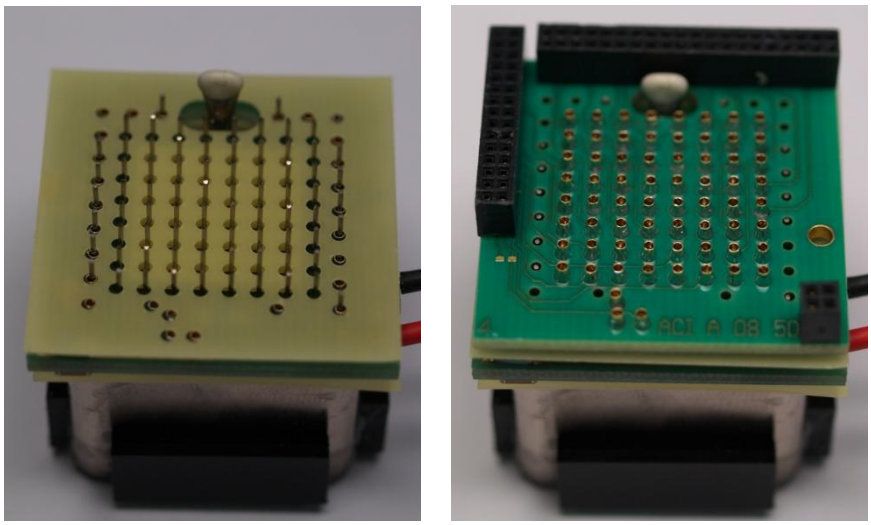

Figure 13.29. LEFT: MAPMT + isolator + spacer + voltage divider + spacer + isolator. RIGHT: MAPMT + isolator + spacer + voltage divider + spacer + isolator + passive board.

13.2.1.3. The active board

The active board is a 10 layer PCB with a FPGA one side and a MultiAnode ReadOut Chip, MAROC, on the other side. The active board is shown in Figure 13.30.

Figure 13.30. MAPMT with full PMF mounted: MAPMT + isolator + spacer + voltage divider + spacer + isolator + passive board + active board.

The MAROC is designed for ALFA [58] and is an evolution of the OPERA_ROC ASIC [59]. The layout of the MAROC 2 is shown in Figure 13.31.

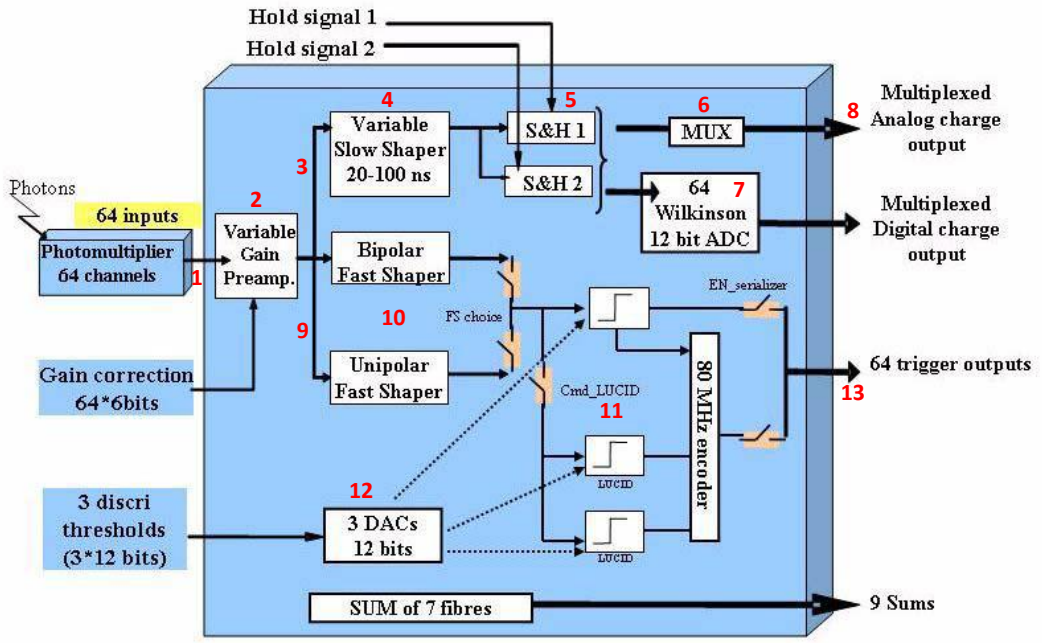

Figure 13.31. The layout of the MAROC 2. The figure is figure 3 in [58]. The red numbers are added to the figure.

The MAROC receives the analog signals from the MAPMT (1). The signals are then amplified individually (2). At this stage the signals are split up to a charge readout patch (3) and a digital readout patch (9).

The charge readout is intended to be used for calibration of the MAPMT gain (determine the needed gain corrections). It can therefore be slow as there is no outside time requirement. The determination of the gain corrections is discussed in Section 16.3.1. For the charge readout the signals are sent to a slow shaper (~100 ns) which consist of a shaper part (4) and a Sample and Hold part (5), which measure the baseline and the charge and store them in capacitors. The signals then go either to a multiplexer output (6) or to an Analog Digital Converter, ADC (7). Originally it was planned to use the MAROC ADC, but at a later stage it was decided to have a better ADC on the motherboard instead. The multiplex output this being used for this (8).

The digital readout is the main readout and has to comply with the speed requirement (requirement number 2) and thereby the overall requirement number 10 in Section 12. The shaper used (10) is therefore fast (15 ns). After the shaper the signal are send to a discriminating part (11). The signal is discriminated with a preset threshold (12). As the discriminating value is the same for all channels it is important that the gain amplifiers have counteracted the different MAPMT channel gains so the discrimination is similar on all channels. At the output (13) a 0 or 1 is send out depending on if the signal was under or over the threshold.

13.2.2. Motherboard

This section is based on [39](section 6.6).

The main task of the motherboard is to collect the data from the 23 PMFs and send it to the DAQ system (see Section 13.2.4). The layout of the motherboard is shown in Figure 13.32.

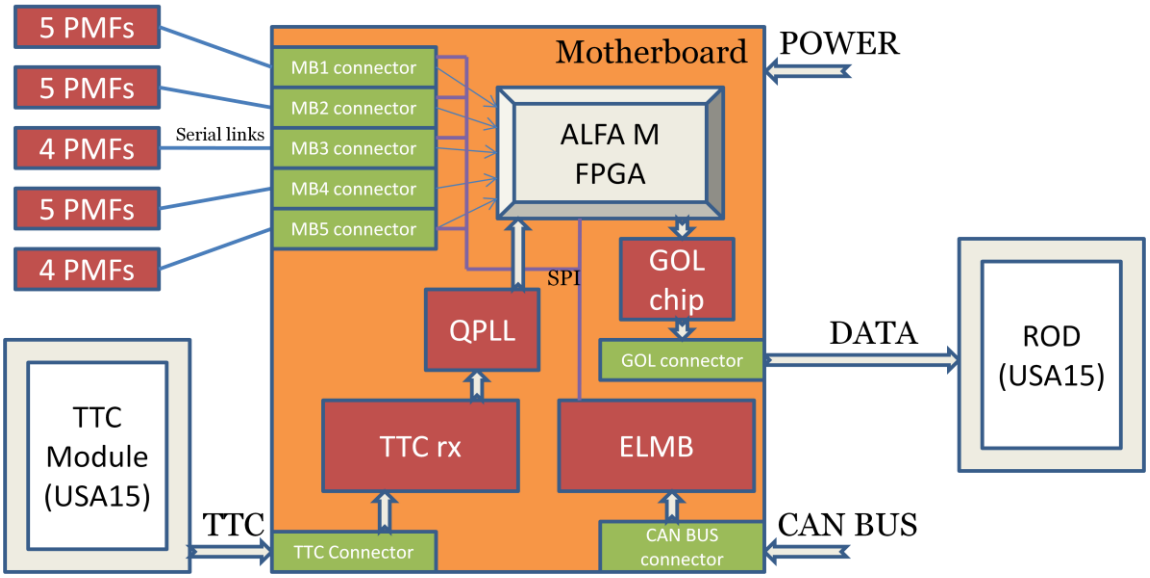

Figure 13.32. Layout of the ALFA motherboard version 4. TTC = Timing, Trigger and Control, ELMB = Embedded Local Monitor Board, CAN = Controller Area Network, ROD = Read Out Driver. The figure is from [42](Roman Pots "ALFA" Motherboard Slide 5, F. Anghinolfi et. al.).

The motherboard receives a trigger (TTC, Timing, Trigger and Control). Then all the PMFs are read out. The date is then send to the Read Out Driver (ROD).

To comply with requirement number 2 and thereby the overall requirement number 10 in Section 12, the motherboard must be able to do this at a rate up to 100 kHz, which is the accepted rate of the ATLAS level 1 trigger (see Section 7.3.6).

The motherboard is controlled over a CAN (Controller Area Network) bus. The CAN bus communicates with the ELMB (Embedded Local Monitor Board) on the motherboard and the ELMB can be used to change or monitor values on the motherboard. It is also possible to send values to the PMFs via the ELMB. This would typical be gain factors and threshold settings. The monitor values would typically be the motherboard voltages and temperature from the sensors.

The motherboard is also used to distribute voltage to the PMFs. A photo of the motherboard is shown in Figure 13.33.

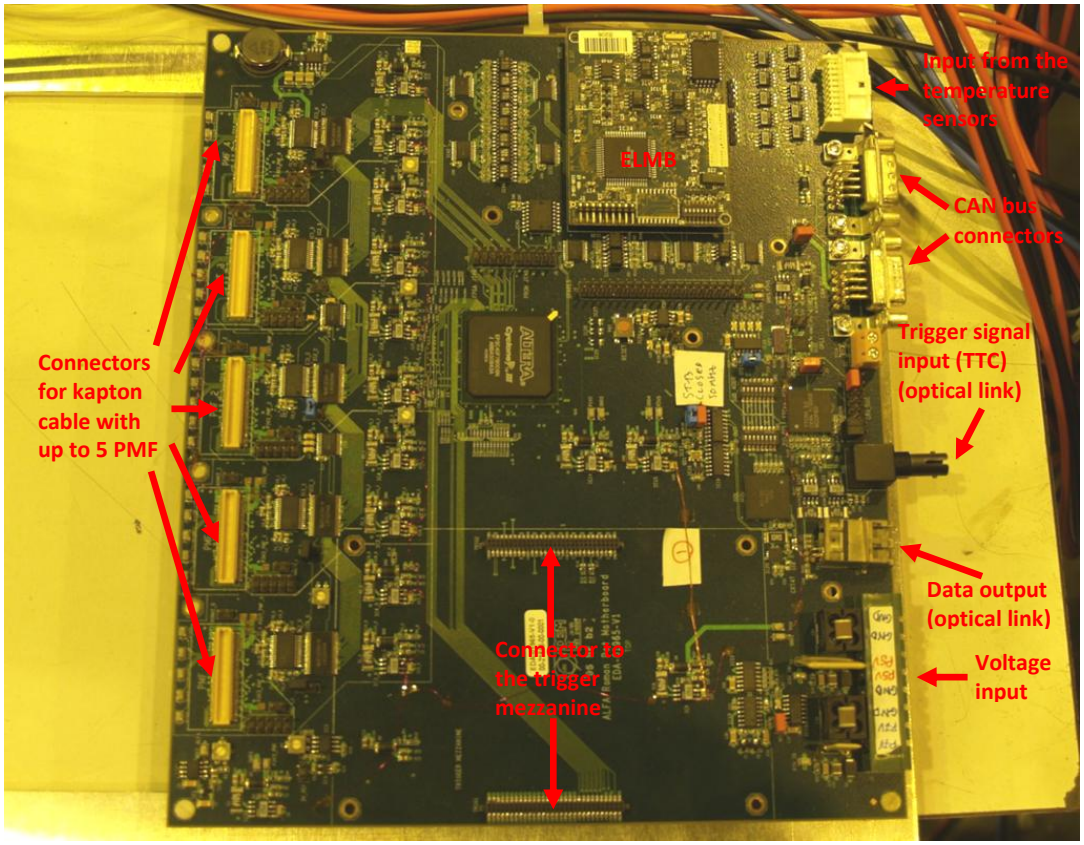

Figure 13.33. The ALFA motherboard.

13.2.3. The trigger mezzanine

The trigger mezzanine is a daughterboard to the motherboard. It houses two modified PMFs that receive input from the trigger PMTs. The signals are shaped and discriminated in the PMF. After that a coincidence is made from the two main triggers. The coincidence signal can be used to trigger the motherboard. The local coincidence is necessary to be fast enough to comply with requirement 2 and thereby the overall requirement number 10 in Section 12. The coincidence signal is also sent to a scaler. The rate can then be monitored when moving the detectors close to the beam to avoid coming too close. There is also a build in safety system that automatic retract the detectors if the rates get too high (see Section 13.4).

From the modified PMFs on the trigger mezzanine the signals from the overlap trigger PMTs are sent to NIM electronic (not locally as it does not need to be very fast) to make coincidences. A coincidence is made from the top and bottom signals on the left side and another coincidence is made from the top and bottom signals on the right side. The coincidences will be used to trigger a readout of the overlap detectors (and the main detectors). The relative top/bottom position will be determined from the reconstructed events in the overlap detectors as discussed in Section 13.1.3.

A photo of the trigger mezzanine is shown in Figure 13.34.

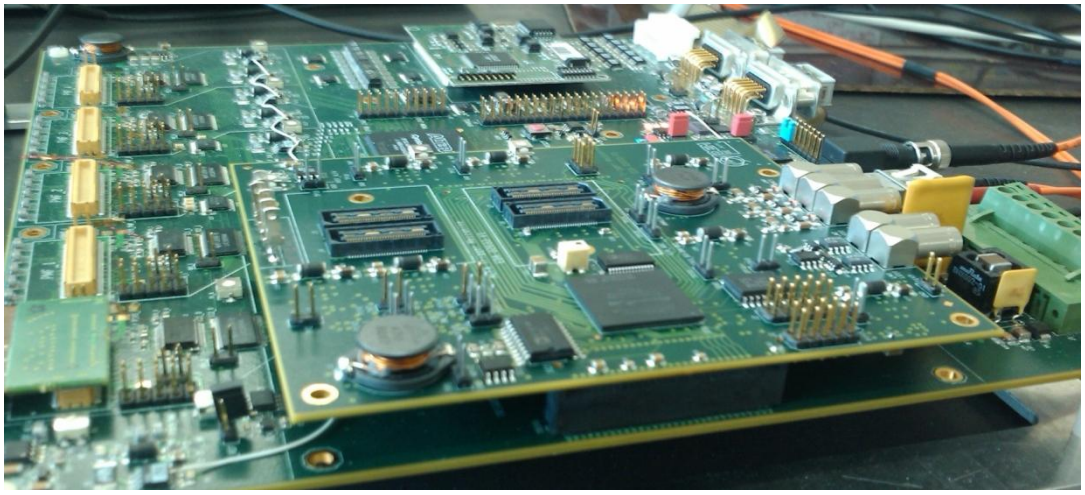

Figure 13.34. The ALFA trigger mezzanine mounted on the ALFA motherboard. The figure is from [60](slide 6).

13.2.4. DAQ

This section is based on [42](Back End and DAQ, G. Blanchot and K. Korcyl).

The data acquisition system, DAQ, is adapted from the ATLAS muon detector (MDT Read Out Driver, MROD) (see Section 7.3.4). This system is capable of complying with the speed requirement (requirement number 2) and thereby the overall requirement number 10 in Section 12. It is also well integrated into the ALTAS readout scheme and thereby complies with requirement number 5. It is based on VME modules as shown in Figure 13.35.

Figure 13.35. The WME create with the DAQ system. The figure is from [42](Back End and DAQ, G. Blanchot and K. Korcyl slide 5).

The DAQ connection to the motherboard is shown in Figure 13.32 page 74.

13.2.5. Power suppliers

This section is based on [39](section 6.7 and 6.8) and [42](HV System for ATLAS/ALFA, Dieter Notz).

The low voltage Power Supply Unit, PSU, for the motherboard, trigger mezzanine, PMF etc needs to supply +7 V at 2 A and +5 V at 12 A per detector. Since the current is high the PSU needs to be located close to the detector. Close to the ALFA stations on both sides of ATLAS there are small caverns mainly used for the LHC cooling system. The low voltage PSUs for ALFA is located here. The low voltage PSU will not be removed with the detectors for high luminosity runs since the cavern has a significantly lower radiation level then the main tunnel. But the low voltage PSU still needs to be moderate radiation hard. Therefore a special designed for LHC experiments low voltage PSU call "MARATON" (MAgnetism Radiation Tolerant New power supply system) will be used. It is made from very basic components and is qualified for radiation levels up to 140 Gy and 10^{12} 1 MeV neutrons. It has 12 channels that each delivers up to 300 W. The control part of the MARATON is a dedicated remote unit in a non radiated area (For ALFA US15).

The high voltage Power Supply Unit, HV PSU, used for ALFA is a modified Iseg EDS 20 130_504. Each module has 32 channels and can supply up to -3 kV and 500 µA. This is well suited for the ALFA need of about -900 V and 360 µA for the MAPMTs as discussed in Section 13.2.1.1. The current of the trigger PMTs 323/344 µA (see Section 13.1.6) and is also will suited to be supplied by the same HV PSU. Because the current is so low the HV PSU can be positioned very far from the ALFA stations and therefore do not have to be radiation hard. The HV PSU will be placed in US15.

13.3. Roman Pot

This section is based on [39](section 1 and 4.2).

In the LHC there is an ultra high vacuum (~10^{-11} mbar) and all equipment therefore has to be "Ultra High Vacuum" equipment. Therefore the ALFA detector must be separated from the LHC primary vacuum. For this ALFA will use a Roman Pot.

A Roman Pot is a vessel which allows a detector in a secondary vacuum to approach the beam inside the beam pipe, but separates the detector from the primary vacuum.

The Roman Pot technology is develop at ISR by a CERN group from Rome (hence the name) [61]. It has been used at the UA4 SPS [41], Tevatron [62] and [63], RHIC [64], HERA [65] and [66] and will be used in TOTEM [9]. Figure 13.36 shows one of the Roman Pot stations from the UA4 (SPS) experiment (currently stored in the north area at CERN).

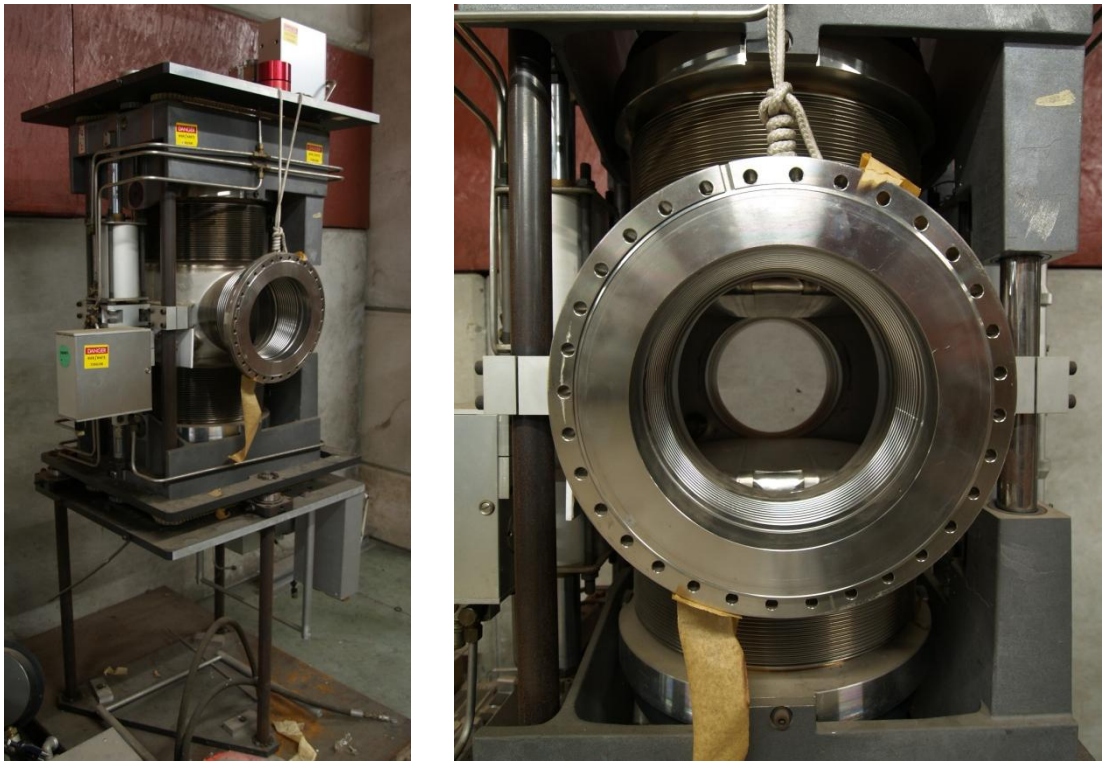

Figure 13.36. *LEFT*: A Roman Pot station from the UA4 (SPS) experiment. *RIGHT*: The Roman Pots from the UA4 (SPS) experiment.

The ALFA Roman Pots have been designed to satisfy requirement number 2 in Section 12 about the very close apache of the detector to the beam and the constraints of the LHC accelerator. One of the ALFA Roman Pots is shown in Figure 13.37.

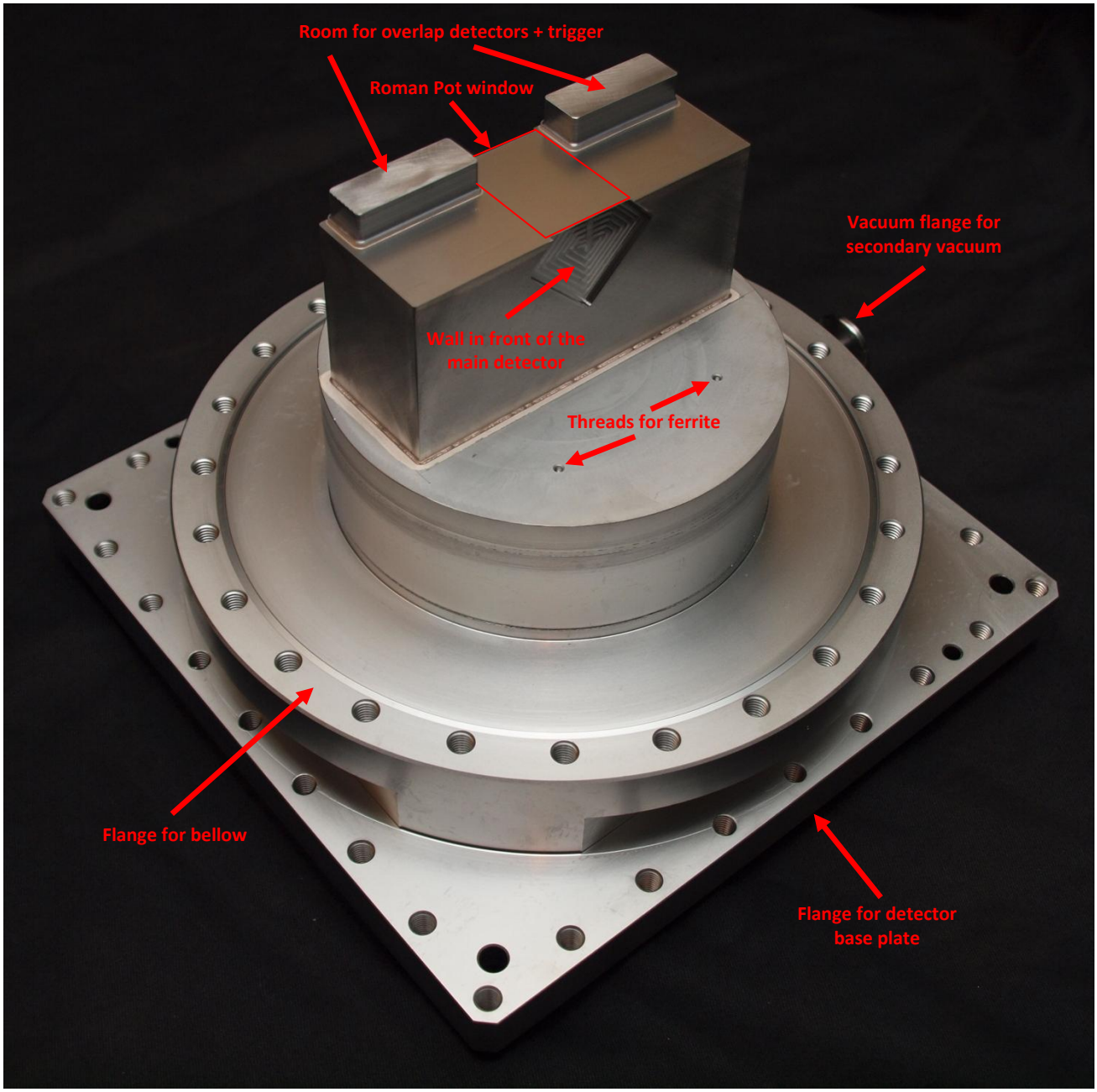

Figure 13.37. An ALFA Roman Pot (A09). The Roman Pot fit around the ALFA detector Figure 13.1.

The thin window which is the direct separation between the detector and the beam has been object of a long R&D phase for TOTEM. ALFA has adopted the results and uses a window of 200 µm thickness. In the studies for TOTEM the window was pressure tested up to 83 bar before it broke. Normally there are vacuum at both sides of the window and it will stay straight. But even if the primary beam vacuum or the secondary vacuum inside the Roman Pot is lost, the pressure difference will only be of the order of 1 bar. So it is safe to assume that the window will not break. It will however bend. This has been studied on an ALFA Roman Pot prototype and in simulations for ALFA and a result is shown in Figure 13.38.

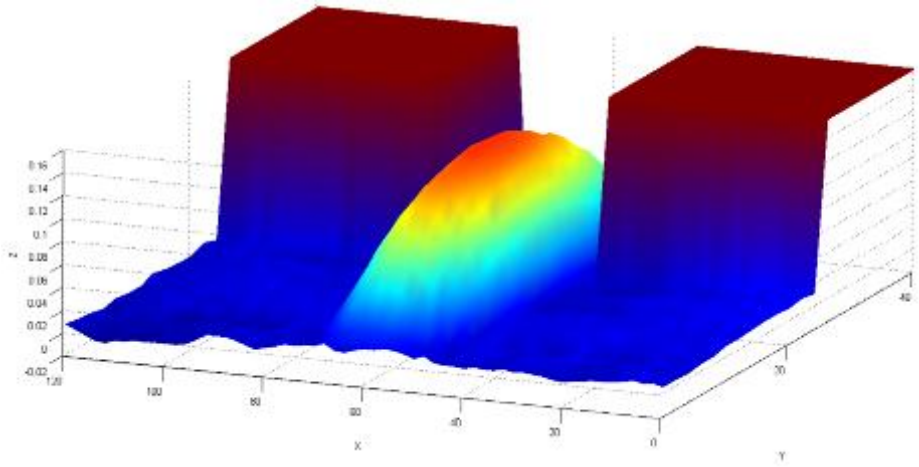

Figure 13.38. Simulation of the bending of the Roman Pot window with the secondary vacuum lost. The window bends into the beam pipe. The window thickness in this simulation was 150 µm. The deformation here is 122 µm (not to scale with the part of the Roman Pot surrounding the overlap detector). Later it was decided to move to 200 µm to reduce the plastic deformation. The figure is from [42](ALFA Roman Pot slide 7, S. Mathot).

Optimally the wall in front of the detector would also have been a very thin window. However this would add a risk of vacuum tightness and require dedicated studies. Therefore it is instead machined down to a thickness of 500 µm.

The impedance of any accelerator is affected by the changes of the beam pipe cross section. A study [39](section 4.3.2) have shown that the effect of the ALFA Roman Pot can be significantly reduced by installing ferrite absorbers. The position of the ferrite absorbers can be seen in Figure 13.37 by the corresponding threads.

To comply with requirement number 9 in Section 12 the detector must be quick and easy to remove and reinstall in the Roman Pot. Therefore the distances between the detector and the Roman Pots inside should not be too small. Only the distance between the window and the detector should be kept to a minimum to comply with requirement number 2 in Section 12. All other distances between the detector and Roman Pot should be kept in the millimeter range. Special tools have been design to be used for the insertion of the detector into the Roman Pot. These reduced significantly the likelihood of damaging the detector (or Roman Pots) under the installation and removing of the detectors.

13.4. Mechanics for movement

This section is based on [42](section 4).

Requirement number 7 in Section 12 states that the central position of the Roman Pots must be adjustable to counteract the different beam height each LHC field might have. To comply with this requirement the Roman Pots are installed in bellows that allow them to move and a mechanical system to adjust the distance to the beam independently of the upper and the lower Roman Pot. The layout of the original ALFA mechanical station is shown in Figure 13.39.

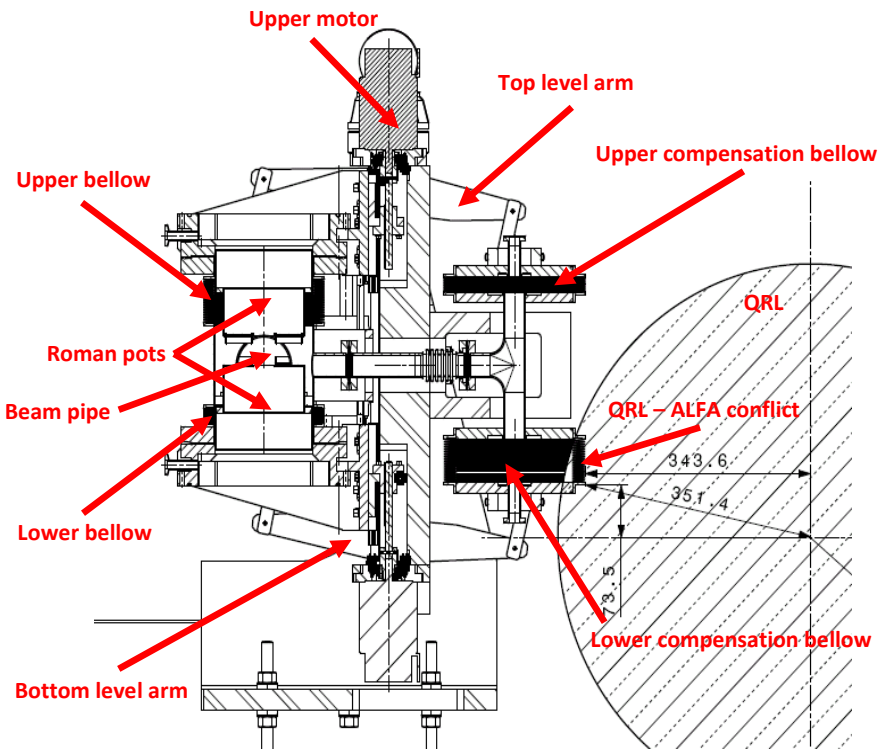

Figure 13.39. Layout of the original ALFA station. The figure is from [42](Summary of the mini-review on mechanics to address solutions about the "conflict" slide 2, G. Spigo). All in red have been added to the figure.

Because of the beam pipe vacuum inside the bellows, the Roman Pots will be pulled in with a force of about 2.7 kN. To compensate for this the ALFA station uses compensation bellows that are a little larger than the bellows around the Roman Pot. The support for the bellows surrounding the Roman Pots and the compensation bellows are connected with an upper and a lower level arm to transfer the forces. The compensation bellows are also connected directly to the beam vacuum so the vacuum, and thereby the force per area, always will be the same in both sets of bellows. As the compensation bellow has a larger surface the net force will be higher. So if no other forces (e.g. the motor torque) influence on the system, the Roman Pots will be retracted to the outer position. In the event of a power cut or other failure this is an important design detail as the Roman Pot will relatively slowly retract to the outer position instead of potentially move into the beam. In the final design springs have been added (to counteract gravity) to retract the upper Roman Pot. The springs were added because the outer position was not always reached with only the force on the bellows.

The Roman Pots are moved by motors connected to a threaded rod. The motors are of the same type as used for the LHC collimators and are radiation qualified up to a dose of 30 MGy. The motors will have 400 steps per revolution and with the threaded rod used this will give a minimum movement of 5 µm.

The position will be monitored with Linear Variable Displacement Transducers, LVDTs. These are radiation hard devises that that determine the position from secondary voltages (3 coils in a steel tube plus a movable core). The LVDTs are shown in Figure 13.40.

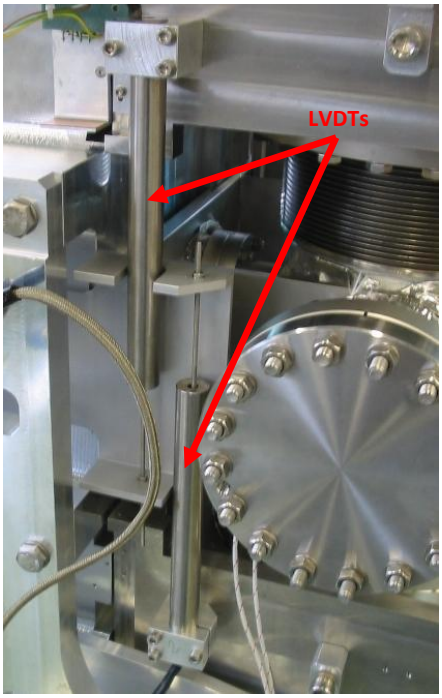

Figure 13.40. LVDT mounted on an ALFA station. The figure is from [42](Status of the ALFA Mechanics slide 29, K. Hiller).

There are a number of safety stoppers in place to prevent a collision of the two pots.

Close to the planed installation time for the stations it was discovered that the cryogenic distribution line, QRL, was enlarged compared to the originally planned size. The real size of the QRL meant that the ALFA station and QRL was now overlapping in space for 3 of the 4 ALFA stations. This is included on Figure 13.39 page 81. As the QRL could not be changed, the ALFA station had too. Therefore a modified design was made where the bellows are lifted to avoid the conflict with the QRL. A photo of the updated mechanics for ALFA is shown in Figure 13.41.

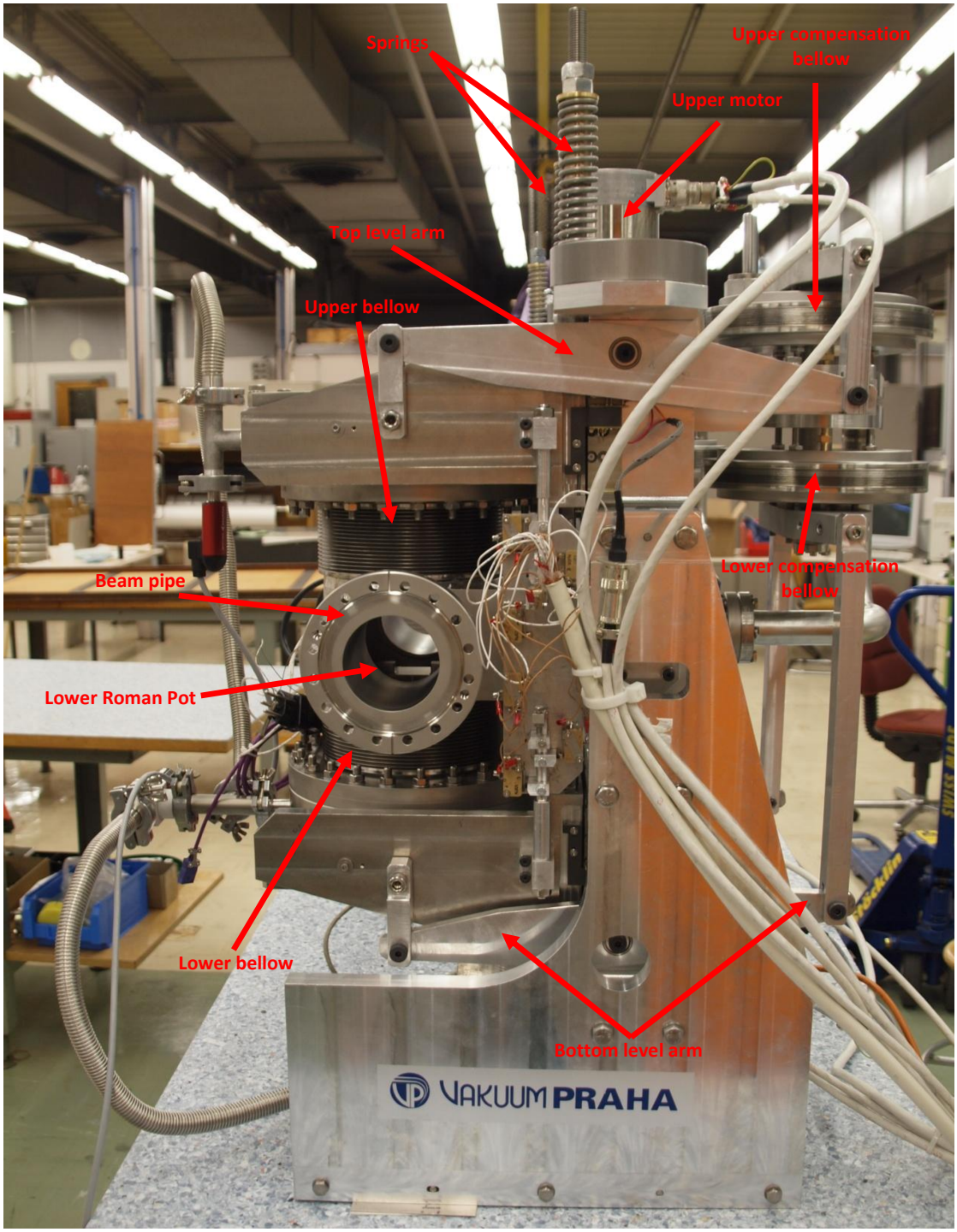

Figure 13.41. Updated mechanics for ALFA.

13.5. Vacuum and cooling

Two stations (4 Roman Pots) share one vacuum pump. The pump is located next to the low voltage power supplied to lower the radiation on the pump. The pump is a KNF N813.3 ANE and can be turn off and one remotely. It is expected that the pump have to undergo maintenance once every year. With one detector installed the pump was able to come to a pressure of about 3 mbar. The pump is included in Figure 16.32 page 210. Electromagnetic valves can be controlled remotely to close the connection between the pump and ether of the two stations (and between the stations).

Each station will have one fan to cool the PMFs of two detectors. This is necessary as the PMFs have a total effect of about 60 W and is housed inside a closed box. The fans can be turned on and off remotely. The filters of the fans should be cleaned periodically. The fan is included in Figure 16.32 page 210.

As there are no active parts inside the Roman Pots no cooling is needed.

13.6. Control and software

This section is based on [39](section 4.4.5).

The Roman Pots will be considered machine elements similar to e.g. the LHC collimators. The control system is therefore the same as for the LHC collimators (NIPXI system) and the Roman Pots will be moved in only from the CERN Control Center, CCC.

The control of the readout, motherboard, PSUs etc will be done from the ATLAS Control Room (luminosity and forward detector disk). The control software is still under development, but a screenshot from a beta version is shown in Figure 13.42.

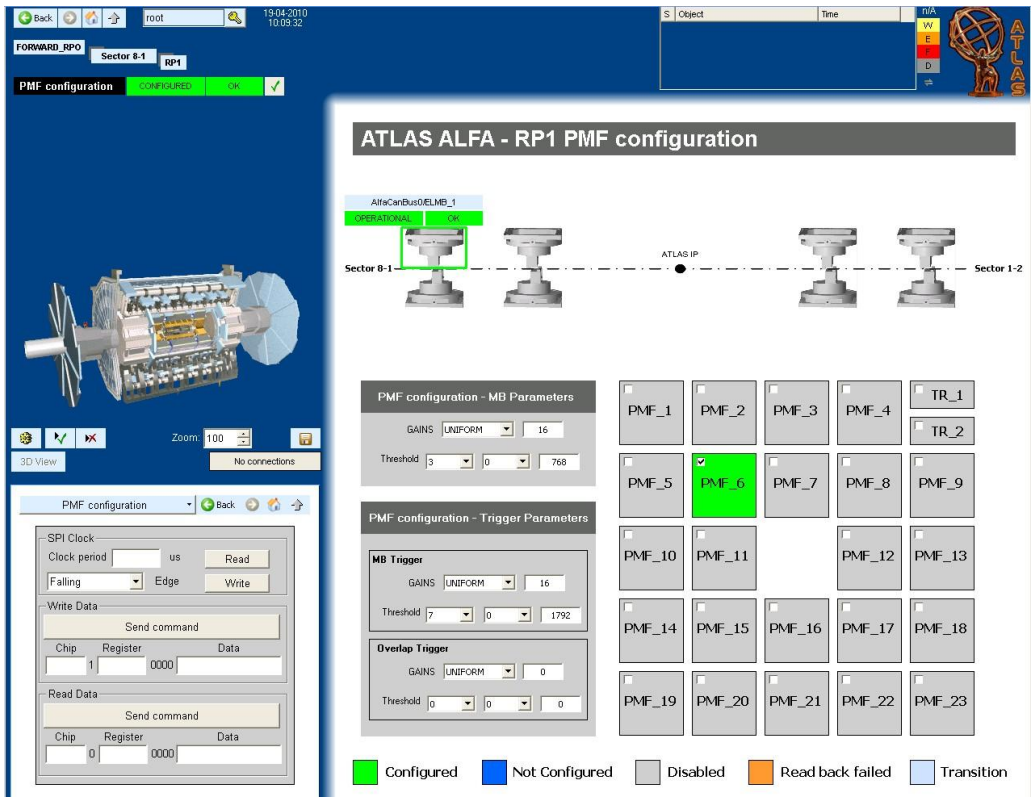

Figure 13.42. Screenshot from the software to control ALFA. This page is used for writing gain factors and threshold to the PMFs. The figure is from slide 7 [67].

14. Laboratory experiments

14.1. Motivation

In the summer of 2008 a beam test of a prototype Roman Pot with a full scintillating fiber detector inside was performed [46]. The readout was done via a prototype ALFA motherboard version 3. In the beam test there were a lot of problems regarding the ALFA motherboard and only a small amount of data was obtained. The data itself has proven difficult to interpret. Some fibers or MAPMT channels that were expected to give signal showed none. In the test beam the readout was digital: under or over a set threshold. Therefore it was not possible to investigate the missing signals in detail. Some of the interpretations done by the ALFA group suggest that significantly less light than expected is seen in a fiber hit by a particle. The scintillating fiber readout by a MAPMT is only expected to make a signal corresponding to 4-5 PhotoElectrons, PEs, so a significant decrease could very well prove devastating for the ALFA project.

Back in 2005 a prototype of a single plane of the detector (2*64 scintillating fibers) was made. This prototype was put in a test beam at DESY II and used to measure the amount of light in the scintillating fibers coupled to two MAPMT. The results are documented by article [68] and showed the expected 4-5 PEs.

The 2008 prototype has however been changed quite a bit. Some changes have been done to the fibers them self (new batch of fiber, new workshop doing the cutting, polishing and assembly) and a lot of changes have been done to the mounting of the fibers. The largest change being the substrate material changed from ceramic to titanium. Therefore something unpredictable could have happened that influence the amount of light which can be detected from a scintillating fiber hit by a particle.

This chapter will mainly describe the buildup of a setup and tests done to measure the detectable amount of light in the scintillating fiber installed in the 2008 prototype detector.

Furthermore questions have also been raised about the scintillator tiles used for triggers. In former prototypes they have a high light yield, about 40 PE, and thereby a near 100% trigger efficiency [39](section 5.2.4). Section 14.6 describes a measurement of the light yield of the trigger scintillator tiles to confirm their high light yield and thereby the high trigger efficiency.

14.2. Analog readout of 64 channel photomultiplier

The readout of the charge from a single PMT could easily be done with an advanced digitally oscilloscope. But the oscilloscopes only have very few channels, so only PMTs connected to maybe 3 fibers could be readout at the same time. The particles used to make a signal in the scintillating fibers are from cosmic rays (mostly muons), so the rate is very low. Combining these two facts makes the desire to use another readout system with more channels available apparent.

14.2.1. Basic setup

Analog readout had been used in a beam test in 2005 [68]. Therefore some components were already made and just needed to be tested and included in the setup.

As a starting point a 64 channel MultiAnode PhotoMultiplier tube (MAPMT) was mounted on a voltage divider. The voltage divider is supplied with a high voltage, HV, (800-1000 V) and sends an appropriate fraction of the voltage to each dynode. Each channel in the MAPMT has an independent pin for readout of the charge.

The MAPMT with the voltage divider was then mounted onto a board for support and to get a connection for each channel in the MAPMT.

To be able to test each channel independently a custom cable was constructed: An alligator clip 15 cm from the end of the cable was connected to the grounding of a coaxial cable. Attached to the end of coaxial cable there was a small hug clip, that was able to grab the soldering connecting the cable to the board. With this cable a single channel of the MAPMT could be chosen and read out by an oscilloscope.

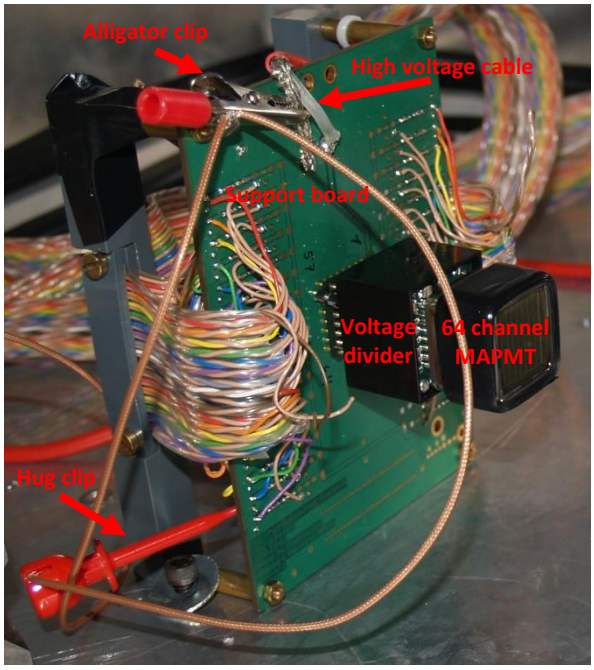

Figure 14.1. Support board with voltage divider and 64 channel photomultiplier. The custom cable is attached.

A quick test setup was made by placing the setup in a dark chamber, connecting HV and lighting the MAPMT with a light emitting diode (LED) powered by a pulse generator. A single channel of the MAPMT was chosen with the custom cable readout by an oscilloscope triggered on the pulse generator. By adjusting the pulse generator and thereby the light emitted by the LED, the amplitude of the MAPMT channel signal changed and it was concluded that the basic setup worked.

14.2.2. 64 channel readout

A schematic of the setup is shown in Figure 14.2. The board with the MAPMT was connected to two data acquisition modules (C.A.E.N. mod. V792, 32 CH QDC) in a Versa Module Europa (VME) crate. These modules measure the charge of each of the 64 channels when the modules are triggered. The triggering is done with a Nuclear Instrumentation Module (NIM) signal. To avoid triggering before the modules were ready after the last readout, the modules sends out an Emitter-Coupled Logic (ECL) signal “busy”. The ECL signals from each data acquisition module and the read-out control board are then converted into a NIM signals and sent through coincidences unit in “or” mode (because no Fan-in Fan-out module was available) to make one busy signal if either module is busy. The common busy signal is then sent to a timer and the inverse output of the timer is used. In this way the timer will send out a “1” NIM signal when there is no busy signal and a “0” NIM signal when there is a busy signal. The output NIM signal from the timer is then sent to a coincidence unit. To the same coincidence unit is connected the device that should trigger the readout, in this case the pulse generator. The coincidence unit will now send out a signal when the pulse generator sends a signal and the VME modules are not busy. This signal is used to trigger the readout of the data acquisition modules.

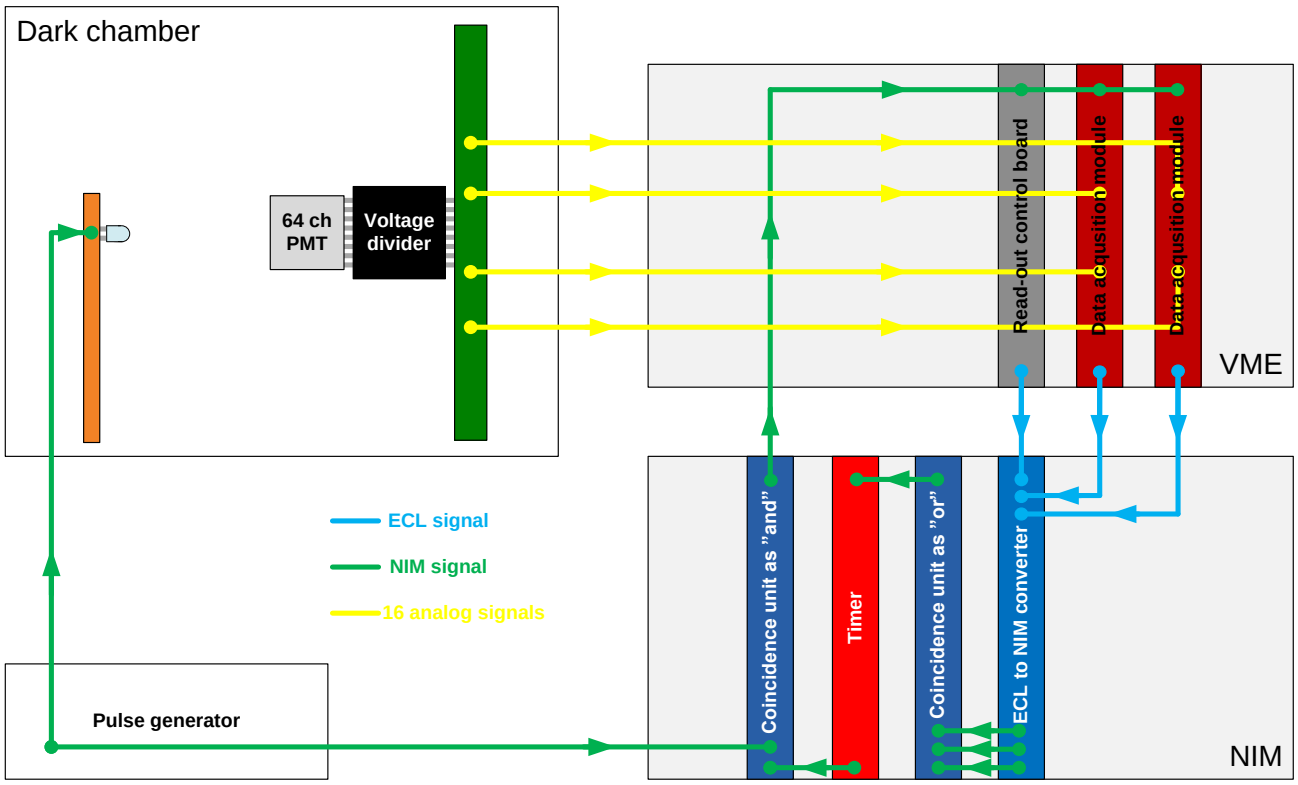

Figure 14.2. A schematic for the VME and NIM connections to the pulse generator and MAPMT.

The data from the VME crate is sent to a Linux-PC running a custom made program for data acquisition for ALFA (used on the 2005 beam test).

The data acquisition window (the time between the trigger and the busy signal) was adjusted to be around 100 ns (see Section 14.3.2). The LED powered by the pulse generator was placed in front of the MAPMT. The custom cable attached was to a random channel and connected to the oscilloscope. By reading out the amplitude of the signal from the MAPMT channel on the oscilloscope, the light amount of the LED was adjusted on the pulse generator to the order of a few photoelectrons (PE) signal in the MAPMT. A data acquisition run was performed for all 64 channels. A run of 150000 triggers take around 17 min with the used frequency of the pulse generator. The HV of the MAPMT was -950 V.

The data is automatically stored on a hard disk on a central server. To be able to look at the data it was filled into ROOT histograms using a script made by the ALFA group. The fill-script, *histos3,* is Appendix C. A raw example of data from one channel put into a histogram by the script is shown as Figure 14.3.

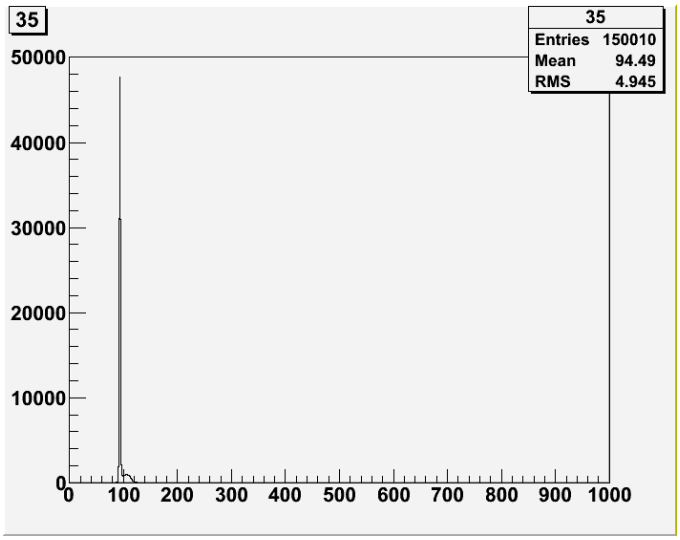

Figure 14.3. Data of channel 36 filled into a histogram by the ALFA group made script. The axes does not have labels and no range is set. The x-axis is charge in ADC counts and the y-axis is number of events.

The numbering of the data starts at 0, so to get the MAPMT channel number, 1 should be added. In the histogram a very high pedestal is shown and then a small bump. The high pedestal corresponds to a lot of zero change measurements because not every channel is hit by light every time the pulse generator sends out a signal. Even if the channel is hit by light, it might not give a signal because the quantum efficiency is not 100 %. Each count in the bump corresponds to a charge measurement higher than zero done be the Analog Digital Converter (ADC) in the data acquisition modules by measuring the area under the signal curve from the MAPMT. To verify the data, the same measurement was done for a single channel using a "histogram of area under curve" function on the oscilloscope and is shown on Figure 14.4.

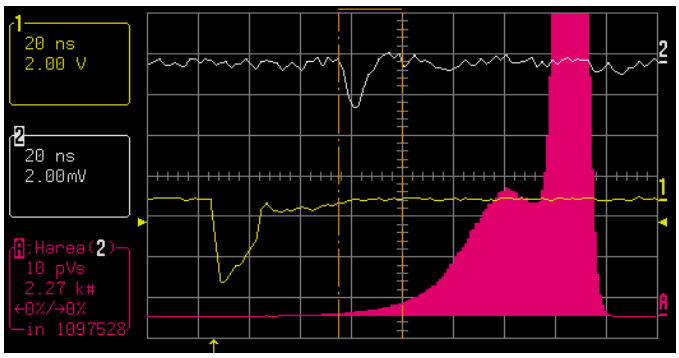

Figure 14.4. Screenshot of the oscilloscope measurement of the charge. The yellow line (1) is the signal from the pulse generator (the trigger) and the white line (2) is the signal from the MAPMT. The area between the two orange vertical lines is the measuring area of the MAPMT signal. The histogram is pink (A) and the x-axis is inverted compared with the one taken with the data acquisition modules because the signals from the MAPMT are negative and here counted as such.

The x-axis is inverted compared to the one taken with the data acquisition modules because the signals from the MAPMT are negative and here counted as such. Else the data seems comparable and it was concluded that the data acquisition setup worked.

14.2.3. First fit equation

The data shown in Figure 14.3 and Figure 14.4 are not just a zero-pedestal and one PE. Even with a small amount of light there will still statically be a chance for 2 PEs, 3 PEs and so on. The number of PEs is expected to be Poisson distributed:

$$P(i) = \frac{e^{-\mu} \cdot \mu^{i}}{i!} \tag{14.1}$$

i Number of photoelectrons

μ Average of signal

A photomultiplier does not give a discrete charge signal when hit by a photon. The signal from a certain number of PEs will come in an interval and is expected to be Gaussian distributed:

$$G(x) = \frac{1}{\sqrt{2\pi} \cdot \sigma} \cdot e^{\frac{-(x-Q)^2}{2 \cdot \sigma^2}} \tag{14.2}$$

Q Average charge

σ Charge deviation

To take both of these properties into account at the same time, a combination of the Poisson distribution and the Gaussian distribution is needed, a Poisson convoluted with a Gaussian [68](equation 2):

$$f(x) = N \cdot \sum_{i=0}^{n} \left[\frac{e^{-\mu} \cdot \mu^{i}}{i!} \cdot \frac{1}{\sqrt{2\pi}\sqrt{i \cdot {\sigma_{1PE}}^2 + {\sigma_{ped}}^2}} \cdot e^{\frac{-(x-Q_{ped}-i \cdot Q_{1PE})^2}{2 \cdot (i \cdot {\sigma_{1PE}}^2 + {\sigma_{ped}}^2)}} \right] \tag{14.3}$$

N Normalizationfactor

i Number of photoelectrons

n Maximum number of photoelectrons

μ Average of signal

Q_{ped} Charge of the pedestal

Q_{1PE} Charge of the 1 photoelectron contribution

σ_{ped} Charge deviation of the pedestal

σ_{1PE} Charge deviation of the 1 photoelectron contribution

In equation (14.3) the charge and the charge deviation have been split up into terms from the pedestal and from the 1 PE. This is done because pedestal is not at zero and therefore the pedestal needs to be used as a starting point for the charge measurement.

14.2.4. First fit

As a starting point a fitting macro for ROOT made by Sebastien Franz (PhD of Universite de Savoie, working at CERN for ALFA) was used. The original fitting macro, *cosmic1pe.C*, is Appendix D. This macro fits the channel called for to:

$$f(x) = N \cdot \sum_{i=0}^{n} \left[\frac{e^{-\mu} \cdot \mu^{i}}{i!} \cdot \frac{1}{\sigma_{1PE}\sqrt{\cdot 2i \cdot \pi}} \cdot e^{\frac{-(x-Q_{ped}-i \cdot (Q_{1PE}-Q_{ped}))^2}{2 \cdot i \cdot {\sigma_{1PE}}^2}} \right] \tag{14.4}$$

N	Normalizationfactor
i	Number of photoelectrons
n	Maximum number of photoelectrons
μ	Lightyeild
Q_{ped}	Charge of the pedestal
Q_{1PE}	Charge of the 1 photoelectron contribution
σ_{1PE}	Charge deviation of the 1 photoelectron contribution

This is a little different from equation (14.3). Besides a difference in the definition of Q_{1PE} equation (14.4) it does not take into account the width of the pedestal. It was tried to fit all the channels in the dataset with the original macro, but it only manage to fit 1 out of the 64 channels. To get it to work the stating values of the fit were changed, which made it able to fit more channels, but soon after it was decided to start almost over and redefined the equation to equation (14.3). The final version (much later than this stage) of *cosmic1pe.C* is Appendix E. At the same time axis labels were added. A second ROOT marco, *All64.C*, was made that just call the *cosmic1pe.C* for all channels (later bad channels were removed). The *All64.C* is Appendix F. To make it faster to look through the 64 plots, picture saving was added to *cosmic1pe*.C so that each plot is saved as a gif file. To make it possible later to change something in the plot, *cosmic1pe*.C also saved each fit as a ROOT file. The part of the plots containing information on the light amount is the bump after pedestal. As it is seen in Figure 14.3 the bump is hardly shown next to the pedestal. To emphasize the bump the range of the y axis is adjusted and further the y axis is set to a logarithmic scale in the *cosmic1pe*.C. A lot of smaller adjustments were done to *cosmic1pe*.C to make it fit all channels and improve the output range etc. An example of the gif-picture output from *cosmic1pe*.C's fit to equation (14.3) is shown as Figure 14.5.

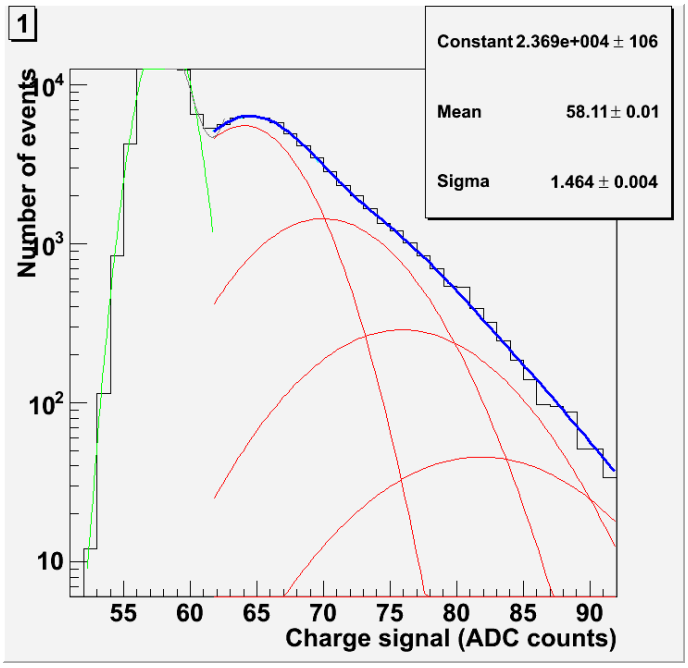

Figure 14.5. Example of the picture output for a single channel of the fitting macro. The green curve is a gaussian fit of the pedestal. The blue curve is the main fit of equation (14.3). The red gaussian curves corresponds to the 1, 2, 3 and 4 PE signal.

14.2.5. BIAS voltage

To make a better separation between the pedestal and the bump the BIAS voltage of the MAPMT was raised (as this will give the MAPMT a higher gain, which should improve the separation). As a starting point -950 V BIAS voltage had been used because that was used in the 2005 beam test. But the MAPMT could safely be operated at a slightly higher voltage. A few different voltage levels were tried, but it turned out that the best separation between the pedestal and the bump was at -1000 V BIAS voltage, which was the highest voltage tested, as it was feared that higher voltage might damaged the MAPMT. After the test the BIAS voltage of the MAPMT were kept on -1000 V.

14.2.6. Mapping

The fill-script *histos3* calls a mapping file that tells the script which ADC channel correspond to which MAPMT channel so that the data is filled into the appropriate channel. The mapping file was already made and used before. But the setup had been moved and might have been changed in some way.

To confirm that the mapping was correct, a simple test was made by placing the LED in one corner of the MAPMT. The data was filled into histograms with the fill-script *histos3* and all the histograms fitted with *cosmic1pe.C*.

Surprisingly the plots that were supposed to correspond to the corner where the LED was positioned did not all show a high amount of light. Further some channels that were supposed to be far from the LED showed large charge signals. It was therefore suspected that something might be wrong with the mapping.

To make a more accurate test the basic setup and 64 channel readout was kept, but the LED setup was changed. To check the mapping it was desirable to only have light on one channel of the MAPMT. To do this a LED mounted in a metal box and connected to a light guide, shown in Figure 14.6 (LEFT), (previously made and used by the author when he was a summer student at CERN) was used. Furthermore an aluminum piece with 64 holes, which previously had been used for testing fibers, was mounted on the MAPMT. The aluminum piece setup is shown in Figure 14.6 (Right).

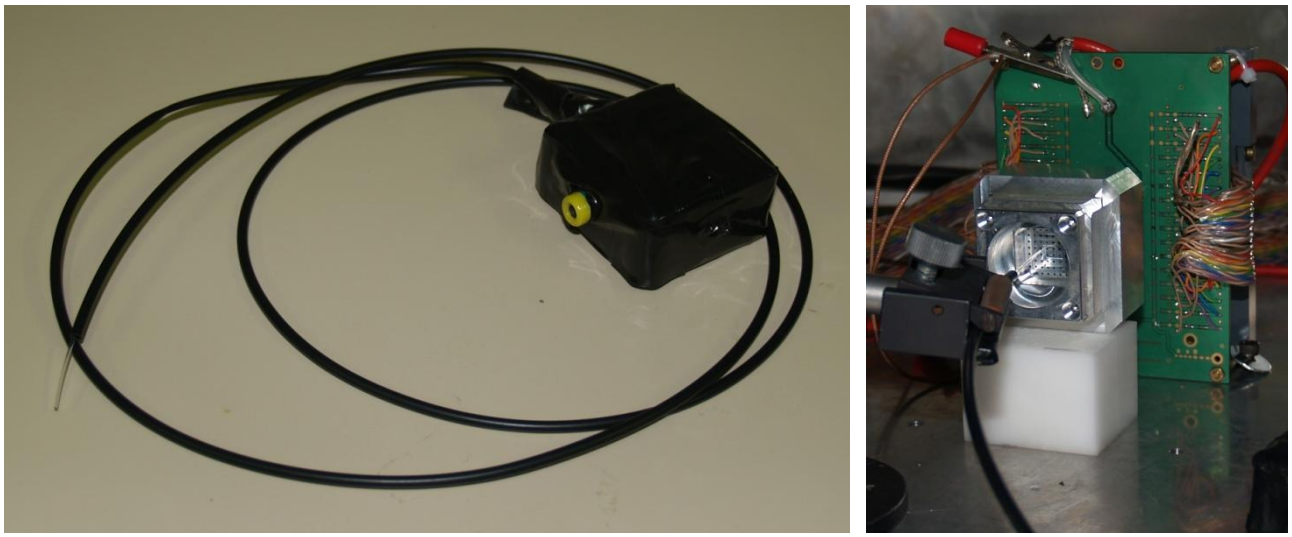

Figure 14.6. *LEFT*: LED mounted in a metal box and a light guide to get the light out of the box. *RIGHT*: Aluminum piece mounted on the MAPMT and the light guide place in front of it.

A series of measurements where the light guide was positioned in front of different holes/MAPMTs channel was made. The data was filled into histograms with *histos3* and analyzed using *cosmic1pe.C*. It was concluded that some of the mapping was correct, but that other parts of the mapping was wrong.

More measurements with light on a single channel were done in a joined effort with Sebastien Franz (PhD of Universite de Savoie, working at CERN for ALFA), whom had made the original mapping file. In the end a pattern was seen: The second half of the mapping file was inverted.

A new mapping file was made to replace the original mapping file. A new series of test with light only to one channel at the time was done and all the tested channels turn out to have the correct mapping. Not all channels were tested (a full test of a channel takes 17 min + data analyze time), but all parts of the MAPMT and all 4 cables (and thereby all 4 inputs on the data acquisition modules) were represented.

As discussed in Section 13.1.4 not all the channels have the same gain. Due to the production method it is expected that there are patterns in the gain and thereby in the charge measured. To look for this, and thereby confirming the mapping file, *cosmic1pe.C* was changed such that the charge difference from the pedestal to the 1 PE Gaussian peak was stored in a file, *1pemean.dat*. Not all channels were fitable. To keep track of which channels that had been fitted the MAPMT channel number were also saved, *index.dat*, in the form of the computer numbering, which is just one lower than the MAPMT channel number.

A plot of the charge difference from the pedestal to the 1 PE Gaussian peak as a function of the MAPMT channel number is shown as Figure 14.7.

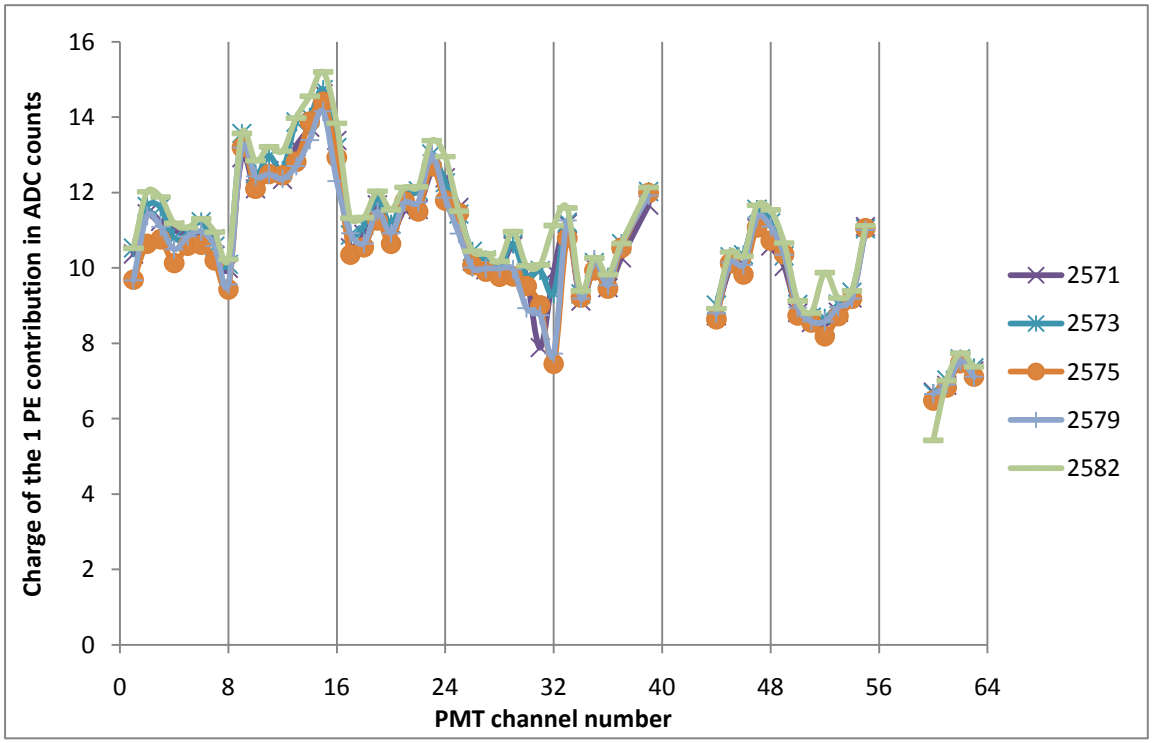

Figure 14.7. The charge difference from the pedestal to the 1 PE Gaussian peak as a function of the MAPMT channel number. The different colors correspond to different measurements. Unfortunately the uncertainties were not stored, but the 5 different data sets give a general idea. There are points missing due to bad channels on the acquisition modules.

The uncertainties were unfortunately not saved, but the 5 data set do give a general idea about the uncertainties and the plot is only used to look for a pattern in the MAPMT channels.

The pattern in the MAPMT channels was not as clear as hope for, however a pattern is seen.

14.2.7. Calibration

A calibration was first done with the MAPMT that originally was used. But later a MAPMT with shims was needed (see Section 17 about shims) and the calibration re-done with this MAPMT. This section will only describe the calibration of the MAPMT with shims, which was the one actually used in the later measurements.

A calibration of the MAPMT is needed to lock all the parameters in equation (14.3) that should not change with the amount of light. This makes it possible to fit only to the amount of light seen, and the results will be more comparable. The parameters that should not change are the position of the pedestal Q_{ped} and its deviation σ_{ped} together with the position of the 1 photoelectron Q_{1PE} and its deviation σ_{1PE}. In equation (14.5) (copy of equation (14.3)) the parameters that should be locked are marked with various colors:

$$f(x) = N \cdot \sum_{i=0}^{n} \left[\frac{e^{-\mu} \cdot \mu^{i}}{i!} \cdot \frac{1}{\sqrt{2\pi}\sqrt{i \cdot \sigma_{1PE}{}^{2} + \sigma_{ped}{}^{2}}} \cdot e^{\frac{-(x - Q_{ped} - i \cdot Q_{1PE})^{2}}{2 \cdot (i \cdot \sigma_{1PE}{}^{2} + \sigma_{ped}{}^{2})}} \right] \tag{14.5}$$

For the calibration, file writing of the charge of the pedestal *ped mean.dat*, the charge deviation of the pedestal *ped RMS.dat*, the position of the 1 PE *1pe mean.dat* and charge deviation of the 1 PE *1pe RMS.dat* were added to *cosmic1pe.C*. To make it easier to distinguish the plot of each PE they were given differed colors in *cosmic1pe.C*.

The calibration itself was made with the setup shown in Figure 14.2. Three data acquisition runs were made with various amount of light. In Figure 14.8 are the data and fit from channel 7 of each run shown. There was no overall tendency in the recorded data files dependant on the amount of light, so the fit seemed to work and the meaningful calibration could be carried out.

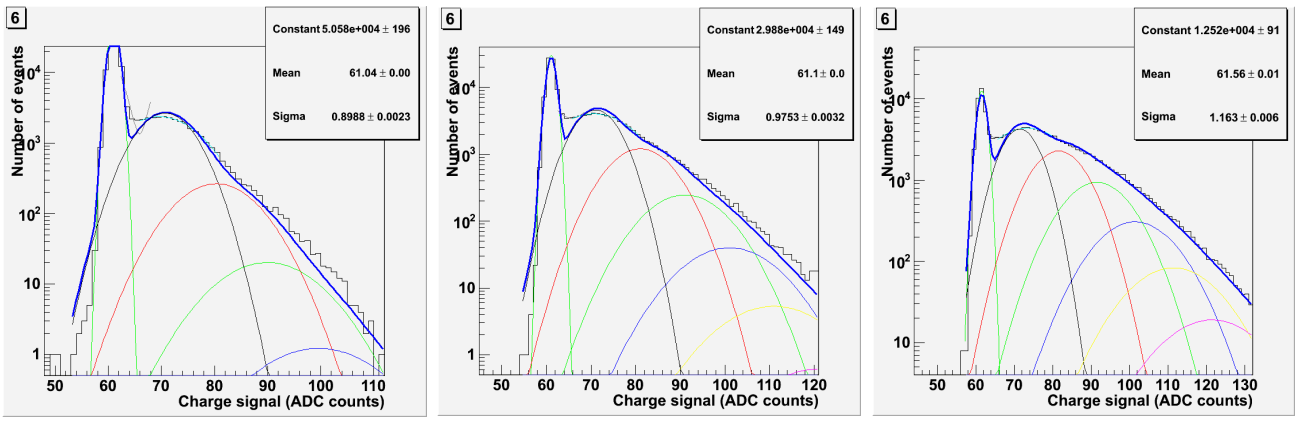

Figure 14.8. Data and fit of MAPMT channel 7 from the 3 calibration runs. The amount of light goes up from the left to the right.

Calibration files were made for pedestal *ped mean.cal*, the charge deviation of the pedestal *ped RMS.cal*, the position of the 1 PE *1pe mean.cal* and charge deviation of the 1 PE *1pe RMS.cal*. This was done by taking the average for the 3 runs of the given parameter. Bad channels and bad fits were disposed of by going through all the fits manually; looking through all the pictures of the data and fits.

Reading of the calibration files and locking of the values of the parameters were added to *cosmic1pe.C*.

14.3. Analog readout on the 2005 prototype setup

The light yield of the fibers in the 2005 prototype have been measured very thoroughly and with good statistic in a beam test and documented in article [68]. Measuring the light yield of the 2005 prototype fibers with the new setup can therefore confirm or disprove the method used.

14.3.1. Setup

A setup was made to measure the light yield of a single layer of 64 fibers in the 2005 prototype. The readout end of the fibers was already mounted in a lattice with 2.3 mm between the centers of each fiber in each direction, corresponding to the distances between each MAPMT channel in the 64 channel MAPMT. The mounted fiber ends are shown in Figure 14.9 (left). Unfortunately the MAPMT channels are not centered on the MAPMT. Therefore the MAPMT have been measured out and 4 custom shims made for it to center the MAPMT channels (see Section 17 about shims). A custom made aluminum piece makes the connection between the 8x8 mounted fiber ends and the MAPMT with spacers as shown in Figure 14.9 (right).

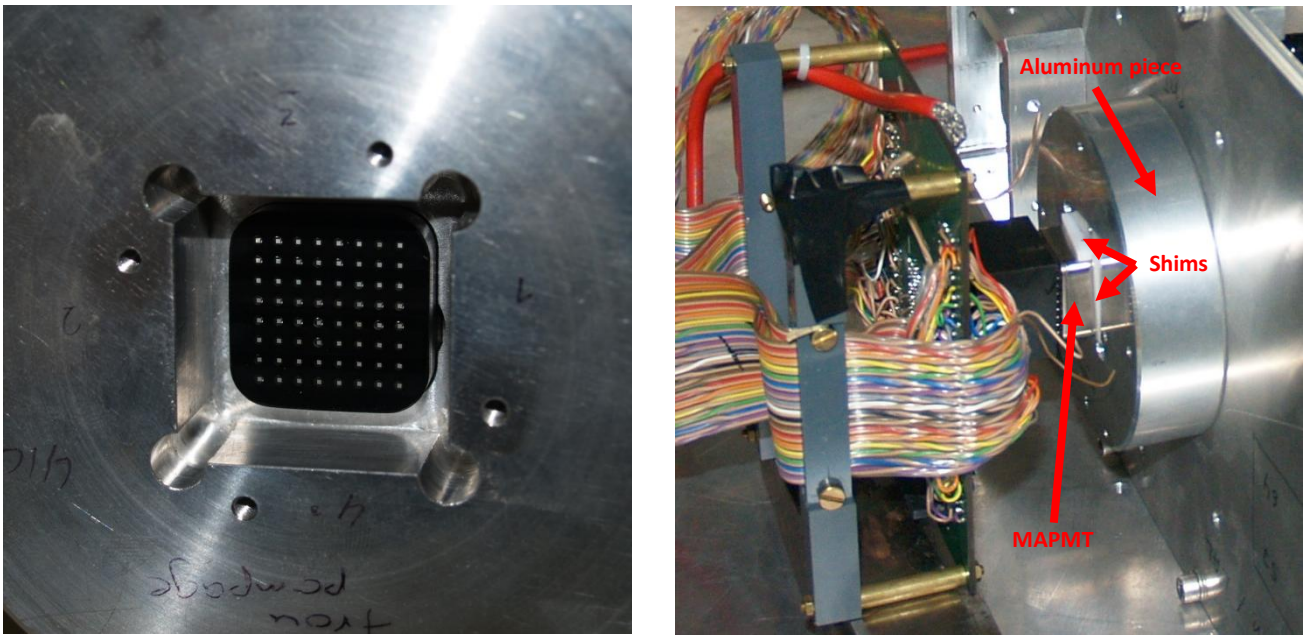

Figure 14.9. *LEFT*: The mounted fiber ends positioned in a custom made aluminum piece. *RIGHT*: The custom made aluminum piece connecting the MAPMT with shims to the mounted fiber ends.

To trigger the readout scintillator tiles with very fast PMTs were used. The trigger scintillator tiles were diamond shaped to correspond to the overlap of two 64 fiber layers shown in Figure 14.10 (left). One of the trigger scintillator tiles and light guides are shown in Figure 14.10 (right) and the shape of the scintillator tile is pointed out.

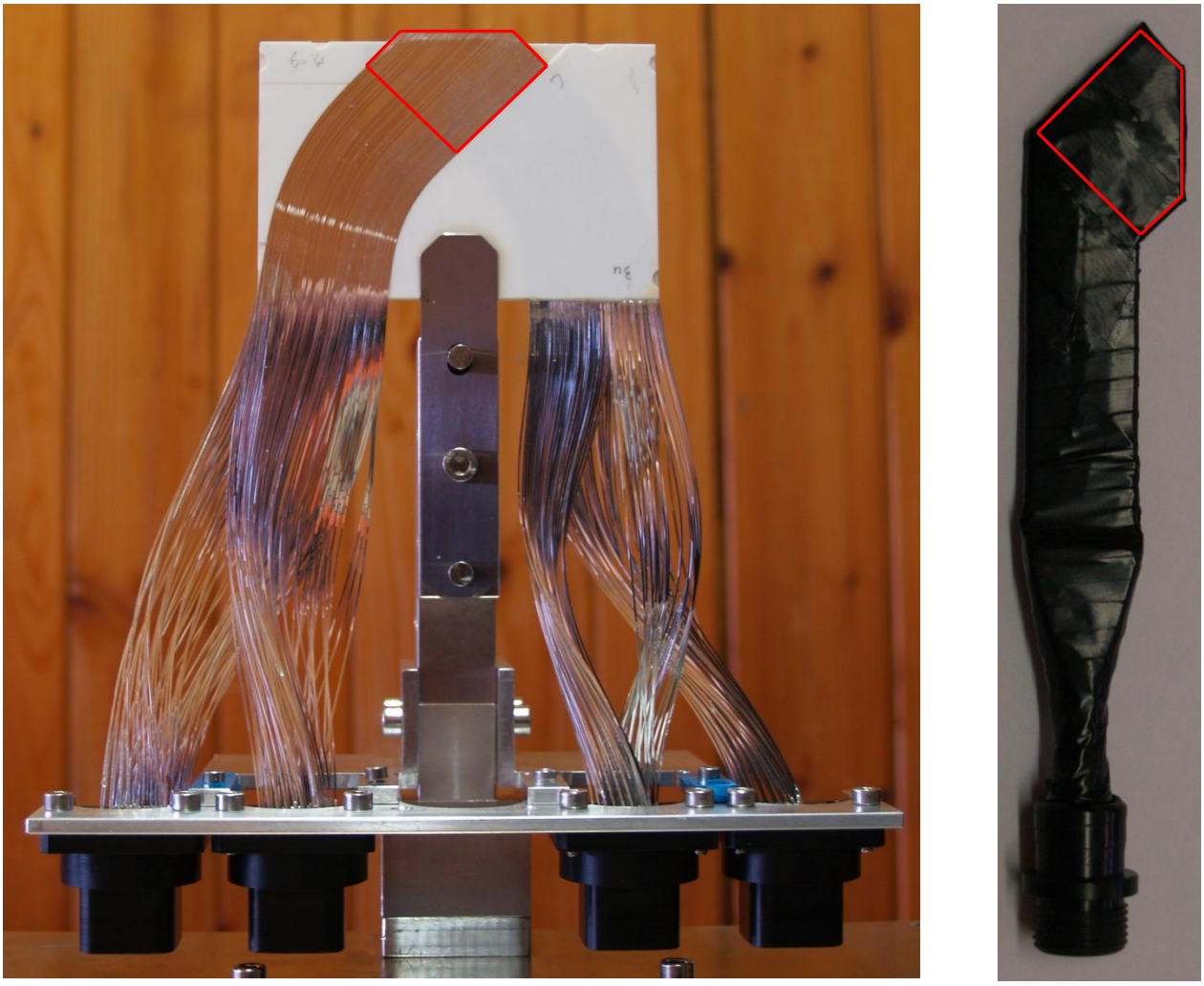

Figure 14.10. *LEFT*: The 2005 prototype with 4 layers of fibers. The overlap (the detecting area) of the fiber layers are pointed out in red. *RIGHT*: Trigger scintillator tile with light guide. The shape of the scintillator tile is pointed out in red.

Two trigger scintillator tiles were used, one on top of the fibers and one below the fibers. This should ensure that if a particle passes both the upper and the lower trigger, it has to have gone though the fibers. The setup of the triggers and prototype were placed in a dark chamber and are shown Figure 14.11 with a strontium-90 source on top. The top trigger PMT was a Hamamatsu R1635 operated at its optimal voltage of -1250 V, and the bottom trigger PMT was a Hamamatsu R7400P operated at its optimal voltage of -800 V.

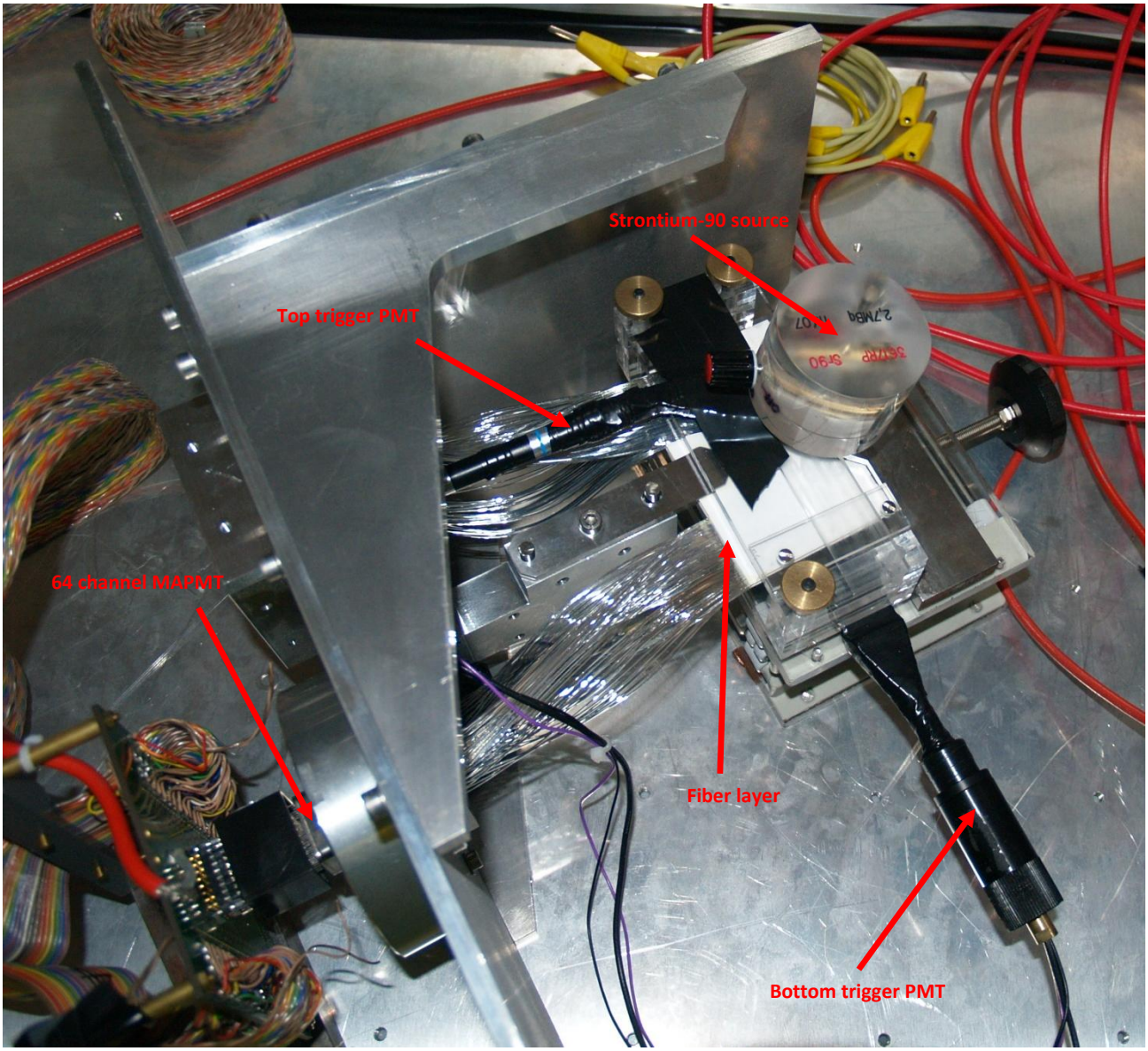

Figure 14.11. The setup in a dark chamber with one trigger scintillator tile with PMT over and one trigger scintillator tile with PMT under the fibers. The MAPMT is connected and shown in the lower left corner. The top of the setup is a strontium-90 source.

The readout system used were basically the same as described in Section 14.2.2. The only difference is the triggering of the readout. Each trigger scintillator tile is readout by a very fast and small PMT, which is connected to a discriminator. If the discriminator receives a signal which is larger than the set threshold (set to 30 mV) it sends out a NIM signal in a width that also can be set (set to 50 ns). These signals then go to the same coincidence unit as the inverted busy signals. Only if there is a signal in both the triggers and there is not a busy signal, a readout of the 64 PMT channels is performed. To keep track of the noise from the trigger PMTs a scaler was added after the discriminator. The common signal from the coincidence unit was also added to the scaler. A schematic for the entire setup with readout is shown in Figure 14.12.

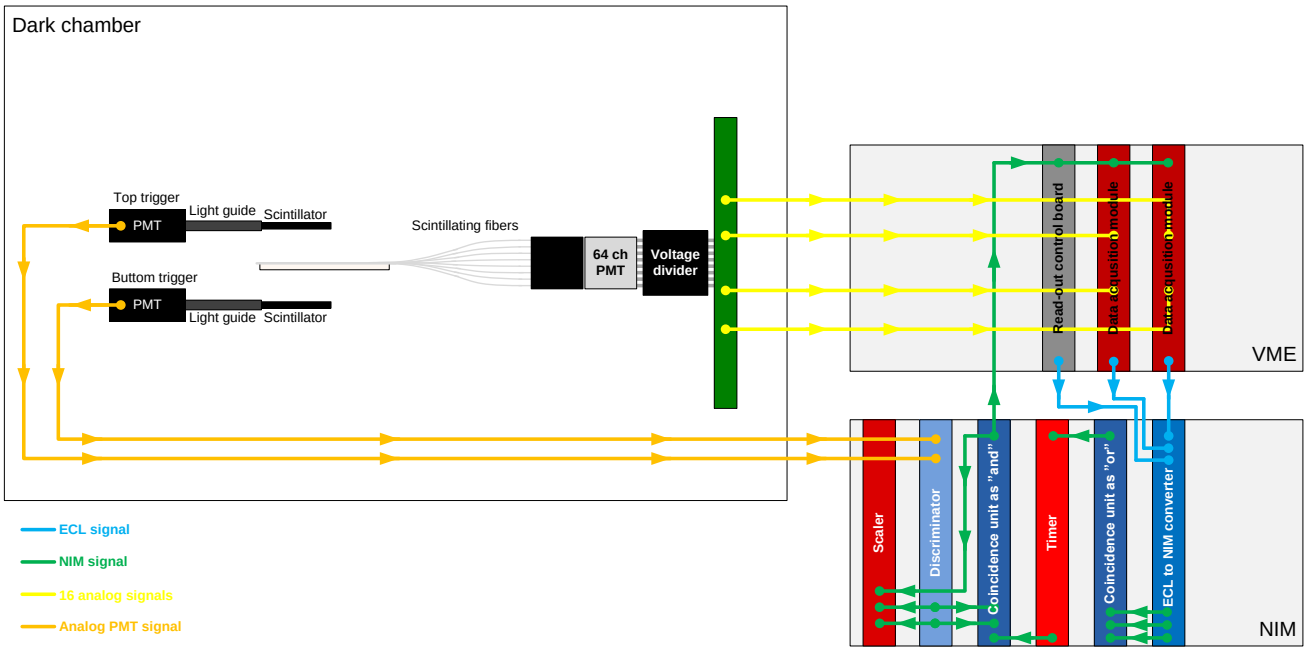

Figure 14.12. A schematic for the setup for measuring the light yield of the fibers in the 2005 prototype.

14.3.2. The data acquisition window

In the manual of the data acquisition module [69](section 3.7) it is specified that the trigger signal (start of the gate) need to be at least 15 ns before the signal that should be recorded. The trigger signals also need to pass through some logic (the discriminators and the coincidence unit) which introduces some delay. Therefore the signals that should be recorded (the MAPMT signals) have to be delayed. In the setup the MAPMT was connected with long 64 twisted pair cables. This introduced some delay. The timing is illustrated in Figure 14.13.

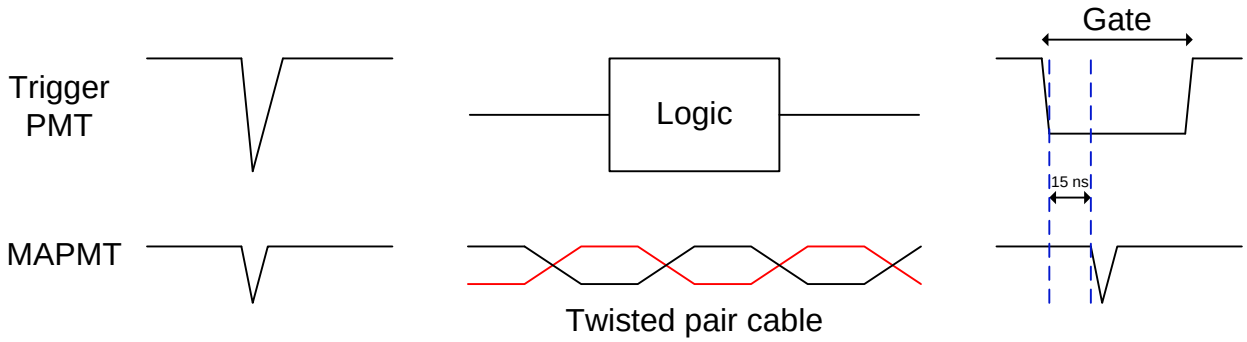

Figure 14.13. Timing for the data acquisition modules.

With a digital oscilloscope it was measured that the trigger signal to start the gate did not arrive 15 ns before the signal from the MAPMT. A further delay of the MAPMT signals was desirable, but the MAPMT readout was connected with 64 twisted pair cables and therefore very difficult to delay. It could of course be done but it would take a lot of work. Also twisted pair cables should not be too long, since noise otherwise will be an issue. Instead the trigger signal needed to arrive faster. All cables for the triggering were shortened as much as possible, but of course kept the same length for both triggers to ensure the trigger signals makes coincidences. The shorter trigger cables made the trigger arrive about 15 ns before the MAPMT signals.

The length of the gate was at the same time adjusted from less than 40 ns to about 50 ns. A too short gate could end the buildup of charge in the data acquisition module before all charge had been recorded (cut the tail of the MAPMT signal).

14.3.3. Data acquisition

First a run with a strontium-90 source (2.8 MBq, beta decay) was performed. The run was carried out by positioning the source on top of the top trigger as shown in Figure 14.11. The test with the source was done to check if the setup was working properly without waiting for good statistic from cosmic. The measurement with the strontium-90 source took about 17 hours and the readout was triggered 151114 times. The results are discussed in Section 14.3.8. The setup seemed to perform well and the source was removed and a 10 days test with cosmic carried out. The readout was trigged 31453 times. The results are discussed in Section 14.3.10.

14.3.4. Rate of cosmic

In this section the expected rate of cosmic particles is calculated and compared to the rate observed in data acquisition in Section 14.3.3.

The cosmic detected in the laboratory are mostly muons as it is shown in Figure 14.14

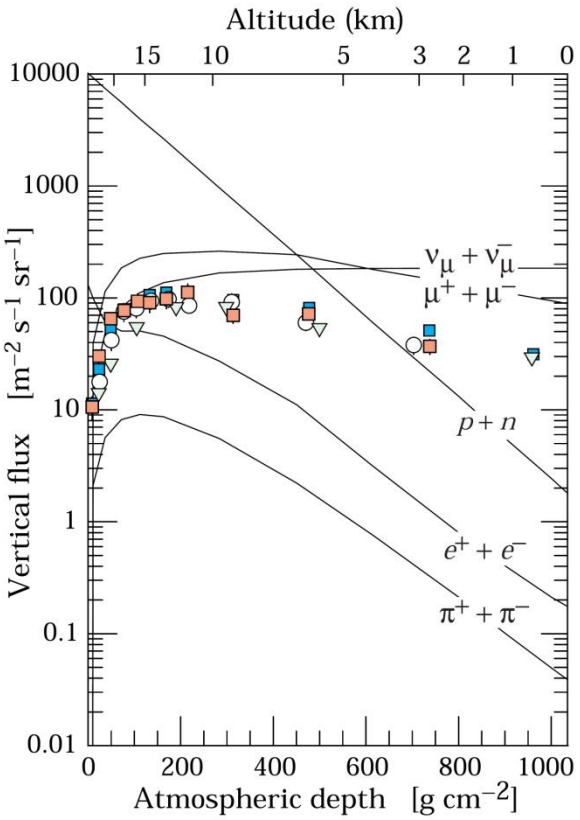

Figure 14.14. Cosmic rays composition depending on altitude. At ground level muons are highly dominating as the neutrinos will not be detected. The figure is figure 24.3 in [28].

The intensity of muons is approximately [28](page 255):

$$I \approx 1 \cdot \frac{counts}{cm^2 \cdot min} \tag{14.6}$$

and the angular distribution is proportional to [28](page 256):

$$\text{Angular distribution} \propto \cos^2\theta \tag{14.7}$$

But not all angles of incoming muons will pass both trigger scintillator tiles. To make the calculations easier and as only an estimate of the intensity of muons is needed, the scintillator tiles are assumed to be flat cylinders.

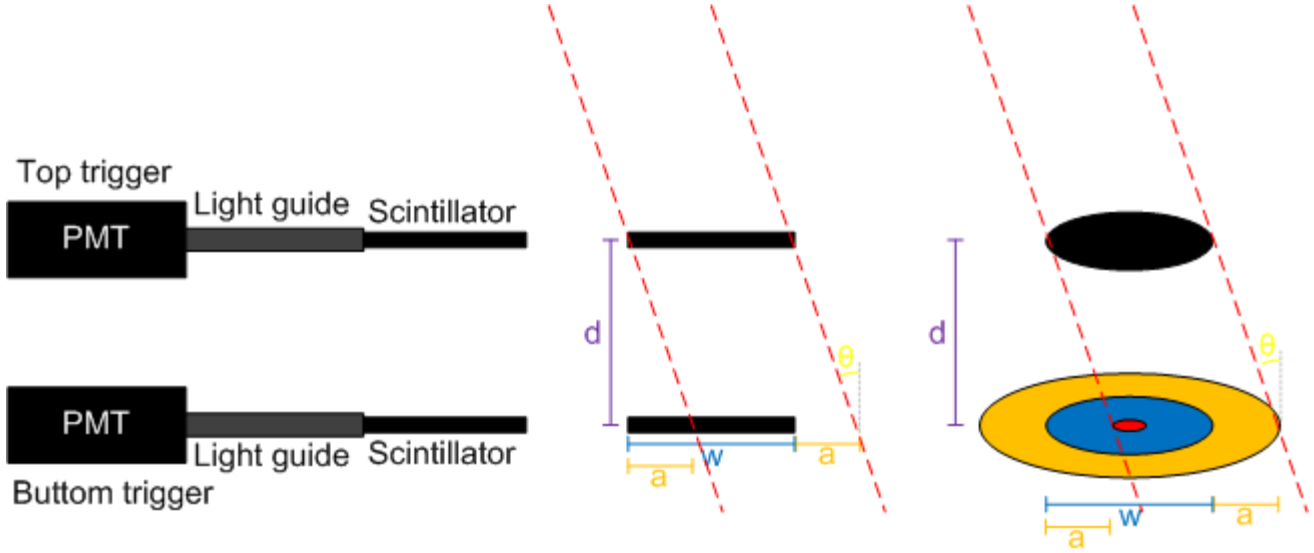

Figure 14.15. To the left are the trigger scintillator tiles with light guides and PMTs. In the middle is the scintillator tiles cut out. To the right is the area of the top scintillator tile, the area of the bottom scintillator tile and the area the muon can pass through in and around the bottom scintillator tile (if the muon passed the top scintillator tile). The red dotted line represents a muon passing the scintillator tile in each edge of the scintillator tile. The labeds: *w* is the width of the scintillator, *d* is the distances between the two scintillators, θ is the incoming angle of the muon, *a* is the distance from the bottom scintillator tile, the muon hits, if the muon hit the outermost part of the top scintillator tile. The red area can be hit for both θ and -θ.

The lager the angle θ gets the less likely it is that the muon passes both scintillator tiles. More precisely, the likelihood of the muons passing the bottom scintillator tile, if it has passed the top scintillator tile, goes as the area of the bottom scintillator tile (the blue area to the right in Figure 14.15) over the area the moun can possible pass at the distance of the bottom scintillator tile (the orange, blue and red area to the right in Figure 14.15). The red area counts double as it can be hit for both θ and - θ. With large θ some part of the bottom scintillator tile will never be hit. This will split the likelihood function into:

For small θ, $\frac{w}{2} > a$, the red counts double and *L* is:

$$\begin{aligned} L &= \frac{\text{Area of the bottom scintillator + double hit area}}{\text{Area of muon pass + double hit area}} \\ &= \frac{\pi\cdot\left(\frac{w}{2}\right)^2 + \pi\cdot\left(\frac{w}{2}-a\right)^2}{\pi\cdot\left(\frac{w}{2}+a\right)^2 + \pi\cdot\left(\frac{w}{2}-a\right)^2} \\ &= \frac{w^2 - 2\cdot a\cdot w + 2\cdot a^2}{w^2 + 4\cdot a^2} \end{aligned} \tag{14.8}$$

For large θ, $\frac{w}{2} < a < w$, some part of the bottom scintillator tile cannot be hit and *L* is:

$$\begin{aligned} L &= \frac{\text{Area of the bottom scintillator} - \text{area that cannot be hit}}{\text{Area of muon pass} - \text{area that cannot be hit}} \\ &= \frac{\pi \cdot \left(\frac{w}{2}\right)^2 - \pi \cdot \left(a - \frac{w}{2}\right)^2}{\pi \cdot \left(\frac{w}{2} + a\right)^2 - \pi \cdot \left(a - \frac{w}{2}\right)^2} \\ &= \frac{w - a}{2 \cdot w} \end{aligned} \tag{14.9}$$

For very large θ, $a > w$, the bottom scintillator tile will never get hit and *L* is:

$$L = 0 \tag{14.10}$$

The distance a can be found geometrically as:

$$\tan\theta = \frac{a}{d} \quad \Rightarrow \quad a = d \cdot \tan\theta \tag{14.11}$$

Equation (14.8), (14.9) and (14.10) then becomes:

$$L = \begin{cases} \dfrac{w^2 - 2 \cdot w \cdot d \cdot \tan\theta + 2 \cdot d^2 \cdot \tan^2\theta}{w^2 + 4 \cdot d^2 \cdot \tan^2\theta} & \text{for} \quad \dfrac{w}{2} > d \cdot \tan\theta \\ \dfrac{w - d \cdot \tan\theta}{2 \cdot w} & \text{for} \quad \dfrac{w}{2} \le d \cdot \tan\theta \le w \\ 0 & \text{for} \quad d \cdot \tan\theta > w \end{cases} \tag{14.12}$$

L is now the weight each angle will be represented by. To find the fraction of the muons which has passed the top scintillator tile and also hit the bottom scintillator tiles, and thereby trigger the readout, an integration of the muon angular distribution, equation (14.7), weight by *L* over all angles is carried out and normalized by an integration over all angles of the angular distribution without weights:

$$f = \frac{\int_0^{90} \cos^2\theta \cdot L d\theta}{\int_0^{90} \cos^2\theta d\theta} \tag{14.13}$$

For the trigger scintillator tiles the distance *d* was 4.0 cm and the width *w* (the long side of the diamond shape) was 3.2 cm. The *f* in equation (14.13) than comes to (integrals are solved in Maple and are included as Appendix G):

$$f_{2005} = \frac{\int_0^{90} \cos^2\theta \cdot L d\theta}{\int_0^{90} \cos^2\theta d\theta} \approx 29.9\ \% \tag{14.14}$$

The diamond shaped of trigger scintillator tile comes from a 3.2cm*3.2cm square were a corner of 2.0cm*2.0cm is cut off. The area of the scintillator tile is therefore:

$$A_{\text{scintillator}} = 3.2cm \cdot 3.2cm - \frac{1}{2} \cdot 2.0cm \cdot 2.0cm = 8.24cm^2 \tag{14.15}$$

From equations (14.6), (14.14) and (14.15) the expected rate of muons can now be calculated:

$$R_{\text{muon, 2005 expected}} = I \cdot f \cdot A_{\text{scintillator}} = 1 \cdot \frac{counts}{cm^2 \cdot min} \cdot 29.9\ \% \cdot 8.24cm^2 = 2.46 \frac{counts}{min} \tag{14.16}$$

The rate of muon seen in the cosmic data acquisition run was:

$$R_{\text{2005 experimental}} = 2.08 \pm 0.04 \frac{counts}{min} \tag{14.17}$$

The rate of muons seen is about the expected and the triggers seem to have a high efficiency as expected.

14.3.5. Source vs. cosmic vs. test beam

It is compelling to just use the source instead of cosmic muons since the rate is so much higher. But the maximum energy of electrons from the strontium-90 source is only 0.546 MeV (primary decay) and 2.28 MeV (secondary decay) [70], so the electron may not be highly relativistic. Passing the air and trigger scintillator tile will further lower the energy of the electrons. At these low energies the ionization will dominate the energy loss, but also bremsstrahlung and others will contribute as show in Figure 14.16 [28](page 273).

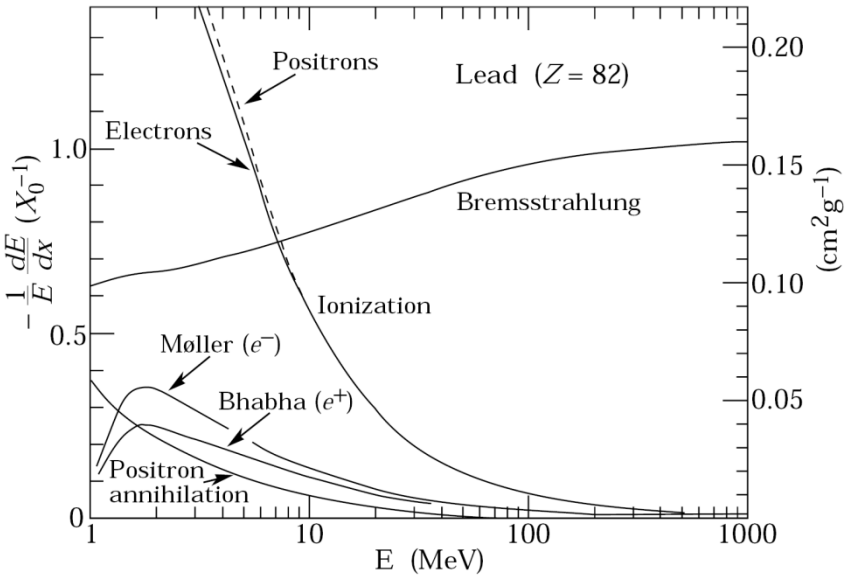

Figure 14.16. Fractional energy loss as a function of the electron (positron) energy. The figure is figure 27.10 in [28].

The electrons may even be completely stopped in fibers. All this adds up to that the relatively slow electrons from the source are very different from the protons that the detector will be used for.

The muons from cosmic on the other hand has a mean energy of about 4 GeV [28](page 255) and is thereby highly relativistic. This energy is higher than the minimum ionizing energy for muons so the mean rate of energy loss (or stopping power) for muons are close to the mean rate of energy loss of protons as they both follow the Bethe-Bloch formula [71](equation 2.26 page 24):

$$-\frac{dE}{dx} = 2\pi N_a r_e^2 m_e c^2 \rho \frac{Z}{A}\frac{z^2}{\beta^2}\left[\ln\left(\frac{2m_e y^2 v^2 W_{\max}}{I^2}\right) - 2\beta^2 - \delta - 2\frac{C}{Z}\right] \quad (14.18)$$

N_a	Avogado's number	β	$\frac{v}{c}$ of incident particle
r_e	Classical electron radius	y	$\frac{1}{\sqrt{1-\beta^2}}$ of incident particle
m_e	Electron mass	$W_{\max}$	Maximum energy transfer in a single collision
c	Speed of light in vacuum	I	Mean excitation potential
ρ	Density of absorbing material	δ	Density correction
Z	Atomic number of absorbing material	C	Shell collision
A	Atomic weight of absorbing material		
z	Charge of incident particle		
v	Speed of incident particle		

Graphically this can be seen in Figure 14.17 which shows the Bethe-Bloch formula for different particles.

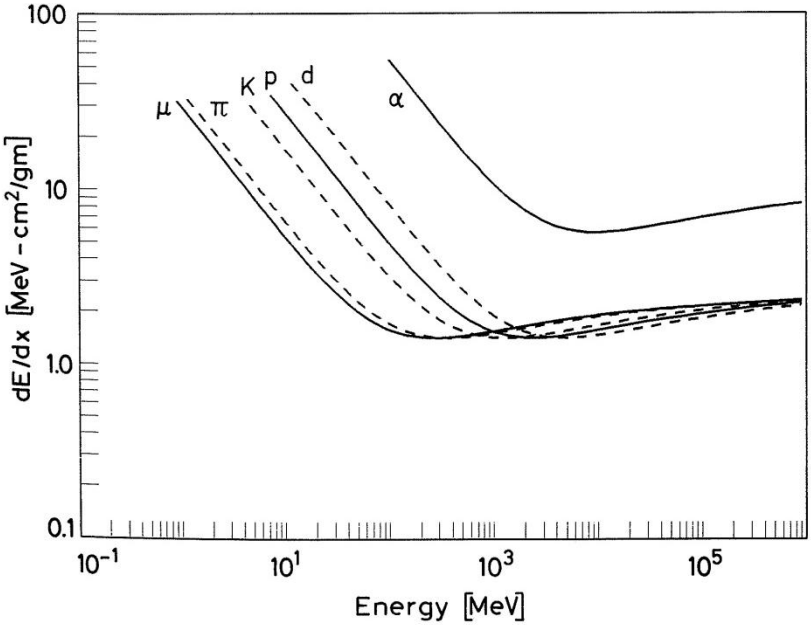

Figure 14.17. The Bethe-Bloch formula for different particles. It is shown that particles of the same charge have almost the same mean rate of energy loss at and above the minimum ionizing energy (the minimum). The figure is figure 2.4 in [71].

The difference in the absorbed energy in a scintillator tile for electrons and muons has previously been investigated by the author in an independent project. This was done by simulating a 2 cm thick plastic scintillator tile in Geant 4. The results for the very low energy range are shown in Figure 14.18.

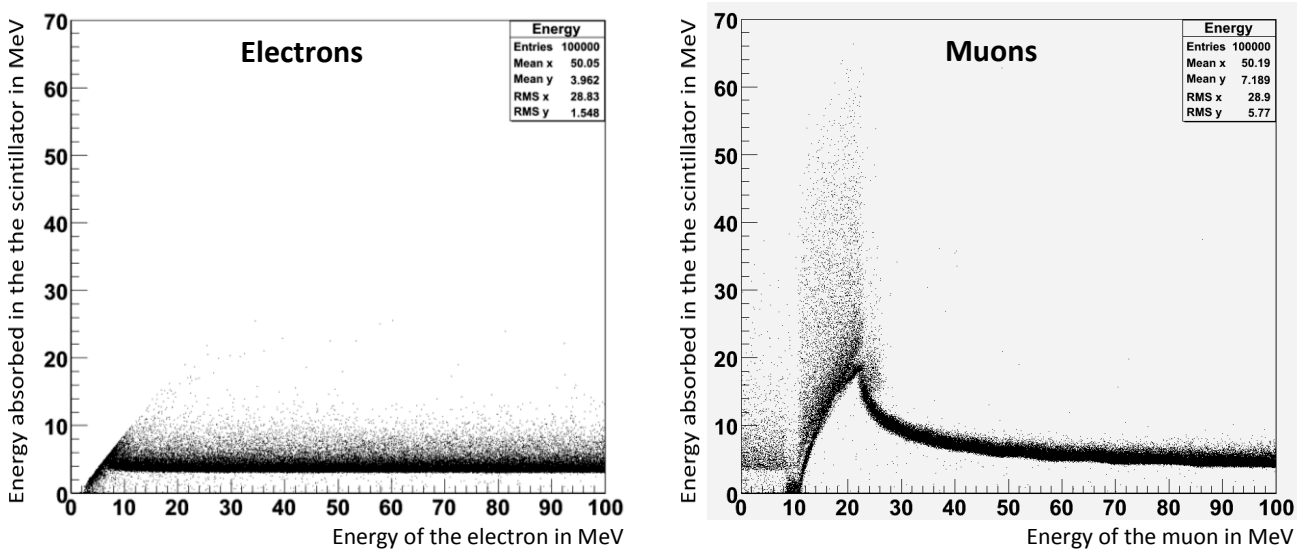

Figure 14.18. Absorbed energy in a 2 cm thick scintillator tile for electrons and muons. Simulation from Geant 4 previously performed by the author.

It is seen that where the electrons get completely absorbed at low energies, the muons have a possibility to decay and thereby deposit much more energy than the potential energy of the incoming muon. At highly relativistic energies the absorbed energy is more alike for electrons and muons. Therefore the results from the cosmic muons should be comparable with data from the 2005 beam test, as this were done at DESY with electrons with an energy of 1 to 6 GeV, which is in the minimal ionizing range of the electron [68]. The difference in the electrons nature at low and high energies is also shown in Figure 14.16.

14.3.6. Optimizing the fit

To be able to fit the data recorded with light coming from the scintillating fibers, some modification is needed to fit equation (14.3). First of all the pedestal should no longer be a part of the overall fit. The pedestal for a single channel will be too high because readout of all channels are triggered every time a particle passes through both trigger scintillator tiles, but only one or two of the fibers will be hit. Therefore changes were made in the fitting macro *cosmic1pe.C* to start the fitting after the pedestal and the fit equation altered not to fit the pedestal (the change is marked in red):

$$f(x) = N \cdot \sum_{i=1}^{n} \left[\frac{e^{-\mu} \cdot \mu^{i}}{i!} \cdot \frac{1}{\sqrt{2\pi}\sqrt{i\sigma_{1PE}{}^{2} + \sigma_{ped}{}^{2}}} \cdot e^{\frac{-(x - Q_{ped} - i \cdot Q_{1PE})^{2}}{2 \cdot (i \cdot \sigma_{1PE}{}^{2} + \sigma_{ped}{}^{2})}} \right] \tag{14.19}$$

Equation (14.19) was fitted to the data and an example is shown as Figure 14.19.

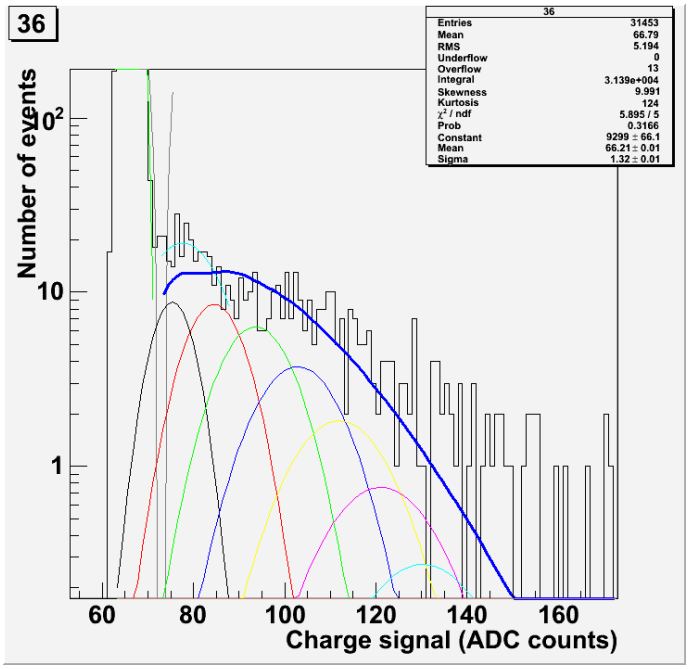

Figure 14.19. Equation (14.19) fitted to data from MAPMT channel 37.

Overall this fit seems satisfactory but near the pedestal the fit is significantly lover then the data. Remember that the y-axis in Figure 14.19 is logarithmic so the difference between data and fit is quite large near the pedestal. It seems there are more events of 1 PE and maybe 2 PE then the Poisson distribution predict. This was also seen in the 2005 test beam and explained as optical crosstalk [68]. The optical crosstalk is explained as a combination of multiple reflections in the entrance window of the MAPMT and direct emission of a small fraction of the light both leading to a small amount of light hitting a neighbor channel on the MAPMT (see also Section 14.7 and Figure 14.53). To take this into account in the fit, a second Poisson distribution convoluted with a Gaussian distribution were added to fit equation (14.19):

$$f(x) = N \cdot \left(\sum_{i=1}^{n} \left[\frac{e^{-\mu} \cdot \mu^{i}}{i!} \cdot \frac{1}{\sqrt{2\pi}\sqrt{i \cdot \sigma_{1PE}{}^{2} + \sigma_{ped}{}^{2}}} \cdot e^{\frac{-(x - Q_{ped} - i \cdot Q_{1PE})^{2}}{2 \cdot (i \cdot \sigma_{1PE}{}^{2} + \sigma_{ped}{}^{2})}} \right] + \sum_{i=1}^{n} \left[\frac{e^{-\mu_{CT}} \cdot \mu_{CT}{}^{i}}{i!} \cdot \frac{1}{\sqrt{2\pi}\sqrt{i \cdot \sigma_{1PE}{}^{2} + \sigma_{ped}{}^{2}}} \cdot e^{\frac{-(x - Q_{ped} - i \cdot Q_{1PE})^{2}}{2 \cdot (i \cdot \sigma_{1PE}{}^{2} + \sigma_{ped}{}^{2})}} \right] \right) \tag{14.20}$$

The only new parameter is μ_{CT} which is the average of the crosstalk signal[1].

The name of the macro was changed to *cosmic.C* (included in a final version as Appendix H) to conserve *cosmic1pe.C* to use for calibration. A new file *All64c.C* was made to call *cosmic.C* for all working channels (like *All64.C* for *cosmic1pe.C*). Equation (14.20) was then fitted to the data and an example is shown as Figure 14.20.

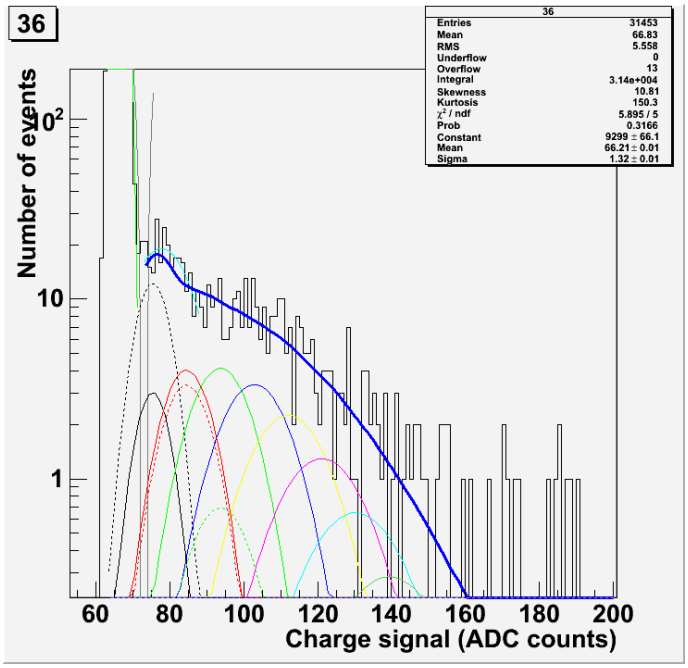

Figure 14.20. Equation (14.20) fitted to data from MAPMT channel 37.

The new fit is very close to the data and is satisfactory.

To readout the information about the amount of light seen in each fit, file writing of the averaged of the signal *Mu.dat*, the error on the averaged of the signal *Mu error.dat*, the averaged crosstalk signal *Mu ct.dat* and the error on the averaged crosstalk signal *Mu ct error.dat* were added to *cosmic.C*.

Finally the standard ROOT stat box (the data and fit information written on the plot) was removed since it only displayed information about the first fit, which is just a Gaussian finding the starting value for the main fit. Instead it was replaced with a manual text box displaying the χ^2 / NDF, the averaged signal μ and the error on μ and the averaged crosstalk signal μ_{CT} and the error on μ_{CT}. An example of the updated look of the ROOT plots are shown in Figure 14.30 page 114.

[1] At first the crosstalk term had its own normalization constant (due to bad notes from 2005) but later this was corrected to one overall normalization constant and thereby minimizing the number for free parameters.

14.3.7. Fiber mapping

The fibers are not arranged fiber 1 to MAPMT channel 1, fiber 2 to MAPMT channel 2 etc. Instead the fibers are arranged in a pattern so no neighbor fibers will be neighbors on the MAPMT. This is done to minimize the effects of crosstalk. A particle can hit two fibers lying next to one another and make a signal in both. In this way crosstalk should not add to a real signal but only make a small signal in an unused channel. But this means that a mapping from the fibers to the MAPMT is needed.

As a starting point a mapping file from the 2005 test beam were used. With the information's from the mapping file the data is split into 45 degrees cut fibers and 90 degree cut fibers to make it easy to look though the fits and distinguish the data. This was done directly in the *cosmic.C* and later had to be redone because a V layer was mistaking for a U layer. The layers are explained in Figure 14.21.

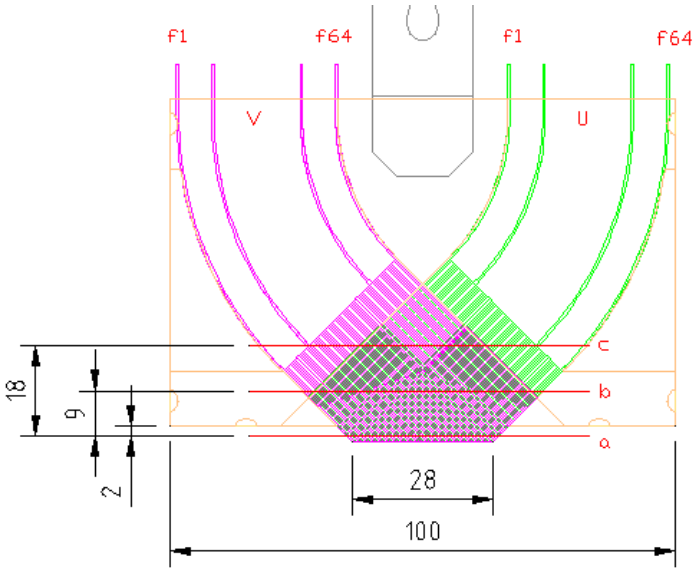

Figure 14.21. The V (purple) and U (green) layers on the detector. All fibers are numbered from left to right. The figure is figure 1 in [72].

It turned out that the MAPMT had not been orientated as in the 2005 test beam, but 180 degrees differently. Therefore the mapping was off by a 180 degree turn. At the time of discovery the data taking for the 2008 prototype (Section 14.4) had begun with the MAPMT orientated as in both the 2005 and 2008 beam tests. Therefore the mapping was not changed in *cosmic.C* as it was ready for the real usage on the 2008 prototype data. Instead the remapping was done directly on the data in Microsoft Excel.

14.3.8. Results from the source setup

The fit described in Section 14.3.6 were used on the data acquired in the run with the strontium-90 source described in Section 14.3.3. The data was remapped as described in Section 14.3.7 and finally each MAPMT channel was mapped to the corresponding fiber. This was done in Microsoft Excel. The results for the light yield and the crosstalk are shown in Figure 14.22 for the 45 degree cut fibers and Figure 14.23 for the 90 degree cut fibers.

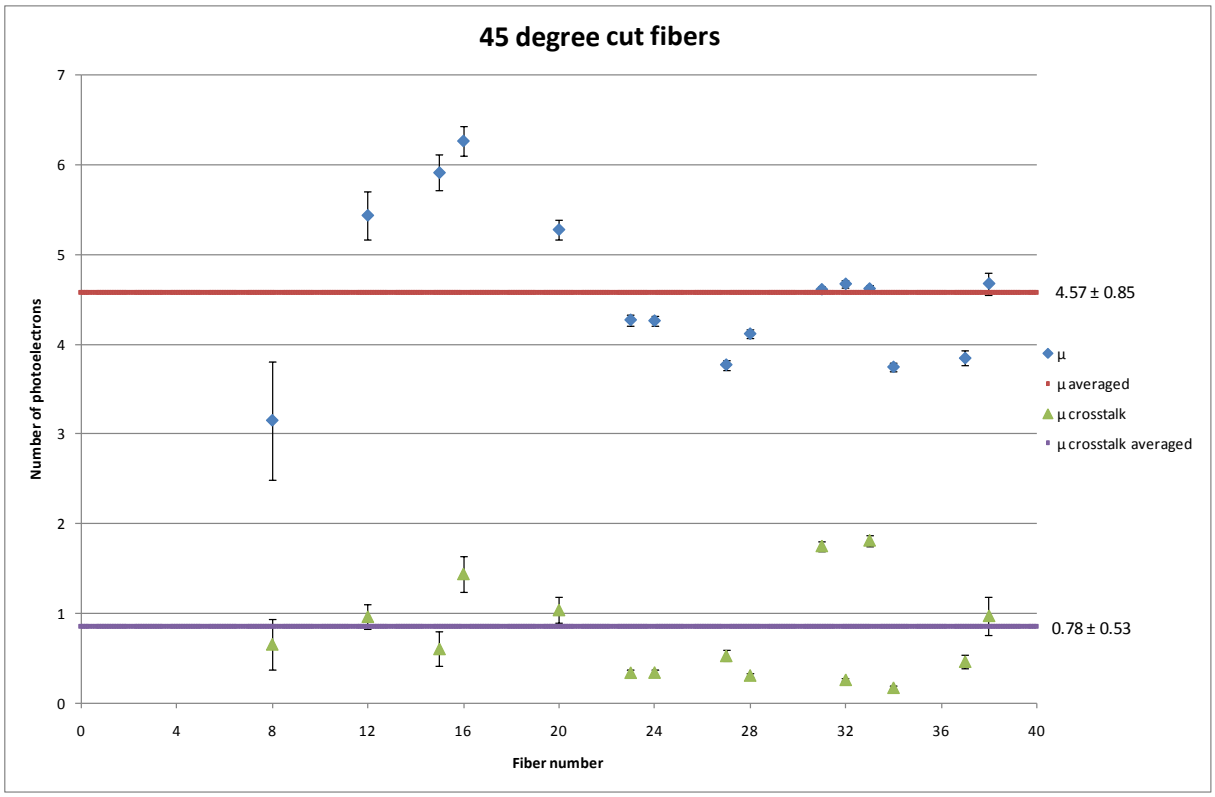

Figure 14.22. Light yield as a function of the fiber number for the 45 degree cut fibers from the run with the strontium-90 source.

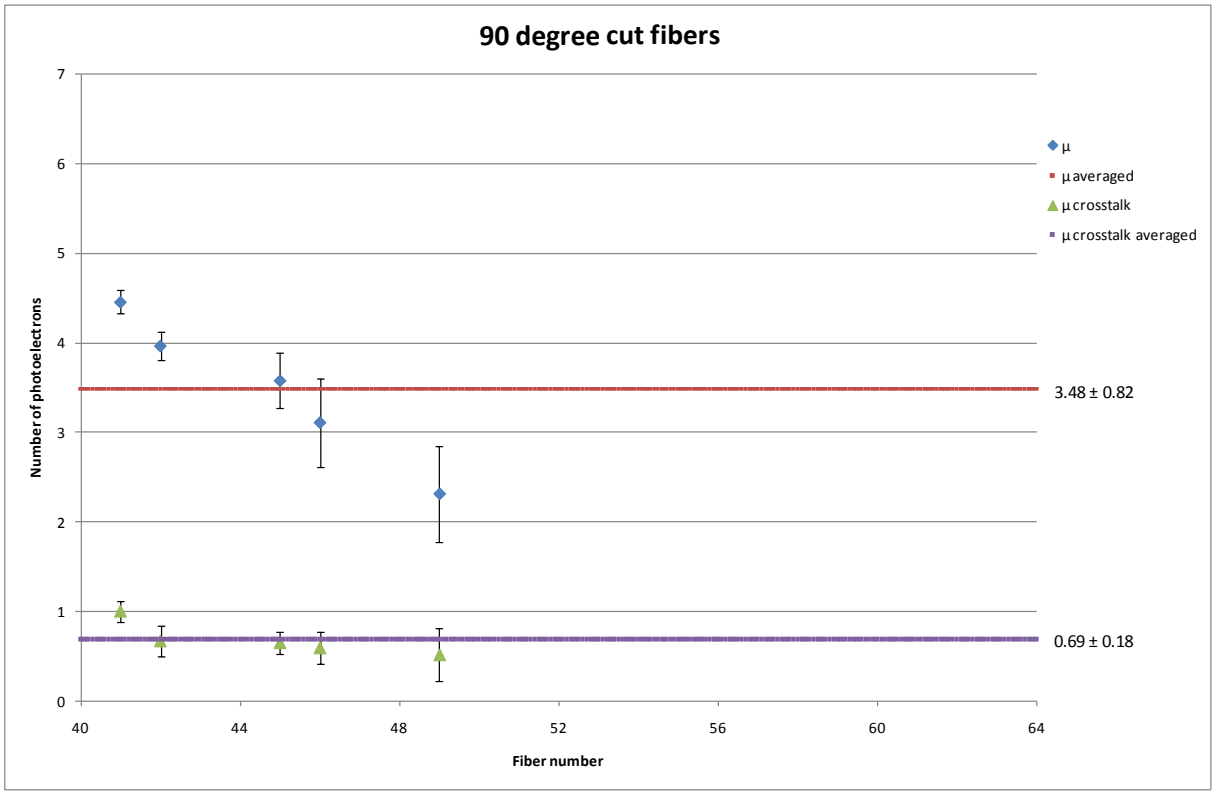

Figure 14.23. Light yield as a function of the fiber number for the 90 degree cut fibers from the run with the strontium-90 source.

14.3.9. Discussion and conclusion on the source setup

Not all channels were fitable. A few due to bad ADC channels in the data acquisition modules. In some channels the pedestal and all the data had changed position relative to the calibration. This was probably because one of the data acquisition modules was damaged and replaced between the acquisition of data and the calibration. These channels were removed by hand.

But there is still a pattern in the channels. None of the lowest and none of the highest numbered fibers had enough data to make a fit. This is because the strontium-90 source was place in the middle of the detector and did not spread out the entire detector area. Also the error bars on the averaged signal μ and the averaged crosstalk signal μ_{CT} are significantly smaller in the centered fibers. This is again because the strontium-90 source were centered here and thereby hitting these fibers with a much higher rate, summing up to much better statistic.

The overall average results for the 45 degrees cut fibers were that 15 channels were fitable with an average of 4.47 ± 0.85 PE. With the restrictions discussed in Section 14.3.5 this could be compared with the 3.93 ± 0.18 PE seen in the 2005 test beam. Within the uncertainties the light yield from the 45 degrees cut fibers in the strontium-90 source run and the light yield from the 45 degrees cut fibers in the 2005 test beam do not differ.

The overall average results for the 90 degrees cut fibers were that only 5 channels were fitable with an average of 3.48 ± 0.82 PE. With the restrictions discussed in Section 14.3.5 this could be compared with the 4.45 ± 0.50 PE seen in the 2005 test beam. Within the uncertainties the light yield from the 90 degrees cut fibers in the strontium-90 source run and the light yield from the 90 degrees cut fibers in the 2005 test beam do not differ.

There seems to be an averaged higher light yield from the 90 degrees cut fibers then from the 45 degrees cut fibers. But within the uncertainties it cannot be concluded conclusively. This is expected as it is seen in the 2005 test beam [68] and described in Section 13.1.

The crosstalk for both the 45 degree cut fibers (μ_{CT} = 0.78 ± 0.53) and the 90 degree cut fibers (μ_{CT} = 0.69 ± 0.18) is significantly higher than seen in the 2005 test beam (μ_{CT} ≈ 0.1). This is discussed further in Section 14.7.

The data for the strontium-90 source could have been improved a lot by simply repeating the measurement with the strontium-90 source placed in different positions on the detector. Thereby the fibers with low statistic in the original run would be hit more often. But the run with the strontium-90 source was primarily made to ensure that the setup was working properly. The results would anyway not be directly comparable to the real application of the detector detecting high energy protons, as discussed in Section 14.3.5. Therefore the measurement was not repeated with other positions of the strontium-90 source, but instead changed to cosmic muons which interactions in the detector are much closer to the interaction of high energy protons.

14.3.10. Results from the cosmic setup

The fit described in Section 14.3.6 was used on the data acquired in the 10 days run with cosmic described in Section 14.3.3. The data was remapped as described in Section 14.3.7 and finally each MAPMT channel was mapped to the corresponding fiber. This was done in Microsoft Excel. The results for the light yield and the crosstalk are shown in Figure 14.24 for the 45 degree cut fibers and Figure 14.25 for the 90 degree cut fibers.

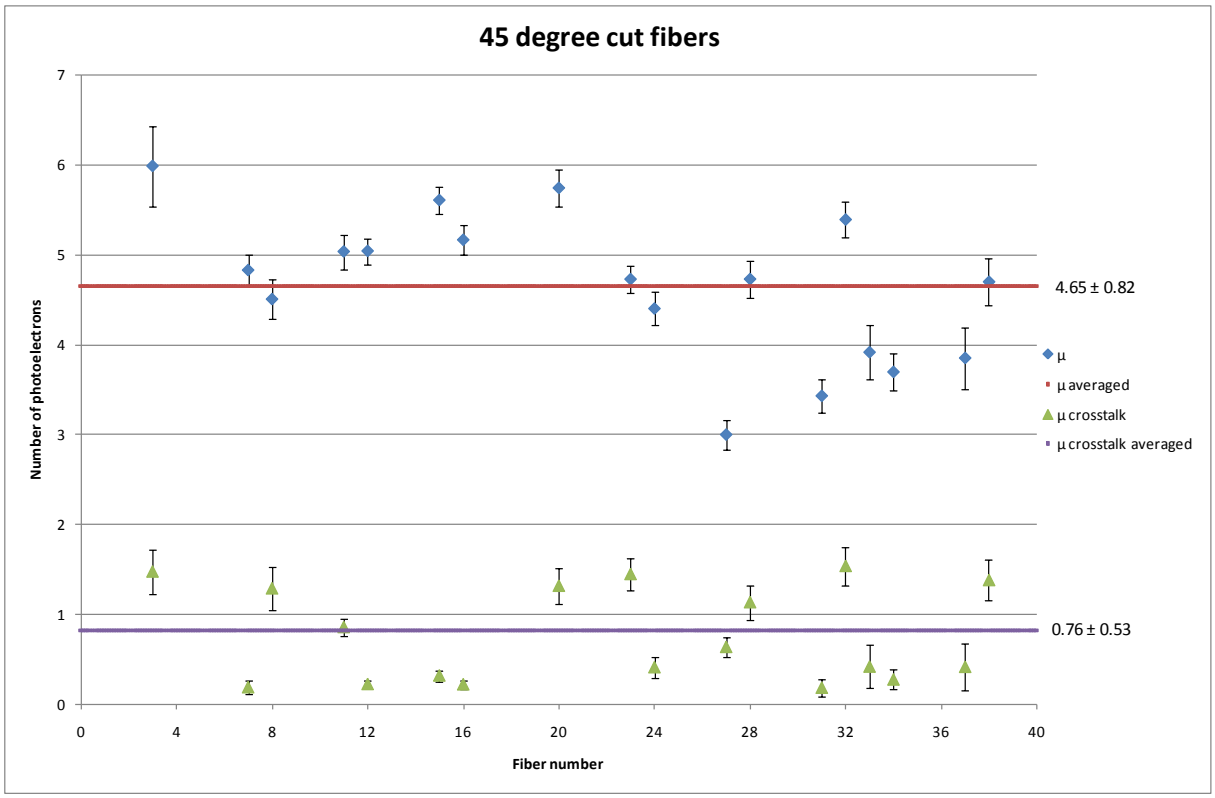

Figure 14.24. Light yield as a function of the fiber number for the 45 degree cut fibers from the run with cosmics.

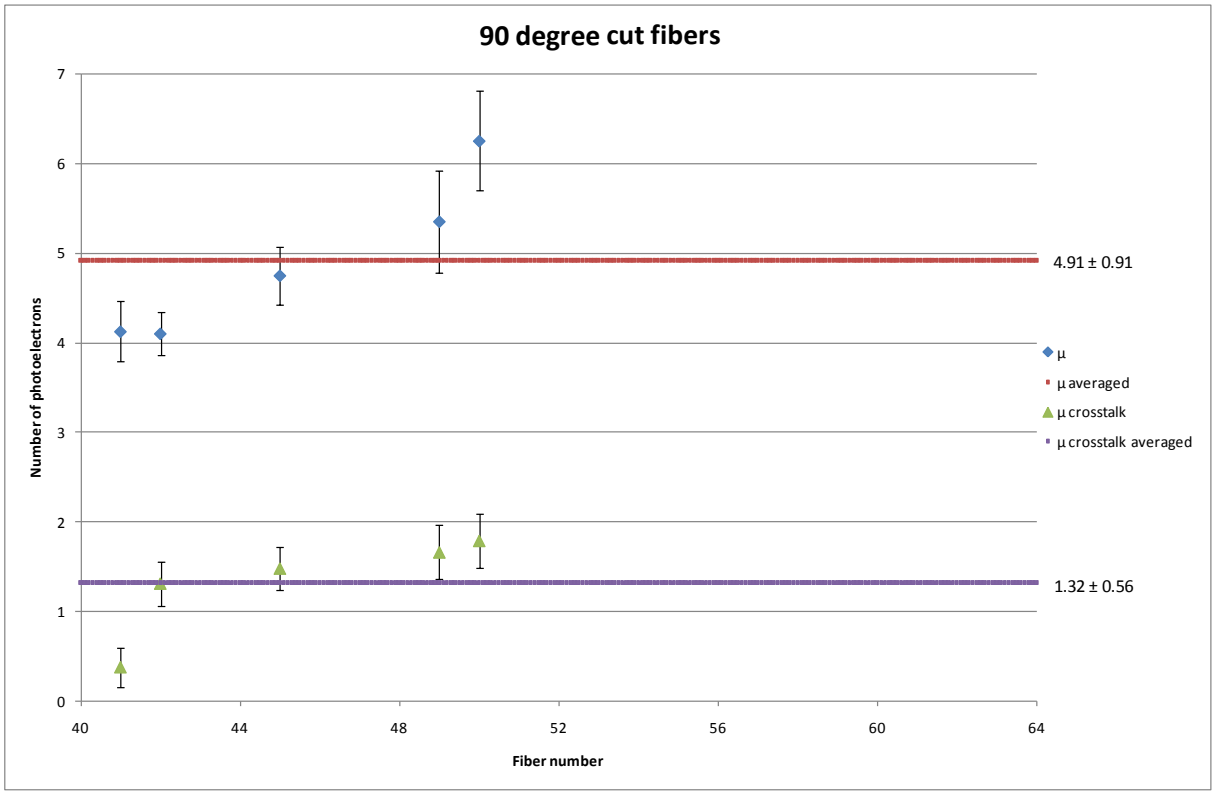

Figure 14.25. Light yield as a function of the fiber number for the 90 degree cut fibers from the run with cosmics.

14.3.11. Discussion and conclusion on the cosmic setup

Again not all channels were fitable. A few due to bad ADC channels in the data acquisition modules. But in some channels the pedestal and all the data had again changed position relative to the calibration. This was probably still because one of the data acquisition modules was damaged and replaced between the acquisition of data and the calibration. These channels were removed by hand.

There is less of a pattern in the cosmic data compared to the source data. Again the outer fibers of the detector had low statistics and could not be fitted. However manually looking at the data plots showed that the amount of data in the outer fibers were more comparable to the amount of data in the central fibers than with the source data. A muon that passes both the top and bottom scinttilator is more likely to pass the center of the detector then the outer part. This explains the lower statistic in the outer fibers. This effect corresponds to the different weighting of the angles Section 14.3.4 and can be seen in Figure 14.15 if one imagines the fibers in between the trigger sicntillators.

The overall average results for the 45 degrees cut fibers were that 18 channels were fitable with an average of 4.65 ± 0.82 PE. As discussed in Section 14.3.5 this should be comparably with the 3.93 ± 0.18 PE seen in the 2005 test beam[68]. Within the uncertainties the light yield from the 45 degrees cut fibers in the cosmic run and the light yield from the 45 degrees cut fibers in the 2005 test beam do not differ.

The overall average results for the 90 degrees cut fibers were that only 5 channels were fitable with an average of 4.91 ± 0.91 PE. As discussed in Section 14.3.5 this should be comparably with the 4.45 ± 0.50 PE seen in the 2005 test beam [68]. Within the uncertainties the light yield from the 90 degrees cut fibers in the cosmic run and the light yield from the 90 degrees cut fibers in the 2005 test beam do not differ.

There seems to be a bit higher averaged light yield from the 90 degrees cut fibers then from the 45 degrees cut fibers. But within the uncertainties it cannot be concluded concussively. This is expected as it is seen in the 2005 test beam [68] and described in Section 13.1.

The crosstalk for both the 45 degree cut fibers ($\mu_{CT} = 0.76 \pm 0.53$) and the 90 degree cut fibers ($\mu_{CT} = 1.32 \pm 0.56$) is significantly higher than seen in the 2005 test beam ($\mu_{CT} \approx 0.1$). This is discussed further in Section 14.7.

The overall number of triggered readouts is only about 1/5 in the cosmic data compared to the source data. More cosmic data is desirable and an amount comparably to the amount of source data would probably make almost all channels fitable. But that would take about 2 month of data acquisition only to re-do a measurement done with very high statistic in the 2005 beam test. The aim in the setup with the 2005 prototype was only to confirm the method used, and that is done satisfactory with the relatively low statistic.

14.4. Analog readout on the 2008 prototype setup

The method to measure the light yield in scintillating fibers has been confirmed by the setup with the 2005 prototype as described in Section 14.3. This method can therefore be applied to the untested 2008 prototype to measure the light yield.

14.4.1. Setup

The 2008 prototype is a complete detector that is ready to be inserted into a Roman Pot. Each of the 20 layers of the detector and the 3 overlap detectors have their own 8x8 fiber mounting to connect to a MAPMT as on the 2005 prototype. The fiber connections are mounted on an aluminum base plate, which also holds the support for the detector layers for both the main detector and the overlap detector. To protect the

detector it is mounted into a black steel box. The black steel box is also useful for support as the detector can be positioned with the detector planes horizontal as shown in Figure 14.26.

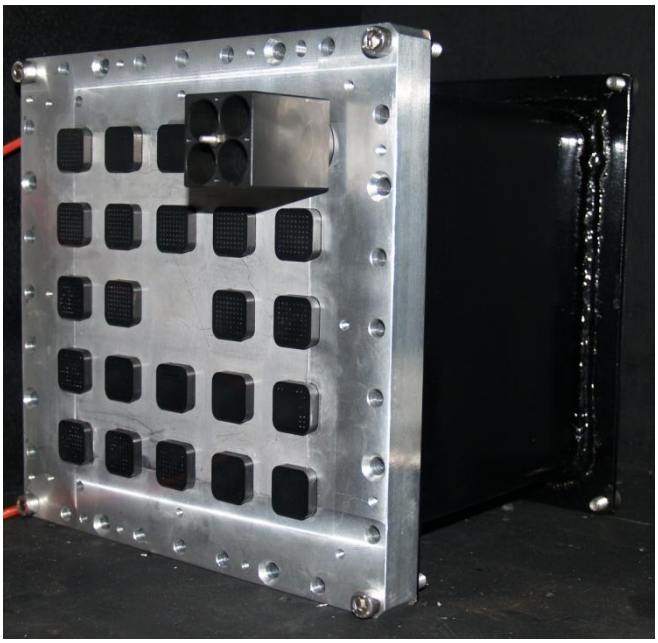

Figure 14.26. Aluminum base plate with 23 8x8 fiber connectors mounted on the black steel box. In the upper right corner of the aluminum plate is the support for the PMTs use for triggering.

There are two scintillators tiles integrated in the detector to do the triggering for the main detector and two smaller scintillator tiles to trigger the overlap detector as shown in Figure 14.27 (left) and discussed in Section 13.1.5. Note that the main detector trigger scintillator tiles are right on top of each other, not on each side of the main detector as on the 2005 prototype setup. This is done to save space in the Roman Pot and has no effect for the triggering of the detector during operation in LHC because the protons trajectory will be almost perpendicular to the detector.

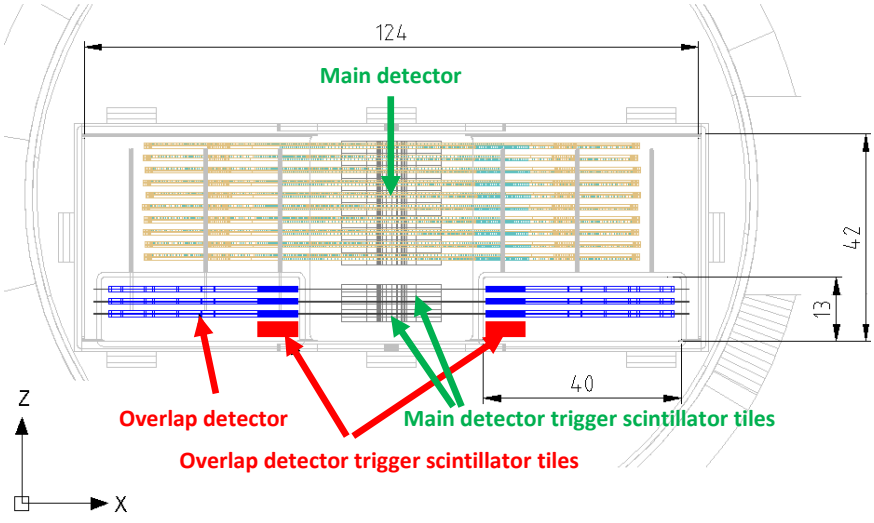

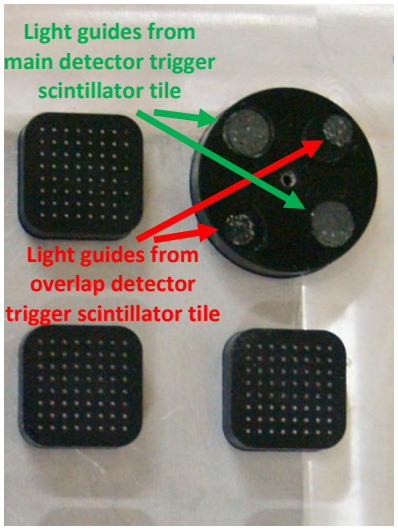

Figure 14.27. *LEFT*: Layout of the detector plates and the trigger scintillator tiles (180 degrees turned compared Figure 14.26). The figure is figure 5-6 in [39]. *RIGHT*: Mounting of the light conducting fibers from the trigger scintillator tiles.

All the trigger scintillator tiles are connected to optical fibers, which are also mounted on the aluminum plate with the 8x8 fiber mountings as shown in Figure 14.27 (right). The main detector trigger scintillator tile is larger than the trigger scintillator tile for the overlap detector, and therefore it has more optical fibers ("as no optical coupling scheme relying on reflection or diffraction alone can transmit photons from a large

source to a small detector with full efficiency", Liouville theorem, reference [73]) as is shown in Figure 14.27 (right). The triggers are read out by ø 8 mm PMTs Hamamatsu R7400P operated at -800 V. To make a good connection between the PMTs and the optical fibers, optical grease was used and springs added to the back of the PMTs thereby forcing the PMTs up against the optical fiber ends.

The custom made aluminum piece, which connects the 8x8 mounted fiber ends and the MAPMT, used in the setup with the 2005 prototype could not be used on the 2008 prototype. This can be seen on Figure 14.9 (right) page 94 and is because it was made for a dismounted 8x8 fiber connection. Therefore a new custom made aluminum piece was needed. This was designed by Andre Braem and produced by Adrian Folley internally in the CERN PH-DT department. The piece can be seen in Figure 14.28 (left) mounted with shims on the MAPMT. Unfortunately the piece was not made exactly to the right sizes and had to be repaired with tape, but in the end it was usable. Using the 4 spacers the MAPMT was connected to the 2008 prototype as shown in Figure 14.28 (right).

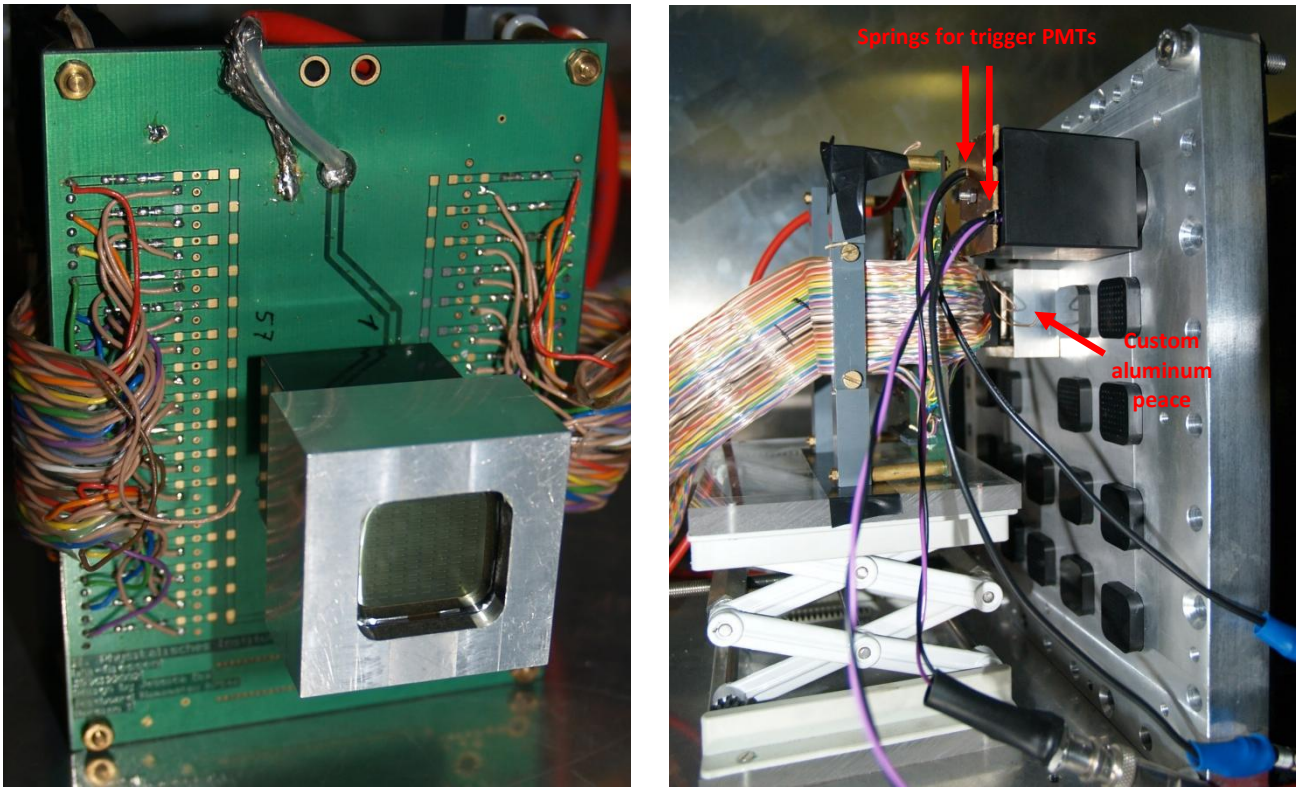

Figure 14.28. *LEFT*: The custom made aluminum piece mounted on the MAPMT. An example of the tape used for repair is seen where the 8x8 fiber connection connects to the MAPMT. *RIGHT*: The MAPMT mounted to the 2008 prototype with the custom made aluminum piece. The springs for mounting the trigger PMTs are also shown.

The MAPMT was connected to the 8x8 mounted fiber connector MAPMT number 7 corresponding to layer 19. This is a U layer (see Figure 14.21) where the layer tested in the 2005 prototype setup in chapter 14.4 was a V layer. This should not have any other effect than a different mapping.

Overall the setup is very close to the setup for the 2005 prototype described in Section 14.3.1 with the main difference being the placement of the trigger scintillator tiles being different. A schematic for the entire setup with readout is shown in Figure 14.29.

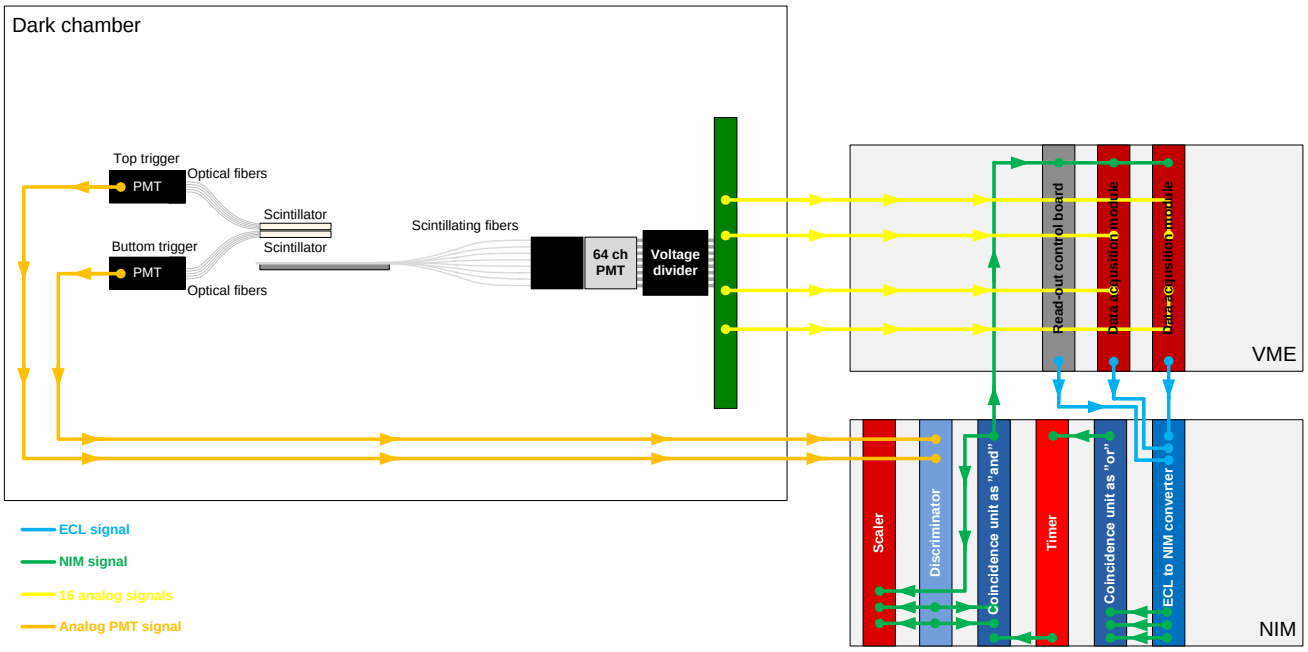

Figure 14.29. A schematic for the setup for measuring the light yield of the fibers in the 2008 prototype.

The readout system is as for the 2005 prototype setup described in Section 14.3.1. The data acquisition window was also comparable to the one used in the 2005 prototype setup described in Section 14.3.3.

14.4.2. Data acquisition

First a few short test runs were carried out to check that the setup worked. These had a higher count rate than expected. To dispose of any noise from the PMTs the threshold for the discriminators was adjusted up to 50 mV. The count rate is discussed further in Section 14.4.3.

A high statistic run was made. The measurement took about 134 hours and the readout was trigged 150001 times. The results are discussed in Section 14.4.4.

14.4.3. Rate of cosmic

As discussed in Section 14.3.4 the cosmic is mostly highly relativistic muons. The rate of the muons is given by equation (14.6). Because the two trigger scintillator tiles are identical in size and they are placed directly on top of each other nearly all muons passing one of the trigger scintillator tiles will also pass the other trigger scintillator tile and thereby trigger a readout. The area of the trigger scintillator tile is the same as for the trigger scintillator tile used in the 2005 setup and is given by equation (14.15). Using equation (14.6) and equation (14.15) the expected rate of muons is therefore:

$$R_{\text{muon, 2008 expected}} = I \cdot A_{\text{scintillator}} = 1 \cdot \frac{counts}{cm^2 \cdot min} \cdot 8.24 cm^2 = 8.24 \frac{counts}{min} \tag{14.21}$$

The rate of muon seen in the cosmic data acquisition run was:

$$R_{\text{2008 experimental}} = 18.67 \pm 0.05 \frac{counts}{min} \tag{14.22}$$

The rate is significantly higher than expected. No immediate explanation was found for the count rate being twice as high as expected. The high rate is discussed further in Section 14.4.7.

14.4.4. Analysis

The fit described in Section 14.3.6 was used by applying the macro *cosmic.C* to the data acquired with cosmic described in Section 14.4.2. An example of the fit is shown in Figure 14.30.

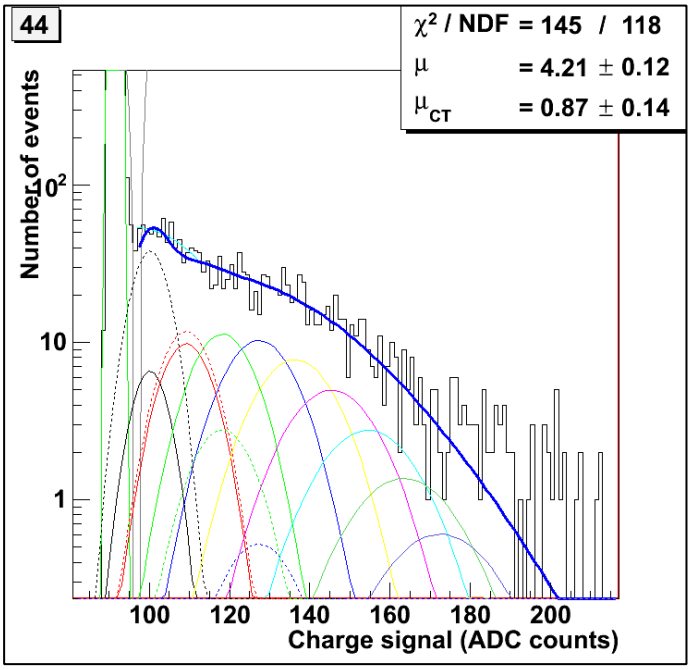

Figure 14.30. MAPMT channel 45 data and fit from the 2008 prototype run.

Each MAPMT channel was mapped to the corresponding fiber as described in Section 14.3.7 taking into account that the tested layer this time was an U layer. This was done in Microsoft Excel.

14.4.5. Results

The results for the light yield and the crosstalk are shown in Figure 14.31 for the 90 degree cut fibers and Figure 14.32 for the 45 degree cut fibers.

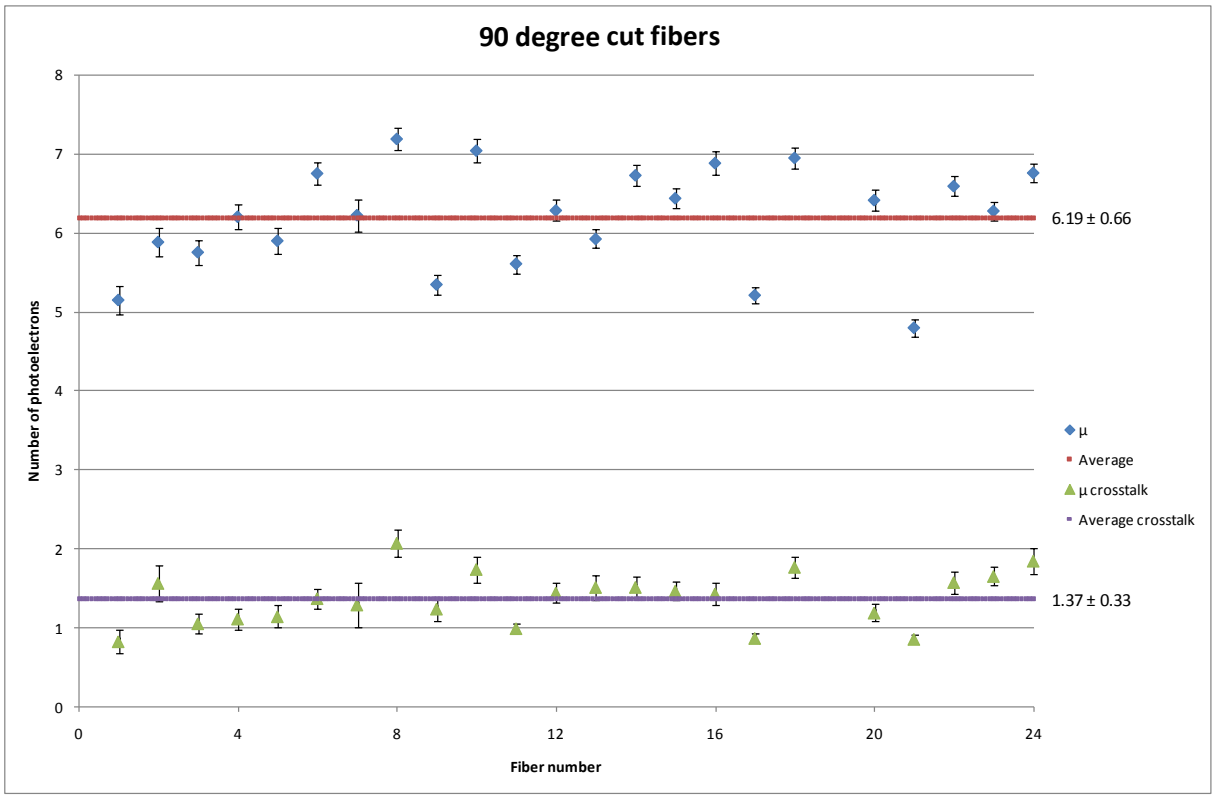

Figure 14.31. Light yield as a function of the fiber number for the 90 degree cut fibers.

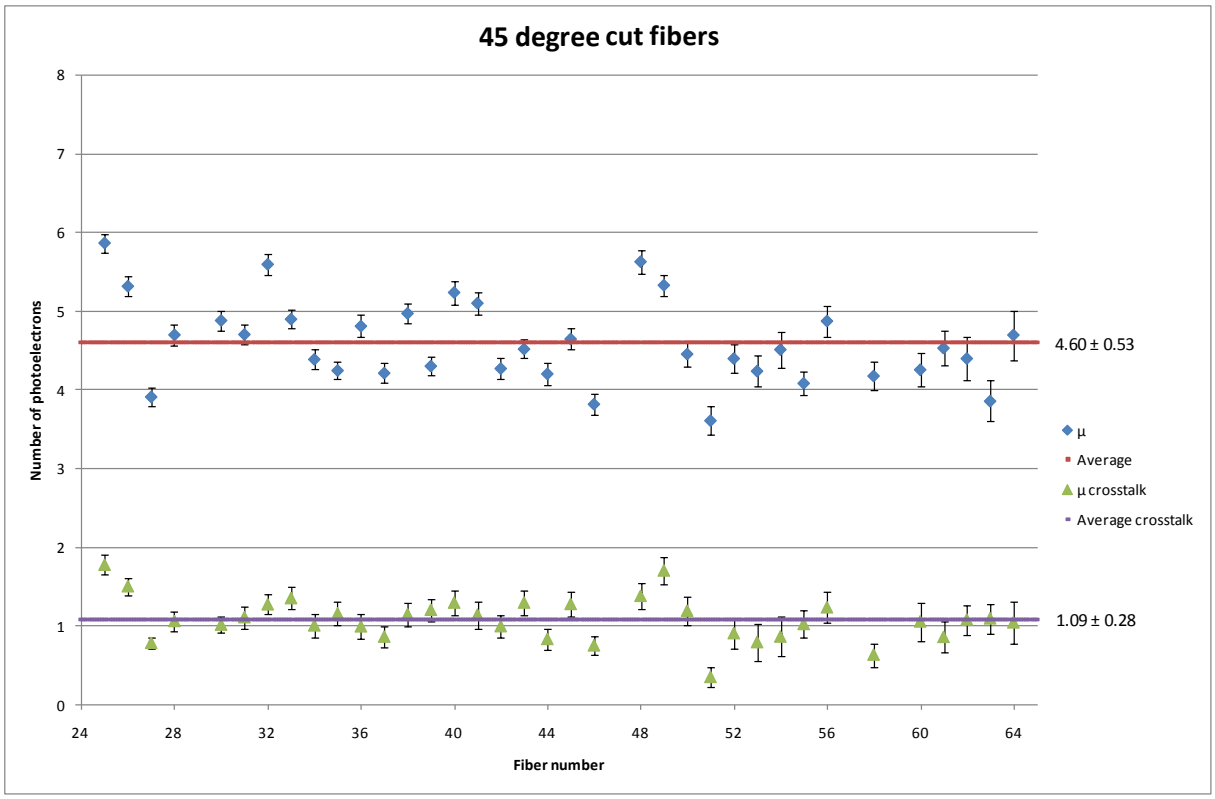

Figure 14.32. Light yield as a function of the fiber number for the 45 degree cut fibers.

14.4.6. Discussion and conclusion

Almost all channels with working ADCs were fit able. The data points seem to be spread randomly around the average. The only pattern seen is larger errors for the outer fibers. This can be explained by less hit statistic for the outer fibers because muons passing the outer fibers are less likely to pass both trigger scintillator tiles, thereby triggering a readout, than muons passing the fibers in the center of the detector as discussed in Section 14.3.10.

The overall average results for the 90 degree cut fibers were that 23 channels were fitable with an average of 6.19 ± 0.66 PE and crosstalk 1.37 ± 0.33 PE. As discussed in Section 14.3.5 this should be comparably with the 4.45 ± 0.50 PE seen in the 2005 test beam [68]. There seems to be significantly higher light yield in the 2008 prototype compared with the 2005 prototype. This could partly be explained by the use of a new version of the MAPMT with higher quantum efficiency than the one used in the 2005 beam setup. The higher light yield should then also be seen in the test performed with the 2005 prototype as the same MAPMT was used. But because of the low number of fitable channels and the relatively large uncertainty in the data it cannot be concluded if the 2005 setup also had a higher light yield than the 2005 beam test.

The overall average results for the 45 degree cut fibers were that 36 channels were fitable with an average of 4.60 ± 0.53 PE and crosstalk 1.09 ± 0.28. As discussed in Section 14.3.5 this should be comparable with the 3.93 ± 0.18 PE seen in the 2005 test beam [68]. Within the uncertainties the light yields from the 45 degrees cut fibers in the 2008 prototype and the light yield from the 45 degree cut fibers in the 2005 test beam do not differ even though there is a tendency for a higher light yield in the 2008 prototype.

The crosstalk for both the 90 degree cut fibers (μ_{CT} = 1.37 ± 0.33) and the 45 degree cut fibers (μ_{CT} = 1.09 ± 0.28) is significantly higher than seen in the 2005 test beam (μ_{CT} ≈ 0.1). This is discussed further in Section 14.7.

There is a significantly higher averaged light yield from the 90 degree cut fibers than from the 45 degree cut fibers. This is expected as it is seen in the 2005 test beam [68] and described in Section 13.1.

See Section 14.7 for notes on comparison of light yields from cosmic data with light yields from beam data.

14.4.7. High count rate

The data is acquired with an unexplained high count rate. This should be taken into consideration before trusting the results. A lot of thoughts were put into explaining the high count rate. Some of the ideas are listed here:

- Noise from PMTs overlapping and making false counts
- Light not from the scintillator tiles triggering readout
- Secondary particles from cosmic made by interaction with the building's roof or with the black steel box
- The detector or the surroundings being slightly radioactive and emitting particles that pass both trigger scintillator tiles and thereby triggering readout.

Noise from the PMTs was ruled out right away. The rate of accidental coincidences can be calculated as [40](equation 2.18):

$$R_{1\ and\ 2} = R_1 \cdot R_2 \cdot (\tau_1 + \tau_2) \tag{14.23}$$

$R_{1\ and\ 2}$ Rate of accidental coincidence

R_1 Rate of signal 1

R_2 Rate of signal 2

τ_1 Width of signal 1

τ_2 Width of signal 2

The rate of the single signals is 0.56 counts/s and 0.83 counts/s respectively and the width of each signal is 50 ns. The rate of accidental coincidences is therefore:

$$R_{1\ and\ 2,\ 2008} = 0.56\frac{counts}{s}\cdot 0.83\frac{counts}{s}\cdot(50ns+50ns) \approx 4.5\cdot 10^{-8}\frac{1}{s} \approx 2.6\cdot 10^{-6}\frac{counts}{\min} \quad (14.24)$$

The rate of accidental coincidences is 7 orders of magnitude smaller than the observed rate and thereby insignificant.

Since the accidental coincidence rate is so low, a lower value of the discriminator threshold could probably be used. The thresholds were lowered to 30 mV, which is the lowest setting for the used discriminator. A run just to test the count rate was performed for about 72 hours to get good statistics. The count rate with the 30 mV discriminator threshold was:

$$R_{2008\ \text{experimental, thr 30 mV}} = 21.83 \pm 0.07\frac{counts}{min} \quad (14.25)$$

As expected the rate was higher with the lower discriminator threshold and the accidental coincidences rate was still comparable to equation (14.24). With an oscilloscope lower threshold was examined, and an even higher rate of coincidences was seen without significant accidental noise rate. A discriminator with a lower threshold limit was desirable since it then would have been possible to trigger on even lower signals and make a measurement to compare the energy deposition in the scintillating fibers. The signals from the trigger PMTs could also have been amplified, but that would delay the readout and thereby give problems with the data acquisition windows as discussed in Section 14.3.2.

Contrary to the trigger system used in the 2005 prototype setup the trigger system used in the 2008 prototype setup is not light tight by is self. If light were somehow coming into the dark chamber with the setup it might trigger the readout. To check for this the essential parts were covered with a piece of cloth and the light switched off in the room. No difference was observed in the count rate.

The detector could have become activated or exposed to radioactive material during the beam test. Particles emitted from radioactive decay would have a very low energy and be completely absorbed by the black steal box. A setup with a 3rd trigger outside the black steal box was therefore made. This will be described in the following sections.

14.4.8. 3rd trigger setup 1

As a 3rd trigger a 40cm·40cm·1cm scintillator was used. First the scintillator was mounted outside the dark chamber under the setup, but it turned out that the scintillator not was light tight so instead it was moved above the setup and into the dark chamber as shown in Figure 14.33.

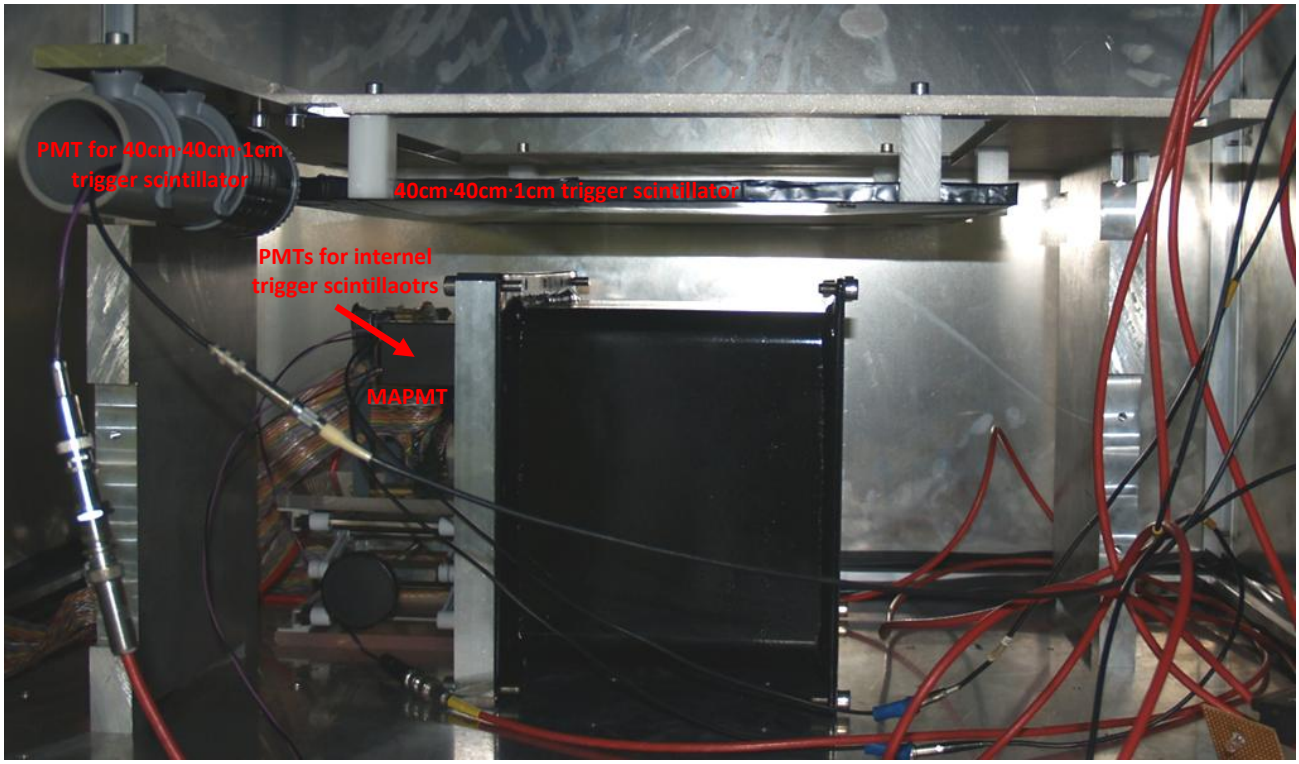

Figure 14.33. Setup with 40cm·40cm·1cm scintillator as 3rd trigger.

The light from the 40cm·40cm·1cm scintillator tile was absorbed and readmitted in a 12 mm square wavelength shifter which was read out by a large PMT, 25 mm Photonis XP3102. The signal from the Photonis XP3102 PMT was added to the NIM trigger electronic by connected it through a discriminator to the coincidence unit in a similar way as the two internal triggers as described in Section 14.4.1 and shown in Figure 14.29. The signal from each of the 3 discriminators use for the trigger PMTs was connected to an oscilloscope as was the signal after the coincidence unit. By triggering on the coincidence the timing of the 3 trigger PMTs could be studied. It turned out that the signal from the Photonis XP3102 PMT, even with the shortest possible cables used, was about 20 ns later then the signal from the Hamamatsu R7400P PMTs used for the internal trigger scintillator tiles. This was probably due to the larger PMT size. The delayed signal meant that the coincidence and thereby the trigger was made about 20 ns later thereby delayed the data acquisition window significantly. As discussed in Section 14.3.2 the signals from the MAPMT could not be delayed easily. Therefore the Photonis XP3102 PMT was removed and replaced by a Hamamatsu R7400P PMT. The window in the Hamamatsu R7400P PMT was only about 40 % of the area of the end of the 12 mm square wavelength shifter, but as the used scintillator tile was thick it should still produce sufficient light. The timing of the 3 PMT signals was tested as described above. Now the 3 PMT signals were well synchronized.

A data acquisition run was started. But it was quickly noted that the trigger rate was too low. Extensive tests were done with the 40cm·40cm·1cm scintillator (which had never been used before), including reinstalling the original Photonis XP3102 PMT and putting a strontium-90 source on top of the scintillator. Even with this setup only few and small signals were observed. In the end it was concluded that the scintillator was badly assembled or had been damaged (properly the scintillator-wave length shifter connection). The setup was therefore given up and replaced by the one described in the next section.

14.4.9. 3rd trigger setup 2

The setup and results, along with a general description of ALFA project, was presented by the author with a poster at Eiroforum School on Instrumentation 2009 (ESI 2009). The poster is Appendix I.

As the new 3rd trigger scintillator a smaller and thoroughly tested 12cm·12cm·0.3cm scintillator was used as shown in Figure 14.34.

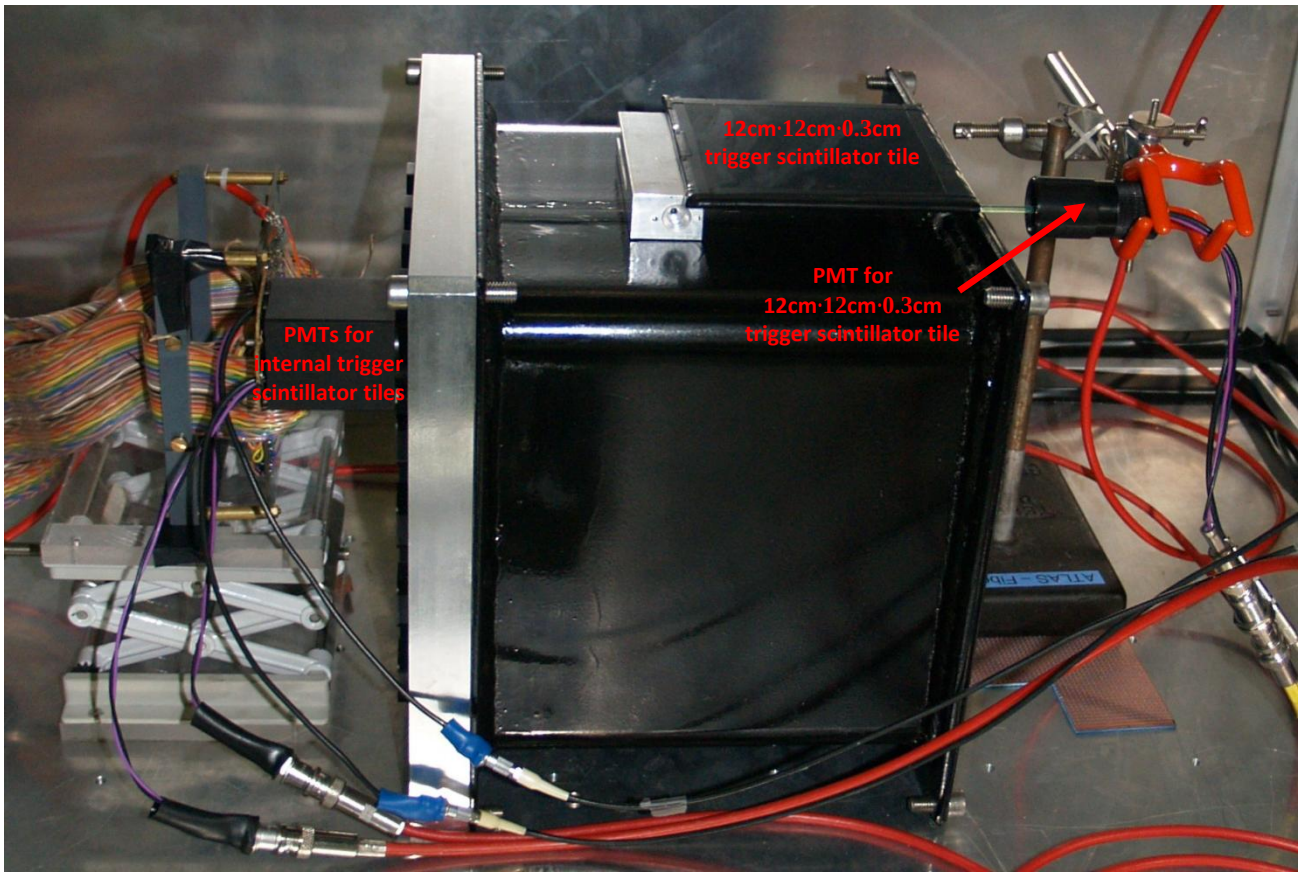

Figure 14.34. Setup with 12cm·12cm·0.3cm scintillator as 3rd trigger.

The light from the 12cm·12cm·0.3cm scintillator tile was absorbed and readmitted in a 3 mm round wavelength shifter which was read out by a Hamamatsu R7400P PMT. A schematic for the setup and readout system is shown in Figure 14.35.

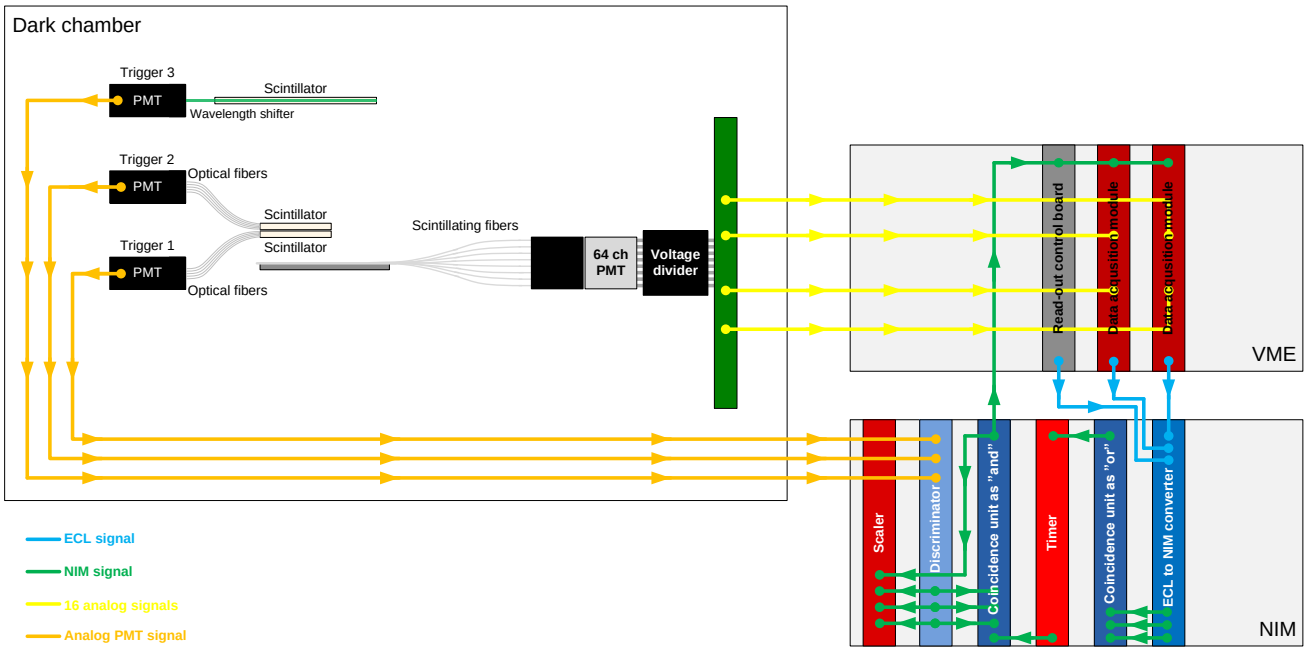

Figure 14.35. A schematic for the setup with a 3rd external trigger for measuring the light yield of the fibers in the 2008 prototype.

The setup is very similar to the one described in Section 14.4.1 and shown in Figure 14.29 just with a 3rd PMT connected in the same manner as the other two.

The coincidence timing of the two PMTs for the internal scintillator tiles and the third external trigger was checked on oscilloscope and proved to be well synchronized and the data acquisition window was therefore as described in Section 14.3.2. The threshold on all the discriminators was set to 30 mV (the minimum of the device) and all trigger PMTs were operated at their optimal voltage of -800 V.

14.4.10. Data acquisition with 3 triggers

First a short run was made to test that everything was working. The count rate was significantly lower than with only the internal triggers. Therefore the data acquisition time had to be much longer.

First a week long run was performed. After a quick look to see if the data made sense the acquisition was continued for another week. This repeated itself until the data acquisition had run for about one month. The readout had then been triggered 89746 times. The rate of the muons is discussed in the next section and the results are discussed in Section 14.4.12.

14.4.11. Expected rate with 3 triggers

The calculation of the expected rate of muons is similar to the rate calculation in Section 14.3.4. But since the triggers are not the same size it is a bit more difficult.

To make the calculations easier and as only an estimate of the intensity of muons is needed, the scintillator tiles are assumed to be flat cylinders. Since the two internal scintillator tiles are placed directly up against each other it is also assumed that all muons passing one of the internal triggers (trigger 1 and 2) will always pass both.

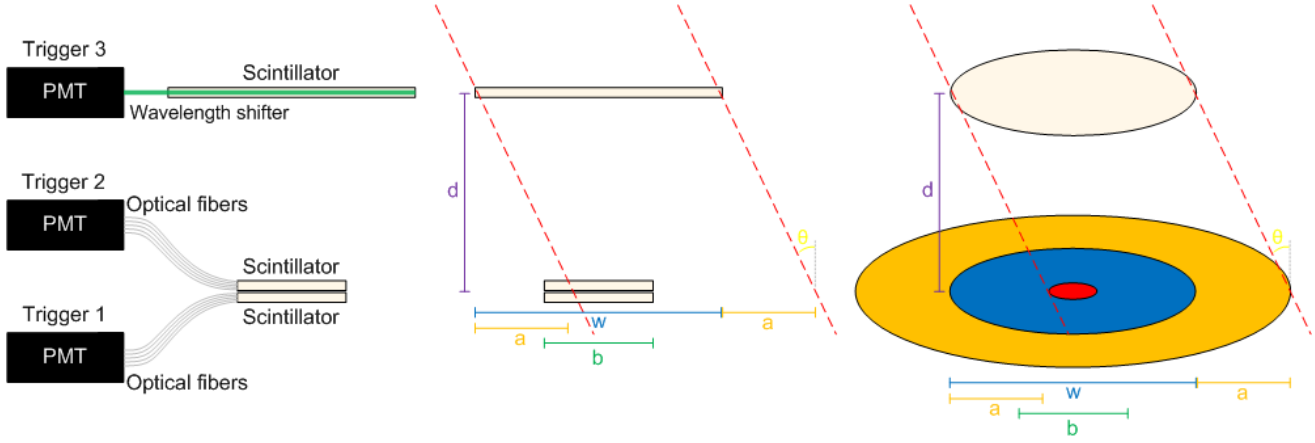

Figure 14.36. To the left are the trigger scintillator tiles with optical fibers or wavelength shifter and PMTs. In the middle is the scintillator tiles cut out. To the right is the area of the top scintillator tile, and the area the muom can pass through in and around the bottom scintillator tile (if the muon passed the top scintillator tile). The red dotted line represents a muon passing the scintillator in each edge of the scintillator tile. The labels: *w* is the width of the top scintillator tile, *b* is the width of the bottom scintillator tile, *d* is the distances between the external scintillator and the internal scintillators, θ is the incoming angle of the muon, *a* are the difference of radius of the top scintillator tile and the outermost radius the muon can hit around the internal scintillator tiles. The red area can be hit for both θ and -θ.

The larger the angle θ gets the less likely is it that the muon passes both the external scintillator tile and the internal scintillators. More precisely, the likelihood of the muons passing the internal scintillator tiles if it has passed the external scintillator tile goes as the area of the internal scintillator tile (the blue area to the right in Figure 14.36) over the area the muon can possible pass at the distance of the internal scintillator tiles (the orange, blue and red area to the right in Figure 14.36). The red area counts double as it can be hit for both θ and - θ. With large θ some part of the internal scintillator tile will never be hit. This will split the likelihood function into:

For small θ, $\frac{w}{2}-a>\frac{b}{2}\Rightarrow a<\frac{w-b}{2}$, all of the bottom detector can be hit for θ and – θ and counts double and *L* is:

$$\begin{aligned} L &= \frac{2\cdot \text{Area of the internal scintillator}}{\text{Area of muon pass + double hit area}} \\ &= \frac{2\cdot\pi\cdot\left(\frac{b}{2}\right)^2}{\pi\cdot\left(\frac{w}{2}+a\right)^2+\pi\cdot\left(\frac{w}{2}-a\right)^2} \\ &= \frac{b^2}{w^2+4\cdot a^2} \end{aligned} \qquad (14.26)$$

For θ a little larger, $\frac{w-b}{2}<a<\frac{w}{2}$, the red counts double but is smaller than the internal scintillator tiles and *L* is:

$$
\begin{aligned}
L &= \frac{\text{Area of the internal scintillators + double hit area}}{\text{Area of muon pass + double hit area}} \\
&= \frac{\pi \cdot \left(\frac{b}{2}\right)^2 + \pi \cdot \left(\frac{w}{2} - a\right)^2}{\pi \cdot \left(\frac{w}{2} + a\right)^2 + \pi \cdot \left(\frac{w}{2} - a\right)^2} \\
&= \frac{w^2 - 4 \cdot a \cdot w + 4 \cdot a^2 + b^2}{2 \cdot (w^2 + 4 \cdot a^2)}
\end{aligned}
\tag{14.27}
$$

For large θ, $\frac{w}{2} < a < \frac{w+b}{2}$, some part of the internal scintillator tiles cannot be hit and *L* is:

$$
\begin{aligned}
L &= \frac{\text{Area of the internal scintillators } - \text{ area that cannot be hit}}{\text{Area of muon pass } - \text{ area that cannot be hit}} \\
&= \frac{\pi \cdot \left(\frac{b}{2}\right)^2 - \pi \cdot \left(a - \frac{w}{2}\right)^2}{\pi \cdot \left(\frac{w}{2} + a\right)^2 - \pi \cdot \left(a - \frac{w}{2}\right)^2} \\
&= \frac{-(w^2 - 4 \cdot a \cdot + 4 \cdot a^2 - b^2)}{8 \cdot a \cdot w}
\end{aligned}
\tag{14.28}
$$

For very large θ, $a > \frac{w+b}{2}$, the internal scintillator tiles will never get hit and *L* is:

$$
L = 0 \tag{14.29}
$$

The distance a can be found geometrically as:

$$
\tan\theta = \frac{a}{d} \quad \Rightarrow \quad a = d \cdot \tan\theta \tag{14.30}
$$

Equation (14.26), (14.27), (14.28) and (14.29) then becomes:

$$
L = \begin{cases}
\dfrac{b^2}{w^2 + 4 \cdot d^2 \cdot \tan^2\theta} & \textit{for} \quad \dfrac{w-b}{2} > d \cdot \tan\theta \\
\dfrac{w^2 - 4 \cdot d \cdot \tan\theta \cdot w + 4 \cdot d^2 \cdot \tan^2\theta + b^2}{2 \cdot (w^2 + 4 \cdot d^2 \cdot \tan^2\theta)} & \textit{for} \quad \dfrac{w-b}{2} \le d \cdot \tan\theta \le \dfrac{w}{2} \\
\dfrac{-(w^2 - 4 \cdot d \cdot \tan\theta \cdot w + 4 \cdot d^2 \cdot \tan^2\theta - b^2)}{8 \cdot d \cdot \tan\theta \cdot w} & \textit{for} \quad \dfrac{w}{2} \le d \cdot \tan\theta \le \dfrac{w+b}{2} \\
0 & \textit{for} \quad d \cdot \tan\theta > w
\end{cases}
\tag{14.31}
$$

L is now the weight each angle will be represented by. To find the fraction of the muons which have passed the top scintillator tile and also hit the bottom scintillator tiles, and thereby trigger the readout, an

integration of the muon angular distribution, equation (14.7), weight by *L* over all angles is carried out and normalized by an integration over all angles of the angular distribution without weights:

$$f = \frac{\int_0^{90} \cos^2\theta \cdot L d\theta}{\int_0^{90} \cos^2\theta d\theta} \tag{14.32}$$

For the trigger scintillator tiles the distance *d* was 115 cm and the width of the external scintillator tile *w* was 120 mm and the width of the internal scintillator tiles *b* were 3.2 cm. The *f* in equation (14.32) then comes to (integrals solved in Maple and are Appendix J):

$$f_{2008,\ 3\ triggers} = \frac{\int_0^{90} \cos^2\theta \cdot L d\theta}{\int_0^{90} \cos^2\theta d\theta} \approx 0.32\ \% \tag{14.33}$$

The external scintillator tile is a square of 12.0cm*12.0cm. But hits in the corners of the scintillator tile will have a much lower likelihood of hitting the internal triggers than any point of the round scintillator tile used in the approximation above. Therefore the area of the external triggers is calculated as was it round with a diameter of 12.0 cm:

$$A_{\text{external scintillator}} = \pi \cdot (6.0cm)^2 \approx 113cm^2 \tag{14.34}$$

From equations (14.6), (14.33) and (14.34) the expected rate of muons can now be calculated:

$$R_{\text{muon, 2008 expected, 3 triggers}} = I \cdot f \cdot A_{\text{scintillator}} = 1 \cdot \frac{counts}{cm^2 \cdot min} \cdot 0.32\ \% \cdot 113cm^2 = 3.63 \frac{counts}{min} \tag{14.35}$$

The rate of muon seen in the cosmic data acquisition run was:

$$R_{\text{2008 experimental, 3 triggers}} = 2.02 \pm 0.01 \frac{counts}{min} \tag{14.36}$$

The rate of muons seen is lower than expected. This can be because the external trigger does not have a 100 % efficiency (probably because of the relatively thin scintillator tile, the use of wave length shifter and the coupling to the PMT). To get an idea about the efficiency of the 3rd trigger a simple test with the strontium-90 source was made. First the source was placed on top of one of the trigger used in the 2005 setup and a simple count was made for 3 min. Then the source was placed on the scintillator used as 3rd trigger and again counted for 3 min. Assuming that the 2005 trigger has 100 % efficiency the efficiency of the 3rd trigger could now be calculated. The test was done for the source in different positions and it turned out that the efficiency was as low as 80 %. Taking this into account the expected rate is:

$$R_{\text{muon, 2008 expected, 3 triggers}} = I \cdot f \cdot A_{\text{scintillator}} \cdot E = 1 \cdot \frac{counts}{cm^2 \cdot min} \cdot 0.32\% \cdot 113cm^2 \cdot 80\% = 2.90 \frac{counts}{min} \tag{14.37}$$

The approximations made to calculate the expected rate may contribute to the difference. The external trigger scintillator was probably not perfectly centered on top of the internal. This can also explain a fraction of the difference.

14.4.12. Results from setup with 3 triggers

The data was analyzed in the same manner as the data from the setup with 2 internal triggers described in Section 14.4.4. First the data was fitted by applying the macro *cosmic.C* to the data as described in Section 14.4.2. An example of the fit is shown in Figure 14.37.

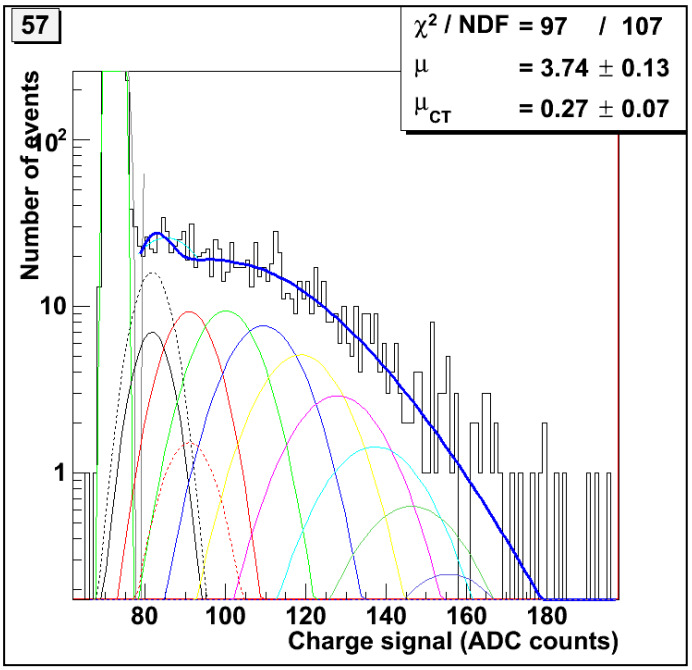

Figure 14.37. MAPMT channel 58 data and fit from the 2008 prototype run with 3 triggers.

Each MAPMT channel was mapped to the corresponding fiber as described in Section 14.3.7 taking into account that the tested layer this time was a U layer. This was done in Microsoft Excel. The results for the light yield and the crosstalk are shown in Figure 14.38 for the 90 degree cut fibers and Figure 14.39 for the 45 degree cut fibers.

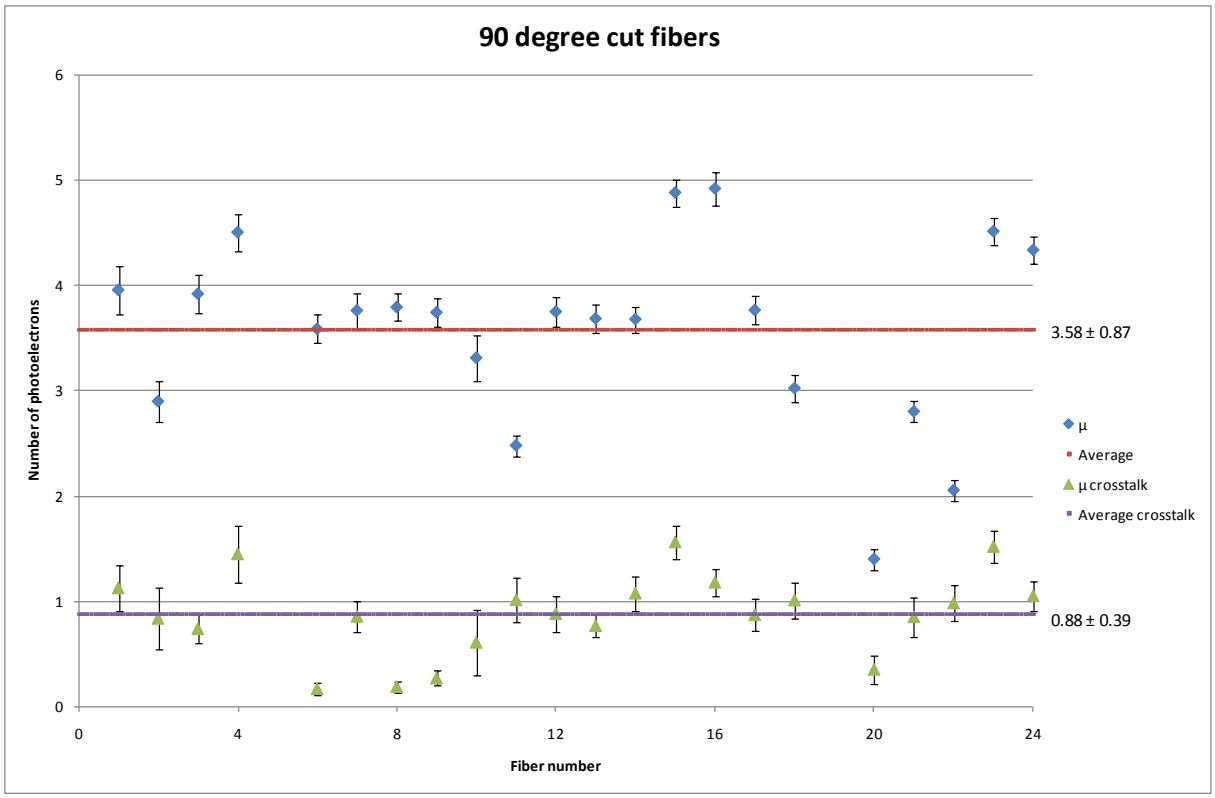

Figure 14.38. Light yield as a function of the fiber number for the 90 degree cut fibers.

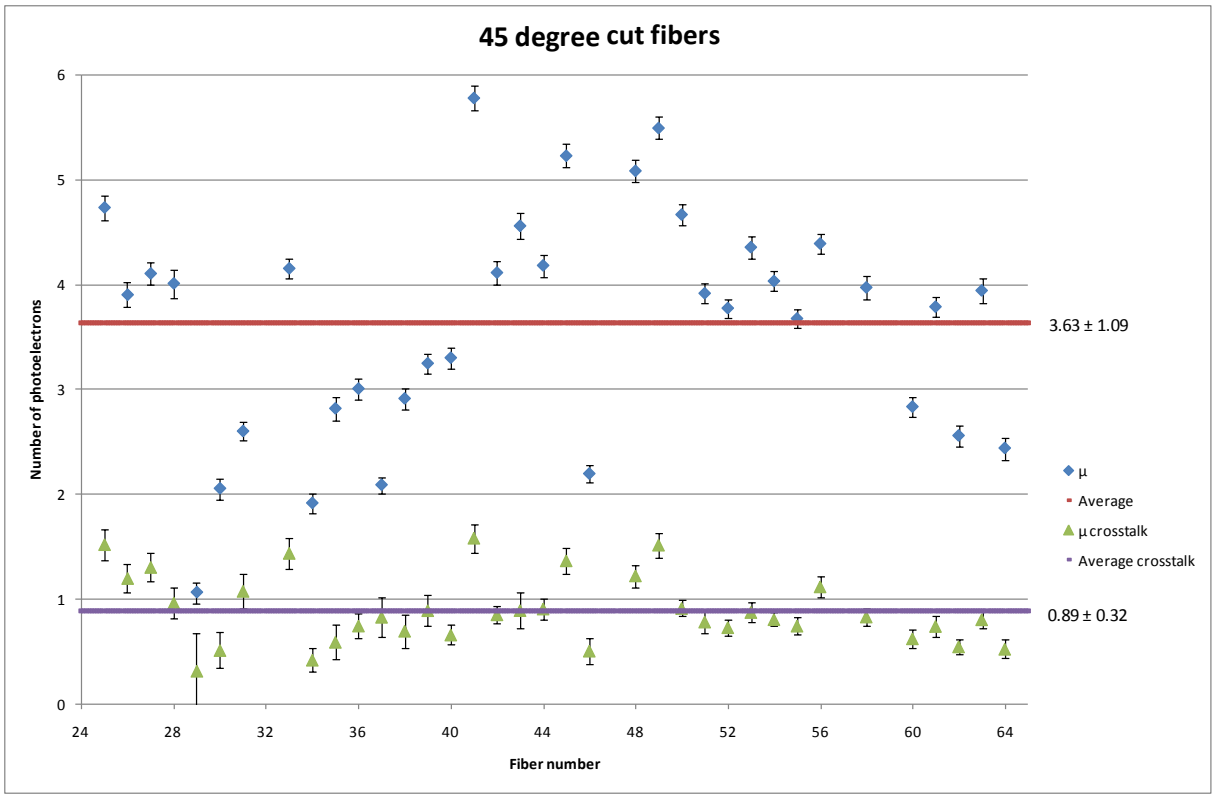

Figure 14.39. Light yield as a function of the fiber number for the 45 degree cut fibers.

14.4.13. Discussion and conclusion

The overall average results for the 90 degree cut fibers were that 22 channels were fitable with an average of 3.58 ± 0.87 PE and crosstalk 0.88 ± 0.39 PE. As discussed in Section 14.3.5 this should be comparable with the 4.45 ± 0.50 PE seen in the 2005 test beam [68]. The results with only the internal triggers were 6.19 ± 0.66 PE, which is significantly higher than with the 3 triggers.

The overall average results for the 45 degree cut fibers were that 36 channels were fitable with an average of 3.63 ± 0.89 PE and crosstalk 0.89 ± 0.32 PE. As discussed in Section 14.3.5 this should be comparable with the 3.93 ± 0.18 PE seen in the 2005 test beam [68]. The results with only the internal triggers were 4.60 ± 0.53 PE.

Some of the difference between the results for only internal trigger vs. 3 triggers can be explained by the accepted angles. The 3 trigger setup accepts only particles almost perpendicular to the detector (as would be the case for the detectors real purpose) where the setup with only internal triggers accepts all angle. If the detected particle does not travels perpendicular to the scintillating fiber the average distance through the fiber will be longer, and the scintillating fiber will send out more light. To get an idea about the magnitude of this effect the following simple calculation was done:

The average incoming angle, y, was found from the angle distribution of muons equation (14.7) by integrating:

$$\bar{\theta} = \frac{\int_0^{90} \theta \cdot \cos^2 \theta d\theta}{\int_0^{90} \cos^2 \theta d\theta} \approx 26.8 \text{ degree} \tag{14.38}$$

The average longer distance through the fiber, L, can now be found from trigonometry to be:

$$L = \frac{1}{\cos 26.8 \text{ degree}} \approx 1.12 \tag{14.39}$$

This shows that the difference in accepted angles should give an effect of the order of 10 % (see also Section 14.7.3.5 for simulations results of the same effect). This is not by itself enough to explain the differences for the runs with internal triggers vs. 3 triggers.

The 3 trigger results are a bit lower than the results from the 2005 test beam. But the difference is not significant.

The crosstalk for both the 90 degree cut fibers (μ_{CT} = 0.88 ± 0.39) and the 90 degree cut fibers (μ_{CT} = 0.89 ± 0.32) is significantly higher than seen in the 2005 test beam (μ_{CT} ≈ 0.1). This is discussed further in Section 14.7.

A pattern in the data for 45 degree cut fiber can be seen with higher values around fiber 40-50. No explanations for this effect or the fact that nothing like it is seen in the data from the setup with internal triggers have been found.

14.4.14. Trigger rate investigation

The observed trigger rate with 3 triggers was as expected or even a bit lower. This is very much in contrast to the rate with only internal triggers which was about 3 times higher than expected. This could indicate that the detector or surroundings had been activated (doing a beam test for instants) or exposit to radioactive material and had to be investigated further.

14.4.14.1. Radioactivity

The count rate was “only” about 3 times higher than expected from cosmic. In respect to radioactivity this would correspond to a very low activation. Therefore it would not be possible just to use a conventional radiation detector to check the detector for this low activation. Instead a setup using the two internal scintillator tiles and an external scintillator tile was made. The idea was to place the external detector close to the internal trigger scintillator tiles without any material in-between. Any radioactive decay from some part of the detector that goes through the internal trigger scintillator tiles should then also hit the external trigger scintillator tile and make a coincidence, which was to be counted. Next a piece of metal should be put in-between the internal and the external triggers scintillator tiles. Almost none of the cosmic high energy muons should be stopped by the metal, but most of the low energetic particles from radioactive decay should be stopped in the metal. Therefore a change in the count rate should be observed when inserting the metal between the internal and the external trigger scintillator tiles. The setup with a piece of aluminum between the internal and external triggers is shown in Figure 14.40.

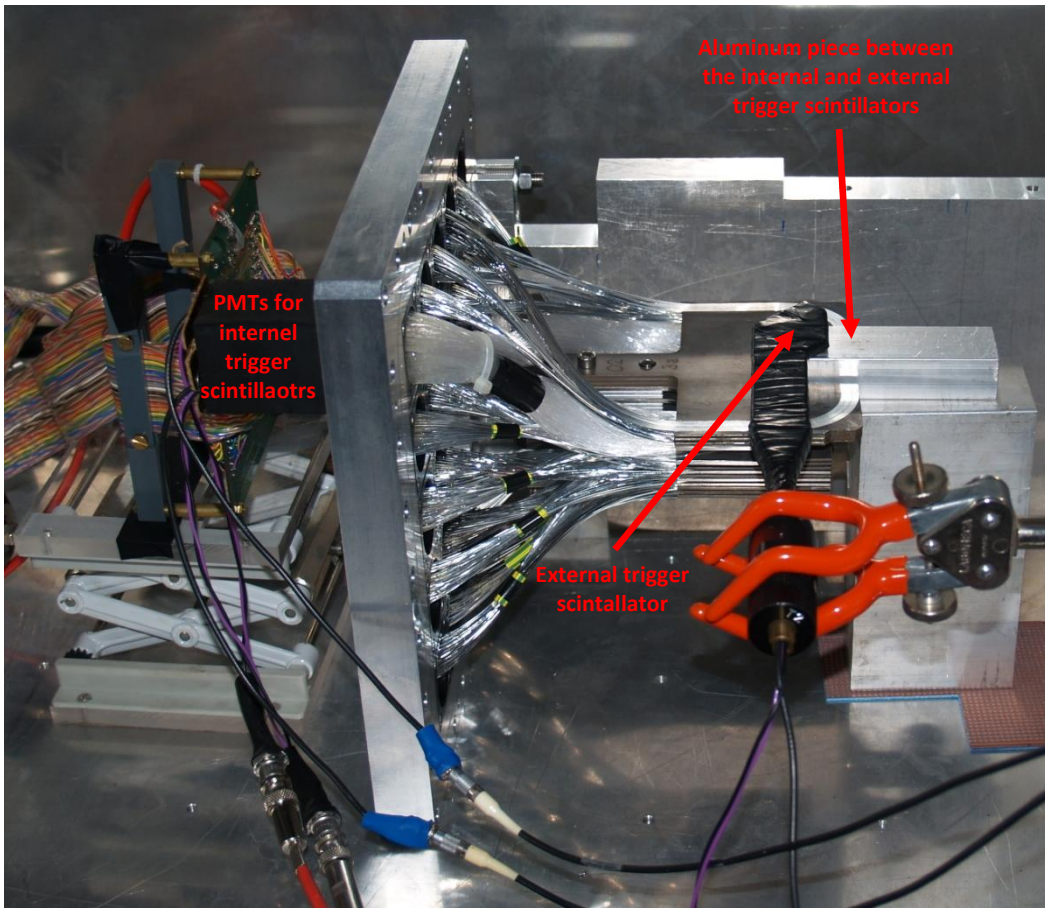

Figure 14.40. Setup for checking the detector for radioactivity.

Each of the PMTs (Hamamatsu R7400P) for the two internal trigger scintillator tiles and the PMT (Hamamatsu R7400P) for the external trigger scintillator tile were connected to a NIM discriminator (threshold 30 mV). The signals from the discriminators were put into a coincidence unit and the coincidence signal was readout by a scaler.

A run with and without the aluminum was made. The count rates were:

$$R_{Air} = 2.8 \pm 0.2 \frac{counts}{\min}$$
$$R_{Aluminum} = 2.7 \pm 0.2 \frac{counts}{\min} \quad (14.40)$$

There is no significant difference between the results with and without the aluminum in-between the internal and external trigger scintillator tiles. What more is, the count rate is very close to the expected calculated from equation (14.35), just with the values for this setup: Distance between the internal and external scintillator tiles 31 mm, Diameter of the internal scintillator tiles 32 mm, Diameter of the external scintillator tile 32 mm:

$$R_{Expected} = 2.9 \frac{counts}{\min} \quad (14.41)$$

Conclusion:

1. The detector does not shown any signs of being radioactive.
2. The too high count rate disappears when adding an external trigger scintillator tile.

14.4.14.2. Close look at the internal scintillator tiles

After the former test had shown that the too high count rate disappeared when adding an external trigger the internal triggers was investigated. After discussions with the leader of the trigger assembly (Karl-Heinz Hiller, DESY Zeuthen (KH)) a scenario was thought of:

There are two bundles of light guides connected to each of the two scintillator tiles (as described in Section 13.1.5). The top scintillator tile has one from the left side and one from the right side. These bundles are supposed to come together to one connection for one PMT for the readout of the top scintillator tile. Likewise the bottom scintillator tile has a left and right light guide bundles both of which are supposed to come together to one PMT connector. It is almost impossible to see the scintilator tiles and light guides on the prototype detector because the overlap detector covers it. Figure 14.41 are therefore of a prototype trigger scintillator system where the two scintillator tiles are taken apart so the light guide bundles are easier seen.

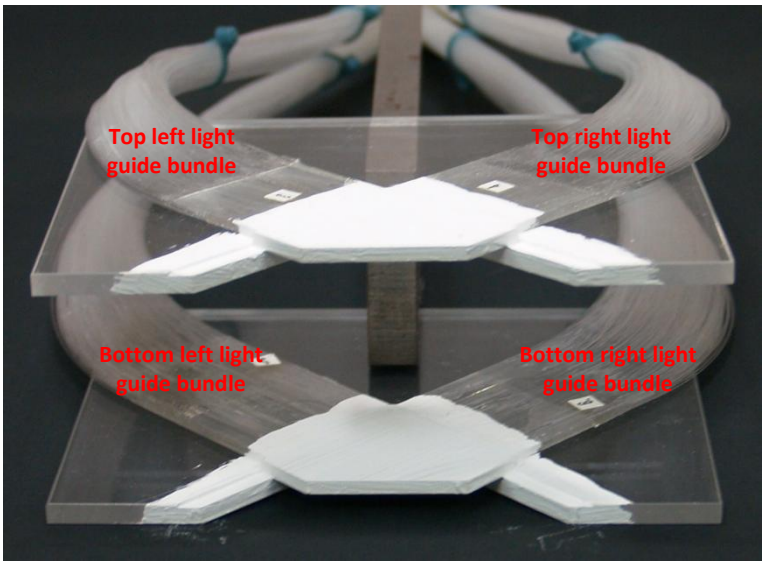

Figure 14.41. Prototype of the trigger system. The different light guide bundles are labeled.

Maybe a wrong assembly has been made where the left light guide bundles from both the top and the bottom scintillator tile have been put to the same PMT connection and the top and bottom right light guide bundles have been put to the other PMT connection.

It was not possible to simply follow the light guides from the scintillator tiles to the PMT connection because of the placement of the overlap detector. So to check if the scenario was correct a direct test of the lights journey was made: A green laser was pointed to one of the scintillator tiles. The light from the laser was intense enough to penetrate the white paint covering the scintillator tile, but too weak to penetrate through to the other scintillator tile. When the green laser light therefore was pointed to only one of the scintillator tiles only light guilds connected to that scintillator tile lights up at the PMT connection.

Figure 14.42 shows results on the light guide connection to a PMT when green laser light is pointed towards one scintillator tile.

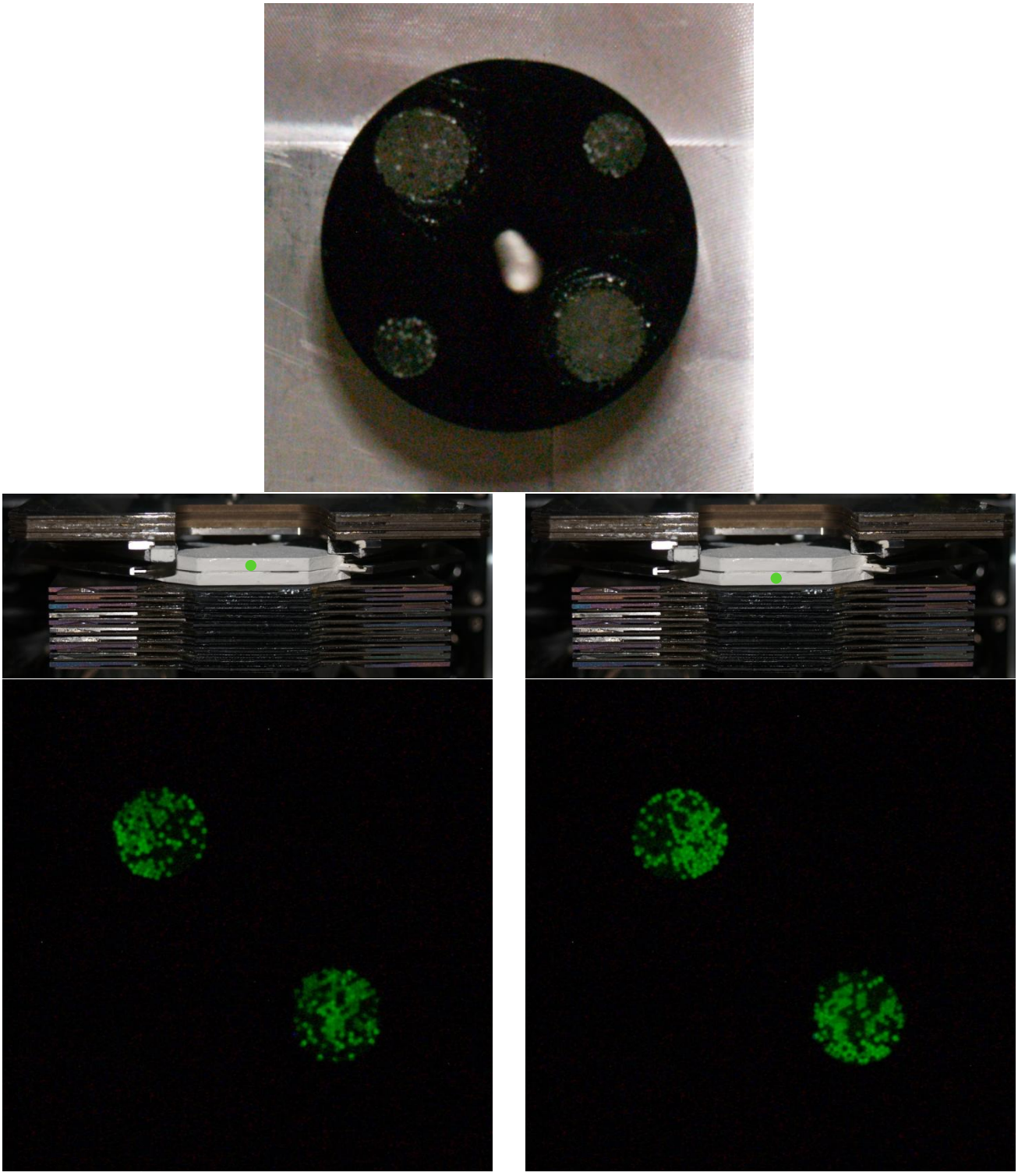

Figure 14.42. *TOP*: PMT connections (as described in Section 13.1). *MIDDLE*: detector with indication of green laser light on top/bottom scintillator tile. *BOTTOM*: Corresponding light in the light guides at the PMT connections.

If the bundles were connected correctly there should only be light on one PMT connection when lighting up one scintillator tile with the green laser. Figure 14.42 clearly shows that light guides on both PMT connection light up when lighting only one scintillator tile. Furthermore Figure 14.42 shows that when the laser is shifted to the other scintillator tile the opposite light guides light up. The conclusion from this is that the scenario is correct; the light guide bundles have been installed incorrectly. Therefore the internal trigger scintillators have not measured coincidences as each PMT have seen light from both scintillator tiles. This is the

explanation for the too high trigger rate. To compensate for this all future measurements will be done with and additional external trigger scintillator.

The finding of this error on the assembly also lead to further checking in the production of the detectors that was to be installed at the LHC/ATLAS so that no such error could occur again.

Further the prototype detector had been used in a test beam and the trigger error explained some abnormalities seen in the data.

14.5. Standard vs. Ultra Bialkali MAPMT

Originally ALFA studied a number of different MAPMTs to select the one with the best performance [75]. This work was mostly done by Sebastien Franz (CERN, PH-ADO) and Christian Joram (CERN, PH-DT). But since the work was done in close collaboration with one of the larger producers of PMTs the results are protected with a none-discloser agreement and therefore not published. In the end ALFA decided to use the Hamamatsu R7600-00-M64 photomultiplier. Since the studies were carried out, Hamamatsu has made a new MAPMT called R7600U-200-M64. This is identical from a mechanical point of view, but the active materials have been upgraded to "Ultra bialkali". This means that the peak quantum efficiency is 43 % where it is 26 % for the standard. But the peak is at a shifted wavelength as seen in Figure 14.43.

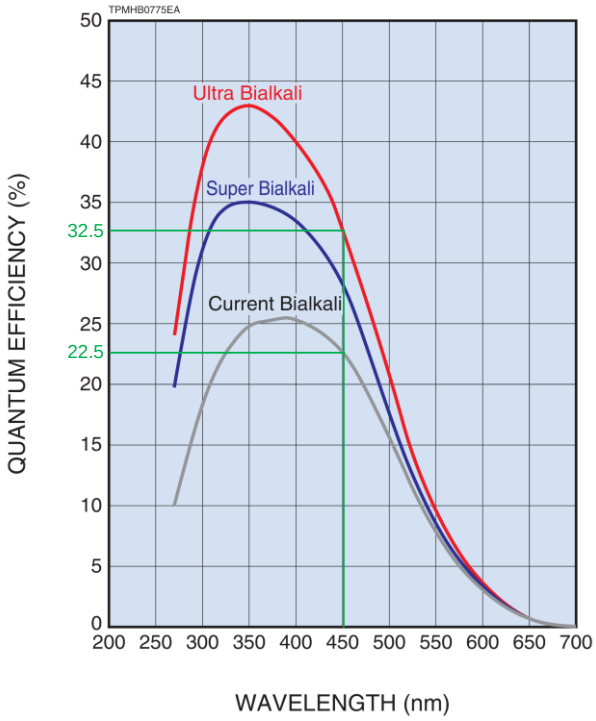

Figure 14.43. Quantum efficiency for Standard, Super and Ultra Bialkali MAPMTs. The figure is a modified version of the original from [58] (also used as Figure 13.25 page 69).

The light from the scintillating fibers peaks at 450 nm [43]. The MAPMT quantum efficiency at 450 nm is added to Figure 14.43; 22.5 % for the Standard Bialkali MAPMT, 32.5 % for the Ultra Bialkali MAPMT. Therefore the average light yield from the fibers would be expected to increase by:

$$\frac{\text{Quantum Efficiency of the Ultra Bialkali MAPMT}}{\text{Quantum Efficiency of the Standard Bialkali MAPMT}} = \frac{32.5\%}{22.5\%} = 1.44 \qquad (14.42)$$

A light yield increase of 44 % would be very comfortable. Especially if the ageing of the detector will decrease the light yield of the fibers. It was therefore decided to purchase a few Ultra Bialkali MAPMTs for testing.

14.5.1. Setup for comparing Standard and Ultra Bialkali MAPMT

The ultimate test for the MAPMTs is the real use for readout of the scintillating fibers. Therefore it was decided to re-use the setup from Figure 14.12 page 97.

The calibration for both the Standard and Ultra Bialkali MAPMT was done as described in Section 14.2.7.

To connect the MAPMT to a prototype detector the MAPMT needed shims to center each fiber on the window of each channel on the MAPMT. As only shims for one MAPMT was needed no effort was put into optimizing the production as this point. The size of the needed shims was measured on a digital microscope (By Christian Joram (CERN PH-DT) and the author) and the 4 shims were produced in the desired sizes by the technician Adrian Folley (CERN PH-DT). The shims used were just loose pieces of Plexiglas and never glued to the MAPMT. For more information about shims see Section 17.

The setup with a prototype detector connected to the MAPMTs was, with a modification in the support, the same as described in Section 14.3. Also the trigger scintillator tiles have been moved closer together for a larger angular acceptance and thereby a higher trigger rate. A photo of the setup is shown in Figure 14.44.

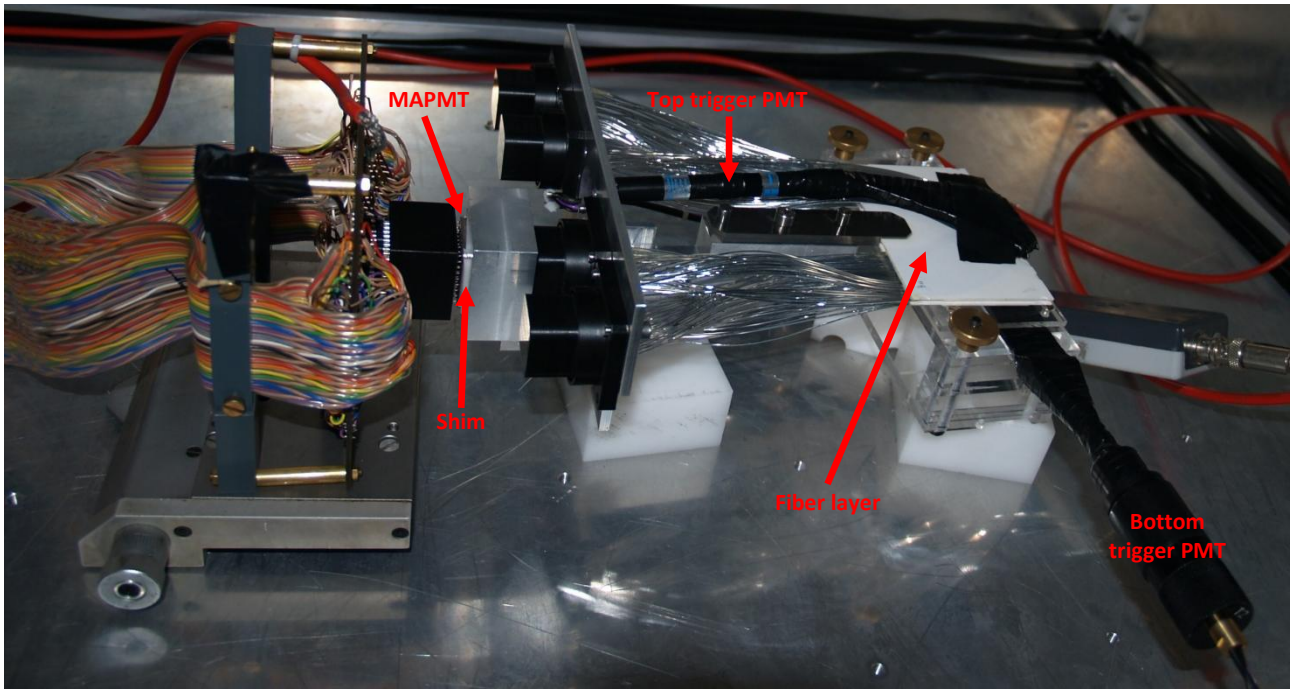

Figure 14.44. Setup for comparing Standard and Ultra Bialkali MAPMTs.

14.5.2. Runs for comparing Standard and Ultra Bialkali MAPMT

First a run with the Standard Bialkali MAPMT was made with cosmic. Data was acquired for about 2 weeks and 100471 triggers were recorded. The DAQ was not stable over that time, so the data was added up from 5 runs.

Then the Standard MAPMT was replaced by the Ultra Bialkali MAPMT and a new run was made. Data was acquired for about 2 weeks and 93312 triggers were recorded. The DAQ was not stable over that time, so the data was added up from 31 runs. The difference in stability had to do with the outside temperature going up and the air-condition turning on and off more frequently. The power consumption of the air-condition was so massive that all 230 V outlet in the laboratory changed a bit and that sometimes made a failure in the DAQ.

14.5.3. Analysis for comparing Standard and Ultra Bialkali MAPMT

The analysis was performed as previously for the similar setup discussed in Section 14.3.6.

14.5.4. Results for comparing Standard and Ultra Bialkali MAPMT

The light yield for all fitable channels for both Standard and Ultra Bialkali MAPMT is shown in Figure 14.45.

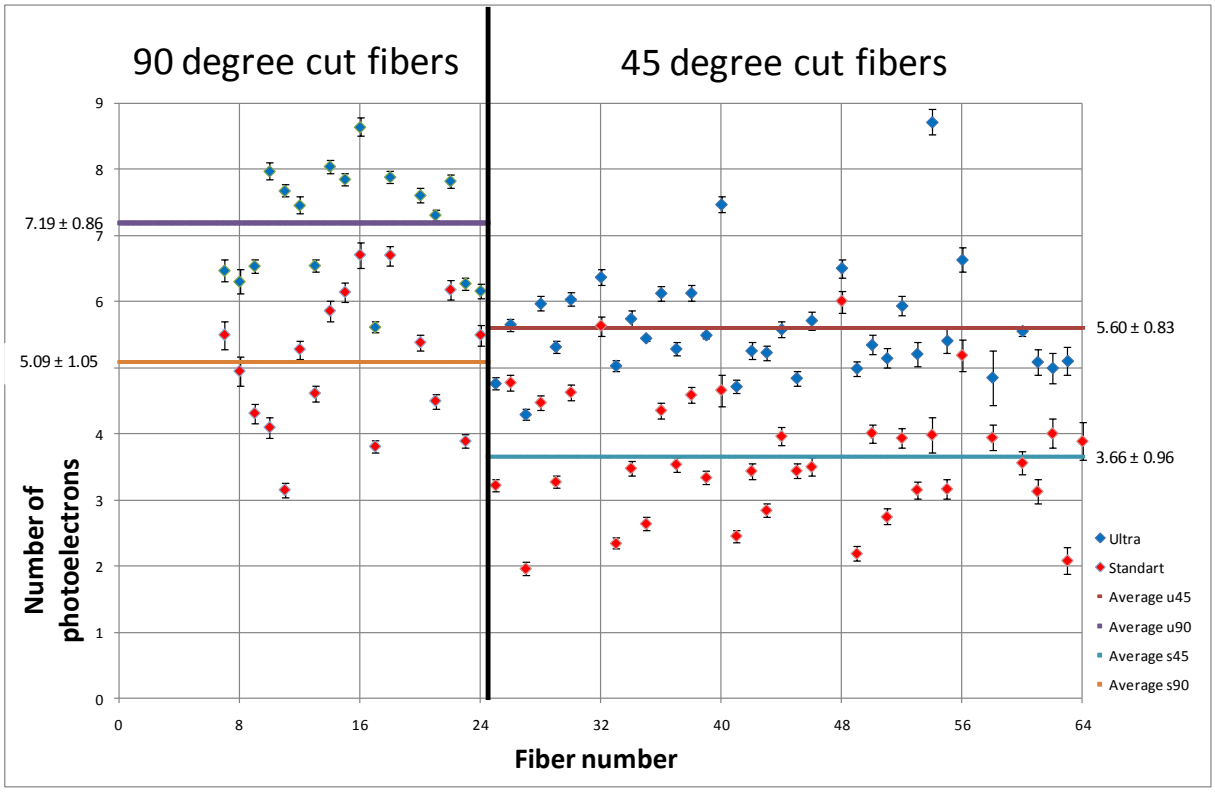

Figure 14.45. Light yield in the ALFA prototype with Standard and Ultra Bialkali MAPMT. The figure has also been presented at an ALFA meeting 14-08-2009.

The average light yield for the 90 degree cut fibers is 5.09 ± 1.05 PE for Standard Bialkali MAPMT and 7.19 ± 1.05 PE for the Ultra Bialkali MAPMT. The data for the first 7 fibers were not fitable. This is most like because they were not covered by the trigger scintillator tiles.

The average light yield for the 45 degree cut fibers is 3.66 ± 0.96 PE for Standard Bialkali MAPMT and 5.60 ± 0.83 PE for the Ultra Bialkali MAPMT. It is seen that the uncertainties for the fits goes up toward the side of the detector. This is because there will be a cut in angles for the cosmic passing both triggers and therefore will the outer fibers have fewer recorded hits and thereby less data. Therefore the fit will have larger uncertainties.

14.5.5. Conclusion for comparing Standard and Ultra Bialkali MAPMT

The average light yield in the fibers measured with the Ultra Bialkali MAPMT has 51 % ± 15 % higher than the average light yield in the fibers measured with the Standard Bialkali MAPMT. This is as expected from Figure 14.43. From this point of view a change to the Ultra Bialkali MAPMT would boost performance. But the Ultra Bialkali MAPMT cost about 50 % more than the Standard Bialkali MAPMT and ALFA is re-using about 100 Standard Bialkali MAPMT from a previous experiment (Hermes at DESY) . A complete change to Ultra Bialkali MAPMT is therefore unrealistic. A change to Ultra Bialkali MAPMT will be an option used to counteract

ageing effect on the fibers if the light yield of the fibers drops significantly over time and the fiber efficiency drops too low.

14.6. Light yield in the trigger scintillator tiles

Several layouts of the trigger scintillator tiles were investigated in a test beam before finally deciding about the design. The test results are discussed in an ATLAS note [53]. The conclusion was that a scintillator tile with a layer of special reflective white paint was the best choice. In the test beam it had a light yield of about 40 PE which should give 100 % trigger efficiency.

A trigger scintillator tile of this kind had been implemented in the 2008 prototype. Both for the main detector trigger and for the overlap detector trigger. The light yield of the installed main trigger had not been measured. There could be a lower light yield due to bending of light guides or other space restrictions. The light yield of the overlap trigger scintillator tile had never been measured. Therefore a cosmic setup was made to measure the light yield of the main and overlap trigger scintillator tiles.

14.6.1. Note about assembly error

The measurements discussed in Section 14.6 were performed before the assembly error with the mix up of the bundles described in Section 14.4.14.2 was discovered. Otherwise the trigger method described in Section 14.6.3 would have used an external trigger.

The averaged light yield of the two main trigger scintillator tiles should still be reliable because the sum of light the two PMT receives still would be the same as if the assembly had been without error.

14.6.2. Calibration of the PMT

To calculate how much light the charge measured from a PMT connected to scintillator tile corresponds to, the charge of the 1 PE needs to be known for the PMT used (as it was the case the MAPMT described in Section 14.2.7). To calibrate the PMT the setup shown in Figure 14.46 was made.

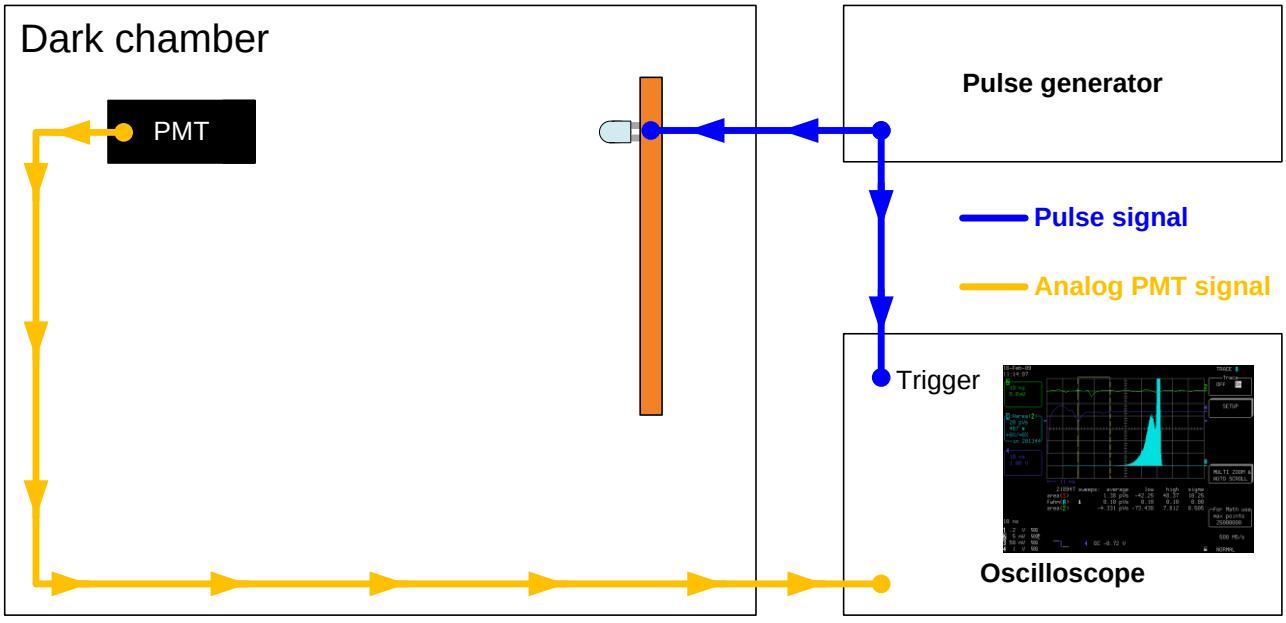

Figure 14.46. A schematic for the setup for calibrating the PMT.

A pulse generator was used to power a LED and to trigger the readout of the PMT (Hamamatsu R7400P used at 800 V). The readout was done directly on an oscilloscope by measuring the area (charge) of the PMT signal. The oscilloscope made a histogram of the charges as shown in Figure 14.47.

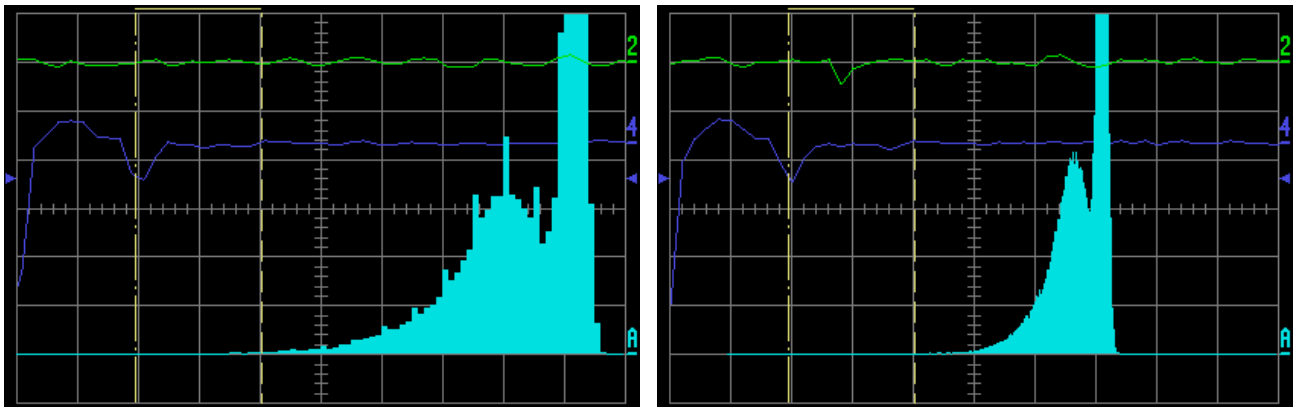

Figure 14.47. Oscilloscope screenshots of 1 PE histograms for PMT calibration of two PMTs. Left: Top PMT, scale 10 pVs. Right: Bottom PMT, scale 20 pVs.

Note that the 1 PE values are negative because the signals from the PMT are negative. As only an estimate of the light yield is needed to conclude that the light yield is high enough to have a 100 % trigger efficiency, the values of the histograms on the oscilloscope will be determined by eye. Both PMTs have a 1 PE peak (distance from the pedestal to the peak) of about 10 pVs.

14.6.3. Setup for measuring the light yield in the main trigger scintillator tiles

The setup is very simple. The PMT corresponding to each scintillator tile is connected to the oscilloscope. The signal from one PMT is used to trigger when a cosmic muon is passing the scintillator tiles. The area of the signal (charge) of the other PMT is then read out and stored in a histogram. A schematic for the setup is shown in Figure 14.48.

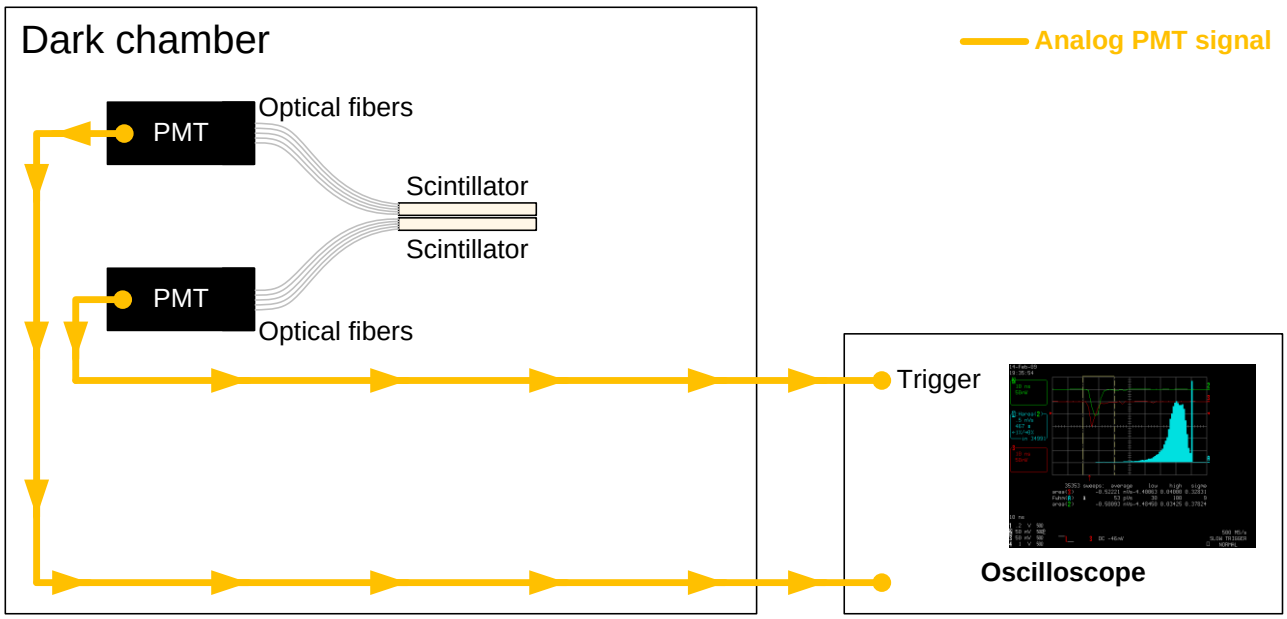

Figure 14.48. A schematic for the setup for measuring the light yield of the main detector scintillator tiles.

14.6.4. Data acquisition and results for the main trigger scintillator tiles light yield measurements

A 26 hours (35353 events) run was made with the bottom scintillator as trigger and readout of the top scintillator PMT. Then a 90 hours (123542 events) run was made with the top scintillator as trigger and readout of the bottom scintillator PMT. The histograms are shown in Figure 14.49.

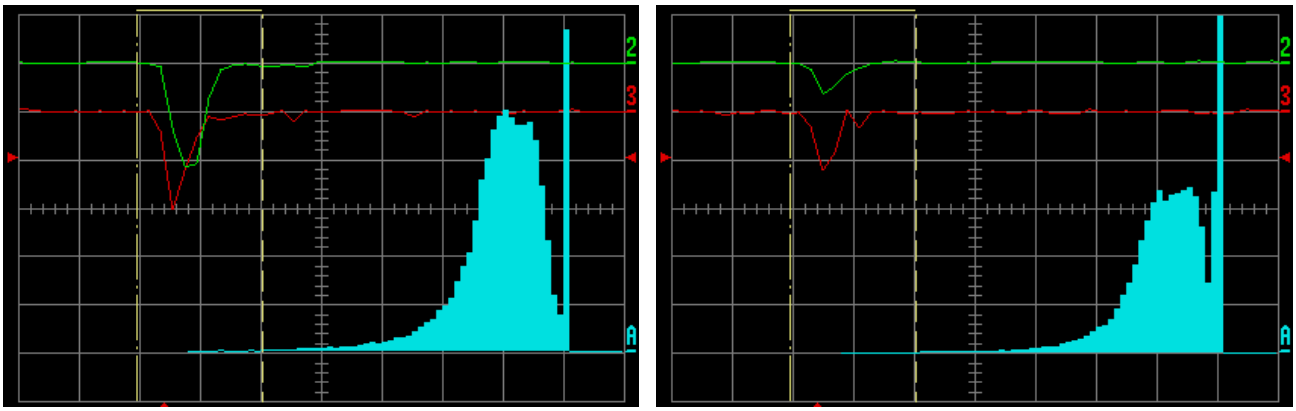

Figure 14.49. Oscilloscope screenshots of cosmic data histograms. Left: Top, scale 500 pVs. Right: Bottom, scale 500 pVs.

Both histograms peak around 400 pVs (distance from pedestal to peak). As the 1 PE for both PMTs were about 10 pVs this corresponds to a light yield of about 40 PE for both triggers.

14.6.5. Conclusion for the main trigger scintillator tiles light yield measurements

The light yield of the main trigger is about 40 PE which was also the light yield found in the beam test on the trigger prototypes discussed in ATLAS note [53]. The light yield is thereby as high as expected and the trigger efficiency should be 100 %. However in Figure 14.49 the signal is not well separated from the pedestal. The signals close the pedestal or even merged with the pedestal cannot be used as triggers and will thereby lower the efficiency. As no such effect was seen at the dedicated test beam it is assumed that these signals are from cosmic particles with inclined angles at the edge of the scintillating tile. Such particles might pass only a small fraction of the scintillating tile and thereby not releasing as many photos as a particle passing the full scintillating tile. A similar test was later made on a final detector at a test beam. Here a good separation of signal and pedestal was observed. See Figure 16.54 and details in Section 16.4.6.3.

14.6.6. Setup for measuring the light yield in the overlap trigger scintillator tile

The 2008 prototype original had two overlap trigger scintillator tiles (as the final detector will have), one for the overlap detector in each side. But at the test beam one of them was hit under insertion in the Roman Pot and fell off. So the light yield measurement was only performed on one overlap trigger scintillator tile.

A schematic for the setup is shown in Figure 14.50.

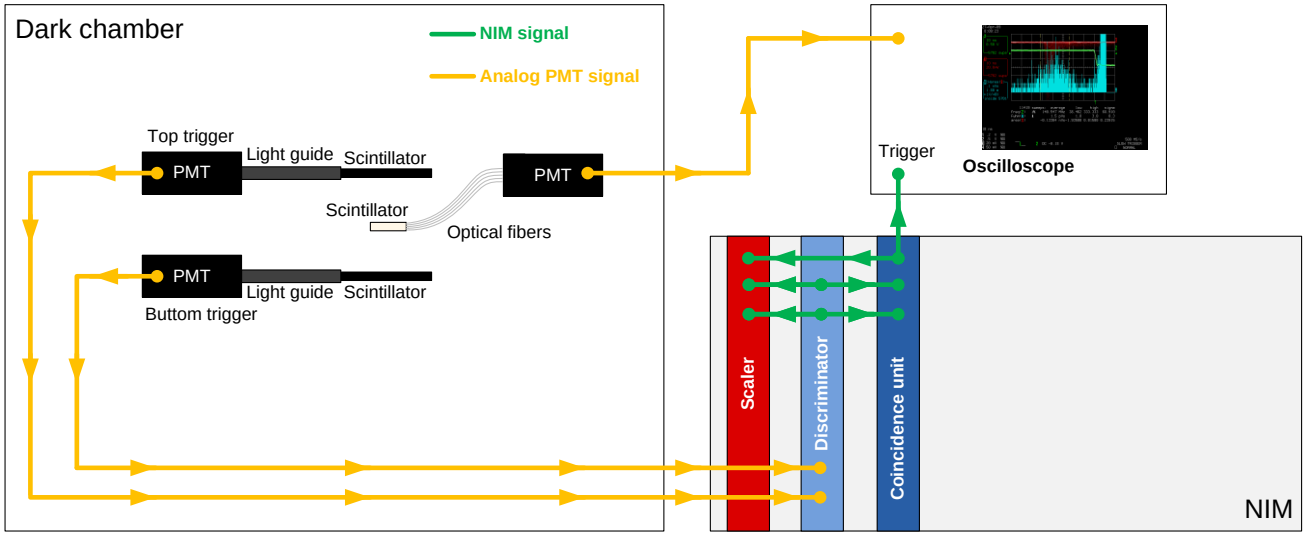

Figure 14.50. A schematic for the setup for measuring the light yield in the overlap detector trigger scintillator tile.

The PMT (Hamamatsu R7400P used at -800 V) measuring the light from the overlap trigger scintillator tile was connected directly to the oscilloscope. Two external scintillators, one below and one above the overlap trigger scintillator tile, was read out by PMTs (Hamamatsu R7400P used at -800 V and Hamamatsu R1635 used at -1250 V) which were connected to NIM discriminators (30 mV threshold). The signal from the discriminators was send to a coincidence unit, which sends the trigger signal to the oscilloscope. The signals from the discriminators and the coincidence signal were also send to a scaler (to look for noise, light leaks etc.).

The setup is shown in Figure 14.51.

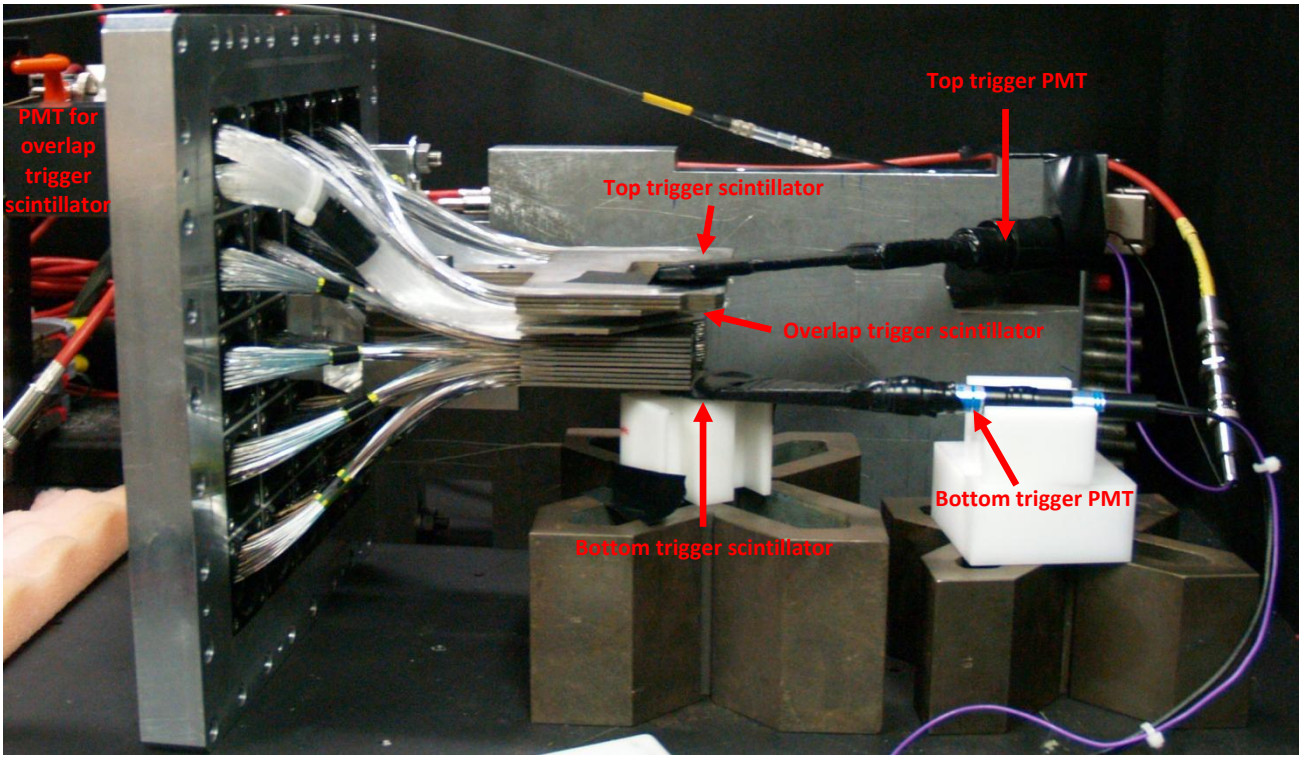

Figure 14.51. Setup for measuring the light yield in the overlap detector trigger scintillator tile.

14.6.7. Data acquisition and results for the overlap trigger scintillator tile light yield measurement

A 90 hours (11419 events) run was made with cosmic. As the trigger scintillator tiles were much larger than the overlap trigger scintillator tile most of the events only contributed to the pedestal. The histogram is shown in Figure 14.52.

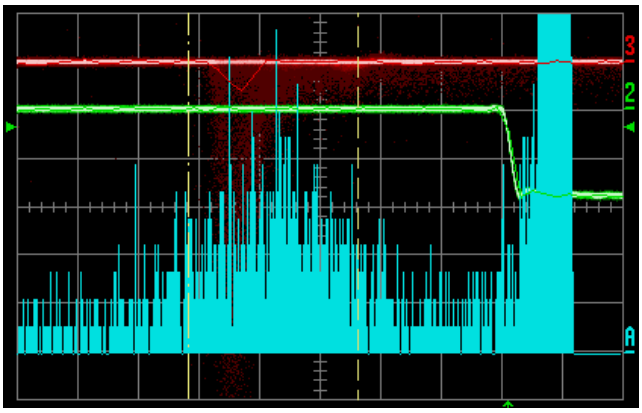

Figure 14.52. Oscilloscope screenshot of cosmic data histogram for the overlap trigger detector. Scale 100 pVs.

The histogram peaks around 400 pVs (distance from pedestal to peak). As the 1 PE for the PMT was about 10 pVs this corresponds to a light yield of about 40 PE.

14.6.8. Conclusion for the overlap trigger scintillator tile light yield measurement

The light yield of the overlap trigger is about 40 PE which was also the light yield found in the main trigger (Section 14.6.5) and in the beam test on the main trigger prototypes discussed in ATLAS note [53]. The design of the overlap trigger is therefore proven to give a very high light yield and the trigger efficiency should be 100 %. (The trigger efficiency of the overlap detector has no direct impact in the overall detector performance (as it is only used for alignment) and does therefore not need to be 100 %. That is the reason why it has not been measured at a test beam).

14.7. Investigation of "crosstalk"

The content of this section has been published as *[74]* which is included as Appendix A.

Figure 14.53 shows in 2D what is meant by crosstalk. A fraction of the light exiting a fiber end might not hit the right PMT channel but the neighbor PMT channel. This fraction is labeled crosstalk. It might not be by direct emission (as in Figure 14.53) but can be due to multiple reflections in the PMT entrance window.

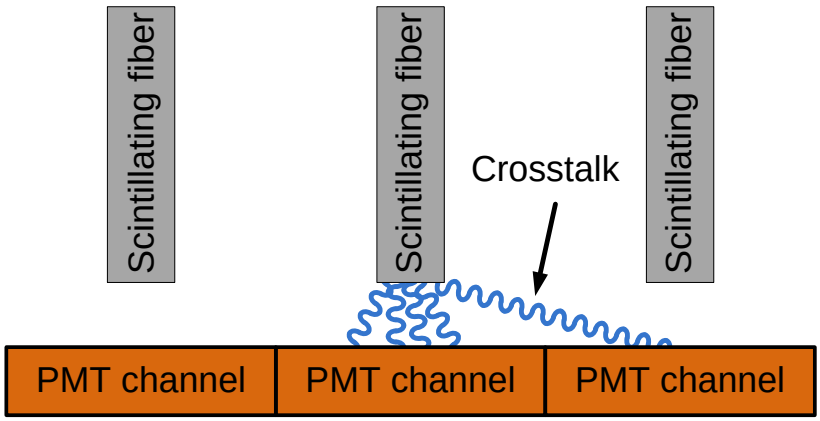

Figure 14.53. Light transition from the scintillating fiber to the MAPMT. A fraction of the light hits a neighbor channel. This fraction is labeled crosstalk.

The crosstalk term in equation (14.20) in all the cosmic charge fits (Figure 14.20, Figure 14.30 and Figure 14.37) which are summed up in the channel plots (Figure 14.22, Figure 14.24, Figure 14.25, Figure 14.31, Figure 14.32, Figure 14.38 and Figure 14.39) are all higher than expected from the 2005 beam test data [68]. A fit of a histogram with data from the 2005 test beam is shown in Figure 14.54.

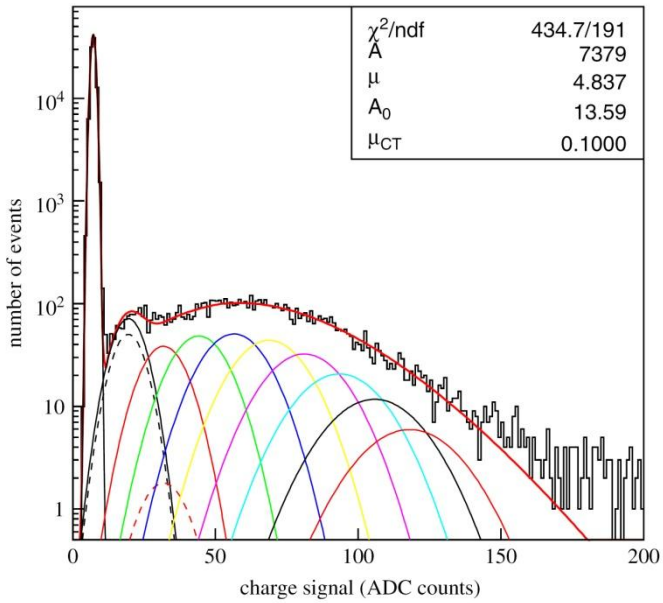

Figure 14.54. Fit of charge histogram with data from the 2005 test beam. The figure is figure 5 in [68].

In the 2005 beam data a crosstalk term of about 0.1 PE was seen where the results from cosmic show a crosstalk term of about 0.7-1.3 PE. The relative crosstalk for the test for the 2008 prototype is:

$$Crosstalk_{\text{cosmic}} = \frac{\mu_{CT}}{\mu + \mu_{CT}} = 19.6 \pm 3.4\% \tag{14.43}$$

In the 2005 test beam the relative crosstalk was:

$$Crosstalk_{\text{beam}} = \frac{\mu_{CT}}{\mu + \mu_{CT}} = 3.4 \pm 1.3\% \tag{14.44}$$

A factor 6 more crosstalk is seen with cosmic compared with the 2005 test beam data and this had to be explained.

14.7.1. Initial investigation

First the high crosstalk was thought to be something artificial from the fit itself. However after some investigation this hypothesis was abandoned.

Then it was thought that the shims for the MAPMT might have been interchanged leading to the fibers not being in the middle of the MAPMT channels, but much closer to the neighbor channel. This would certainly induce more crosstalk. The MAPMT was placed under a microscope and it was concluded that the spaces were in the right positions and that the fibers should be very close to center on the MAPMT channels.

14.7.2. Cosmic vs. Beam

An idea originated that the different crosstalk value was not due to something artificial or wrong with the setup, but a real physical difference with using cosmic instead of a beam. A beam comes from a very well defined direction and in the 2005 setup the detector was placed perpendicular to the beam. The particles in the beam (6 GeV electrons) would therefore hit one fiber per layer (the particle could also hit in the inactive space between to fibers and thereby not hit any fibers in a layer). A particle from a beam will never hit more than one fiber per layer and will always go the shortest path through the fiber layer. But the cosmic particles have an angular destitution (equation (14.7)). Therefore one cosmic particle can hit more than one fiber per layer and the particles path through a fiber layer will in general be longer. The difference is illustrated in Figure 14.55.

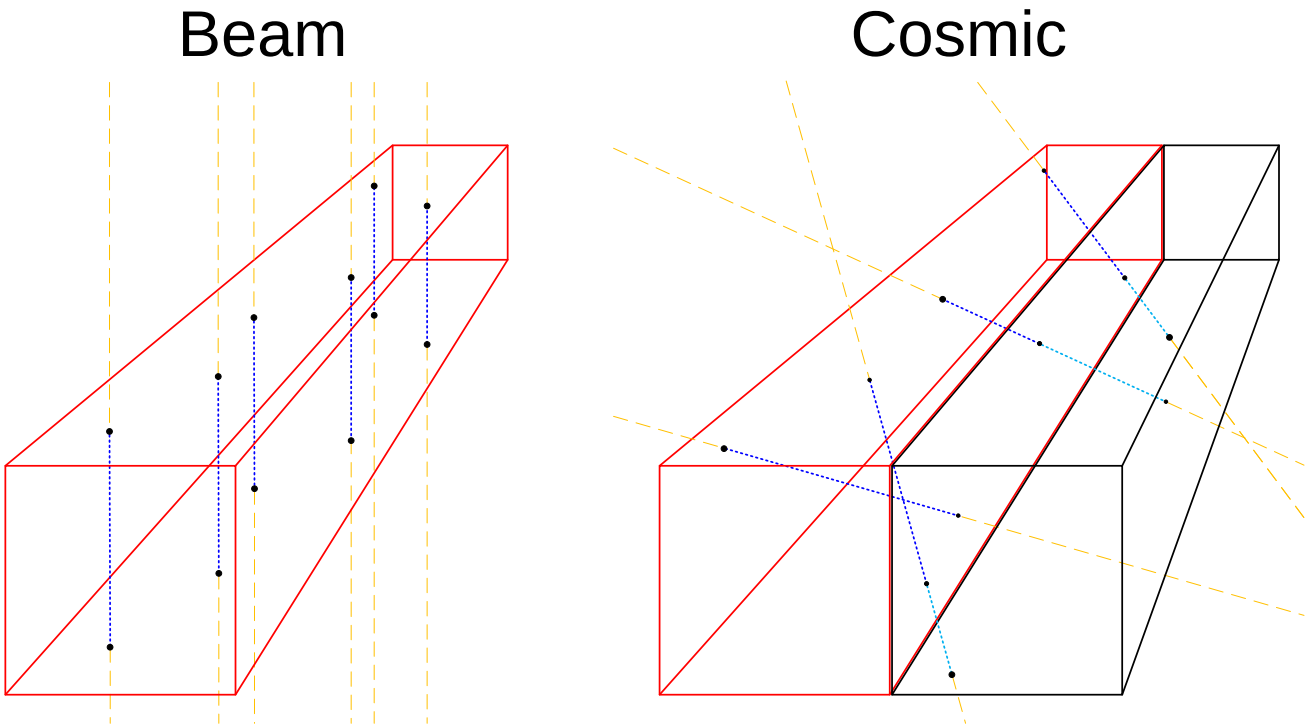

Figure 14.55. Illustration of the difference between particles from a beam and from cosmic. For easier comparison the beam is coming from above in the illustration. The fibers are made in red and black. The particle track outside the fiber is yellow and the particle tracks inside the fibers are blue in different shades depending on fiber.

Scintillating fibers being passed though only partly of a particle will obviously send out fewer photons. The MAPMT channel receiving the photons will therefore in average make a smaller signal. This will make a pileup of small charge signals, which in the fit with equation (14.20) will come out as crosstalk. This could be an explanation for the larger crosstalk term seen in the cosmic data compared to the data from a beam.

14.7.3. Simulation

To investigate the hypothesis that the larger crosstalk term seen the cosmic data compared to the data from the beam test was due to the angular destitution of the cosmic, a small simulation was made.

The simulation was made in C++ and run inside ROOT, using ROOTs histograms as an output. Also ROOTs TRandom3 was used for random numbers. The simulation code version 2 is included as Appendix K.

14.7.3.1. Generation of particles

To simplify the geometry the fibers are assumed to be infinity long so that a particle never will exit from the end of a fiber. It is also assumed that the fiber first hit will always have 5 fibers next to it. This means that the fiber simulated will not be on the edge of the detector and that a particle will never pass though more than 6 fibers (θ (see Figure 14.57) up to about 80 degrees).

The simulation first generates a random position on a fiber where the particle hits. The width and height of the squared fiber is call b, so the position, p, on the fiber is made by multiplying a random number between 0 and 1 with b. b and p are shown in Figure 14.56.

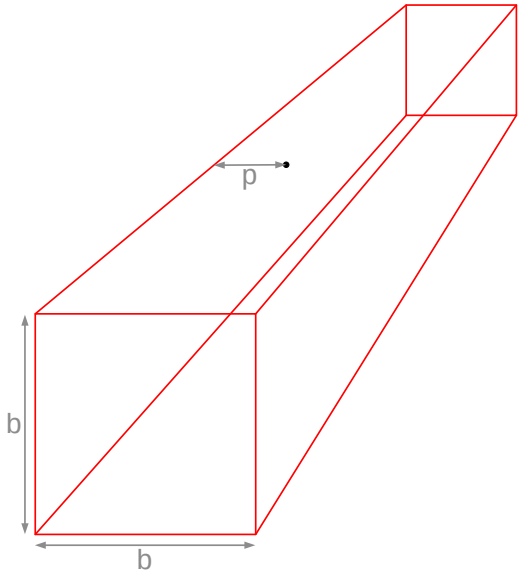

Figure 14.56. b and p in the simulation.

The simulation then generates the angle perpendicular to the fiber (the polar angle), θ. This is generated randomly from the angular distribution of cosmic muons (copy of equation (14.7)) in an interval:

$$\text{Angular distribution} \propto \cos^2\theta \tag{14.45}$$

The interval is from 0 to $\pi/2$ (or another smaller angle if cuts from triggers are wanted). The definition of θ is shown in Figure 14.57.

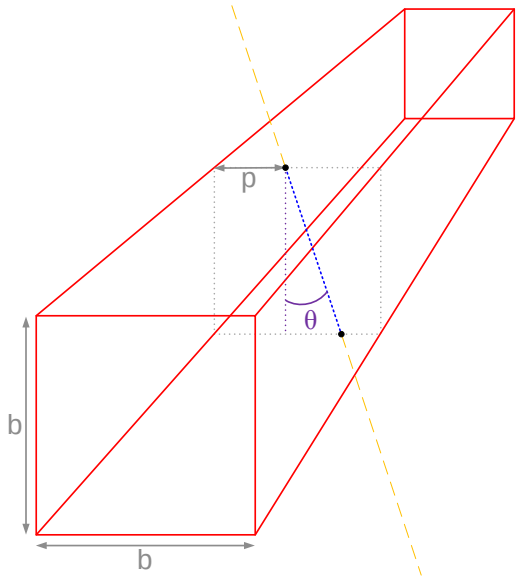

Figure 14.57. The angle θ in the simulation.

Next the simulation generates randomly the angle φ, which is the azimuthal angle. In principle φ should be in the interval from 0 to 2π. But since there should be no differences between each fiber end, and since it should not matter if a second fiber hit is on one side or the other of the first, the interval for φ is only going from 0 to π/2. This will make the geometry much easier and should not change the simulation in any way. φ is made by generating a random number between 0 and 1 and multiplying it with π/2. The definition of φ is shown in Figure 14.58.

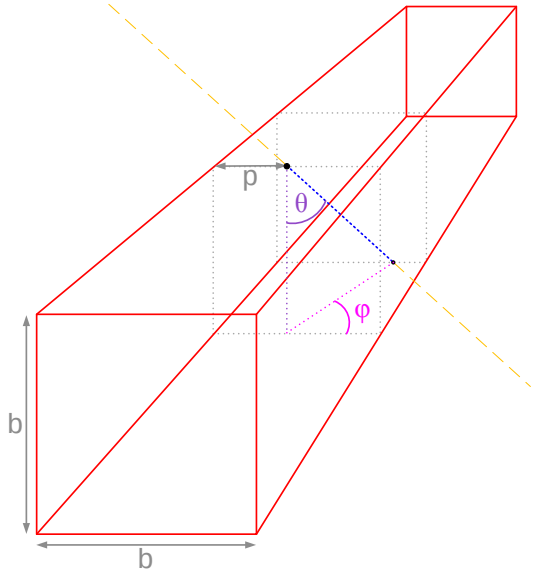

Figure 14.58. The angle φ in the simulation.

14.7.3.2. Simulation version 1

Particles are assumed to never be stopped in the fibers and always induce the same number of photons per length travelled inside a fiber.

The simulation first determined how many fibers a particle will hit. The limit for only one fiber being hit is found as the maximum for θ as seen in Figure 14.59.

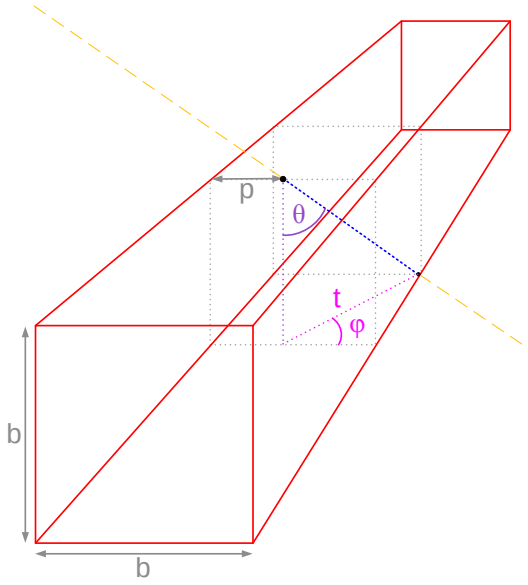

Figure 14.59. Maximum θ for only one fiber being hit.

To determine the maximum angle for θ where only one fiber is hit the length of t is first calculated:

$$\cos\varphi = \frac{b-p}{t} \Rightarrow$$
$$t = \frac{b-p}{\cos\varphi} \tag{14.46}$$

θ can then be found as:

$$\tan\theta_{\max 1} = \frac{t}{b}$$
$$= \frac{b-p}{\cos\varphi \cdot b} \quad \Rightarrow \tag{14.47}$$
$$\theta_{\max 1} = \arctan\frac{b-p}{\cos\varphi \cdot b}$$

The limit for two fibers being hit is shown in Figure 14.60.

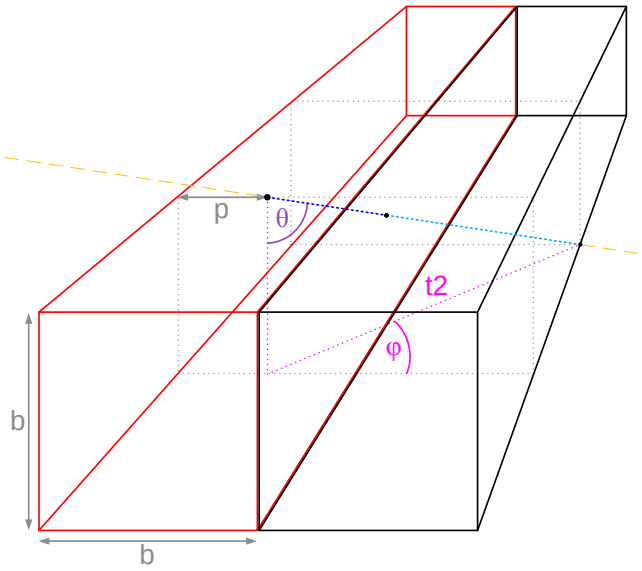

Figure 14.60. Maximum θ for two fibers being hit.

To determine the maximum angle θ where only two fibers are being hit the length of t2 is first calculated:

$$\cos\varphi = \frac{2\cdot b - p}{t2} \Rightarrow$$
$$t2 = \frac{2\cdot b - p}{\cos\varphi} \tag{14.48}$$

θ can then be found as:

$$\tan\theta_{\max 2} = \frac{t2}{b}$$
$$= \frac{2\cdot b - p}{\cos\varphi \cdot b} \Rightarrow \tag{14.49}$$
$$\theta_{\max 2} = \arctan\frac{2\cdot b - p}{\cos\varphi \cdot b}$$

In the same fashion the rest of the limits are found:

$$\theta_{\max 3} = \arctan\frac{3\cdot b - p}{\cos\varphi \cdot b} \tag{14.50}$$

$$\theta_{\max 4} = \arctan\frac{4\cdot b - p}{\cos\varphi \cdot b} \tag{14.51}$$

$$\theta_{\max 5} = \arctan\frac{5\cdot b - p}{\cos\varphi \cdot b} \tag{14.52}$$

For each scenario of the number of fibers hit the length the particle travels inside each fiber is calculated.

For only one fiber hit, $\theta < \arctan\frac{b - p}{\cos\varphi \cdot b}$, the distance, lr, the particle travels inside the fiber is shown in Figure 14.61.

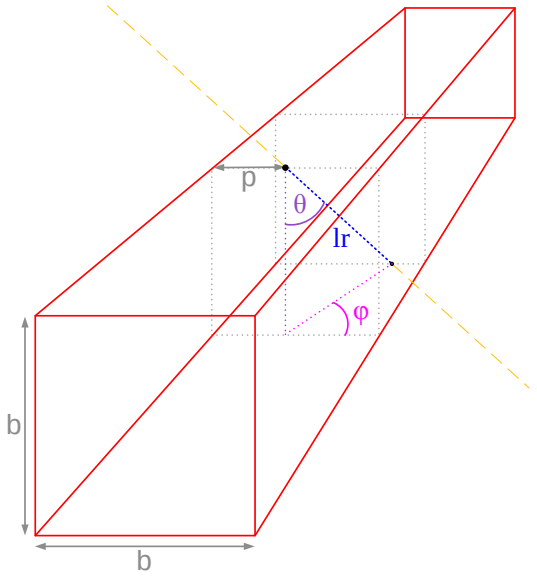

Figure 14.61. Distance lr for one fiber hit in the simulation.

lr can be calculated as:

$$lr = \frac{b}{\cos\theta} \tag{14.53}$$

For two fibers hit, $\arctan\frac{b-p}{\cos\varphi\cdot b} < \theta < \arctan\frac{2\cdot b-p}{\cos\varphi\cdot b}$, the distances, lr and lr2, the particles travels inside each of the fibers are shown in Figure 14.62.

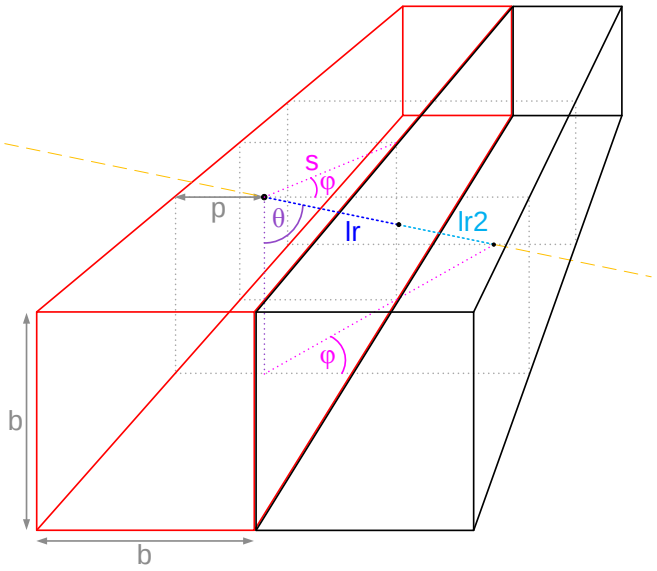

Figure 14.62. lr and lr2 for 2 fibers hit in the simulation.

lr can be calculated via s:

$$\cos\varphi = \frac{b-p}{s} \quad \Rightarrow \qquad s = \frac{b-p}{\cos\varphi} \tag{14.54}$$

$$\cos\left(\frac{\pi}{2}-\theta\right)=\frac{s}{lr} \qquad \Rightarrow$$

$$lr=\frac{s}{\cos\left(\frac{\pi}{2}-\theta\right)} \qquad (14.55)$$

$$=\frac{b-p}{\cos\varphi\cdot\cos\left(\frac{\pi}{2}-\theta\right)}$$

lr2 can now be calculated using lr:

$$\cos\theta=\frac{b}{lr+lr2} \qquad \Rightarrow$$

$$lr2=\frac{b}{\cos\theta}-lr \qquad (14.56)$$

For three fibers hit, $\arctan\frac{2\cdot b-p}{\cos\varphi\cdot b}<\theta<\arctan\frac{3\cdot b-p}{\cos\varphi\cdot b}$, the distances, lr, lr2 and lr3, the particles travels inside each of the fibers is shown in Figure 14.63.

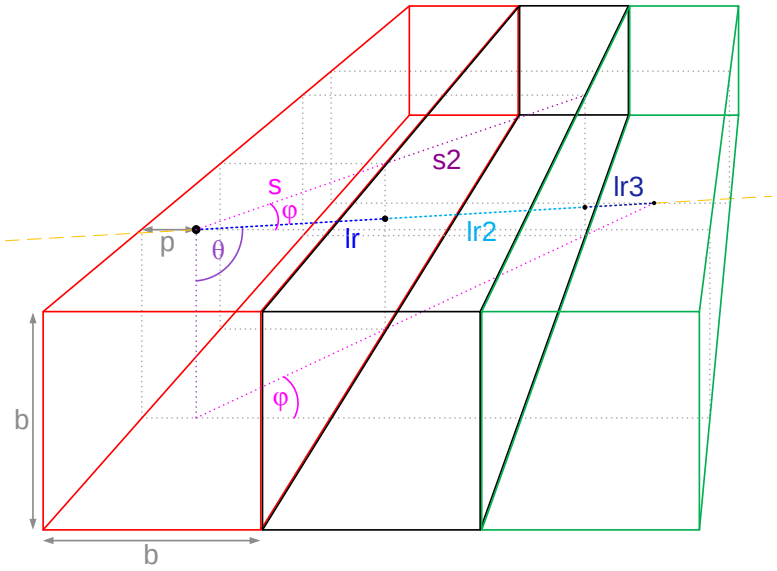

Figure 14.63. lr, lr2 and lr2 for three fibers hit in the simulation.

lr can be calculated as for two fibers according to equation (14.56).

lr2 can be calculated via s and s2 and using lr:

$$\cos\varphi=\frac{2\cdot b-p}{s+s2} \qquad \Rightarrow$$

$$s+s2=\frac{2\cdot b-p}{\cos\varphi} \qquad (14.57)$$

$$\cos\left(\frac{\pi}{2}-\theta\right)=\frac{s+s2}{lr+lr2} \quad \Rightarrow$$

$$lr2=\frac{s+s2}{\cos\left(\frac{\pi}{2}-\theta\right)}-lr \tag{14.58}$$

$$=\frac{2\cdot b-p}{\cos\varphi\cdot\cos\left(\frac{\pi}{2}-\theta\right)}-lr$$

lr3 can now be calculated using lr and lr2:

$$\cos\theta=\frac{b}{lr+lr2+lr3} \quad \Rightarrow$$

$$lr3=\frac{b}{\cos\theta}-lr2-lr \tag{14.59}$$

The distances the particles travels inside the fibers in the cases where 4, 5 and 6 fibers are hit are calculated in a similar fashion.

For all the events where less than 6 fibers are hit, the distances lr*i* (*i* being the number of a fiber not hit) should in principle be set to zero. This will give the pedestal. Instead of exactly zero it is set to a value very close to zero (0.03, ~ 0.75 % of main light). This will simulate the noise from the MAPMTs and the events where the photoelectrons created inside the MAPMT miss the first dynode but hit the second.

The simulation takes a random number, p_i, from a Poisson distribution with a mean value proportional to lr*i*. The program generates a Gaussian distribution with mean p_i and width $\sqrt{p_i}\cdot\sigma_1$, where σ_1 is the measured width of the 1 PE peak. The electronic pedestal width $\sigma_{pedestal}$ is added to all σ_{p_i} values in quadrature:

$$\sigma_{p_i}=\sqrt{{\sigma_{pedestal}}^2+p_i\cdot{\sigma_1}^2} \tag{14.60}$$

The program now chooses a random value from this distribution and fills it into a histogram.

14.7.3.3. Results for simulation version 1

The histogram from the simulated values was fitted with *Cosmic.C* modified to work with the simulated data. The histogram and fit is shown in Figure 14.64.

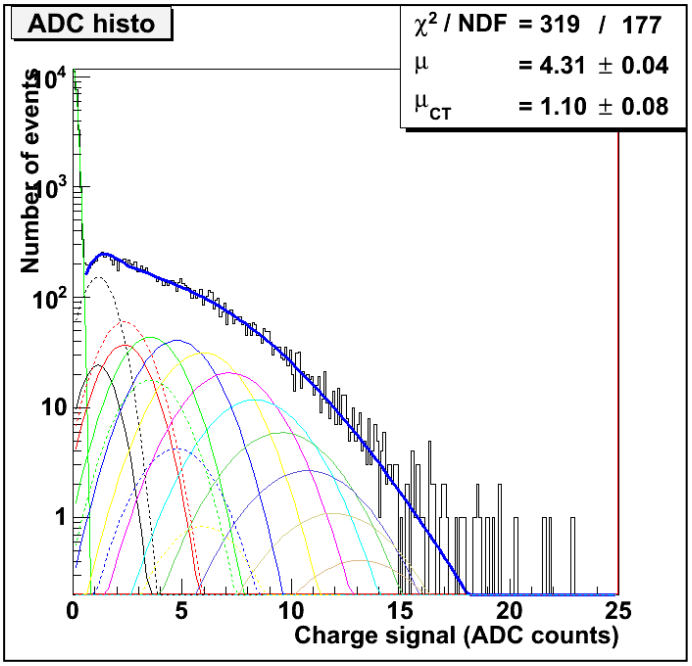

Figure 14.64. Histogram from simulation with geometry 1 fitted with equation (14.20).

The fit was with equation (14.20). The results from the fit are a main light yield of 4.31 ± 0.04 PE and a "crosstalk" term of 1.10 ± 0.08 PE. The absolute values themselves have no direct physical meaning as they just scale with the inputted "width of fiber in PE", b, in the simulation. But the relative crosstalk can be compared to real data. The ratio is:

$$Crosstalk_{\text{Simulated cosmic 1}} = \frac{\mu_{CT}}{\mu + \mu_{CT}} = \frac{1.10\ PE}{4.31\ PE + 1.10\ PE} = 20.3 \pm 1.3\ \% \qquad (14.61)$$

This is comparable to what was seen in the cosmic data ~20 %. To make a control that this is really a difference between cosmic and beam and not for example an artificial effect from the noise term the simulation was repeated for beam. This was done keeping all parameters at the same value but locking the angle θ to zero, as it would be in a beam. The result for the control beam simulation is shown in Figure 14.65.

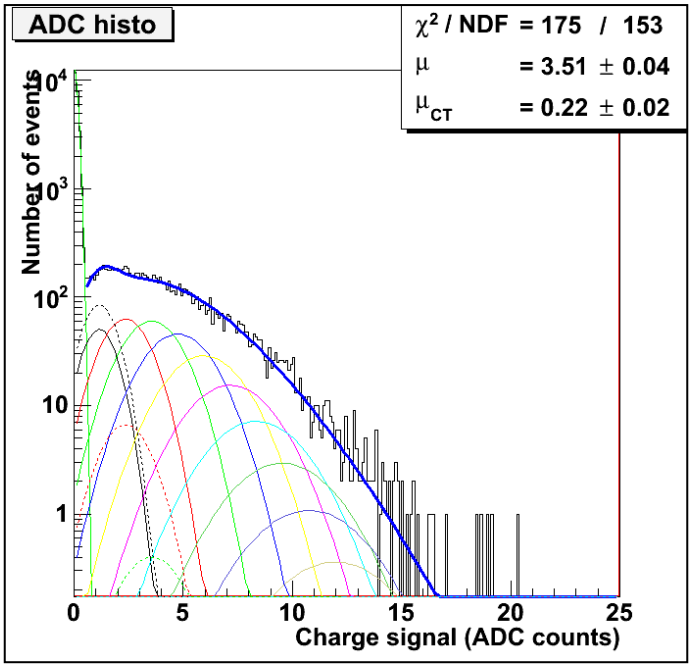

Figure 14.65. Simulation for beam with the same settings as for the cosmic simulation.

The results from the fit are a main light yield of 3.51 ± 0.04 PE and a "crosstalk" term of 0.22 ± 0.02 PE. The ratio of crosstalk over main light yield is therefore:

$$Crosstalk_{\text{Simulated beam 1}} = \frac{\mu_{CT}}{\mu + \mu_{CT}} = \frac{0.22\ PE}{3.51\ PE + 0.22\ PE} = 5.9 \pm 0.6\ \% \qquad (14.62)$$

It is hereby shown that a significant difference between cosmic and beam "crosstalk" light yield is to be expected.

The cosmic has a higher main light yield term because the particles on average will always travel longer through the fiber when they are not hitting the fiber perpendicularly. More about this effect in simulation version 2 Section 14.7.3.5.

As the "crosstalk" term for cosmic is more a term of light in secondary fibers, it could be argued to add the crosstalk term to the main light yield to get a more realistic overall light yield.

This first version of the simulation clearly demonstrated that a difference between beam and cosmic in the MAPMT "crosstalk" charge distribution is to be expected. However the simulation is very rough in the assumptions on geometry and with the noise term introduced. This could explain why the simulation has a larger crosstalk term for beam than the beam data. To make a more realistic simulation a second version was made.

14.7.3.4. Simulation version 2

In the first simulation the fibers were assumed be active in the entire volume and to be staked with no space between them. In reality the active part of the fiber is about 480 µm out of the 500 µm widths and on average there are 10 µm between the fibers. This can have an impact for all particles hitting more than one fiber as the distances the particle travels inside the fibers will be shorter.

Also the noise term from version 1 is reduced to a more realistic value and a small optical crosstalk term is introduced. This will be described in details later in this section.

Particles are again assumed to never be stopped in the fibers and always induce the same number of photons per length travelled inside a fiber.

The simulation again first determines how many fibers a particle will hit given with the angle θ. The limit for hitting only one fiber is the same as in geometry 1 and is shown in Figure 14.59 and is given by equation (14.48).

The limit for entering fiber number 2 is shown in Figure 14.66.

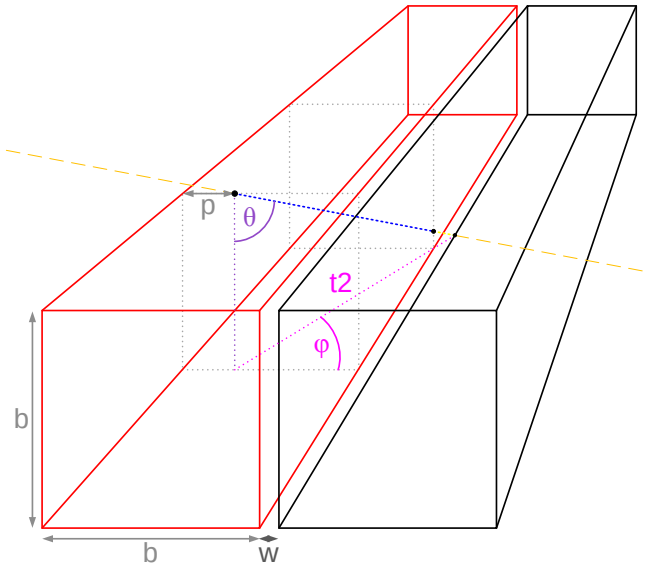

Figure 14.66. Maximum θ before entering fiber two.

This limit can be found in a fashion similar to the second limit in geometry 1:

$$\begin{aligned} \tan\theta_{\max\ 1+w} &= \frac{t2}{b} \\ &= \frac{2\cdot b + w - p}{\cos\varphi \cdot b} \qquad \Rightarrow \\ \theta_{\max\ 1+w} &= \arctan\frac{2\cdot b + w - p}{\cos\varphi \cdot b} \end{aligned} \tag{14.63}$$

In a similar fashion the rest of the needed limits are found:

$$\theta_{\max\ 2} = \arctan\frac{2\cdot b + w - p}{\cos\varphi \cdot b} \tag{14.64}$$

$$\theta_{\max\ 2+w} = \arctan\frac{2\cdot b + 2\cdot w - p}{\cos\varphi \cdot b} \tag{14.65}$$

$$\theta_{\max\ 3} = \arctan\frac{3\cdot b + 2\cdot w - p}{\cos\varphi \cdot b} \tag{14.66}$$

$$\theta_{\max\ 3+w} = \arctan\frac{3\cdot b + 3\cdot w - p}{\cos\varphi \cdot b} \tag{14.67}$$

$$\theta_{\max\ 4} = \arctan\frac{4\cdot b + 3\cdot w - p}{\cos\varphi \cdot b} \tag{14.68}$$

$$\theta_{\max\ 4+w} = \arctan\frac{4\cdot b + 4\cdot w - p}{\cos\varphi\cdot b} \tag{14.69}$$

$$\theta_{\max\ 5} = \arctan\frac{5\cdot b + 4\cdot w - p}{\cos\varphi\cdot b} \tag{14.70}$$

$$\theta_{\max\ 5+w} = \arctan\frac{5\cdot b + 5\cdot w - p}{\cos\varphi\cdot b} \tag{14.71}$$

For each scenario of number of fibers hit, the length the particle travels inside each fiber is calculated.

For only one fiber hit, $\theta < \arctan\frac{b-p}{\cos\varphi\cdot b}$, the distance, lr, the particle travels inside the fiber is the same as for geometry 1 and is shown in Figure 14.61 and is calculated in equation (14.53).

For the particle exiting the side of fiber one but not hitting fiber two, $\arctan\frac{b-p}{\cos\varphi\cdot b} < \theta < \arctan\frac{b+w-p}{\cos\varphi\cdot b}$, the distance, lr, the particles travels inside the fiber is shown in Figure 14.67.

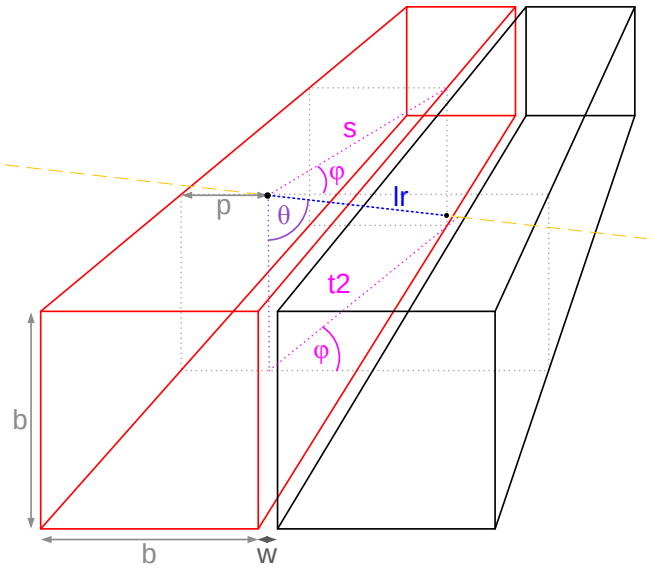

Figure 14.67. Distance lr for the particle exiting between fiber one and two.

lr can be calculated via s:

$$\cos\varphi = \frac{b-p}{s} \quad \Rightarrow \quad s = \frac{b-p}{\cos\varphi} \tag{14.72}$$

$$\cos\left(\frac{\pi}{2}-\theta\right)=\frac{s}{lr} \qquad \Rightarrow$$

$$lr=\frac{s}{\cos\left(\frac{\pi}{2}-\theta\right)} \qquad (14.73)$$

$$=\frac{b-p}{\cos\varphi\cdot\cos\left(\frac{\pi}{2}-\theta\right)}$$

For two fibers hit, $\arctan\frac{b+w-p}{\cos\varphi\cdot b}<\theta<\arctan\frac{2\cdot b+w-p}{\cos\varphi\cdot b}$, the distances, lr and lr2, the particles travel inside each of the fibers is shown in Figure 14.68.

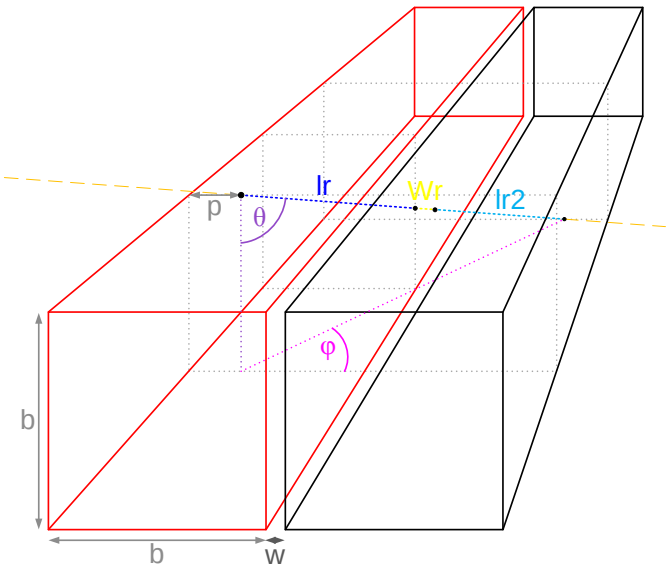

Figure 14.68. lr and lr2 for 2 fibers hit in the simulation.

lr can be calculated as for the particle exiting between fiber one and two equation (14.73).

The distance the particles travels in the inactive area between the fibers, Wr, is needed to calculate lr2 and can be calculated similar to lr:

$$Wr=\frac{W}{\cos\varphi\cdot\cos\left(\frac{\pi}{2}-\theta\right)} \qquad (14.74)$$

lr2 can now be calculated using lr and Wr:

$$\cos\theta=\frac{b}{lr+lr2+Wr} \qquad \Rightarrow$$

$$lr2=\frac{b}{\cos\theta}-lr-Wr \qquad (14.75)$$

The distances the particles travels inside the fibers in the cases where 3, 4, 5 and 6 fibers or the space in between is hit is calculated in a similar fashion.

The effect of the photomultiplier and the filling into a histogram are done as in version 1.

The noise from the MAPMTs and the events where the photoelectrons created inside the MAPMT miss the first dynode but hit the second, are simulated as in version 1; by putting all distances, lrx, for fibers not hit to a low value. But in version 2 this value is 0.006 (0.15 % of the main light), which is the charge measured in none hit channels in a real MAPMT [75](used with permission). Also a crosstalk term is introduced. The 4 MAPMT channels surrounding the main channel will see a little of the light of the main channel. The crosstalk amount have been measured with a pulsed LED to 0.96 %, 0.73 %, 1.00 % and 0.77 % of the main light (for around 4 PE)[75] (used with permission). To take this into account every lrx is multiplied, in turn, with the 4 percentages. The 4 results correspond to the light the MAPMT will see in the neighboring channels and the effects of the MAPMT are simulated by a Poisson and a Gaussian distribution, as for the main light. Finally the crosstalk values are added to the main histogram.

14.7.3.5. Results for simulation version 2

The histogram from the simulated values was fitted with *Cosmic.C* as for geometry 1. The histogram and fit are shown in Figure 14.69.

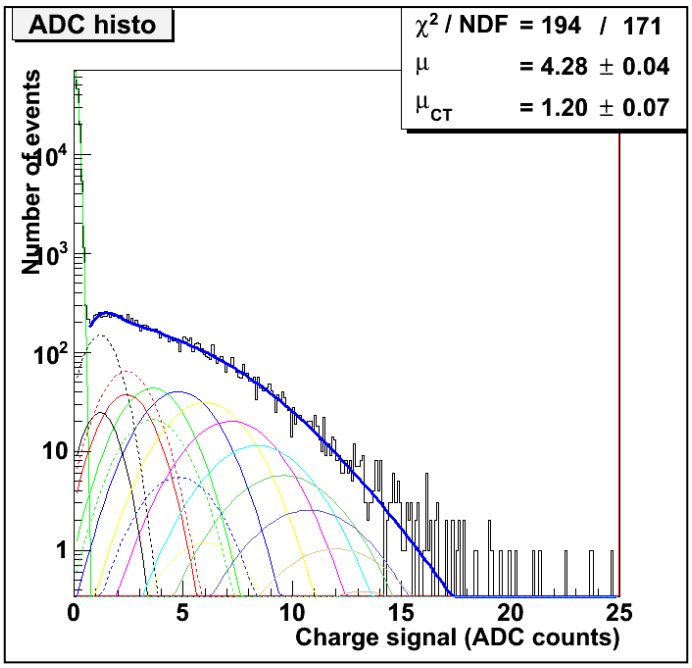

Figure 14.69. Histogram from simulation version 2 fitted with equation (14.20).

The fit was done with equation (14.20). The results from the fit are a main light yield of 4.28 ± 0.04 PE and a "crosstalk" term of 1.20 ± 0.07 PE. The absolute values themselves have no direct physical meaning as they just scale with the inputted "width of fiber in PE", b, in the simulation. But the ratio between the main and the "crosstalk" term can be compared to real data. The ratio is:

$$Crosstalk_{\text{Simulated cosmic 2}} = \frac{\mu_{CT}}{\mu + \mu_{CT}} = \frac{1.20\ PE}{4.28\ PE + 1.20\ PE} = 21.9 \pm 1.2\ \% \qquad (14.76)$$

This is comparable to what was seen in the cosmic data ~20 %. To make a control that this is really a difference between cosmic and beam and not for example an artificial effect from the noise term the simulation was repeated for beam. This was done keeping all parameters at the same value but locking the angle θ to zero, as it would be in a beam. The result for the control beam simulation is shown in Figure 14.70.

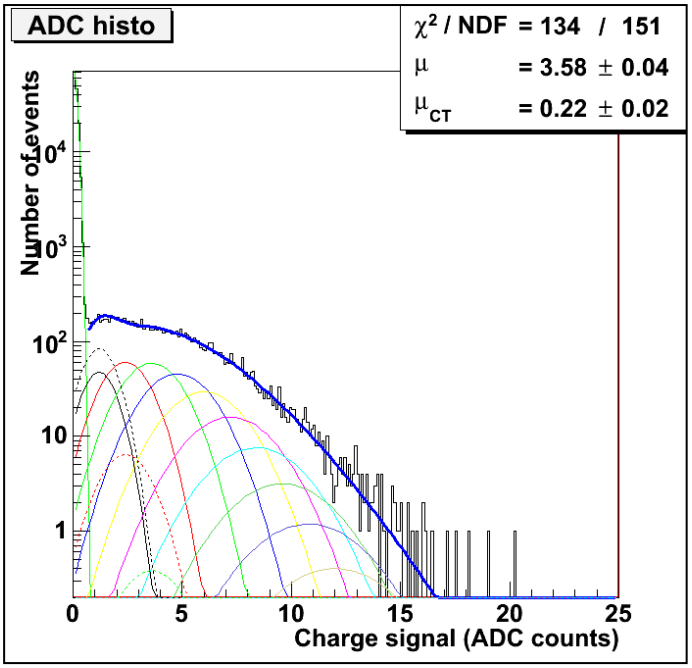

Figure 14.70. Simulation for beam with the same settings as for the cosmic simulation.

The results from the fit are a main light yield of 3.58 ± 0.04 PE and a "crosstalk" term of 0.22 ± 0.02 PE. The ratio of crosstalk over main light yield is therefore:

$$Crosstalk_{\text{Simulated beam 2}} = \frac{\mu_{CT}}{\mu + \mu_{CT}} = \frac{0.22\ PE}{3.58\ PE + 0.22\ PE} = 5.8 \pm 0.6\ \% \qquad (14.77)$$

This is very close to the beam simulation results in version 1, as it should be. 5.8 % is a bit higher than the results from the beam test in 2005. Some of the difference might be explained by different fitting methods: In the 2005 fit a extra fit parameter was added to allow for an independent normalization of the pedestal peak, because not every fiber was hit in each recorded beam event [68](section 3.2). In the cosmic fits no such parameter was introduced, but the fit was started after the pedestal as described in Section 14.3.6.

The more realistic version 2 once more shows a significant difference between cosmic and beam "crosstalk" light yield. The differences to version 1 are small.

The cosmic have a higher main light yield term because the particles on average will always travel longer through the fiber when they are not hitting the fiber perpendicularly. The effect seems to be larger than the first approximation of 10 % made in Section 14.4.13:

$$\text{average higher light yeild} = \frac{\mu_{\text{cosmic}}}{\mu_{\text{beam}}} = \frac{4.28\ PE}{3.58\ PE} = 1.20 \pm 0.02 \qquad (14.78)$$

In the simulation there is an average of 20 % more light in the fibers due to the longer average path travelled inside the fiber compared to a perpendicular beam. The approximation made in Section 14.4.13 and the simulation is in fact not directly comparable: The approximation in Section 14.4.13 finds the average angle and then the length through the fiber at that angle. But since the pass length through the fiber does not grow linearly with the angle this cannot be directly compared to the average light yield.

As the "crosstalk" term for cosmic are more a term of light in secondary fibers, it could augured to add the crosstalk term to the main light yield to get a more realistic overall light yield.

15. Cosmic setup with Orsay test board readout

15.1. Motivation

The cosmic test aims at testing as many aspect of the equipment as possible before moving to a test beam or installation. By making a cosmic test the parts have been in real use and problems can be found and dealt with without missing beam time or installation opportunities. As the timescale for correcting problems is also much larger if the problems are found already on the cosmic test, more time demanding and better solutions can also incorporated.

In particular the ALFA detectors need to be tested after they are assembled. Fibers can be broken or cut badly which would give either no light or a low light yield. To find errors in production and to know which fibers are bad a test of the light yield of all fibers are needed. This could be done in a test beam, but since it is important to find and correct production errors fast and it is unrealistic to have a test beam each time a new detector is produced, a cosmic test of all ALFA detectors was planed.

The setup described in Section 14 can only readout one MAPMT and thereby one layer of an AFLA detector (see Section 13.1). To get sufficient statistics with cosmics takes about 2-3 weeks. If all 20 main detector layers + the 3 overlap detector layers had to be tested one by one it would therefore take about 1 year/detector. This is clearly not an option with 8 detectors + 2 spares to test.

The best option would be to use the final readout system that will also be used after everything is installed. This would also be a check of everything from the particle is detected to it is reconstructed by the analysis software. Unfortunately the motherboard version 4 was still under development and was only expected fully ready shortly before the detectors had to be installed. Therefore this option was not possible.

In the 2008 test beam, two test boards developed in Orsay for testing PMFs had been used for readout (taking over for the motherboard version 3 that proofed to have a lot of problems). Each board was able to read out 5 PMF (see Section 13.2.1 about PMFs) and had proved to run reliably. They had some frequency limitations (maximum about 120 Hz), but for a cosmic this would not be a problem. Therefore it was decided to use 5 Orsay test boards, OB, for a cosmic setup for testing of the detectors.

15.2. Preparation of the setup

The board design for the OBs was updated a little and the PCB ordered. The boards were then assembled at CERN PCB assembly workshop.

15.2.1. The Orsay test board

Figure 15.1 shows one of the OBs in real size.

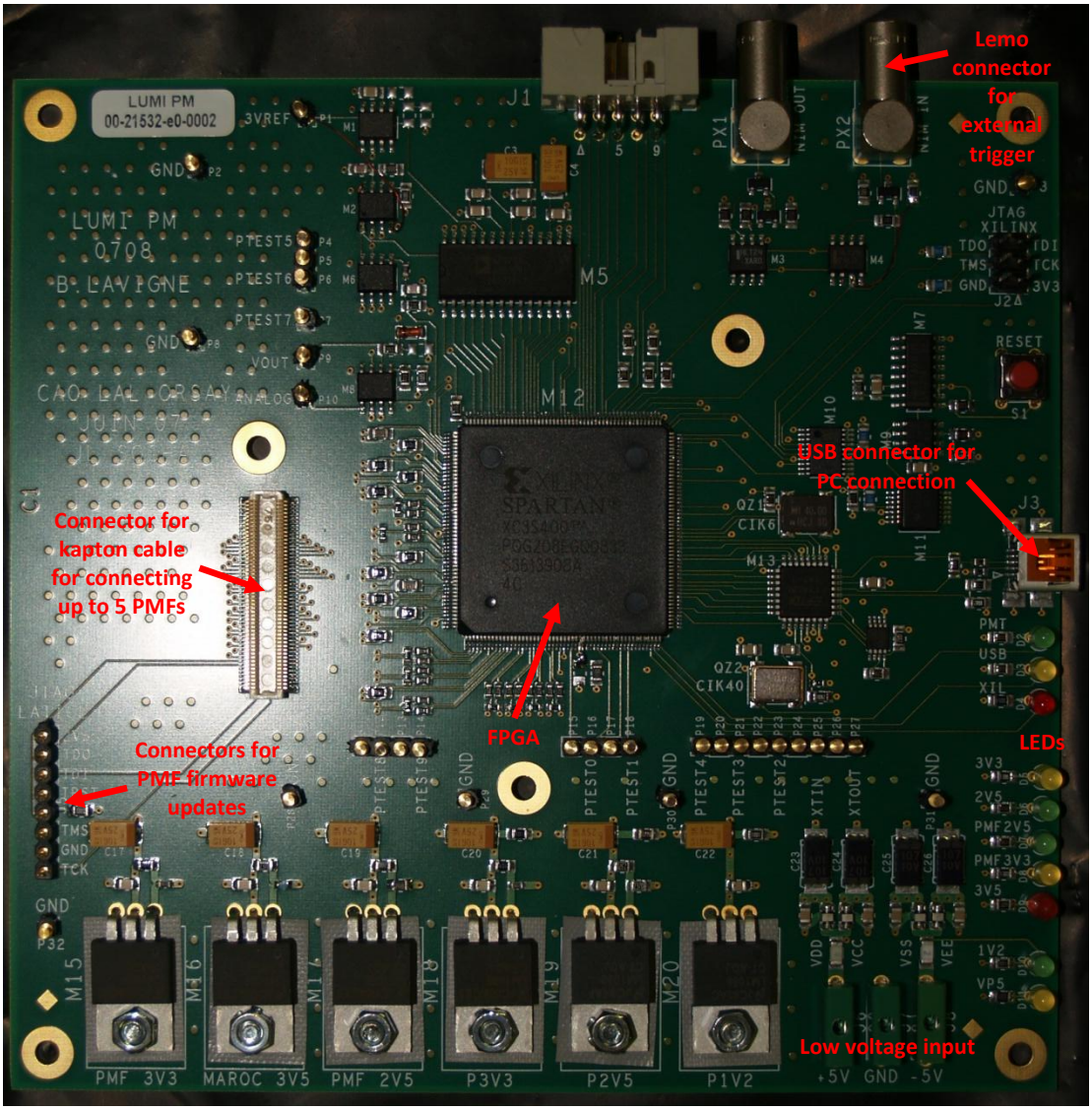

Figure 15.1. Orsay test board in real size.

The key component is a FPGA of type Xilinx SPARTAN-3 XC3S400.

The OBs is powered by + 5 V and – 5 V. The + 5 V is also used for the connected PMFs. The OB has internal voltage dividers and a series of LEDs indicate that all voltages are within limits.

The readout of the board can be triggered externally with a NIM signal. The OBs are read out by a Windows based computer connected via a USB connection.

The firmware of the connected PMFs can be updated by a lattice cable connection. The up to 5 PMFs themselves are connected via a kapton cable to a connector central on the board. The PMFs are powered through these kapton cables and the signals travels through other wires in the same kapton cable (see Section 13.2 for details).

15.2.2. Support for the Orsay test boards

When the 5 kapton cables are connected to the 23 PMFs in the black box, the kapton cables will be parallel and close together. To connect all 5 kapton cables to 5 OB therefore takes some kind of stacking of the OBs because the kapton cables have a limited length and can only be bent in one direction. The author therefore designed support for the 5 OBs. The idea sketch is shown in Figure 15.2.

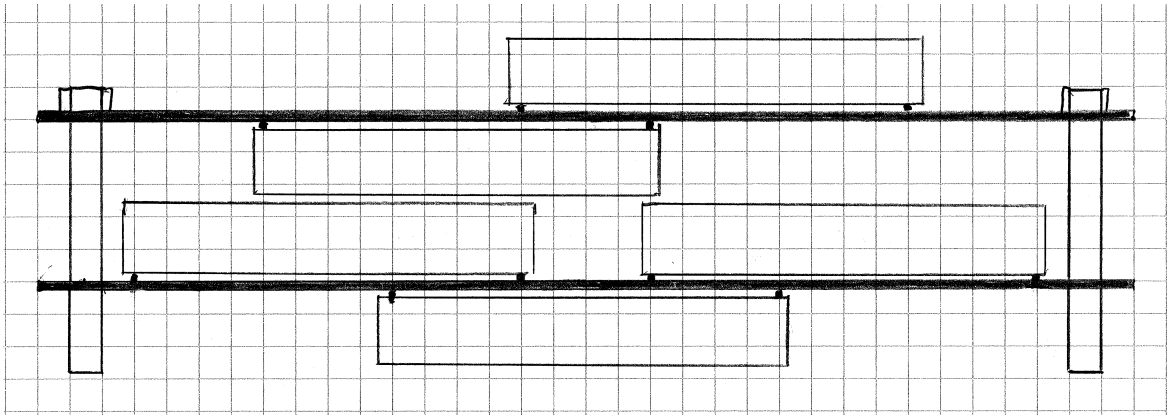

Figure 15.2. Sketch of the support for the 5 Orsay boards.

The handmade technical drawings are included as Appendix L. The support was designed to allow easy access to all connectors on all OBs. Therefore the upper aluminum support plate has a hole in it for easy access to the OB hanging under it and the top support plate can be lifted off (due to the segmented brass spacers) to allow access to the top OB on the lower support plate. The lowest OB is on the drawing supported on the lower aluminum support plate, but can as well be standing on its own. The latter allows easy access to the lowest OB possible by lifting the two support plates.

As the design was composed of relatively simple pieces and with standard tolerances the author made them himself as shown in Figure 15.3.

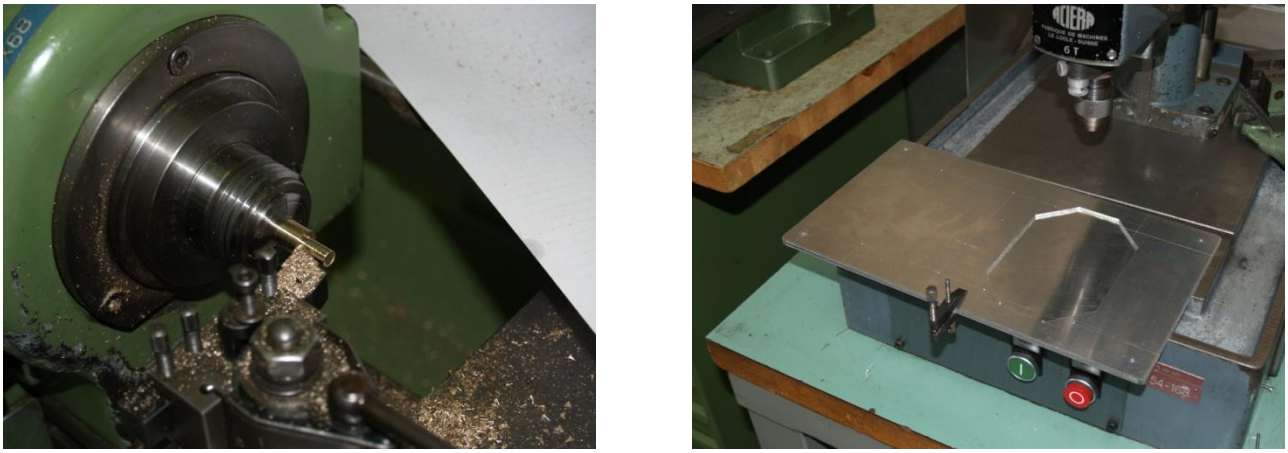

Figure 15.3. *LEFT*: One of the brass spacer being made on a lathe. *RIGHT*: Holes being drilled in the aluminum plates.

The support with 5 OBs installed is shown in Figure 15.4.

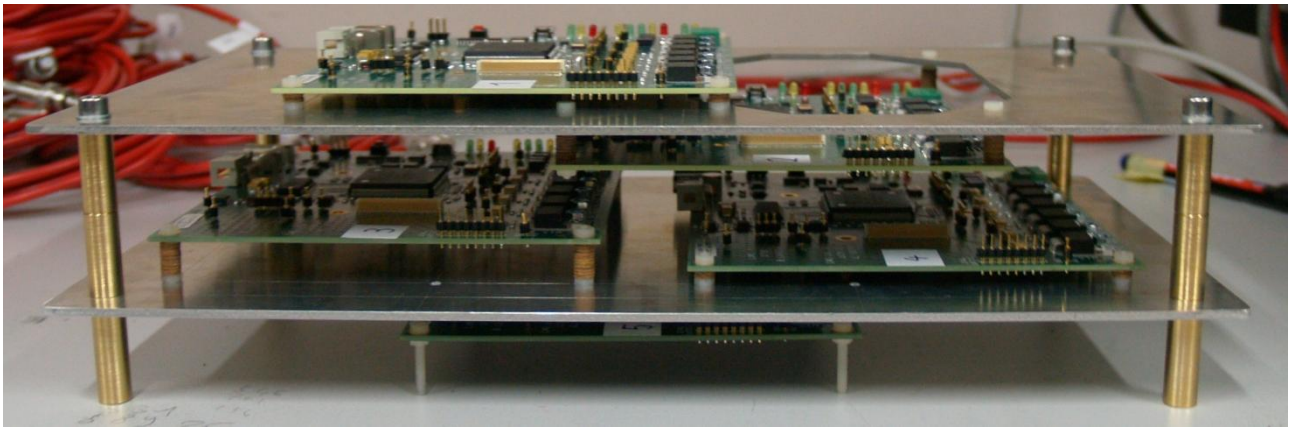

Figure 15.4. The support with 5 OBs installed.

15.2.3. Cooling for the setup

In the final installation the mu-metal grid frame is covered with a black box to keep light out. Through the box is a high air flow to keep the temperature down (see Section 13.5). The PMFs total power comsomtion is of the order of 60 W. So also for the cosmic setup cooling is needed, but as the cooling was not available and anyway would be complicated to fit into the dark chamber, a different solution was adopted.

3 fans of 12 cm were added for the overall setup and a 8 cm fan for the OBs. The cooling is shown in Figure 15.5

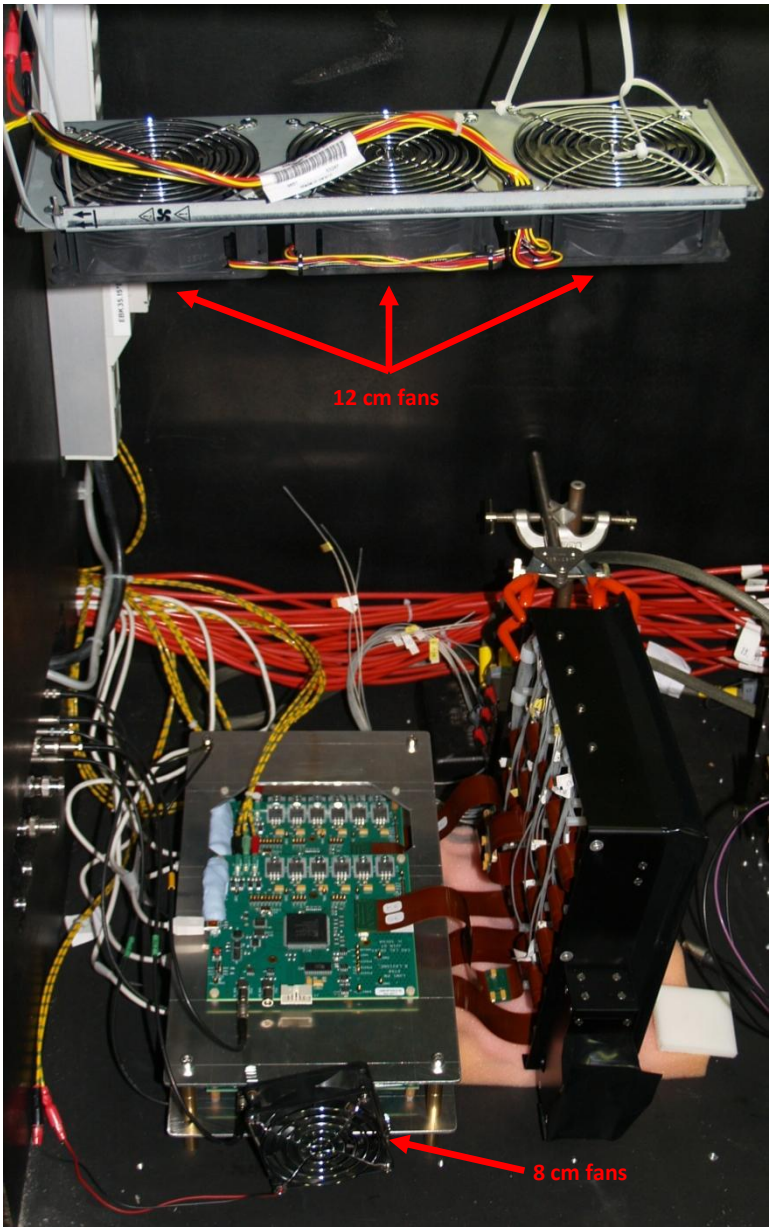

Figure 15.5. Cooling for the setup.

With these fans installed the electronics were kept at a suitable temperature.

15.2.4. Low and high voltage

For low voltage - 5 V, 0 V and + 5 V was needed. This was provided by two standard laboratory PSUs (TTi TSX1820p). A custom cable was made to connect the PSUs and the OBs.

The custom made ALFA high voltage PSUs (see Section13.2.5) were unavailable because they were being used for testing the motherboard. Therefore a standard HV multichannel PSU was used (CAEN SY 527 mainframe + CAEN A732N + CAEN A734N). The CAEN PSU used standard MHV connectors and not the Redel connectors used for the ALFA HV. Fortunately 2 patch boxes had already been made (The patch boxes were originally made for testing high voltage).

Figure 15.6 shows the low and high voltages connectors.

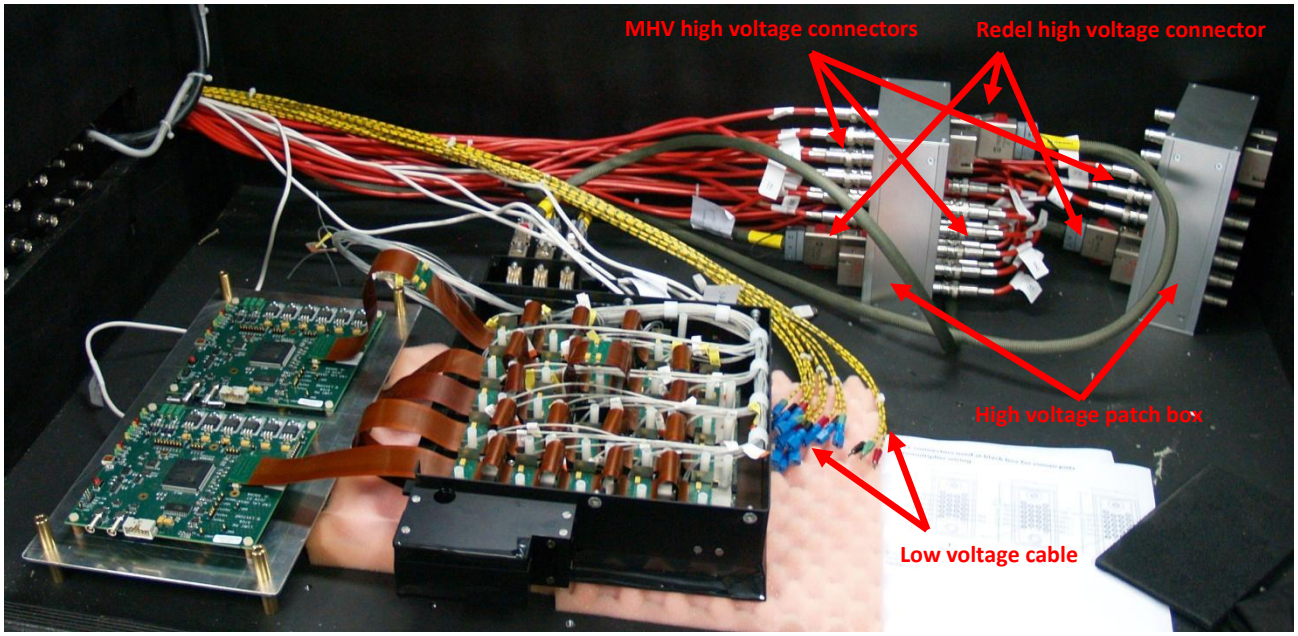

Figure 15.6. The low- and high voltage connectors and the high voltage patch boxes.

15.2.5. Setup for hardware and software testing

To verify the newly produced boards and the software the key persons from Orsay (Bernard Lavigne (Designer of the OBs), Pierre Barrillo (PMF expert), Chafik Cheikali (Maker of the OB software)) came to CERN.

First the boards were tested for production errors. Miner errors were found on two of them. The two OBs were handed back to the CERN PCB assembly workshop and the errors were corrected.

To test the software a basic setup was made. The setup is shown in Figure 15.7.

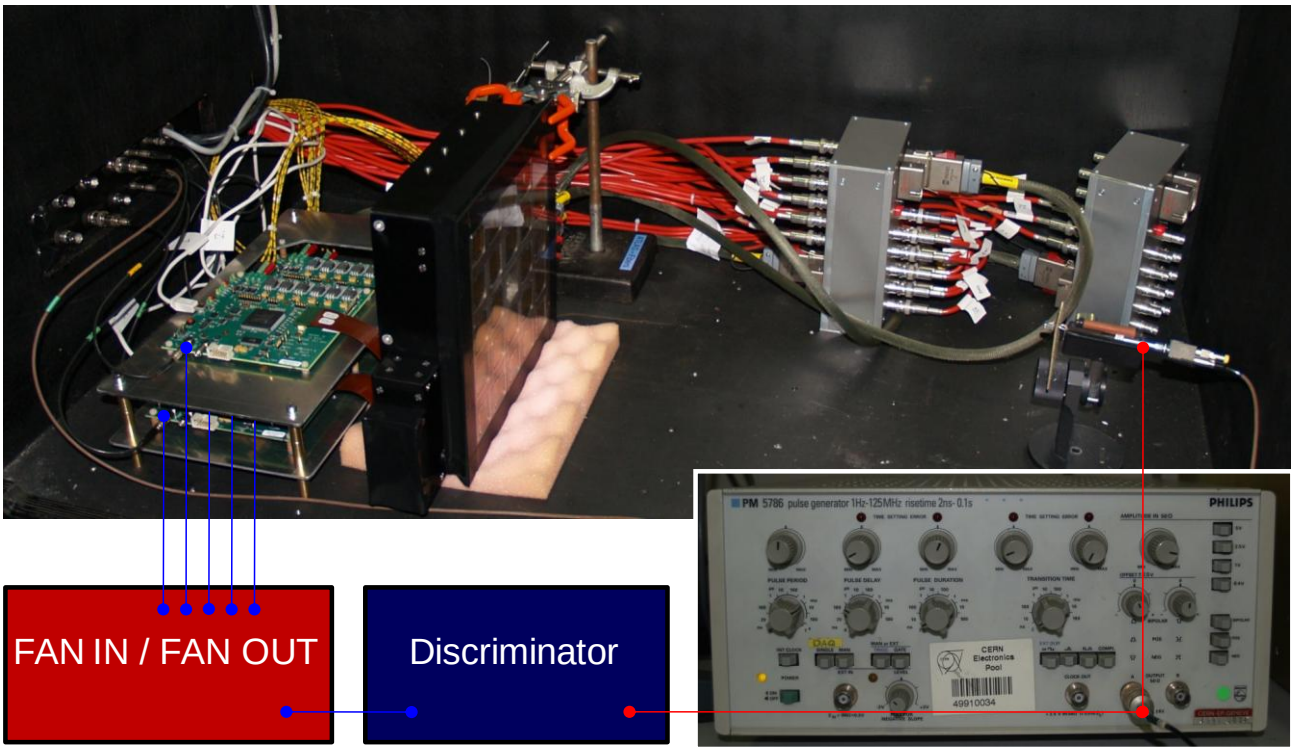

Figure 15.7. The basic setup for testing the software for the OBs. The figure is original presented at an ALFA meeting in DESY Zeuthen 7th May 2009.

A pulse generator lights a LED and sends a signal to a discriminator. The discriminator sends out a NIM signal to a FAN IN/FAN OUT to multiply the signal into 5. Each of the 5 OBs receives a signal and trigger a readout. All MAPMTs are read out via PMFs and the data stored on a computer. (A similar setup was later used to calibrate the MAPMTs. See Section 16.3.1 for a more detailed description of the setup).

The pulse generator was adjusted so the LED sends out a lot of light to be sure to get some signal even if some settings were far from optimal.

A few runs were made with the setup. Some of the runs give meaningful result in the form of number of hits vs triggers in each MAPMT channel in the online software as shown in Figure 15.8.

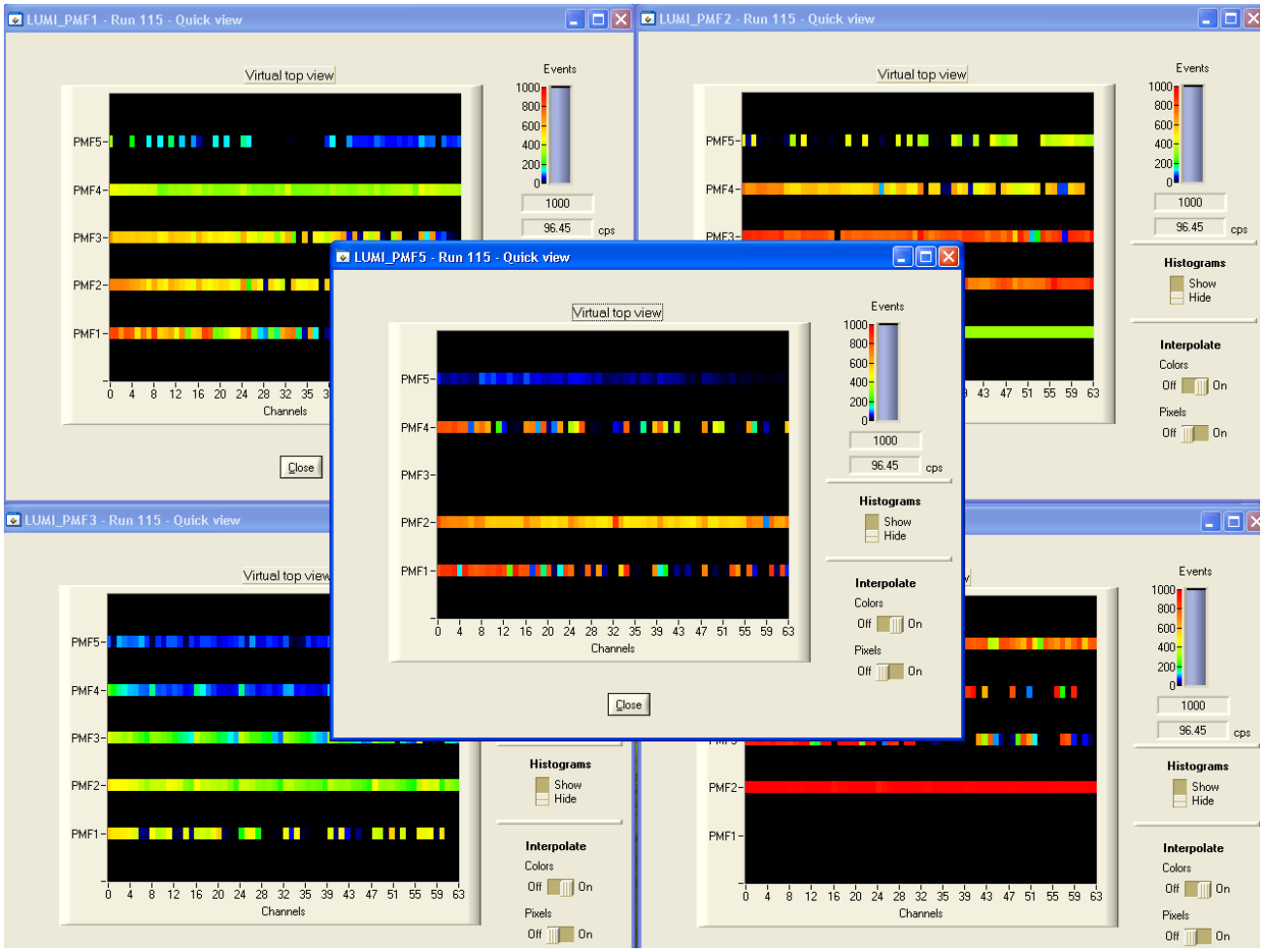

Figure 15.8. Screenshot from the PC controlling the 5 OBs. Each row represents a MAPMT. Each point in the row is a MAPMT channel.

However a high fraction of the runs failed after some time.

This turn out to be a software problem. The software was originally made to run only one board and had later been scaled to use in the cosmic setup. But some counting was not split up correctly and let to the failures. Chafik Cheikali (Orsay) corrected the problems (over some weeks) and a new software version was developed.

With the new software and a new computer to remove any failures from lack of computer resources the setup ran reasonably stable.

15.2.6. Debugging the setup

From the point of view of the OBs hardware and software the setup now seemed to work. But it turned out that a lot of things still had to be corrected before the setup was useful for physical testing.

15.2.6.1. LEDs on Orsay boards

The OBs were originally made for testing PMFs (without MAPMTs). For this there is no need to work in darkness. Therefore 10 LEDs were placed on the board to indicate correct voltages present etc. But since the OBs had to be inside the black box, due to the limited length and flexibility of the kapton cables, the light from the LEDs would detected by the MAPMTs. The LED can be seen in the lower right side of Figure 15.1 page 156.

First it was tied to cover the LEDs with black tape, but that solution was not light tight enough.

In the end a low-tech solution found: A bubblegum like product that could make a tight seal at the uneven surface of the PCB. The solution is shown in Figure 15.9.

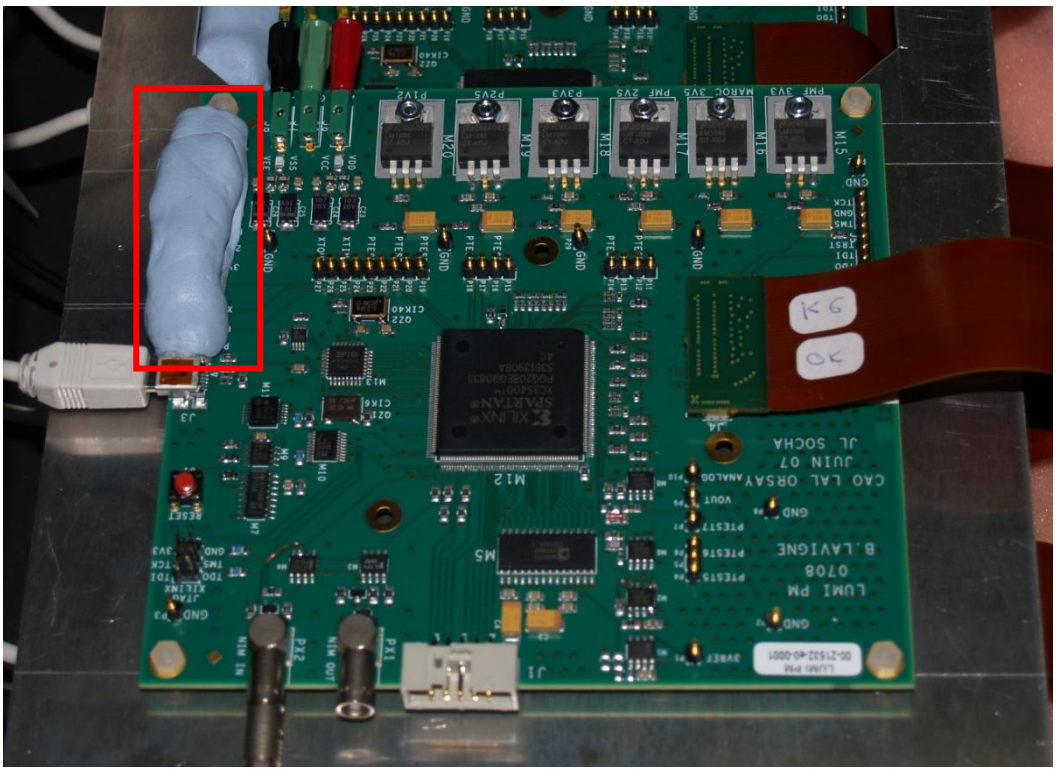

Figure 15.9. The OB with the LEDs covered with a bubblegum like product.

Also the back of the PCB had to be covered because the LED was so intense that light propagated though the PCB.

15.2.6.2. Plexiglas spacers

When installed on a detector the fiber connectors will push back the MAPMT/PMF, which is just held in place by springs. But before installation nothing kept the MAPMT inside the mu-metal grid frame. Therefore a clear Plexiglas plate was placed in front of the MAPMTs. But it turned out that the HV-board in some cases hit the mu-metal grid frame and thereby short-circuit the high voltage. Another problem with the same origin was that the MAPMT/PMF lost contact because they were not pushed together. To take care of these problems 4mm*29mm*29mm Plexiglas pieces were installed between the Plexiglas plate and the MAPMT as a substitute for the fiber connector. This cured the problems. But the solution was not perfect. The light now had to go through two layers of Plexiglas with unknown reflections before arriving at the MAPMT windows. So this alone would make the light uneven over the MAPMTs. However for analog readout it did not matter too much as long all channels received about the same amount of light. But for testing of the binary output it could be a serious problem. More about this in Section 16.3.1.1. Figure 15.10 shows the Plexiglas installed in front of the MAPMTs.

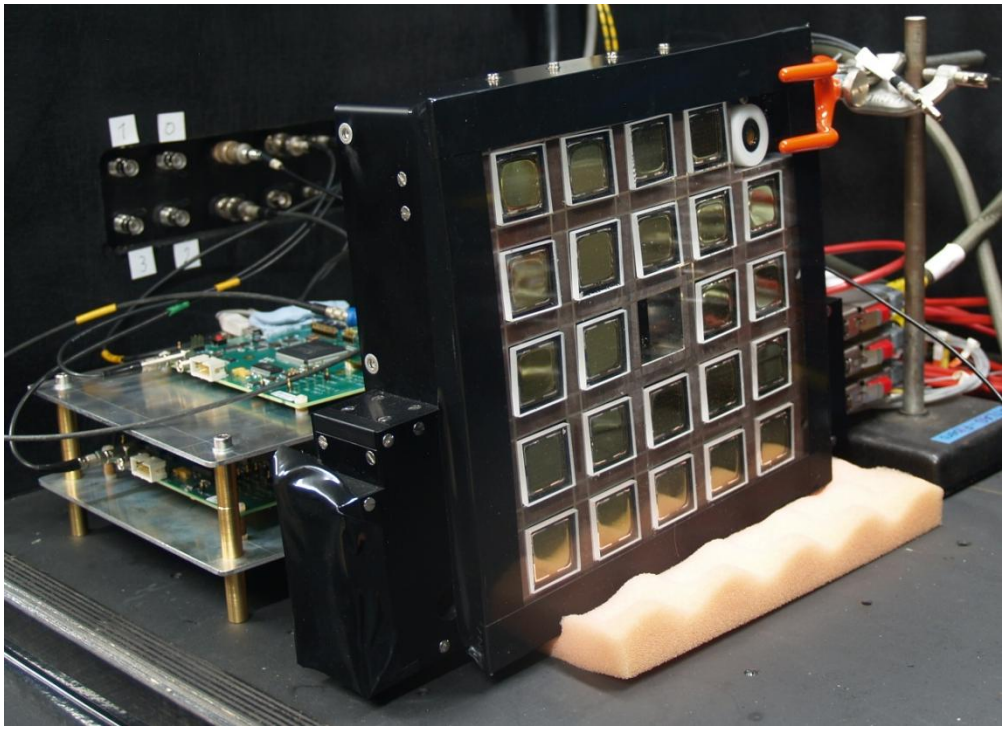

Figure 15.10. Mu-metal grid frame with a Plexiglas plate in front. Between the Plexiglas plate and the MAPMTs are smaller pieces of Plexiglas to add space before the MAPMT.

The problem that the MAPMTs can fall out of the mu-metal grid frame was corrected on the final mu-metal grid frame by adding an edge inside the mu-metal grid frame. Additionally the MAPMTs shims were corrected so the shims will be pressed against the edge inside the mu-metal grid frame in a distance so the HV-board will not hit the mu-metal grid frame.

15.2.6.3. Mapping problems

A number of tests were now made with the setup and it was tried to make a first equal gain calibration (calibrations are discussed in Section 16.3.1 page 183). The calculated gain factors were applied but the gain did not get equalized.

A number of tests were made to investigate the problem. One that proved useful was the loading of the maximum gain 63 to one channel and keeping the rest at gain 16. This made even very small signals to be over the threshold on the channels with gain 63. By adjusting the threshold the channels with gain 63 fired almost on every trigger (amplified noise) but the rest only fired on a small fraction of the triggers. In this way the mapping of the gain corrections could be checked.

Directly on the online software (screenshot Figure 15.8 page 161) it could be observed that the channel with the high gain factor loaded did not correspond to the channel that fired very often. A mapping mismatch was found.

It was quite surprising that the mapping mismatch had not been discovered before as 2 OBs had been used, among other things, in the test beam in 2008. But due the many other problems in the test beam, the equal gain option had not really been used.

The online monitoring results were found also in the stored data. But this did not tell whether it was the gain tables mapping, the mapping of the results or both that were wrong.

To identify the mapping error the following setup was made. One MAPMT was removed from the mu-metal grid frame and mounted in an aluminum support structure for connection to one empty fiber connector. The MAPMT was still connected to a PMF and read out by an OB.

The fiber connector made a grid of holes in the position of each MAPMT channel. Light from a pulsed LED was connected via a light guide to only one of the holes (using the previously discussed author made tool, Section 14.2.6 and shown in Figure 14.6 page 91).

The setup is shown in Figure 15.11.

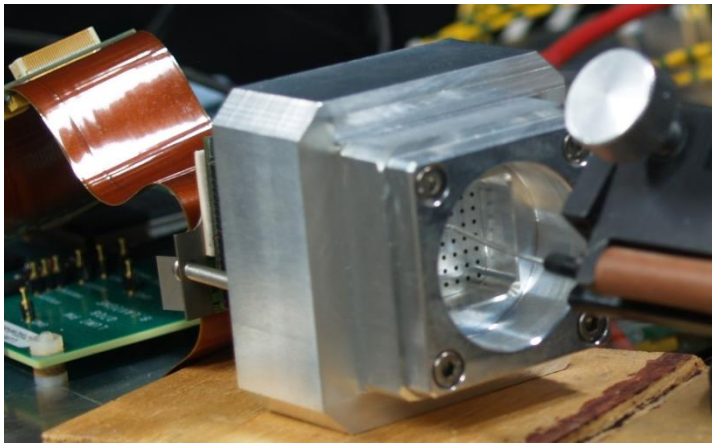

Figure 15.11. The setup for determining the correct mapping.

A few runs were made with light at different positions and the correct mapping noted.

The mapping results were sent to Chafik Cheikali (Orsay) (who made the OB software) and Matthieu Heller (PhD student at Laboratoire de l'Accelerateur Lineaire), MH, (who has done the mapping for most of the ALFA test beams). From the few correctly mapped channels from the measurements they were able to find the mapping errors in the software and make a new version. The new software was tested the same fashion and proved to have the correct mapping.

15.3. Optimization of the setup

To get the setup discussed in Section 15.2.5 to work a very high light level from the LED was used. This was necessary because the setup was not optimized yet. The optimization of the readout of the slow shaper and the threshold in the MAROC chip on the PMF is discussed in the following sub-sections.

15.3.1. Optimization of the Q-delay

The slow shaper received the charge from the amplifier in the PMF. Simplified, the charge is built up on a capacitor. To a given time the capacitor is discharged into an ADC (See details in Section 13.2.1). But the time at which the charge is released from the capacitor to the ADC is critical. If the charge is transferred too soon not all the charge has been stored in the capacitor. However on the capacitor the charge will degrade over time, so if it is read out to late some of the charge might be lost. The time at which the charge is sent to the ADC is called Q-delay.

To optimize the Q-delay a number of runs were made on the basic setup discussed in Section 15.2.5 (and in detail in Section 16.3.1). The high voltages on the MAPMTs were -900 V. The light level was kept at the same level on the LED and only the Q-delay was changed. The charge spectrums for Q-delay = 0 ns, 37.5 ns and 100 ns is shown in Figure 15.12.

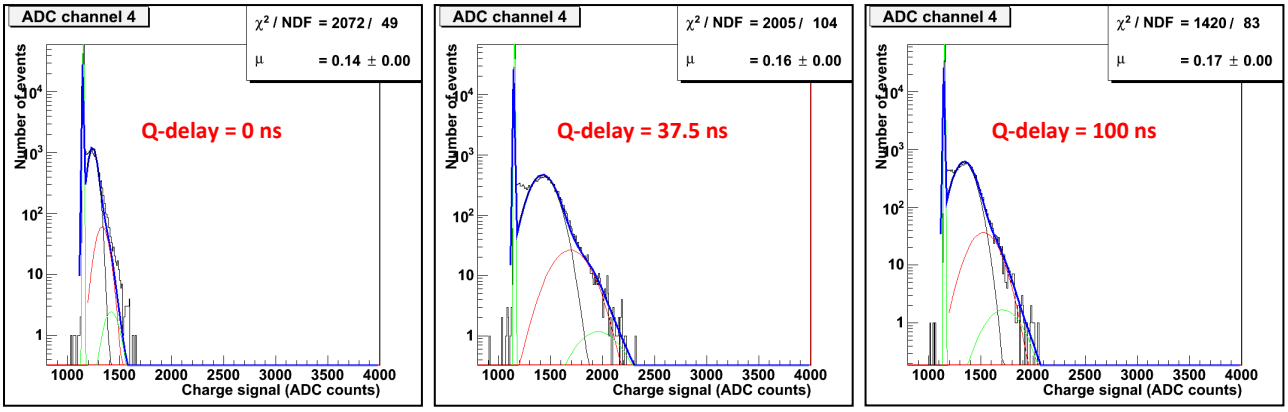

Figure 15.12. Charge spectrums for Q-delay = 0 ns, 37.5 ns and 100 ns.

It is clearly seen that less charge is collected at 0 ns compared to 37.5 ns and that the charge has degraded for 100 ns. The charges spectrums are again fitted with equation (14.3) using macro *Cal1PE.C* (included in Appendix M) (see section 16.3.1.5). As a measure of the charge the position of the 1 PE peak is used. The 1 PE position is plotted vs. the Q-delay in Figure 15.13, which is made in Microsoft Excel.

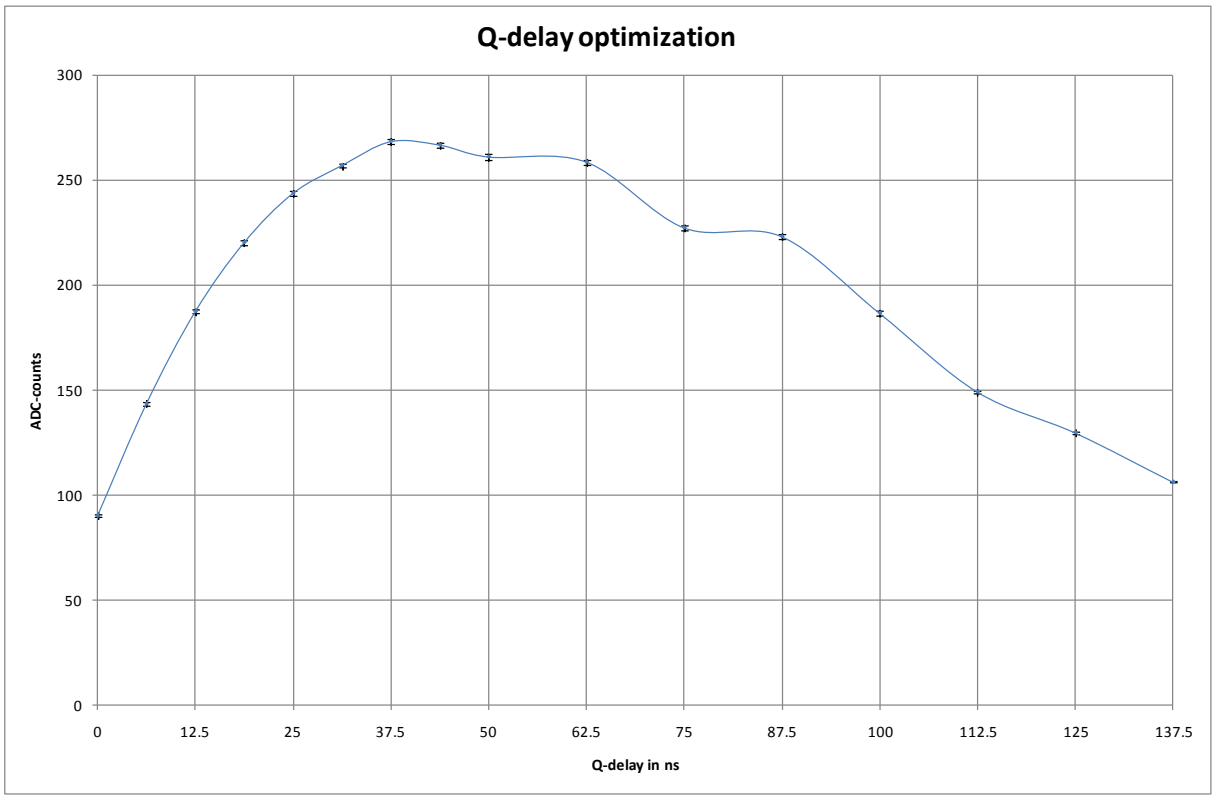

Figure 15.13. Graph of the 1 PE position as a function of the Q-delay.

The peak value is at a Q-delay of 37.5 ns and therefore this was chosen as the Q-delay to use. But the Q-delay curve is rather flat from 25 ns to 62.5 ns, so any value inside this interval could be used. For the cosmic setup discussed in Section 15.5.2 the cables and electronic makes a delay for about 25 ns. To compensate for that a 25 ns lower Q-delay value is used for the cosmic setup.

15.3.2. Optimization of the threshold

For making a meaningful threshold scan the gains of the channels have to be equalized. This was done as described in Section 16.3.1. All the channels should now have the same gain and the threshold should have the same effect on all channels.

To optimize the threshold a number of runs were made on basic setup discussed in Section 15.2.5 (and in detail in Section 16.3.1). The light was kept on a very low level with an average around 0.05 PE. This should insure that (almost) only 1 PEs was seen.

A threshold scan was made by manually setting the threshold to the wanted value and then making a run. 10000 triggers were used for each run.

The digital readout was stored in a binary file (one for each PMF). Built into the software controlling the Orsay test boards is a tool to convert the binary files to text files with 0 or 1 for each trigger and each MAPMT channel. However the build-in converter only convert one files at the time, so for each run it is necessary to convert the data for each PMF manually. Therefore the runs were made with 23 MAPMTs, but only data from one was converted.

To analyze the data a summation of the hits in each channel was made and the rate calculated by dividing by the number of triggers. This was done in Microsoft Excel for all channels and all threshold settings. The rates were then plotted as a function of the threshold. The threshold is defined in DAC (Digital Analog Converter) channels which correspond to a certain voltage (mV range). The plot is shown in Figure 15.14.

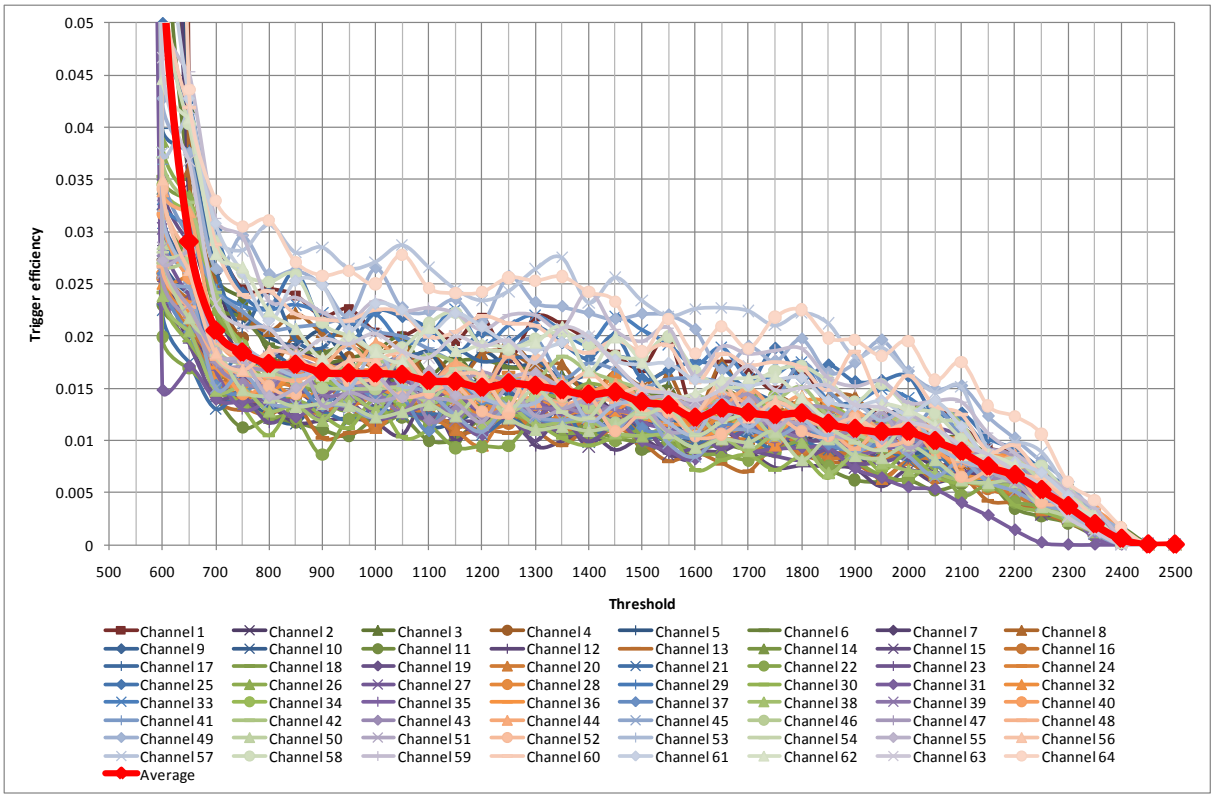

Figure 15.14. S-curve for all channels in one PMF. Light average is about 0.05 PE.

Because of the shape these efficiency plots are called “S-curves”. Below around threshold 700 noise from electronics is dominating. Then there is a plateau from threshold 750 to 2000. There is only s small change in trigger efficiency in this range and the threshold should be selected in this range not to lose any events (even those with only 1 PE) but still be out of the noise from electronics. A threshold of 1000 was selected for use in the cosmic setup.

15.4. Gain equalization and calibration

The gains of all the MAPMTs channels were equalized as described in Section 16.3.1. A final run was made to make sure that all the gains were equalized sufficiently. This proved to be the case (as seen in Section 16.3.1.6). The position of the pedestal, the width of the pedestal, the position of the 1 PE and the width of the 1 PE were saved for all channels. These are needed for correct fitting of the charge spectrums from the fiber light.

15.5. Cosmic test of a full ALFA detector

Apart from a general test of as many as possible of the part that will later be used in a test beam or be installed, the cosmic setup characterizes light yield of all fibers in the detectors.

15.5.1. Concept of the light yield measurements

The idea about the light yield measurement is very similar to the one described in Section 14.3.6: Use the MAPMT charge spectrum made from the scintillator light from cosmic particles passing a fiber together with pre calibrated 1 PE charge spectrum for each MAPMT channel to determent the average light coming from each fiber. Figure 15.15 shows a MAPMT charge spectrum made from cosmic particles passing a scintillating fiber.

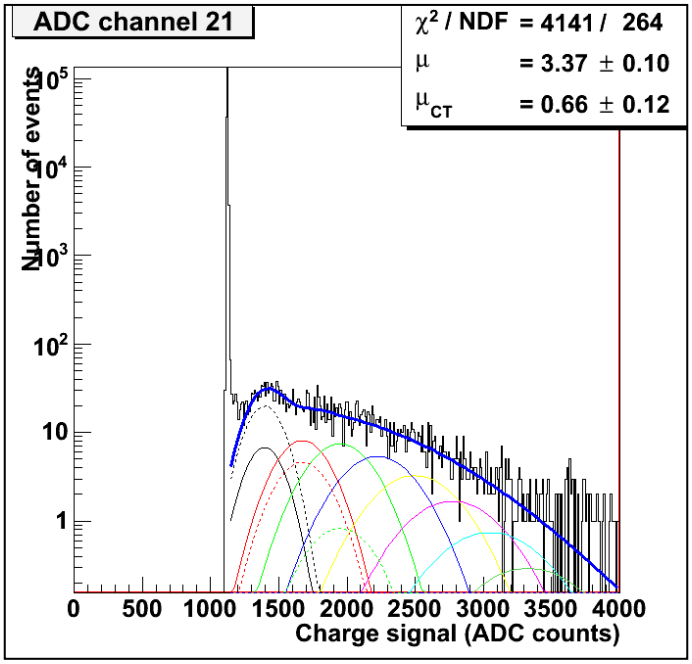

Figure 15.15. MAPMT charge spectrum for one scintillating fiber being passed by cosmic particles.

The MAPMT charge spectrum is fitted with equation (14.20) using the position of the pedestal, the width of the pedestal, the position of the 1 PE and the width of the 1 PE from the calibration of that particular MAPMT channel. The light yield for this particular channel is 3.37 ± 0.10 PE.

15.5.2. Setup for measuring the scintillating fiber light yield with cosmics

A schematic of the setup is shown in Figure 15.16.

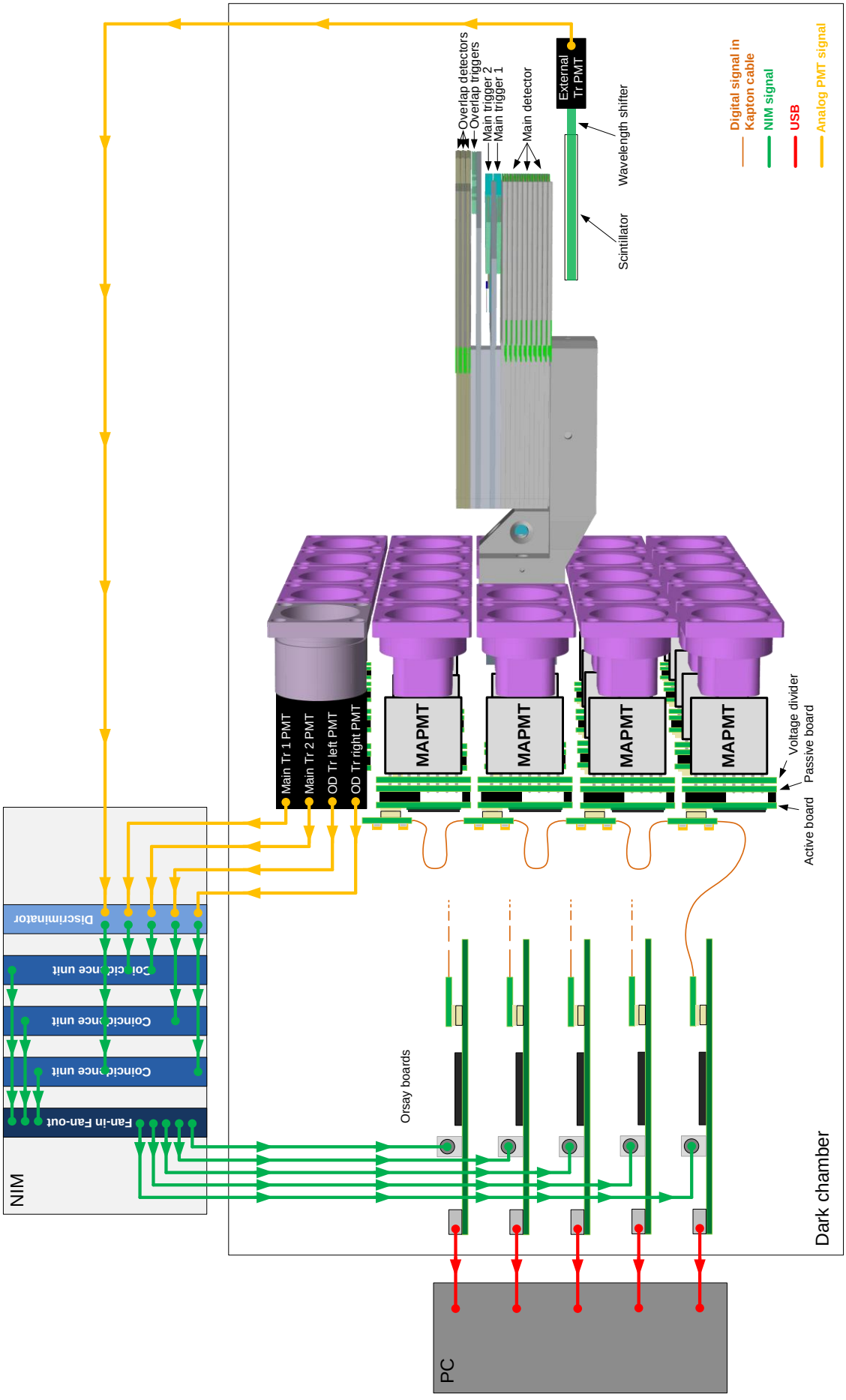

Figure 15.16. The cosmic setup for determining the light yield in the scintillating fibers. The detector part is a modified copy of the AutoCAD drawing made by Andre Beam CERN. On the figure the scintillating fibers are light green, the trigger scintillator tiles are turquoise, the clear fibers are olive green and the fiber connectors are purple. The part of the fiber going from the titanium plate to the fiber connector is left out to make the figure clearer.

A cosmic particle passes through the main area of the detector or one of the overlap detectors. Ultraviolet light is emitted in the fibers the particles passes through. The ultraviolet light is absorbed in the fiber and re-emitted with a longer wavelength (blue) that can propagate through the fiber. The blue light hits the photo-cathode of a MAPMT and some is converted into photoelectrons. The MAPMTs are powered with -900 V through a one-board voltage divider. Next to this is a passive board which sends the charges from the MAPMTs to the active board, where the signal is amplified with a preset gain correcting factor. The signals are then put in analog memory. One after one these are then send through a kapton cable to a Analog-Digital-Converter, ADC, on a Orsay test board. Details about the front end electronic are discussed in Section 13.2.1.

The cosmic particle also passes through the trigger detectors. Either the two main trigger scintillator tiles and the external trigger scintillator tile, or one of the overlap triggers and the external trigger. In the scintillator tiles passed through by the cosmic particle, ultraviolet light is emitted. The ultraviolet light is absorbed in the scintillator tile and reemitted with a longer wavelength (blue) that can propagate through the scintillator tile. For the internal triggers the blue light travels though clear fibers to a PMT and some of the light is converted into photoelectrons. In the much thicker external scintillator tile the blue light is absorbed in a wavelength shifter connected to one side of the scintillator tile. The light is reemitted as green light and travels though the wavelength shifter to a PMT where some of the light is converted into photoelectrons.

The analog signals from the PMTs are sent into discriminators, which sent out NIM signals instead. The NIM signals are sent to a coincidence unit, which send out one NIM signals if the incoming NIM signals are overlapping in time. For the main detector the coincidence is made from both main trigger detectors + the external trigger. For the overlap the coincidence is made from one of the overlap trigger detectors + the external trigger. The NIM signal from the coincidence units are send to a Fan-in Fan-out unit, which sent out 5 identical NIM signals, one to each OB. These NIM signals trigger a readout of all MAPMTs.

When the Orsay boards receive a trigger it reads out the charge, in turn, of all the channels of the up to 5 MAPMTs it has attached. After the charges have been digitalized, the Orsay boards save the data on a Windows based PC connected via USB. The USB connection is also used to set up most parameters (gain, threshold etc) on the Orsay board.

A photo of the setup is shown in Figure 15.17.

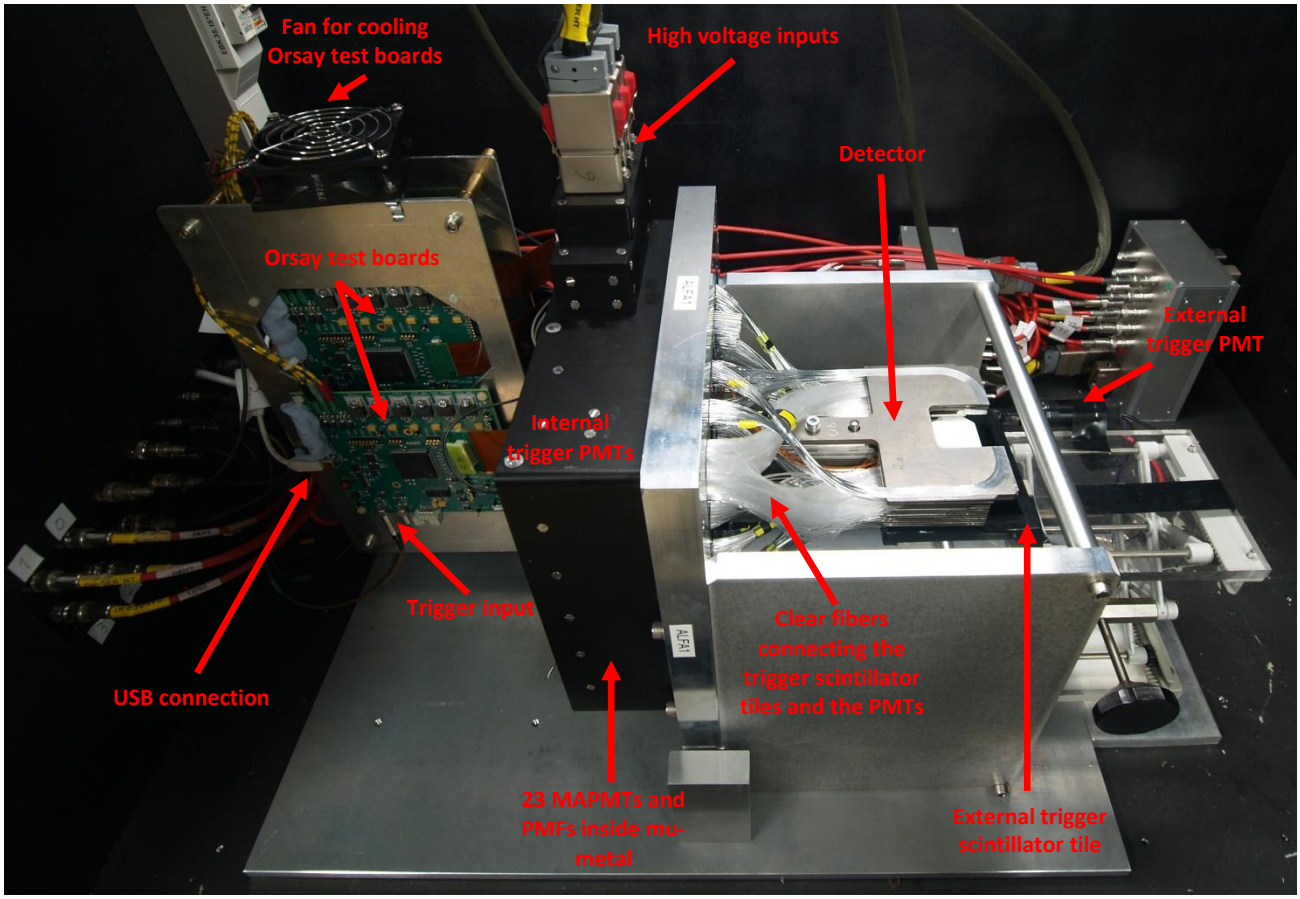

Figure 15.17. The cosmic setup for a full ALFA detector inside a dark chamber.

The support (shown in Figure 15.17) used for the detector, which also supports the 90 degree tilt of the structure for the Orsay boards (discussed in Section 15.2.2) is design by Andre Bream (CERN PH-DT) after idea discussions with the author.

15.5.3. Run with cosmic

For the cosmic run the HV was -950 V on the trigger PMTs and -900 V the MAPMTs. The threshold in the discriminators for triggering, see Figure 15.16 page 168, was set to 30 mV. The delay of the readout, the Q-delay, was set to 12.5 ns, which was 25 ns less than for the calibration to counteract the longer delays as discussed in Section 15.3.1.

The cosmic test went on for about two weeks. The OB was not stable over this time causing a split up of the cosmic test into many runs. In total 178773 triggers was stored. The average rate for the main triggers was 5.76 hit/min, 0.73 hit/min for the left overlap trigger (trigger 3) and 1.04 hit/min for the right overlap trigger (trigger 1). For the overlaps (area ~0.9 cm^2) this is about expected from cosmic (see Section 14.3.4), but for the main trigger (area ~8.3 cm^2) it is a bit too low. This might be because the used triggers PMTs were a lower gain model (Hamamatsu R7400U) rather than the high gain model normally used (Hamamatsu R7400P). This could make some signals too small to extend over the discriminator threshold. The trigger PMTs was replaced before the ALFA1 was installed.

15.5.4. Analysis of cosmic data

As for the calibration runs (Section 16.3.1.5) the data from the Orsay boards are stored as binary data. To do any data processing the data is filled into histograms using a macro called *histCOSMICS.C* (included as

Appendex O) made by MH. The macro makes a folder with the run number. Inside that folder the macro makes a sub-folder for each MAPMT. In the folder for each MAPMT the macro makes a ROOT file containing a histogram for each channel on the MAPMT. These ROOT histograms need to be analyzed as described in Section 14.3.6 with *cosmic.C* in a modified version (see details below in this section) using the calibration files made previously (Section 15.2.4). To analyze all channels on a MAPMT a macro, *AllCH.C* (Appendix N), that just run *cosmic.C* for each MAPMT channel. To analyze all MAPMTs in a mu-metal grid frame (an entire detector) 4 run macros, *Run1.C*, *Run2.C*, *Run3*.C and *Run4.C* (Appendix O), were made. Each runs *AllCH.C* for 5-6 MAPMTs. They are used to spread out the fitting to 4 CPU cores in a very easy way simply by running ROOT 4 times, one per Run-macro. This made the fitting almost 4 times faster and it could still be run on only one PC.

The modifications to *cosmic.C* (Appendix P) were necessary because the binning of the histograms was different. Also some smaller improvements were made. The changes made the fit more reliable and made it fail less. Also the overall fitting time went down.

The analysis gave out the light yield with errors and the "cross talk" (see Section 14.7) light yield with errors in 4 separate files for each MAPMT. In order to achieve faster implementation into Microsoft Excel a C++ macro (run inside ROOT) was made, *Data4.C* (Appendix Q), to combine these 4 files into one for each MAPMT.

15.5.5. Results of the cosmic test on ALFA1

For each layer on the ALFA1 detector a plot was made with the light yield of each channel ordered by fiber numbering. An example from the main layers is shown in Figure 15.18.

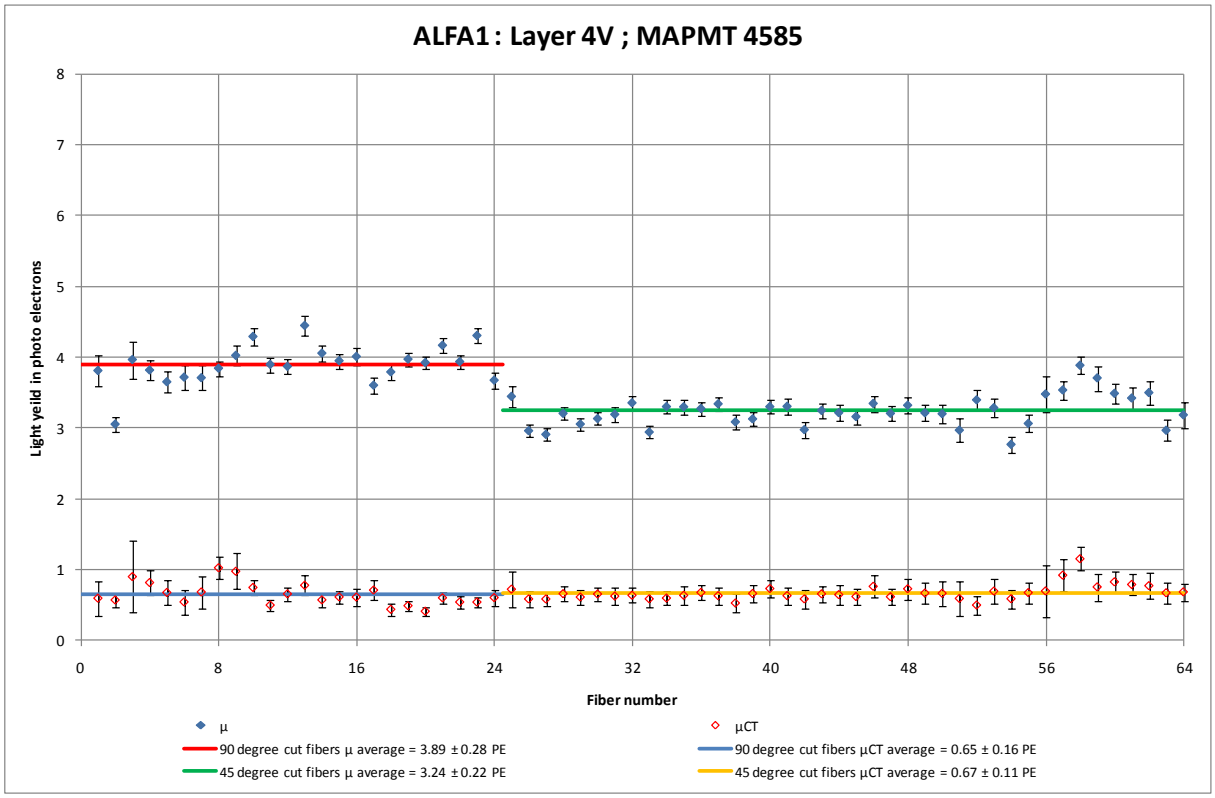

Figure 15.18. Light yield in layer 4V in ALFA1.

The fibers numbered 1-24 are 90 degree cut fibers and have an average light yield of 3.89 ± 0.28 PE. The fibers numbered 25-64 are 45 degree cut fibers and have an average light yield of 3.24 ± 0.22 PE. This means

that the light yield in the 90 degree cut fibers are higher, as expected. The uncertainties go down towards the centre of the detector. This is due to two effects:

1. The external trigger limits the angles of cosmic particles that make a trigger. Because of the angular distribution of the cosmic muons (see Section 14.3.4) the central fibers will have more hits. Therefore the central fibers have more data and the fit will have smaller errors.
2. The triggers only cover a part of the scintillation fibers. For the 45 degree cut fibers these parts become shorter closer to the edge. This is illustrated in Figure 15.19. Therefore these fibers will have fewer hits and thereby less data so the fits will have larger errors.

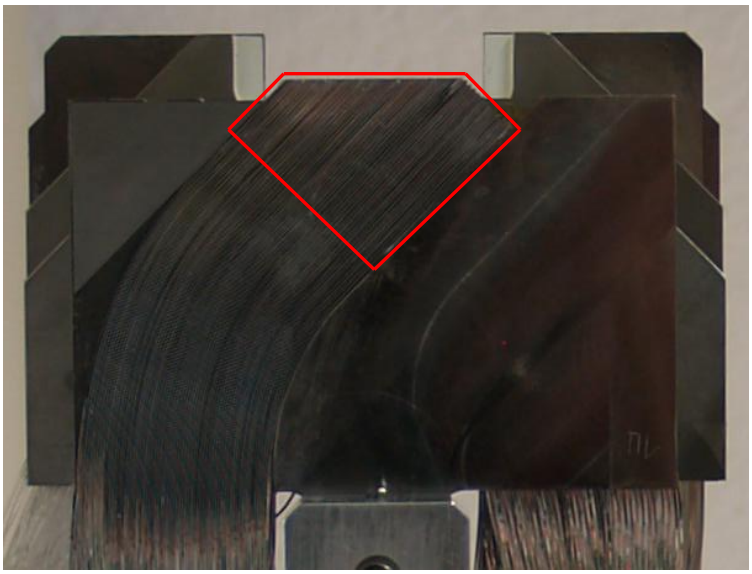

Figure 15.19. The fibers to the left in the photo have a shorter overlap with the trigger. Therefore these fibers have fewer hits and thereby less data, so the fits will have larger errors.

The crosstalk term for the main detector in Figure 15.18 is 0.65 ± 0.16 PE for the 90 degree cut fibers and 0.67 ± 0.11 PE for the 45 degree fibers. As discussed in Section 14.7 the cross talk term for cosmic is dominated by particles hitting more than one fiber and is here in the expected range.

All average light yields measured with cosmic should be normalized by diverting with a factor of about 1.2 before comparison with light yield from a beam, as discussed in Section 14.7 and *[74]*.

An example from the overlap layers are shown in Figure 15.20.

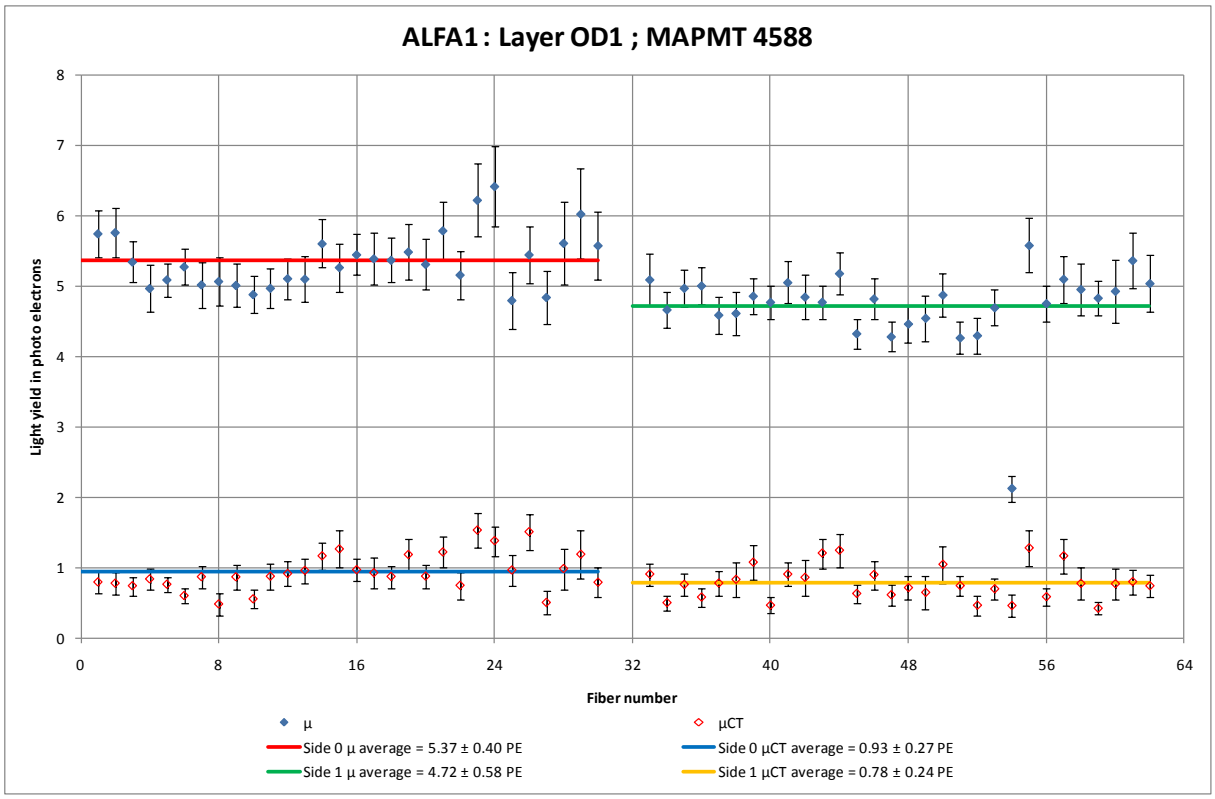

Figure 15.20. Light yield in overlap layer 1 in ALFA1.

The light yield in the in the overlap is about 5 PE which is a bit higher than expected compared to the main layers. The uncertainties are larger compared to the uncertainties in main layers. This is due to only 6 mm of the fibers are covered by the triggers scintillator tiles. Therefore these fibers will have fewer hits and thereby less data so the fits will have larger errors.

The crosstalk term for the overlap detector layer in Figure 15.20 is 0.93 ± 0.27 PE for side 0 and 0.78 ± 0.24 PE for side 1. As discussed in Section 14.7 the cross talk term for cosmic is dominated by particles hitting more than one fiber and is here in the expected range.

All average light yields measured with cosmic should be normalized by diverting with a factor of about 1.2 before comparison with light yield from a beam, as discussed in Section 14.7 and *[74]*.

An overview of the averaged light yield for all layers is shown in Figure 15.21.

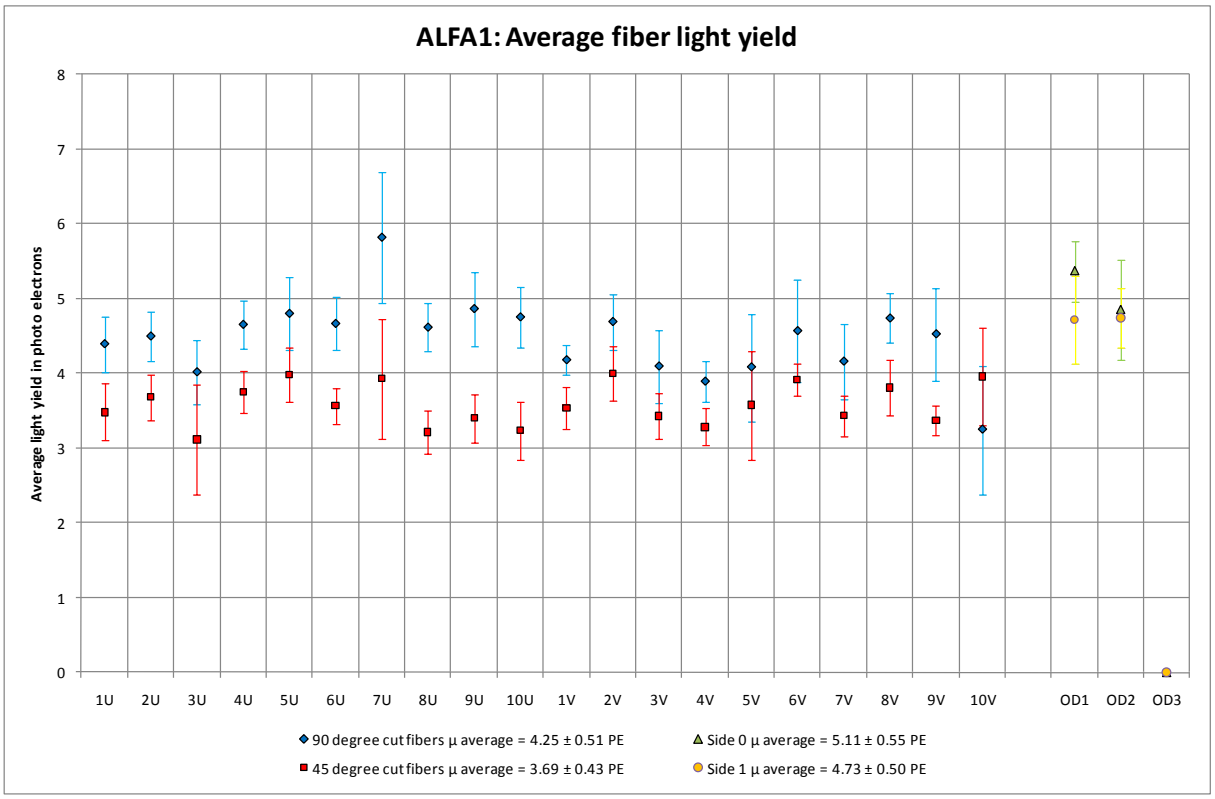

Figure 15.21. Average light yield for all layers in ALFA1. In the tested configuration OD3 was not installed.

There is consistency in the light yields of the fibers with the same cut. The light yields of the main detector are a bit lower than what was hoped, but it is still sufficient to use the detector.

As a quality check of the detector a plot of the number of bad fibers was made. This is shown in Figure 15.22.

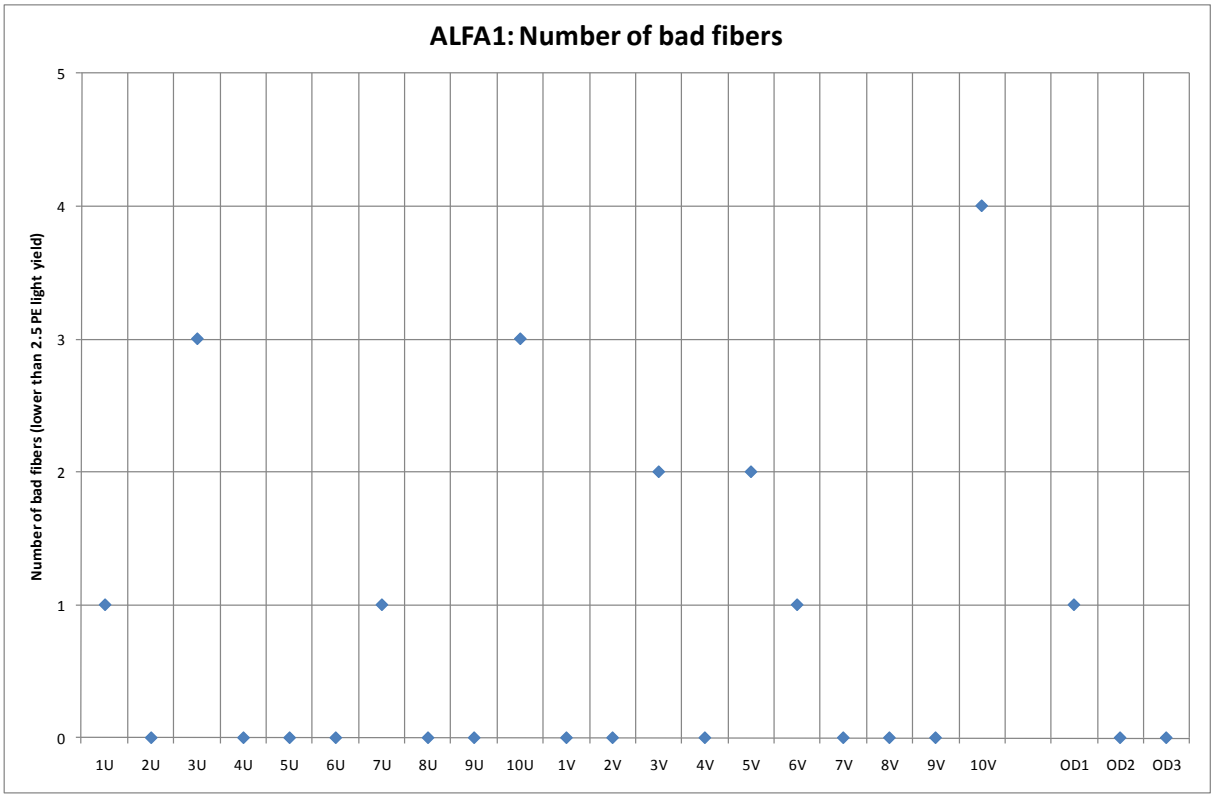

Figure 15.22. Number of bad fibers per layer in ALFA1. A bad fiber is here defined have lower light yield than 2.5 PE.

A bad fiber is here defined ad a fiber with a light yield lower than 2.5 PE. 18 bad fibers out of 1400 fibers is 1.3 % of the channels, which is acceptable. Also none of the layers had very many bad fibers, even though layer 10V is a bit high with 4 bad fibers.

The plots for all layers and a short description of the setup were combined for internal use in ALFA and are Appendix R.

15.6. Cosmic test of prototype overlap detectors

The content of this section has been published as *[50]* which is included as Appendix B.

In August 2009 there was a readiness review of ALFA. One of the issues raised was the possible ageing of scintillation fibers used for the overlap triggers.

The scintillating fibers (Kuraray SCSF-78, S-type (see Section 13.1.1)) have a recommended minimum bending radius of 25 mm [43] for round fibers. A larger minimum bending radius is to be expected on square fibers as the outer corners will have more stress than the outside center on a round fiber. In the ALFA overlap detector layers a radius between 22.5 mm and 30 mm is needed. Therefore there were originally some tests made to investigate the fiber behavior with small bending radius [48]. It concluded that already at bending radius 30 mm there were significant degradation of the light transport performance and under microscope cracks in the fibers could even be seen. Following studies [49] was made to bend the fibers to the needed radius by heating the fibers under the bending. The bent fibers were visually inspected and transmission tests were performed. An optimal temperature of 85 ˚C was found at which the transmission of the fiber did not change over a period of 20 days. This temperature was later used to bend the fibers for 2·2 layer prototype. The prototype was tested with a strontium-90 source and later in the ALFA test beam October 2006. All tests indicated performance comparable to that of un-bent fibers.

The stability of the performance of the bent scintillating fibers have been proven for a period of the order of a month, but the ALFA detectors will be used for many years. In order to verify that there are no ageing effects for the bent fibers a long term test of the performance was needed.

15.6.1. Method to verify performance

Back in 2006 a number of test were done to verify the performance of the prototype overlap detector [49]. At that time there was no analog readout available for all fibers (all MAPMT channels). The light yield in the scintillating fibers hit by electrons from a strontium source was estimated on a few fibers with readout directly on an oscilloscope. However the method was only valid for cross checking with other fibers and not for the absolute light yield.

At the test beam in October 2006 the readout was of all channels, but only binary: Over or under a threshold. Here it was verified that all fibers gave enough light to make the MAPMT give a signal over threshold.

This test could off cause be repeated, but the fibers could potentially have suffered from some loss of light but still give enough light so the MAPMT makes a signal over the threshold.

It would therefore be better to measure the light yield in each fiber. But since no such measurement was performed right after the prototype was build, a direct comparison is not possible. But as described in Section 15.5 the first final ALFA detectors have been build and the light yield of all fibers (including the overlap detector fibers) have been measured in a cosmic setup. A light yield comparison can therefore be made between the about 3 year old bent fibers in the prototype overlap detector and the newly bent fibers in the overlap detectors on the final ALFA detector. The un-bent fibers in the final ALFA detector could also be included in the comparison.

15.6.2. Setup for measuring scintillating fiber light yield in the prototype overlap detectors

The method to determining the light yield is the same as described in Section 15.5.1.

A schematic of the setup is shown in Figure 15.23.

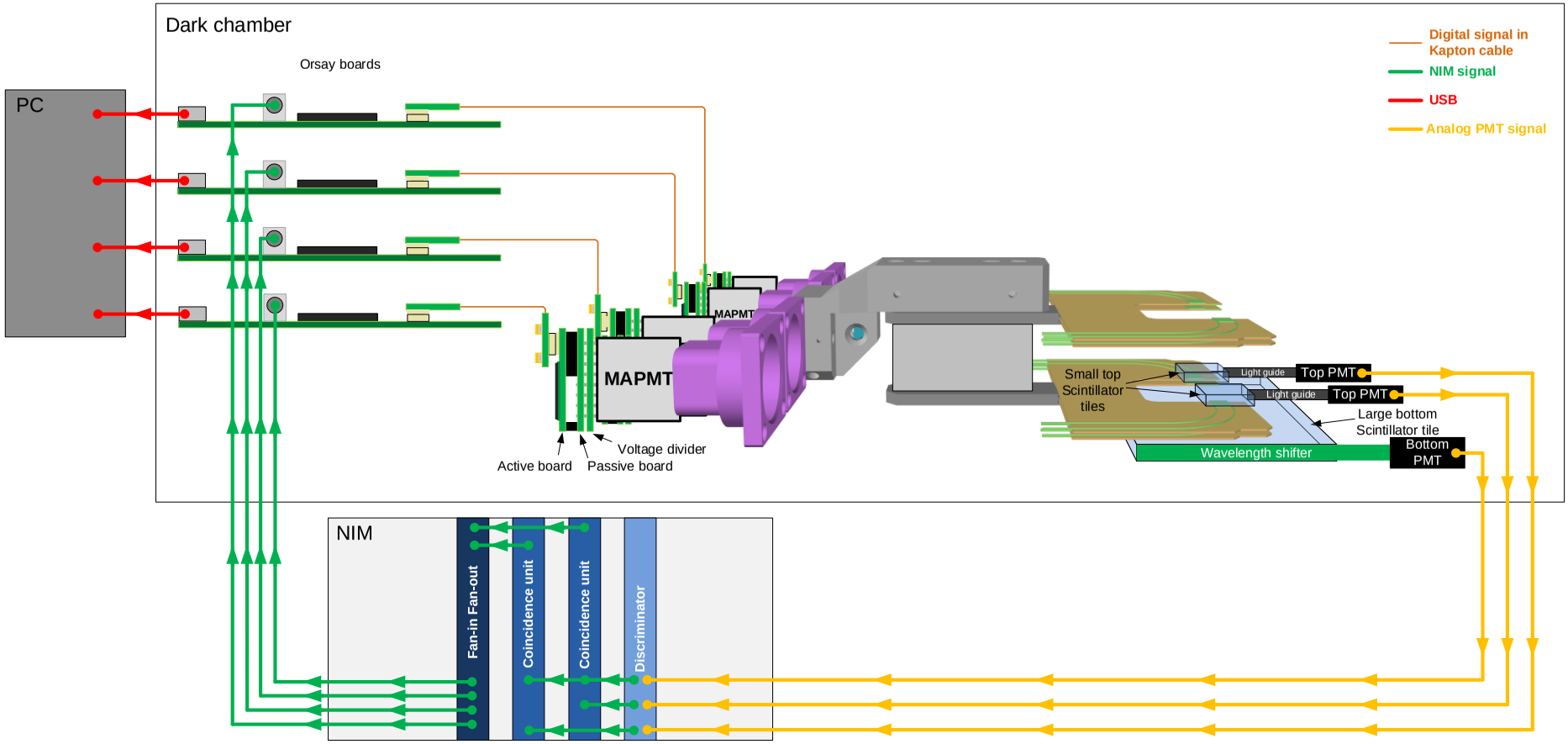

Figure 15.23. The cosmic setup for determining the light yield in the scintillating fibers for the prototype overlap detector. The detector part pieced together from AutoCAD drawings made by Andre Beam (CERN, PH-DT). On the figure the scintillating fibers are light green, the trigger scintillator tiles are transparent light blue and the fiber connectors are purple. The part of the fiber going from the titanium plate to the fiber connector is left out to make the figure clearer.

A cosmic particle passes through the overlap detectors. Ultraviolet light is emitted in the fibers the particles passes through. The ultraviolet light is absorbed in the fiber and reemitted in a longer wavelength (blue) that can propagate though the fiber. The blue light hits the photo-cathode of a MAPMT and some are converted into photoelectrons. The MAPMTs are powered trough a one-board voltage divider. Next to this is a passive board which sent the charges from the MAPMTs to the active board, where the signal is amplified with a preset gain correcting factor. The signals are then put in analog memory. One after one these are then sent though a kapton cable to an Analog-Digital-Converter (ADC) on an Orsay test board.

The cosmic particle also passes through one of the small top trigger scintillating tiles and the large bottom trigger scintillating tile. In the scintillator tiles pass through by the cosmic particle ultraviolet light is emitted. The ultraviolet light is absorbed in the scintillator tile and reemitted in a longer wavelength (blue) that can propagate though the scintillator tile. For the small top triggers the blue light travels through a clear light guide to a PMT and some of the light is converted into photoelectrons. In the much thicker large bottom scintillator tile the blue light is absorbed in a wavelength shifter connected to one side of the scintillator tile. The light is reemitted as green light and travels though the wavelength shifter to a PMT where some of the light is converted into photoelectrons.

The analog signals from the PMTs are sent into discriminators, which sent out NIM signals instead. The NIM signals are sent to a coincidence unit, which sent out one NIM signals if the incoming NIM signals are overlapping in time. Coincidences are made with the large trigger and either of the small triggers. The NIM signal from the coincidence units is send to a Fan-in Fan-out unit, which sends out 4 identical NIM signals, one to each OB. These NIM signals trigger a readout of all MAPMTs.

When the Orsay boards receive a trigger it reads out the charge, in turn, of all the channels of the MAPMT it has attached. After the charges have been digitalized, the Orsay boards saves the data on a Windows based PC connected via USB. The USB connection is also used to set up most parameters (gain, threshold etc) on the Orsay board.

A photo of the setup is shown in Figure 15.24.

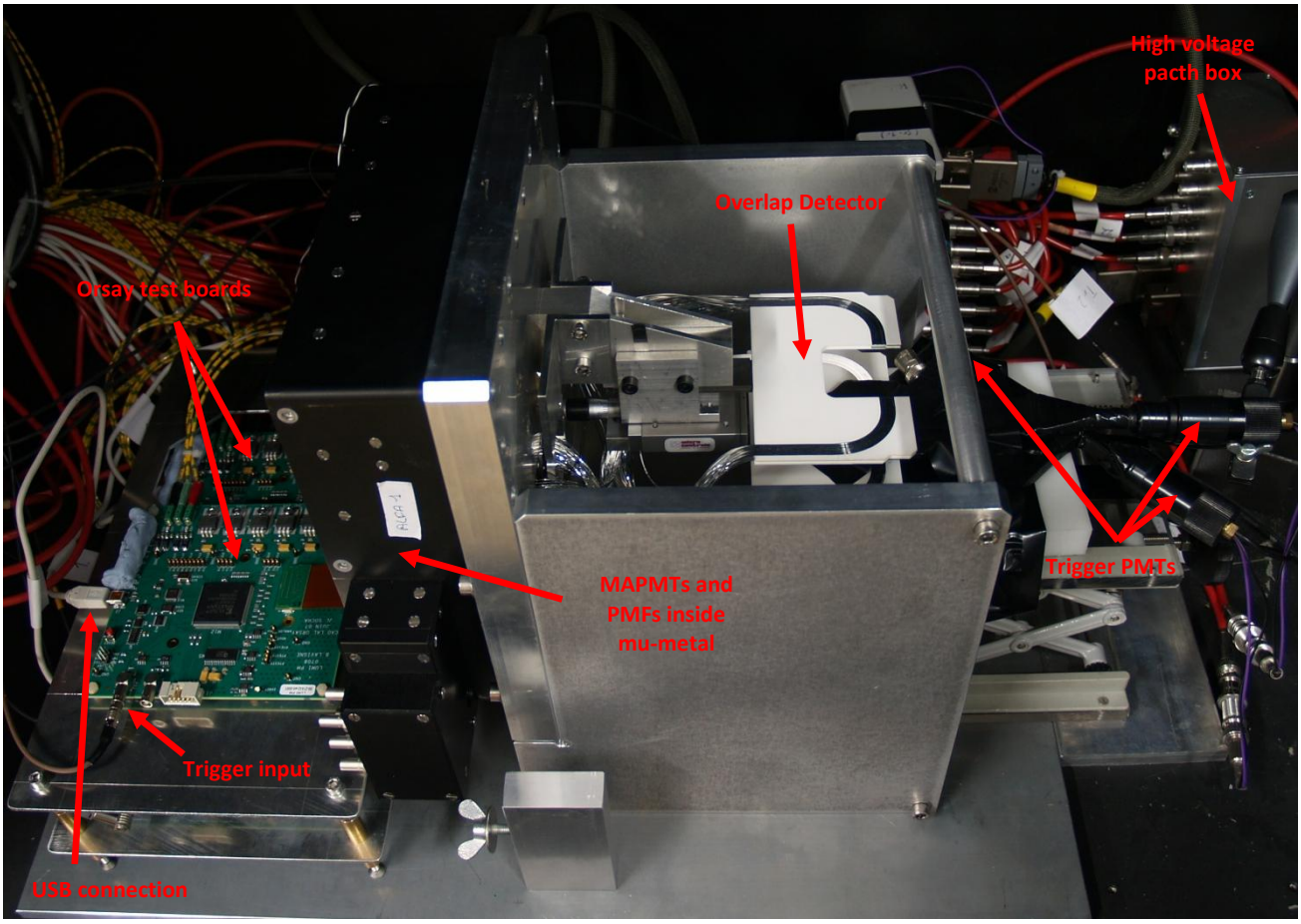

Figure 15.24. The cosmic setup for the overlap detectors.

The small triggers are placed so only the used part for the scintillating fibers are covered, see Figure 15.23 and Figure 15.25.

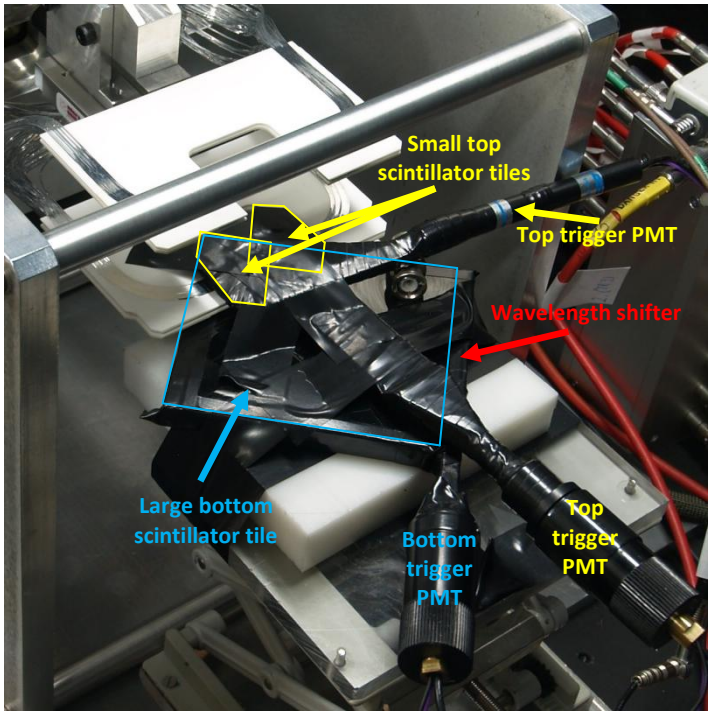

Figure 15.25. Scintillator tiles for triggering on the cosmic setup for the overlap detectors. The active part of the small top scintillator tiles is indicated with yellow. The active part large bottom scintillator tile is indicated with light blue.

For the two lower layers this means that the triggering will be done only for particles passing the part of the scintillating fibers actually intended to be used. However the two upper layers have a distance of about 44 mm to the lower layers. Combined with the angular distribution of the cosmic, triggers will be made for particles passing part of the scintillating fibers not intended to be used. Therefore only the results of the lower layers can be trusted.

15.6.3. Run with cosmic for the prototype overlap detector

For the PMTs used for triggering the HV were -1250 V (Hamamatsu R1635 used for one small top trigger) and -800 V (Hamamatsu R7400P used for one small top trigger and the large bottom trigger). For the MAPMTs the HV was -900 V. The threshold in the discriminators for triggering, see Figure 15.23 and Figure 15.25, was set to 30 mV. The delay of the readout, the Q-delay, was set to 12.5 ns, which was 25 ns less than for the calibration to counteract the longer delays as discussed in Section 15.3.1.

The cosmic test went on for about 3 weeks. The OB was not stable over this time so the cosmic test was split into many runs. Over all 557573 triggers was stored, but many of the triggers was made with particles not passing the scintillation fibers but only the triggers (as the triggers was much larger than the area used on the overlap detectors).

15.6.4. Analysis of cosmic on the prototype overlap detector

As for the calibration runs (Section 16.3.1.5) and the cosmic test of a full ALFA detector (15.5) the data from the Orsay boards are stored as binary data. To do any data processing the data is filled into histograms using a macro called *histCOSMICS.C (Appendix N)* made by MH. The macro makes a folder with the run number. Inside that folder the macro makes a sub-folder for each MAPMT. In the folder for each MAPMT the macro makes a ROOT file containing a histogram for each channel on the MAPMT. These ROOT files were all analyzed as described in Section 15.5.4.

15.6.5. Results of the cosmic test of the prototype overlap detector

For each layer on the prototype overlap detector a plot was made with the light yield of each channel ordered by fiber numbering. For layer 1 and 2 (the two lower layers in the setup with correct triggering) the results is shown in Figure 15.26 and Figure 15.27.

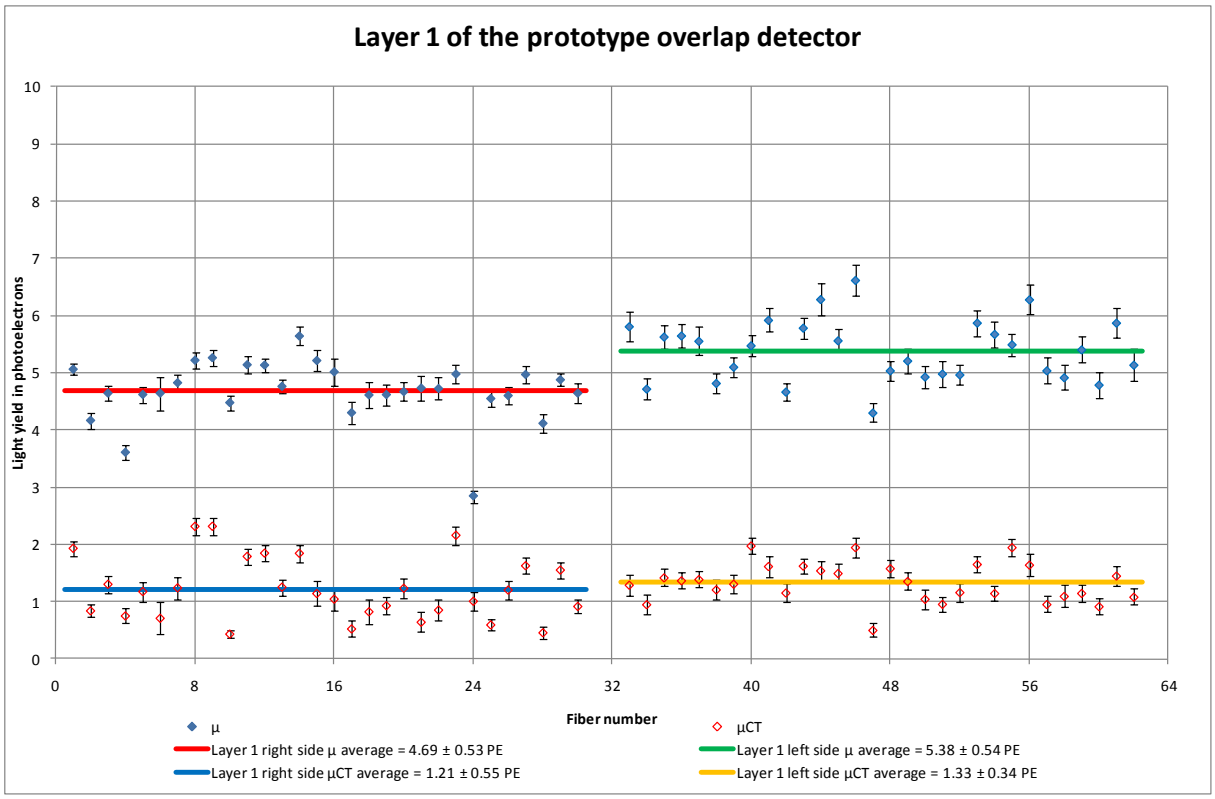

Figure 15.26. Light yield in each fiber of layer 1 in the prototype overlap detector.

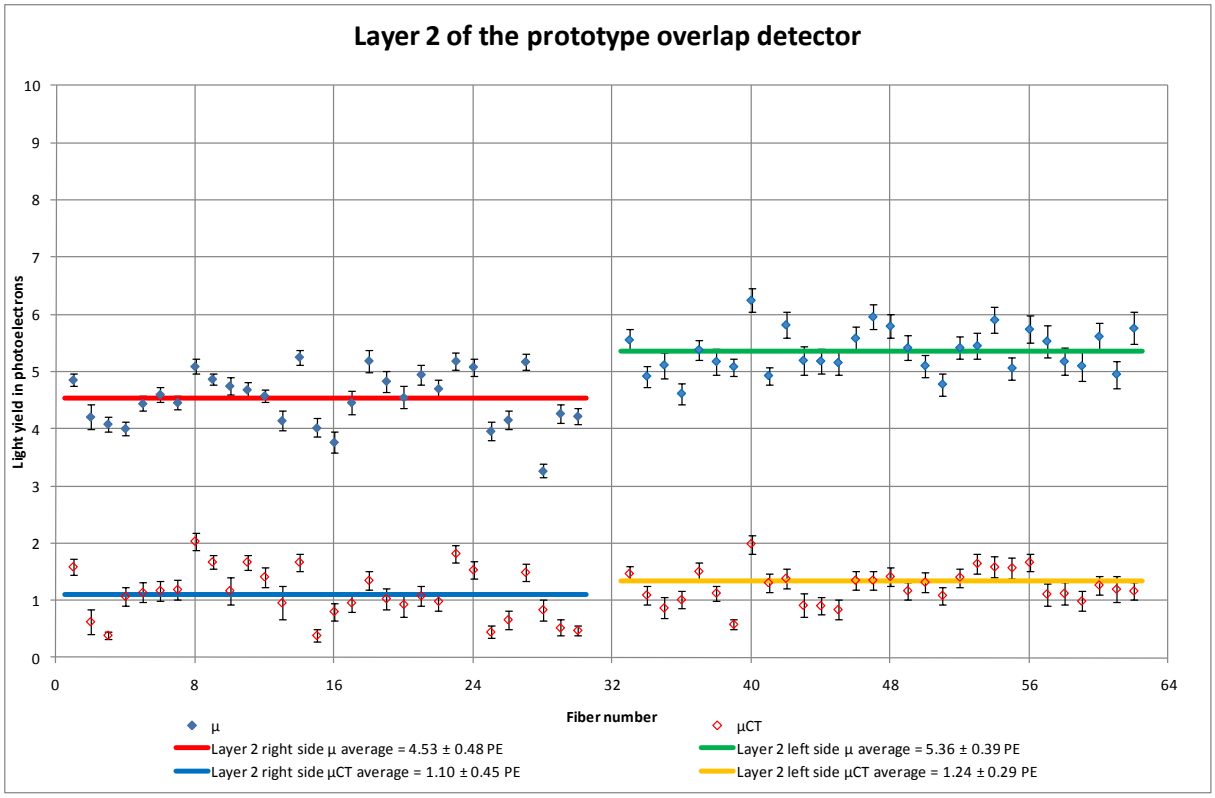

Figure 15.27. Light yield in each fiber of layer 2 in the prototype overlap detector.

The results of layer 3 and 4 of the prototype overlap detector are Appendix S, but for this there is not only triggered on the part of the scintillating fibers used and the results can therefore not be used directly.

15.6.6. Conclusion on the performance of the prototype overlap detector

The light yields of all scintillating fibers of the 3 years old overlap detector are high. The average light yield per side is 4.69 ± 0.53 PE, 5.38 ± 0.54 PE, 4.53 ± 0.48 PE and 5.36 ± 0.39 PE which is directly comparable to the newly produced ALFA1 detector with average light yield per side 5.37 ± 0.40 PE, 4.72 ± 0.58 PE, 4.85 ± 0.67 PE and 4.74 ± 0.39 PE.

The crosstalk term for the overlap detector layer in Figure 15.27 is 1.10 ± 0.45 PE for the right side and 1.24 ± 0.29 PE for the left side. As discussed in Section 14.7. the cross talk term for cosmic is dominated by particles hitting more than one fiber and is here in the expected range.

All average light yields measured with cosmic should be normalized by diverting with a factor of about 1.2 before comparison with light yield from a beam, as discussed in Section 14.7 and *[74]*.

Also no fibers in the prototype overlap detector are dead or have and very low light yield. The conclusion is therefore that no ageing effects are seen on the bent scintillating fibers over a period of 3 years.

16. Test beam 2009

16.1. Preface

The 2009 beam test involved almost all of the ALFA collaboration and thereby years of manpower. This section will therefore only give an overview of all the tasks done to make the test beam possible. Some more emphasis will be put on the tasks where the author was directly involved.

16.2. Test beam motivation

The test beam in 2009 had many sub goals, but the main goal was to read out an entire ALFA station very close to the way it will be done in the final installation. For this to be possible every sub device had to be ready:

- The support structure for everything had to work (primarily the stations discussed in Section 13.4)
- The detectors themselves had to be operational.
- The MAPMTs had to be calibrated.
- The MAPMTs had to be mounted on top of the scintillating fiber ends.
- The high voltage for the individual PMTs had to be operational.
- The PMFs had to work.
- The motherboards had to be operational (had never been used for real tests before).
- The data acquisitions system had to be operational.
- The software to control everything had to be operational.
- The online (or semi-online) analysis software had to work.

So the beam test was first and foremost a check that everything was working and that the development was on the right track.

Of the more directly physical goals were scans of parameters to find the optimal settings. Also a test of the entire detector surface and especially edge near the beam was desired to investigate the detector performance.

At the end of the test beam it was planned to make vacuum tests including a test where the Roman Pot window would touch the detector. This test was to check that the detector not would be harmed if the beam vacuum was lost accidentally.

16.3. Before the test beam

In the weeks leading up to the test beam a lot of things had to be made ready and tested. This section discusses the most important of them.

16.3.1. Calibration of the MAPMTs

The gain of the different channels on a MAPMT can vary up to a factor 2-3. Furthermore the mean gain of two different MAPMTs can also vary a factor 2-3. All in all this can lead to a huge difference in gain. The default readout is binary; over or under a set threshold. For this threshold to have the same effect on all MAPMT channels the gains need to be equalized. This was foreseen in the electronic design and the PMFs have 64 charge amplifiers (as discussed in Section 13.2.1). Each amplifier has 6 bits which resolve in 64 levels

of amplification. Gain factor 16 leaves the charge untouched. Gain factor 32 amplifies the charge by a factor of 2 and so on.

To find the right gain factor of each channel, the charges from the MAPMT needed to be measured. The PMFs have a mode for this, but the motherboards were still in an early stage where only the binary readout was operational. Therefore the calibration needed to be performed with the 5 Orsay boards used in the cosmic setup. This task was exclusively given to the author as he knew the setup.

16.3.1.1. Preparation for calibration

At the point when the calibration needed to be performed neither of the mu-metal grid frame with MAPMTs, PMFs and so on had been assembled jet. The only mu-metal grid frame where the high voltage boards where connected was the old one from prototype 2008 used to test the cosmic setup. As there were also not enough MAPMTs with shims available the old ones from the prototype had to be re-used.

The first task before the calibration could be performed was therefore to interchange MAPMTs in the prototype mu-metal grid frame and pair them with active PMF boards. To keep track of the MAPMT/PMF mapping a photo was taking and the names of the MAPMTs added to it. Later more information was added and it proved to be a very useful tool. During the test beam a copy was even attached to the black box shielding the MAPMTs from light to always have it close to the actual MAPMTs/PMFs. The mapping slides are included as Appendix T.

The new MAPMTs had an epoxy shim, which was a design that was later abandoned. See also Section 17 about shims. None of the shims was really good, but some of them were directly bad. So a selection was made by looking at the shims, looking at the measurements of the shims, seeing how they fitted in the mu-metal grid frame and so on. Also 3 Ultra BiAlkali, UBA, MAPMTs was included in ALFA2 to investigate their behavior under the test beam.

It proved to be non-trivial to interchange the MAPMTs. This should normally never be done and therefore no way to remove the HV-board from the mu-metal grid frame had been prepared. Because of that the MAPMT/PMF had to be assembled around the already connected HV-board. The HV-cables to the HV-boards is quite stiff and has a tendency to break next to the soldering when the HV-board is moved. This happen a few times during the interchange and the cables then had to be exposed and re-soldered.

Figure 16.1 shows the work in progress to assemble the pieces inside an ALFA mu-metal grid frame.

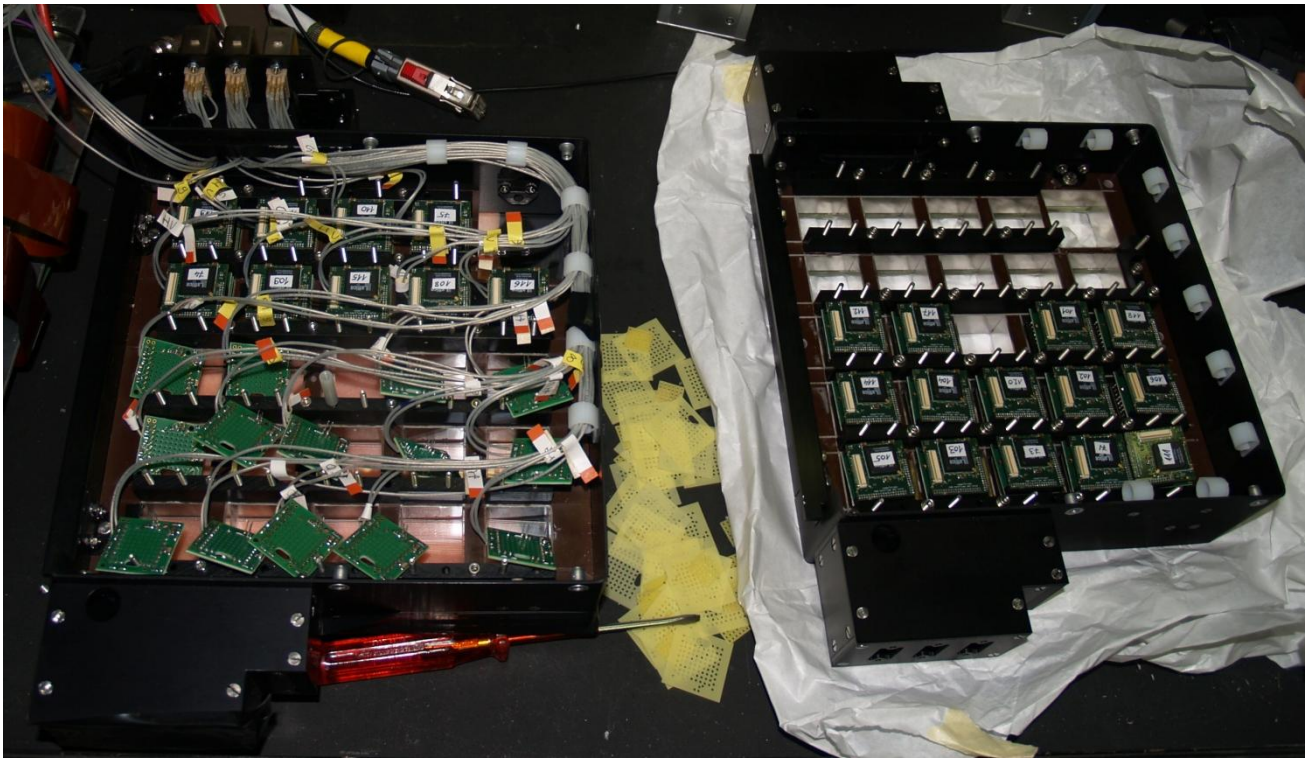

Figure 16.1. Assembly of the pieces inside an ALFA mu-metal grid frame. The mu-metal grid frame to the right (without HV-cables) is used to keep track of the MAPMT/PMF mapping.

16.3.1.2. Concept of the calibration

The concept of the calibration was similar to the one in Section 14.2.7: Use a pulsed LED at very low light level (<0.1 PE average) to determine the position of the 1 PE as shown in Figure 16.2.

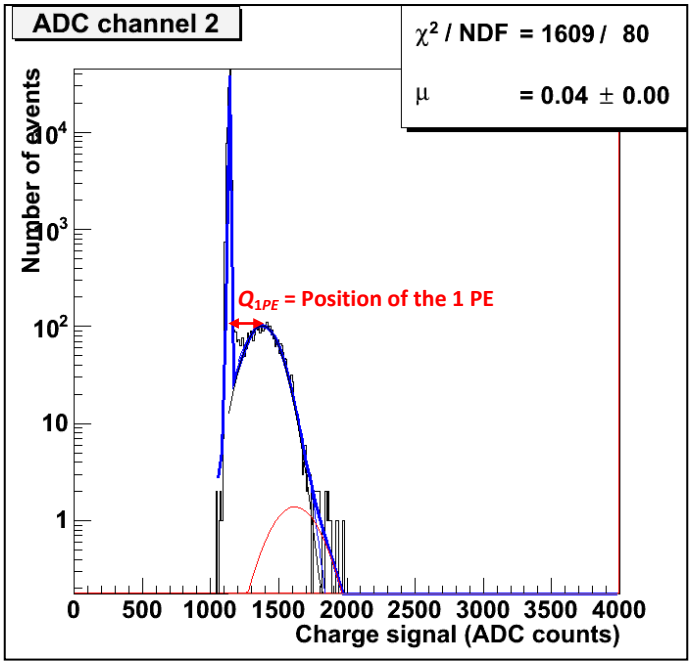

Figure 16.2. Fit to the charge spectrum from a MAPMT channel. The position of the 1 PE is highlighted.

The MAPMT charge spectrum is here again fitted with equation (14.3). The gain factor can then be calculated as:

$$\text{Gain factor} = \frac{\text{Wanted } Q_{1PE}}{\text{Fitted } Q_{1PE}} \cdot 16 \qquad (16.1)$$

The calculations of the gain factors were included in the ROOT macro *Cal1PE.C* that automatically made a list of the calculated gain factors that could be loaded to the amplifiers in the PMFs.

16.3.1.3. Setup for calibration of a full ALFA detector

A schematic of the calibration setup is shown in Figure 16.3.

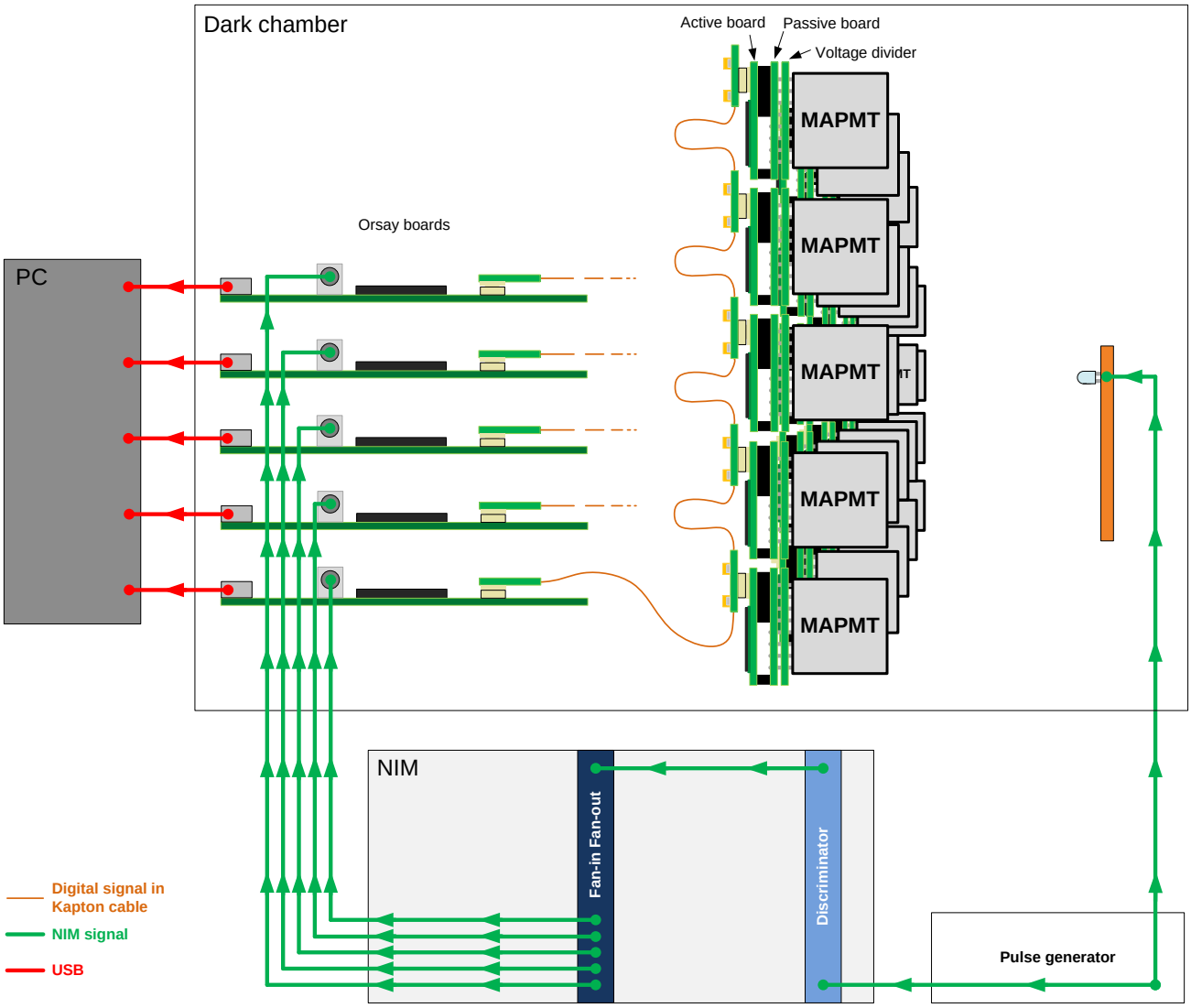

Figure 16.3. A schematic of the setup for calibration of a full ALFA detector.

The pulse generator sends out a signal of about -3.7 V and about 10 ns wide to the LED. The LED emits a short light pulse. A fraction of the light hits the MAPMTs windows and some is converted into PhotoElectrons, PE. The MAPMTs are powered trough a one-board voltage divider. Next to this is a passive board which just sends the charges from the MAPMTs to the active board, where the signals are amplified (in the first calibration the amplification gain factor is 16 (no amplification)). The signals are then stored in analog memory. One after one, they are then sent though a kapton cable to a Analog-Digital-Converter (ADC) on an Orsay test board.

The signal from the pulse generator is also sent to a discriminator to convert it into a standard NIM signal. This signal is then sent to a Fan-in Fan-out for splitting it into 5 identical NIM signals. Each of this are sent to an Orsay board to trigger the readout.

When the Orsay boards receive a trigger signal they read out the charge, in turn, of all the channels of the up to 5 MAPMTs they have attached. After the charges have been digitalized the Orsay test boards save the data on a Windows based PC connected via USB. The USB connection is also used to set up most parameters (gain, threshold etc) on the Orsay test board.

A photo of the setup is shown in Figure 16.4.

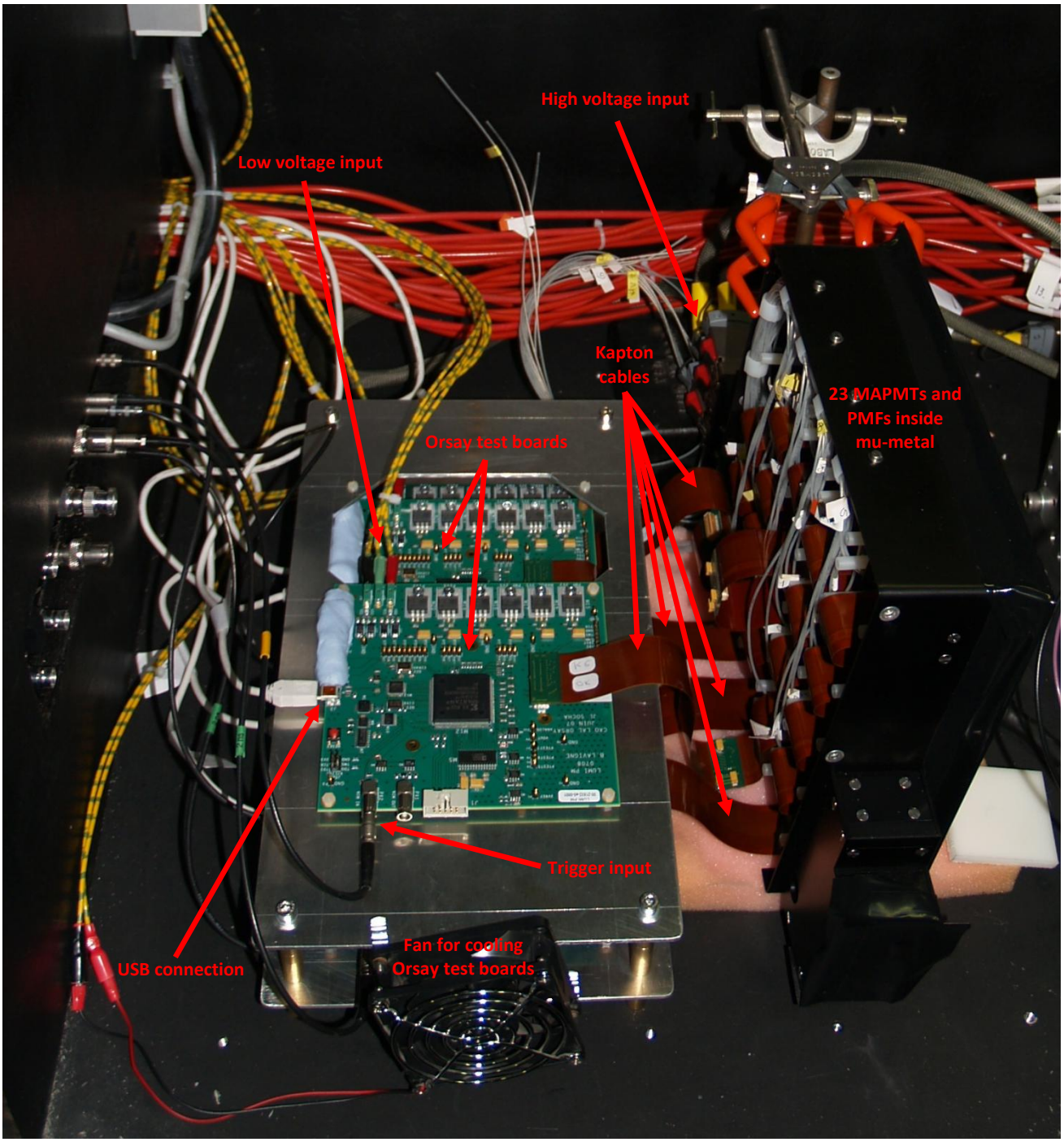

Figure 16.4. Calibration setup inside a dark chamber used to calibrate ALFA1 and ALFA2 for the test beam in 2009. The LED is not shown.

16.3.1.4. Calibration runs for ALFA1 and ALFA2

The high voltage of all MAPMTs was -900 V. All amplifier channels were first set to gain factor 16. Then a run was performed with 100000 triggers. This took about 15 min. Then the data was filled into histograms, which took about 15 min, and the gain factors calculated (see Section 16.3.1.2), which took about 25 min using 4 CPU cores. The gain factors were then loaded onto the amplifiers on the PMFs and a new run was made again with 100000 triggers. Again the data was filled into histograms and analyzed, see Section 16.3.1.5 for details. If everything was perfect with the first fit all channels should now have equal gain. But a few fits were bad (this actual lead to the fit improvements described in Section 16.3.1.5) and also channels that started out with very low gain, where the 1 PE peak was almost included in the pedestal as in Figure 16.5, did not get the correct gain factor.

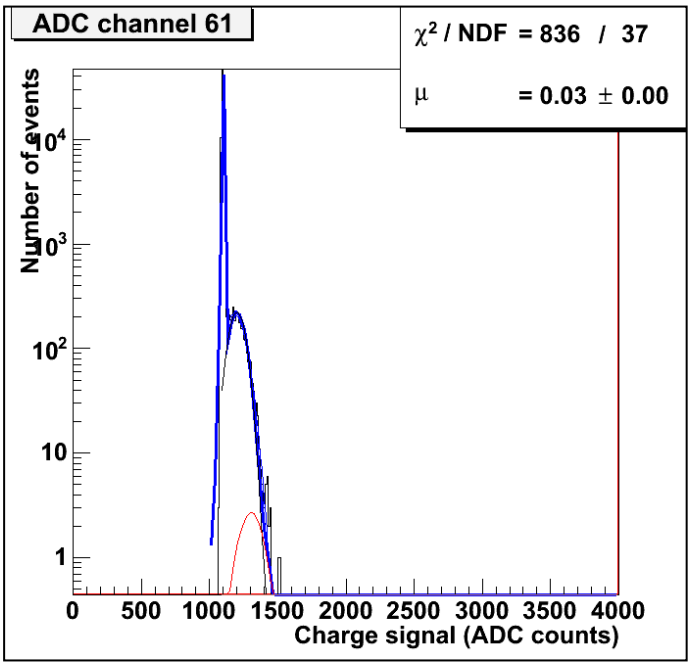

Figure 16.5. 1 PE charge spectrum with low gain. The 1 PE peak is almost merged with the pedestal and the calculated gain factor is therefore a bit off.

Therefore new gain factors were calculated from the second run. A new run with 100000 triggers was made, filled into histograms and analyzed. This time most of the channels were equalized. New gain factors were calculated for the few channels that were still a bit off. It would have been good to make a final run to verify that all channels were now indeed equalized, but the MAPMTs and PMFs were needed for test of the motherboard.

The calibration to get equalized gain was done on both ALFA1 and ALFA2. The results of the before equalization, equalization step one and two are shown in Section 16.3.1.6 for ALFA1 and in Section 16.3.1.7 for ALFA2.

16.3.1.5. Calibration analysis

The data from the Orsay boards are stored as binary data. To do any data processing the data is filled into histograms using a macro called *histCOSMICS.C (included ad Appenedix O)* made by MH. The macro makes a folder with the run number. Inside that folder the macro makes a sub-folder for each MAPMT. In the folder for each MAPMT the macro makes a ROOT file containing a histogram for each channel on the MAPMT. These ROOT histograms all needs to be analyzed with *cosmic1pe.C* (from Section 14.2.4) in a modified version renamed to *Cal1PE.C (Appendix M)*(see details below in this section). To analyze all channels on a

MAPMT a macro, *AllCH.C* (similar to Appendix O), that just run *Cal1PE.C* for each MAPMT channels. To analyze all MAPMTs in a mu-metal grid frame (an entire detector) 4 run macros, *Run1.C*, *Run2.C*, *Run3*.C and *Run4.C (similar to Appendix O)*, were made. These each just run *AllCH.C* for 5-6 MAPMTs. They are used to spread out the fitting to 4 CPU cores in a very easy way simply by running ROOT 4 times, one per Run-macro. This made the fitting almost 4 times faster and it could still be run on only one PC.

The modifications to *Cal1PE.C* were necessary because the binning of the histograms and the pedestal position was different. Also some improvements were made: Stating values for the fits were changed from fixed values to values found by pre-fitting/calculation. For instance the starting value for μ was calculated by integrating all bins after the pedestal and dividing by the integral of the pedestal. The changes made the fit more reliable and made it fail less. Also the overall fitting time went down because of the starting values now was very close to the final value.

The calculation of the gain factor from equation (16.1) was also included in *Cal1PE.C*. The gain factors were saved as a file. Another addition to *Cal1PE.C* was that it makes a list of dead channels. A dead channel is here defined as a channel with no data or with only pedestal. The list of dead channels is very useful to quickly check for errors.

The results (Section 16.3.1.6 and 16.3.1.7) are plotted in Microsoft Excel. To implement the 92 files (23 MAPMTs*4: the position of the 1 PE, error on the position of the 1 PE, width of the 1 PE and error on width of the 1 PE) fast into Microsoft Excel, C++ macros (run inside ROOT) were made. The C++ macros, *DataCal.C* and *DataCalAll.C* (Appendix U), made one file of all the data and also took care of a PMF-mapping difference between the motherboard and the OB.

Also a C++ macro (run inside ROOT) was made to split one file with all 1472 gain factors up into separate one gain factor file per PMF that could be loaded on the OBs, *SplitGainFactors.C* (Appendix U).

To make the calibration files (position of the pedestal, the width of the pedestal, the position of the 1 PE and the width of the 1 PE) and place them in the right folders a C++ macro (run inside ROOT) was made, *CalibrationFiles.C* (Appendix U).

16.3.1.6. ALFA1 results for the gain equalization calibration

The 1 PE position of the MAPMT channels of the MAPMTs in ALFA1 as they were before the calibration can be seen in Figure 16.6.

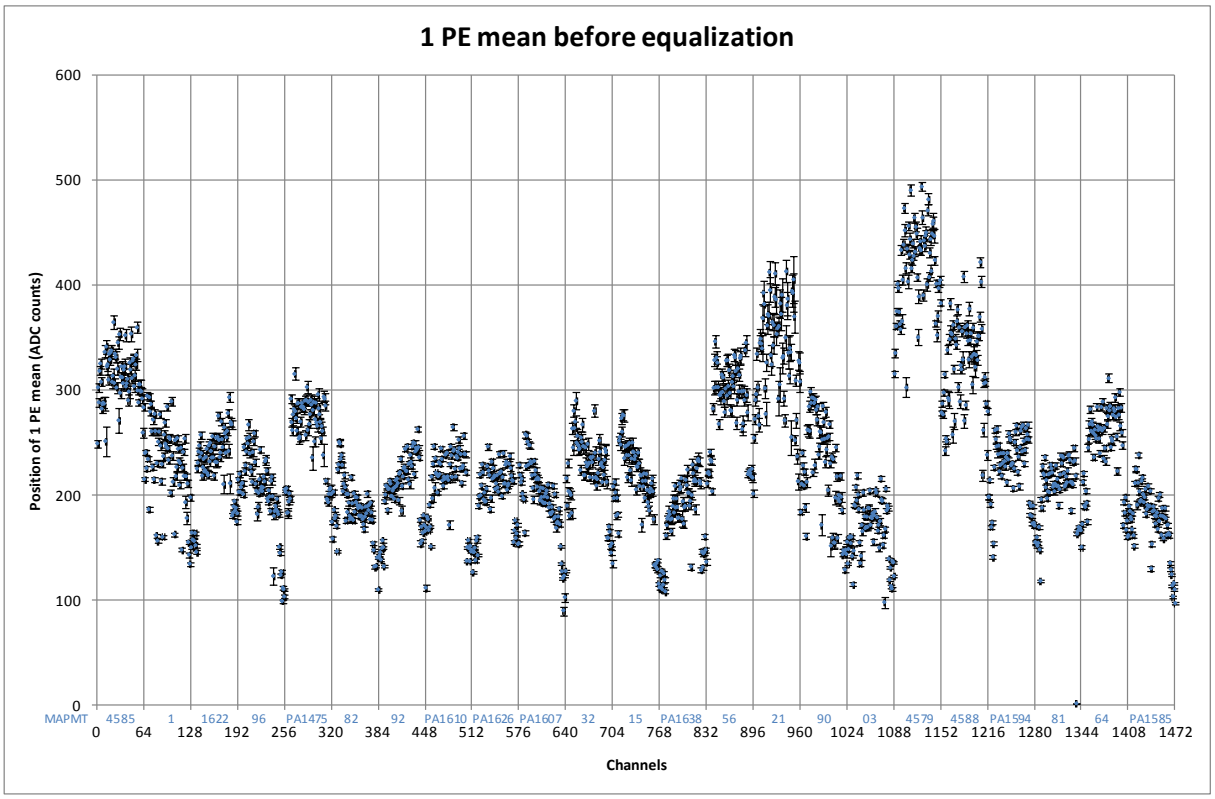

Figure 16.6. 1 PE position of the MAPMT channels of ALFA1 before the calibration.

Differences up to a factor 5 are seen in the gains. It is also seen that the first and the last channels on a MAPMT has a tendency to have a lower gain, which is also expected from the layout of the MAPMTs. The very low gain channel in MAPMT 81 needs a gain factor of more than 63 to be equalized to the rest. As this is out of the range for the amplifier the gain factor was set to the maximum of 63. It could be considered to increase the high voltage for MAPMT 81. That would raise the gain off all channels. The low gain channel could therefore be brought to the common gain value and the rest of the channels could be adjusted to the common gain value with a lower amplification.

The 1 PE position of the MAPMT channels of the MAPMTs in ALFA1 after the first step of the calibration is seen in Figure 16.7.

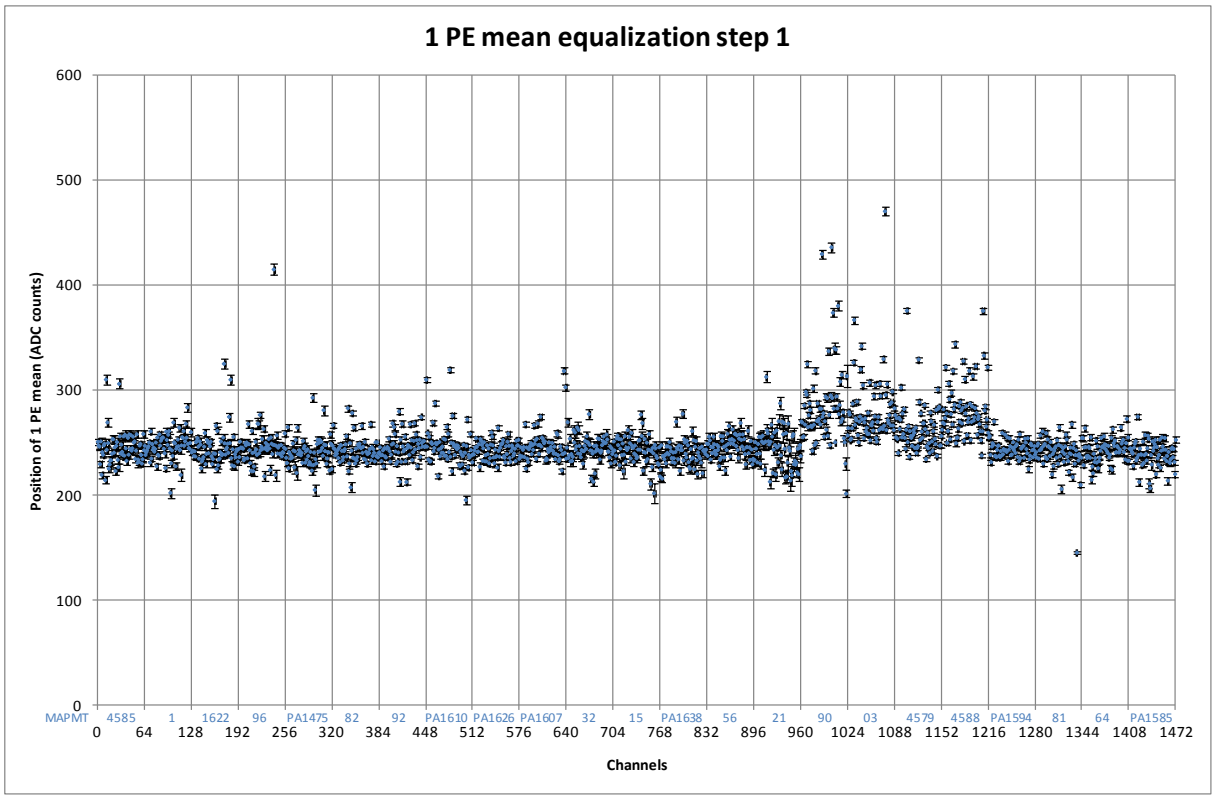

Figure 16.7. 1 PE position of the MAPMT channels of ALFA1 after the first step of the calibration.

The effect of the calibration is clearly visible, but a few channels are still a different.

The 1 PE position of the MAPMT channels in ALFA1 after the final step of the calibration are seen in Figure 16.8.

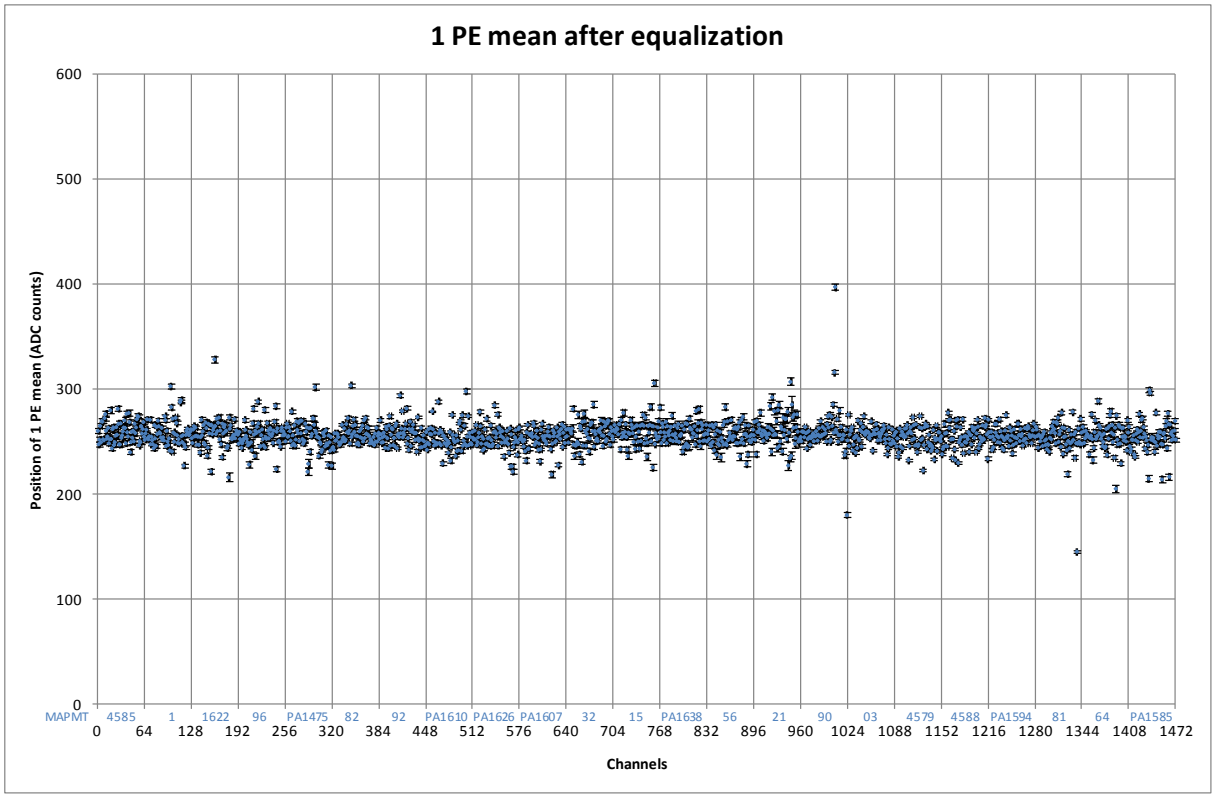

Figure 16.8. 1 PE position of the MAPMT channels of ALFA1 after the final step of the calibration.

Almost all the channels are here equalized within step size of the amplifiers. New gain factors were calculated for the few channels that not equalized. Compared to the gains before equalization in Figure 16.6 a huge improvement it seen.

16.3.1.7. ALFA2 results for the gain equalization calibration

The 1 PE position of the MAPMT channels in ALFA2 as they were before the calibration can be seen in Figure 16.9.

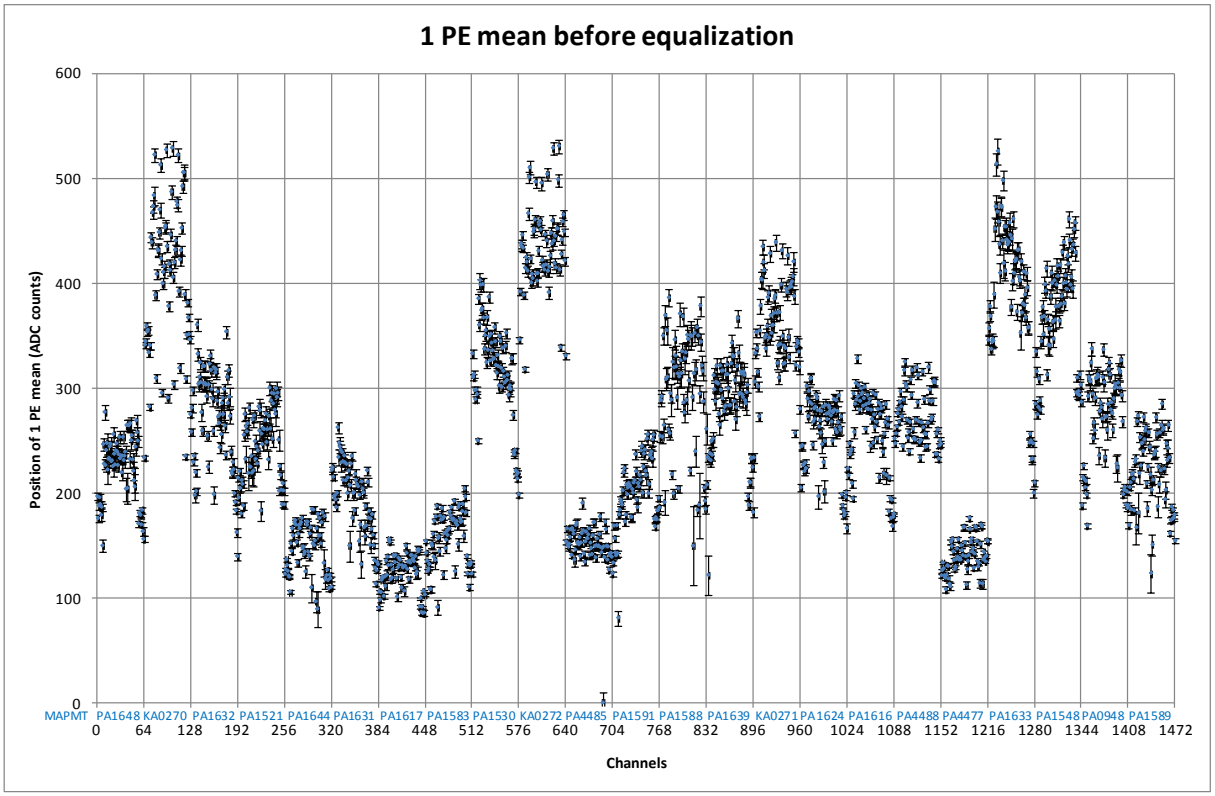

Figure 16.9. 1 PE position of the MAPMT channels of ALFA2 before the calibration.

Differences of over a factor 5 are seen in the gains. It is also seen that the first and the last channels on a MAPMT has a tendency to have a lower gain, which is also expected from the layout of the MAPMTs. The MAPMTs with names starting with KA is UBA MAPMTs.

The 1 PE position of the MAPMT channels in ALFA2 after the first step of the calibration is seen in Figure 16.10.

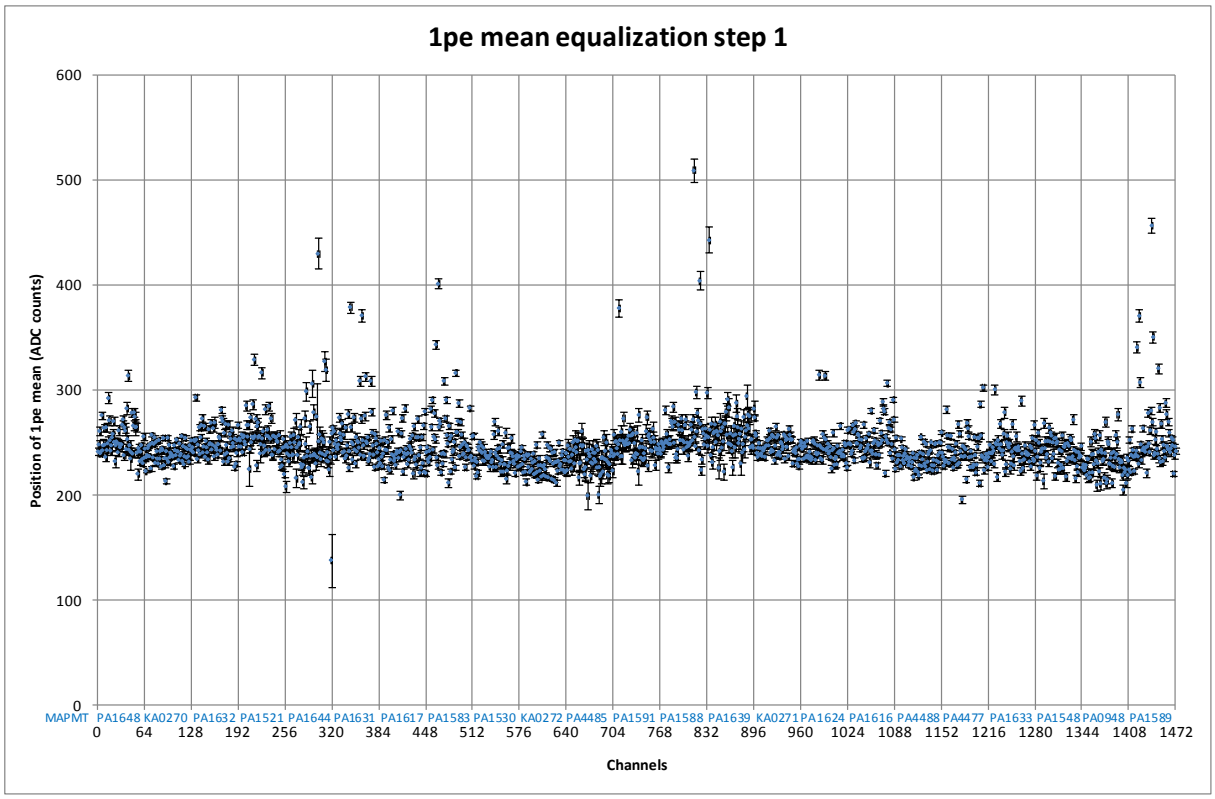

Figure 16.10. 1 PE position of the MAPMT channels of ALFA2 after the first step of the calibration.

The effect of the calibration is clearly visible, but a few channels are still a different.

The 1 PE position of the MAPMT channels of the MAPMTs in ALFA2 after the final step of the calibration are seen in Figure 16.11.

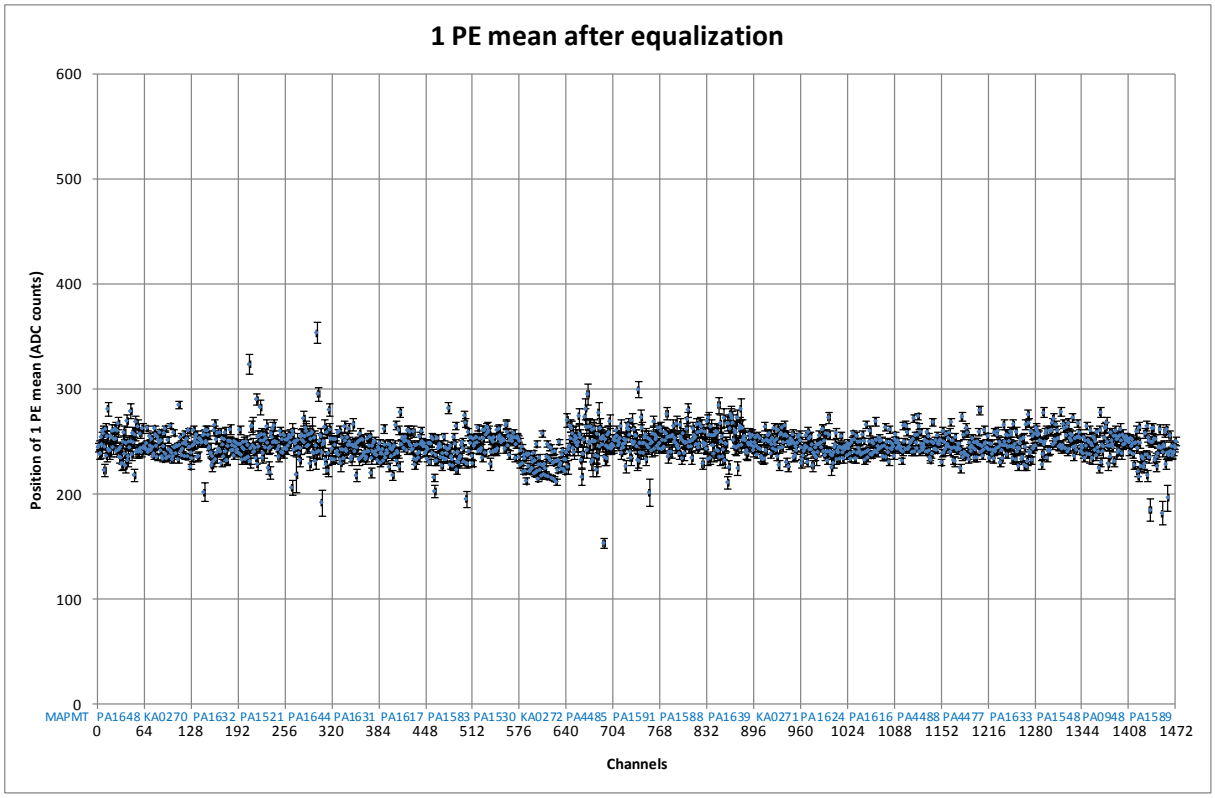

Figure 16.11. 1 PE position of the MAPMT channels of ALFA2 after the final step of the calibration.

Almost all the channels are here equalized within step size of the amplifiers. New gain factors were calculated for the few channels that not equalized. Compared to the gains before equalization in Figure 16.9 a huge improvement is seen.

The manufacturer of the MAPMTs, Hamamatsu, provides a gain table for the channels in each MAPMT. However since this is only a relative measurement for the channels in the measured MAPMT this cannot be used to cross calibrate MAPMTs. A comparison of Hamamatsu gain tables and the gain factors (actually the reciprocal gain factors) found in the calibration would however be a nice further check of the calibration method and the found gain factors. Such a comparison is shown in Figure 16.12.

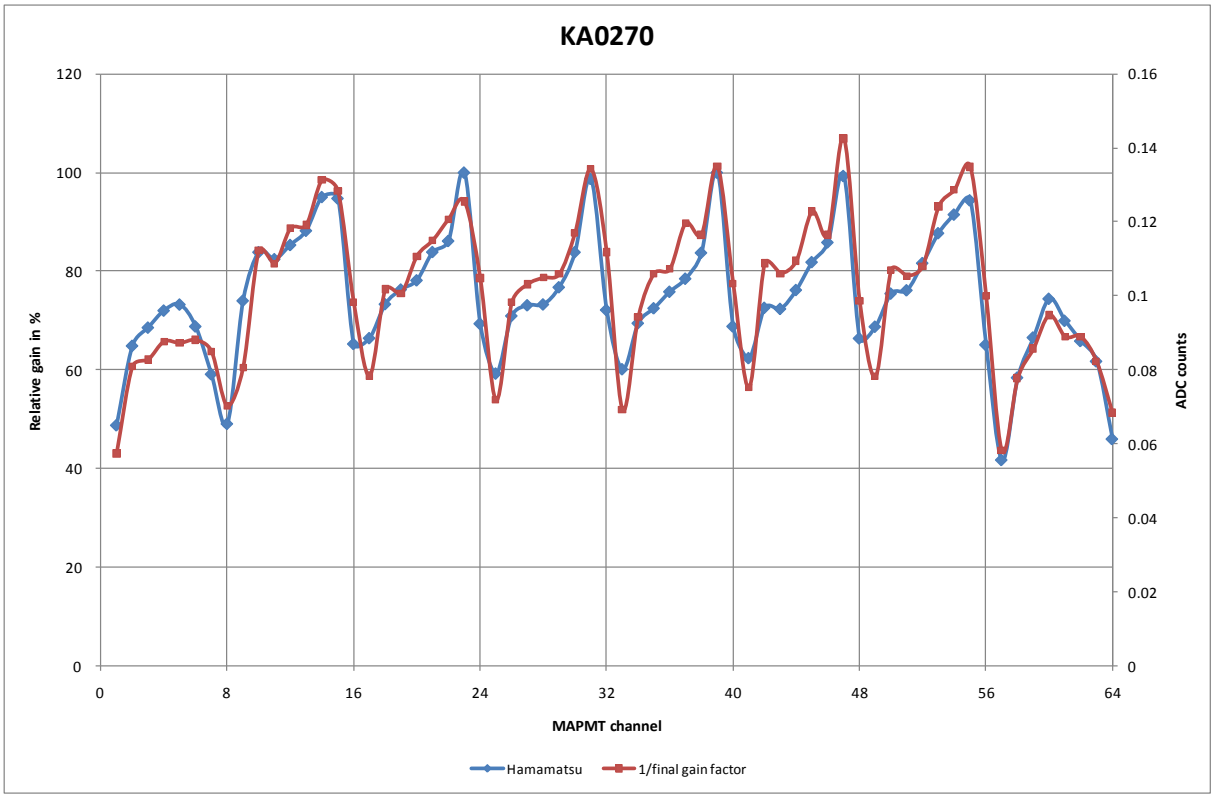

Figure 16.12. Comparison of the Hamamatsu gain values and the found gain factors for one MAPMT. Note that the scaling is done by using to different secondary axes.

An excellent correspondence is seen between the gain Hamamatsu have measured and the gain factors found in the calibration. This further underlines the correctness of the method and the found gain factors.

Hamamatsu data were not available for all MAPMTs, but for the ones where the Hamamatsu data were available comparisons diagrams were made. These are included as Appendix V.

16.3.2. Equal light source for testing and calibration

For testing the MAPMTs they are normally put in a dark chamber to shield them from unwanted light. But this is very inconvenient because the readout board(s), high voltage, low voltage and so on also have to be in the dark chamber or to be connected through the dark chamber somehow. Space is also limited in a dark chamber and since it is only accessible from one side some charges might be unnecessary hard to perform. If any changed is needed on something inside a dark chamber the high voltage to the PMTs has to be unplugged. In a testing phase a lot of small charges have to be made all over the setup and therefore a normal dark chamber would be inconvenient. To make access easier and limit the number of times the PMTs have to be unplugged (and therefore the potential number of failure to remember to unplug the PMTs), Karl-Heinz Hiller (DESY Zeuthen), KH, suggested to put a LED inside one of the prototype Roman Pots and connect

the mu-metal grid frame with content on top. This would be a light tight and very convenient structure. However for the test of the binary readout the light level over all MAPMTs needed to be very identical.

16.3.2.1. LED in Roman Pot

The first suggestion by KH was to use light guides to transport the light from the LED to the windows of the MAPMTs. This was soon realized to be very difficult and it was not clear if the light level would be even enough at the MAPMTs.

There were some ideas to use multiple LEDs, but KH did not like this because the LED might age differently and thereby change the light distribution over time.

KHs next idea was to put the LED in the bottom of a prototype Roman Pot and put one (or more) “diffuser plate(s)” in between the LED and the MAPMTs. The author joined the project and this idea was tried out.

Wide angle LEDs was purchased. This had a 60 degree cone. To make this cone even wider a LED lens mount (a small lens attached directly on the LED) was also purchased. The LED and the lens were installed on a Plexiglas support in the bottom of the Roman Pot. The LED was connected in parallel to a 50 ohm resister (minimize signal reflections) and a lemo cable was connected though the pumping hole in the Roman Pot. The setup is shown inFigure 16.13 (left).

The workshop made a diffuser plate. This was simply a 10 mm Plexiglas plate which had been de-polished on both sides with sandpaper. The diffuser plate inside the Roman Pot is shown in Figure 16.13 (right).

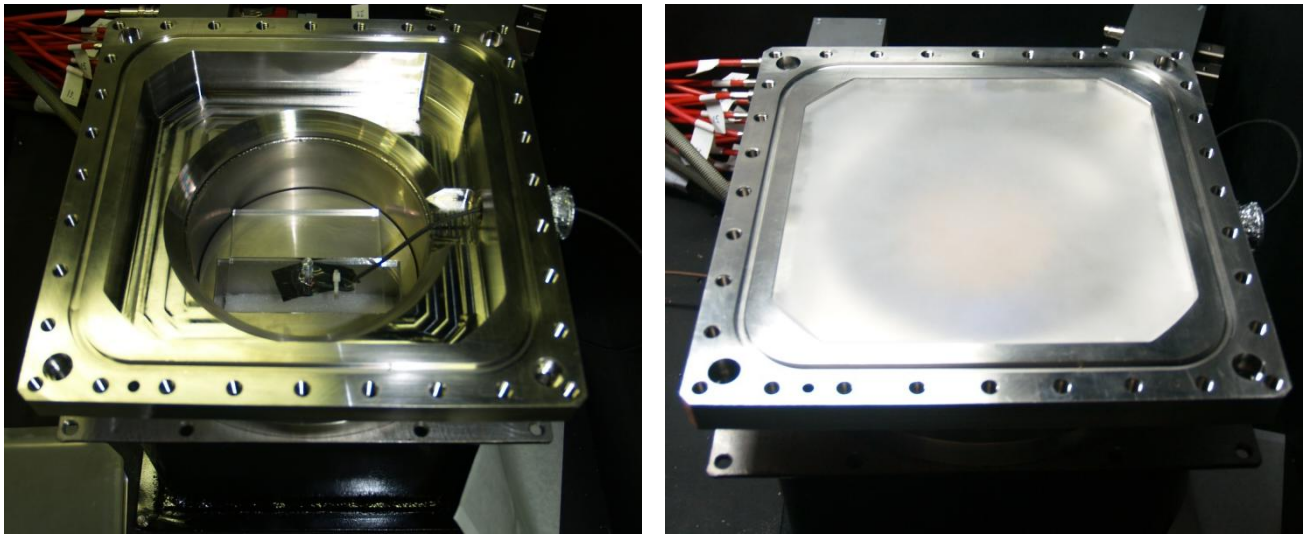

Figure 16.13. *LEFT*: LED and LED lens mount inside the Roman Pot. *RIGHT*: Diffuser plate inside the Roman Pot.

This configuration was tested with high intensity LED light. By eye it was visible that the light was not equally distributed over the surface. There was too much light in center compared to the sides.

It was discussed to put another diffuser plate in between the LED and the current diffuser plate. Also some kind of lens to defocus the light was discussed, but that would have been hard to make or expensive to buy. Instead the author suggested a cone of Plexiglas. A cone is fairly easy and fast to produce. It was decided to try it and the author made the piece. Figure 16.14 (left) shows the Plexiglas cone installed in the Roman Pot. By eye the cone seemed to have made the light distribution much more equal. To judge anything by eye it was necessary to cover the diffuser plate with paper (or something else with a suitable transparency). Else it was not the amount of light that was seen over the diffuser surface but rather where the light was coming from (because the diffuser is fairly transparent). Figure 16.14 (right) demonstrates this as it seems like the

amount of light is many times higher in the center than to the sides, but the light is really rather close to be evenly distributed, and what is really seen is just that the light comes from the center.

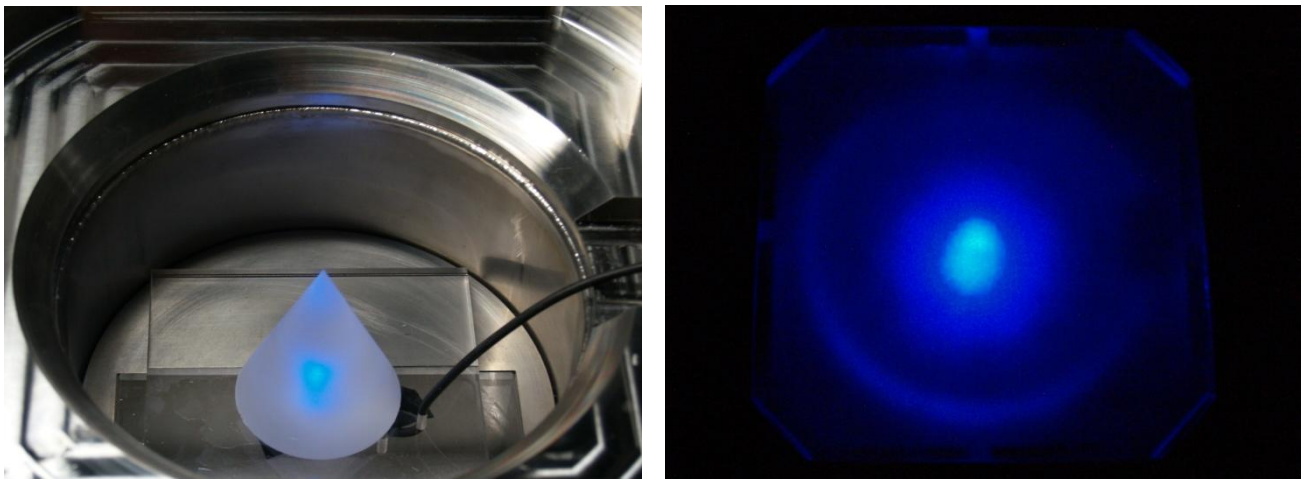

Figure 16.14. *LEFT*: The Plexiglas cone installed in the Roman Pot. *RIGHT*: Light distribution on the diffuser plate.

It was decided to adjust the LED to give a light amount comparable per area to the light of the used scintillating fibers and measure the light intensity in the positions of the MAPMTs. To measure the light intensity it would have been perfect to use a full ALFA mu-metal grid frame, but the readout was not yet operational. Therefore it was decided to use a trigger PMT (Hamamatsu R7400P). To get all the positions of the MAPMTs a base plate (the plate normally holding the fiber connectors) was installed on top of the diffuser plate. The author made a Teflon piece that fitted the size of the trigger PMT to the size of the fiber connectors (and the inside of a mu-metal grid frame). The base plate and Teflon piece with the PMT inside is shown in Figure 16.15.

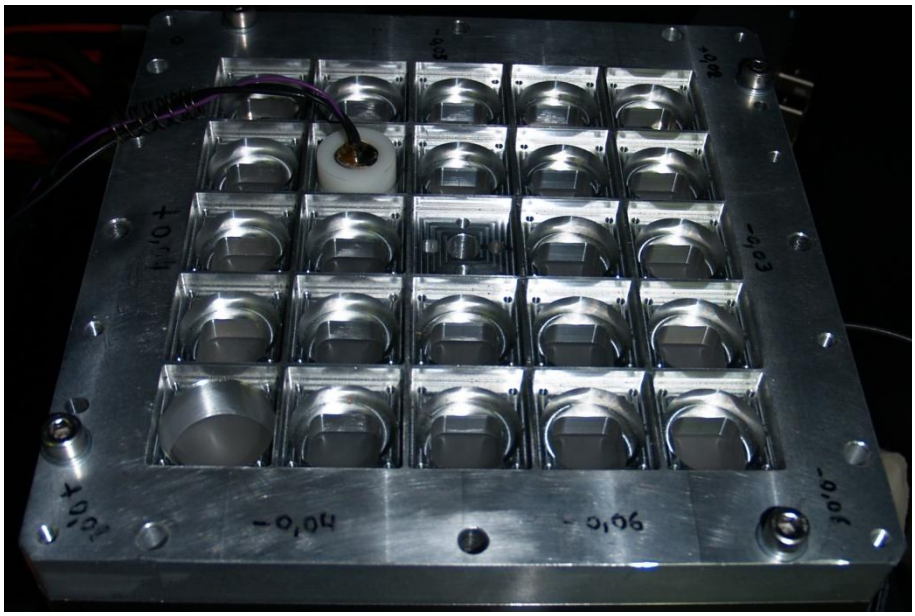

Figure 16.15. The base plate for positioning of the PMT on top of the diffuser plate inside the Roman Pot. The PMT is mounted inside a Teflon piece for correct centering.

The PMT was in turn placed in all MAPMT positions. The relative amount of light was measured by measuring the average charge of the PMT. The readout was done directly on a digital oscilloscope trigged on the pulse generator. The setup was basically the same as the PMT calibration for the trigger scintillator tiles shown in Figure 14.46 in Section 14.6.2.

On the oscilloscope charge-histograms was made. The relative amount of light is given as the distance from the pedestal to the mean of the charge peak. The results are given in Figure 16.16.

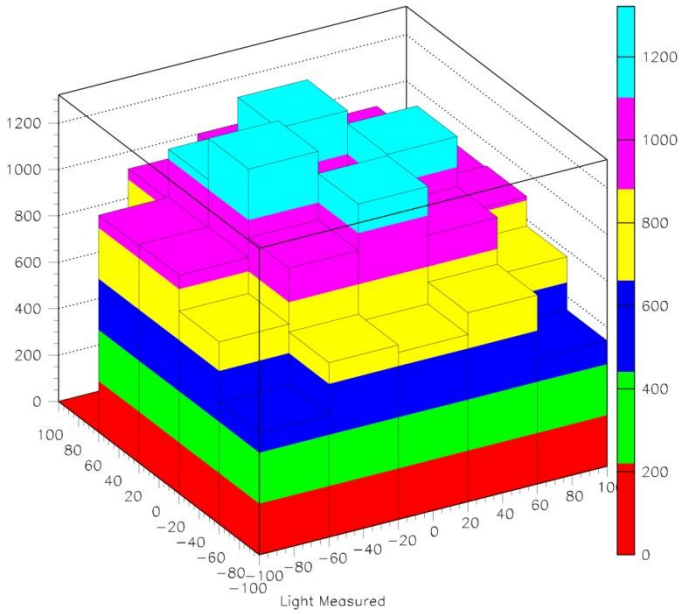

Figure 16.16. The relative amount of light in the different MAPMT positions for the LED in the Roman Pot. The plot is made by KH.

As the plot shows the corner MAPMTs sees about 40 % of the light amount seen in the center MAPMTs and thereby a there are a difference of about 250 %. The aim was less than a 20 % difference. Also it was discovered that the outer channels on the corner MAPMTs might not see any light at all. Therefore the work to improve the design of the LED inside a Roman Pot stopped.

The LED inside the Roman Pot was used in few early test of the motherboard where a light source was needed, but where it did not matter too much how much light reached each MAPMT.

16.3.2.2. Calibration box

A new approach to an equal light source for all MAPMTs in a convenient fashion was needed. KH had no more time for the project and the author therefore took over almost completely.

The new idea shame was very simple: Get long enough away from the light source (the LED) and the light distribution will be (almost) flat over a small surface. No optics at all.

It would be most convenient to have the mu-metal grid frame horizontally as it would be for the top detector in the installation. This pretty much made the design: A horizontal detector with a LED far away => a box with a LED at ground level and the detector outside on top of the box in a convenient working height. Figure 16.17 (left) shows a sketch of the calibration box.

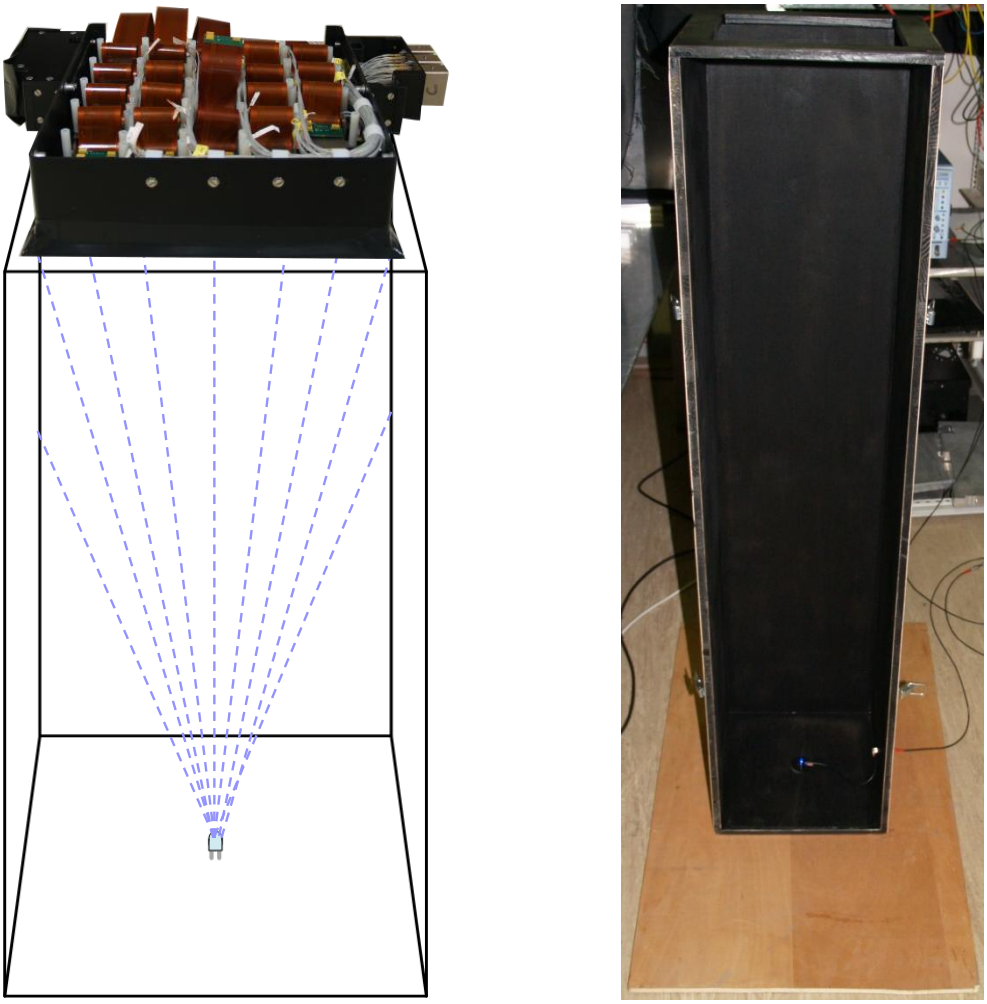

Figure 16.17. *LEFT*: Sketch of the calibration box. *RIGHT*: The calibration box. The box is open so the LED is shwon.

This was presented at an ALFA meeting and approved. As no real high precision was needed, no technical drawings were made. The sketch was given directly to a technician together with the size of the mu-metal grid frame and he made the calibration box from that. Figure 16.17(right) shows the open calibration box.

To check the distribution of light on the MAPMTs position a measurement like the one described in the LED in a Roman Pot in Section 16.3.2.1 was made. Since the base plate was no longer availably the MAPMT position was found via a mu-metal grid frame made out of POM. The other end of the Teflon piece was made to fit in the mu-metal grid frame and the PMT was again mounted inside the Teflon piece. The setup is shown in Figure 16.18.

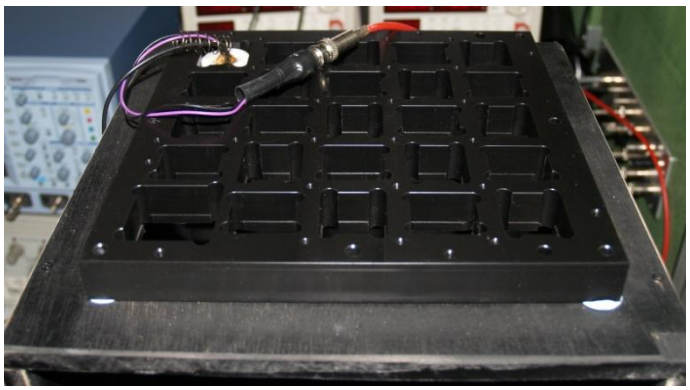

Figure 16.18. The mu-metal grid frame made in PMT whit the Teflon piece holding the PMT.

The top of the box was covered with black fabric and measurements like for the LED in the Roman Pot was started. After e few measuring points it was clear directly from the data on the oscilloscope that the light was not evenly distributed. This time the light was not more intense in the center but to one side. This was very unexpected and instead of wasting time finishing the rest of the measuring point, error finding was started.

It turned out that a particular bad LED had been used. The LED is shown in Figure 16.19.

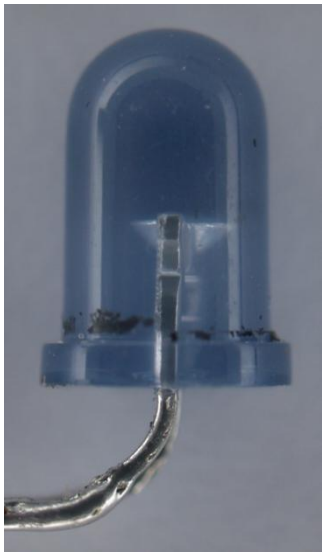

Figure 16.19. The LED with badly center light emission point.

As can be seen in Figure 16.19 the position where the light is made inside the LED is not centered but much to one side. The optics of the LED itself will therefore make the LED send light to one side.

A selection process was made over all availably LEDs and the one with the best centering was used to replace the LED in the calibration box.

The measurement was repeated for all position of MAPMTs. The results were sent to KH who then made the plot shown in Figure 16.20.

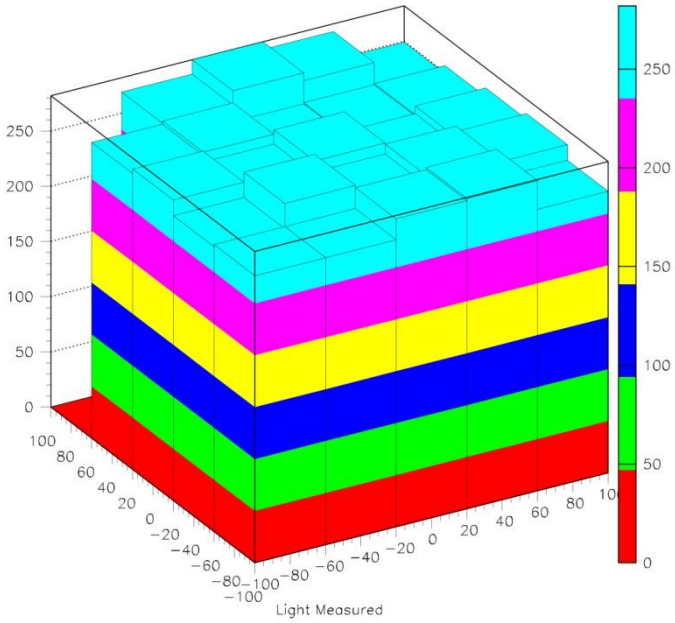

Figure 16.20. The relative amount of light in the different MAPMT positions for the calibration box. The plot is made by KH.

It is seen that the light levels are the same within about 10 %. Also no real pattern in the light distribution is seen. The fluctuations might reflect the uncertainties of the measurements itself. The calibration box was therefore taking into use in the motherboard test and was intended to later be used for the calibration of all ALFA detectors.

16.3.3. Equipment test prior to the test beam

The motherboard had never been tested with real MAPMTs. Only artificial injection of charge. Such a test was of cause needed before a beam test. This would at the same time be a test of almost all systems needed in the test beam.

The author participated in this and made comparisons to what was know from the cosmic setup with 5 Orsay boards.

16.3.3.1. The equipment test setup

The mu-metal grid frame was mounted on top of the calibration box. Even though the mu-metal grid frame was a final version with the edge inside preventing the MAPMTs to fall out, it was necessary to put a spacer in to push the MAPMT back because the shims on the MAPMTs was made wrong with the spacer sitting to low on the MAPMT so there was a danger for short circuit the high voltage on the mu-metal grid frame.

The motherboard was mounted on the side of the calibration box as on an ALFA station. The setup is shown in Figure 16.21.

Figure 16.21. The setup use for equipment test prior to the test beam.

The mu-metal grid frame is covered with a black box to protect the MAPMTs against light. A large fan is connected through a hose to the black box to provide cooling for the electronics.

The readout of the motherboard is done over a fiber optical link. For the tests two data acquisition, DAQ, systems was used: The old system Filar was used to make S-curves (see Section 16.3.3.6 page 204) and the new system MROD was used for everything else. Physically Filar is a direct connection on a PC interference card, while MROD is VME modules (sse Section 13.2.4).

The triggering was done using a TLU-box from EUDET [76]. Sending a NIM signal (or an analog signal) would trigger a readout. The TLU-box could also make coincidences of up to 4 signals or work as “or”.

Low voltage was supplied by two standard laboratory power supply units, PSUs.

High voltage was connected with multi wire cables from an ISEG custom made multichannel high voltage PSU (See Section 13.2.5). The HV PSU could solely be controlled via computer interferences, where all information about voltage, current, rise time and so on could be viewed and changed.

16.3.3.2. Basic test

The first test was very basic: See a difference in data with and without LED light on the MAPMTs. After some debugging this was achieved.

16.3.3.3. Light tight

A very basic test was made to with no LED light to see if the black box was light tight. It turned out that it was not. Signals were seen in MAPMTs in one side of the black box. After some small adjustment the test was repeated and the black box was light tight.

16.3.3.4. Mapping test

Next a check of the MAPMT mapping and channels mapping was made. This was done by simply covering half of the MAPMTs in the mu-metal grid frame with black paper and making a run. The setup is shown in Figure 16.22.

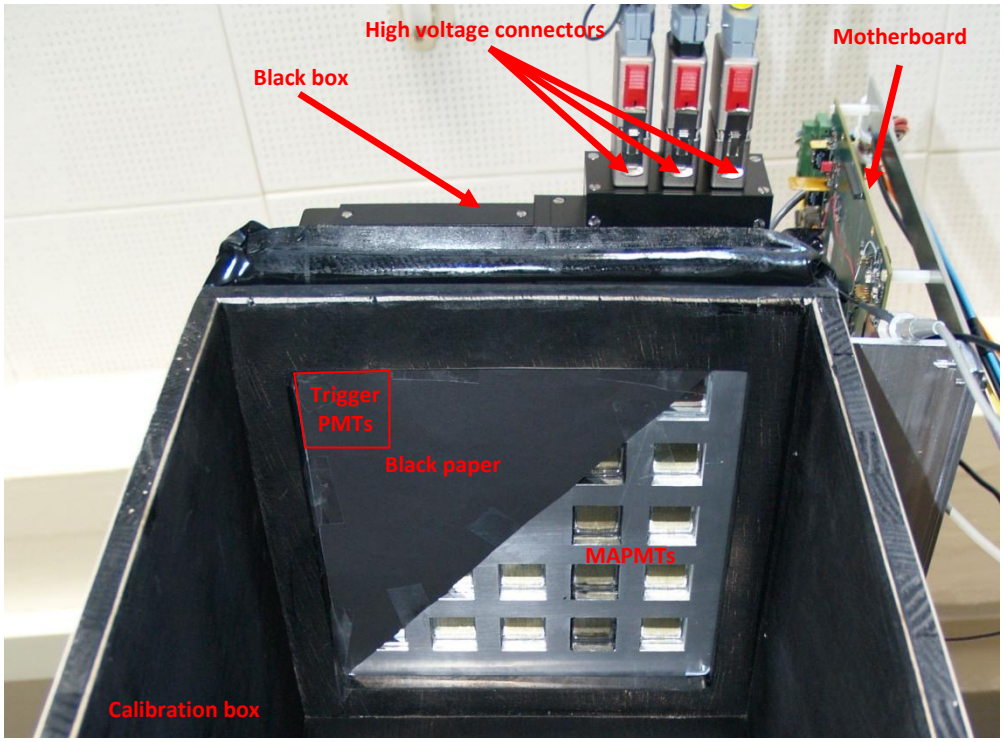

Figure 16.22. Setup on top of the calibration box. Half for the MAPMTs are covered with black paper.

The readout result is shown in Figure 16.23.

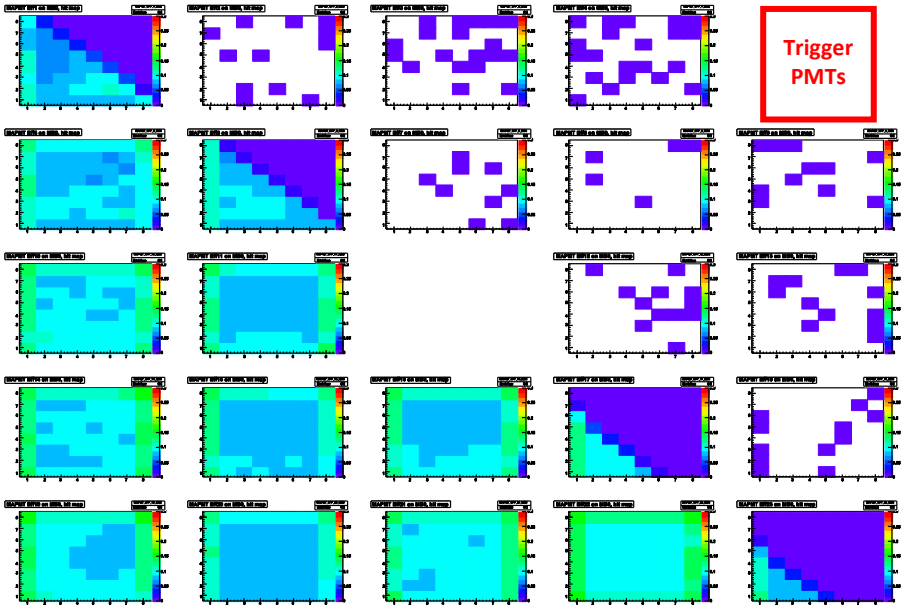

Figure 16.23. Result from the mapping test. The hotter the color the more triggers with signal over the threshold. The figure is made by MH.

The shape of the black paper is clearly seen. Both on the overall MAPMT position and on the channels position in the MAPMTs. Therefore it was concluded that the mapping was correct.

The mapping test was repeated for the other mu-metal grid frame with similar results.

16.3.3.5. Edge effect

In Figure 16.23 the MAPMTs that are not covered seem to have a higher rate of signal over the threshold in the edge channels compared to the central channels (this are actually from the test of the second mu-metal grid frame, but the effect was discovered on the test of the first mu-metal grid frame). This effect could be due to the aluminum frame supporting the spacers to push back the MAPMTs. These spacers was necessary because the shims used was not positioned correctly and therefore did not keep the MAPMT in a distance that would secure the high voltage board from touching the mu-metal grid frame. Some reflections in the spacers or in the aluminum support might make the light distribution un-equal. Therefore the setup was disassembled and the aluminum and the side of the spacers colored black to eliminate reflections. This can be seen on Figure 16.24 and on Figure 16.23 (as the photo is from the test of the second mu-metal grid frame and made later).

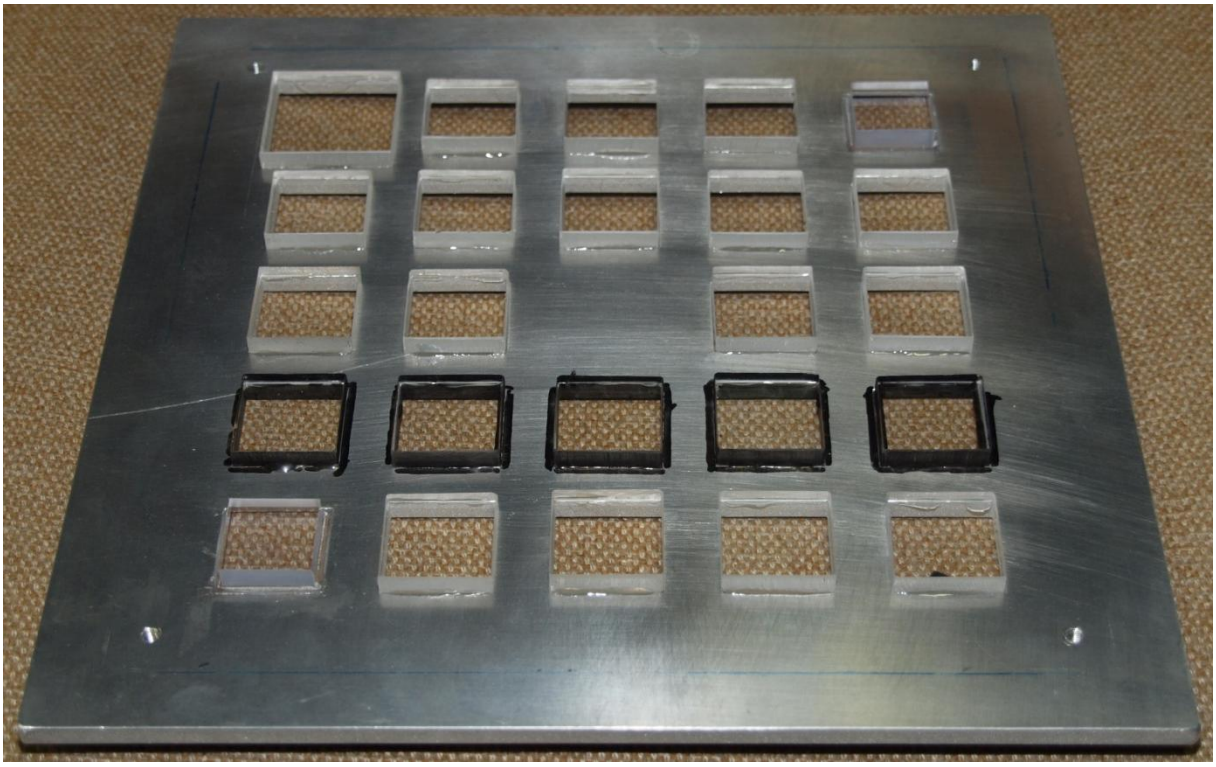

Figure 16.24. Aluminum with spacers. The sides of the spacers and on the aluminum are colored black on the 4th row.

A run was made and the results after offline reconstructions are shown in Figure 16.25.

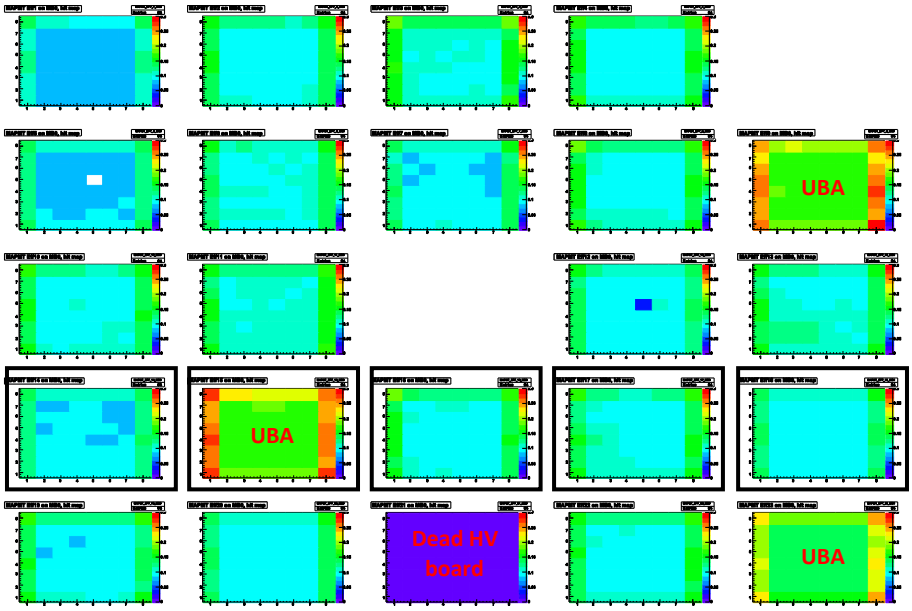

Figure 16.25. Result from the reflection test. The row with colored sides are marked with black. One MAPMT had a bad high voltage board. There are 3 Ultra Bialkali MAPMTs. The original plot is made by MH.

There is no visible effect from the coloring. Furthermore a similar effect was observed with the perpetration of the cosmic setup. In Figure 16.26 is shown the charge (average light) and the binary (rate of triggers over threshold) data from a test on the cosmic setup.

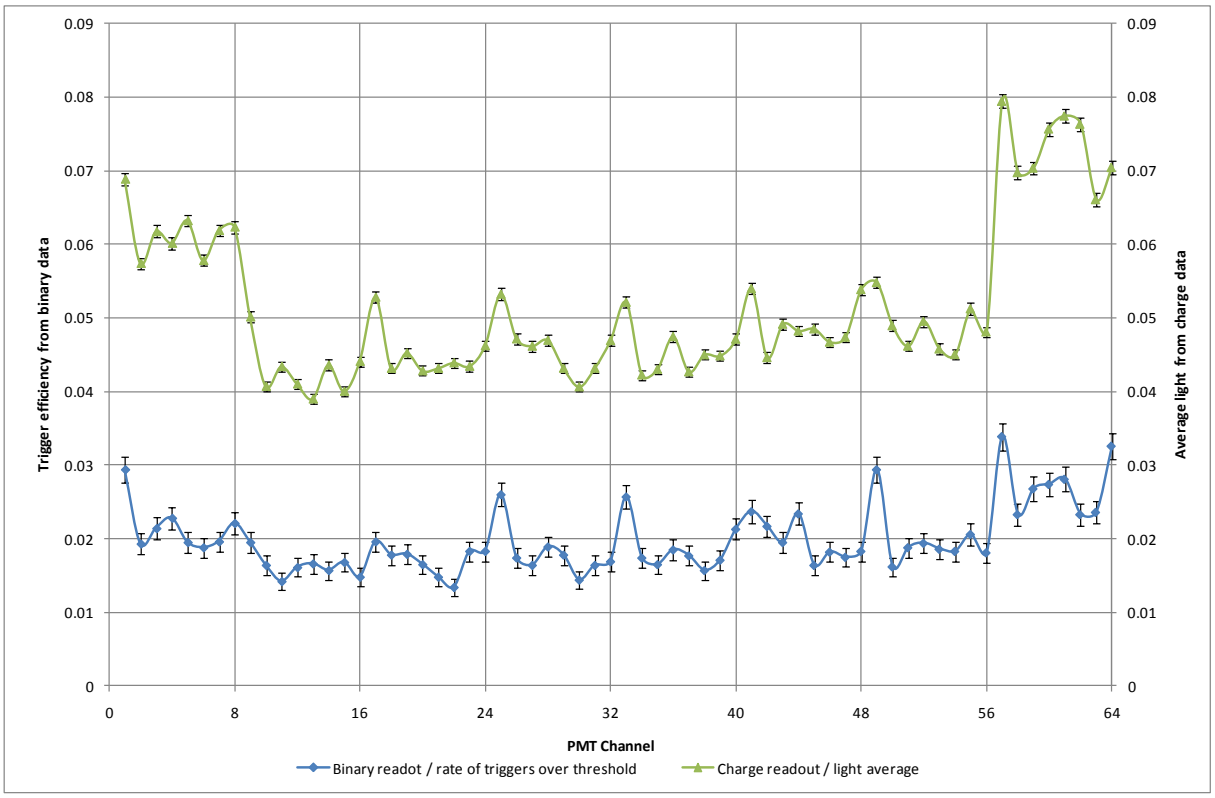

Figure 16.26. Charge and binary data from a test on the cosmic setup.

The test was done with a pulsed LED at low light level. It is clearly seen that the first and last 8 channels on the MAPMT have a higher average light level and rate of triggers over threshold. These channels correspond to the left and right edge on the MAPMT seen in Figure 16.25. Channel 17, 25, 33, 41, 49 also shows higher levels than the surrounding channels. This correspond to the higher edge on MAPMTs in Figure 16.25. It was therefore concluded that the effect was a property of the MAPMT. Likely a higher electron capture probability of the first dynode. (Figure 16.26 was originally made to compare charge and digital readout. The rate of triggers over threshold was lower than expected compared to the average light seen in the charge readout. This was later explained because the readout time of the digital data was not optimized under the test).

16.3.3.6. S-curves

The main tool to verify the performance for the electronics and MAPMTs had the in previously test beam been threshold scan of trigger efficiency call S-curves. S-curves made with the cosmic setup is discussed in Section 15.3.2 and shown in Figure 15.14 page 166. For the cosmic setup on the Orsay test board it was time demanding to make as it had to be done manually. But with the motherboards this had been atomized so only the number of point of threshold and the number of triggers at each threshold had to be input and software then made all the changes and stored the S-curves.

The average light level was adjusted to about 0.2 PE and a number of runs were made. An example of an S-curve is shown in Figure 16.27.

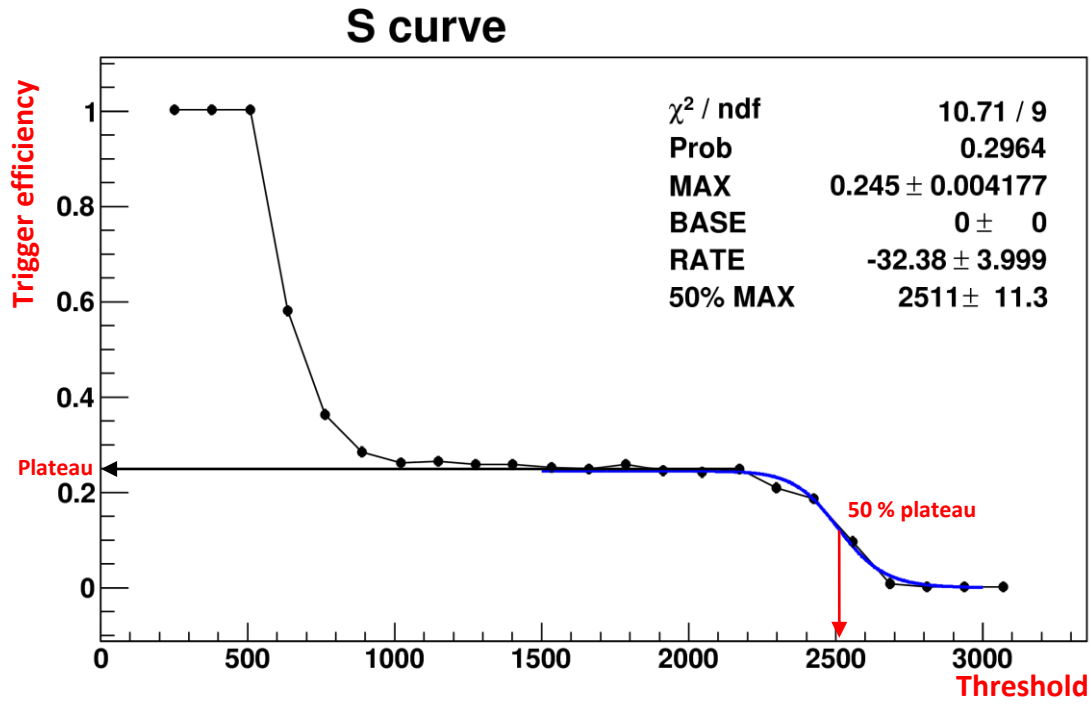

Figure 16.27. S-curve with plateau and 50 % plateau. The light level average was about 0.2 PE. The graph is original made by MH.

In the previous test beam a difference of the plateau height for different MAPMT channels had always been observed and explained by the different gain. It was therefore expected that the plateau height should be equalized with the gain. A run with all gain set to 16 was therefore made and compared to a run where the gains was equalized. The results are shown in Figure 16.28.

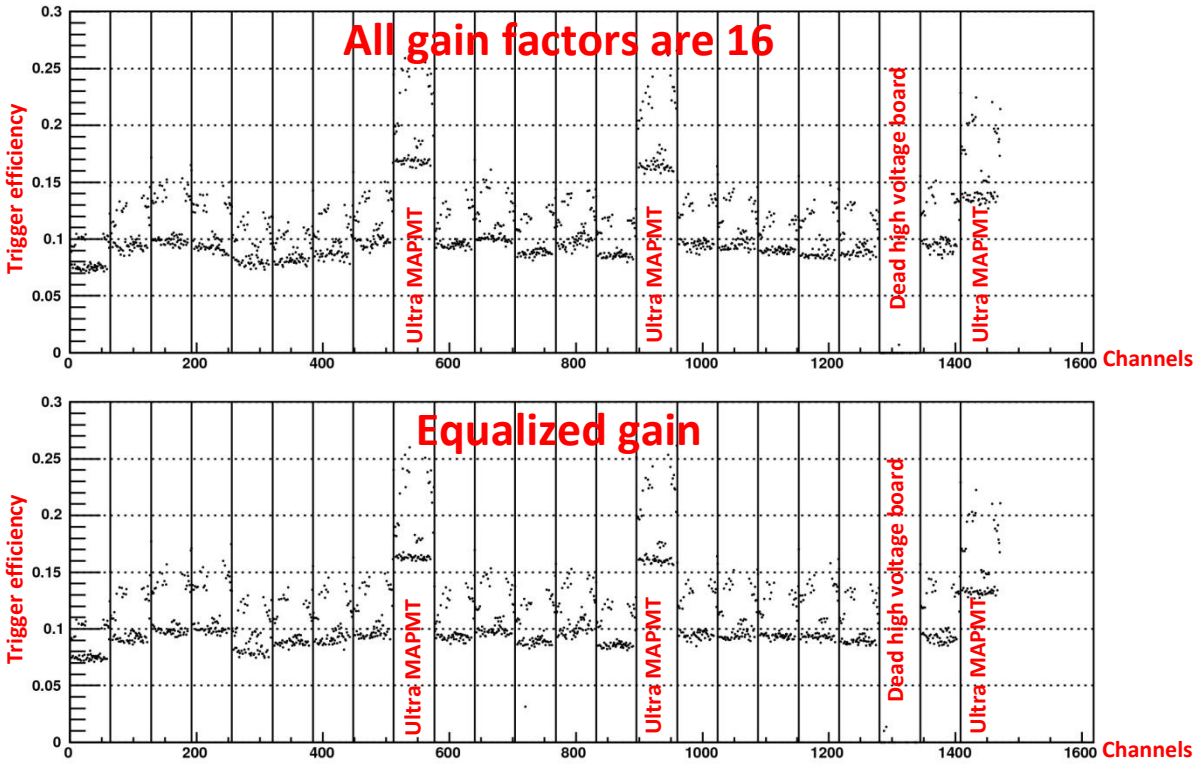

Figure 16.28. Plateau height for all channels in ALFA2. On top all gain factors are set to 16. On bottom the gain are equalized. The average light level is about 0.1 PE. Black part of the figure is made by MH.

There are no significant differences seen by equalizing the gains, which was rather unexpected.

This result led to a lot of discussion and small test:

Was the mapping of the gain factors correct? This was checked by setting same gain factors to 0 and look for which channels had no data. The gain factor mapping was correct.

Was the gain factors themselves correct? This was very hard to check as the motherboard did not have support for charge readout.

Did the gain factors work at all? A test was made where all gain factors were multiplied by 1.5. No significant difference was observed. But putting the gain factors to 0 did make the signals disappear. So the gain factors did have some kind of impact.

Why was there a similar pattern for the distribution of each MAPMT? The answer was the edge effect discussed in Section 16.3.3.5. The higher light yield is of course also seen in the trigger efficiency and this more than anything else explains the differences between different channels. Furthermore the overall MAPMT differences in the trigger efficiency of about 10 % can be expected from the quantum efficiency.

It was suggested that it might be better to look for difference between gain equalization and all gain set to 16 in the slope from the plateau to 0. There the fit of 50 % plateau was introduced as shown in Figure 16.27 page 205. The results from the 50 % plateau are shown in Figure 16.29.

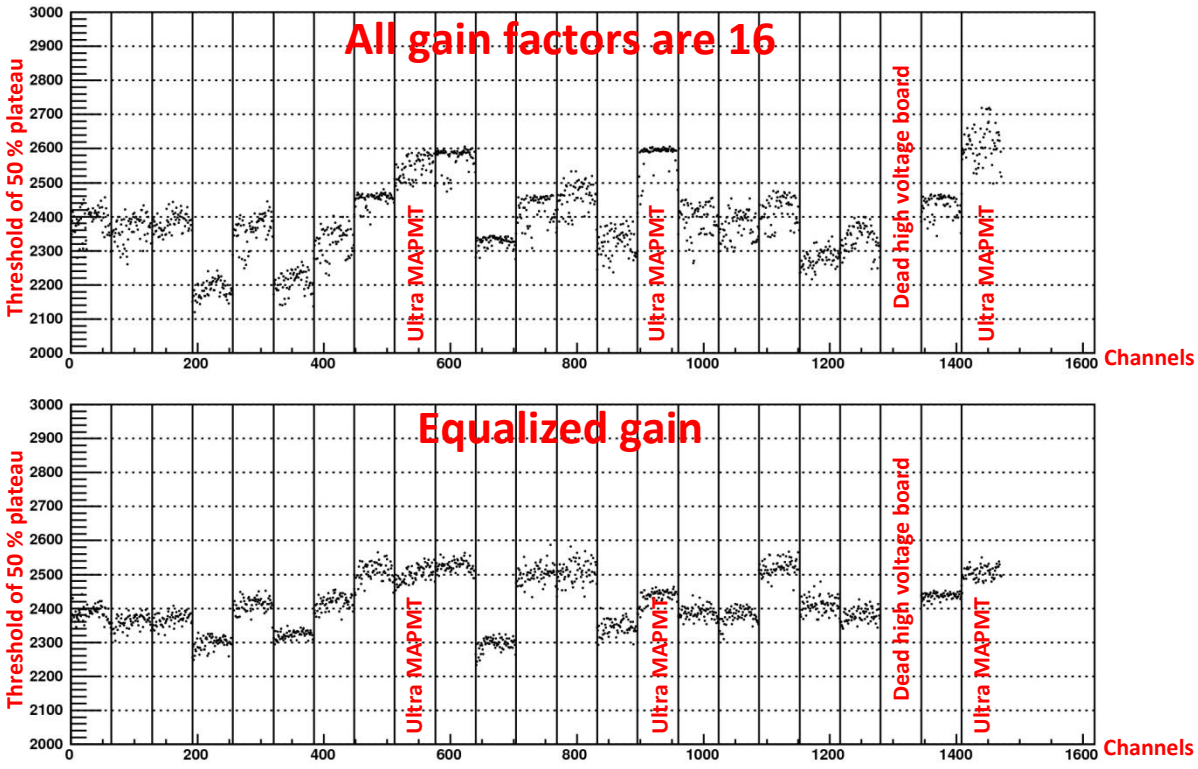

Figure 16.29. Threshold at 50 % plateau for all channels in ALFA2. On top all gain factors are set to 16. On bottom the gain are equalized. The average light level is about 0.1 PE. Black part of the figure is made by MH.

Here some improvement is seen in going from all channels at gain factor 16 to equalized gain: With all gain factors 16 the threshold at 50 % plateau is between 2130 and 2730. With equalized gain the threshold at 50 % plateau is between 2250 and 2570. Also there is a tendency that inside each MAPMT the values are less spread. This gave confidence to the gain factors and the way they were applied. But it was still not understood why the gain equalization did not help more.

The final answer came some time after the test beam (partly by investigating a suggestion from the author). The range in the binary readout was not well fitted to the range of the signal from the MAPMT. The linear part of the range only goes up to about 1/3 of the signal from 1 PE. After that the rage becomes closer to logarithmic. This means that even a small signal will be over threshold in the linear part. At high threshold the shape of the S-curve is mainly determent by the range limitations and only partly by the gain settings. A test was later made with about 5 times higher gain. It would have been expected (if the range was linear) that the plateau should end at a higher value, but no significant difference was observed at high threshold. This verified the range limitations.

The range mismatch between charge from the MAPMT and the digital readout was not fatal. It just meant that the threshold could not be used to cut noise and crosstalk in a range as large as expected.

16.3.3.7. Short cosmic run with motherboard readout

In the last days leading up to the test beam it was decided to make a short cosmic run with readout done by the motherboard. This would not give enough data to evaluate any performance of the detector or electronics, but it would be valuable to test that everything was working. Also some real data from particles crossing the detector is valuable to optimize the software needed under the test beam.

The setup was adopted from the cosmic setup with Orsay test boards discussed in Section 15.5.2 with a schematic shown in Figure 15.16 page 168. But here the readout was done with a motherboard and only the internal main trigger tiles were used to make a coincidence to trigger a readout. The setup is shown in Figure 16.30.

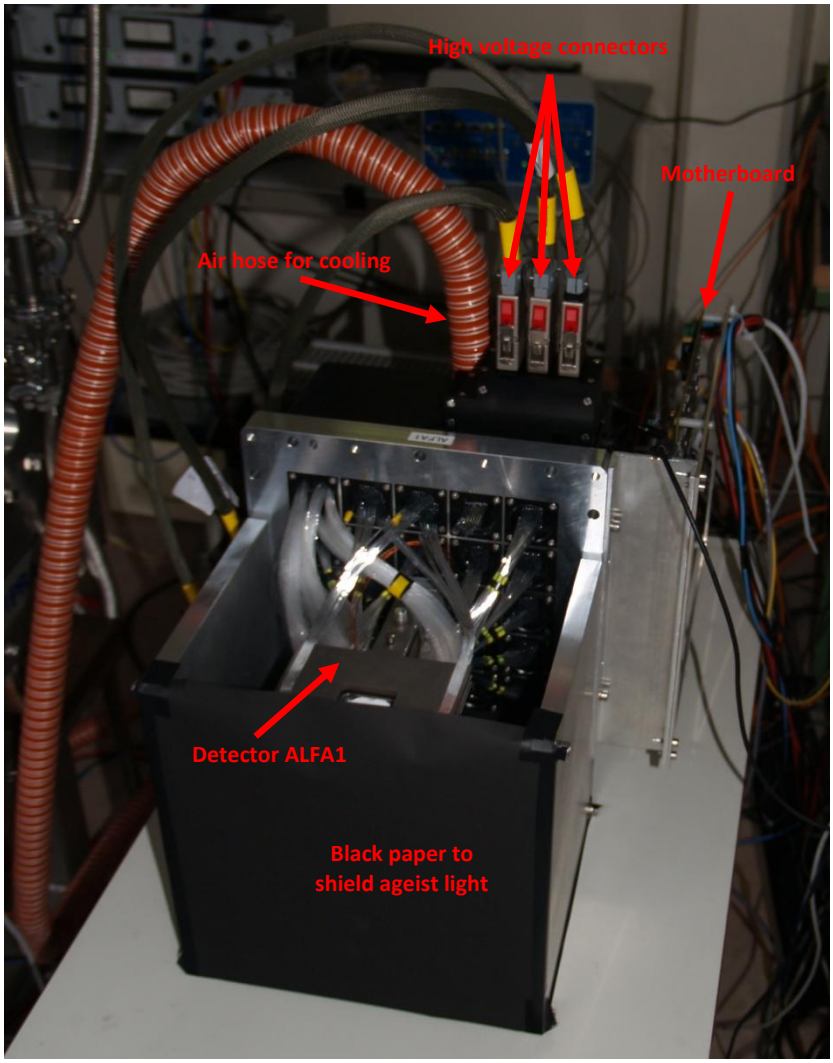

Figure 16.30. Setup for cosmic run with motherboard.

It was not possible to place the setup in a black chamber, so instead it was covered with black paper and tape and later black fabric.

The readout time (pipeline delay) had to be optimized. To optimize this with low rate cosmic would be very painful and time consuming. So a Sr-90 source was placed on top of the main triggers and the first main layer of scintillating fibers after the trigger tiles was readout. The electrons from the source did only penetrate the first few layers of the full detector, but for optimization of the readout time the first layer was sufficient.

A scan of the delay was made to optimize readout time. This was done by setting a delay and then taking data for a given time. The highest numbers of hits was then used as optimal readout time. See Section 16.4.6.1 for the optimization of the pipeline delay at the test beam.

After the trigger delay optimization a cosmic run was made. Figure 16.31 shows a screenshot of the first cosmic event.

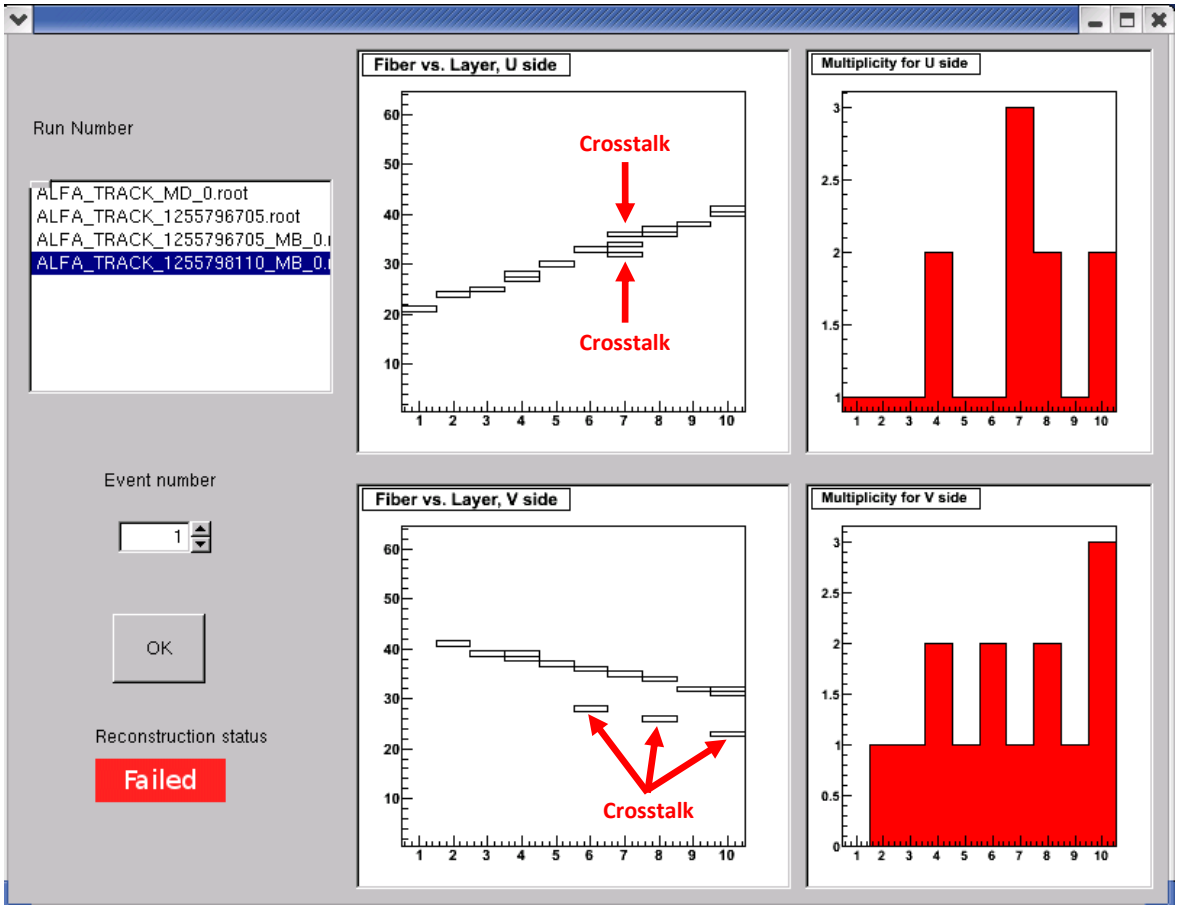

Figure 16.31. Screenshot of the first cosmic event. Software made by MH.

The central plots show the layers in the detector (x-axis) and the fibers in each layer (y-axis). A track is clearly visible. This gave great confidence that everything was working. It also showed that all mappings were applied correctly. A few extra hits are visible. From the fiber/MAPMT mapping this is clearly crosstalk (light from one fiber hitting the neighbor MAPMT channel as shown in Figure 14.53 page 139).

A cosmic run was made for about 2 days. The trigger rate was much lower than expected from cosmic (see Section 14.3.4). An investigation revealed that the average signals from the trigger PMTs were much smaller than previously seen. It turned out that the PMTs installed were Hamamatsu type 7400U where the ones previously used had been Hamamatsu type 7400P. The main difference between the two types is the gain. Therefore the signals were much smaller than previously seen and often below the threshold of the discriminator. At the test beam amplifiers were therefore added.

Over the last night of the cosmic run a high voltage module tripped. It turned out to be because of too high temperature. Therefore fans were added at the test beam.

The data from the cosmic run was used to optimize some of the software later used at the test beam.

16.4. The test beam

The 3 first days of the test beam time was used to transport everything to the test beam area (H6B (PPE 156) SPS at CERN with a beam of 120 GeV pions), set it up and test everything without beam (or only with muons). On the 3rd day everything was aligned to the theoretical beam axis by the CERN alignment group. Figure 16.32 shows the final setup for the test beam. The details of each part are described in the following sections.

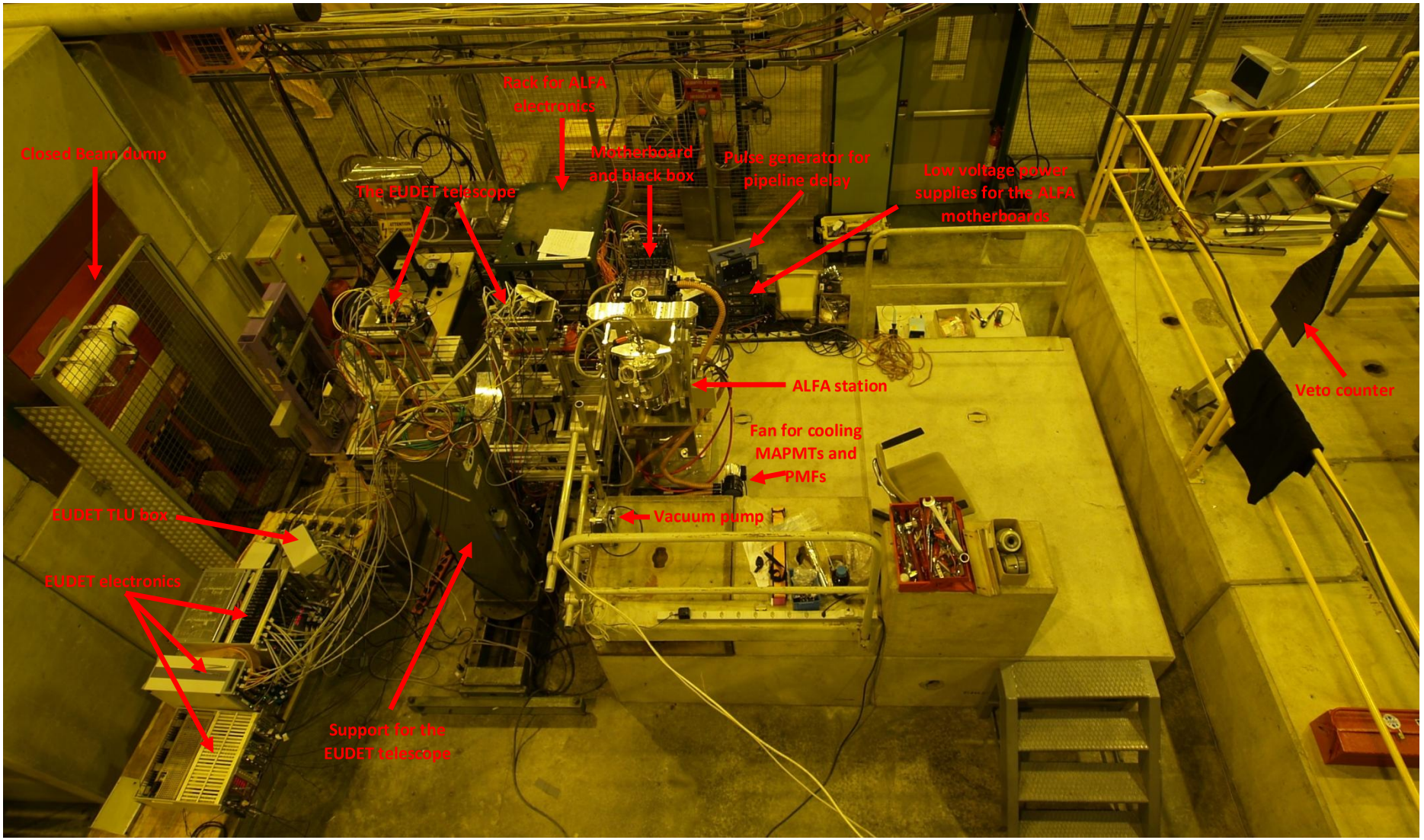

Figure 16.32. Final setup for the test beam 2009. The beam is coming from the left side.

16.4.1. The test beam setup

The idea of the setup was to test a complete ALFA station in conditions as close as possible to the working conditions in the tunnel. Therefore the detectors were installed in Roman Pots and the Roman Pots in the station. The installation of a detector in a Roman Pot is difficult as the gaps between the detector and the Roman Pot are of the order of 100 µm and pieces are fragile. Custom made insertion tools (that later was perfected to be used in the installation in the tunnel) was therefore used and the detectors was installed successfully. The Roman Pots (and thereby the detectors) were locked in the most inner position. The position is shown in Figure 16.33. The beam is coming directly toward the spectator.

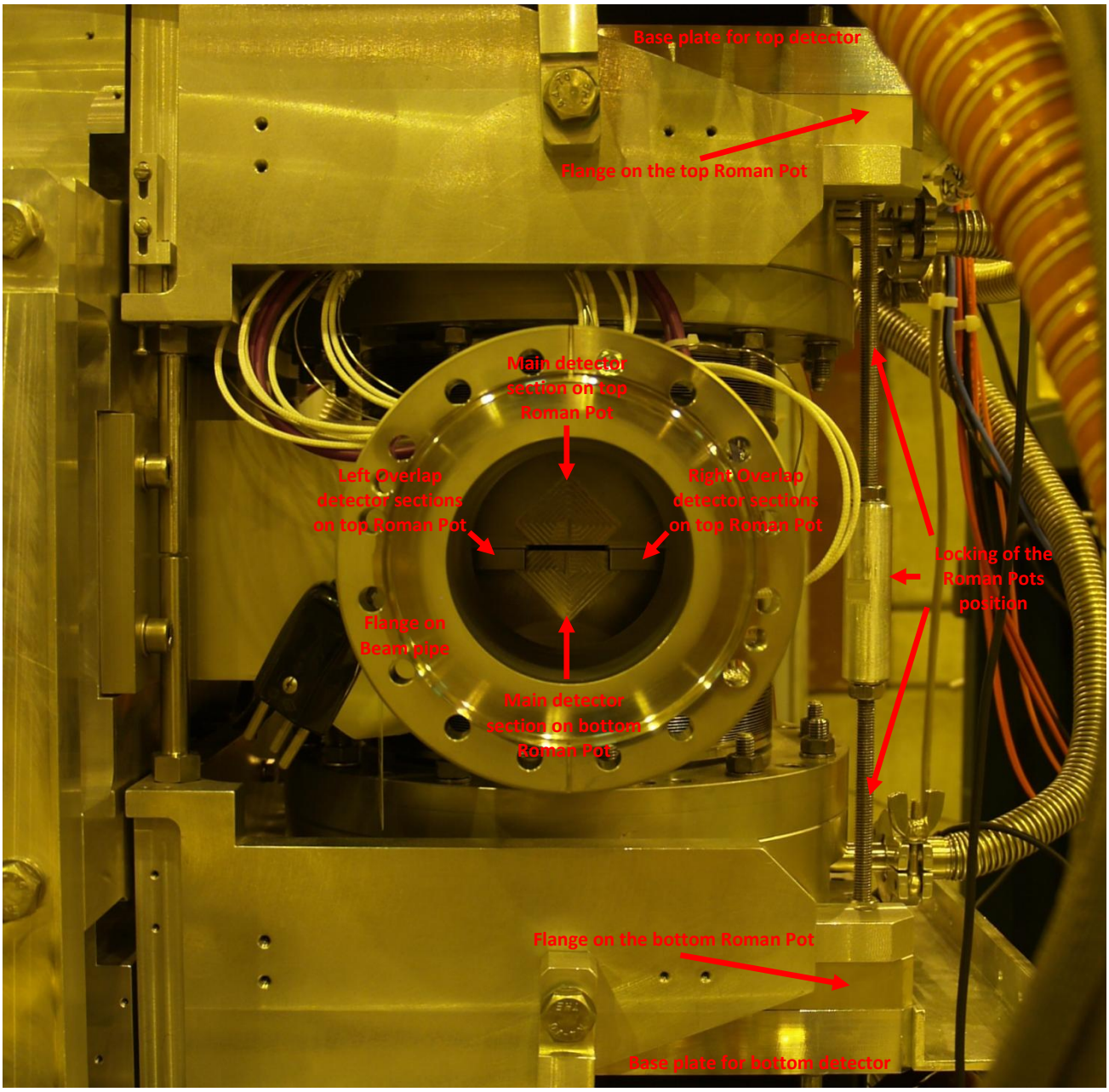

Figure 16.33. Roman Pot (and thereby detector) position under the test beam.

The idea was to keep the detectors in the same relative position to avoid uncertainties induced by the moving mechanism. The beam is only a few millimeters wide. It was therefore not possible to irradiate the entire detector at the same time. To keep the relative detector position the entire station was therefore made adjustable in both directions perpendicular to the beam. The movable table that made it possible is

shown in Figure 16.34. The adjustments were measured with a digital sliding caliper and a two-directional weather leveler.

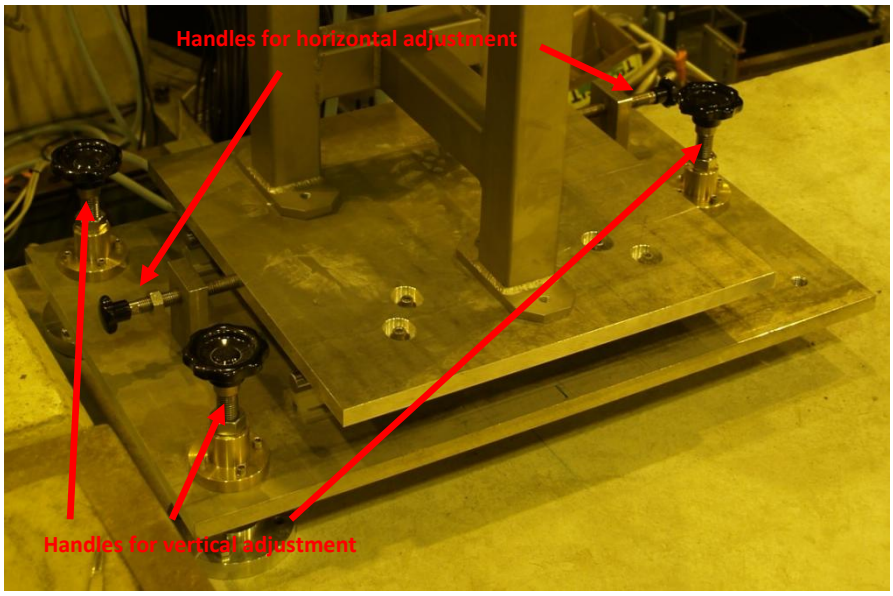

Figure 16.34. Movable table for adjusting height and position of the station.

Afterwards the black boxes with MAPMTs etc. were installed and then the motherboards. The motherboards were connected to the MROD DAQ system via a fiber optic link. All electronic were tested and was working almost immediately.

Figure 16.35 shows the station with all parts installed.

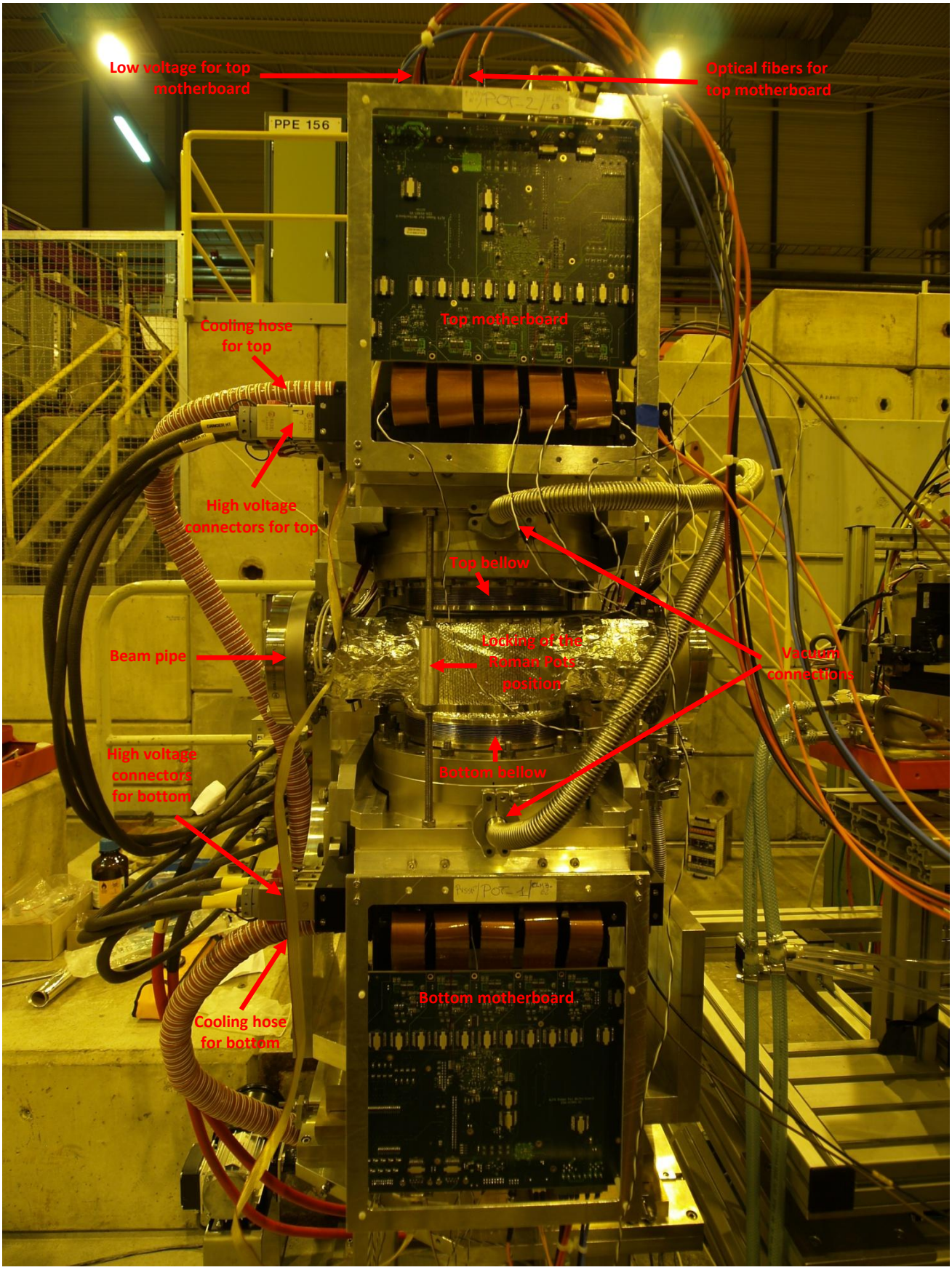

Figure 16.35. Station with all parts installed. The beam comes from the right side.

16.4.2. The EUDET telescope

This section is based on [77].

In order to make resolution, edge etc. studies it is needed (or at least preferable) to know the position of each particles very well (an external tracking reference). ALFA is by far not the only user at test beams that need to know the particles position with very high resolution and therefore the European Union has funded the making of a beam telescope called EUDET [77] with is shown in Figure 16.36.

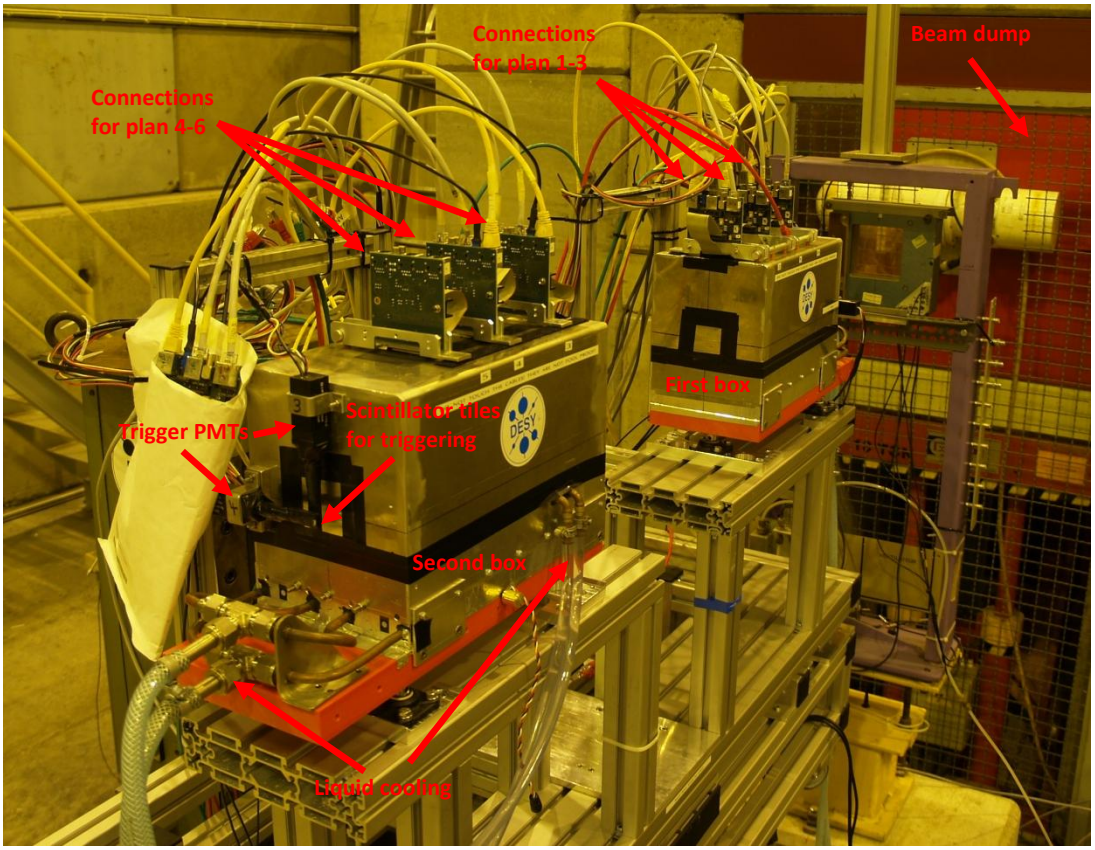

Figure 16.36. The EUDET telescope.

The EUDET telescope has 6 planes (only 5 were working when it was used by ALFA) of pixel sensors spread over two boxes. The sensors had just been upgraded to Mimosa 26 with an active area of 21.2 mm · 10.6 mm and 1152 · 576 pixels. The pixel pitch is 18.4 µm. ALFA was the first user to use the new sensors.

The sensors are cooled with liquid.

The readout is done with WME x64 boards with build in zero-suppressing.

It is supported on a platform that can be moved by motors in both directions perpendicular to the beam. This makes it possible to make adjustment of the position from outside with the beam on. This option was not used by ALFA.

The triggering is normally done by 4 scintillator tiles (2 perpendicular to each other in front and 2 perpendicular to each other after the telescope) readout by PMTs. As the sensors had been upgraded to larger ones also the scintillaor tiles had to be changed to larger piece.

EUDET has developed their own trigger logic unit (TLU) with 4 inputs. The TLU includes discriminators and coincidences units. But the most essential task of the TLU is to provide event numbers and timestamps.

Normally the devise under testing is put between the two boxes with plans. This means that the track is interpolated between the two EUDET boxes and this gives a very high resolution of about 3 µm. But for ALFA it was unfortunately not an option to put a station between the two boxes as the spaces was insufficient. Therefore ALFA was put after EUDET and the tracks had to be extrapolated, which would mean a lower resolution in the end.

16.4.3. Triggering

The custom made triggering boards (the trigger mezzanine, see Section 13.2.3) that will be used in the final installation at LHC were not available at the test beam. Therefore the trigger system had to be built out of standard NIM electronic. The author made the triggering system in cooperation with Christian Joram (CERN PH-DT).

As triggers there where: 4 scintillator tiles surrounding EUDET, 2x2 main scintillator tiles in the ALFA detectors, 2x2 overlap scintillator tiles in the ALFA detectors. All read out by PMTs.

A first test in the test beam zone revealed that the signal from all PMTs in the ALFA detectors was much smaller than normally seen. As discussed in Section 16.3.3.7 it turned out that the PMTs installed was of a lower gain type than was intended. To counteract this all ALFA trigger signals had to be amplified.

The overall trigger logic is shown in Figure 16.37.

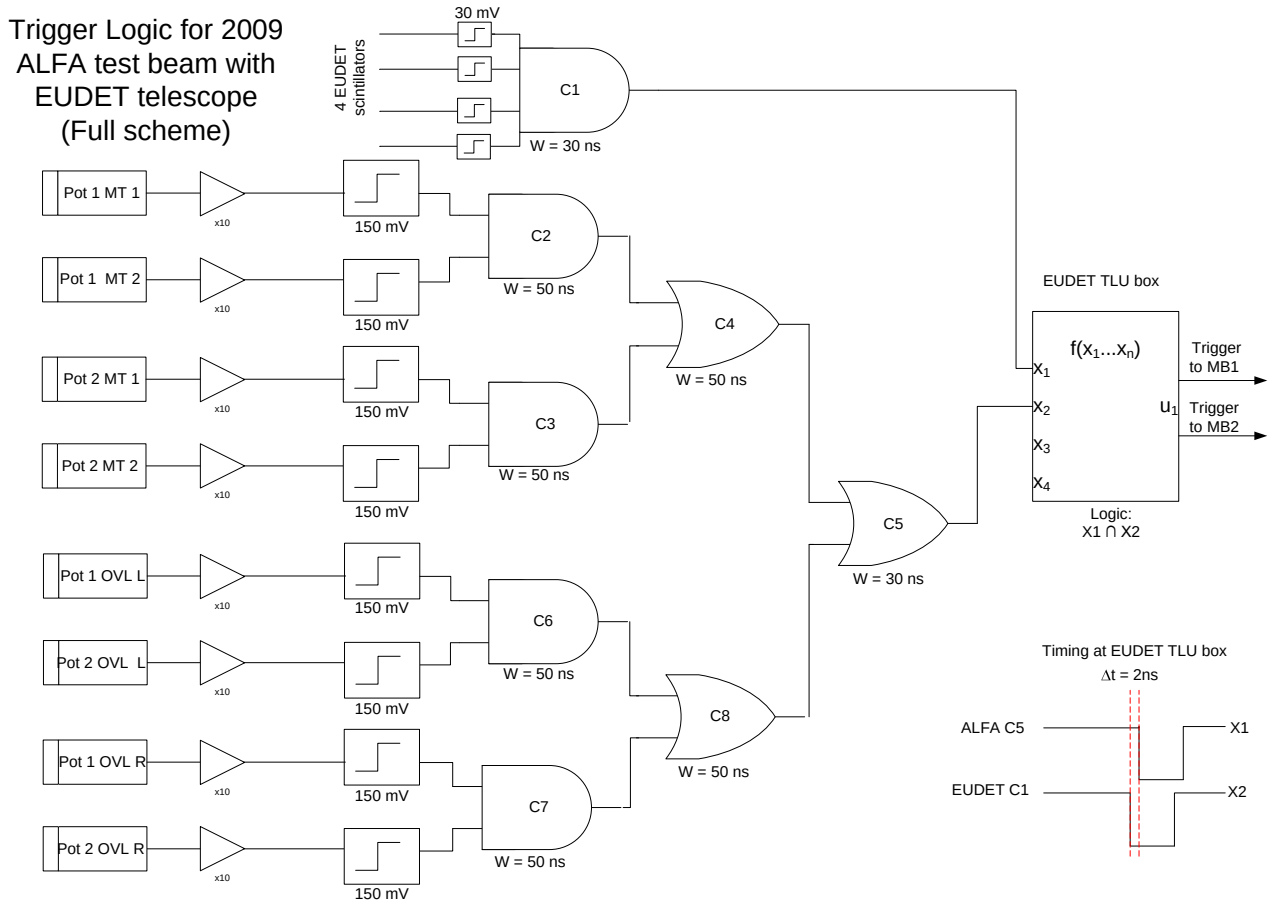

Figure 16.37. Main trigger logic used for ALFA test beam. The figure is a modified version original made by Christian Joram (CERN PH-DT).

The signals from the EUDET trigger PMTs were discriminated with a threshold of 30 mV. Then a coincidence (C1) was made of all of them and a NIM signal send to the EUDET TLU box.

The signals from the ALFA main triggers were first amplified by a factor of 10 and were then discriminated at 150 mV threshold. A coincidence (C2) was made of signals from two main triggers from the same detector. Then the signal passed thought an “or” unit (C4) to be combined with the coincidence (C3) of the other mean trigger.

The signals from the ALFA overlap triggers were first amplified by a factor of 10 and were then discriminated at 150 mV threshold. A coincidence (C6) was made of signals from left overlaps of both detectors. Then the signal passed thought an “or” (C8) unit to be combined with the coincidence (C7) of the right overlap triggers.

The combined main trigger signal (C4) and the combined overlap trigger signal (C8) were then combined in an “or” unit (C5) and sent to the EUDET TLU.

The EUDET TLU then triggered in case of a coincidence from the coincidence from EUDET triggers (C1) and the combined ALFA trigger (C5). The delays were made so that the combined ALFA signal (C5) was about 2 ns later than the EUDET coincidence (C1). This was done so the coincidence would always be defined by the combined ALFA signal (C5), and not sometimes the combined ALFA signal (C5) and sometimes the EUDET coincidence (C1).

The TLU box sends a trigger to the motherboards, make a timestamp and event number.

The timing of all signals was checked and optimized using a digital oscilloscope. As the zone is not accessible when the pion beam is on, so this was done by shooting a low intensity pion beam into the last beam dump before the setup. The secondary muons from the beam dump were then used for timing studies. See Section 16.4.4 for more information about the beam setup.

Figure 16.38 shows the rack with the trigger system, high voltage, DAQ system etc.

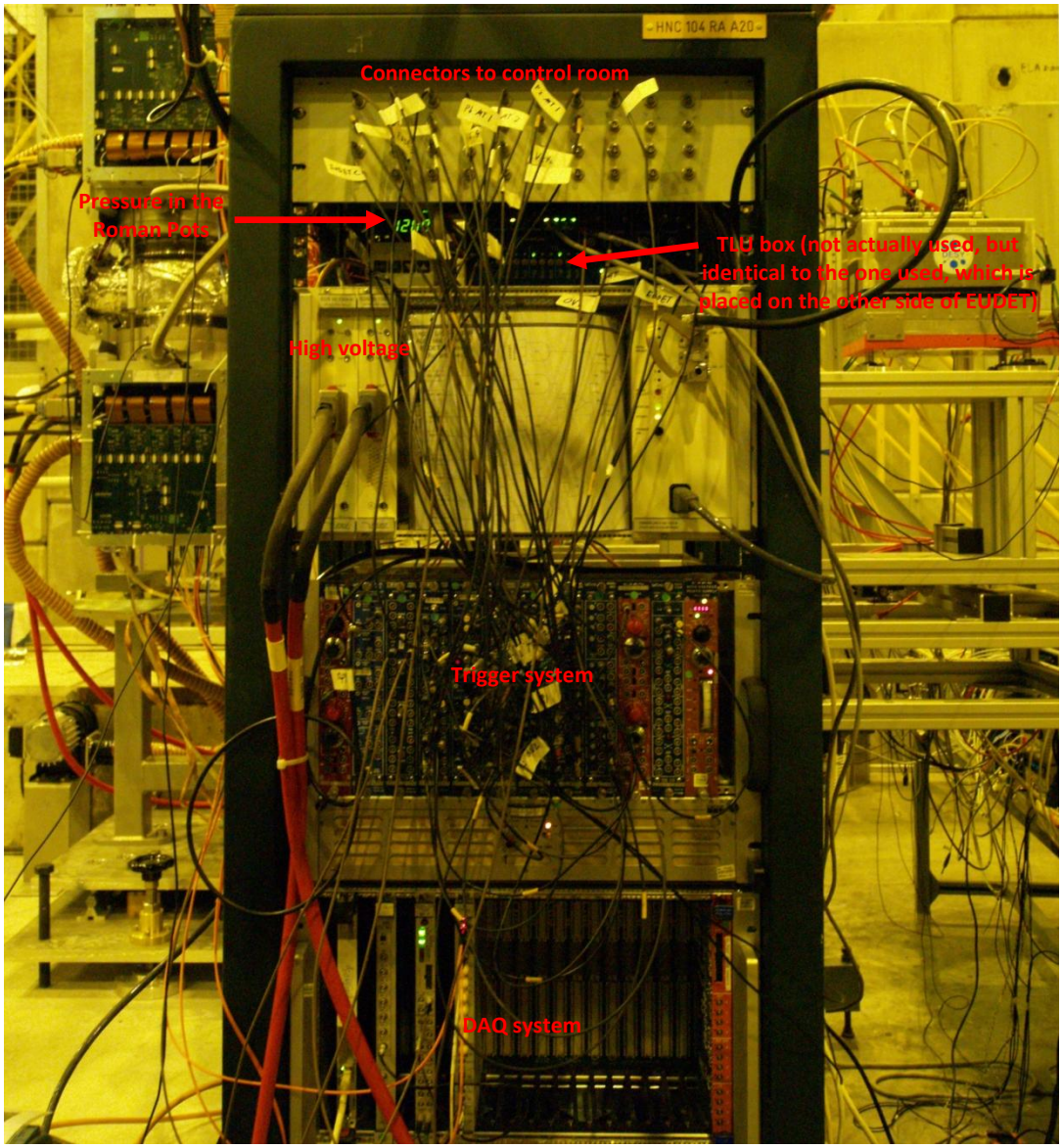

Figure 16.38. Rack setup from the test beam.

The discriminated signal for all PMTs and all outputs for logic units (CX) was doubled and the spare signals send all the way to the control room. These made it possible to check signals from outside with beam on. This proved very useful. Many checks were made. The most imported discovery was that there was no coincidences for the overlap triggers (C8 = 0). From the checks from outside (made by the author) with beam on, it was found that there was a right-left swop for the lower detector. This was quickly counteracted by going in and interchanging the connections from the two overlap PMTs. Much later it was discovered the right-left swop was because of a wrong mapping of the clear fibers from the overlap triggers tiles to the PMT connectors in the detector.

The signals arriving in the control room could be feed to a scaler in the beam setup system to have for example the number of EDUET coincidences (C1), the combined main trigger signal (C4) and the combined trigger signal (C8) directly on the monitor when setting up the beam (see Section 16.4.4).

For some runs the trigger system was modified. For instances runs were made with only the EUDET triggers. As the TLU box needed to be re-configured to trigger only on one input and the trigger modification was done at times were no EUDET support was available, the trigger modification was done by simply doubling the EUDET coincidence (C1) signal and put both into the EUDET TLU.

For other runs it was wanted to trigger only on the ALFA trigger (C5). This was done by doubling the signal and sending both to the EUDET TLU box.

Also for some runs the veto (see Section 16.4.4) was wanted, for others not. So it was added or taken away a few times.

All modifications done to the triggering system after the test beam started was done by the author.

16.4.4. The beam

The particles in the beam are 120 GeV pions. The spill length is about 60 s. Of that about 10 s are delivered to H6. The reference conditions for the beam were not useable for the ALFA beam test. The readout of EUDET is rather slow and with a too high occupancy (to many signals in each frame) EUDET would not be able to reconstruct the tracks. Normally EUDET did not adjust the beam but only adjusted the position of EUDET to be in the halo of the beam. But beam halo particles have a less pure signature and also the main beam would still hit the ALFA station. Therefore the beam adjustments were required. The initial beam adjustments were made by Per Grafstrom (CERN PH-ADO) and followed closely by the author. During the test beam period smaller adjustments were needed to counteract changes in the beam. These adjustments were made by the author.

16.4.4.1. Controlling and monitoring the beam

The beam can be controlled from a dedicated small control room close to the test beam zone. From here the current of all relevant magnets can be adjusted and the position of the collimators can be set etc. To not adjust the beam blindly a number of detectors are in place inside the beam along the beam axis. In Appendix W there is a full beam optical drawing of beamline H6 including beam detectors. Appendix W is the official H6 drawing. The access to the zone with the ALFA station was also controlled from the beam control room.

There are scintillator tiles read out by PMTs, which are primarily used to count the number of particles in the beam. In the optical drawing and the beam setup software they are called SCINX (X being the number of the scintillator).

There are wire chambers which gives the beam profile and position. The high voltage of the wire chambers can be adjusted to adjust the sensitivity, but at very small and low intensity beams they are not sensitive and accurate enough to be used. In the beam optical drawing and the beam setup software they are called MWPCX (X being the number of the wire chamber).

For the best beam profile there is a drift chamber (in the software also called a delayed wire chamber). This can be used at very low intensities.

As discussed in Section 16.4.3 the beam control system also have 4 scaler inputs for NIM signals. This was normally connected to the EUDET coincidence (C1), the coincidence of the top main triggers (C2), the coincidence of the bottom main triggers (C3) and the veto (see Section 16.4.5). For runs with beam on the overlap detectors, the coincidence of the overlap (C6 or C7) was connected instead of the coincidence of one of the main triggers (C2 or C3).

The first beam setup was done when the ALFA station was still being installed in the area. This was possible because there was a beam dump (DMP in the optical drawings) just in front of the area with the ALFA station inside. The muons from the pion decay in the beam dump were also used for timing studies (see Section 16.4.3 for details).

16.4.4.2. Initial setup of the beam

To reduce the intensity of the beam collimator 5 and 6 (horizontal/vertical acceptance collimators) were set to the most closed positions (± 2 mm). This gave a reduction of the number of particles per spill going from about $6 \cdot 10^5$ particles/spill to about $8 \cdot 10^4$ particles/spill. The beam profile seen by the wire chamber still look good as shown in Figure 16.39.

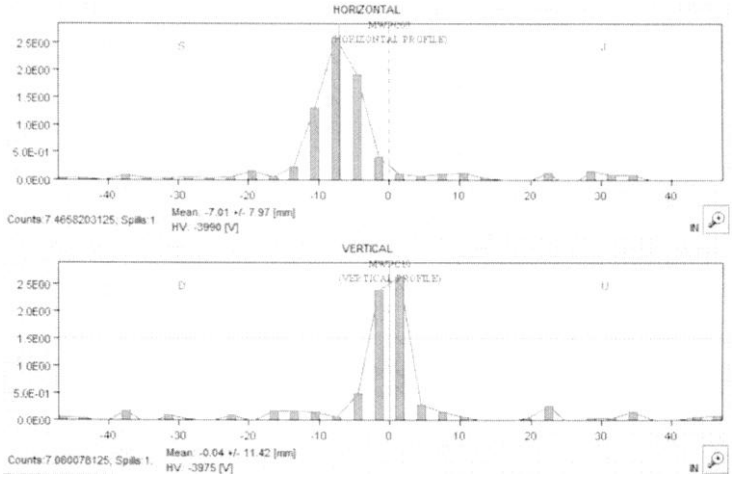

Figure 16.39. Beam profile in wire chamber 9 and 10 after moving collimator 5 and 6 to ± 2 mm. The x-axis is distance in mm. The y-axis is number of counts. The figure is a scan from the beam log book.

The beam is not exactly centered but close enough and the beam has a full width of about 10 mm.

To further decrease the intensity of the beam it was decided to defocus the beam with quadrupole number 5. The current in quadrupole number 5 was adjusted from 149.9 A to 145 A. This reduced the number of particles per spill from about $8 \cdot 10^4$ particles/spill to about $8 \cdot 10^3$ particles/spill. The wire chambers were now not sensitive enough to measure the beam profiled, so instead the drift chamber was use. The profiles in the drift champers are shown in Figure 16.40.

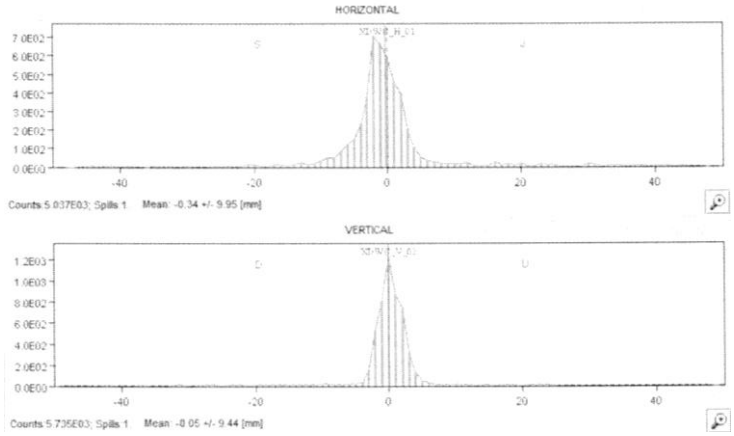

Figure 16.40. Beam profile in the drift chambers after adjusting the current of quadrupole 5 to 145 A. The x-axis is distance in mm. The y-axis is number of counts. The figure is a scan from the beam log book.

This rate and profile were satisfying. To make sure that the beam was well aligned to the center of EUDET a scan was needed of the trigger rate in EUDET as function of the beam position in the two directions perpendicular to the beam. This was done by first scanning the current of bending magnet Trim 6 (horizontal scan) and storing the number of coincidences in the EUDET triggers (C1) (normalized by the number of particles in each spill) for each current value. The result of the scan is shown in Figure 16.41.

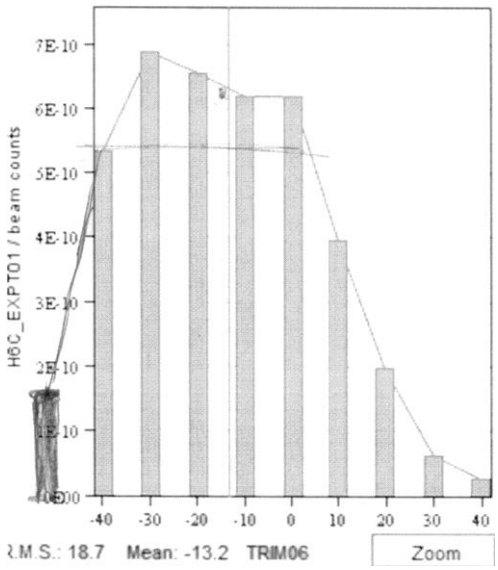

Figure 16.41. Scan of the current of Trim 6 as a function of the number of coincidences in the EUDET triggers (C1). The x-axis is current in Trim 6 in A. The y-axis is coincidences in the EUDET trigger (C1) normalized by the number of particles in the spill. The figure is a scan from the beam log book.

A back of an envelope fit gave an optimum value of the current of Trim 6 of -15 A. This was set as new reference. Next a vertical scan was made by scanning the current of Trim5 and storing the number of coincidences in the EUDET triggers (C1) (normalized by the number of particles in each spill) for each current value. The result of the scan is shown in Figure 16.42.

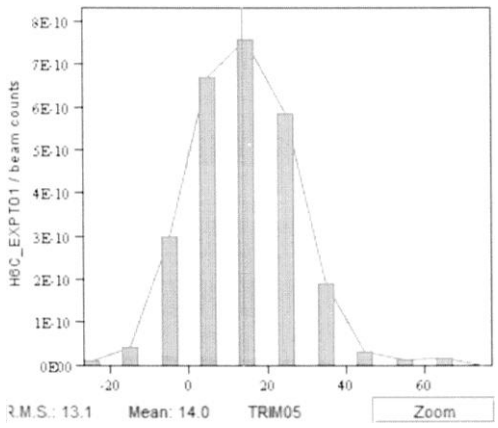

Figure 16.42. Scan of the current of Trim 5 as a function of the number of coincidences in the EUDET triggers (C1). The x-axis is current in Trim 5 in A. The y-axis is coincidences in the EUDET trigger (C1) normalized by the number of particles in the spill. The figure is a scan from the beam log book.

A back of an envelope fit gave an optimum value of the current of Trim 5 of 15 A. This was set as new reference. A check of the beam profile was made and there were no significant changes. The occupancy in EUDET was checked in a short run of 9981 triggers. The result is shown in Figure 16.43.

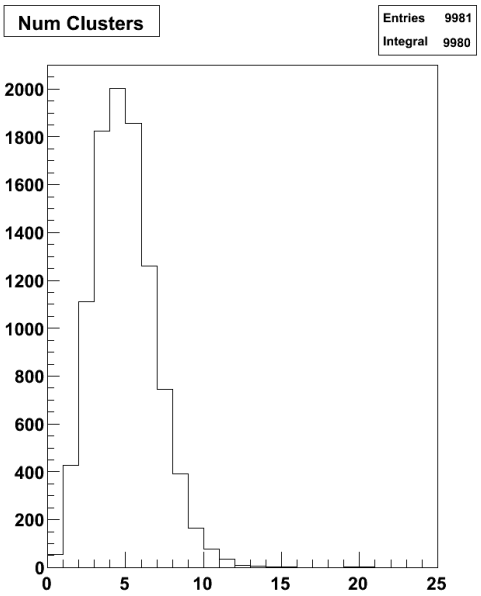

Figure 16.43. Occupancy in EUDET. The x-axis is number of clusters (tracks + noise). The y-axis is number of events. The figure is a screenshot from the EUDET control PC.

The EUDET group wants less than 10 clusters per trigger to be able to reconstruct tracks. From the distribution in Figure 16.43 it is seen that the beam intensity is well adjusted for this. It correspond to about $4 \cdot 10^4$ EUDET C1 trigges/spill.

The beam was declared ready for use and combined data taking of ALFA and the EUDET telescope began. See Section 16.4.6 for an overview of the different runs made.

In the Figure 16.53(Left) page 229 the beam profile is clearly seen in the ALFA detector.

16.4.4.3. Maintenance of the beam

The beam needed to undergo some maintenance under the entire time of the test beam. The number of particles in a spill changes. The beam position changes a little and thereby the effect of the collimators. The multiplicity changed (because the primary target changed (The primary target is hit with 400 GeV protons from the SPS to make secondary pions)) some times etc. As the EUDET sensors were very sensitive about too high intensity and it was desirable to keep the intensity up to get most events out of the beam time, it was needed to keep an eye on the beam and to counteract any changes. This was mainly done by the author. The counteracting was most often an adjustment of the current in quadrupole number 5 followed by checking the rates of scintilaltors, the rate on the scalers and the beam profile.

16.4.4.4. Muon beam

Pions were desired for most runs because pions are hadrons, and have similar properties to the protons the detector will be used for. However the pion beam had to be kept at a small width if the rate in EUDET should not be too high. To irradiate the entire detector (or most of it) in one run it was therefore suggested (by the author) to make a wider beam and dump it into the beam dump in front of the detector. In that way only muons would reach EUDET and the ALFA station. This would reduce the rate significantly. The modification to the beam was made by the author and used for a long night to have high statistic.

To make the beam wider the collimators was moved:

Collimator 3: From ± 1.0 mm to ± 1.5 mm.

Collimator 5: From ± 2.0 mm to ± 10.0 mm

Collimator 6: From ± 2.0 mm to ± 10.0 mm

Collimator 8: From ± 1.0 mm to ± 2.0 mm

To give a higher rate the current of quadrupole number 5 was adjusted from 145 A to 146 (closer to good focus).

This gave a rate of $1.6 \cdot 10^3$ EUDET C1 trigges/spill which EUDET easily could handle. The rate in combined ALFA triggers (C5) was $5.9 \cdot 10^3$ EUDET C1 trigges/spill. This clearly shows that the beam was wider than the EUDET trigger tiles (or in principal off centered).

EUDET could handle about 3 times higher rate, but with the current setting about $1.2 \cdot 10^6$ particles/spill (number of particles in scintillator 9) were dumped at the beam dump. This is about the upper limit allowed.

The beam profile was checked with the wire chambers and shown in Figure 16.44.

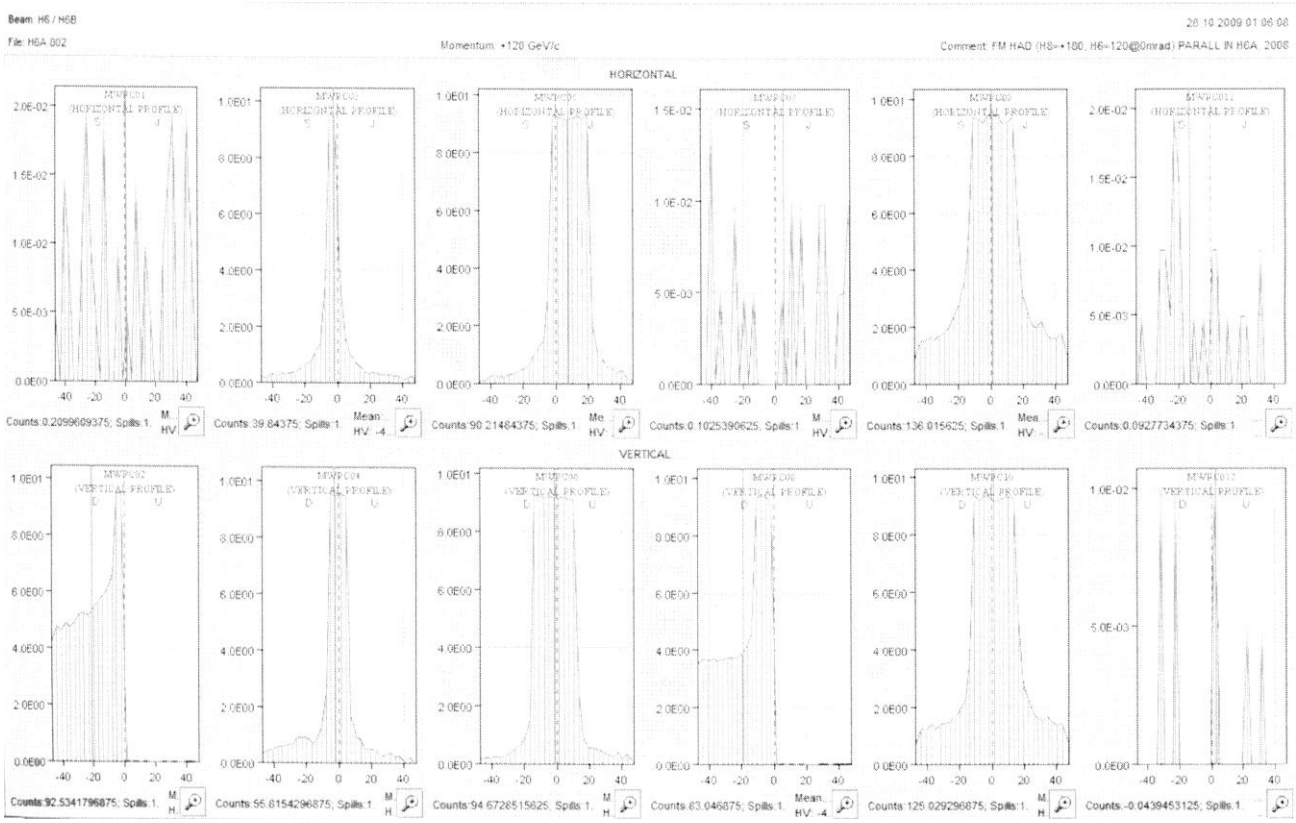

Figure 16.44. Beam profile in all wire chamber. The x-axis is distance in mm. The y-axis is number of counts. As there were no time for adjusting (or wanting for auto adjusting) of the high voltage of the wire chambers, not all are well adjusted. Therefore some of profiles are missing. The figure is a scan from the beam log book.

The detailed beam profile from the drift chamber is shown in Figure 16.45.

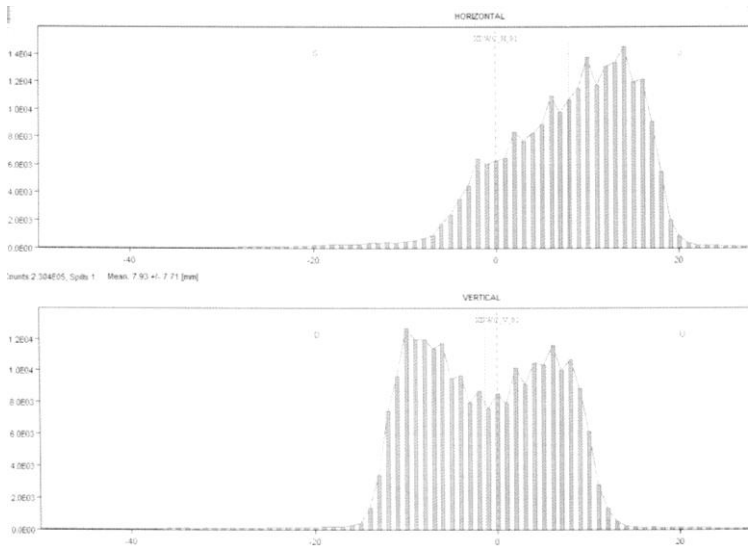

Figure 16.45. Beam profile in the drift chambers. The x-axis is distance in mm. The y-axis is number of counts. The figure is a scan from the beam log book.

The beam now had a full width of about 25 mm and was a bit of center horizontally. The muons from the pion decays would have a (small) angular distribution. Therefore the beam would be even wider at the ALFA station and should cover both detectors.

The ALFA station was positioned so EUDET was covered completely inside the lower detector. The triggering was set to only combined AFLA (C5) (see Section 16.4.3 for details) and the veto counter signal was removed (see Section 16.4.5 about the veto counter). A long high statistic run was made over night. Over 2 million triggers were recorded.

The next morning the beam was set back to the normal conditions.

16.4.5. The veto counter

When a particle from the beam (120 GeV pions) hit objects (Roman Pot, trigger scintillator tiles, EUDET sensor, scintillating fibers etc.) there is a change that they can interact and produce a shower. It is desirable to exclude these events. Else they will later be hard to distinguish from nose, crosstalk etc. Therefore it was planned to use a veto counter.

The veto counter at disposal was simply a 40 cm*40 cm scintillator tile with a 30 mm hole in the center. The center of the hole is aligned to the beam. Particles from a shower will not all fit in the hole and some of them will pass though the scintillator tile and thereby give a signal in the connected PMT.

A rough alignment of the veto counter was made by holding a laser pointer to the theoretical beam line and shining though the hole in the veto counter and hitting another point on the theoretical beam line. Later fine adjustments to the theoretical beam line were made by the CERN alignment group. The veto counters position relative to the ALFA station and EUDET is shown in Figure 16.46.

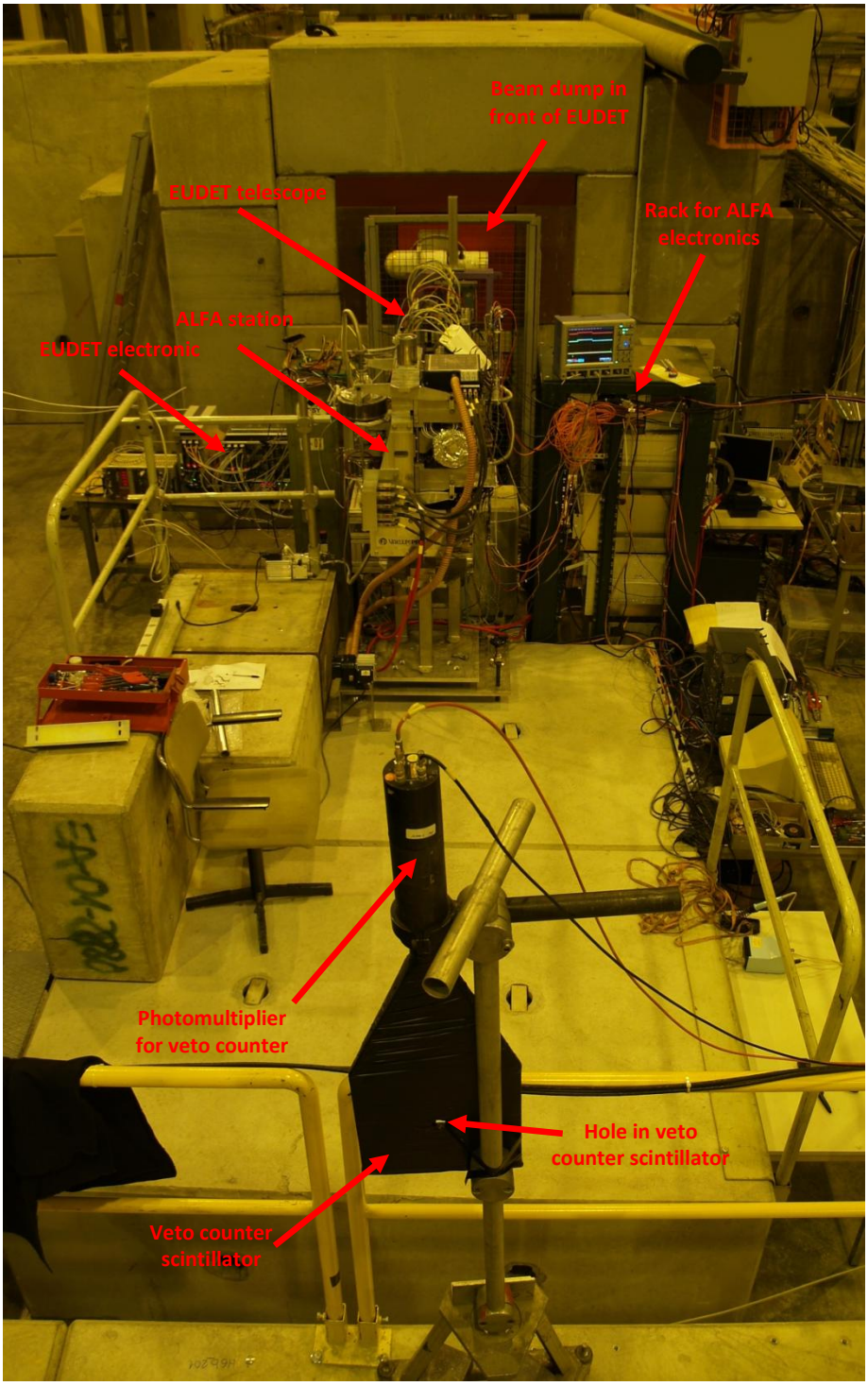

Figure 16.46. Veto counter aligned after EUDET and the ALFA station.

The PMT was connected to high voltage (2200 V). The signal from the PMT was discriminated. The signal was then connected to the veto input of C5. If there is a signal on the veto input when the leading edge of signal comes to any input, nothing will get to the output (veto). But since the veto counter was positioned a far away from the triggering system it had to be connected with a long cable, which introduced a delay to the signal. Therefore the signal arrived at C5 after the trigger signal had already passed though. To counteract this, the signal C1-TLU, C4-C5 and C8-C5 was all delayed by 48 ns. Then it was possible to have the veto signal arrive and make a veto as intended. To counteract the delayed trigger the delay between the TLU and the motherboard (in ALFA normally called pipeline delay) was reduced with 48 ns (see also Section 16.4.6.1 about pipeline delay).

It was needed to verify that the veto counter was well aligned to the beam. To do this the beam position was scanned horizontally by scanning the current in Trim 6 and look at the number of counts in the veto counter normalized by the number of particles in the spill. The result is shown in Figure 16.47.

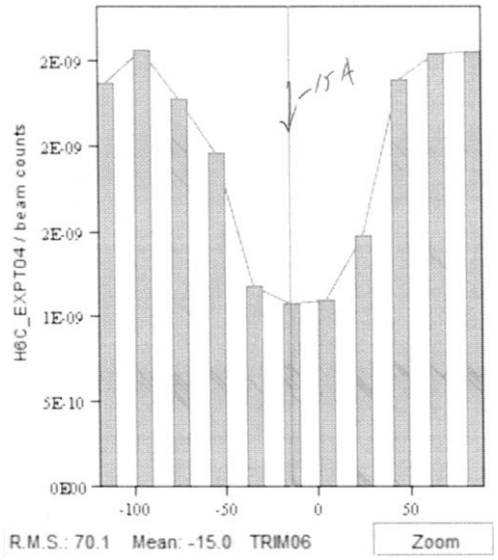

Figure 16.47. Scan of the current of Trim 6 as a function of the number of counts in the veto counter. The x-axis is current in Trim 6 in Amperes. The y-axis is number of count in the veto counter normalized by the number of particles in the spill. The figure is a scan from the beam log book.

The result was an optimal current value of -15 A, which was the same as the alignment with EUDET. It was therefore concluded that the veto counter was well aligned horizontally.

The beam position was hereafter scanned vertically by scanning the current in Trim 5 and look at the number of counts in the veto counter normalized by the number of particles in the spill. The result is shown in Figure 16.48.

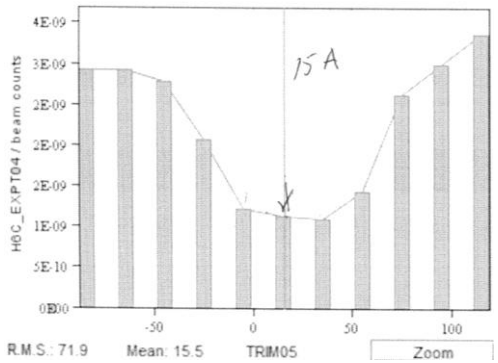

Figure 16.48. Scan of the current of Trim 5 as a function of the number of counts in the veto counter. The x-axis is current in Trim 5 in Amperes. The y-axis is number of count in the veto counter normalized by the number of particles in the spill. The figure is a scan from the beam log book.

The result was an optimal current value of 15 A, which was the same as the alignment with EUDET. It was therefore concluded that the veto counter was also well aligned vertically.

The veto counter was hereafter used in most runs.

It is worth noticing the high rate in the veto counter even with the beam in the central position. It correspond to about $2 \cdot 10^3$ count/spill. This was noise from the PMT on the veto counter. But the noise should be equally distributed over the spill of about 10 s and the width of the signal was only about 100 ns the fraction of lost events from fake vetos is neglectible.

16.4.6. Run strategy and preliminary results

About $3 \cdot 10^7$ events were recorded in the test beam. In this section the strategy behind and some preliminary results are discussed.

16.4.6.1. Pipeline delay

The first runs after everything was working were dedicated to find the optimal pipeline delay. The pipeline delay is the time from a trigger is made in the trigger system to the data is at the end of the digital pipeline and has to be stored. If not set up correctly the DAQ will only get empty blocks for data.

The value from the short cosmic run (corrected for the new cables lengths) (see Section 16.3.3.7) before the test beam was used as a starting point for the pipeline delay. A good evaluation for the pipeline delay is the layer multiplicity (reconstructed tracks would be the perfect choice, but the time it takes to reconstruct the tracks would give a too long feedback time). MH had root macros from previous ALFA test beam that calculated the multiplicity. As the readout follows the LHC frequency of 40 MHz the window size of the readout is 25 ns.

A scan was made with of the readout time in steeps of 5 ns. The delay is made by a pulse generator which sends out a pulse at a given time after an incoming pulse has arrived. Since the pulse generator can only be adjusted in the zone next to the ALFA station each steep required an access. Since it takes about 7 min from access requested until it is possible to go in, and then again about 7 min to get the beam on after, this scan was quite time demanding. 6 points was made with different delay. The results for 4 layers are shown in Figure 16.49.

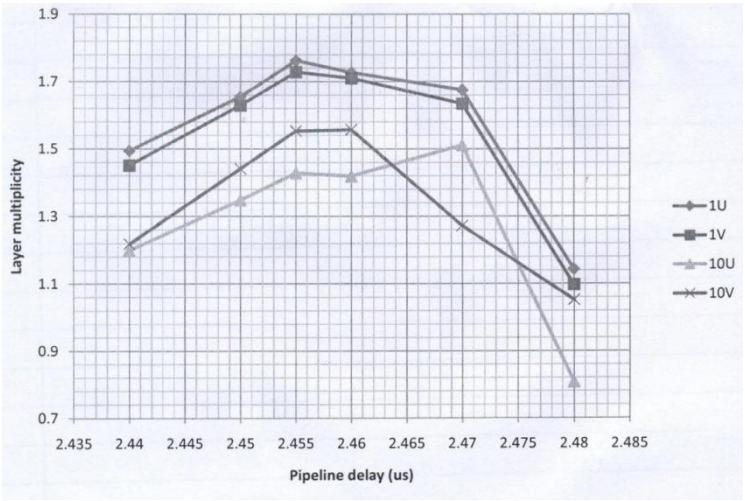

Figure 16.49. Scan for the pipeline delay as a function of the layer multiplicity in 4 layers of an ALFA detector. The figure is a scan from the ALFA test beam logbook 2009.

The multiplicity peeks at dealy 2.455 µs, and this value was used here after. When the veto counter was added the trigger system had to be delayed by 48 ns. To counteract this, the author adjusted the pipeline delay to 2.407 µs as discussed in Section 16.4.5.

16.4.6.2. Alignment scan

In the test beam in 2006 it was discovered that the alignment of a detector perpendicular to the beam could be done by looking at the resolution of the detector [78]. The resolution could be measured by the ALFA detector alone by using the first half of the detector as a telescope for the second half. This was done by looking separately at the residuals in x or y directions. Since the algorithm used for the reconstruction

assumes that the track is perpendicular to the ALFA planes, the presence of an angle (an unaligned detector) will imply a shift in the mean value. An example is shown in Figure 16.50. The width of the peak is the resolution of the half detector.

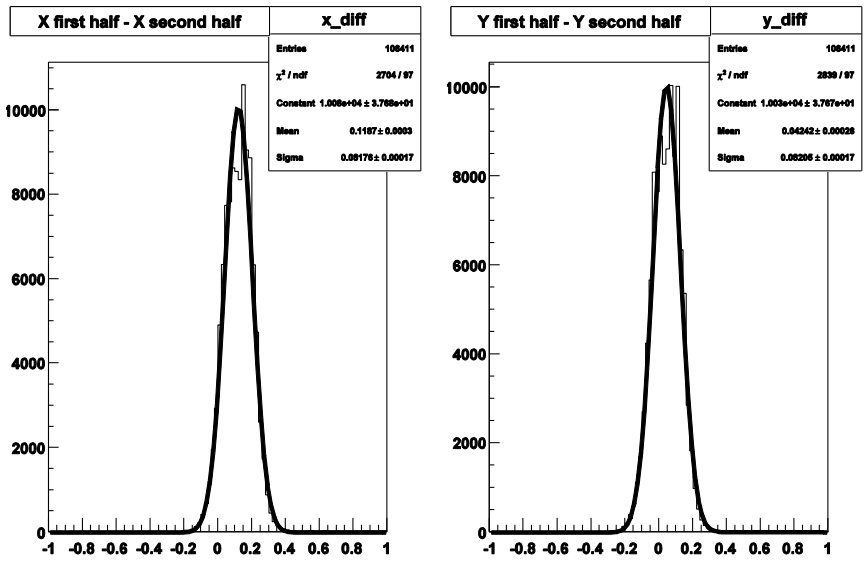

Figure 16.50. Resolution plot with the detector tilted. An offset of the x-mean value is clearly seen. The figure is made on data from run 1256661389 with a macros made by MH.

To adjust the detector perpendicular to the beam a scan was made where the station and thereby the detectors was tilted. This was done in both x and y direction. Figure 16.50 is form the most outer point in the x-direction. The tilt was thereafter plotted as a function of the residual offset from zero. An example of a plot for the x-direction is shown in Figure 16.51.

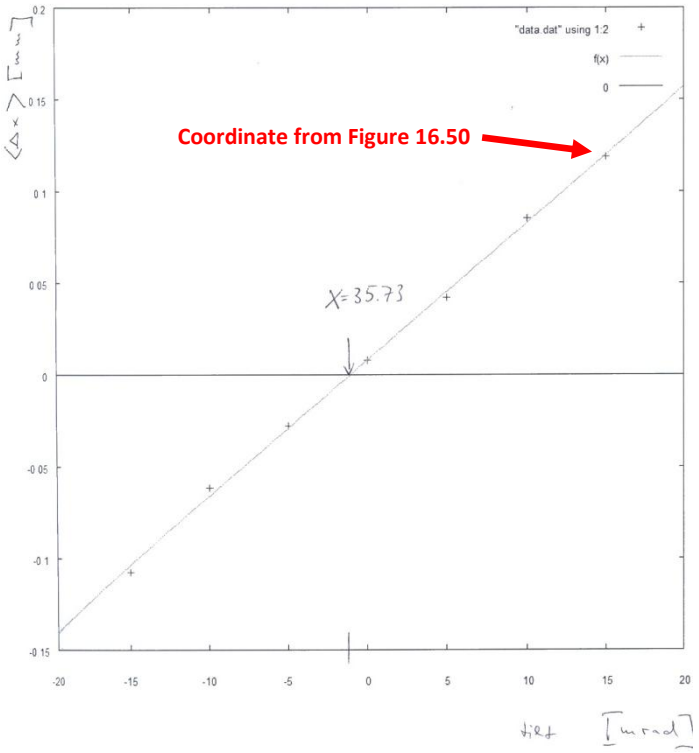

Figure 16.51. Results from scan of the resolution. The figure is a scan from the ALFA test beam logbook 2009.

After the scan the detector was adjusted to the optimal value of about -1 mrad. The same was done for the y-direction. The scan was repeated for the other detector to find the relative inclination of the detectors. The inclination was about 3 mrad. From the 2006 test beam it is known that the resolution of an ALFA detector is stable within ± 7 mrad [78](page 6), so an inclination between the upper and the lower detector of 3 mrad is acceptable.

16.4.6.3. Position scan

The EUDET telescope is much smaller than the ALFA detectors. To test the entire detector with the EUDET telescope in front it was therefore necessary to move the ALFA station. It was also very imported to determine the precise position of the overlap detectors relative to the main detectors, as the overlap in the final installation will be used to give the relative position of the detectors with a position of about 10 µm [39](section 5.2.3) (see Section 13.1.3). The relative overlap- main detector position was determent by position the EUDET telescope so it covered some of the overlap detector and some of the main detector. Figure 16.52 shows the relative position of the ALFA overlap triggers to the main triggers in ALFA seen in a EUDET sensor.

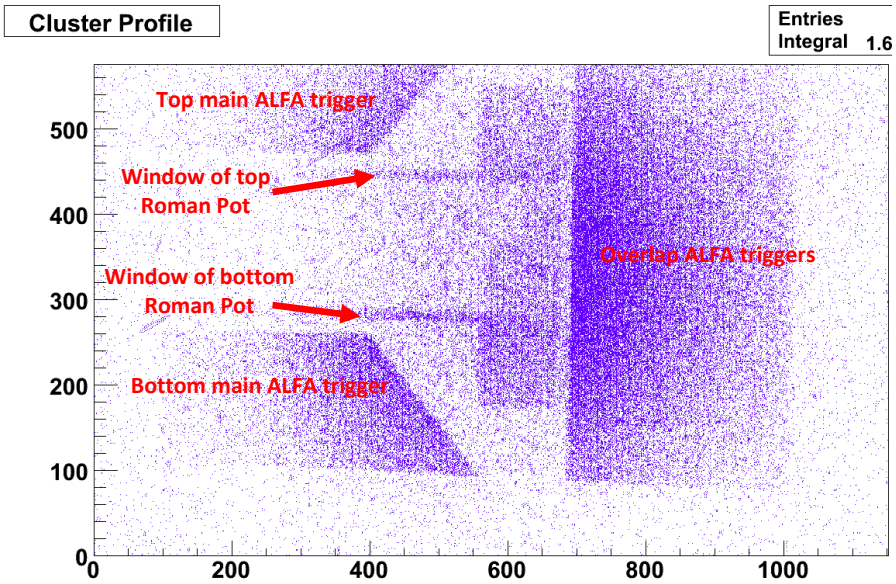

Figure 16.52. Relative overlap trigger and main trigger position seen in EUDET. The figure is a screenshort from the EUDET control PC of the cluster seen in one EUDET sensor. Cutoff due to miss alignment of the EUDET triggers and the EUDET sensors is clearly visible.

The windows on the Roman Pots are also clearly seen. This is most likely due to particles passing the EUDET triggers and then hitting a window of a Roman Pot. This will produce a shower of particles where some hit the ALFA trigger tiles.

From the analysis of the data the relative position of each fiber in the ALFA main detector to each fiber in ALFA overlap detectors can be determent. The ALFA analysis team is currently working on this.

To check the position the ALFA detectors MH reconstructed the tracks in ALFA and made a hit map of the detectors. Examples are shown in Figure 16.53.

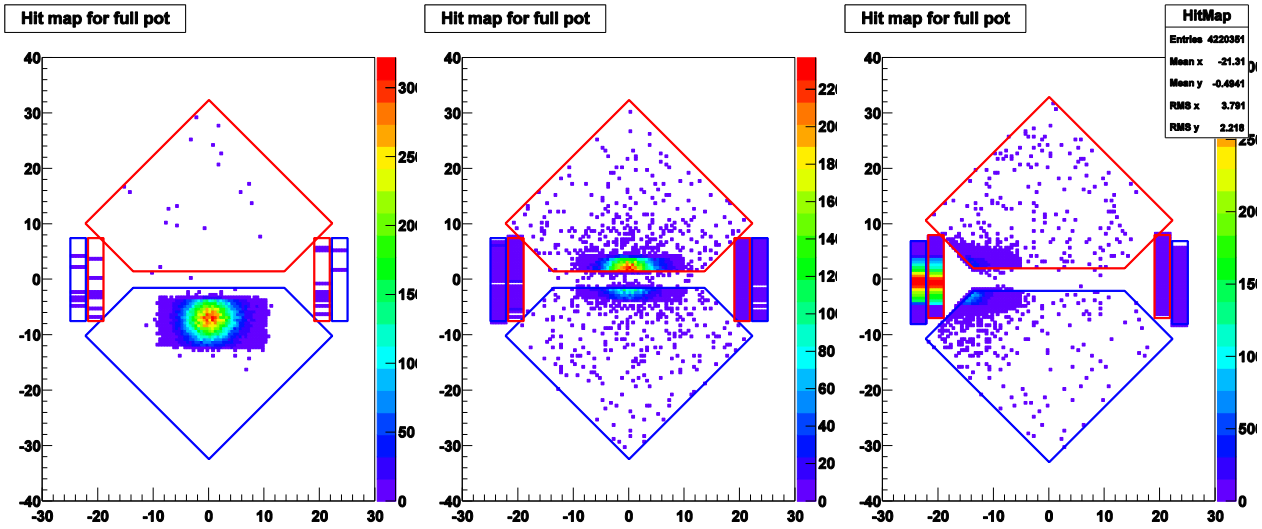

Figure 16.53. Hit maps of the detector. *LEFT*: EUDET and the beam are in front of the lower detector. The shape of the EUDET triggers is clearly shown. The beam profile is also clearly seen. *CENTER*: EUDET and the beam are centered between the upper and lower detector. *RIGHT*: EUDET and the beam are covering part of the overlap detector and the main detector. The hit maps are made with macros made by MH.

A position scan was made so that the entire detector was covered. During the position scan the author added a none-foreseen test: Light yield of the main triggers in all positions.

The measurement is similar to the one described in Section 14.6 and the setup was close to the setup in Figure 14.48 page 135: The analog signal from both the main trigger PMTs was amplified and readout by an oscilloscope. The triggering of the scope was done by the trigger signal also send to the EUDET TLU box. The charge measured in each trigger PMT was stored in a histogram directly on the oscilloscope. This was done for each position of the beam on the lower detector. An example is shown in Figure 16.54.

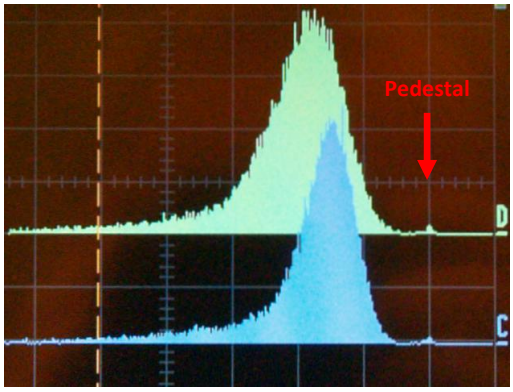

Figure 16.54. Oscilloscope screenshots of beam data histograms. C (main trigger 1) scale: 1 nVs, D (main trigger 2) scale: 2 nVs.

The signal is well separated from the signal (unlike the similar cosmic test Section 14.6) indicating ~100 % trigger efficiency if the trigger threshold is set close to the pedestal.

After the test beam the 1 PE signal was determent with a setup like the one in Figure 14.46 page 134. As the PMTs used was of the low gain type (Hamamatsu R7400U) the position of the 1 PE was half inside the pedestal. This gave a large uncertainty on the 1 PE calibration of about 25 %. The light yield for both main triggers was calculated and the result is shown in Figure 16.55.

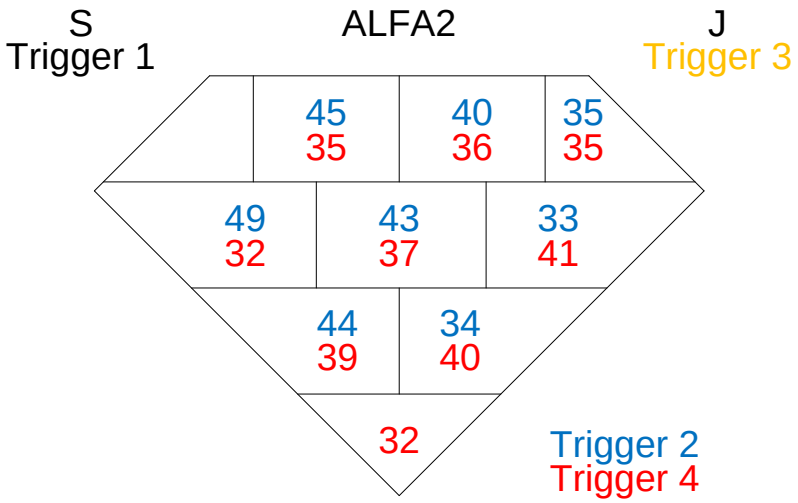

Figure 16.55. Light yield in the main triggers for the lower detector (ALFA2) in PhotoElectrons. The relative uncertainty for position to position is about 5 %. The absolute uncertainty of the light yield is of the order of 25 % (because of the 1 PE calibration).

The difference in light yield from 33 PE to 49 PE (about 33 % lower) for two symmetric points in the trigger tile was quite surprising. This had not been observed in the prototypes in dedicated trigger test beam in 2007 [53]. Something in the production of the triggers must have led to losses of some of the light. The light level should still be high enough to ensure almost 100 % trigger efficiency. But the trigger light yield in different position should be measured in all detectors produces to insure no dead sports or too low light yield. This could be included in the 2010 test beam.

16.4.6.4. Gain, high voltage and threshold scans

Much of the test beam time was dedicated to optimize the gain, high voltage of the MAPMTs and the threshold of the readout of the MAPMTs. These parameters are directly correlated and to find the optimal settings takes therefore a lot of combinations.

First the gain was looked at gain factors equalized (or gain factor = 16) and the threshold at thermo 7 (thermo 1 = threshold 256, thermo 2 = threshold 521 etc in Figure 15.14 page 166). The high voltage scanned at values: -800 V, -850 V, -900 V and -950 V.

Next the gain was looked at gain factors = equalized (or gain factor = 16) and the high voltage at -900 V. The threshold was scanned at values thermo: 6, 7, 8, 9, 10, 11 and 12.

Then the threshold was looked at thermo 7 and the high voltage at -900 V. The gain factors were scanned at values: 12, 16, 24, equalized and 1.5·equalized.

Even more combinations were made.

The data is being analyzed by the ALFA test beam analyzing team to find the optimal setting of the combination of gain, high voltage and threshold.

16.4.6.5. Vacuum test

As the last test in the test beam a vacuum pump was added to the setup. The idea was to test different scenarios of losing the vacuum and see the effect (possible destruction) on an ALFA detector.

First a test was made with vacuum in the beam pipe and in the lower Roman Pot (due to a later repaired leak it was not possible to have vacuum in the upper Roman Pot). For the upper pots this simulates loss of vacuum in the Roman Pot. Because of particles going through the EUDET triggers and then hitting the Roman

Pot window making a shower the bending of the Roman Pot window could be observed directly in the online EUDET software (hit pattern in one sensor) as shown in Figure 16.56.

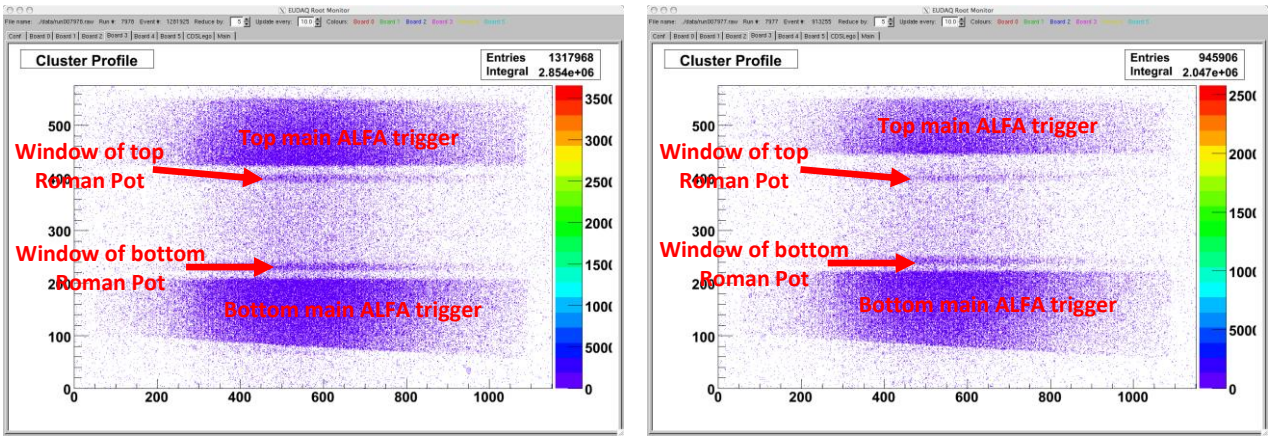

Figure 16.56. *LEFT*: Reference before any vacuum was applied. The windows of both the top and bottom Roman Pot are straight. *RIGHT*: Vacuum in the beam pipe and in the lower Roman Pot. The top Roman Pot window bends into the beam pipe. The figures are screenshot from the EUDET control PC of the hit pattern of one sensor.

Next a run with vacuum only in the lower Roman Pot was made. This should simulate vacuum loss in the beam pipe. The window of the Roman Pot is expected to bend and hit the ALFA detector. In the EUDET online software it was clearly seen that the Roman Pot window indeed was touching the detector.

At the end the complete station was again pressurized and a long run was made to verify the performance after the simulated vacuum losses. The preliminary results indicate no change in performance and the detector and Roman Pot would therefore probably survive a loss of vacuum without damage.

16.4.6.6. Data analysis

The data from the test beam will be analyzed of the ALFA analysis team. This work is still ongoing and have been delayed because EUDET usually uses interpolate track, not extrapolate as it is needed for the setup with ALFA. It is expected that ALFA will publish the results from the 2009 test beam in the fall of 2010. Included in the results should be:

- The resolution of a full ALFA detector measured with EUDET.
- The edge sensitivity of the ALFA detector.
- The relative overlap – main detector position
- The fiber layer efficiency
- The overlap efficiency
- Cross talk studies
- Optimal setting for gain factors, MAPMT high voltage and threshold
- Verify no performance degradation after the vacuum tests

17. Shims

The grid of channels on the MAPMTs is not in a well defined position relative to the sides of the MAPMT. Each piece is centered differently with up to 500 µm deviations. To counteract the different centering so the MAPMT channels are well centered on the scintillating fiber ends, it was decided to equip each MAPMT with custom shims. With the shims attached the channel-grid of the MAPMT should be well centered relative to the outside of the shims. The position of the channel-grid is defined by 4 precision points as shown in Figure 17.1.

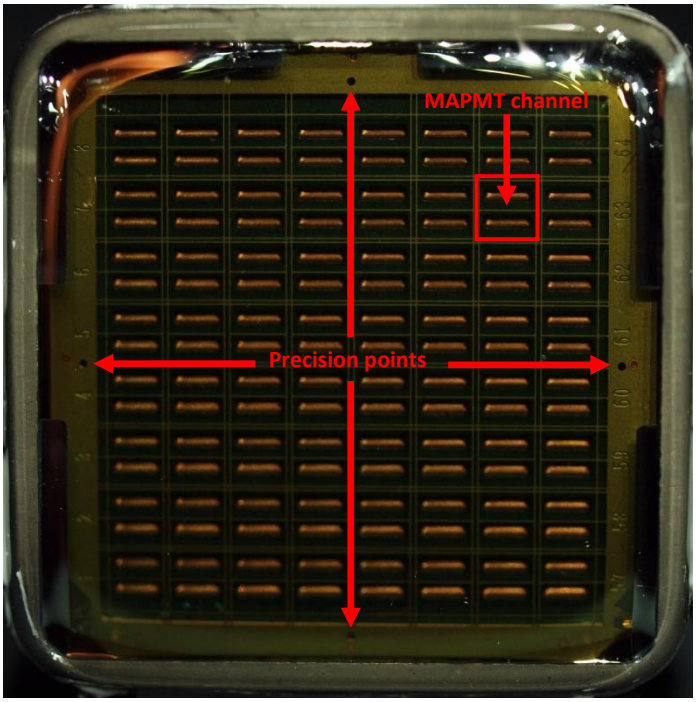

Figure 17.1. Channel-grid on a MAPMT. The precision points are clearly visible. Also the numbering of the channels can be read directly on the channel-grid.

17.1. 1st generation shims

The 1st generation shims used for test of MAPMTs and the first detector prototypes were just loose pieces of Teflon or Plexiglas. The used of the first generation shims are included in Section 14.3.1 and Section 14.5.1. In Section 14.5.1 it is also described how they were made.

17.2. 2nd generation shims

The original proposal for production of shims was to use pieces of POM (Polyoxymethylene, a plastic often used for precision part) glued with silicon glue to the MAPMTs. This was done at DESY for the 23 MAPMTs in prototype 2 and an example for this second generation of shims is shown in Figure 17.2.

Figure 17.2. 2nd generation shim: Flat piece of POM glued to the MAPMT.

The second generation shims were used at the test beam of prototype 2 in 2008. Due to production problems with generation 3, the MAPMTs with generation 2 shims were re-used for ALFA1 in the 2009 test beam.

Generation 2 shims were too short which might allow the MAPMT to turn, which would introduce more crosstalk. Also the thickness of the glue makes the positioning imprecise.

17.3. 3rd generation shims

The design of generation 3 shims was proposed by DESY and was a shim consisting of epoxy glue. An example of 3rd generation shims is shown in Figure 17.3.

Figure 17.3. 3rd generation shim: Epoxy glue.

The MAPMT was aligned under a microscope and glue was field in to make a shim. This was again done at DESY (Hamburg).

There were objections to this design. Some feared that the drying of the epoxy surrounding the MAPMT might squeeze the metal part of the MAPMT and damage it. The effect might not come immediately so a simple check of the MAPMT properties would not rule out some damage. Also the epoxy was not easily removable (as the silicon glue is). If any MAPMTs with shims are not within the wanted precision and has to be redone (which happened to 30 MAPMTs because of a bad microscope) the MAPMT might be damaged from the removal of the shims (which happened to 2 MAPMTs).

The 3rd generation shims was used for 23 MAPMTs in ALFA2 for the test beam 2009. The distance from the shim to the window of the MAPMT was too large. This gave some problems when the MAPMTs were not connected to a detector. For example in the setting up of the cosmic (see Section 15.2.6.2) and in the equipment test before the beam test 2009 (see Section 16.3.3.5).

17.4. Proof of method at CERN

It was decided to go back to the originally idea of POM + silicon glue. DESY (who were responsible for the MAPMT shims) did not believe in this design.

17.4.1. Design of a shim tool

To proof that POM shims + silicon could work and be produced quickly with high precision, it was decided to make a tool at CERN for shim production.

The general idea of the tool was discussed between Christian Joram (CERN PH-DT), Andre Bream (CERN PH-DT) and the author. Next the author worked out the details and designed the tool with handmade drawing for each piece. These are included as Appendix X. The design idea is described in Section 17.4.2.

The tool was implemented in AutoCAD Mechanical 2010 by Andre Bream (CERN PH-DT) to check that everything fitted in 3 dimensions. No errors were found. The thickness of some of the plates was adjusted to a standard size to make the pieces easier (and thereby cheaper) to produce. The 3D drawing is shown in Figure 17.4. The micrometer screws were not implemented.

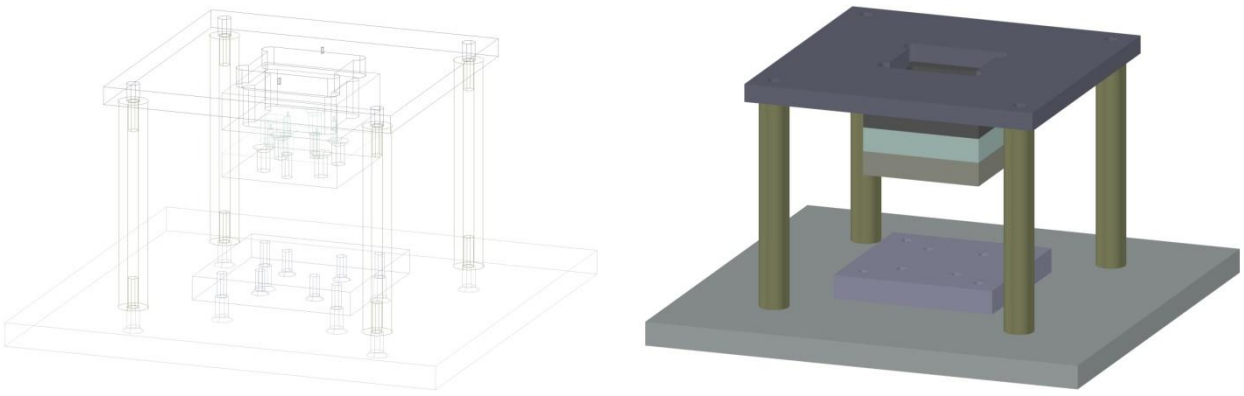

Figure 17.4. *LEFT*: 3D AutoCAD drawing of the shim tool. The micrometer screws were not implemented. *RIGHT*: Rendered version of Andre Breams AutoCAD drawing made by the author.

Digital drawings were made for production. These are very similar to the original handmade drawings and are included in Appendix Y. The pieces were produced in a CERN workshop under the Detector Technology department. The final pieces were assembled by the author. The shim tool is shown in Figure 17.5.

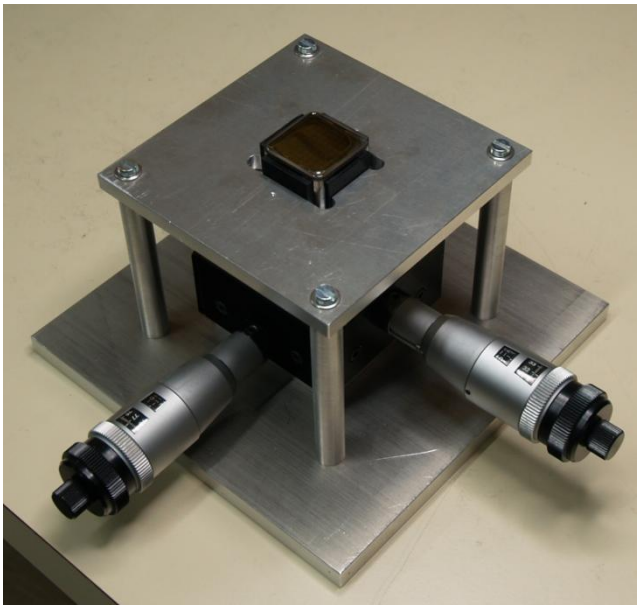

Figure 17.5. Final assembled shim tool with MAPMT and shims installed.

17.4.2. Method for using the shim tool

First the MAPMT was installed by fitting 4 pins from the MAPMT into the support fitted on the bi-directional micrometer screws. The support is shown in Figure 17.6.

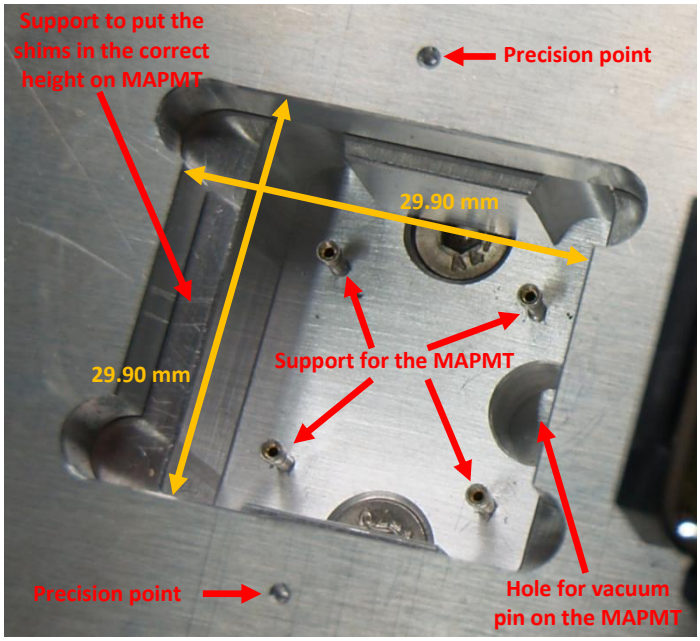

Figure 17.6. Close up of the shim tool.

The MAPMT can now be moved with the micrometer screws relative to the top plate, in which there are made a precision square hole (with round corners to make the machining possible) with a side length of 29.90 mm. On the top plate there is furthermore made two precision points.

The idea is now to put the shim tool on a microscope and find the two precision points on the top plate (alignment of the shim tool). Next step is to move the microscope to the position where the precision point on the channel-grid of the MAPMT should be. Then move the MAPMT with the micrometer screws until the precision point of channel-grid of the MAPMT is in the correct position in 2D. The channels of the MAPMT

are now aligned to the hole in the top plate. As a check the microscope should move to the other precision points on the MAPMT. Figure 17.7 shows a screenshot from the digital microscope used.

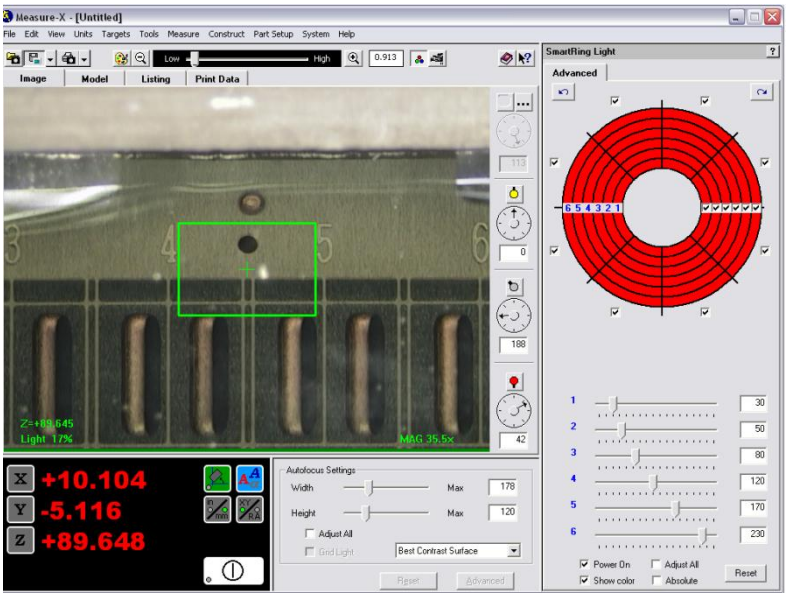

Figure 17.7. Screenshot from the digital microscope used for finding the position point on the top plate and the moved to the position where the precision point of the MAPMT channel-grid should be.

Shims were pre-made (see Appendix X for handmade drawing for production) in a variety of thicknesses with 0.1 mm step size (full production the steep size should be 0.05 mm, but for the proof of method this was not needed). As the channel-grid of the MAPMT was centered it was only a matter of trying out shims and selects the thickest ones that still fitted.

For production a tool for supporting the MAPMT and the shims under gluing was foreseen. But for the proof of method the gluing was done by hand. The MAPMT with shims are shown in Figure 17.8.

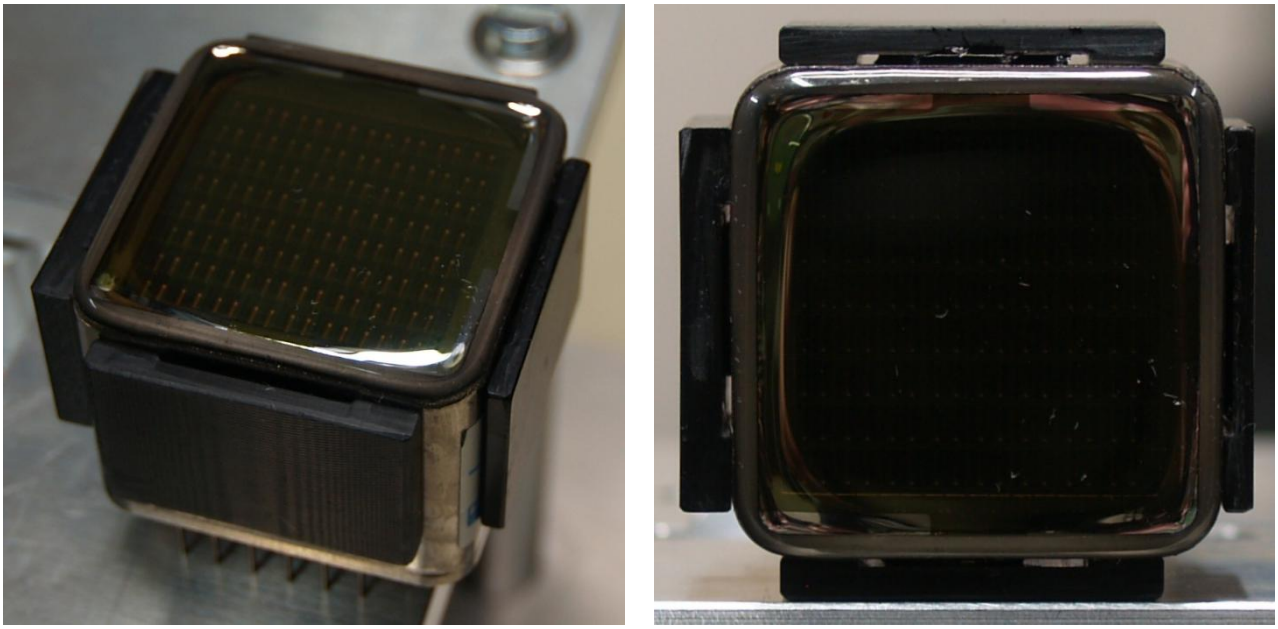

Figure 17.8. *LEFT*: MAPMT with shims as "proof of method". *RIGHT*: MAPMT with shims as "proof of method". It is shown that the glue fill out the space foreseen for it and the distance is defined by the shim (not the shim + glue).

The result was very good. The shims were well connected to the MAPMT and the glue did not add any distance as can be seen in Figure 17.8. The shims were put to a realistic force test to see that they stayed connected, and they did. The relative distances of the sides of the shims and the channel-grid on the MAPMT

was checked under a microscope, and was very good (less than 0.1 mm off). For production this could be expected to be better as the steep size of the shims would be smaller. The overall size of the MAPMT + shims was good (29.76 mm·29.76 mm), but for production it would be even better to make the precision square hole 30.00 mm·30.00 mm as the steep size of the shims always will add some spare room, so the MAPMT + shims still would fit without any problems into the mu-metal grid frame with holes of 30.00 mm·30.00 mm.

This proofed that design and method of production was good and should be used. If a high end digital microscope is used, the finding of the precisions point on the top plate and the movement to the position were the precision point(s) on the MAPMT channel-grid should be, could even be automated. Then the shim production could be really fast and still with very good results.

17.5. 4th generation shims

The shim design and method described in the previous section was partly adapted by DESY for the shim production. They thought that the use of micrometer screws was too expensive a made a hand adjusted production tool instead.

The idea of the shim design with the glue in an indentation in the shim was kept. Also the distance from the shims to the window have been corrected since generation 3.

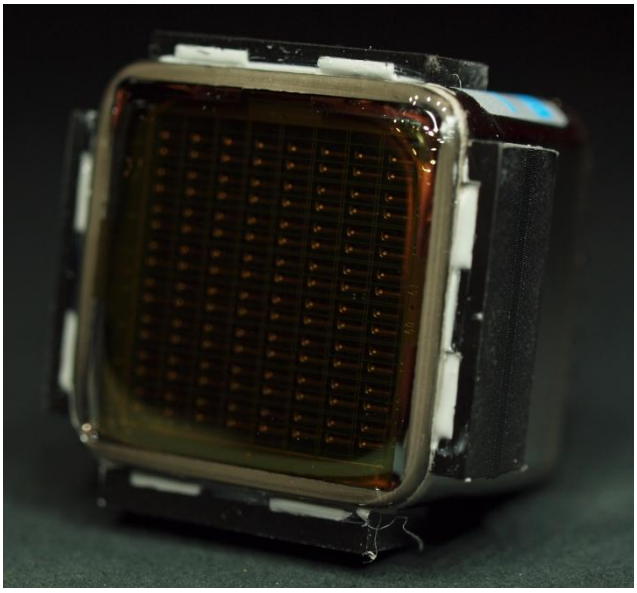

Figure 17.9. 4th generation shim: POM with indentations for glue.

40 MAPMT was equipped with the new shims at DESY and send to CERN. 23 of them were to be used in ALFA2 that was to be installed in LCH sector 8-1 a few weeks later as a first test of detector etc. installation. When the shims were installed and a minimum of force applied to the shims (when connecting the kapton cables on the PMFs) many of the shims fell off. It turned out that the glue did not fill out the indentation in the shim nicely as shown in Figure 17.10.

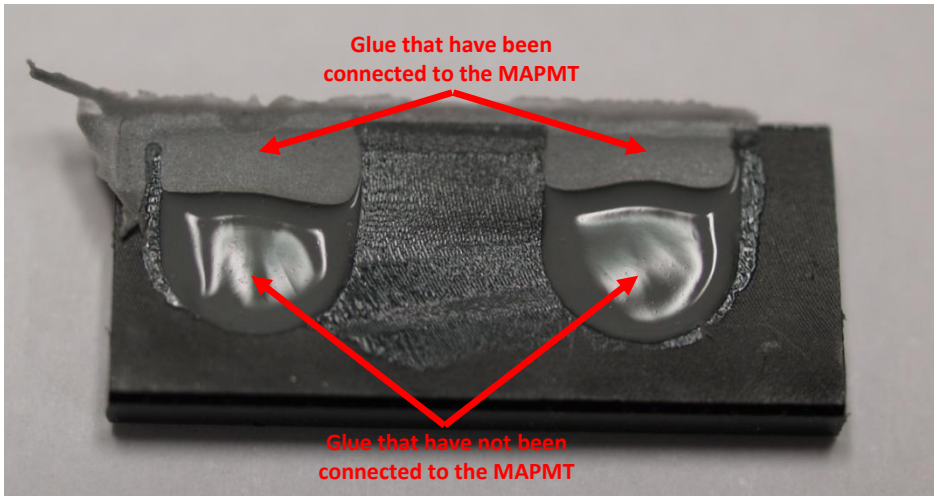

Figure 17.10. Shims that fall off an MAPMT. The lack of glue in the lower part of the indentation is clearly seen.

As there were no time for any new shims before ALFA2 had to be installed, the MAPMTs that had lost shims were just replaced with others from the same production steep. Hugh effort was made not to apply any force on the shims. The installation did succeed without losing any shims.

By chance the author was at DESY (for a Geant4 workshop on beam telescopes) shortly after and used the opportunity to go over the steps of attaching shims to the MAPMTs. A small change in the gluing procedure and a force test on the final MAPMT + shim was suggested and afterwards implemented in the production.

Since over 100 MAPMT have been equipped with shims at DESY. All have passed a final force test at CERN. The positioning of the MAPMT channel-grid relative to the sides of the shims is also good as is the distance from the shims to the MAPMT window. The 4th generation shims will be used for all ALFA detectors.

18. Radiation detectors

It is planned to remove the ALFA detectors and frontend electronic when they are not being used and the LHC runs with high luminosity. The scintillating fibers can take an accumulated dose of about 300 krad (=3 kGy) before any significant performance degradation is observed [45] (see also Sector 13.1.1). Simulations of the radiation levels at the ALFA detectors, electronic, stations etc. are being made. But better than simulation would be a real measurement of the radiation at the detector position and around the station.

Therefore it was decided to install radiation monitors at the position of the ALFA station before the LHC started to operate.

18.1. The radiation detectors

As radiation sensors it was decided to use Thermo Luminescent Dosimeters, TLDs, which is a passive dosimeter for ionizing radiation. The TLDs are consisting of $CaSO_4$ crystals. When heated the crystals emits light proportional to the dose of radiation in the TLD.

As a passive dosimeter TLDs are cheap and easy to install, but have the disadvantage that they have to be removed in order to be read out.

The TLDs was donated by DESY and will go back to DESY for read out.

KH designed the radiation detectors to have two windows. Each window would be equipped with 6 TLDs. 3 of type TLD800 with a range of 0.0005-100000 Gy and 3 of type TLD100 with a range of 0.00001-10 Gy. This should ensure redundant measurements and a large range. Figure 18.1 shows a radiation detector.

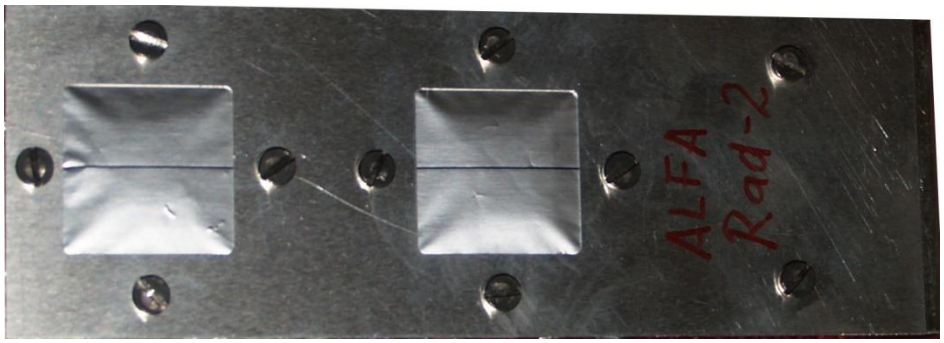

Figure 18.1. Radiation detector with 2 windows.

18.2. LHC sector 1-2

The feet of the ALFA stations were already installed but the ALFA stations were not. Therefore it was decided to install the first radiation detectors on an ALFA foot. The first radiation detectors were installed on an ALFA foot in LHC sector 1-2 by KH and the author. Figure 18.2 shows the installed radiation detectors.

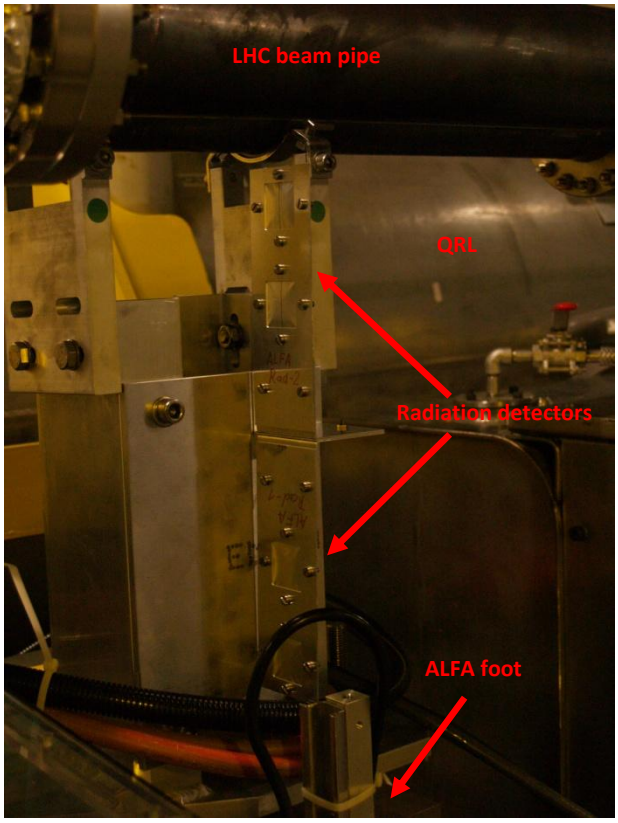

Figure 18.2. Radiation detector 1 and 2 installed on an ALFA foot in LHC sector 1-2.

18.3. LHC sector 8-1

For LHC sector 8-1 it was uncertain what should be done. The ALFA group wanted to install the first station (as the other stations needed modifications to fit because the cryogenic distribution line, QRL, took up the room originally planned for ALFA stations as discussed in Section 13.4) to gain experience. It would also be the best check if there were any more unforeseen problems and to know all the steps in the process and how long time each installation step actually takes. But the LHC group would only allow installation if the Roman Pots were installed in the station. The reasoning was that the cavity left if no Roman Pot was installed would disturb the RF system. The delivery date of the Roman Pots was very close to the final close down of LHC access before startup 2009, so it was unknown to the very end if the ALFA station would be installed or not.

Therefore it was also unknown where the radiation detectors should be installed. If the station was installed it was desirable to place some of the radiation detectors inside the Roman Pots in the actual position of the detector. It had also been decided that one of the radiation detectors should be installed between the two beam pipes of LHC rather than under it (as in LHC section 1-2).

Support similar to the one used in sector 1-2 was already ready. But no support was foreseen if the radiation detectors should be installed in the Roman Pots. The author pointed out that the radiation detectors without support might get in a position to damage the Roman Pot window and that the position of the radiation detectors would be very undefined without any support. Especially for the lower Roman Pot. The author therefore designed support for the radiation detectors inside the Roman Pots. Handmade drawings are included as Appendix Z. As the support was needed fast (and did not need very high precision) the author also produced the pieces. The drawings could not be followed completely as the aluminum plates delivered was thicker than the one ordered (3 mm rather than 1 mm) and there was no time to get the desired thickness.

After the support was made it was suggested to add springs to it to insure that it would not move. As the beam pipe and the Roman Pot are baked out for vacuum at several hundred degrees Celsius the spring material has to be of high quality (low quality spring losses the spring characteristic at high temperature [79](section 2.2.5). The author therefore added two plates of copper beryllium to act as springs. The final support is shown in Figure 18.3.

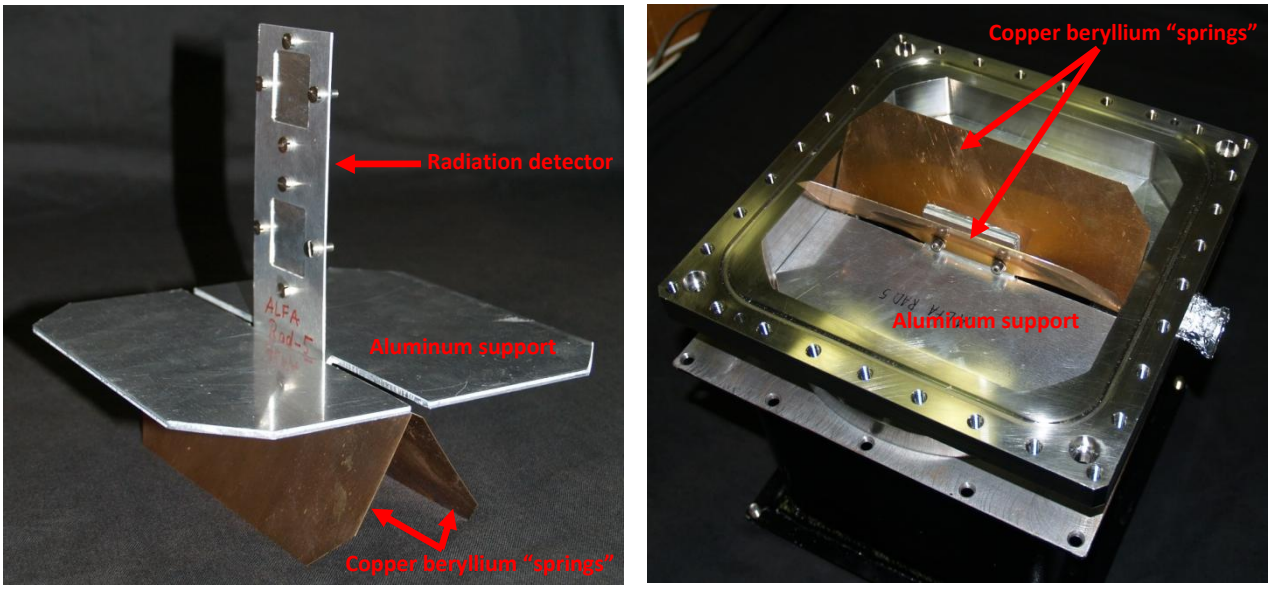

Figure 18.3. *LEFT*: Final support for installing a radiation detector inside a Roman Pot. *RIGHT*: The support tested inside a prototype Roman Pot.

In the end the Roman Pots was delivered in time and the first ALFA station installed. All of the installation was closely followed by the author.

Before the final vacuum test at ground level (before installation) a radiation detector was installed in each of the two pots using the support shown in Figure 18.3.

The last radiation detector was installed (by the author) on the foot with no ALFA station in LHC sector 8-1 between the beam pipes using support made by the author.

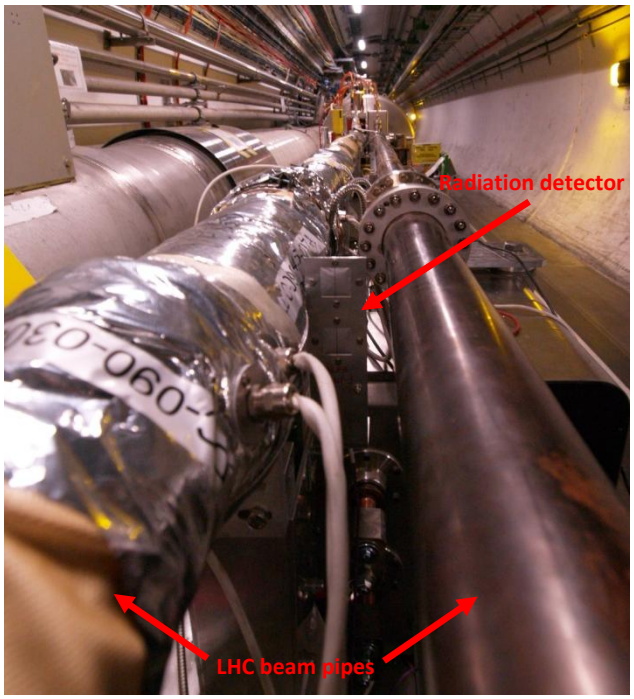

Figure 18.4. Radiation detector installed between the LHC beam pipes in LHC sector 8-1.

18.4. Results from radiation detectors

In the technical stop 2009-2010 ALFA decided to install the first detector to gain experience and check for any problems in the installation presidia. Also the fist detector with full readout could be used to commission many systems.

The installation was done one the 26th of January 2010 and was followed closely by the author. The installed station with a detector, black box with PMF, MAPMTs etc and a motherboard is shown in the front page.

To install the detector in the (top) Roman Pot the radiation detector with support had to be removed. This was done by the author as the person knowing the radiation support design best.

After passing the radiation control for removing materials from LHC, the TLDs were removed from the support and send to DESY Hamburg for analysis.

The results from all the TLDs were no radiation within the sensitive range. For the most sensitive TLD100 this meant a dose of less than 20 µGy. This was after the 2009 LHC run which had an integrated luminosity of about 20 μb^{-1}. To check if the ALFA detectors could be left in the Roman Pots for the 18-24 month run plan in 2011-2012 with and integrated luminosity of up to 1 fb^{-1} the following back-of-an-envelope calculation was made by KH:

$$\frac{L_{2010-2011}}{L_{2009}} = \frac{Dose_{2010-2011}}{Dose_{2009}} \Rightarrow$$

$$Dose_{2010-2012} = Dose_{2009} \cdot \frac{L_{2010-2011}}{L_{2009}} \qquad (18.1)$$

$$= 20\ \mu Gy \cdot \frac{20\ \mu b^{-1}}{1\ fb^{-1}} = 4 \cdot 10^5\ Gy = 40000\ krad$$

This is more than a 100 times more than the scintillating fibers can withstand. But it might easily be an over estimation because the lowest sensitive values of the TLDs used and the radiation might in reality have been much lower.

The rest of the radiation detectors are currently still installed and will not be removed before a more significant luminosity (dose) has been accumulated. The radiation detector installed in the lower Roman Pot will not be removed until the remaining ALFA detectors (and stations) are installed. The current estimate is that it will be done in the technical shut down end of 2010. However it might first be in the long shutdown in the end of 2011 if ALFA will not be permitted to break the beam vacuum for station installation before.

19. Conclusion

This thesis has discussed the importance for precise absolute luminosity measurements at ATLAS, the varies ATLAS sub-detectors and how some of them will be used measure luminosity. This lead to the need for the ALFA detector system. From the physics needs come the performance specification of the ALFA detector. The performance needs lead to the design of the ALFA detector and the support systems.

To check that the detector operates at the design specification a setup consisting of standard readout parts have been build. This has been used with cosmic rays to measure the light yield of 64 fibers at a time and thereby verifying the method. The setup have also been used to proof the potential 51 % ± 15 % higher light yield by using Ultra Bialkali MAPMTs rather than the standard Bialkali MAPMTs. Also it was discovered that the term previously introduced to describe cross talk with cosmic particles are totally dominated by effect of the inclined tracks. This was verified with a simple Monte Carlo simulation and is published as *[74]*.

The light yield of the trigger tiles was measured on a full prototype with cosmic particles and it was verified that the light yield was high enough to expect ~100 % efficiency. Similar measurement was later repeated at a test beam where a position scan of the triggers was possible. The results showed an unexpected pattern in the light yield over the surface of the trigger, but the overall light yield should still be sufficient to expect ~100 % efficiency.

The standard readout components have afterward been replaced with 5 custom made Orsay test boards, which made it possible to readout a full detector. The setup have been made and optimized. Afterwards gain equalization calibrations of all the MAPMT channels have been made for two detectors. One of the detectors has been submitted to a full cosmic rays test and the light yield measured in all fibers. Fibers with low light yield have been mapped for later explanation of low efficiency. The setup has also been used to verify the light yield stability of an old prototype overlap detector with over bent squared scintillating fibers. No ageing effect was observed. The result is published as *[50]*.

In October of 2009 ALFA had 3 weeks of test beam. Before a large number of tests was made to check and understand the equipment. A tool with equal light level over the surface of the MAPMT grid was design and used extensively during the equipment test. Among the tests were check of light tightness, mapping and S-curves (efficiency curves). The final check before going to the test beam was a cosmic run, whished verified that all involved systems worked, and that the mapping for the tracker was well understood.

At the test beam area an ALFA station was equipped with two detectors with readout. A silicon pixel beam telescope was installed in front of the ALFA station to give a precise position of each particle. The gain calibration of the detectors made with the 5 Orsay board was used in a large fraction of the test beam runs. A veto counter was used to exclude particles making showers. The beam was set up to meet the requirements for rate and size and continuously fine adjusted to keep the data taking at the optimal rate. A number of parameters were varied and the full area of both detectors was covered with beam and the beam telescope. The data is still being analyzed by the ALFA test beam data group, but the preliminary results looks promising and is expected to be published in the fall of 2010.

The LHC has started taking data for physics and the first papers have been published. In the first ATLAS paper *[33]* the absolute luminosity has an uncertainty of 17 %. This underlines the need for improvement in the luminosity determination and the need for ALFA to be installed. The cosmic testing, calibration etc. makes the installation and operation of the full ALFA detector system one step closer to be a reality.

20. List of equipment and software

The laboratory equipment is included in the text.

20.1. Photos

All photos without reference are taking by the author using some of the listed equipment.

20.1.1. DSLR

Olympus E-500

Olympus E-30

20.1.2. Lenses

Olympus Zuiko Digital 14-45 mm

Olympus Zuiko Digital 40-150 mm

Olympus Zuiko Digital 9-18 mm

Olympus Zuiko Digital 18-180 mm

Olympus Zuiko Digital 35 mm (Macro)

20.1.3. Photo light

Olympus FL-36R flash

Hama LED Macro Light, DSLR

20.2. Software

Microsoft Word 2007

MathType 6.5

Microsoft Excel 2007

Microsoft Visio 2007

GNU Emacs 23.1.50.1

ROOT 5.18-5.26

Maple 9.5

Autodesk AutoCAD Mechanical 2010

21. References

Reference where the author is on the author list is marked with *italic*.

[1] Webpage: http://public.web.cern.ch

[2] Webpage: http://en.wikipedia.org/wiki/CERN

[3] Webpage: http://public.web.cern.ch/public/en/About/Mission-en.html

[4] CERN Document Server (http://cdsweb.cern.ch/)

[5] Webpage: http://lhc-machine-outreach.web.cern.ch/lhc-machine-outreach/

[6] Booklet: The LHC guide (Materials for CERN guides), CERN.

[7] Webpage: http://en.wikipedia.org/wiki/A_Large_Ion_Collider_Experiment

[8] The CMS and TOTEM diffractive and forward physics working group, *Prospects for Diffractive and Forward Physics at the LHC*, CERN/LHCC 2006-039/G-124. (21 December 2006).

[9] TOTEM Collaboration, *TOTEM Technical Design Report, Total Cross Section, Elastic Scattering and Diffraction Dissociation at the Large Hadron Collider at CERN*, CERN-LHCC-2004-002. (7 January 2004).

[10] Webpage: http://en.wikipedia.org/wiki/Compact_Muon_Solenoid

[11] Webpage: http://www.atlas.ch/detector.html

[12] Booklet: ATLAS factsheet (http://www.atlas.ch/fact-sheets.html)

[13] Webpage: http://www.atlas.ch/etours_exper/experiment-07.html

[14] ATLAS LARG Unit, *Liquid Argon Calorimeter Technical Design Report*, CERN/LHCC 96-41. (15 December 1996).

[15] Webpage: http://www.hep.lu.se/atlas//thesis/egede/thesis-node43.html

[16] Webpage: http://www.atlas.ch/calorimeter.html

[17] J. Maneira (on behalf of the TileCal community), *Commissioning of the ATLAS Tile Calorimeter*, ATL-TILECAL-PROC-2010-001, (25 January 2010).

[18] L. Pontecorvo (on behalf of the ATLAS Collaboration), *The ATLAS Muon Spectrometer*, SN-ATLAS-2003-030. (28 July 2003).

[19] Andrej Gorišek, J. Stefan Institute, Ljubljana, Slovenia, *ATLAS Week / Luminosity WG*, CERN (4 December 2008).

[20] Webpage: https://twiki.cern.ch/twiki/bin/view/Atlas/BcmWiki#The_ATLAS_Diamond_Beam_Condition

[21] David Berge et al., *Luminosity measurement using the ATLAS Minimum Bias Trigger Scintillator System*, ATL-LUM-INT-2010-004. (31 March 2010).

[22] Mauro Villa (for the ATLAS LUCID group), *The Luminosity Monitor of the ATLAS Experiment*, ATL-LUM-PROC-2009-004. (16 November 2009).

[23] Pavel Ruzicka (on behalf of the ATLAS collaboration), *Forward physics at the ATLAS experiment*, ATL-LUM-PROC-2010-001. (21 January 2010).

[24] A. Sbrizzi, *Measurement of Luminosity with LUCID in ATLAS*, San Carlos de Bariloche, Argentina, (14-21 January 2009).

[25] The ATLAS Collaboration, *Zero Degree Calorimeters for ATLAS, Letter of Intent*, The ATLAS Experiment at the CERN Large Hadron Collider, JINST3 (2008) S08003. (2008).

[26] R. Hauser (on behalf of the ATLAS Collaboration), *The ATLAS Trigger System*, SN-ATLAS-2003-027. (24 July 2003).

[27] F. Pastore (on behalf of the ATLAS Collaboration), *ATLAS Trigger: design and commissioning*, ATL-DAQ-SLIDE-2009-303. (September 29th - October 4th 2009).

[28] PDG (Physics Letter B, Review of Particle Physics, (July 2008)).

[29] Book: *an introduction to PARTICLE ACCELERATORS*, EDMUND WILSON, OXFORD.

[30] H. Burkhardt and P. Grafstrom, *Absolute Luminosity from Machine Parameters*, LHC Project Report 1019 (23 May 2007).

[31] ATLAS Collaboration, *ATLAS DETECTOR AND PHYSICS PERFORMANCE, Technical Design Report*, ATLAS TDR 14, CERN/LHCC 99-14. (25 May 1999).

[32] Viatcheslav Sharyy (for CDF and D0 callaboration), *Top Quark Pair Production Cross Section at Tevatron*, Rencontres de Moriond QCD and High Energy Interactions. (17 March 2009).

[33] ATLAS Collaboration, *Charged-particle multiplicities in pp interactions at sqrt(s) = 900 GeV measured with the ATLAS detector at the LHC*, Phys Lett B 688, Issue 1, 21-42. (15 March 2010).

[34] Beate Heinemann, Eric Torrence and Guillaume Unal, *Determination of the Luminosity using the Liquid-Argon Calorimeter Endcaps*. ATL-COM-LUMI-2010-002. (9 March 2010).

[35] W.Bonivento, *Online luminosity monitoring with liquid Argon calorimeters at ATLAS and D0*, ATL-LARG-2001-001. (8 January 2001).

[36] Gerhard Brandt, Beate Heinemann and Lauren Tompkins, *Determination of the Event Rates and Luminosity using Events with Charged Particles*, ATL-COM-LUMI-2010-012. (4 May 2010).

[37] S.M White, R. Alemany-Fernandez, H. Burkhardt and M. Lamont, *First Luminosity Scans in the LHC*, to be published.

[38] S. van der Meer, *Calibration of the effective beam height in the Intersecting Storage Ring, ISR*, CERN-ISR-PO-68-31. (1968).

[39] ATLAS Luminosity and Forward Physics Community, *ATLAS Forward Detectors for Measurement of Elastic Scattering and Luminosity*, ATLAS TDR 018, CERN/LHCC 2008-04. (17 January 2008).

[40] Book: Dan Green, *The Physics of Particle Detectors*, Cambridge monographs on particle physics, nuclear physics and cosmology.

[41] UA4 Collaboration, D. Bernard et. al., *The Real Part of the Forward Proton Antiproton Elastic Scattering Amplitude at the Centre of Mass Energy of 546 GeV*, Phys. Lett. B 198 (1987) 583- 589. (1987).

[42] ALFA readiness review. (13 August 2009) (http://indico.cern.ch/conferenceDisplay.py?confId=62776).

[43] Scintillation Materials brochure from Kuraray.

[44] E. C. Aschenauer et al., *Measurements of the radiation hardness of selected scintillating and light guide fiber materials*, physics/9907018, DESY-99-078 (1999).

[45] A. Mapelli et al., *Development of a detector (ALFA) to measure the absolute LHC luminosity at ATLAS*, presented at the 10th International Conference on Advanced Detector and Particle Physics, Como, Italia, ATL-LUM-PUB-2007-006. (11 December 2007).

[46] B. Allongue et. Al, *Test Beam 2008: First measurements with an ALFA Roman Pot Prototype*, Internal ATLAS note: ATL-LUM-INT-2010-001. (2010)

[47] Webpage: https://twiki.cern.ch/twiki/bin/view/Main/AlfaDetectorProduction

[48] A. Braem, A. Folley, C. Joram, L. Kottelat. *Characterization studies on scintillating fibers*, lum-pub-2006-004. (2006).

[49] A. Braem, C. David, A. Folley, C. Joram, L. Kottelat, A. Mapelli, M. van Stenis, H. Stenzel, M. Szauter. *Design, Construction and Metrology of the Overlap Detectors for the ALFA system*, lum-pub-2007-004. (2007).

[50] S. Jakobsen and C. Joram. *Light yield stability over time in bent squared scintillating fibers*, Internal ATLAS note: ATL-LUM-INT-2009-004. (20 May 2010). Included as Appendix B.

[51] C. Joram et al., *Basic Considerations on the Overlap Detectors of the ATLAS ALFA system*, ATL-LUM-PUB-2007-002. (12 March 2007).

[52] Webpage: http://sales.hamamatsu.com/en/products/electron-tube-division/detectors/photomultiplier-tubes/part-r7600-00-m64.php

[53] A. Braem et. al. *Trigger Counter Studies for the ALFA Detector*, ATL-LUM-PUB-2009-001. (14 April 2009).

[54] Eljen EJ-200 Datasheet (http://www.eljentechnology.com/datasheets/EJ200%20data%20sheet.pdf),

[55] Webpage: http://sales.hamamatsu.com/en/products/electron-tube-division/detectors/photomultiplier-tubes/part-r7401.php

[56] Webpage: http://sales.hamamatsu.com/en/products/electron-tube-division/detectors/photomultiplier-tubes/part-r9880u-110.php

[57] Broche: *Hamamatsu UBA (Ultra Bialkali) SBA (Super Bialkali) Photomultiplier Tube Series*.

[58] P. Barrillon, S. Blin, M. Bouchel, T. Caceres, C. de La Taille, G. Martin-Chassard, P. Puzo, and N. Seguin-Moreau, *MAROC: Multi-Anode ReadOut Chip for MaPMTs*, proceedings IEEE 2006. (2006).

[59] A. Lucotte et al., *A front-end read out chip for the OPERA scintillator tracker*, Nucl. Instr. And Meth. A 521 (2004) 378-392.

[60] F. Anghinolfi, *ALFA Electronics Status*, ALFA detector meeting 24 februar 2010.

[61] CERN-Rome collaboration, *The Real Part of the Forward Proton Proton Scattering Amplitude Measurement at the CERN Intersecting Storage Rings*, Phys. Lett. 66 B (1977) 390-394. (1977).

[62] F. Abe et al., *Measurement of small angle antiproton-proton elastic scattering at = 546 and 1800 GeV*, Phys. Rev. D 50, 5518 (1994).

[63] A. Brandt et al., *A Forward Proton Detector at DØ*, FERMILAB-PUB-97/377. (1997).

[64] PP2PP Collaboration, *The PP2PP experiment at RHIC: silicon detectors installed in Roman Pots for forward proton detection close to the beam*, Nucl. Instrum. and Meth. A 535, 415-420. (2004).

[65] P. van Esch et al., *The H1 forward proton spectrometer at HERA*, Nucl. Instrum. and Meth. A, 446, 409-425. (2000).

[66] ZEUS Collaboration, M. Derrick et al., *The ZEUS Leading Proton Spectrometer and its Use in the Measurement of Elastic Rho0 Photoproduction at HERA*, DESY 96-183, Zeitschrift f. Physik C73 (1997) 2, 253-268.

[67] S. Franz, *Update on ALFA controls*, ALFA Technical meeting April 19th 2010.

[68] S. Ask et. Al., *Luminosity measurement at ATLAS—Development, construction and test of scintillating fibre prototype detectors*, Nuclear Instruments and Methods in Physics Research A 568 (2006) 588–600.

[69] CAEN, *Technical Information Manual, MOD. 792 series*, 00102/97:V792x.MUTx/06 (15 Nobember 2002).

[70] Webpage: http://en.wikipedia.org/wiki/Strontium-90

[71] Book: W.R. Leo, *Techniques for Nuclear and Particle Physics Experiments, A How-to Approach*, Secound Revised Edition, Springer-Verlag (1994).

[72] A. Braem, C. Joram, A. Mapelli, A. Kocnar and J. Pospichal, *Metrology results of the ALFA 2006 prototype detectors*. lum-pub-2006-007. (27 November 2006).

[73] Helmuth Spieler, *Introduction to Radiation Detectors and Electronics, IV. Scintillation Detectors – 3*. (2 February 1999).

[74] S. Jakobsen and C. Joram. *Differences in light yield and crosstalk in a scintillating fiber tracker between beam- and cosmic measurements*, Internal ATLAS note: ATL-LUM-INT-2009-004. (14 December 2009). Included as Appendix A.

[75] Unpublished work by Sebastien Franz (CERN, PH-ADO) and Christian Joram (CERN, PH-DT) protected by none-discloser agreement.

[76] Daniel Haas, *The DAQ for the EUDET pixel telescope*, LCWS/ILC2007. (2007).

[77] Webpage: http://www.eudet.org/

[78] S. Ask, S.Hoffmann and H. Stenzel, *Spatial Resolution Study of ALFA from the CERN Testbeam in 2006*. ATL-LUM-PUB-2007-003. (21 May 2007).

[79] Book: Yoshirō Yamada, *Materials for Springs*, Japan Society of Spring Engineers, Springer. (2007).

22. Appendix list

Appendix A

Differences in light yield and crosstalk in a scintillating fiber tracker between beam- and cosmic measurements

S. Jakobsen (CERN, PH-ADO) and C. Joram (CERN, PH-DT)

Abstract

The Absolute Luminosity For ATLAS, ALFA, detector aims for measuring LHC luminosity with high precision by using pp-scattering under small angles [1]. The tracking detector is made from scintillating fibers readout by MultiAnode PhotoMultiplier Tubes, MAPMTs. It is essential that the scintillating fibers send out enough light to give clear signals from the MAPMTs and that only the intended MAPMT channel receive light from the scintillating fiber. All ALFA detectors will be tested with cosmic before installation to determined, among other things, the light yield of all scintillating fibers. This note describes differences in fiber light yield and crosstalk between beam and cosmic.

ATL-LUM-INT-2009-004
14 December 2009

1. Introduction

In 2005 a beam test of a prototype for the Absolute Luminosity For ATLAS, ALFA, was performed at DESY [2]. The prototype detector had 10 layers of 6 squared scintillating fibers each. The light yield of the scintillating fibers was measured using MultiAnode PhotoMultiplier Tubes, MAPMTs pre-calibrated with low intensity LED. The calibration was done by fitting the 1 photo electron charge spectrum with a Poisson distribution convoluted with a Gauss function [2]:

$$f(x) = N \cdot \left(\sum_{i=0}^{n} \left[\frac{e^{-\mu} \cdot \mu^{i}}{i!} \cdot \frac{1}{\sqrt{2\pi}\sqrt{i \cdot {\sigma_{1PE}}^{2} + {\sigma_{ped}}^{2}}} \cdot e^{\frac{-(x - Q_{ped} - i \cdot Q_{1PE})^{2}}{2 \cdot (i \cdot {\sigma_{1PE}}^{2} + {\sigma_{ped}}^{2})}} \right] \right) \quad \text{(I)}$$

N	Normalizationfactor	Q_{1PE}	Charge of the 1 photoelectron
i	Number of photoelectrons	σ_{ped}	Charge deviation of the pedestal
n	Maximum number of photoelectrons	σ_{1PE}	Charge deviation of the 1 photoelectron
Q_{ped}	Charge of the pedestal	μ	Main light yield

To describe light exiting one fiber, but hitting the neighbor MAPMT channel a crosstalk term (the second sum) was introduced in the fiber light yield fit formula:

$$f(x) = N \cdot \left(\sum_{i=1}^{n} \left[\frac{e^{-\mu} \cdot \mu^{i}}{i!} \cdot \frac{1}{\sqrt{2\pi}\sqrt{i \cdot {\sigma_{1PE}}^{2} + {\sigma_{ped}}^{2}}} \cdot e^{\frac{-(x - Q_{ped} - i \cdot Q_{1PE})^{2}}{2 \cdot (i \cdot {\sigma_{1PE}}^{2} + {\sigma_{ped}}^{2})}} \right] + \sum_{i=1}^{n} \left[\frac{e^{-\mu_{CT}} \cdot {\mu_{CT}}^{i}}{i!} \cdot \frac{1}{\sqrt{2\pi}\sqrt{i \cdot {\sigma_{1PE}}^{2} + {\sigma_{ped}}^{2}}} \cdot e^{\frac{-(x - Q_{ped} - i \cdot Q_{1PE})^{2}}{2 \cdot (i \cdot {\sigma_{1PE}}^{2} + {\sigma_{ped}}^{2})}} \right] \right) \quad \text{(II)}$$

μ_{CT} Crosstalk light yield

The light hitting a neighbor channel can have a direct pass as in Figure 1, or it can have multiple reflections in the MAPMT entrance window.

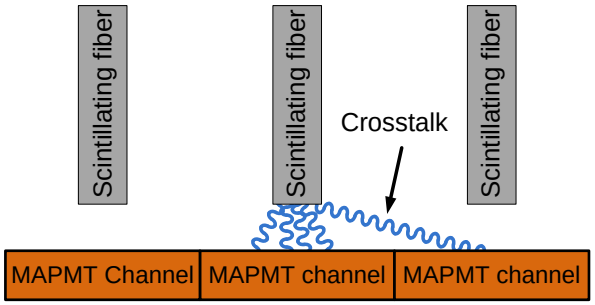

Figure 1. Light transition from the scintillating fiber to the MAPMT. A fraction of the light hits a neighbor MAPMT channel. This fraction is label crosstalk.

In [2] the relative crosstalk was determined to:

$$Crosstalk_{\text{beam}} = \frac{\mu_{CT}}{\mu + \mu_{CT}} = 3.4 \pm 1.3\% \quad \text{(III)}$$

An example of the data and fit is shown in Figure 2.

In 2009 a cosmic setup was made at CERN to test all ALFA detectors before installation. In a cosmic test performed on a full size prototype detector the relative crosstalk was determined to:

$$Crosstalk_{\text{cosmic}} = \frac{\mu_{CT}}{\mu + \mu_{CT}} = 19.6 \pm 3.4\% \quad \text{(IV)}$$

An example of the cosmic data and fit is shown in Figure 3.

Appendix A

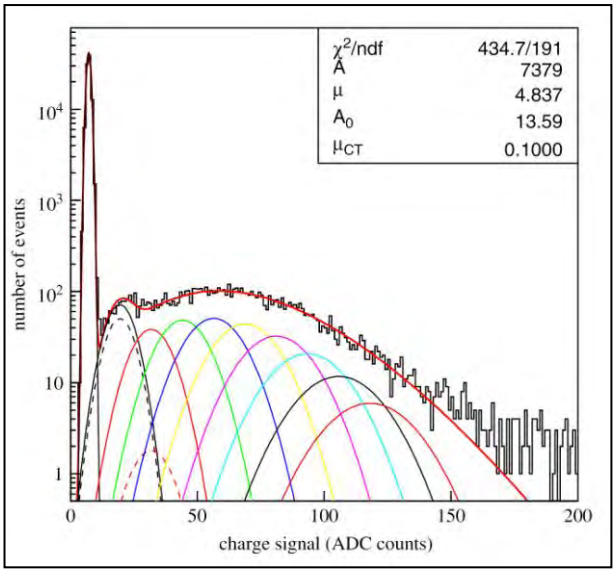

Figure 2. Fit of charge histogram with data from the 2005 test beam. (Figure 5 from [2]).

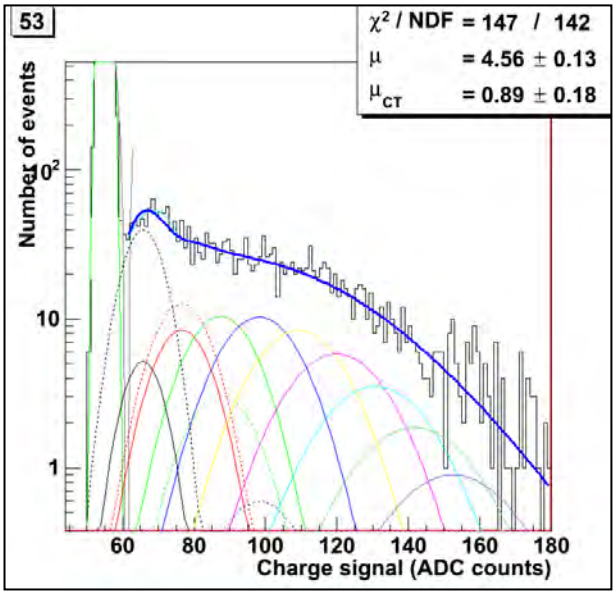

Figure 3. Fit of charge histogram with data from a cosmic test.

2. Hypothesis

A beam comes from a very well defined direction and in the 2005 setup the detector was placed perpendicular to the beam. The particles in the beam (6 GeV electrons) will never hit more than one fiber per layer. The particles will always go the shortest path through the fiber layer. But the cosmic particles (primarily muons) have an angular destitution [3]:

$$\text{Angular distribution} \propto \cos^2\theta \qquad \text{(V)}$$

Therefore one cosmic particle can hit more than one fiber per layer. Also the distance a particle travels inside a fiber layer will in general be longer. The difference is illustrated in Figure 4.

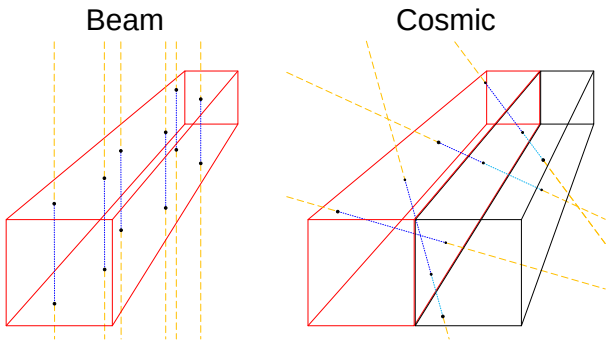

Figure 4. Illustration of the difference between particles from a beam and from cosmic. For easier comparison the beam is coming from above in the illustration. The fibers are made in red and black. The particle track outside the fiber is yellow and the particle tracks inside the fibers are blue in different shades depending on fiber.

Scintillating fibers being passed though only partly of a particle will obvious send out fewer photons. The MAPMT channel receiving the photons will therefore in average make a smaller signal. This will make a pileup of small charge signals, which in the fit with equation (II) will come out as crosstalk. This could be an explanation for the larger crosstalk term seen in the cosmic data compeered to the data from a beam.

3. Simulation

To investigate the hypothesis a simple Monte Carlo simulation was made.

The Monte Carlo simulation was made in C++ and run inside ROOT, using ROOTs histograms as an output. Also ROOTs TRandom3 was used for random numbers.

3.1. Generation of particles

To simplify the geometry the fibers are assumed to be infinity long. Therefore a particle will never exit from the end of a fiber. It is also assumed that the fiber first hit will always have 5 fibers next to it. This means that fiber simulated will not be on the edge of the detector and that a particle will never pass though more than 6 fibers (θ (see below) up to about 80 degrees).

The simulation first generates a random position on a fiber where the particle hits. The width and height of the squared fiber is call *b*, so the position, *p*, on the fiber is made by multiplying a random number between 0 and 1 with *b*. *b* and *p* are shown in Figure 5.

Appendix A

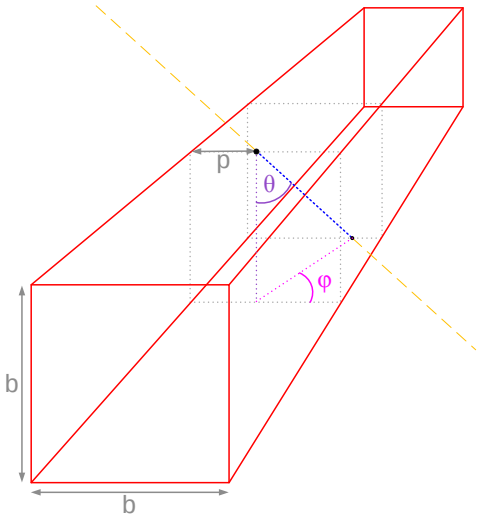

Figure 5. The angle ϕ in the simulation.

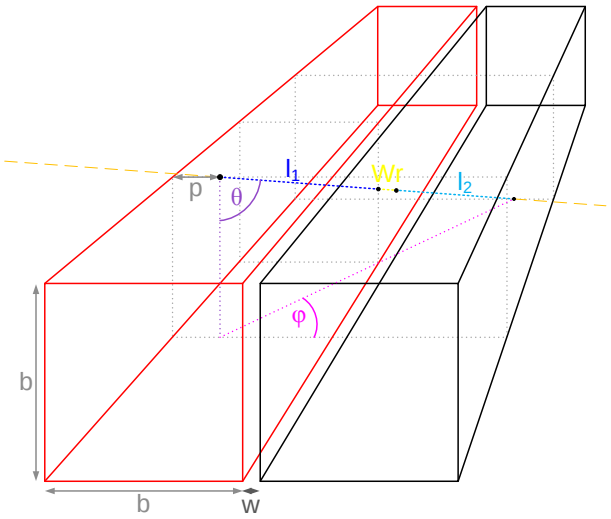

Figure 6. Length a particles travels inside fiber 1 and fiber 2.

The simulation then generates the angle perpendicular to the fiber (the polar angle), θ. This is generates randomly from the angular distribution of cosmic particles equation (V).

The interval is going from 0 to π/2. The definition of θ is shown in Figure 5.

Next the simulation generates randomly the angle φ, which is the azimuthal angle. In principle φ should be in the interval from 0 to 2π. But since there should be no differences between each end of the fiber, and since it should not matter if a second fiber hit is on one side or the other of the first, the interval for φ is only going from 0 to π/2. This makes the geometry much easier and should not change the simulation in any way. φ is made by generating a random number between 0 and 1 and multiply it with π/2. The definition of φ is shown in Figure 5.

3.2. Particle interaction

Particles are assumed to never be stopped in the fibers. It is also assumed that particles always induce the same number of photons per length travelled inside a fiber.

The simulation first determines how many fibers will be hit by a generated particle. Then the length a generated particle travels inside each fiber is fund by geometrically calculations as shown in Figure 6.

The active part of the fiber, *b*, is assumed to be 480 µm out of the 500 µm widths and the inactive part between active fibers, *W*, is assumed to be 30 µm. The length a particle travel inside fiber *i* is labeled l_i.

The number of photo electrons, PE, detected by the MAPMT follows a Poisson distribution due to the statistical nature of the involved processes.

The simulation starts off by taking a random number, p_i, from a Poisson distribution with a mean value proportional to l_i. The program generates a Gaussian distribution with mean p_i and width $\sqrt{p_i}\cdot\sigma_1$, where σ_1 is the measured width of the 1 PE peak. The electronic pedestal width $\sigma_{pedestal}$ is added to all σ_{p_i} values in quadrature:

$$\sigma_{p_i} = \sqrt{\sigma_{pedestal}^{\,2} + p_i \cdot \sigma_1^{\,2}} \qquad \text{(VI)}$$

The program chooses now a random value from this distribution and fills it into a histogram.

3.3. Noise and crosstalk

The noise from the MAPMTs and the events where the PE created inside the MAPMT miss the first dynode but hit the second, is included in the simulation. This is done by introducing a noise value for MAPMT channels for fibers not hit. The value is ~0.15 % of the main light, which is the charge measured in none hit channels in a real MAPMT [4]. The 4 MAPMT channels surrounding the main channel will see crosstalk. The crosstalk amount has been measured with a LED pulsed thought a clear fiber to one MAPMT channel. The 4 neighbors

channel got 0.96 %, 0.73 %, 1.00 % and 0.77 % of the main light (for around 4 PE in the main MAPMT channel) [4]. To take this into account every l_i is multiplied, in turn, with the 4 percentages. The 4 results correspond to the light the MAPMT will see in the neighboring channels. The effects of the MAPMT are simulated by a Poisson and a Gaussian, as for the main light. Finally the crosstalk values are added to the main histogram.

3.4. Fit and results

The histograms with the simulated data are fitted with equation (II) in the same manner as the real data.

The results corresponding to cosmic are shown in Figure 7.

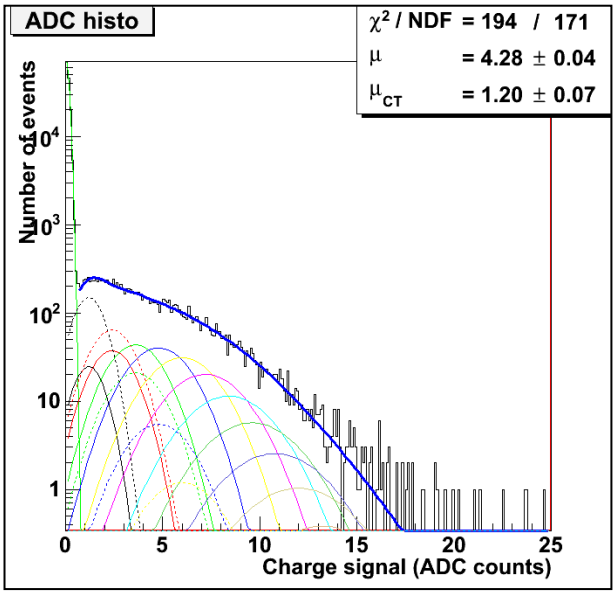

Figure 7. Histogram from simulation cosmic data fitted with equation (II).

The results from the fit are a main light yield of 4.28 ± 0.04 PE and the "crosstalk" term is 1.20 ± 0.07 PE. The absolute values themselves have no direct physical meaning as they just scale with the inputted "number of PE per length" used in the simulation. But the relative crosstalk can be compared to real data. The relative crosstalk is:

$$Crosstalk_{\text{MC cosmic}} = \frac{\mu_{CT}}{\mu + \mu_{CT}} = 21.9 \pm 1.2\ \% \quad \text{(VII)}$$

This is comparable to what was seen in the cosmic data, 19.6 ± 3.4 %. To make a control that this is really a difference between cosmic and beam and not for example an artificial effect from the noise term the simulation was repeated for beam. This was done by keeping all parameters at the same value but locking the angle θ to zero, as it would be in a beam. The result for the control beam simulation is shown in Figure 8.

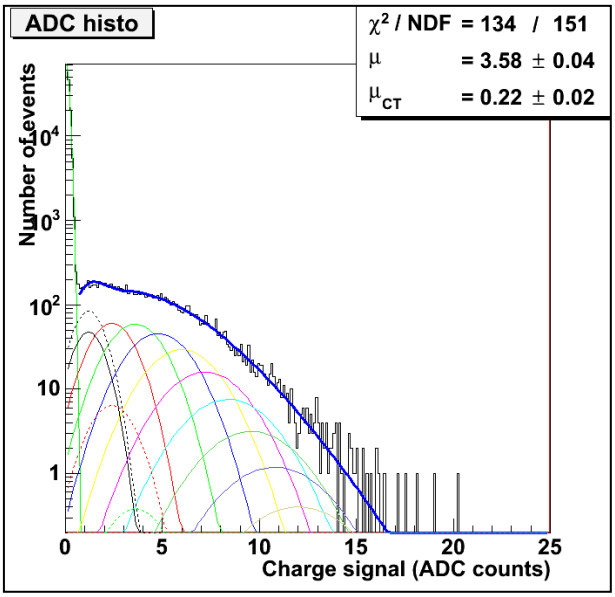

Figure 8. Histogram from simulation of beam with the same settings as for the cosmic simulation.

The results from the fit are a main light yield of 3.58 ± 0.04 PE and the crosstalk term is 0.22 ± 0.02 PE. The relative crosstalk is therefore:

$$Crosstalk_{\text{MC beam}} = \frac{\mu_{CT}}{\mu + \mu_{CT}} = 5.8 \pm 0.6\ \% \quad \text{(VIII)}$$

This is a little higher but still comparable to what was seen in the beam data, 3.4 ± 1.3 %.

The cosmic have a higher main light yield term. This is because the particles on average will always travel longer trough the fiber when they are not hitting the fiber perpendicular:

$$\frac{\mu_{\text{cosmic}}}{\mu_{\text{beam}}} = \frac{4.28\ PE}{3.58\ PE} = 1.20 \pm 0.02 \quad \text{(IX)}$$

4. Conclusion

A cosmic setup for measuring of the light yield of an ALFA scintillating fiber detector was tested in 2009. The results for the relative crosstalk term of the light yield, $\frac{\mu_{CT}}{\mu + \mu_{CT}}$, was munch higher, 19.6 ± 3.4 %, than what was previous seen in a beam test in 2005, 3.4 ± 1.3 %. A

hypothesis that the much larger crosstalk term seen in cosmic data is not due to crosstalk, but a property for the angular distribution of cosmic particles, was investigated by making a Monte Carlo simulation. The simulation data had a relative crosstalk term of 21.9 ± 1.2 % for cosmic and 5.8 ± 0.6 % for beam. Thereby the simulation substantiated the hypothesis.

The simulation also showed that the average light yield of a fiber will be 20 ± 2 % larger for cosmic compared to beam.

5. References

[1] ATLAS Coll.: ATLAS Forward Detectors for Measurement of Elastic Scattering and Luminosity, ATLAS TDR 018, CERN/LHCC 2008-04.

[2] Nuclear Instruments and Methods in Physics Research A 568 (2006) 588-600.

[3] Physics Letters B, Review of Particle Physics, July 2008, page 256.

[4] Unpublished work done by Sebastien Franz (CERN, PH-ADO) and Christian Joram (CERN, PH-DT) (used with permission).

Appendix B

Light yield stability over time in bent squared scintillating fibers

S. Jakobsen[1] and C. Joram[2]

[1] *The Niels Bohr Institute, Copenhagen University*
[2] *CERN, PH-DT*

07-05-2010

Abstract

The ALFA (Absolute Luminosity For ATLAS) project aims at measuring luminosity in LHC with high precision by using pp-scattering under small angles [1]. This will be done by moving an upper and a lower tracking detector inside Roman Pots very close to the beam. To align the upper and lower tracking detector a dedicated part overlaps and the alignment will be done with particles passing both the upper and the lower detector.

The tracking detectors and the overlapping part are made up from scintillating fibers. Because of spatial constraints the scintillating fibers used for the overlapping part have a smaller bending radius than recommended by the manufacture. Previous studies have showed that no significant performance degradation is seen if the scintillating fibers are bent at elevated temperature [2]. This note describes the investigation of long term ageing effects on the bent scintillating fibers. The light yields of the scintillating fibers of a 3 years old prototype have been measured with cosmics. A similar measurement has been performed on a newly produced detector. The results show no significant difference in the light yields between the 3 years old prototype and the newly produced detector.

Introduction

An ALFA (Absolute Luminosity For ATLAS) station consists of an upper and a lower detector that can move independently and therefore compensate for the different beam positions that each LHC fill might have. The alignment for the upper and lower detector is foreseen to be done using the halo particles of the beam. Dedicated parts of the ALFA detectors overlap in the beam direction. This part is called the overlap detector. The halo particles will pass both the upper and the lower overlap detectors (as seen in Figure 1) and thereby provide alignment information as described in [2].

The overlap detector is constructed from 0.5x0.5 mm^2 square scintillating fibers (Kuraray SCSF-78, S-type) read out by MultiAnode PhotoMultiplier Tubers, MAPMTs (as is the main ALFA detector). The recommended minimum bending radius is 25 mm for round fibers [3]. A larger minimum bending radius is to be expected on square fibers as the outer corners will have more stress than the center of a round fiber. In the ALFA overlap layers, bending radii between 22.5 mm and 30 mm are needed, which is much less than for the main detectors as shown in Figure 1. Therefore, there were originally some tests made to investigate the fiber behavior under small bending radius [4]. Already at a bending radius of 30 mm significant degradation of the light transport performance was observed and cracks in the fibers could

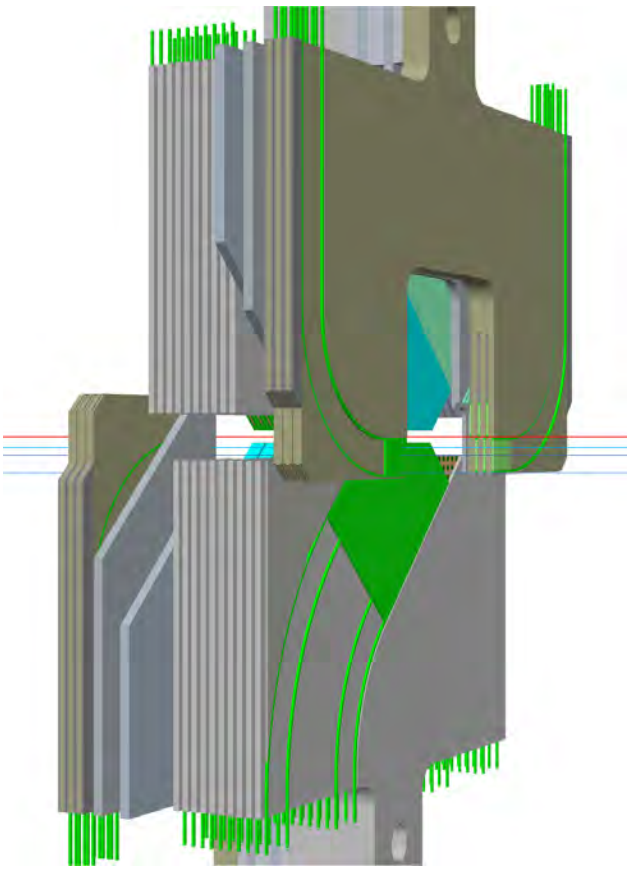

Figure 1. Upper and lower ALFA detector. The aluminized scintillating fibers are here light green and the trigger scintillator tiles are turquoise. The center of the beam is marked with a red trajectory. The 3 trajectories for halo particles hitting the overlap detectors are deference shades of blue. The figure is a modified version of the original AutoCAD drawings made by A. Bream (CERN PH-DT).

ATL-LUM-INT-2010-007
20 May 2010

even be seen under a microscope. Further studies were made to bend the fibers to the needed radius at elevated temperature [2]. An optimal temperature of 85 ˚C was fund at which the transmission of the fiber did not change over a period of 20 days. This temperature was later in 2006 used to bend the fibers for a 2·2 layer prototype detector. The prototype was tested with a Strontium-90 source and later in the ALFA test beam in October 2006. All tests indicated performance comparable to that of un-bent fibers.

The stability of the performance of the bent scintillating fibers has been proven for a period of the order of a month, but the ALFA detectors will be used for many years. To verify that there are no ageing effects for the bent fibers, a long term test of the performance was needed. This note describes the test made to verify the long term performance for the bent scintillating fibers used in the overlap detector.

Method for validating performance

All ALFA detectors and frontend electronic will undergo a cosmic test after their final assembly and before installation. This is done to make a final validation of as many parts as possible in their final assembly and potentially replace bad parts. For the detectors themselves, the light yields of all scintillating fibers are determined and bad fibers are mapped. The first ALFA detector, ALFA1, has already been trough the cosmic test and the light yield of all scintillating fibers was determined.

The overlap prototype made in 2006 now has an age of over 3 years. To validate if the performance has degraded over this period in time, a cosmic test similar to the ones used for validating the final detectors was performed on the prototype. As no such measurements were done when the prototype overlap detector was built in 2006, the performance (light yield of each fiber) will instead be compared to the recently produced overlap layers of ALFA1.

Concept and setup for the light yield measurements

The charge gain of the different MAPMT channels can differ by up to a factor 6 (this includes variations from MAPMT to MAPMT of a factor ~3). To compensate for this, there are amplifiers with adjustable gain for each MAPMT channel integrated in the frontend electronics. The calibration of the amplifiers was made with a setup where very low light levels from a pulsed LED gave on average about 0.05 photoelectrons, PE, to each MAPMT channel. Because the readout motherboard was not operational yet, the readout was done with test boards designed by the Orsay group. A schematic and photo of the setup is shown in appendix A and detailed information can be found in [5]. The charge histograms from the calibration were fitted with Poisson distributions convoluted with Gauss functions [6]:

$$f(x) = N \cdot \sum_{i=0}^{n} \left[\frac{e^{-\mu} \cdot \mu^{i}}{i!} \cdot \frac{1}{\sqrt{2\pi}\sqrt{i \cdot \sigma_{1PE}{}^{2} + \sigma_{ped}{}^{2}}} \cdot e^{\frac{-(x - Q_{ped} - i \cdot Q_{1PE})^{2}}{2 \cdot (i \cdot \sigma_{1PE}{}^{2} + \sigma_{ped}{}^{2})}} \right] \quad (1)$$

N	Normalizationfactor	Q_{1PE}	Charge of the 1 PE
i	Number of PEs	σ_{ped}	Charge deviation of the pedestal
n	Maximum number of PEs	σ_{1PE}	Charge deviation of the 1 PE
Q_{ped}	Charge of the pedestal	μ	Main light yield

The amplifiers were adjusted so that the measured 1 PE charge from each MAPMT channel was the same. An example of a 1 PE fit is shown in Figure 2.

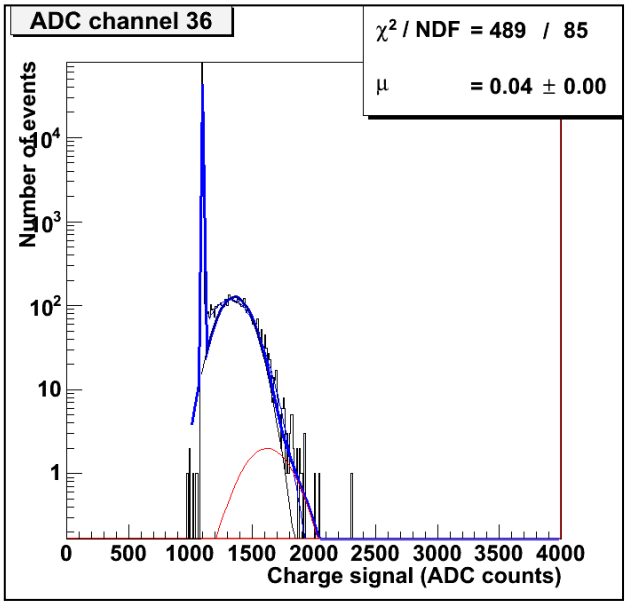

Figure 2. 1 PE charge spectrum form calibration. The pedestal represents triggers with no charge in the MAPMT channel. A small 2 PE (red) contribution is also shown.

After this calibration, the setup was changed for cosmics particles. The LED was removed and the triggering changed to scintillating tiles readout by PMTs. For the full ALFA1 detector, the internal trigger scintillator tiles were used together with an external larger scintillator tile. The measurements were performed for only two (middle and lower) of the three overlap fiber layers. A schematic and photo of the setup is shown in appendix B and detailed information can be found in [5]. The prototype overlap detector did not have built-in trigger scintillator tiles, so the triggering was done with 2 small scintillator tiles together with a large scintillator tile. This assured triggering on only the part of the scintillating fibers which are intended to be active for the lower two layers. For the upper two layers the triggering was not restricted to only the part of the scintillating fibers intended to be active. A schematic and photo of the setup is shown in appendix C and detailed information can be found in [5].

Appendix B

For the full ALFA1 detector, a cosmic run of about 2 weeks was made. For the prototype overlap detector, a cosmic run of about 3 weeks was made.

The light yield of each fiber was determined by fitting the charge distribution with the following expression:

$$f(x) = N \cdot \left(\sum_{i=1}^{n} \left[\frac{e^{-\mu} \cdot \mu^{i}}{i!} \cdot \frac{1}{\sqrt{2\pi}\sqrt{i \cdot \sigma_{1PE}{}^{2} + \sigma_{ped}{}^{2}}} \cdot e^{\frac{-(x - Q_{ped} - i \cdot Q_{1PE})^{2}}{2 \cdot (i \cdot \sigma_{1PE}{}^{2} + \sigma_{ped}{}^{2})}} \right] + \sum_{i=1}^{n} \left[\frac{e^{-\mu_{CT}} \cdot \mu_{CT}{}^{i}}{i!} \cdot \frac{1}{\sqrt{2\pi}\sqrt{i \cdot \sigma_{1PE}{}^{2} + \sigma_{ped}{}^{2}}} \cdot e^{\frac{-(x - Q_{ped} - i \cdot Q_{1PE})^{2}}{2 \cdot (i \cdot \sigma_{1PE}{}^{2} + \sigma_{ped}{}^{2})}} \right] \right) \quad \text{(II)}$$

μ_{CT} Crosstalk light yield

All parameters marked with red are locked to the calibration values (from the 1 PE fit). The second sum was originally introduced for beam measurements to describe crosstalk, however for cosmic particles it describes primarily effects due to the angular distribution of the cosmic particles as discussed in [7]. An example of a fit of cosmic data is shown in Figure 3.

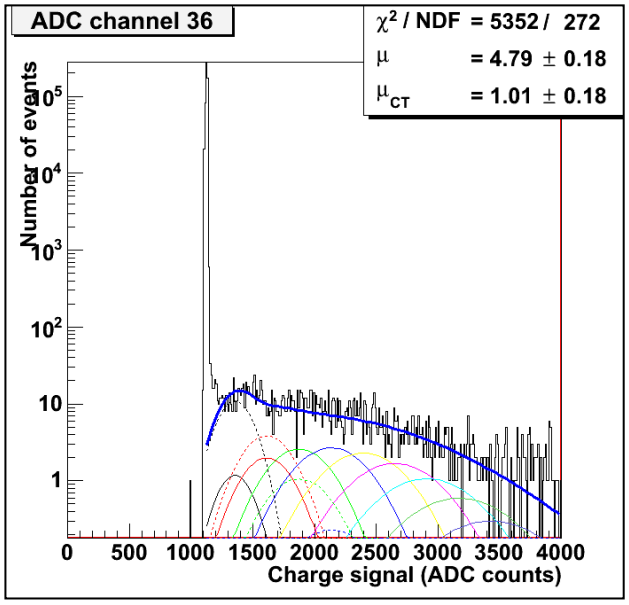

Figure 3. Charge spectrum from cosmic particles.

Results

The light yields for all fibers in the two lower layers of the prototype overlap detector are shown in Figure 4 and Figure 5.

The average overall light yield is 4.99 ± 0.62 PE. The differences seen between the right and the left sides are most likely due to variations in the quantum efficiency from one MAPMT to another (fibers 1-30 on layer 1 and 2 were connected to one MAPMT, and fibers 33-62 on layer 1 and 2 were connected to another MAPMT).

The results for layer 3 and 4 are shown in Figure 6 and Figure 7. For these measurements, however, the triggering scheme was not selecting only the area intended to be active. The results can therefore not be used for direct comparison.

The light yields for all fibers in the 2 overlap layers of the ALFA1 detector are shown in Figure 8 and Figure 9.

The overall light yield average is 4.92 ± 0.58 PE.

Conclusions

The light yields of all scintillating fibers of the 3 years old overlap detector are high. The average light yield is 4.99 ± 0.62 PE which is directly comparable to the newly produced ALFA1 detector with average light yield of 4.92 ± 0.58 PE. All average light yields measured with cosmics should be normalized by dividing by a factor of about 1.2 before comparison with light yield from a beam, as explained in [7]. No fibers in the prototype overlap detector are dead or show particularly low light yield. The conclusion is therefore that, over a period of 3 years, no ageing effects have occurred on the bent scintillating fibers.

References

[1] ATLAS Coll.: ATLAS Forward Detectors for Measurement of Elastic Scattering and Luminosity, ATLAS TDR 018, CERN/LHCC 2008-04.

[2] A. Braem, C. David, A. Folley, C. Joram, L. Kottelat, A. Mapelli, M. van Stenis, H. Stenzel, M. Szauter. Design, Construction and Metrology of the Overlap Detectors for the ALFA system, lum-pub-2007-004.

[3] Scintillation Materials brochure from Kuraray.

[4] A. Braem, A. Folley, C. Joram, L. Kottelat. Characterization studies on scintillating fibers, lum-pub-2006-004.

[5] S. Jakobsen. Master Thesis 'Commissioning of the luminosity detector ALFA', 2010, to be published.

[6] S. Ask et al., Luminosity measurement at ATLAS—Development, construction and test of scintillating fibre prototype detectors, Nuclear Instruments and Methods in Physics Research A 568 (2006) 588-600.

[7] S. Jakobsen and C. Joram. Differences in light yield and crosstalk in a scintillating fiber tracker between beam- and cosmic measurements, ATL-LUM-INT-2009-004.

Appendix B

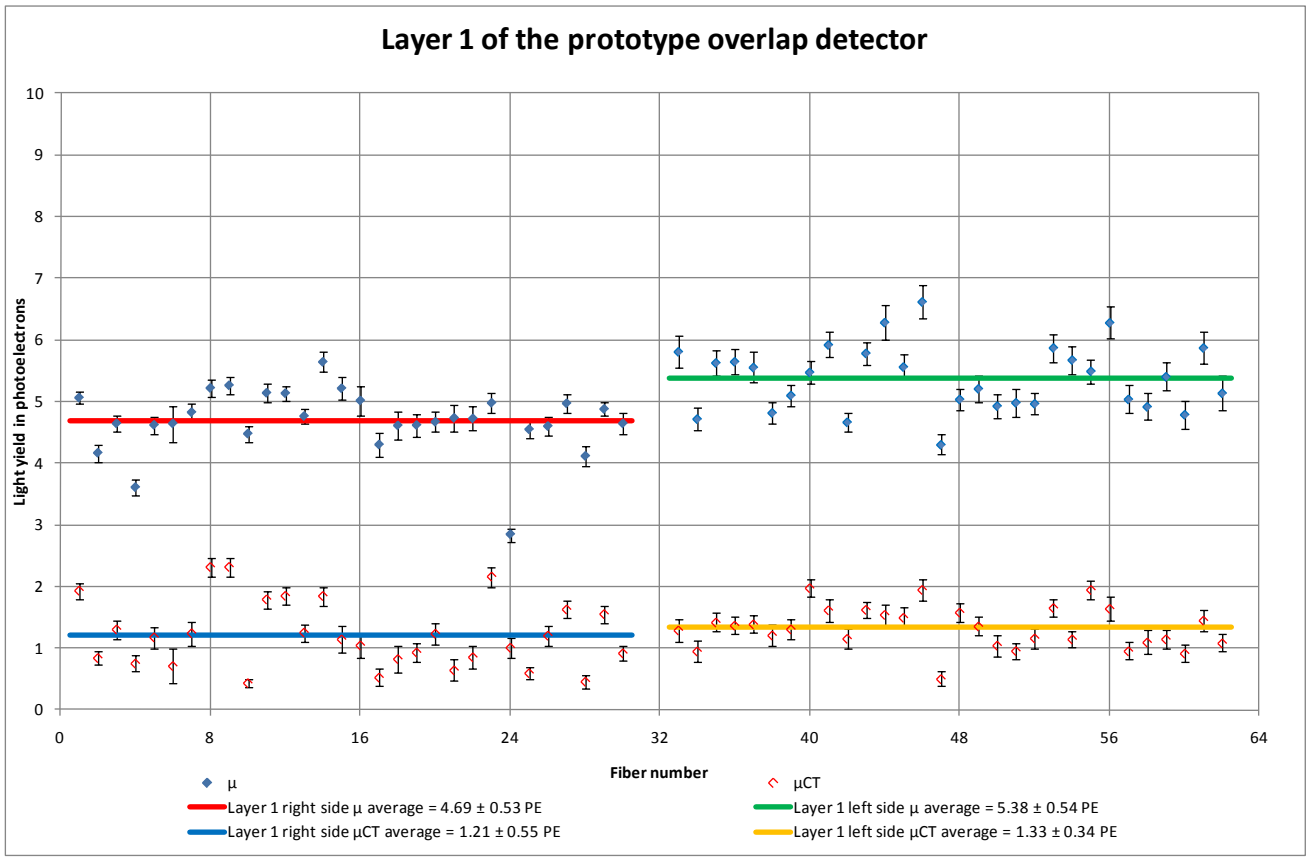

Figure 4. Light yield in each fiber of layer 1 in the prototype overlap detector.

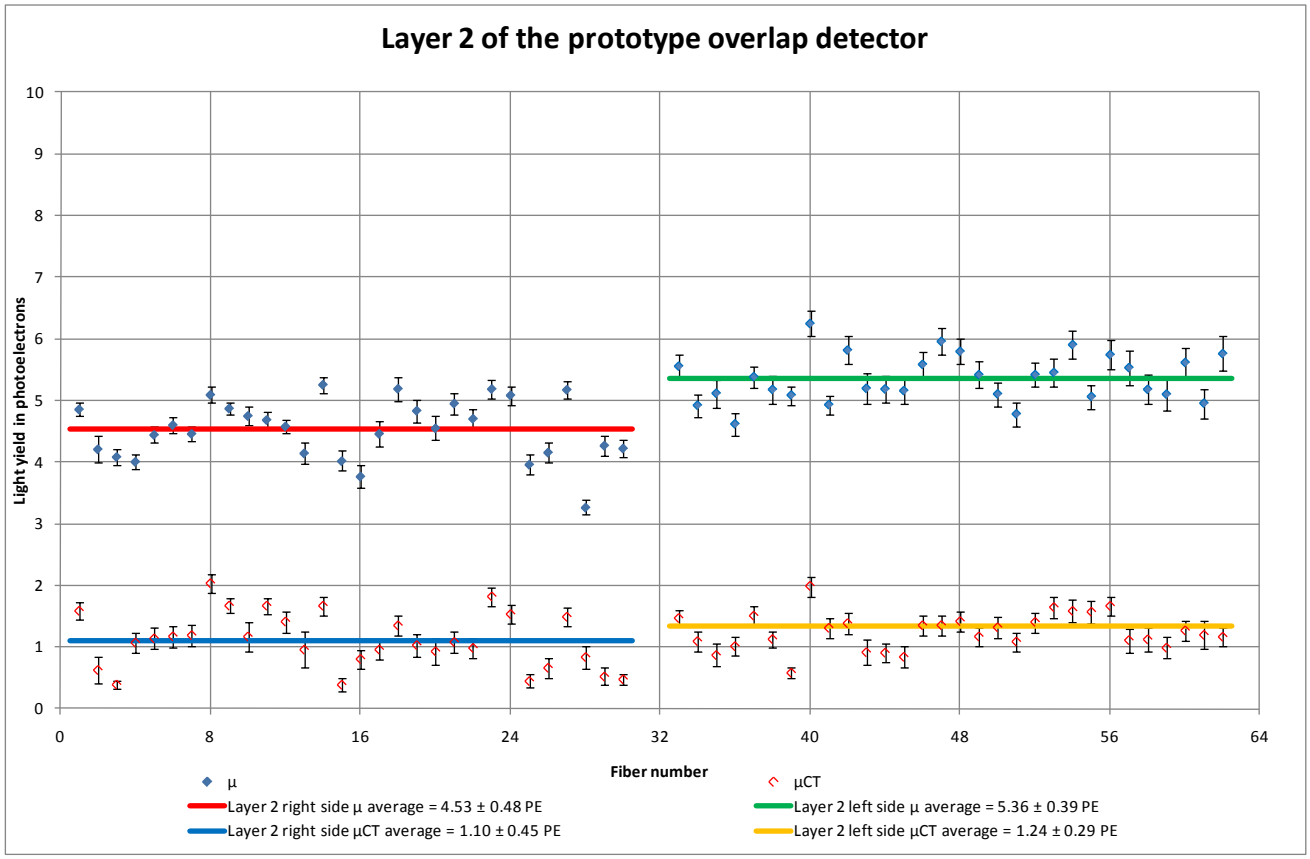

Figure 5. Light yield in each fiber of layer 2 in the prototype overlap detector.

Appendix B

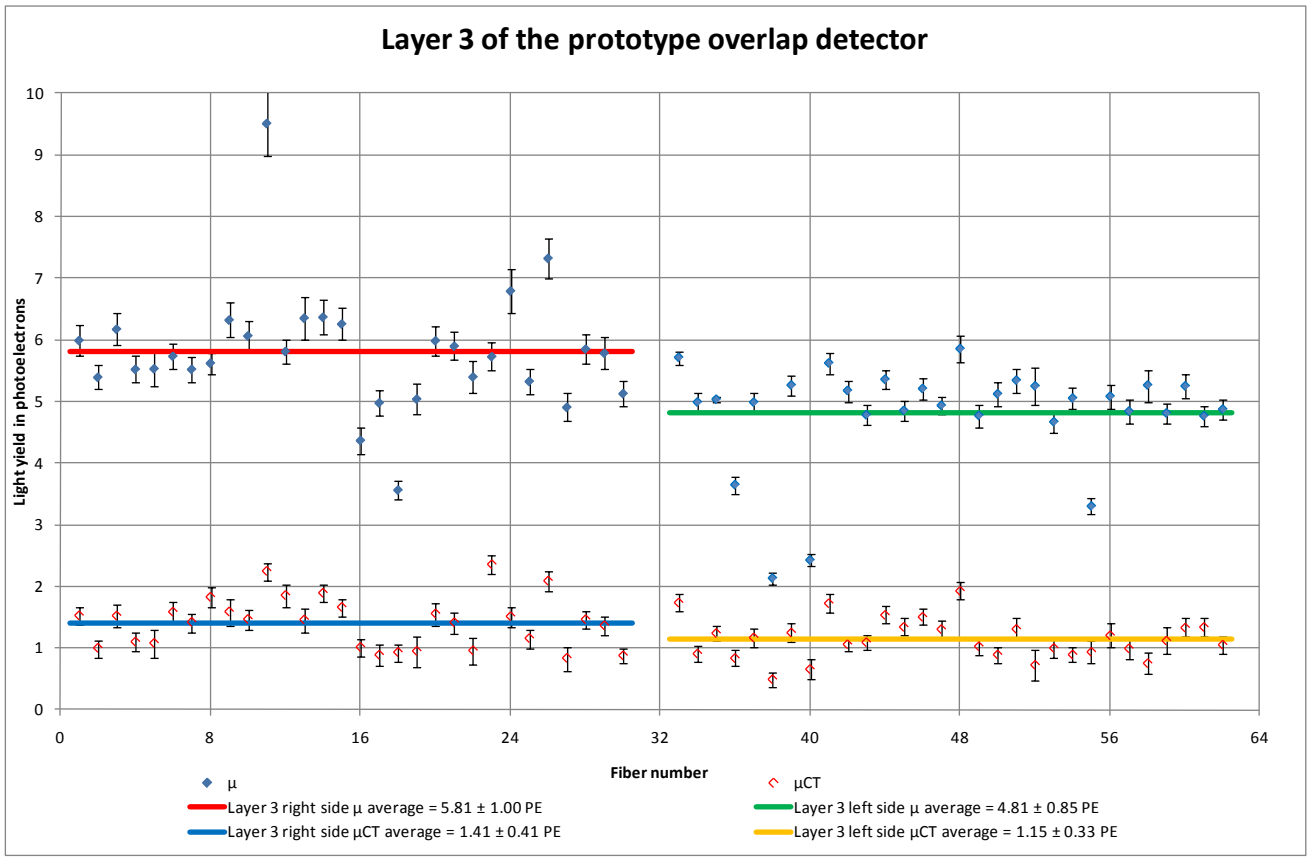

Figure 6. Light yield in each fiber of layer 3 in the prototype overlap detector. The very high light yield in fiber number 11 is artificial because of a range overflow.

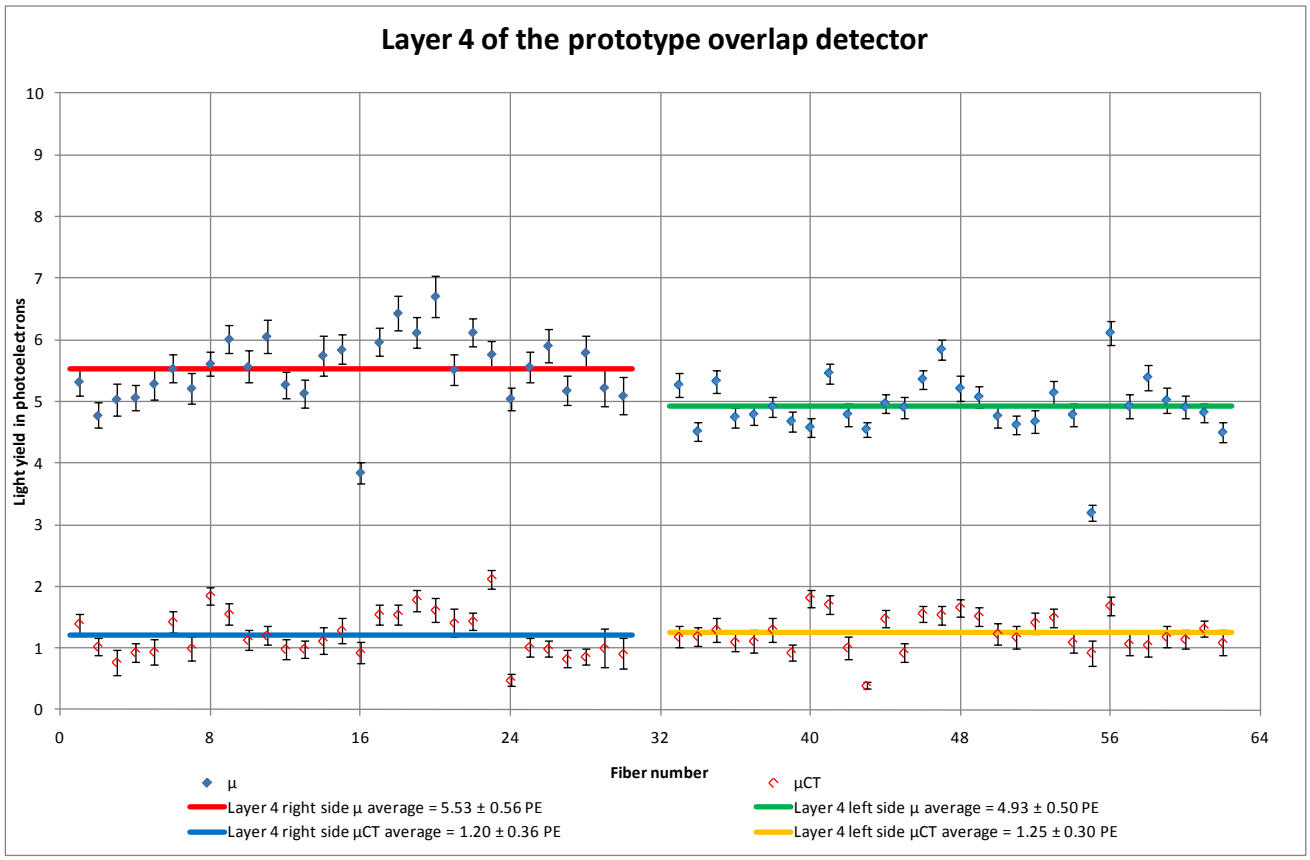

Figure 7. Light yield in each fiber of layer 4 in the prototype overlap detector

Appendix B

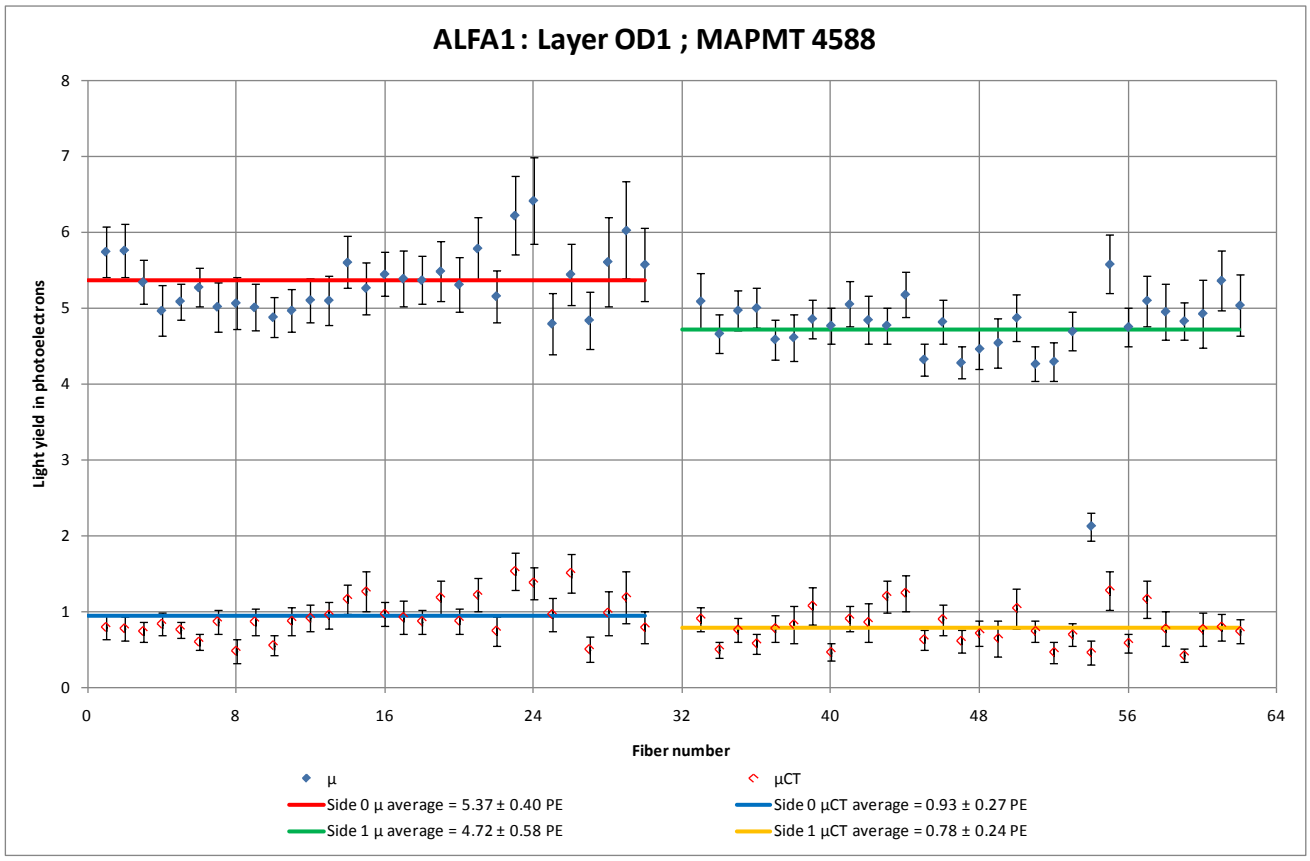

Figure 8. Light yield in each fiber of layer 1 in the ALFA1 overlap detector.

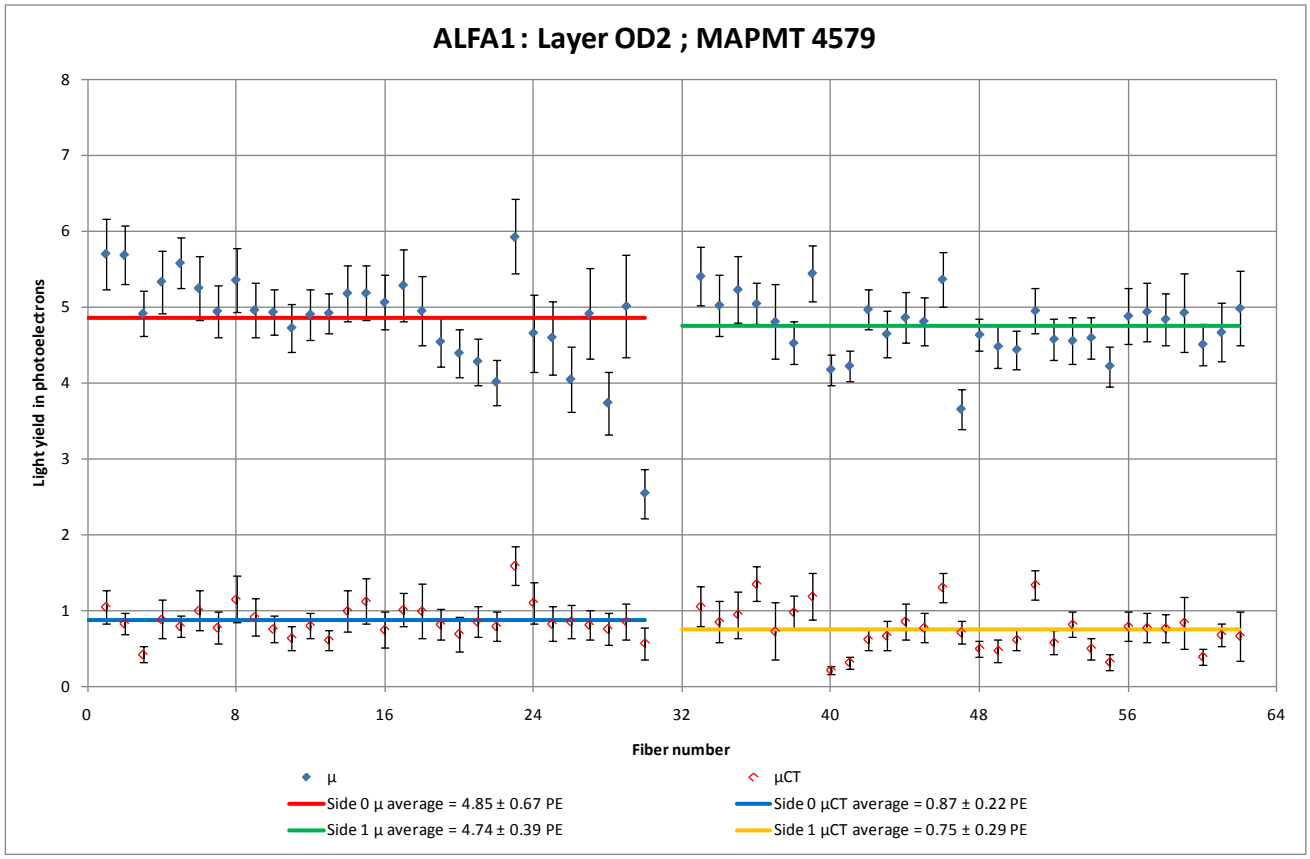

Figure 9. Light yield in each fiber of layer 2 in the ALFA1 overlap detector.

Appendix B

Appendix

A. Setup for calibration of a full ALFA detector

A schematic of the setup is shown in Figure 10.

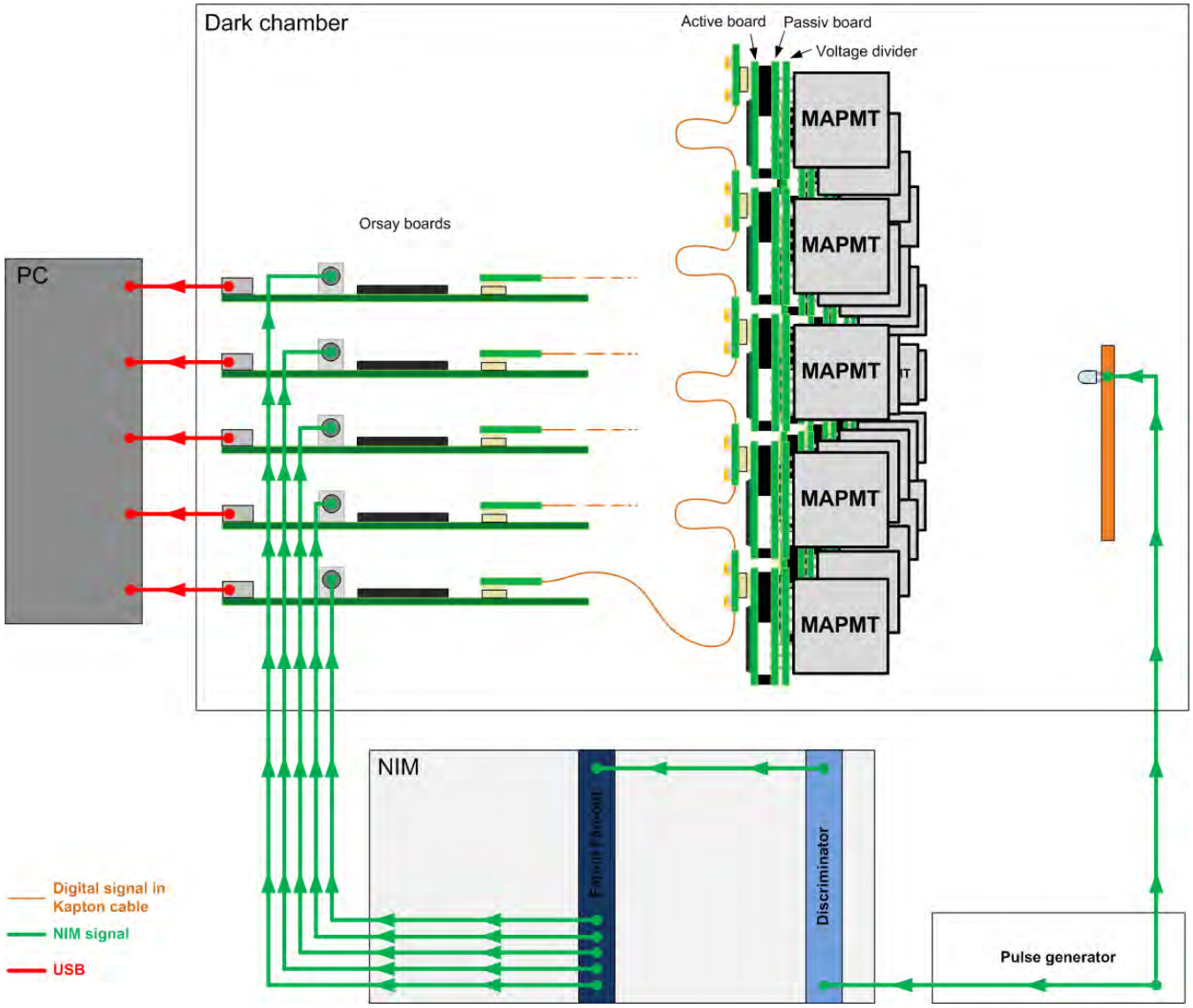

Figure 10. Schematic of the setup for calibration of a full ALFA detector.

Appendix B

A photo of the setup is shown in Figure 11.

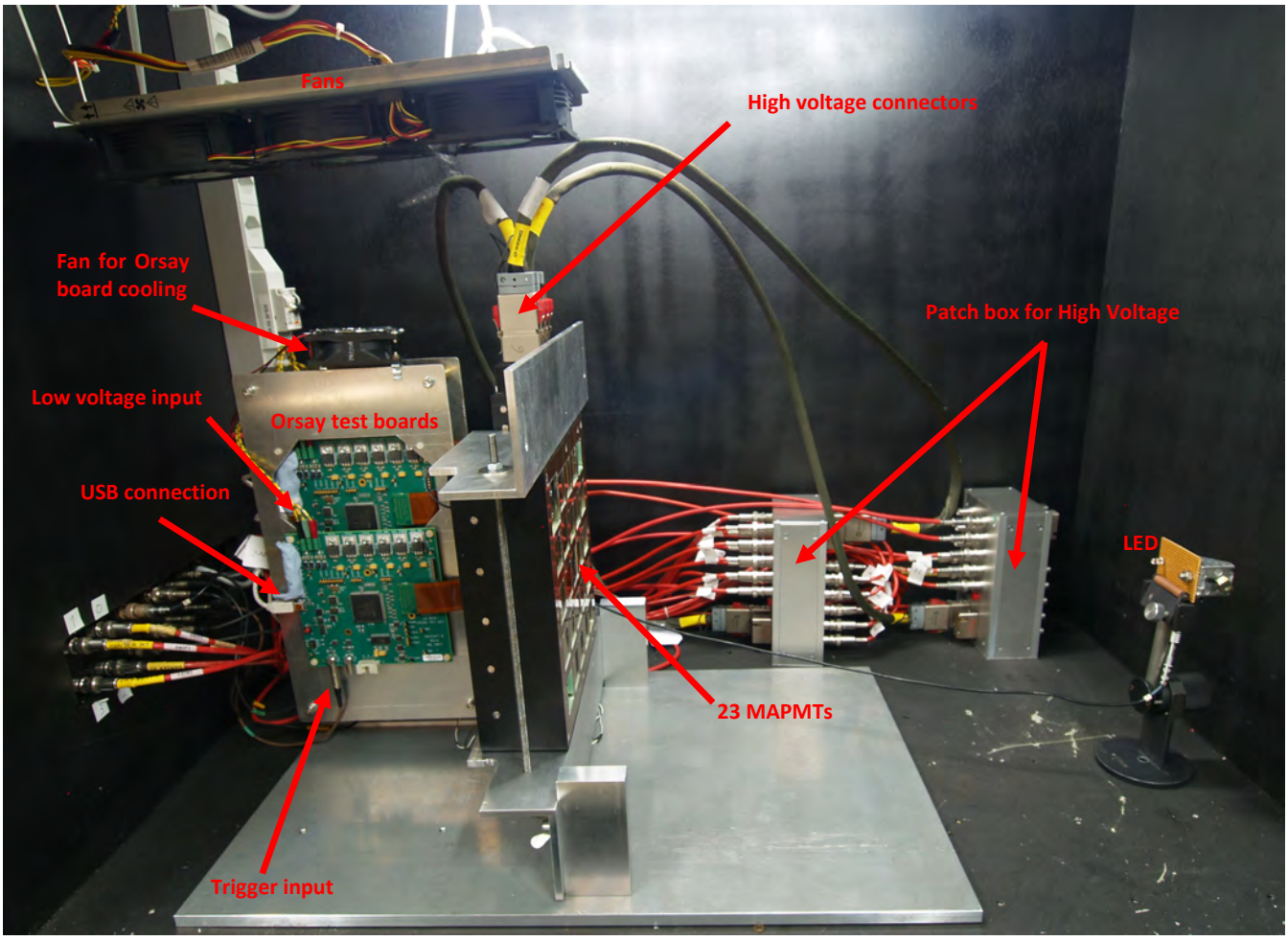

Figure 11. Setup inside a dark chamber used to calibrate the MAPMTs.

Appendix B

B. Setup for measuring the scintillating fiber light yield with cosmic of a full ALFA detector

A schematic of the setup is shown in Figure 12.

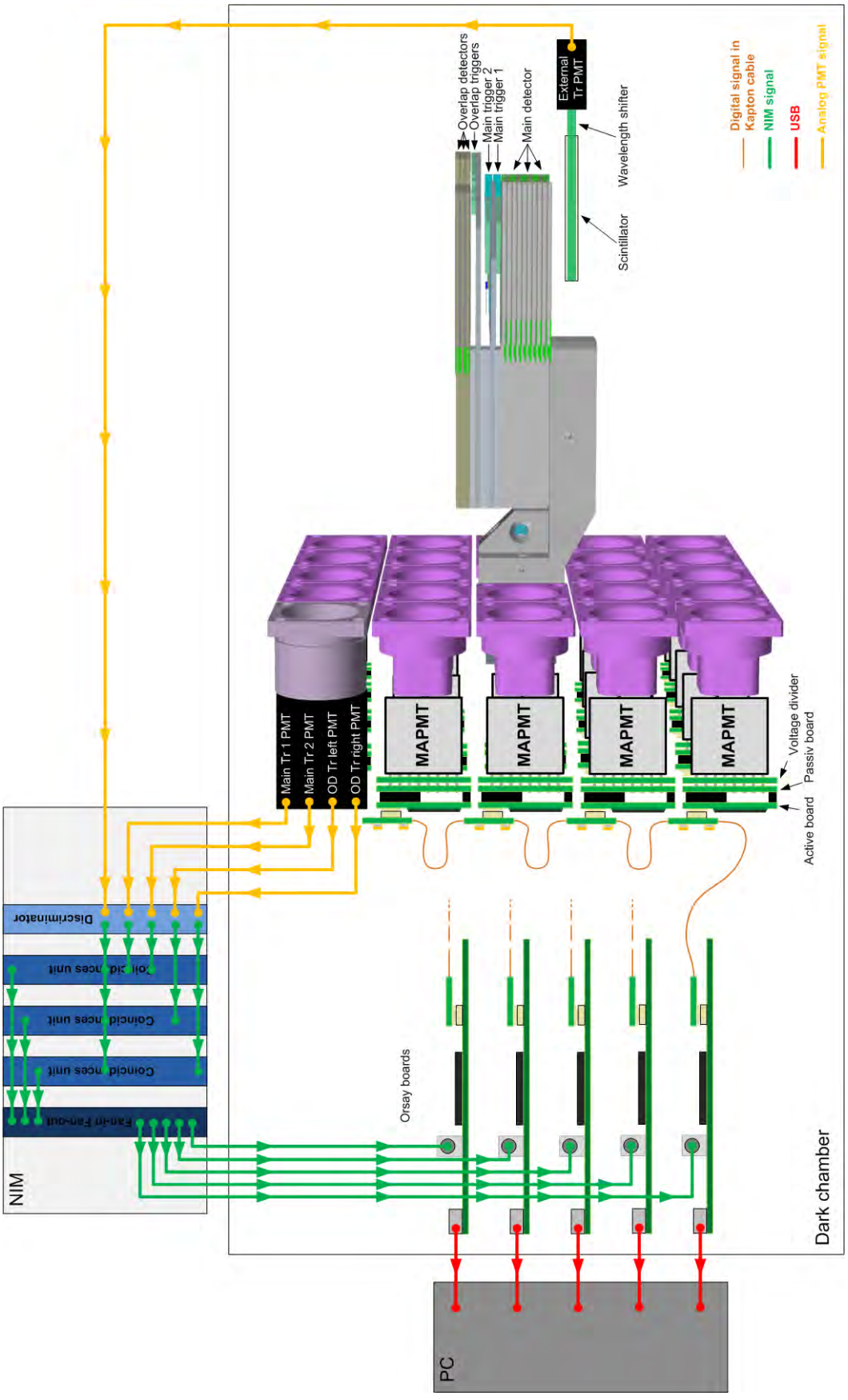

Figure 12. The cosmic setup for determining the light yield in the scintillating fibers. The detector part is a modified copy of the AutoCAD drawing made by A. Beam (CERN PH-DT). On the figure the scintillating fibers are light green, the trigger scintillator tiles are turquoise, the clear fibers are olive green and the fiber connectors are purple. The part of the fiber going from the titanium plate to the fiber connector is left out to make the figure clearer.

Appendix B

A photo of the setup is shown in Figure 13.

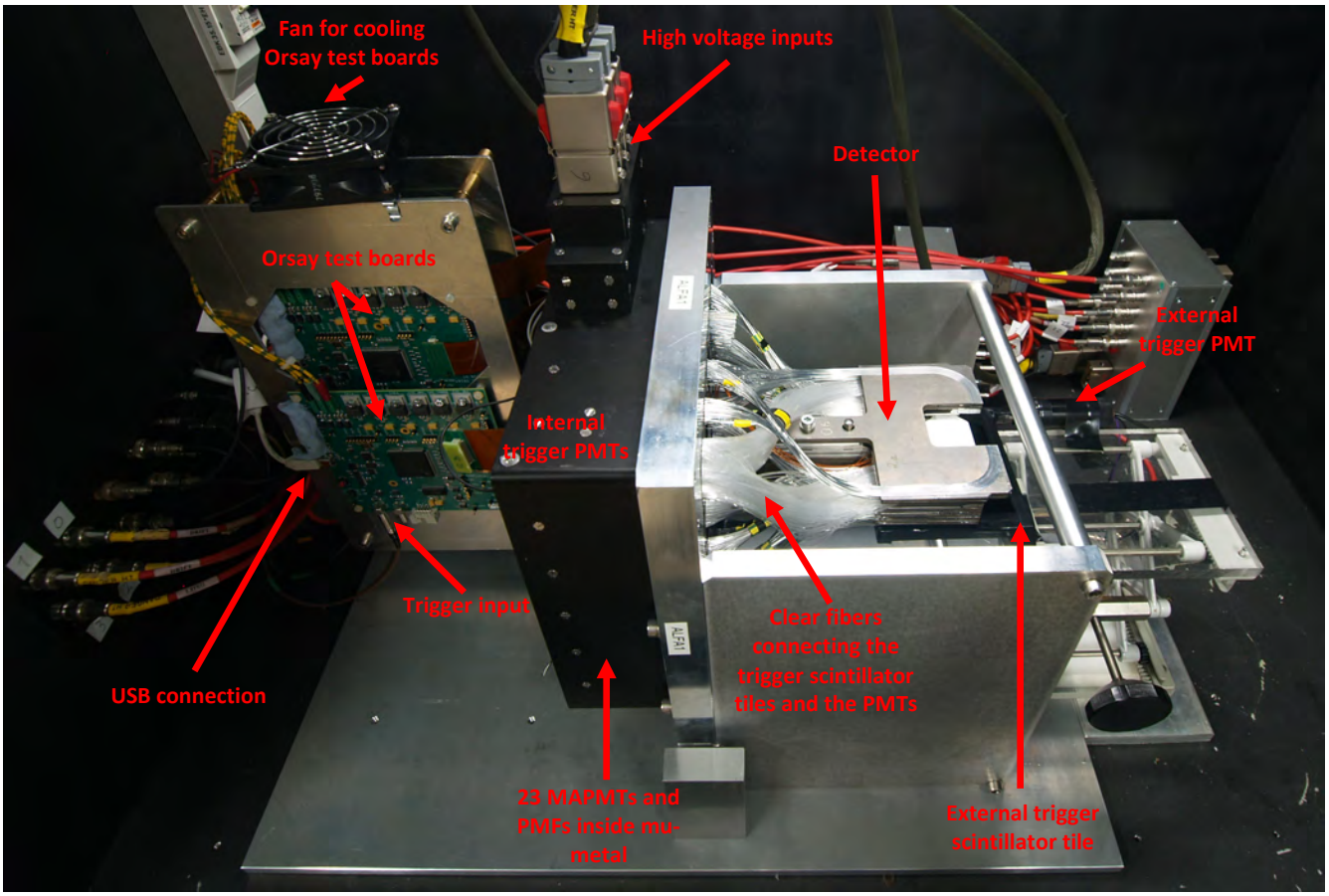

Figure 13. The cosmic setup for a full ALFA detector inside a dark camber.

Appendix B

C. Setup for measuring scintillating fiber light yield in the prototype overlap detectors

A schematic of the setup is shown in Figure 14.

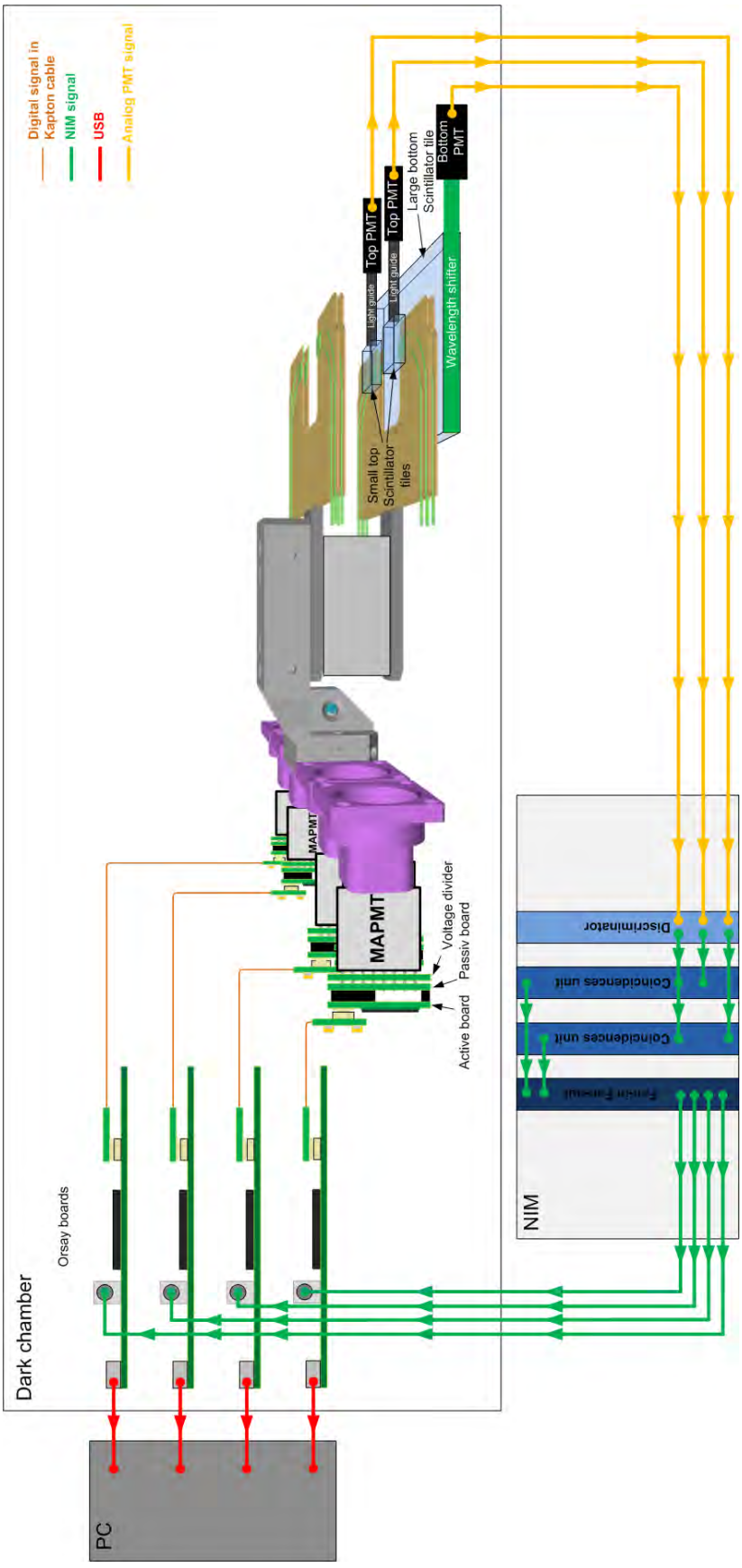

Figure 14. The cosmic setup for determining the light yield in the scintillating fibers for the prototype overlap detector. The detector part pieced together from AutoCAD drawings made by A. Beam (CERN PH-DT). On the figure the scintillating fibers are light green, the trigger scintillator tiles are transparent light blue and the fiber connectors are purple. The part of the fiber going from the titanium plate to the fiber connector is left out to make the figure clearer.

Appendix B

A photo of the setup is shown in Figure 15.

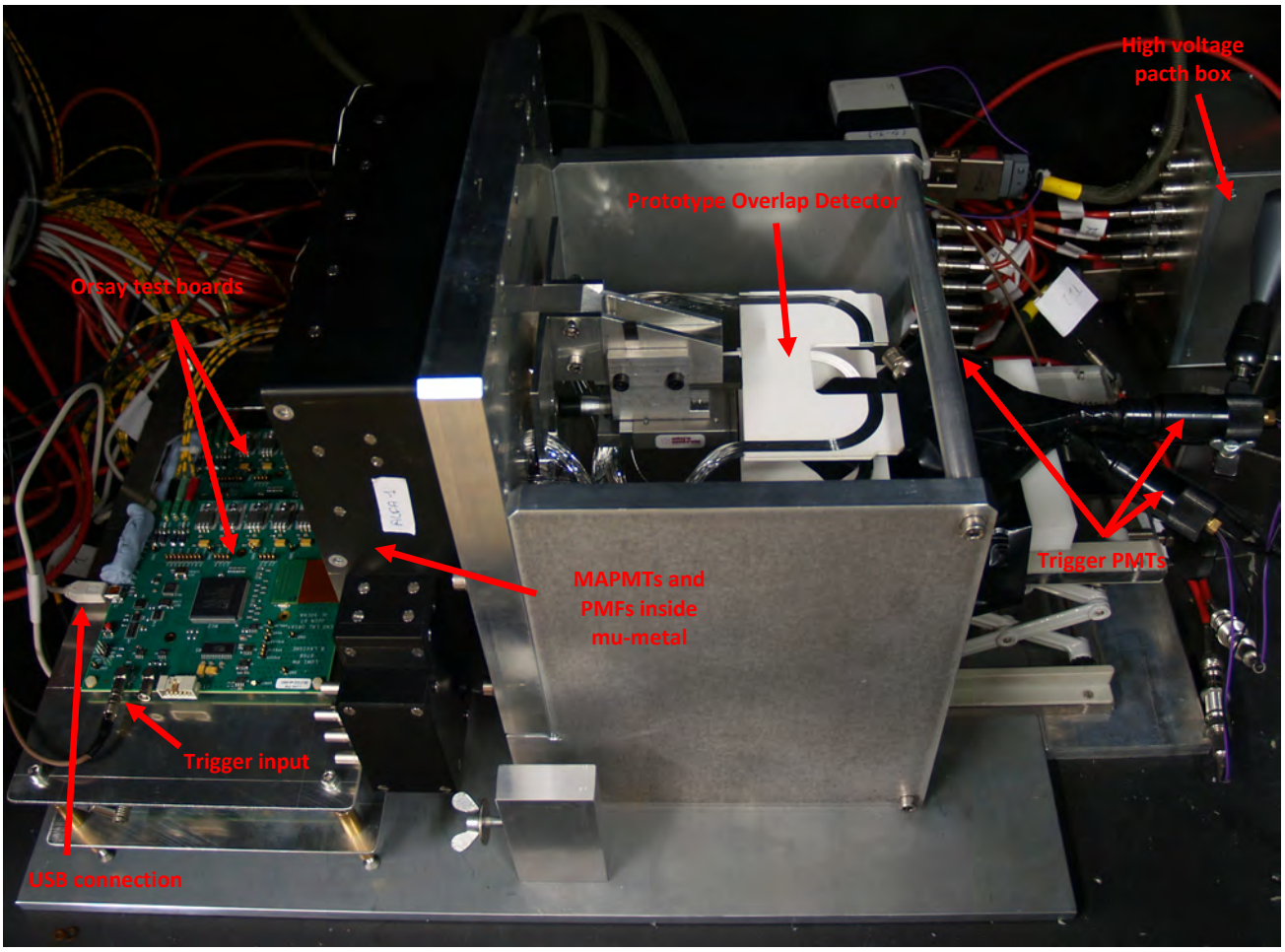

Figure 15. The cosmic setup for the overlap detectors.

The small triggers are placed such that only the used part of the scintillating fibers is covered. This is illustrated on Figure 14 and Figure 16.

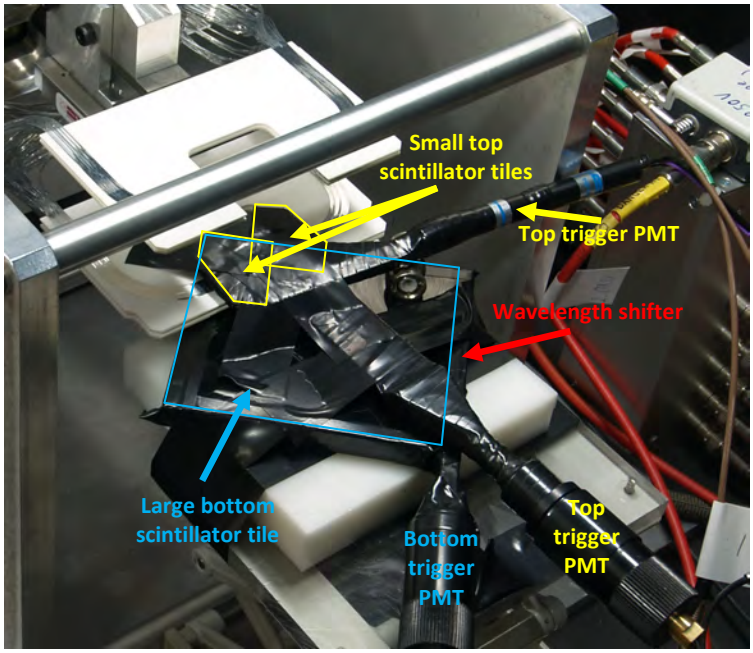

Figure 16. Scintillator tiles for triggering on the cosmic setup for the overlap detectors. The active part of the small top scintillator tiles is indicated with yellow. The active part large bottom scintillator tile is indicated with light blue.

Appendix C

histos3.cxx:

```
#include <iostream.h>
#include <fstream.h>
#include <ostream.h>
#include <iomanip.h>

#include "histos3.h"
#include "readAlfa.h"


const char* MAPADCPMT = "map-adc-pmt.txt";


int readAlfa(int argc, char** argv)
{
  int NUMPMF = 2;
  filename = argv[1];
  char* ROOTname = argv[2];

  tFileOut = new TFile(ROOTname,"RECREATE");
  TH1I* histo = new TH1I("histo","ADC histo",1000,0.,1000.);
  TH2I* histo2 = new TH2I("histo2", "ADC 2D histo",10,-1,9,10,-1,9);
  TTree* tree = new TTree("ADC data","");

  unsigned int notUsed,word[2][32];

  //read mapping file
  int mapping[64];
  readMapping(mapping);
  float res2[64];
  char str[2];
  TH1I* histoAll[64];;
  for(int i=0;i<64;i++){
    sprintf(str,"%d",i);
    tree->Branch(str,&res2[i],"res2[1]/F");
    histoAll[i] = new TH1I(str,str,1000,0.,1000.);
  }
  float res;
  tree->Branch("res",&res,"res/F");


  int nuSize = sizeof(notUsed);
  //ifstream file(filename,ios::binary);
  ifstream file(filename);
  //TODO maybe buffering is better
  for(int i=0;i<23;i++){
    file.read((char*)&notUsed,nuSize);   //read some ...
  }
  int writePMF = 0;


  while(file.good()){
  //TODO READ WHOLE OEN EVENT !!! into buffer
    for(int i=0;i<34;i++){
      file.read((char*)&notUsed,nuSize);   //read some ...
    }

    for(int i=0;i<NUMPMF;i++){  //here shouled be for(int i=0;i<nReadPmf;i++){
      writePMF = 0;
      file.read((char*)&notUsed,nuSize);  // read start flag
      file.read((char*)&notUsed,nuSize);  // read ??
      file.read((char*)&notUsed,nuSize);  // read ??
      for(int j=0;j<32;j++){
         file.read((char*)&word[i][j],nuSize);   //read word data
      }
      file.read((char*)&notUsed,nuSize); // read end flag
```

```
    }
    file.read((char*)&notUsed,nuSize);    //read ???
    file.read((char*)&notUsed,nuSize);    //read ???
    file.read((char*)&notUsed,nuSize);    //read ???


    for(int i=0;i<NUMPMF;i++){
      for(int j=0;j<32;j++){
        unsigned int mask = 4095;  // we need last 12 bits, 4095 is binary
00000000000000000000111111111111, we get it by bit AND with num
        //unsigned int res = word[i][j] & mask;
        res = word[i][j] & mask;
        histo->Fill(res);
        //std::cout << "vysledek je " << std::dec << res << std::endl;
        int num = 32*i + j;
        int mapTo = mapping[num] - 1;
        //std::cout << "mapTo: " << std::dec << mapTo << std::endl;
        histoAll[mapTo]->Fill(res);
        res2[mapTo] = res;
        int x = mapTo/8;
        int y = mapTo%8;
        //std::cout << "x, y and res: " << x << " " << y << " " << res <<
std::endl;


        histo2->Fill(x,y,res);
        //if(x==1 && y==1)
        //  histo11->Fill(res);
      }
    }
    //for(int i=0;i<64;i++)
    //  std::cout << res2[i] << std::endl;


    tree->Fill();
  }

  /*
  tTreeOut->Write();
  tTreeOut->AutoSave();
  file.close();
  tFileOut->Close();
  */
  tree->Write();
  tFileOut->Write();
  tFileOut->Close();
  return 0;
}


void readMapping(int mapping[64])
{
  ifstream mapFile;
  mapFile.open(MAPADCPMT);
  if(mapFile.good())
    {
      for(int i=0;i<64;i++)
        {
          mapFile >> mapping[i];
        }
    }
  else
    {
      cout << "methode 'void readMapping(int mapping[64])'" << endl;
      cout << "je ne trouve pas le fichier : " << MAPADCPMT << endl;
      cout << " EXIT du programme !" << endl;
      exit(1);
    }
```

```
}



void histos3(char* ROOTname)
{
  TFile* file = new TFile(ROOTname);
  TH1I* hists[64];
  //must be 3!! two chars and one for the string end
  char str[3];
  for(int i=0;i<64;i++)
    {
      sprintf(str,"%d",i);
      std::cout << "remplissage histo " << str << std::endl;
      hists[i] = (TH1I*)file->Get(str);
    }
}

int main(int argc, char** argv)
{
  char* ROOTname = argv[2];

  if(argc != 3)
    {
      cout << "utilisation de la commande 'histos3' :" << endl;
      cout << "histos3 FichierDeDonnees NomFichierSortieROOT" << endl;
      return 1;
  }
  readAlfa(argc,argv);
  histos3(ROOTname);
  return 0;
}
```

histos3.h:

```
#include <TQObject.h>
#include <RQ_OBJECT.h>

#include <TApplication.h>
#include <TGClient.h>
#include <TCanvas.h>
#include <TGButton.h>
#include <TGFrame.h>
#include <TRootEmbeddedCanvas.h>
#include <TH1I.h>
#include <TH2I.h>
#include <TFile.h>
#include <TCanvas.h>
#include <TVirtualPad.h>
#include <TF1.h>
//#include <RQ_OBJECT.h>



class TGWindow;
class TGMainFrame;
class TRootEmbeddedCanvas;
```

readAlfa.h:

```
//INCLUDES
// Standard libraries
#include <fstream.h>
```

Appendix C

```
#include <iostream>
#include <stdlib.h>
#include <cmath>
// TDAQ release
// Root
#include "TFile.h"
#include "TTree.h"
#include "TH1I.h"
#include "TH2I.h"
#include <string.h>
// File I/O (found in /usr/include/ )
#include <unistd.h>
#include <sys/types.h>
#include <sys/stat.h>
#include <fcntl.h>


//CONSTANTS
//include constats file
//#include "constants.h"

//GLOBAL VARIABLES
char* filename = NULL;   // File name
int nPmf = 0;   //number of pmfs
bool verbose = false;   //switch silent/verbose mode
// Maximum NUMPMF PMFs with 64 char
//bool pmfData[NUMPMF][32];   //pmf data
bool pmfData[2][32];
//size of one event
int eventSize = 0;
int nReadPmf = 0;
TFile *tFileOut;
TTree *tTreeOut;

//FUNCTIONS
//reaqd mapping between cable and pmt
void readMapping(int mapping[64]);
//init pmf data array to zeros
void initPmf();
//check agruments and sets file name, number of pmfs and mode
int checkArgs(int argc, char** argv);
//init root file, tree etc.
void initRoot();
//write PMF values
void writeEvents(int n,unsigned int word1);
//main
int readAlfa(int argc, char** argv);
```

Appendix D

Original Cosmic1pe.C:

```
#include "TMultiGraph.h"
#include "TFile.h"
#include "TTree.h"
#include "TBrowser.h"
#include "TH2.h"
#include "TRandom.h"
#include "TMath.h"


Double_t fit1pe(Double_t *x, Double_t *par)
{

  Double_t result=0.;

  for (Int_t i=1;i<10;i++)
    {

      Double_t fact=1;
      for (Int_t var=1;var<i+1;var++)
         {
           fact *= var;
         }

      Double_t P = (TMath::Exp((-1.)*par[0])*par[0]**i)/fact;
      Double_t G1 = 1./(par[3]*TMath::Sqrt(2.*i*TMath::Pi())) ;
      Double_t G2 = TMath::Exp( ( (-1.) * (x[0] - par[5] - i*(par[1]-par[5]))**2
)/(2.*i*par[3]**2));
      result += P * G1 * G2;
    }
 result *= par[4];
 return result;
}

Double_t peFct(Double_t *x, Double_t *param)
{
  Double_t result = 0.;
  Double_t fact = 1;
  for (Int_t var=1;var<param[6]+1;var++)
    fact *= var;

 Double_t P = (TMath::Exp((-1.) * param[0]) * param[0]**param[6])/fact;
 Double_t G1 = 1./(param[3]*TMath::Sqrt(2.*param[6]*TMath::Pi())) ;
 Double_t G2 = TMath::Exp(((-1.) * (x[0] - param[5] - param[6]*(param[1]-
param[5]))**2 )/(2.*param[6]*param[3]**2));
 result += P * G1 * G2;
 result *= param[4];
 return result;
}

void cosmic1pe(int index)
{
  //Create, fill and display raw data
  TFile *file = new TFile("ped_1pe.root");
  TH1I *pedestal;
  char str[2];
  sprintf(str,"%d",index);
  pedestal = (TH1I*) gDirectory->Get(str);

  TF1* gaussPE;

  TCanvas *pedestalDisp = new TCanvas("canvas1","pedestal - 1pe",200,60,600,600);

  pedestalDisp->cd();
  pedestal->Draw();
```

Appendix D

```
  //Evaluate 1pe characteristics
  cout << "Pedestal " << index << endl;
  Double_t pedX,singleX,pedRMS,singleRMS;
  pedX = pedestal->GetMaximumBin();

  Float_t MinFit = pedestal->GetMaximumBin()-3.;
  Float_t MaxFit = pedestal->GetMaximumBin()+2.;

  TF1* G1 = new TF1("G1","gaus",MinFit,MaxFit);
  G1->SetLineColor(3);
  G1->SetLineWidth(1);
  pedestal->Fit(G1,"R");
  pedX = G1->GetParameter(1);
  pedRMS = G1->GetParameter(2);

  TF1* G2 = new TF1("G2","gaus",MaxFit,pedX + 12.);
  G2->SetLineColor(2);
  G2->SetLineWidth(1);
  pedestal->Fit(G2,"R+");
  singleX = G2->GetParameter(1);
  singleRMS = G2->GetParameter(2);

  TF1* fct3    = new TF1("fct3",fit1pe,MaxFit,150,6);
  fct3->SetParameter(0,singleX);
  fct3->SetParameter(1,singleX);
  fct3->FixParameter(2,pedRMS);
  fct3->SetParameter(3,singleRMS);
  fct3->SetParameter(4,1000);
  fct3->FixParameter(5,pedX);
  fct3->SetLineColor(4);
  fct3->SetParName(0,"Mu");
  fct3->SetParName(1,"1pe mean");
  fct3->SetParName(2,"ped RMS");
  fct3->SetParName(3,"1pe RMS");
  fct3->SetParName(4,"Norm");
  fct3->SetParName(5,"ped mean");

  pedestal->Fit(fct3,"R+") ;
  gStyle->SetOptStat("");
  gStyle->SetOptFit(0101);


  for (Int_t ii=1;ii<5;ii++)
    {
      TF1 *fit = new TF1("Npe",peFct,MaxFit,150,7);
      fit->FixParameter(0,fct3->GetParameter(0));
      fit->FixParameter(1,fct3->GetParameter(1));
      fit->SetParameter(2,fct3->GetParameter(2));
      fit->FixParameter(3,fct3->GetParameter(3));
      fit->SetParameter(4,fct3->GetParameter(4));
      fit->FixParameter(5,fct3->GetParameter(5));
      fit->FixParameter(6,ii);
      fit->SetLineColor(2);
      fit->SetLineWidth(1);
      fit->DrawCopy("same");
    }


  pedestal->SetMaximum(2*(G2->GetParameter(0)));
  pedestal->SetAxisRange(singleX-3.*singleRMS,singleX+6.*singleRMS);

}
```

Final Cosmic1pe.C:

```
#include "TMultiGraph.h"
#include "TFile.h"
#include "TTree.h"
#include "TBrowser.h"
#include "TH2.h"
#include "TRandom.h"
#include "TMath.h"


Double_t fit1pe(Double_t *x, Double_t *par)
{

  Double_t result=0.;

  for (Int_t i=0;i<10;i++)
    {

      Double_t fac=1;
         if(i<1)
        {fac=1;}
      else{
 for (Int_t var=1;var<i+1;var++)
        {
          fac *= var;
        }}


      //  Double_t P = (TMath::Exp((-1.)*par[0])*par[0]**i)/fact;
      //  Double_t G1 = 1./(par[3]*TMath::Sqrt(2.*i*TMath::Pi())) ;
      // Double_t G2 = TMath::Exp( ( (-1.) * (x[0] - par[5] - i*(par[1]-par[5]))**2
)/(2.*i*par[3]**2));

      //Factorial
      /*
  Int_t b;
  Double_t fac;
  if(i==0)
  {
    fac=1.0;
    return fac;
  }
  else{
  fac=1;
  b=0;
  do
  {
    b=b+1;
    fac=fac*b;
  }while(b!=i);
  return fac;
  }
      */
      /*
      if (i=0)
        {Double_t fac=1;}
      else{}
      if (i=1)
        {Double_t fac=1;}
      else{}
      if (i=2)
        {Double_t fac=2;}
      else{}
      if (i=3)
        {Double_t fac=6;}
      else{}
```

```
      if (i=4)
        {Double_t fac=24;}
      else{}
      if (i=5)
        {Double_t fac=120;}
      else{}
      if (i=6)
        {Double_t fac=720;}
      else{}
      if (i=7)
        {Double_t fac=5040;}
      else{}
      if (i=8)
        {Double_t fac=40320;}
      else{}
      if (i=9)
        {Double_t fac=362880;}
      else{}
      if (i=10)
        {Double_t fac=3628800;}
      else{}
*/

      Double_t P = (TMath::Exp((-1.)*par[0])*par[0]**i)/(fac);
      // Double_t G1 =
1./((TMath::Sqrt(par[3]**2+par[2]**2))*TMath::Sqrt(2.*i*TMath::Pi())) ;
      //   if (i<1){ Double_t G1 = 1./(par[2]) ;}
      //else{Double_t G1 =
1./((TMath::Sqrt(par[3]**2+par[2]**2))*TMath::Sqrt(2.*i*TMath::Pi())) ;}
      //  Double_t G1 =
1./((TMath::Sqrt(2.*i*TMath::Pi()*par[3]**2+2.*TMath::Pi()*par[2]**2))) ;
      // Double_t G1 =
1./((TMath::Sqrt(2.*TMath::Pi())*(TMath::Sqrt(TMath::Sqrt(i)*par[3]**2+par[2]**2)))
) ;
      Double_t G1 =
1./((TMath::Sqrt(2.*TMath::Pi())*(TMath::Sqrt((i*par[3]**2+par[2]**2))))) ;
      Double_t G2 = TMath::Exp( ( (-1.) * (x[0] - par[5] - i*(par[1]))**2
)/(2.*(i*par[3]**2+par[2]**2)));

      result += P * G1 * G2;
    }
 result *= par[4];
 return result;
}
/*
Double_t peFct(Double_t *x, Double_t *param)
{
  Double_t result = 0.;
  Double_t fact = 1;
  for (Int_t var=1;var<param[6]+1;var++)
    fact *= var;

   // Double_t P = (TMath::Exp((-1.) * param[0]) * param[0]**param[6])/fact;
   // Double_t G1 = 1./(param[3]*TMath::Sqrt(2.*param[6]*TMath::Pi())) ;
   // Double_t G2 = TMath::Exp(((-1.) * (x[0] - param[5] - param[6]*(param[1]-
param[5]))**2 )/(2.*param[6]*param[3]**2));

      Double_t P = (TMath::Exp((-1.) * param[0]) * param[0]**param[6])/fact;
      //  Double_t G1 =
1./((TMath::Sqrt(param[3]**2+param[2]**2))*TMath::Sqrt(2.*param[6]*TMath::Pi())) ;
      Double_t G1 =
1./((TMath::Sqrt(2.*TMath::Pi())*(TMath::Sqrt((param[6]*param[3]**2+param[2]**2))))
) ;
      Double_t G2 = TMath::Exp( ( (-1.) * (x[0] - param[5] -
param[6]*(param[1]))**2 )/(2.*(param[6]*param[3]**2+param[2]**2)));

result += P * G1 * G2;
 result *= param[4];
```

```
 return result;
}
*/
Double_t peFct(Double_t *x, Double_t *param)
{
  Double_t result = 0.;
  Double_t fact = 1;
  for (Int_t var=1;var<param[6]+1;var++)
    fact *= var;

      Double_t P = (TMath::Exp((-1.) * param[0]) * param[0]**param[6])/fact;
      Double_t G1 =
1./((TMath::Sqrt(2.*TMath::Pi())*(TMath::Sqrt((param[6]*param[3]**2+param[2]**2))))
) ;
      Double_t G2 = TMath::Exp( ( (-1.) * (x[0] - param[5] -
param[6]*(param[1]))**2 )/(2.*(param[6]*param[3]**2+param[2]**2)));

result += P * G1 * G2;
 result *= param[4];
return result;
}
void cosmic1pe(int index)
{
  //Create, fill and display raw data
  TFile *file = new TFile("ped_1pe.root");
  TH1I *pedestal;
  char str[2];
  sprintf(str,"%d",index);
  pedestal = (TH1I*) gDirectory->Get(str);
  pedestal->GetYaxis()->SetTitle("Number of events");
  pedestal->GetXaxis()->SetTitle("Charge signal (ADC counts)");


   TF1* gaussPE;

  TCanvas *pedestalDisp = new TCanvas("cavas","pedestal - 1pe",200,60,700,700);
 pedestalDisp->SetLogy();
   pedestalDisp->cd();
   pedestal->Draw();


  //Evaluate 1pe characteristics
  cout << "Pedestal " << index << endl;
  Double_t pedX,singleX,pedRMS,singleRMS,Mina,Minb;
  pedX = pedestal->GetMaximumBin();

  Float_t MinFitInt = pedestal->GetMaximumBin()-TMath::Sqrt(pedestal-
>GetMaximum())/30-1.;
  Float_t MaxFitInt = pedestal->GetMaximumBin()+TMath::Sqrt(pedestal-
>GetMaximum())/30+1.;

TF1* G1 = new TF1("G1","gaus",MinFitInt,MaxFitInt);
  G1->SetLineColor(3);
  G1->SetLineWidth(1);
  pedestal->Fit(G1,"R");
  pedX = G1->GetParameter(1);
  pedRMS = G1->GetParameter(2);

  if(0.8<pedRMS)
    {  TF1* Min = new TF1("Min","pol2",pedX+1.5*pedRMS, pedX+5.5*pedRMS+2);}
  else{  TF1* Min = new TF1("Min","pol2",pedX+1, pedX+8);}

  //  TF1* Min = new TF1("Min","pol2",pedX+1.5*pedRMS, pedX+10*pedRMS+0.1);
 Min->SetLineColor(14);
 Min->SetLineWidth(1);
 pedestal->Fit(Min,"R+");
 Mina = Min->GetParameter(2);
 Minb = Min->GetParameter(1);
```

```
  if (30<-Minb/(2*Mina))
    {if (-Minb/(2*Mina)<200)
   {Float_t MaxFit =  -Minb/(2*Mina);}
         else {Float_t MaxFit =  pedX+4;}}
         else {Float_t MaxFit =  pedX+4;}

 /*
if (-Minb/(2*Mina)<200)
   {Float_t MaxFit =  -Minb/(2*Mina);}
         else {Float_t MaxFit =  pedX+4;}
 */
 // Float_t MaxFit =  -Minb/(2*Mina);
 //   Float_t MaxFit =  pedX+4;

TF1* G2 = new TF1("G2","gaus",MaxFit,MaxFit +35);
  G2->SetLineColor(7);
  G2->SetLineWidth(1);
  pedestal->Fit(G2,"R+");
  singleX = G2->GetParameter(1);
  singleRMS = G2->GetParameter(2);

  TF1* fct3    = new TF1("fct3",fit1pe,MinFitInt+20,300,6);

  fct3->SetParLimits(0,0,100);
  fct3->SetParLimits(1,0,10000000);
  // fct3->SetParLimits(2,pedRMS-0.00000000001,pedRMS+0.00000000001);
  fct3->SetParLimits(3,0,10000000);
  fct3->SetParLimits(4,0,1000000);
  // fct3->SetParLimits(5,0,100000000);
  //  fct3->SetParLimits(5,pedX-0.000000001,pedX+0.000000001);

  fct3->SetParameter(0,0.1);
  if (singleX>1)
    {fct3->SetParameter(1,singleX-pedX);}
  else {fct3->SetParameter(1,pedX+3);}
  fct3->FixParameter(2,pedRMS);
  //fct3->SetParameter(2,pedRMS);
  if (singleRMS>0.1)
    {fct3->SetParameter(3,singleRMS);}
  else{fct3->SetParameter(3,pedRMS);}
  fct3->SetParameter(4,110000);
  // fct3->SetParameter(5,pedX);
      fct3->FixParameter(5,pedX);
    fct3->SetLineColor(4);

  fct3->SetParName(0,"Mu");
  fct3->SetParName(1,"1pe mean");
  fct3->SetParName(2,"ped RMS");
  fct3->SetParName(3,"1pe RMS");
  fct3->SetParName(4,"Norm");
  fct3->SetParName(5,"ped mean");

  pedestal->Fit(fct3,"R+") ;
  gStyle->SetOptStat("");
  gStyle->SetOptFit(0101);


  /*
    for (Int_t ii=1;ii<10;ii++)
    {
      TF1 *fit = new TF1("Npe",peFct,MinFitInt,300,7);
      fit->FixParameter(0,fct3->GetParameter(0));
      fit->FixParameter(1,fct3->GetParameter(1));
      //fit->SetParameter(2,fct3->GetParameter(2));
      fit->FixParameter(3,fct3->GetParameter(3));
      fit->SetParameter(4,fct3->GetParameter(4));
      fit->FixParameter(5,fct3->GetParameter(5));
```

```
      fit->FixParameter(6,ii);
      fit->SetLineColor(ii);
      fit->SetLineWidth(1);
      fit->DrawCopy("same");
    }

 */
  for (Int_t ii=1;ii<15;ii++)
    {
      TF1 *fit = new TF1("Npe",peFct,MinFitInt+20,300,7);
      //TF1 *fit = new TF1("Npe",peFct,MaxFit,300,7);
      fit->FixParameter(0,fct3->GetParameter(0));
      fit->FixParameter(1,fct3->GetParameter(1));
      //fit->SetParameter(2,fct3->GetParameter(2));
      fit->FixParameter(3,fct3->GetParameter(3));
      fit->SetParameter(4,fct3->GetParameter(4));
      fit->FixParameter(5,fct3->GetParameter(5));
      //  fit->FixParameter(7,fct3->GetParameter(6));
      //fit->FixParameter(8,fct3->GetParameter(7));
      fit->FixParameter(6,ii);
      // fit->SetLineColor(ii);
      if(10>ii){ fit->SetLineColor(ii);}
      else{fit->SetLineColor(ii+31);}
      fit->SetLineWidth(1);
      fit->DrawCopy("same");
    }

    if(singleX>1)
      { pedestal->SetMaximum(10*(G2->GetParameter(0)));
        pedestal->SetAxisRange(singleX-3.*singleRMS,singleX+6.*singleRMS);}
    else {pedestal->SetMaximum(pedestal->GetMaximum()+500);
        pedestal->SetAxisRange(pedX-8.*pedRMS,pedX+16.*pedRMS);}
 //read out

Double_t pemean=1;
pemean = fct3->GetParameter(1) -  fct3->GetParameter(5);


ofstream myfile;            //SJ
 myfile.open ("D:/CERN temp/analyze-Sune/Output/1pemean.dat", ios::app);   //SJ
 myfile << pemean;   //SJ
 myfile<<"\n";   //SJ
 myfile.close();

ofstream myfile2;            //SJ
 myfile2.open ("D:/CERN temp/analyze-Sune/Output/index.dat", ios::app);   //SJ
 myfile2 << index;   //SJ
 myfile2<<"\n";   //SJ
 myfile2.close();

ofstream myfile3;            //SJ
 myfile3.open ("D:/CERN temp/analyze-Sune/Output/Mu.dat", ios::app);   //SJ
 myfile3 << fct3->GetParameter(0);   //SJ
 myfile3<<"\n";   //SJ
 myfile3.close();

ofstream myfile4;            //SJ
 myfile4.open ("D:/CERN temp/analyze-Sune/Output/1pe mean.dat", ios::app);   //SJ
 myfile4 << fct3->GetParameter(1);   //SJ
 myfile4<<"\n";   //SJ
 myfile4.close();

ofstream myfile5;            //SJ
 myfile5.open ("D:/CERN temp/analyze-Sune/Output/1pe RMS.dat", ios::app);   //SJ
 myfile5 << fct3->GetParameter(3);   //SJ
 myfile5<<"\n";   //SJ
 myfile5.close();
```

```
 ofstream myfile6;            //SJ
  myfile6.open ("D:/CERN temp/analyze-Sune/Output/Norm.dat", ios::app);   //SJ
  myfile6 << fct3->GetParameter(4);   //SJ
  myfile6<<"\n";   //SJ
  myfile6.close();

 ofstream myfile7;            //SJ
  myfile7.open ("D:/CERN temp/analyze-Sune/Output/ped mean.dat", ios::app);   //SJ
  myfile7 << fct3->GetParameter(5);   //SJ
  myfile7<<"\n";   //SJ
  myfile7.close();

ofstream myfile8;            //SJ
  myfile8.open ("D:/CERN temp/analyze-Sune/Output/ped RMS.dat", ios::app);   //SJ
  myfile8 << fct3->GetParameter(2);   //SJ
  myfile8<<"\n";   //SJ
  myfile8.close();


    /*
    TFile("1pemean.dat", "RECREATE");
    Write(1pem);
    */
  /*
TFile *hfile = new TFile(indextestfil.root, "RECREATE");
hfile->Append(pedestalDisp);
hfile->Write();
  */

  // File saving

  if (index<1)
    {pedestalDisp->SaveAs("D:/CERN temp/analyze-Sune/Output/gif/0.gif");
    pedestalDisp->SaveAs("D:/CERN temp/analyze-Sune/Output/root/0.root");}
  else{ }

   if (index<2)
    {if (index>0)
        {pedestalDisp->SaveAs("D:/CERN temp/analyze-Sune/Output/gif/1.gif");
       pedestalDisp->SaveAs("D:/CERN temp/analyze-Sune/Output/root/1.root");}
      else{}}
   else{}
   if (index<3)
    {if (index>1)
        {pedestalDisp->SaveAs("D:/CERN temp/analyze-Sune/Output/gif/2.gif");
       pedestalDisp->SaveAs("D:/CERN temp/analyze-Sune/Output/root/2.root"); }
      else{}}
   else{}
   if (index<4)
    {if (index>2)
        {pedestalDisp->SaveAs("D:/CERN temp/analyze-Sune/Output/gif/3.gif");
       pedestalDisp->SaveAs("D:/CERN temp/analyze-Sune/Output/root/3.root");}
      else{}}
   else{}
   if (index<5)
    {if (index>3)
        {pedestalDisp->SaveAs("D:/CERN temp/analyze-Sune/Output/gif/4.gif");
       pedestalDisp->SaveAs("D:/CERN temp/analyze-Sune/Output/root/4.root"); }
      else{}}
   else{}
   if (index<6)
    {if (index>4)
        {pedestalDisp->SaveAs("D:/CERN temp/analyze-Sune/Output/gif/5.gif");
       pedestalDisp->SaveAs("D:/CERN temp/analyze-Sune/Output/root/5.root");}
      else{}}
   else{}
   if (index<7)
    {if (index>5)
```

```
      {pedestalDisp->SaveAs("D:/CERN temp/analyze-Sune/Output/gif/6.gif");
     pedestalDisp->SaveAs("D:/CERN temp/analyze-Sune/Output/root/6.root"); }
   else{}}
else{}
if (index<8)
 {if (index>6)
      {pedestalDisp->SaveAs("D:/CERN temp/analyze-Sune/Output/gif/7.gif");
     pedestalDisp->SaveAs("D:/CERN temp/analyze-Sune/Output/root/7.root");}
   else{}}
else{}
if (index<9)
 {if (index>7)
      {pedestalDisp->SaveAs("D:/CERN temp/analyze-Sune/Output/gif/8.gif");
     pedestalDisp->SaveAs("D:/CERN temp/analyze-Sune/Output/root/8.root"); }
   else{}}
else{}
if (index<10)
 {if (index>8)
      {pedestalDisp->SaveAs("D:/CERN temp/analyze-Sune/Output/gif/9.gif");
     pedestalDisp->SaveAs("D:/CERN temp/analyze-Sune/Output/root/9.root"); }
   else{}}
else{}
if (index<11)
 {if (index>9)
      {pedestalDisp->SaveAs("D:/CERN temp/analyze-Sune/Output/gif/10.gif");
     pedestalDisp->SaveAs("D:/CERN temp/analyze-Sune/Output/root/10.root"); }
   else{}}
else{}
if (index<12)
 {if (index>10)
   { pedestalDisp->SaveAs("D:/CERN temp/analyze-Sune/Output/gif/11.gif");
     pedestalDisp->SaveAs("D:/CERN temp/analyze-Sune/Output/root/11.root"); }
   else{}}
else{}
if (index<13)
 {if (index>11)
   { pedestalDisp->SaveAs("D:/CERN temp/analyze-Sune/Output/gif/12.gif");
     pedestalDisp->SaveAs("D:/CERN temp/analyze-Sune/Output/root/12.root"); }
   else{}}
else{}
if (index<14)
 {if (index>12)
   { pedestalDisp->SaveAs("D:/CERN temp/analyze-Sune/Output/gif/13.gif");
     pedestalDisp->SaveAs("D:/CERN temp/analyze-Sune/Output/root/13.root");}
   else{}}
else{}
if (index<15)
 {if (index>13)
  {  pedestalDisp->SaveAs("D:/CERN temp/analyze-Sune/Output/gif/14.gif");
     pedestalDisp->SaveAs("D:/CERN temp/analyze-Sune/Output/root/14.root"); }
   else{}}
else{}
if (index<16)
 {if (index>14)
      {pedestalDisp->SaveAs("D:/CERN temp/analyze-Sune/Output/gif/15.gif");
     pedestalDisp->SaveAs("D:/CERN temp/analyze-Sune/Output/root/15.root"); }
   else{}}
else{}
if (index<17)
 {if (index>15)
      {pedestalDisp->SaveAs("D:/CERN temp/analyze-Sune/Output/gif/16.gif");
     pedestalDisp->SaveAs("D:/CERN temp/analyze-Sune/Output/root/16.root"); }
   else{}}
else{}
if (index<18)
 {if (index>16)
      {pedestalDisp->SaveAs("D:/CERN temp/analyze-Sune/Output/gif/17.gif");
     pedestalDisp->SaveAs("D:/CERN temp/analyze-Sune/Output/root/17.root"); }
```

```
   else{}}
else{}
if (index<19)
 {if (index>17)
      {pedestalDisp->SaveAs("D:/CERN temp/analyze-Sune/Output/gif/18.gif");
     pedestalDisp->SaveAs("D:/CERN temp/analyze-Sune/Output/root/18.root"); }
   else{}}
else{}
if (index<20)
 {if (index>18)
      {pedestalDisp->SaveAs("D:/CERN temp/analyze-Sune/Output/gif/19.gif");
     pedestalDisp->SaveAs("D:/CERN temp/analyze-Sune/Output/root/19.root");}
   else{}}
else{}
if (index<21)
 {if (index>19)
      {pedestalDisp->SaveAs("D:/CERN temp/analyze-Sune/Output/gif/20.gif");
     pedestalDisp->SaveAs("D:/CERN temp/analyze-Sune/Output/root/20.root"); }
   else{}}
else{}
if (index<22)
 {if (index>20)
      {pedestalDisp->SaveAs("D:/CERN temp/analyze-Sune/Output/gif/21.gif");
     pedestalDisp->SaveAs("D:/CERN temp/analyze-Sune/Output/root/21.root"); }
   else{}}
else{}
if (index<23)
 {if (index>21)
      {pedestalDisp->SaveAs("D:/CERN temp/analyze-Sune/Output/gif/22.gif");
     pedestalDisp->SaveAs("D:/CERN temp/analyze-Sune/Output/root/22.root"); }
   else{}}
else{}
if (index<24)
 {if (index>22)
      {pedestalDisp->SaveAs("D:/CERN temp/analyze-Sune/Output/gif/23.gif");
     pedestalDisp->SaveAs("D:/CERN temp/analyze-Sune/Output/root/23.root");}
   else{}}
else{}
if (index<25)
 {if (index>23)
      {pedestalDisp->SaveAs("D:/CERN temp/analyze-Sune/Output/gif/24.gif");
     pedestalDisp->SaveAs("D:/CERN temp/analyze-Sune/Output/root/24.root"); }
   else{}}
else{}
if (index<26)
 {if (index>24)
      {pedestalDisp->SaveAs("D:/CERN temp/analyze-Sune/Output/gif/25.gif");
     pedestalDisp->SaveAs("D:/CERN temp/analyze-Sune/Output/root/25.root"); }
   else{}}
else{}
if (index<27)
 {if (index>25)
      {pedestalDisp->SaveAs("D:/CERN temp/analyze-Sune/Output/gif/26.gif");
     pedestalDisp->SaveAs("D:/CERN temp/analyze-Sune/Output/root/26.root"); }
   else{}}
else{}
if (index<28)
 {if (index>26)
      {pedestalDisp->SaveAs("D:/CERN temp/analyze-Sune/Output/gif/27.gif");
     pedestalDisp->SaveAs("D:/CERN temp/analyze-Sune/Output/root/27.root"); }
   else{}}
else{}
if (index<29)
 {if (index>27)
      {pedestalDisp->SaveAs("D:/CERN temp/analyze-Sune/Output/gif/28.gif");
     pedestalDisp->SaveAs("D:/CERN temp/analyze-Sune/Output/root/28.root"); }
   else{}}
else{}
```

```
if (index<30)
 {if (index>28)
      {pedestalDisp->SaveAs("D:/CERN temp/analyze-Sune/Output/gif/29.gif");
     pedestalDisp->SaveAs("D:/CERN temp/analyze-Sune/Output/root/29.root"); }
   else{}}
else{}
if (index<31)
 {if (index>29)
      {pedestalDisp->SaveAs("D:/CERN temp/analyze-Sune/Output/gif/30.gif");
     pedestalDisp->SaveAs("D:/CERN temp/analyze-Sune/Output/root/30.root"); }
   else{}}
else{}
if (index<32)
 {if (index>30)
      {pedestalDisp->SaveAs("D:/CERN temp/analyze-Sune/Output/gif/31.gif");
     pedestalDisp->SaveAs("D:/CERN temp/analyze-Sune/Output/root/31.root"); }
   else{}}
else{}
if (index<33)
 {if (index>31)
      {pedestalDisp->SaveAs("D:/CERN temp/analyze-Sune/Output/gif/32.gif");
     pedestalDisp->SaveAs("D:/CERN temp/analyze-Sune/Output/root/32.root");}
   else{}}
else{}
if (index<34)
 {if (index>32)
      {pedestalDisp->SaveAs("D:/CERN temp/analyze-Sune/Output/gif/33.gif");
     pedestalDisp->SaveAs("D:/CERN temp/analyze-Sune/Output/root/33.root"); }
   else{}}
else{}
if (index<35)
 {if (index>33)
      {pedestalDisp->SaveAs("D:/CERN temp/analyze-Sune/Output/gif/34.gif");
     pedestalDisp->SaveAs("D:/CERN temp/analyze-Sune/Output/root/34.root"); }
   else{}}
else{}
if (index<36)
 {if (index>34)
      {pedestalDisp->SaveAs("D:/CERN temp/analyze-Sune/Output/gif/35.gif");
     pedestalDisp->SaveAs("D:/CERN temp/analyze-Sune/Output/root/35.root");}
   else{}}
else{}
if (index<37)
 {if (index>35)
      {pedestalDisp->SaveAs("D:/CERN temp/analyze-Sune/Output/gif/36.gif");
     pedestalDisp->SaveAs("D:/CERN temp/analyze-Sune/Output/root/36.root"); }
   else{}}
else{}
if (index<38)
 {if (index>36)
      {pedestalDisp->SaveAs("D:/CERN temp/analyze-Sune/Output/gif/37.gif");
     pedestalDisp->SaveAs("D:/CERN temp/analyze-Sune/Output/root/37.root"); }
   else{}}
else{}
if (index<39)
 {if (index>37)
      {pedestalDisp->SaveAs("D:/CERN temp/analyze-Sune/Output/gif/38.gif");
     pedestalDisp->SaveAs("D:/CERN temp/analyze-Sune/Output/root/38.root"); }
   else{}}
else{}
if (index<40)
 {if (index>38)
      {pedestalDisp->SaveAs("D:/CERN temp/analyze-Sune/Output/gif/39.gif");
     pedestalDisp->SaveAs("D:/CERN temp/analyze-Sune/Output/root/39.root"); }
   else{}}
else{}
if (index<41)
 {if (index>39)
```

```
      {pedestalDisp->SaveAs("D:/CERN temp/analyze-Sune/Output/gif/40.gif");
     pedestalDisp->SaveAs("D:/CERN temp/analyze-Sune/Output/root/40.root");}
   else{}}
else{}
if (index<42)
 {if (index>40)
      {pedestalDisp->SaveAs("D:/CERN temp/analyze-Sune/Output/gif/41.gif");
     pedestalDisp->SaveAs("D:/CERN temp/analyze-Sune/Output/root/41.root"); }
   else{}}
else{}
if (index<43)
 {if (index>41)
      {pedestalDisp->SaveAs("D:/CERN temp/analyze-Sune/Output/gif/42.gif");
     pedestalDisp->SaveAs("D:/CERN temp/analyze-Sune/Output/root/42.root"); }
   else{}}
else{}
if (index<44)
 {if (index>42)
      {pedestalDisp->SaveAs("D:/CERN temp/analyze-Sune/Output/gif/43.gif");
     pedestalDisp->SaveAs("D:/CERN temp/analyze-Sune/Output/root/43.root"); }
   else{}}
else{}
if (index<45)
 {if (index>43)
      {pedestalDisp->SaveAs("D:/CERN temp/analyze-Sune/Output/gif/44.gif");
     pedestalDisp->SaveAs("D:/CERN temp/analyze-Sune/Output/root/44.root"); }
   else{}}
else{}
if (index<46)
 {if (index>44)
      {pedestalDisp->SaveAs("D:/CERN temp/analyze-Sune/Output/gif/45.gif");
     pedestalDisp->SaveAs("D:/CERN temp/analyze-Sune/Output/root/45.root"); }
   else{}}
else{}
if (index<47)
 {if (index>45)
      { pedestalDisp->SaveAs("D:/CERN temp/analyze-Sune/Output/gif/46.gif");
     pedestalDisp->SaveAs("D:/CERN temp/analyze-Sune/Output/root/46.root"); }
   else{}}
else{}
if (index<48)
 {if (index>46)
      {pedestalDisp->SaveAs("D:/CERN temp/analyze-Sune/Output/gif/47.gif");
     pedestalDisp->SaveAs("D:/CERN temp/analyze-Sune/Output/root/47.root"); }
   else{}}
else{}
if (index<49)
 {if (index>47)
      {pedestalDisp->SaveAs("D:/CERN temp/analyze-Sune/Output/gif/48.gif");
     pedestalDisp->SaveAs("D:/CERN temp/analyze-Sune/Output/root/48.root"); }
   else{}}
else{}
if (index<50)
 {if (index>48)
      {pedestalDisp->SaveAs("D:/CERN temp/analyze-Sune/Output/gif/49.gif");
     pedestalDisp->SaveAs("D:/CERN temp/analyze-Sune/Output/root/49.root");}
   else{}}
else{}
if (index<51)
 {if (index>49)
      {pedestalDisp->SaveAs("D:/CERN temp/analyze-Sune/Output/gif/50.gif");
     pedestalDisp->SaveAs("D:/CERN temp/analyze-Sune/Output/root/50.root");}
   else{}}
else{}
if (index<52)
 {if (index>50)
      { pedestalDisp->SaveAs("D:/CERN temp/analyze-Sune/Output/gif/51.gif");
     pedestalDisp->SaveAs("D:/CERN temp/analyze-Sune/Output/root/51.root"); }
```

```
      else{}}
    else{}
    if (index<53)
     {if (index>51)
          { pedestalDisp->SaveAs("D:/CERN temp/analyze-Sune/Output/gif/52.gif");
         pedestalDisp->SaveAs("D:/CERN temp/analyze-Sune/Output/root/52.root"); }
      else{}}
    else{}
    if (index<54)
     {if (index>52)
          { pedestalDisp->SaveAs("D:/CERN temp/analyze-Sune/Output/gif/53.gif");
         pedestalDisp->SaveAs("D:/CERN temp/analyze-Sune/Output/root/53.root"); }
      else{}}
    else{}
    if (index<55)
     {if (index>53)
          { pedestalDisp->SaveAs("D:/CERN temp/analyze-Sune/Output/gif/54.gif");
         pedestalDisp->SaveAs("D:/CERN temp/analyze-Sune/Output/root/54.root");}
      else{}}
    else{}
    if (index<56)
     {if (index>54)
          {pedestalDisp->SaveAs("D:/CERN temp/analyze-Sune/Output/gif/55.gif");
         pedestalDisp->SaveAs("D:/CERN temp/analyze-Sune/Output/root/55.root"); }
      else{}}
    else{}
    if (index<57)
     {if (index>55)
          {pedestalDisp->SaveAs("D:/CERN temp/analyze-Sune/Output/gif/56.gif");
         pedestalDisp->SaveAs("D:/CERN temp/analyze-Sune/Output/root/56.root"); }
      else{}}
    else{}
    if (index<58)
     {if (index>56)
          {pedestalDisp->SaveAs("D:/CERN temp/analyze-Sune/Output/gif/57.gif");
         pedestalDisp->SaveAs("D:/CERN temp/analyze-Sune/Output/root/57.root");}
      else{}}
    else{}
    if (index<59)
     {if (index>57)
          {pedestalDisp->SaveAs("D:/CERN temp/analyze-Sune/Output/gif/58.gif");
         pedestalDisp->SaveAs("D:/CERN temp/analyze-Sune/Output/root/58.root"); }
      else{}}
    else{}
    if (index<60)
     {if (index>58)
          {pedestalDisp->SaveAs("D:/CERN temp/analyze-Sune/Output/gif/59.gif");
         pedestalDisp->SaveAs("D:/CERN temp/analyze-Sune/Output/root/59.root"); }
      else{}}
    else{}
    if (index<61)
     {if (index>59)
{         pedestalDisp->SaveAs("D:/CERN temp/analyze-Sune/Output/gif/60.gif");
         pedestalDisp->SaveAs("D:/CERN temp/analyze-Sune/Output/root/60.root"); }
      else{}}
    else{}
    if (index<62)
     {if (index>60)
          {pedestalDisp->SaveAs("D:/CERN temp/analyze-Sune/Output/gif/61.gif");
         pedestalDisp->SaveAs("D:/CERN temp/analyze-Sune/Output/root/61.root"); }
      else{}}
    else{}
    if (index<63)
     {if (index>61)
          { pedestalDisp->SaveAs("D:/CERN temp/analyze-Sune/Output/gif/62.gif");
         pedestalDisp->SaveAs("D:/CERN temp/analyze-Sune/Output/root/62.root"); }
      else{}}
    else  {  }
```

```
    if (index<64)
     {if (index>62)
          {pedestalDisp->SaveAs("D:/CERN temp/analyze-Sune/Output/gif/63.gif");
          pedestalDisp->SaveAs("D:/CERN temp/analyze-Sune/Output/root/63.root"); }
       else{}}
    else{  }

}
```

Appendix F

All64.C:

```
.x cosmic1pe.C(0);
.x cosmic1pe.C(1);
.x cosmic1pe.C(2);
.x cosmic1pe.C(3);
.x cosmic1pe.C(4);
.x cosmic1pe.C(5);
.x cosmic1pe.C(6);
.x cosmic1pe.C(7);
.x cosmic1pe.C(8);
.x cosmic1pe.C(9);
.x cosmic1pe.C(10);
.x cosmic1pe.C(11);
.x cosmic1pe.C(12);
.x cosmic1pe.C(13);
.x cosmic1pe.C(14);
.x cosmic1pe.C(15);
.x cosmic1pe.C(16);
.x cosmic1pe.C(17);
.x cosmic1pe.C(18);
.x cosmic1pe.C(19);
.x cosmic1pe.C(20);
.x cosmic1pe.C(21);
.x cosmic1pe.C(22);
.x cosmic1pe.C(23);
.x cosmic1pe.C(24);
.x cosmic1pe.C(25);
.x cosmic1pe.C(26);
.x cosmic1pe.C(27);
.x cosmic1pe.C(28);
.x cosmic1pe.C(29);
.x cosmic1pe.C(30);
.x cosmic1pe.C(31);
.x cosmic1pe.C(32);
.x cosmic1pe.C(33);
.x cosmic1pe.C(34);
//.x cosmic1pe.C(35); //bad channel
.x cosmic1pe.C(36);
//.x cosmic1pe.C(37); //bad channel
.x cosmic1pe.C(38);
.x cosmic1pe.C(39);
.x cosmic1pe.C(40);
.x cosmic1pe.C(41);
.x cosmic1pe.C(42);
.x cosmic1pe.C(43);
.x cosmic1pe.C(44);
.x cosmic1pe.C(45);
.x cosmic1pe.C(46);
.x cosmic1pe.C(47);
.x cosmic1pe.C(48);
.x cosmic1pe.C(49);
.x cosmic1pe.C(50);
.x cosmic1pe.C(51);
.x cosmic1pe.C(52);
.x cosmic1pe.C(53);
.x cosmic1pe.C(54);
//.x cosmic1pe.C(55); //bad channel
.x cosmic1pe.C(56);
.x cosmic1pe.C(57);
.x cosmic1pe.C(58);
.x cosmic1pe.C(59);
.x cosmic1pe.C(60);
.x cosmic1pe.C(61);
.x cosmic1pe.C(62);
//.x cosmic1pe.C(63); //bad channel
```

Appendix G

From Maple:

Find the limits:

```
> limit1:=solve(w/2=d*tan(theta),theta);limit2:=solve(w=d*tan(theta),theta);
```

$$limit1 := \arctan\left(\frac{w}{2\,d}\right)$$

$$limit2 := \arctan\left(\frac{w}{d}\right)$$

Integrating until the fist limit:

```
> I1:=int(cos(theta)^2*(w^2-2*w*d*tan(theta)+2*d^2*tan(theta)^2)/(w^2+4*d^2*tan(theta)^2),theta=0..limit1);
```

$$I1 := \int_0^{\arctan\left(\frac{w}{2\,d}\right)} \frac{\cos(\theta)^2\,(w^2 - 2\,w\,d\,\tan(\theta) + 2\,d^2\,\tan(\theta)^2)}{w^2 + 4\,d^2\,\tan(\theta)^2}\,d\theta$$

Integrating between the limits:

```
> I2:=Int(cos(theta)^2*(w-d*tan(theta))/(2*w),theta=limit1..limit2);
```

$$I2 := \int_{\arctan\left(\frac{w}{2\,d}\right)}^{\arctan\left(\frac{w}{d}\right)} \frac{\cos(\theta)^2\,(w - d\,\tan(\theta))}{2\,w}\,d\theta$$

Integrating after the 2ed. limit until 90 degree (Pi/2) (just for the principle. It is know that this should be zero):

```
> I3:=int(cos(theta)^2*0,theta=limit2..Pi/2);
```

$$I3 := 0$$

Adding the integrals to one:

```
> Iall:=I1+I2+I3;
```

$$Iall := \int_0^{\arctan\left(\frac{w}{2\,d}\right)} \frac{\cos(\theta)^2\,(w^2 - 2\,w\,d\,\tan(\theta) + 2\,d^2\,\tan(\theta)^2)}{w^2 + 4\,d^2\,\tan(\theta)^2}\,d\theta + \int_{\arctan\left(\frac{w}{2\,d}\right)}^{\arctan\left(\frac{w}{d}\right)} \frac{\cos(\theta)^2\,(w - d\,\tan(\theta))}{2\,w}\,d\theta$$

Appendix G

Calculating f:

```
> f:=Iall/Int(cos(theta)^2,theta=0..Pi/2);
```

$$f := \frac{\int_0^{\arctan\left(\frac{w}{2\,d}\right)} \frac{\cos(\theta)^2\,(w^2 - 2\,w\,d\,\tan(\theta) + 2\,d^2\,\tan(\theta)^2)}{w^2 + 4\,d^2\,\tan(\theta)^2}\,d\theta + \int_{\arctan\left(\frac{w}{2\,d}\right)}^{\arctan\left(\frac{w}{d}\right)} \frac{\cos(\theta)^2\,(w - d\,\tan(\theta))}{2\,w}\,d\theta}{\int_0^{\frac{1}{2}\pi} \cos(\theta)^2\,d\theta}$$

Input variabels:

```
> d:=40;
```

$$d := 40$$

```
> w:=32;
```

$$w := 32$$

Numerical result of f:

```
> evalf(f);
```

$$0.2994223735$$

Appendix H

cosmic.C:

```
#include "TMultiGraph.h"
#include "TFile.h"
#include "TTree.h"
#include "TBrowser.h"
#include "TH2.h"
#include "TRandom.h"
#include "TMath.h"
#include <iostream>
#include <fstream>
#include "TStyle.h"
#include "TText.h"



Double_t fit1pe(Double_t *x, Double_t *par)
{

  Double_t result1=0.;

  for (Int_t i=1;i<15;i++)
    {

      Double_t fac=1;
         if(i<1)
        {fac=1;}
      else{
 for (Int_t var=1;var<i+1;var++)
        {
          fac *= var;
        }}

      Double_t P = (TMath::Exp((-1.)*par[0])*par[0]**i)/(fac);
      Double_t G1 =
1./((TMath::Sqrt(2.*TMath::Pi())*(TMath::Sqrt((i*par[3]**2+par[2]**2))))) ;
      Double_t G2 = TMath::Exp( ( (-1.) * (x[0] - par[5] - i*(par[1]))**2
)/(2.*(i*par[3]**2+par[2]**2)));

      result1 += P * G1 * G2;
    }
  // result1 *= par[4];
 // return result;

 Double_t result2=0.;
  for (Int_t iiii=1;iiii<5;iiii++)
    {

      Double_t fac2=1;
         if(iiii<1)
        {fac2=1;}
      else{
 for (Int_t var=1;var<iiii+1;var++)
        {
          fac2 *= var;
        }}
      Double_t Pct = (TMath::Exp((-1.)*par[6])*par[6]**iiii)/(fac2);
      Double_t G1ct =
1./((TMath::Sqrt(2.*TMath::Pi())*(TMath::Sqrt((iiii*par[3]**2+par[2]**2))))) ;
      Double_t G2ct = TMath::Exp( ( (-1.) * (x[0] - par[5] - iiii*(par[1]))**2
)/(2.*(iiii*par[3]**2+par[2]**2)));

      result2 += Pct * G1ct * G2ct;
    }
  // result2 *= par[7];
 Double_t result = result1 + result2;
```

```
 result *= par[4];
  return result;
 // return  result2;
}



Double_t peFct(Double_t *x, Double_t *param)
{
  Double_t result = 0.;
  Double_t fact = 1;
  for (Int_t var=1;var<param[6]+1;var++)
    fact *= var;

      Double_t P = (TMath::Exp((-1.) * param[0]) * param[0]**param[6])/fact;
      Double_t G1 =
1./((TMath::Sqrt(2.*TMath::Pi())*(TMath::Sqrt((param[6]*param[3]**2+param[2]**2))))
) ;
      Double_t G2 = TMath::Exp( ( (-1.) * (x[0] - param[5] -
param[6]*(param[1]))**2 )/(2.*(param[6]*param[3]**2+param[2]**2)));

result += P * G1 * G2;
 result *= param[4];
return result;
}
Double_t peFctCT(Double_t *x, Double_t *param)
{
Double_t result2=0.;
 Double_t fact = 1;
  for (Int_t var=1;var<param[6]+1;var++)
    fact *= var;

      Double_t Pct = (TMath::Exp((-1.)*param[7])*param[7]**param[6])/(fact);
      Double_t G1ct =
1./((TMath::Sqrt(2.*TMath::Pi())*(TMath::Sqrt((param[6]*param[3]**2+param[2]**2))))
) ;
      Double_t G2ct = TMath::Exp( ( (-1.) * (x[0] - param[5] -
param[6]*(param[1]))**2 )/(2.*(param[6]*param[3]**2+param[2]**2)));

      result2 += Pct * G1ct * G2ct;

 result2 *= param[4];
 return result2;
}

void cosmic(int index)
{
  //Create, fill and display raw data
  TFile *file = new TFile("ped_1pe.root");
  TH1I *pedestal;
  char str[2];
  sprintf(str,"%d",index);
  pedestal = (TH1I*) gDirectory->Get(str);
  pedestal->GetYaxis()->SetTitle("Number of events");
  pedestal->GetXaxis()->SetTitle("Charge signal (ADC counts)");



   TF1* gaussPE;

  TCanvas *pedestalDisp = new TCanvas("cavas","pedestal - 1pe",200,60,700,700);
 pedestalDisp->SetLogy();
  pedestalDisp->cd();
  pedestalDisp->SetFillColor(0);
  pedestalDisp->SetFrameFillColor(0);
  pedestal->Draw();
```

```
  //Evaluate 1pe characteristics
  cout << "Pedestal " << index << endl;
  Double_t pedX,singleX,pedRMS,singleRMS,Mina,Minb;
  pedX = pedestal->GetMaximumBin();

  Float_t MinFitInt = pedestal->GetMaximumBin()-TMath::Sqrt(pedestal-
>GetMaximum())/30-1.;
  Float_t MaxFitInt = pedestal->GetMaximumBin()+TMath::Sqrt(pedestal-
>GetMaximum())/30+1.;

TF1* G1 = new TF1("G1","gaus",MinFitInt,MaxFitInt);
  G1->SetLineColor(3);
  G1->SetLineWidth(1);
  pedestal->Fit(G1,"R");
  pedX = G1->GetParameter(1);
  pedRMS = G1->GetParameter(2);


  if(0.8<pedRMS)
    {  TF1* Min = new TF1("Min","pol2",pedX+1.5*pedRMS, pedX+5.5*pedRMS+2);}
  else{  TF1* Min = new TF1("Min","pol2",pedX+1, pedX+8);}

  //  TF1* Min = new TF1("Min","pol2",pedX+1.5*pedRMS, pedX+10*pedRMS+0.1);
 Min->SetLineColor(14);
 Min->SetLineWidth(1);
 pedestal->Fit(Min,"R+");
 Mina = Min->GetParameter(2);
 Minb = Min->GetParameter(1);

  if (30<-Minb/(2*Mina))
    {if (-Minb/(2*Mina)<200)
   {Float_t MaxFit =  -Minb/(2*Mina);}
         else {Float_t MaxFit =  pedX+4;}}
         else {Float_t MaxFit =  pedX+4;}


TF1* G2 = new TF1("G2","gaus",MaxFit,MaxFit +15);
  G2->SetLineColor(7);
  G2->SetLineWidth(1);
  pedestal->Fit(G2,"R+");
  singleX = G2->GetParameter(1);
  singleRMS = G2->GetParameter(2);

  //TF1* fct3    = new TF1("fct3",fit1pe,MinFitInt,300,6);
  TF1* fct3    = new TF1("fct3",fit1pe,MaxFit,500,7);
  fct3->SetParLimits(0,0,20);
  fct3->SetParLimits(1,0,10000000);
  fct3->SetParLimits(3,0,10000000);
  fct3->SetParLimits(4,0,1000000);
  fct3->SetParLimits(6,0.0001,5);
  fct3->SetParLimits(7,1,1000000);
  // fct3->SetParLimits(5,0,100000000);


  //read Fit calibration files.
   ifstream in1pemean; //Declare the stream variable
   Double_t buffer1pemean;
   in1pemean.open("1pe mean.cal"); //Open the file.
   for(int iii = 0; iii < index+1; iii++){
   in1pemean>>buffer1pemean;}  //Read the number.
   in1pemean.close();//Close the file.

   ifstream in1peRMS; //Declare the stream variable
   Double_t buffer1peRMS;
   in1peRMS.open("1pe RMS.cal");   //Open the file.
   for(int iii = 0; iii < index+1; iii++){
   in1peRMS>>buffer1peRMS;} //Read the number.
```

```
    in1peRMS.close(); //Close the file.

    ifstream inpedmean; //Declare the stream variable
    Double_t bufferpedmean;
    inpedmean.open("ped mean.cal");   //Open the file.
    for(int iii = 0; iii < index+1; iii++){
    inpedmean>>bufferpedmean;} //Read the number.
    inpedmean.close(); //Close the file.

    ifstream inpedRMS; //Declare the stream variable
    Double_t bufferpedRMS;
    inpedRMS.open("ped RMS.cal");   //Open the file.
    for(int iii = 0; iii < index+1; iii++){
    inpedRMS>>bufferpedRMS;} //Read the number.
    inpedRMS.close(); //Close the file.

    fct3->SetParameter(0,7);
    fct3->FixParameter(1,buffer1pemean);
    fct3->FixParameter(2,bufferpedRMS);
    fct3->FixParameter(3,buffer1peRMS);
    fct3->SetParameter(4,110000);
    // fct3->FixParameter(5,bufferpedmean);
    fct3->SetParameter(6,0.7);
    fct3->SetLineColor(4);


    // fct3->SetParameter(0,4);
    // fct3->FixParameter(1,buffer1pemean);
    //fct3->FixParameter(2,pedRMS);
    //  fct3->FixParameter(3,buffer1peRMS);
    //  fct3->SetParameter(4,1100);
     fct3->FixParameter(5,pedX);
    // fct3->SetParameter(6,0.01);
    //  fct3->SetParameter(7,800);

    fct3->SetLineColor(4);

  fct3->SetParName(0,"Mu");
  fct3->SetParName(1,"1pe mean");
  fct3->SetParName(2,"ped RMS");
  fct3->SetParName(3,"1pe RMS");
  fct3->SetParName(4,"Norm");
  fct3->SetParName(5,"ped mean");
  fct3->SetParName(6,"Mu CT");
  // fct3->SetParName(7,"Norm CT");

  pedestal->Fit(fct3,"R+") ;
   gStyle->SetOptStat("");
   // gStyle->SetOptStat(1111111111);
   // gStyle->SetOptFit(1111);
    gStyle->SetOptStat(0000000000);
    gStyle->SetOptFit(0000);
// TPaveStats(Min[0]);
//  TPaveText ();


//Print of mu and mu CT vaules on plot

pt = new TPaveText(1.0,1.0,0.58,0.81, "NDC"); // NDC sets coords
                                              // relative to pad dimensions
pt->SetFillColor(0); // text is black on white
pt->SetTextSize(0.04);
pt->SetTextAlign(12);
text = pt->AddText("#chi^{2} / NDF");
text = pt->AddText("#mu");
text = pt->AddText("#mu_{CT}");
pt->Draw();       //to draw your text object
```

Appendix H

```
pt2 = new TPaveText(1.0,1.0,0.741,0.812, "NDC"); // NDC sets coords
pt2->SetFillColor(0);
pt2->SetLineColor(0); // text is black on white
pt2->SetTextSize(0.04);
pt2->SetTextAlign(12);
char buf0[10];
 sprintf(buf0, "= %.0f", fct3->GetChisquare());
 text = pt2->AddText(buf0);
char buf[10];
sprintf(buf, "= %.2f", fct3->GetParameter(0));
 text = pt2->AddText(buf);
char buf2[10];
sprintf(buf2, "= %.2f", fct3->GetParameter(6));
 text = pt2->AddText(buf2);
 // text = pt->AddText("#pm ");
pt2->Draw();       //to draw your text object


pt3 = new TPaveText(1.0,1.0,0.865,0.812, "NDC"); // NDC sets coords
pt3->SetFillColor(0);
pt3->SetLineColor(0); // text is black on white
pt3->SetTextSize(0.04);
pt3->SetTextAlign(12);
 text = pt3->AddText("/ ");
 text = pt3->AddText("#pm ");
 text = pt3->AddText("#pm ");
pt3->Draw();       //to draw your text object

pt4 = new TPaveText(1.0,1.0,0.9,0.812, "NDC"); // NDC sets coords
pt4->SetFillColor(0);
pt4->SetLineColor(0); // text is black on white
pt4->SetTextSize(0.04);
pt4->SetTextAlign(12);
char buf5[10];
sprintf(buf5, "%.0f", fct3->GetNDF());
 text = pt4->AddText(buf5);
char buf3[10];
sprintf(buf3, "%.2f", fct3->GetParError(0));
 text = pt4->AddText(buf3);
char buf4[10];
sprintf(buf4, "%.2f", fct3->GetParError(6));
 text = pt4->AddText(buf4);
 // text = pt->AddText("#pm ");
pt4->Draw();       //to draw your text object


    for (Int_t ii=1;ii<15;ii++)
    {
      TF1 *fit = new TF1("Npe",peFct,MinFitInt,500,9);
      //TF1 *fit = new TF1("Npe",peFct,MaxFit,300,7);
      fit->FixParameter(0,fct3->GetParameter(0));
      fit->FixParameter(1,fct3->GetParameter(1));
      //fit->SetParameter(2,fct3->GetParameter(2));
      fit->FixParameter(3,fct3->GetParameter(3));
      fit->SetParameter(4,fct3->GetParameter(4));
      fit->FixParameter(5,fct3->GetParameter(5));
      fit->FixParameter(7,fct3->GetParameter(6));
      // fit->FixParameter(8,fct3->GetParameter(7));
      fit->FixParameter(6,ii);
      // fit->SetLineColor(ii);
      if(10>ii){ fit->SetLineColor(ii);}
      else{fit->SetLineColor(ii+31);}
      fit->SetLineWidth(1);
      fit->DrawCopy("same");
    }

    for (Int_t ii=1;ii<5;ii++)
    {
```

```
        TF1 *fit2 = new TF1("Npe",peFctCT,MinFitInt,500,9);
        //TF1 *fit = new TF1("Npe",peFct,MaxFit,300,7);
        fit2->FixParameter(0,fct3->GetParameter(0));
        fit2->FixParameter(1,fct3->GetParameter(1));
        //fit->SetParameter(2,fct3->GetParameter(2));
        fit2->FixParameter(3,fct3->GetParameter(3));
        fit2->SetParameter(4,fct3->GetParameter(4));
        fit2->FixParameter(5,fct3->GetParameter(5));
        fit2->FixParameter(7,fct3->GetParameter(6));
        // fit2->FixParameter(8,fct3->GetParameter(7));
        fit2->FixParameter(6,ii);
        fit2->SetLineColor(ii);
        fit2->SetLineStyle(2);

        fit2->SetLineWidth(1);
        fit2->DrawCopy("same");
      }

      if(singleX>1)
        { pedestal->SetMaximum(10*(G2->GetParameter(0)));
          //       pedestal->SetAxisRange(singleX-2.*singleRMS,singleX+fct3-
>GetParameter(0)*2.5*singleRMS);}
          //       pedestal->SetAxisRange(bufferpedmean-2.*bufferpedRMS,200);}
          //       pedestal->SetAxisRange(bufferpedmean-10,bufferpedmean+350);}
          pedestal->SetAxisRange(pedX-10,pedX+350);}
      //pedestal->SetAxisRange(bufferpedmean-2.*bufferpedRMS,bufferpedmean+(fct3-
>GetParameter(0))*(buffer1pemean-bufferpedmean));}
          //pedestal->SetAxisRange(singleX-2.*singleRMS,200);}
      else {pedestal->SetMaximum(pedestal->GetMaximum()+500);
        //  pedestal->SetAxisRange(pedX-8.*pedRMS,pedX+16.*pedRMS);}
           pedestal->SetAxisRange(pedX-8.*pedRMS,pedX+350);}



 //read out

 Double_t pemean=1;
 pemean = fct3->GetParameter(1) -  fct3->GetParameter(5);

 if(index==0 || index==1 || index==2|| index==8|| index==9|| index==10||
index==16|| index==17|| index==18|| index==24|| index==25|| index==26|| index==32||
index==33|| index==34|| index==40|| index==41|| index==42|| index==48|| index==49||
index==50|| index==56|| index==57|| index==58)
 {
 ofstream myfile;            //SJ
  myfile.open ("D:/CERN temp/analyze-Sune/Output/90/1pemean.dat", ios::app);   //SJ
  myfile << pemean;   //SJ
  myfile<<"\n";   //SJ
  myfile.close();

 ofstream myfile2;            //SJ
  myfile2.open ("D:/CERN temp/analyze-Sune/Output/90/index.dat", ios::app);   //SJ
  myfile2 << index;   //SJ
  myfile2<<"\n";   //SJ
  myfile2.close();

 ofstream myfile3;            //SJ
  myfile3.open ("D:/CERN temp/analyze-Sune/Output/90/Mu.dat", ios::app);   //SJ
  myfile3 << fct3->GetParameter(0);   //SJ
  myfile3<<"\n";   //SJ
  myfile3.close();

 ofstream myfile4;            //SJ
  myfile4.open ("D:/CERN temp/analyze-Sune/Output/90/1pe mean.dat", ios::app);
//SJ
  myfile4 << fct3->GetParameter(1);   //SJ
  myfile4<<"\n";   //SJ
  myfile4.close();
```

```
 ofstream myfile5;            //SJ
  myfile5.open ("D:/CERN temp/analyze-Sune/Output/90/1pe RMS.dat", ios::app);
//SJ
  myfile5 << fct3->GetParameter(3);   //SJ
  myfile5<<"\n";   //SJ
  myfile5.close();

 ofstream myfile6;            //SJ
  myfile6.open ("D:/CERN temp/analyze-Sune/Output/90/Norm.dat", ios::app);   //SJ
  myfile6 << fct3->GetParameter(4);   //SJ
  myfile6<<"\n";   //SJ
  myfile6.close();

 ofstream myfile7;            //SJ
  myfile7.open ("D:/CERN temp/analyze-Sune/Output/90/ped mean.dat", ios::app);
//SJ
  myfile7 << fct3->GetParameter(5);   //SJ
  myfile7<<"\n";   //SJ
  myfile7.close();

ofstream myfile8;            //SJ
  myfile8.open ("D:/CERN temp/analyze-Sune/Output/90/ped RMS.dat", ios::app);
//SJ
  myfile8 << fct3->GetParameter(2);   //SJ
  myfile8<<"\n";   //SJ
  myfile8.close();

ofstream myfile9;            //SJ
  myfile9.open ("D:/CERN temp/analyze-Sune/Output/90/Mu ct.dat", ios::app);   //SJ
  myfile9 << fct3->GetParameter(6);   //SJ
  myfile9<<"\n";   //SJ
  myfile9.close();

ofstream myfile10;            //SJ
  myfile10.open ("D:/CERN temp/analyze-Sune/Output/90/Mu Error.dat", ios::app);
//SJ
  myfile10 << fct3->GetParError(0);   //SJ
  myfile10<<"\n";   //SJ
  myfile10.close();

ofstream myfile11;            //SJ
  myfile11.open ("D:/CERN temp/analyze-Sune/Output/90/Mu ct Error.dat", ios::app);
//SJ
  myfile11 << fct3->GetParError(6);   //SJ
  myfile11<<"\n";   //SJ
  myfile11.close();
  /*
char bufindexgif[10];
sprintf(bufindexgif, "D:/CERN temp/analyze-Sune/Output/90/gif/%f.gif", index);
char bufindexroot[10];
sprintf(bufindexroot, "D:/CERN temp/analyze-Sune/Output/90/gif/%f.gif", index);
    pedestalDisp->SaveAs(bufindexgif);
    pedestalDisp->SaveAs(bufindexroot);
  */
}
 else{
 ofstream myfile;            //SJ
  myfile.open ("D:/CERN temp/analyze-Sune/Output/45/1pemean.dat", ios::app);   //SJ
  myfile << pemean;   //SJ
  myfile<<"\n";   //SJ
  myfile.close();

 ofstream myfile2;            //SJ
  myfile2.open ("D:/CERN temp/analyze-Sune/Output/45/index.dat", ios::app);   //SJ
  myfile2 << index;   //SJ
  myfile2<<"\n";   //SJ
  myfile2.close();
```

```
 ofstream myfile3;            //SJ
  myfile3.open ("D:/CERN temp/analyze-Sune/Output/45/Mu.dat", ios::app);   //SJ
  myfile3 << fct3->GetParameter(0);   //SJ
  myfile3<<"\n";   //SJ
  myfile3.close();

 ofstream myfile4;            //SJ
  myfile4.open ("D:/CERN temp/analyze-Sune/Output/45/1pe mean.dat", ios::app);
//SJ
  myfile4 << fct3->GetParameter(1);   //SJ
  myfile4<<"\n";   //SJ
  myfile4.close();

 ofstream myfile5;            //SJ
  myfile5.open ("D:/CERN temp/analyze-Sune/Output/45/1pe RMS.dat", ios::app);
//SJ
  myfile5 << fct3->GetParameter(3);   //SJ
  myfile5<<"\n";   //SJ
  myfile5.close();

 ofstream myfile6;            //SJ
  myfile6.open ("D:/CERN temp/analyze-Sune/Output/45/Norm.dat", ios::app);   //SJ
  myfile6 << fct3->GetParameter(4);   //SJ
  myfile6<<"\n";   //SJ
  myfile6.close();

 ofstream myfile7;            //SJ
  myfile7.open ("D:/CERN temp/analyze-Sune/Output/45/ped mean.dat", ios::app);
//SJ
  myfile7 << fct3->GetParameter(5);   //SJ
  myfile7<<"\n";   //SJ
  myfile7.close();

ofstream myfile8;            //SJ
  myfile8.open ("D:/CERN temp/analyze-Sune/Output/45/ped RMS.dat", ios::app);
//SJ
  myfile8 << fct3->GetParameter(2);   //SJ
  myfile8<<"\n";   //SJ
  myfile8.close();

ofstream myfile9;            //SJ
  myfile9.open ("D:/CERN temp/analyze-Sune/Output/45/Mu ct.dat", ios::app);   //SJ
  myfile9 << fct3->GetParameter(6);   //SJ
  myfile9<<"\n";   //SJ
  myfile9.close();

ofstream myfile10;            //SJ
  myfile10.open ("D:/CERN temp/analyze-Sune/Output/45/Mu Error.dat", ios::app);
//SJ
  myfile10 << fct3->GetParError(0);   //SJ
  myfile10<<"\n";   //SJ
  myfile10.close();

ofstream myfile11;            //SJ
  myfile11.open ("D:/CERN temp/analyze-Sune/Output/45/Mu ct Error.dat", ios::app);
//SJ
  myfile11 << fct3->GetParError(6);   //SJ
  myfile11<<"\n";   //SJ
  myfile11.close();
 }



  // File saving

  if (index<1)
```

Appendix H

```
  {pedestalDisp->SaveAs("D:/CERN temp/analyze-Sune/Output/90/gif/0.gif");
  pedestalDisp->SaveAs("D:/CERN temp/analyze-Sune/Output/90/root/0.root");}
else{ }

 if (index<2)
  {if (index>0)
       {pedestalDisp->SaveAs("D:/CERN temp/analyze-Sune/Output/90/gif/1.gif");
       pedestalDisp->SaveAs("D:/CERN temp/analyze-Sune/Output/90/root/1.root");}
    else{}}
 else{}
 if (index<3)
  {if (index>1)
       {pedestalDisp->SaveAs("D:/CERN temp/analyze-Sune/Output/90/gif/2.gif");
       pedestalDisp->SaveAs("D:/CERN temp/analyze-Sune/Output/90/root/2.root"); }
    else{}}
 else{}
 if (index<4)
  {if (index>2)
       {pedestalDisp->SaveAs("D:/CERN temp/analyze-Sune/Output/45/gif/3.gif");
       pedestalDisp->SaveAs("D:/CERN temp/analyze-Sune/Output/45/root/3.root");}
    else{}}
 else{}
 if (index<5)
  {if (index>3)
       {pedestalDisp->SaveAs("D:/CERN temp/analyze-Sune/Output/45/gif/4.gif");
       pedestalDisp->SaveAs("D:/CERN temp/analyze-Sune/Output/45/root/4.root"); }
    else{}}
 else{}
 if (index<6)
  {if (index>4)
       {pedestalDisp->SaveAs("D:/CERN temp/analyze-Sune/Output/45/gif/5.gif");
       pedestalDisp->SaveAs("D:/CERN temp/analyze-Sune/Output/45/root/5.root");}
    else{}}
 else{}
 if (index<7)
  {if (index>5)
       {pedestalDisp->SaveAs("D:/CERN temp/analyze-Sune/Output/45/gif/6.gif");
       pedestalDisp->SaveAs("D:/CERN temp/analyze-Sune/Output/45/root/6.root"); }
    else{}}
 else{}
 if (index<8)
  {if (index>6)
       {pedestalDisp->SaveAs("D:/CERN temp/analyze-Sune/Output/45/gif/7.gif");
       pedestalDisp->SaveAs("D:/CERN temp/analyze-Sune/Output/45/root/7.root");}
    else{}}
 else{}
 if (index<9)
  {if (index>7)
       {pedestalDisp->SaveAs("D:/CERN temp/analyze-Sune/Output/90/gif/8.gif");
       pedestalDisp->SaveAs("D:/CERN temp/analyze-Sune/Output/90/root/8.root"); }
    else{}}
 else{}
 if (index<10)
  {if (index>8)
       {pedestalDisp->SaveAs("D:/CERN temp/analyze-Sune/Output/90/gif/9.gif");
       pedestalDisp->SaveAs("D:/CERN temp/analyze-Sune/Output/90/root/9.root"); }
    else{}}
 else{}
 if (index<11)
  {if (index>9)
       {pedestalDisp->SaveAs("D:/CERN temp/analyze-Sune/Output/90/gif/10.gif");
       pedestalDisp->SaveAs("D:/CERN temp/analyze-Sune/Output/90/root/10.root"); }
    else{}}
 else{}
 if (index<12)
  {if (index>10)
    { pedestalDisp->SaveAs("D:/CERN temp/analyze-Sune/Output/45/gif/11.gif");
      pedestalDisp->SaveAs("D:/CERN temp/analyze-Sune/Output/45/root/11.root"); }
```

```
    else{}}
  else{}
  if (index<13)
   {if (index>11)
     { pedestalDisp->SaveAs("D:/CERN temp/analyze-Sune/Output/45/gif/12.gif");
       pedestalDisp->SaveAs("D:/CERN temp/analyze-Sune/Output/45/root/12.root"); }
     else{}}
  else{}
  if (index<14)
   {if (index>12)
     { pedestalDisp->SaveAs("D:/CERN temp/analyze-Sune/Output/45/gif/13.gif");
       pedestalDisp->SaveAs("D:/CERN temp/analyze-Sune/Output/45/root/13.root");}
     else{}}
  else{}
  if (index<15)
   {if (index>13)
    {  pedestalDisp->SaveAs("D:/CERN temp/analyze-Sune/Output/45/gif/14.gif");
       pedestalDisp->SaveAs("D:/CERN temp/analyze-Sune/Output/45/root/14.root"); }
     else{}}
  else{}
  if (index<16)
   {if (index>14)
        {pedestalDisp->SaveAs("D:/CERN temp/analyze-Sune/Output/45/gif/15.gif");
       pedestalDisp->SaveAs("D:/CERN temp/analyze-Sune/Output/45/root/15.root"); }
     else{}}
  else{}
  if (index<17)
   {if (index>15)
        {pedestalDisp->SaveAs("D:/CERN temp/analyze-Sune/Output/90/gif/16.gif");
       pedestalDisp->SaveAs("D:/CERN temp/analyze-Sune/Output/90/root/16.root"); }
     else{}}
  else{}
  if (index<18)
   {if (index>16)
        {pedestalDisp->SaveAs("D:/CERN temp/analyze-Sune/Output/90/gif/17.gif");
       pedestalDisp->SaveAs("D:/CERN temp/analyze-Sune/Output/90/root/17.root"); }
     else{}}
  else{}
  if (index<19)
   {if (index>17)
        {pedestalDisp->SaveAs("D:/CERN temp/analyze-Sune/Output/90/gif/18.gif");
       pedestalDisp->SaveAs("D:/CERN temp/analyze-Sune/Output/90/root/18.root"); }
     else{}}
  else{}
  if (index<20)
   {if (index>18)
        {pedestalDisp->SaveAs("D:/CERN temp/analyze-Sune/Output/45/gif/19.gif");
       pedestalDisp->SaveAs("D:/CERN temp/analyze-Sune/Output/45/root/19.root");}
     else{}}
  else{}
  if (index<21)
   {if (index>19)
        {pedestalDisp->SaveAs("D:/CERN temp/analyze-Sune/Output/45/gif/20.gif");
       pedestalDisp->SaveAs("D:/CERN temp/analyze-Sune/Output/45/root/20.root"); }
     else{}}
  else{}
  if (index<22)
   {if (index>20)
        {pedestalDisp->SaveAs("D:/CERN temp/analyze-Sune/Output/45/gif/21.gif");
       pedestalDisp->SaveAs("D:/CERN temp/analyze-Sune/Output/45/root/21.root"); }
     else{}}
  else{}
  if (index<23)
   {if (index>21)
        {pedestalDisp->SaveAs("D:/CERN temp/analyze-Sune/Output/45/gif/22.gif");
       pedestalDisp->SaveAs("D:/CERN temp/analyze-Sune/Output/45/root/22.root"); }
     else{}}
  else{}
```

Appendix H

```
if (index<24)
 {if (index>22)
      {pedestalDisp->SaveAs("D:/CERN temp/analyze-Sune/Output/45/gif/23.gif");
     pedestalDisp->SaveAs("D:/CERN temp/analyze-Sune/Output/45/root/23.root");}
   else{}}
else{}
if (index<25)
 {if (index>23)
      {pedestalDisp->SaveAs("D:/CERN temp/analyze-Sune/Output/90/gif/24.gif");
     pedestalDisp->SaveAs("D:/CERN temp/analyze-Sune/Output/90/root/24.root"); }
   else{}}
else{}
if (index<26)
 {if (index>24)
      {pedestalDisp->SaveAs("D:/CERN temp/analyze-Sune/Output/90/gif/25.gif");
     pedestalDisp->SaveAs("D:/CERN temp/analyze-Sune/Output/90/root/25.root"); }
   else{}}
else{}
if (index<27)
 {if (index>25)
      {pedestalDisp->SaveAs("D:/CERN temp/analyze-Sune/Output/90/gif/26.gif");
     pedestalDisp->SaveAs("D:/CERN temp/analyze-Sune/Output/90/root/26.root"); }
   else{}}
else{}
if (index<28)
 {if (index>26)
      {pedestalDisp->SaveAs("D:/CERN temp/analyze-Sune/Output/45/gif/27.gif");
     pedestalDisp->SaveAs("D:/CERN temp/analyze-Sune/Output/45/root/27.root"); }
   else{}}
else{}
if (index<29)
 {if (index>27)
      {pedestalDisp->SaveAs("D:/CERN temp/analyze-Sune/Output/45/gif/28.gif");
     pedestalDisp->SaveAs("D:/CERN temp/analyze-Sune/Output/45/root/28.root"); }
   else{}}
else{}
if (index<30)
 {if (index>28)
      {pedestalDisp->SaveAs("D:/CERN temp/analyze-Sune/Output/45/gif/29.gif");
     pedestalDisp->SaveAs("D:/CERN temp/analyze-Sune/Output/45/root/29.root"); }
   else{}}
else{}
if (index<31)
 {if (index>29)
      {pedestalDisp->SaveAs("D:/CERN temp/analyze-Sune/Output/45/gif/30.gif");
     pedestalDisp->SaveAs("D:/CERN temp/analyze-Sune/Output/45/root/30.root"); }
   else{}}
else{}
if (index<32)
 {if (index>30)
      {pedestalDisp->SaveAs("D:/CERN temp/analyze-Sune/Output/45/gif/31.gif");
     pedestalDisp->SaveAs("D:/CERN temp/analyze-Sune/Output/45/root/31.root"); }
   else{}}
else{}
if (index<33)
 {if (index>31)
      {pedestalDisp->SaveAs("D:/CERN temp/analyze-Sune/Output/90/gif/32.gif");
     pedestalDisp->SaveAs("D:/CERN temp/analyze-Sune/Output/90/root/32.root");}
   else{}}
else{}
if (index<34)
 {if (index>32)
      {pedestalDisp->SaveAs("D:/CERN temp/analyze-Sune/Output/90/gif/33.gif");
     pedestalDisp->SaveAs("D:/CERN temp/analyze-Sune/Output/90/root/33.root"); }
   else{}}
else{}
if (index<35)
 {if (index>33)
```

```
      {pedestalDisp->SaveAs("D:/CERN temp/analyze-Sune/Output/90/gif/34.gif");
     pedestalDisp->SaveAs("D:/CERN temp/analyze-Sune/Output/90/root/34.root"); }
   else{}}
else{}
if (index<36)
 {if (index>34)
      {pedestalDisp->SaveAs("D:/CERN temp/analyze-Sune/Output/45/gif/35.gif");
     pedestalDisp->SaveAs("D:/CERN temp/analyze-Sune/Output/45/root/35.root");}
   else{}}
else{}
if (index<37)
 {if (index>35)
      {pedestalDisp->SaveAs("D:/CERN temp/analyze-Sune/Output/45/gif/36.gif");
     pedestalDisp->SaveAs("D:/CERN temp/analyze-Sune/Output/45/root/36.root"); }
   else{}}
else{}
if (index<38)
 {if (index>36)
      {pedestalDisp->SaveAs("D:/CERN temp/analyze-Sune/Output/45/gif/37.gif");
     pedestalDisp->SaveAs("D:/CERN temp/analyze-Sune/Output/45/root/37.root"); }
   else{}}
else{}
if (index<39)
 {if (index>37)
      {pedestalDisp->SaveAs("D:/CERN temp/analyze-Sune/Output/45/gif/38.gif");
     pedestalDisp->SaveAs("D:/CERN temp/analyze-Sune/Output/45/root/38.root"); }
   else{}}
else{}
if (index<40)
 {if (index>38)
      {pedestalDisp->SaveAs("D:/CERN temp/analyze-Sune/Output/45/gif/39.gif");
     pedestalDisp->SaveAs("D:/CERN temp/analyze-Sune/Output/45/root/39.root"); }
   else{}}
else{}
if (index<41)
 {if (index>39)
      {pedestalDisp->SaveAs("D:/CERN temp/analyze-Sune/Output/90/gif/40.gif");
     pedestalDisp->SaveAs("D:/CERN temp/analyze-Sune/Output/90/root/40.root");}
   else{}}
else{}
if (index<42)
 {if (index>40)
      {pedestalDisp->SaveAs("D:/CERN temp/analyze-Sune/Output/90/gif/41.gif");
     pedestalDisp->SaveAs("D:/CERN temp/analyze-Sune/Output/90/root/41.root"); }
   else{}}
else{}
if (index<43)
 {if (index>41)
      {pedestalDisp->SaveAs("D:/CERN temp/analyze-Sune/Output/90/gif/42.gif");
     pedestalDisp->SaveAs("D:/CERN temp/analyze-Sune/Output/90/root/42.root"); }
   else{}}
else{}
if (index<44)
 {if (index>42)
      {pedestalDisp->SaveAs("D:/CERN temp/analyze-Sune/Output/45/gif/43.gif");
     pedestalDisp->SaveAs("D:/CERN temp/analyze-Sune/Output/45/root/43.root"); }
   else{}}
else{}
if (index<45)
 {if (index>43)
      {pedestalDisp->SaveAs("D:/CERN temp/analyze-Sune/Output/45/gif/44.gif");
     pedestalDisp->SaveAs("D:/CERN temp/analyze-Sune/Output/45/root/44.root"); }
   else{}}
else{}
if (index<46)
 {if (index>44)
      {pedestalDisp->SaveAs("D:/CERN temp/analyze-Sune/Output/45/gif/45.gif");
     pedestalDisp->SaveAs("D:/CERN temp/analyze-Sune/Output/45/root/45.root"); }
```

```
   else{}}
else{}
if (index<47)
 {if (index>45)
      { pedestalDisp->SaveAs("D:/CERN temp/analyze-Sune/Output/45/gif/46.gif");
     pedestalDisp->SaveAs("D:/CERN temp/analyze-Sune/Output/45/root/46.root"); }
   else{}}
else{}
if (index<48)
 {if (index>46)
      {pedestalDisp->SaveAs("D:/CERN temp/analyze-Sune/Output/45/gif/47.gif");
     pedestalDisp->SaveAs("D:/CERN temp/analyze-Sune/Output/45/root/47.root"); }
   else{}}
else{}
if (index<49)
 {if (index>47)
      {pedestalDisp->SaveAs("D:/CERN temp/analyze-Sune/Output/90/gif/48.gif");
     pedestalDisp->SaveAs("D:/CERN temp/analyze-Sune/Output/90/root/48.root"); }
   else{}}
else{}
if (index<50)
 {if (index>48)
      {pedestalDisp->SaveAs("D:/CERN temp/analyze-Sune/Output/90/gif/49.gif");
     pedestalDisp->SaveAs("D:/CERN temp/analyze-Sune/Output/90/root/49.root");}
   else{}}
else{}
if (index<51)
 {if (index>49)
      {pedestalDisp->SaveAs("D:/CERN temp/analyze-Sune/Output/90/gif/50.gif");
     pedestalDisp->SaveAs("D:/CERN temp/analyze-Sune/Output/90/root/50.root");}
   else{}}
else{}
if (index<52)
 {if (index>50)
      { pedestalDisp->SaveAs("D:/CERN temp/analyze-Sune/Output/45/gif/51.gif");
     pedestalDisp->SaveAs("D:/CERN temp/analyze-Sune/Output/45/root/51.root"); }
   else{}}
else{}
if (index<53)
 {if (index>51)
      { pedestalDisp->SaveAs("D:/CERN temp/analyze-Sune/Output/45/gif/52.gif");
     pedestalDisp->SaveAs("D:/CERN temp/analyze-Sune/Output/45/root/52.root"); }
   else{}}
else{}
if (index<54)
 {if (index>52)
      { pedestalDisp->SaveAs("D:/CERN temp/analyze-Sune/Output/45/gif/53.gif");
     pedestalDisp->SaveAs("D:/CERN temp/analyze-Sune/Output/45/root/53.root"); }
   else{}}
else{}
if (index<55)
 {if (index>53)
      { pedestalDisp->SaveAs("D:/CERN temp/analyze-Sune/Output/45/gif/54.gif");
     pedestalDisp->SaveAs("D:/CERN temp/analyze-Sune/Output/45/root/54.root");}
   else{}}
else{}
if (index<56)
 {if (index>54)
      {pedestalDisp->SaveAs("D:/CERN temp/analyze-Sune/Output/45/gif/55.gif");
     pedestalDisp->SaveAs("D:/CERN temp/analyze-Sune/Output/45/root/55.root"); }
   else{}}
else{}
if (index<57)
 {if (index>55)
      {pedestalDisp->SaveAs("D:/CERN temp/analyze-Sune/Output/90/gif/56.gif");
     pedestalDisp->SaveAs("D:/CERN temp/analyze-Sune/Output/90/root/56.root"); }
   else{}}
else{}
```

Appendix H

```
    if (index<58)
     {if (index>56)
          {pedestalDisp->SaveAs("D:/CERN temp/analyze-Sune/Output/90/gif/57.gif");
         pedestalDisp->SaveAs("D:/CERN temp/analyze-Sune/Output/90/root/57.root");}
       else{}}
    else{}
    if (index<59)
     {if (index>57)
          {pedestalDisp->SaveAs("D:/CERN temp/analyze-Sune/Output/90/gif/58.gif");
         pedestalDisp->SaveAs("D:/CERN temp/analyze-Sune/Output/90/root/58.root"); }
       else{}}
    else{}
    if (index<60)
     {if (index>58)
          {pedestalDisp->SaveAs("D:/CERN temp/analyze-Sune/Output/45/gif/59.gif");
         pedestalDisp->SaveAs("D:/CERN temp/analyze-Sune/Output/45/root/59.root"); }
       else{}}
    else{}
    if (index<61)
     {if (index>59)
{        pedestalDisp->SaveAs("D:/CERN temp/analyze-Sune/Output/45/gif/60.gif");
         pedestalDisp->SaveAs("D:/CERN temp/analyze-Sune/Output/45/root/60.root"); }
       else{}}
    else{}
    if (index<62)
     {if (index>60)
          {pedestalDisp->SaveAs("D:/CERN temp/analyze-Sune/Output/45/gif/61.gif");
         pedestalDisp->SaveAs("D:/CERN temp/analyze-Sune/Output/45/root/61.root"); }
       else{}}
    else{}
    if (index<63)
     {if (index>61)
          { pedestalDisp->SaveAs("D:/CERN temp/analyze-Sune/Output/45/gif/62.gif");
         pedestalDisp->SaveAs("D:/CERN temp/analyze-Sune/Output/45/root/62.root"); }
       else{}}
    else  {  }
    if (index<64)
     {if (index>62)
          {pedestalDisp->SaveAs("D:/CERN temp/analyze-Sune/Output/45/gif/63.gif");
         pedestalDisp->SaveAs("D:/CERN temp/analyze-Sune/Output/45/root/63.root"); }
       else{}}
    else{  }

}
```

Light Yield in the ALFA Detector

NIELS BOHR INSTITUTE, UNIVERSITY OF COPENHAGEN, CERN, PH-ADO, Sune Jakobsen, jakobsen@nbi.dk

Absolute Luminosity For ATLAS

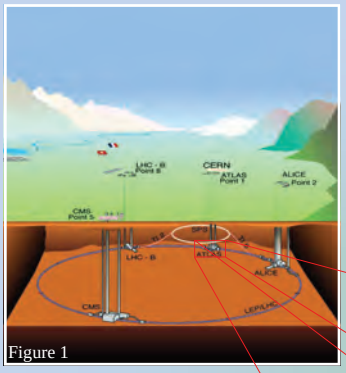

Figure 1

The large Hadron Collider (LHC) (figure 1)

- 50-175 m underground
- 27 km circumference circle
- 8.33 Tesla bending magnets
- 12 kA
- 1.9 Kelvin
- 14 TeV center of mass energy
- Proton-proton collision every 25 ns
- 4 large detectors
- Search for new physics

ATLAS (figure 2)

- Multipurpose detector
- The larges detector ever build: 46 m long and 26 m high
- Weighs about 7000 tons
- Inner part: tracking of particles
- Center part: energy calorimeters
- Outer part: Muon detection
- 3 level trigger system
- About 100 millions electrical readout channels
- About 200 Tbytes of data per year

ALFA – Absolute Luminosity For ATLAS

- Detected very small angels (~µrad)
- Detectors are about 240 m from the interaction point (figure 3 and 4)
- Detectors are about 1.5 mm from the beam
- One detector above the beam and one below the beam
- The positions of the detectors is adjustable both relative to the beam and relative to each other (figure 5)
- Secondary vacuum inside a Roman pot (figure 6) makes positioning very close to the beam possible

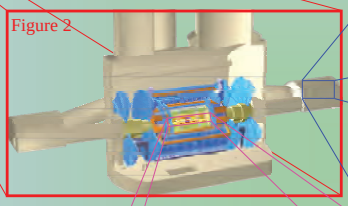
Figure 2

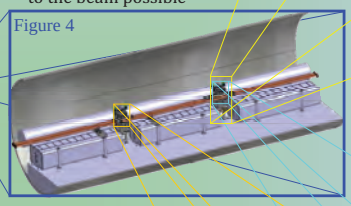
Figure 4

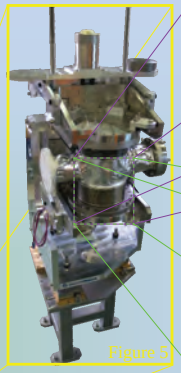
Figure 5

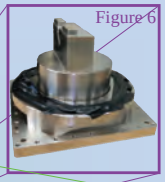
Figure 6

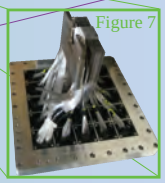
Figure 7

Luminosity

To know at what rate an interesting event occurs it is very imported to know how many protons actually collide head-on. One way to measure the rate of head-on collisions, the luminosity, is via Coulomb scattering. A well known fraction of the protons will not hit head-on, but scatter on one another. By measuring the angle and number of the scatted protons the absolute luminosity can be determined by fitting to the formula below.

$$\frac{dN}{dt} \approx L\pi \left| -\frac{2\alpha_{EM}}{|t|} + \frac{\sigma_{tot}}{4\pi}(i+\rho)\, e^{\frac{-b|t|}{2}} \right|^2$$

N	Number of interactions
$-t$	Four momentum transfer squared
L	Luminosity
α_{EM}	Electrometric cobbling constant
σ_{tot}	Totel cross section
ρ	Describs inelastic term (absorption)

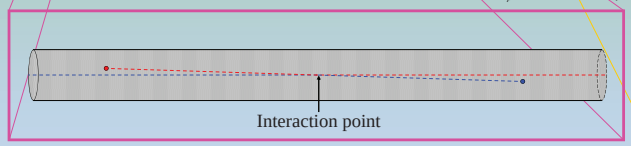

Figure 3

240 m 240 m

The detector (figure 7)

- 500 µm squared scintillating fibers
- 64 fibers in a layer
- Every second layer perpendicular to make a pixel like lattice
- 20 layers. Each layer shifted in position to get higher accumulated precision
- 2 scintillator tiles of full detector size for triggering the mean detector
- Read out by 64 channel multianode photomultipliers (MAPMT) (figure 8)
- Overlap detectors to determine the relative detector positions

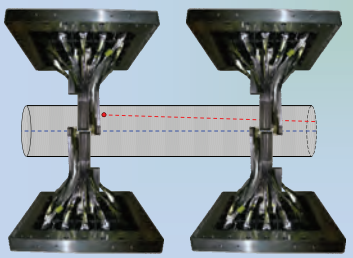

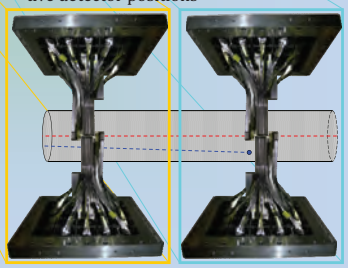

Light Yield Measurement

Motivation

In the summer of 2008 a proton beam test of a prototype Roman pot with the scintillating fiber detector inside was performed. The setup allowed only binary readout of the charge: over or under threshold. Some of the data interpretations done by the ALFA group suggest that significantly less light than expected is seen in a fiber hit by a particle. The detector has two types of fibers: 45° and 90° end cut, which could have different light yield. To investigate further a cosmic setup with analog charge readout was prepared.

Figure 8

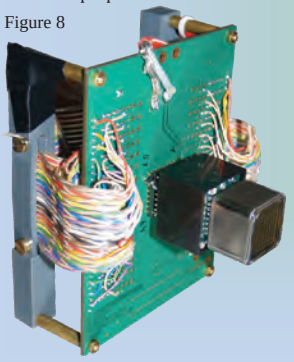

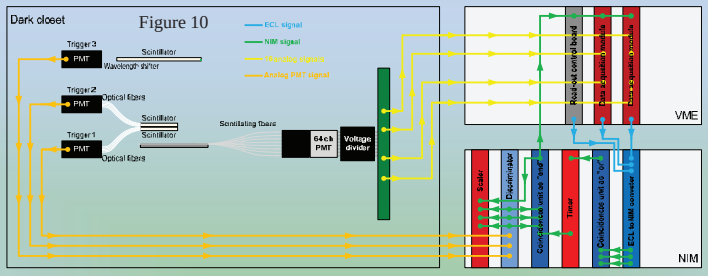

Figure 10

The cosmic setup (figure 9)

- One MAPMT (figure 8) calibrated with single photons from a pulsed LED
- Readout of a single detector layer
- The detector mounted in a black steel box for protection and support
- Triggering on the two built-in trigger scintillators and one external scintillator
- The connections and signal types are shown in figure 10.
- Data acquisition for one month due to low cosmic rate ,1 $\frac{counts}{cm^2 \cdot min}$, and small detector surface

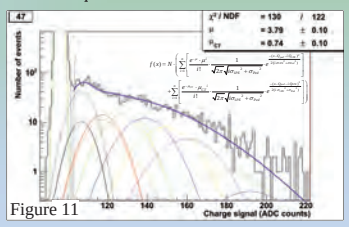

Figure 11

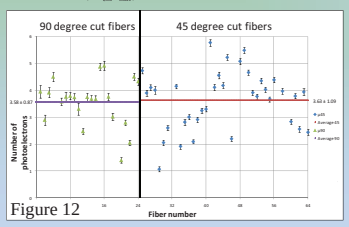

Figure 12

Data analyses and concussion

The charge histograms where fitted with a Poisson convoluted with a Gaussian (with an extra term for crosstalk where a fraction of light from a fiber is detected by an adjacent channel of the MAPMT) using the measured one photoelectron charge spectrum. A fit for one channel is shown in figure 11. The results for all channels are shown in figure 12. There is an average of about 3.6 photoelectrons for both 45° and 90° cut fibers, which is about the expected. It was therefore concluded that (most) fibers seems to have sufficient light yield.

Figure 9

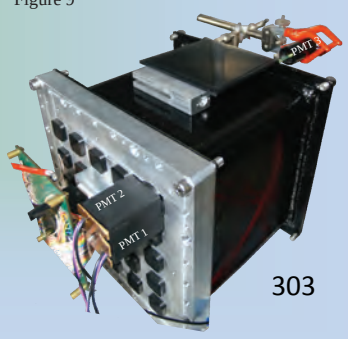

Figure references: Figure 1 and 2 are from the CERN webpage. Figure 4 and the luminosity formula are from "ATLAS Forward Detectors for Measurement of Elastic Scattering and Luminosity, Technical Design Report", ATLAS TDR 018, CERN/LHCC

Appendix J

From Maple:

Find the limits:

```
> limit1:=solve((w-
b)/2=d*tan(theta),theta);limit2:=solve(w/2=d*tan(theta),theta);limit
3:=solve((w+b)/2=d*tan(theta),theta);
```

$$limit1 := \arctan\left(\frac{w - b}{2\,d}\right)$$

$$limit2 := \arctan\left(\frac{w}{2\,d}\right)$$

$$limit3 := \arctan\left(\frac{w + b}{2\,d}\right)$$

Integrating until the fist limit:

```
>
I1:=int(cos(theta)^2*b^2/(w^2+4*(d*tan(theta))^2),theta=0..limit1);
```

$$I1 := \int_0^{\arctan\left(\frac{w - b}{2\,d}\right)} \frac{\cos(\theta)^2\, b^2}{w^2 + 4\,d^2\,\tan(\theta)^2}\, d\theta$$

Integrating between the limit1 and limit2:

```
> I2:=int(cos(theta)^2*(w^2-
4*d*tan(theta)*w+4*(d*tan(theta))^2+b^2)/(2*(w^2+4*(d*tan(theta))^2)
),theta=limit1..limit2);
```

$$I2 := \int_{\arctan\left(\frac{w - b}{2\,d}\right)}^{\arctan\left(\frac{w}{2\,d}\right)} \frac{\cos(\theta)^2\,(w^2 - 4\,d\,\tan(\theta)\,w + 4\,d^2\,\tan(\theta)^2 + b^2)}{2\,w^2 + 8\,d^2\,\tan(\theta)^2}\, d\theta$$

Integrating between the limit2 and limit3:

```
I3:=int(cos(theta)^2*(-w^2+4*d*tan(theta)*w-
4*(d*tan(theta))^2+b^2)/(8*d*tan(theta)*w),theta=limit2..limit3);
```

$$I3 := \int_{\arctan\left(\frac{w}{2\,d}\right)}^{\arctan\left(\frac{w+b}{2\,d}\right)} \frac{\cos(\theta)^2\,(-w^2 + 4\,d\,\tan(\theta)\,w - 4\,d^2\,\tan(\theta)^2 + b^2)}{8\,d\,\tan(\theta)\,w}\,d\theta$$

Integrating after the 2ed. limit until 90 degree (Pi/2) (just for the principle. It is know that this should be zero):

```
> I4:=int(cos(theta)^2*0,theta=limit2..Pi/2);
```

$$I4 := 0$$

Adding the integrals to one:

```
> Iall:=I1+I2+I3+I4;
```

$$Iall := \int_{0}^{\arctan\left(\frac{w-b}{2\,d}\right)} \frac{\cos(\theta)^2\,b^2}{w^2 + 4\,d^2\,\tan(\theta)^2}\,d\theta + \int_{\arctan\left(\frac{w-b}{2\,d}\right)}^{\arctan\left(\frac{w}{2\,d}\right)} \frac{\cos(\theta)^2\,(w^2 - 4\,d\,\tan(\theta)\,w + 4\,d^2\,\tan(\theta)^2 + b^2)}{2\,w^2 + 8\,d^2\,\tan(\theta)^2}\,d\theta + \int_{\arctan\left(\frac{w}{2\,d}\right)}^{\arctan\left(\frac{w+b}{2\,d}\right)} \frac{\cos(\theta)^2\,(-w^2 + 4\,d\,\tan(\theta)\,w - 4\,d^2\,\tan(\theta)^2 + b^2)}{8\,d\,\tan(\theta)\,w}\,d\theta$$

Calculating f:

```
> f:=Iall/Int(cos(theta)^2,theta=0..Pi/2);
```

Appendix J

$$f := \frac{1}{\int_0^{\frac{1}{2}\pi} \cos(\theta)^2 \, d\theta} \left(\int_0^{\arctan\left(\frac{w-b}{2d}\right)} \frac{\cos(\theta)^2 b^2}{w^2 + 4d^2 \tan(\theta)^2} \, d\theta + \int_{\arctan\left(\frac{w}{2d}\right)}^{\arctan\left(\frac{w-b}{2d}\right)} \frac{\cos(\theta)^2 (w^2 - 4d\tan(\theta) w + 4d^2 \tan(\theta)^2 + b^2)}{2w^2 + 8d^2 \tan(\theta)^2} \, d\theta + \int_{\arctan\left(\frac{w}{2d}\right)}^{\arctan\left(\frac{w+b}{2d}\right)} \frac{\cos(\theta)^2 (-w^2 + 4d\tan(\theta) w - 4d^2 \tan(\theta)^2 + b^2)}{8d\tan(\theta) w} \, d\theta \right)$$

Input variabels:

Distance between the scintillators:

```
> d:=115;
```

$$d := 115$$

Diameter of the top scintillator:

```
> w:=120;
```

$$w := 120$$

Diameter of the bottom scintillator:

```
> b:=32;
```

$$b := 32$$

Numerical result of f:

```
> evalf(f);
```

$$0.03210526657$$

Count rate:

```
> evalf(f)*(w/20)^2*3.14159265359;
```

$$3.631020106$$

Appendix K

MC.C:

```
#include "TMultiGraph.h"
#include "TFile.h"
#include "TTree.h"
#include "TBrowser.h"
#include "TH2.h"
#include "TRandom.h"
#include "TMath.h"
#include <iostream>
#include <fstream>
#include "TStyle.h"
#include "TText.h"
#include <TRandom1.h>
#include <TRandom2.h>
#include <TRandom3.h>
#include <TStopwatch.h>
#include <TF1.h>
#include <TUnuran.h>
#include <TUnuranContDist.h>
#include <TFile.h>

#ifndef ROOT_TRandom3
#define ROOT_TRandom3
#ifndef ROOT_TRandom
#include "TRandom.h"
#endif

#include <TRandom3.h>

#include <TH1I.h>
#include <TH1F.h>
//#include <TH2I.h>
#include <TFile.h>
#include <TCanvas.h>
#include <TVirtualPad.h>
//#include <TF1.h>

//Number of event
Double_t N = 10000;

void MC(int Seed){
 TRandom3* ran = new TRandom3(Seed);
 TRandom* ran2 = new TRandom(Seed);
  char* ROOTname = "ped_1pe.root";
  tFileOut = new TFile(ROOTname,"RECREATE");
  TH1I* histo = new TH1I("0","ADC histo",250,0.,25);
 for (int i=0; i<N; ++i){

   Double_t phi =ran->Rndm()*TMath::Pi()/2;
   Double_t b =4;//wide of active fiber
   Double_t w =30/480*b;//wide of inactive area between fibers
   Double_t p =ran->Rndm()*b;

   //Cosmic
   TF1 *f1 = new TF1("f1","pow(cos(x),2)",0,TMath::Pi()/2);

   //Beam
// TF1 *f1 = new TF1("f1","pow(cos(x),2)",0,0.0001);


Double_t theta = f1->GetRandom();


 Double_t ziro=0.006;
 //Fiber 1.
  if(theta > 0 || theta < atan((b-p)/(b*cos(phi))))
```

```
      {
        Double_t lr=b/(cos(theta));
        Double_t lr2=ziro;
        Double_t lr3=ziro;
        Double_t lr4=ziro;
        Double_t lr5=ziro;
        Double_t lr6=ziro;
      }
     //Space between fiber 1 and 2.
    if(theta >= atan((b-p)/(b*cos(phi))))
      {if( theta < atan((b+w-p)/(b*cos(phi))))
          {
       Double_t lr=(b-p)/((cos(phi)*cos(TMath::Pi()/2-theta)));
       Double_t lr2=ziro;
       Double_t lr3=ziro;
       Double_t lr4=ziro;
       Double_t lr5=ziro;
       Double_t lr6=ziro;
     }}
    //Fiber 2.
    if(theta >= atan((b+w-p)/(b*cos(phi))))
      {if( theta < atan((2*b+w-p)/(b*cos(phi))))
          {
       Double_t lr=(b-p)/((cos(phi)*cos(TMath::Pi()/2-theta)));
       Double_t lr2=b/(cos(theta))-lr-w/((cos(phi)*cos(TMath::Pi()/2-theta)));
       Double_t lr3=ziro;
       Double_t lr4=ziro;
       Double_t lr5=ziro;
       Double_t lr6=ziro;
    }}
    //Space between fiber 2 and 3.
    if(theta >= atan((2*b+w-p)/(b*cos(phi))))
      {if( theta < atan((2*b+2*w-p)/(b*cos(phi))))
          {
       Double_t lr=(b-p)/(cos(phi)*cos(TMath::Pi()/2-theta));
       Double_t lr2=(2*b-p)/(cos(phi)*cos(TMath::Pi()/2-theta))-lr-
w/((cos(phi)*cos(TMath::Pi()/2-theta)));
       Double_t lr3=Ziro;
       Double_t lr4=ziro;
       Double_t lr5=ziro;
       Double_t lr6=ziro;
    }}
    //Fiber 3.
    if(theta >= atan((2*b+2*w-p)/(b*cos(phi))))
      {if( theta < atan((3*b+2*w-p)/(b*cos(phi))))
          {
       Double_t lr=(b-p)/(cos(phi)*cos(TMath::Pi()/2-theta));
       Double_t lr2=(2*b-p)/(cos(phi)*cos(TMath::Pi()/2-theta))-lr-
w/((cos(phi)*cos(TMath::Pi()/2-theta)));
       Double_t lr3=b/(cos(theta))-lr2-lr-2*w/((cos(phi)*cos(TMath::Pi()/2-theta)));
       Double_t lr4=ziro;
       Double_t lr5=ziro;
       Double_t lr6=ziro;
    }}
    //Space between fiber 3 and 4.
    if(theta >= atan((3*b+2*w-p)/(b*cos(phi))))
      {if( theta < atan((3*b+3*w-p)/(b*cos(phi))))
          {
       Double_t lr=(b-p)/(cos(phi)*cos(TMath::Pi()/2-theta));
       Double_t lr2=(2*b-p)/(cos(phi)*cos(TMath::Pi()/2-theta))-lr-
w/((cos(phi)*cos(TMath::Pi()/2-theta)));
       Double_t lr3=(3*b-p)/(cos(phi)*cos(TMath::Pi()/2-theta))-lr2-lr-
2*w/((cos(phi)*cos(TMath::Pi()/2-theta)));
       Double_t lr4=ziro;
       Double_t lr5=ziro;
       Double_t lr6=ziro;
    }}
    //Fiber 4.
```

Appendix K

```
 if(theta >= atan((3*b+3*w-p)/(b*cos(phi))))
    {if( theta < atan((4*b+3*w-p)/(b*cos(phi))))
         {
     Double_t lr=(b-p)/(cos(phi)*cos(TMath::Pi()/2-theta));
     Double_t lr2=(2*b-p)/(cos(phi)*cos(TMath::Pi()/2-theta))-lr-
w/((cos(phi)*cos(TMath::Pi()/2-theta)));
     Double_t lr3=(3*b-p)/(cos(phi)*cos(TMath::Pi()/2-theta))-lr2-lr-
2*w/((cos(phi)*cos(TMath::Pi()/2-theta)));
     Double_t lr4=b/(cos(theta))-lr3-lr2-lr-3*w/((cos(phi)*cos(TMath::Pi()/2-
theta)));
     Double_t lr5=ziro;
     Double_t lr6=ziro;
 }}
 //Space between fiber 4 and 5.
 if(theta >= atan((4*b+3*w-p)/(b*cos(phi))))
    {if( theta < atan((4*b+4*w-p)/(b*cos(phi))))
         {
     Double_t lr=(b-p)/(cos(phi)*cos(TMath::Pi()/2-theta));
     Double_t lr2=(2*b-p)/(cos(phi)*cos(TMath::Pi()/2-theta))-lr-
w/((cos(phi)*cos(TMath::Pi()/2-theta)));
     Double_t lr3=(3*b-p)/(cos(phi)*cos(TMath::Pi()/2-theta))-lr2-lr-
2*w/((cos(phi)*cos(TMath::Pi()/2-theta)));
     Double_t lr4=(4*b-p)/(cos(phi)*cos(TMath::Pi()/2-theta))-lr3-lr2-lr-
3*w/((cos(phi)*cos(TMath::Pi()/2-theta)));
     Double_t lr5=ziro;
     Double_t lr6=ziro;
 }}
 //Fiber 5.
 if(theta >= atan((4*b+4*w-p)/(b*cos(phi))))
    {if( theta < atan((5*b+4*w-p)/(b*cos(phi))))
         {
     Double_t lr=(b-p)/(cos(phi)*cos(TMath::Pi()/2-theta));
     Double_t lr2=(2*b-p)/(cos(phi)*cos(TMath::Pi()/2-theta))-lr-
w/((cos(phi)*cos(TMath::Pi()/2-theta)));
     Double_t lr3=(3*b-p)/(cos(phi)*cos(TMath::Pi()/2-theta))-lr2-lr-
2*w/((cos(phi)*cos(TMath::Pi()/2-theta)));
     Double_t lr4=(4*b-p)/(cos(phi)*cos(TMath::Pi()/2-theta))-lr3-lr2-lr-
3*w/((cos(phi)*cos(TMath::Pi()/2-theta)));
     Double_t lr5=b/(cos(theta))-lr4-lr3-lr2-lr-4*w/((cos(phi)*cos(TMath::Pi()/2-
theta)));
     Double_t lr6=ziro;
 }}
 //Space between fiber 5 and 6.
 if(theta >= atan((5*b+4*w-p)/(b*cos(phi))))
    {if( theta < atan((5*b+5*w-p)/(b*cos(phi))))
         {
     Double_t lr=(b-p)/(cos(phi)*cos(TMath::Pi()/2-theta));
     Double_t lr2=(2*b-p)/(cos(phi)*cos(TMath::Pi()/2-theta))-lr-
w/((cos(phi)*cos(TMath::Pi()/2-theta)));
     Double_t lr3=(3*b-p)/(cos(phi)*cos(TMath::Pi()/2-theta))-lr2-lr-
2*w/((cos(phi)*cos(TMath::Pi()/2-theta)));
     Double_t lr4=(4*b-p)/(cos(phi)*cos(TMath::Pi()/2-theta))-lr3-lr2-lr-
3*w/((cos(phi)*cos(TMath::Pi()/2-theta)));
     Double_t lr5=(5*b-p)/(cos(phi)*cos(TMath::Pi()/2-theta))-lr3-lr2-lr-
4*w/((cos(phi)*cos(TMath::Pi()/2-theta)));
     Double_t lr6=ziro;
 }}
//Fiber 6.
if(theta >= atan((5*b+5*w-p)/(b*cos(phi))))
   {
     Double_t lr=(b-p)/(cos(phi)*cos(TMath::Pi()/2-theta));
     Double_t lr2=(2*b-p)/(cos(phi)*cos(TMath::Pi()/2-theta))-lr-
w/((cos(phi)*cos(TMath::Pi()/2-theta)));
     Double_t lr3=(3*b-p)/(cos(phi)*cos(TMath::Pi()/2-theta))-lr2-lr-
2*w/((cos(phi)*cos(TMath::Pi()/2-theta)));
     Double_t lr4=(4*b-p)/(cos(phi)*cos(TMath::Pi()/2-theta))-lr3-lr2-lr-
3*w/((cos(phi)*cos(TMath::Pi()/2-theta)));
```

Appendix K

```
     Double_t lr5=(5*b-p)/(cos(phi)*cos(TMath::Pi()/2-theta))-lr4-lr3-lr2-lr-
4*w/((cos(phi)*cos(TMath::Pi()/2-theta)));
     Double_t lr6=(6*b-p)/(cos(phi)*cos(TMath::Pi()/2-theta))-lr5-lr4-lr3-lr2-lr-
5*w/((cos(phi)*cos(TMath::Pi()/2-theta)));
 }


 Double_t p1 = ran->Poisson(lr);
 Double_t p2 = ran->Poisson(lr2);
 Double_t p3 = ran->Poisson(lr3);
 Double_t p4 = ran->Poisson(lr4);
 Double_t p5 = ran->Poisson(lr5);
 Double_t p6 = ran->Poisson(lr6);


 Double_t sigmaPed = 0.15;
 Double_t sigma = 1.0;

 Double_t g1 =ran->Gaus(p1,sqrt(pow(sigmaPed,2)+p1*pow(sigma,2)));
 Double_t g2 =ran->Gaus(p2,sqrt(pow(sigmaPed,2)+p2*pow(sigma,2)));
 Double_t g3 =ran->Gaus(p3,sqrt(pow(sigmaPed,2)+p3*pow(sigma,2)));
 Double_t g4 =ran->Gaus(p4,sqrt(pow(sigmaPed,2)+p4*pow(sigma,2)));
 Double_t g5 =ran->Gaus(p5,sqrt(pow(sigmaPed,2)+p5*pow(sigma,2)));
 Double_t g6 =ran->Gaus(p6,sqrt(pow(sigmaPed,2)+p6*pow(sigma,2)));


 //Histogram


 histo->Fill(g1);
 histo->Fill(g2);
 histo->Fill(g3);
 histo->Fill(g4);
 histo->Fill(g5);
 histo->Fill(g6);

 Double_t CT1 = 0.0081;
 Double_t CT2 = 0.0085;
 Double_t CT3 = 0.0062;
 Double_t CT4 = 0.0058;

 //Crosstalk from 1st fiber hit
Double_t pCT1 =ran->Poisson(lr*CT1);
Double_t pCT2 =ran->Poisson(lr*CT2);
Double_t pCT3 =ran->Poisson(lr*CT3);
Double_t pCT4 =ran->Poisson(lr*CT4);
Double_t gCT1 =ran->Gaus(pCT1,sqrt(pow(sigmaPed,2)+pCT1*pow(sigma,2)));
Double_t gCT2 =ran->Gaus(pCT2,sqrt(pow(sigmaPed,2)+pCT2*pow(sigma,2)));
Double_t gCT3 =ran->Gaus(pCT3,sqrt(pow(sigmaPed,2)+pCT3*pow(sigma,2)));
Double_t gCT4 =ran->Gaus(pCT4,sqrt(pow(sigmaPed,2)+pCT4*pow(sigma,2)));
histo->Fill(gCT1);
histo->Fill(gCT2);
histo->Fill(gCT3);
histo->Fill(gCT4);

 //Crosstalk from 2nd fiber hit
Double_t pCT1 =ran->Poisson(lr2*CT1);
Double_t pCT2 =ran->Poisson(lr2*CT2);
Double_t pCT3 =ran->Poisson(lr2*CT3);
Double_t pCT4 =ran->Poisson(lr2*CT4);
Double_t gCT1 =ran->Gaus(pCT1,sqrt(pow(sigmaPed,2)+pCT1*pow(sigma,2)));
Double_t gCT2 =ran->Gaus(pCT2,sqrt(pow(sigmaPed,2)+pCT2*pow(sigma,2)));
Double_t gCT3 =ran->Gaus(pCT3,sqrt(pow(sigmaPed,2)+pCT3*pow(sigma,2)));
Double_t gCT4 =ran->Gaus(pCT4,sqrt(pow(sigmaPed,2)+pCT4*pow(sigma,2)));
histo->Fill(gCT1);
histo->Fill(gCT2);
histo->Fill(gCT3);
histo->Fill(gCT4);
```

Appendix K

```
 //Crosstalk from 3th fiber hit
Double_t pCT1 =ran->Poisson(lr3*CT1);
Double_t pCT2 =ran->Poisson(lr3*CT2);
Double_t pCT3 =ran->Poisson(lr3*CT3);
Double_t pCT4 =ran->Poisson(lr3*CT4);
Double_t gCT1 =ran->Gaus(pCT1,sqrt(pow(sigmaPed,2)+pCT1*pow(sigma,2)));
Double_t gCT2 =ran->Gaus(pCT2,sqrt(pow(sigmaPed,2)+pCT2*pow(sigma,2)));
Double_t gCT3 =ran->Gaus(pCT3,sqrt(pow(sigmaPed,2)+pCT3*pow(sigma,2)));
Double_t gCT4 =ran->Gaus(pCT4,sqrt(pow(sigmaPed,2)+pCT4*pow(sigma,2)));
histo->Fill(gCT1);
histo->Fill(gCT2);
histo->Fill(gCT3);
histo->Fill(gCT4);

 //Crosstalk from 4th fiber hit
Double_t pCT1 =ran->Poisson(lr4*CT1);
Double_t pCT2 =ran->Poisson(lr4*CT2);
Double_t pCT3 =ran->Poisson(lr4*CT3);
Double_t pCT4 =ran->Poisson(lr4*CT4);
Double_t gCT1 =ran->Gaus(pCT1,sqrt(pow(sigmaPed,2)+pCT1*pow(sigma,2)));
Double_t gCT2 =ran->Gaus(pCT2,sqrt(pow(sigmaPed,2)+pCT2*pow(sigma,2)));
Double_t gCT3 =ran->Gaus(pCT3,sqrt(pow(sigmaPed,2)+pCT3*pow(sigma,2)));
Double_t gCT4 =ran->Gaus(pCT4,sqrt(pow(sigmaPed,2)+pCT4*pow(sigma,2)));
histo->Fill(gCT1);
histo->Fill(gCT2);
histo->Fill(gCT3);
histo->Fill(gCT4);

 //Crosstalk from 5th fiber hit
Double_t pCT1 =ran->Poisson(lr5*CT1);
Double_t pCT2 =ran->Poisson(lr5*CT2);
Double_t pCT3 =ran->Poisson(lr5*CT3);
Double_t pCT4 =ran->Poisson(lr5*CT4);
Double_t gCT1 =ran->Gaus(pCT1,sqrt(pow(sigmaPed,2)+pCT1*pow(sigma,2)));
Double_t gCT2 =ran->Gaus(pCT2,sqrt(pow(sigmaPed,2)+pCT2*pow(sigma,2)));
Double_t gCT3 =ran->Gaus(pCT3,sqrt(pow(sigmaPed,2)+pCT3*pow(sigma,2)));
Double_t gCT4 =ran->Gaus(pCT4,sqrt(pow(sigmaPed,2)+pCT4*pow(sigma,2)));
histo->Fill(gCT1);
histo->Fill(gCT2);
histo->Fill(gCT3);
histo->Fill(gCT4);

 //Crosstalk from 6th fiber hit
Double_t pCT1 =ran->Poisson(lr6*CT1);
Double_t pCT2 =ran->Poisson(lr6*CT2);
Double_t pCT3 =ran->Poisson(lr6*CT3);
Double_t pCT4 =ran->Poisson(lr6*CT4);
Double_t gCT1 =ran->Gaus(pCT1,sqrt(pow(sigmaPed,2)+pCT1*pow(sigma,2)));
Double_t gCT2 =ran->Gaus(pCT2,sqrt(pow(sigmaPed,2)+pCT2*pow(sigma,2)));
Double_t gCT3 =ran->Gaus(pCT3,sqrt(pow(sigmaPed,2)+pCT3*pow(sigma,2)));
Double_t gCT4 =ran->Gaus(pCT4,sqrt(pow(sigmaPed,2)+pCT4*pow(sigma,2)));
histo->Fill(gCT1);
histo->Fill(gCT2);
histo->Fill(gCT3);
histo->Fill(gCT4);


 ofstream myfiletheta;            //SJ
  myfiletheta.open ("D:/CERN temp/MC fiber/Output/theta.dat", ios::app);   //SJ
  myfiletheta << theta;   //SJ
  myfiletheta<<"\n";   //SJ
  myfiletheta.close();

 ofstream myfilephi;            //SJ
  myfilephi.open ("D:/CERN temp/MC fiber/Output/phi.dat", ios::app);   //SJ
  myfilephi << phi;   //SJ
  myfilephi<<"\n";   //SJ
```

```
 myfilephi.close();

ofstream myfilep;            //SJ
 myfilep.open ("D:/CERN temp/MC fiber/Output/p.dat", ios::app);   //SJ
 myfilep << p;   //SJ
 myfilep<<"\n";   //SJ
 myfilep.close();

ofstream myfilelr;            //SJ
 myfilelr.open ("D:/CERN temp/MC fiber/Output/lr.dat", ios::app);   //SJ
 myfilelr << lr;   //SJ
 myfilelr<<"\n";   //SJ
 myfilelr.close();

ofstream myfilelr2;            //SJ
 myfilelr2.open ("D:/CERN temp/MC fiber/Output/lr2.dat", ios::app);   //SJ
 myfilelr2 << lr2;   //SJ
 myfilelr2<<"\n";   //SJ
 myfilelr2.close();

ofstream myfilelr3;            //SJ
 myfilelr3.open ("D:/CERN temp/MC fiber/Output/lr3.dat", ios::app);   //SJ
 myfilelr3 << lr3;   //SJ
 myfilelr3<<"\n";   //SJ
 myfilelr3.close();

ofstream myfilelr4;            //SJ
 myfilelr4.open ("D:/CERN temp/MC fiber/Output/lr4.dat", ios::app);   //SJ
 myfilelr4 << lr4;   //SJ
 myfilelr4<<"\n";   //SJ
 myfilelr4.close();

ofstream myfilelr5;            //SJ
 myfilelr5.open ("D:/CERN temp/MC fiber/Output/lr5.dat", ios::app);   //SJ
 myfilelr5 << lr5;   //SJ
 myfilelr5<<"\n";   //SJ
 myfilelr5.close();

ofstream myfilelr6;            //SJ
 myfilelr6.open ("D:/CERN temp/MC fiber/Output/lr6.dat", ios::app);   //SJ
 myfilelr6 << lr6;   //SJ
 myfilelr6<<"\n";   //SJ
 myfilelr6.close();

ofstream myfilep1;            //SJ
 myfilep1.open ("D:/CERN temp/MC fiber/Output/p1.dat", ios::app);   //SJ
 myfilep1 << p1;   //SJ
 myfilep1<<"\n";   //SJ
 myfilep1.close();

ofstream myfilep2;            //SJ
 myfilep2.open ("D:/CERN temp/MC fiber/Output/p2.dat", ios::app);   //SJ
 myfilep2 << p2;   //SJ
 myfilep2<<"\n";   //SJ
 myfilep2.close();

ofstream myfilep3;            //SJ
 myfilep3.open ("D:/CERN temp/MC fiber/Output/p3.dat", ios::app);   //SJ
 myfilep3 << p3;   //SJ
 myfilep3<<"\n";   //SJ
 myfilep3.close();

ofstream myfilep4;            //SJ
 myfilep4.open ("D:/CERN temp/MC fiber/Output/p4.dat", ios::app);   //SJ
 myfilep4 << p4;   //SJ
 myfilep4<<"\n";   //SJ
 myfilep4.close();
```

Appendix K

```
 ofstream myfilep5;            //SJ
  myfilep5.open ("D:/CERN temp/MC fiber/Output/p5.dat", ios::app);   //SJ
  myfilep5 << p5;   //SJ
  myfilep5<<"\n";   //SJ
  myfilep5.close();

 ofstream myfilep6;            //SJ
  myfilep6.open ("D:/CERN temp/MC fiber/Output/p6.dat", ios::app);   //SJ
  myfilep6 << p6;   //SJ
  myfilep6<<"\n";   //SJ
  myfilep6.close();

 ofstream myfileg1;            //SJ
  myfileg1.open ("D:/CERN temp/MC fiber/Output/g1.dat", ios::app);   //SJ
  myfileg1 << g1;   //SJ
  myfileg1<<"\n";   //SJ
  myfileg1.close();


}
  tFileOut->Write();
  tFileOut->Close();
}
```

Version 2

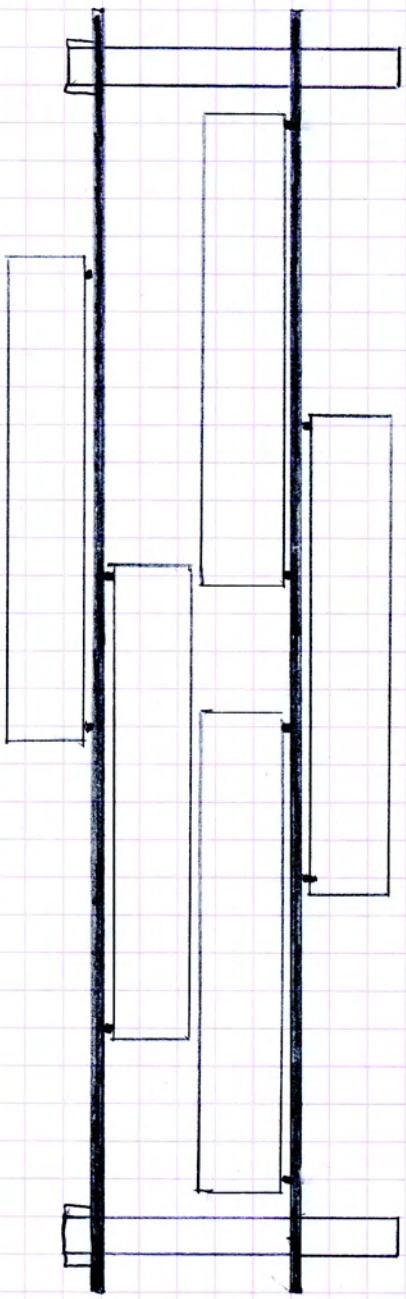

50

1:2

version 2

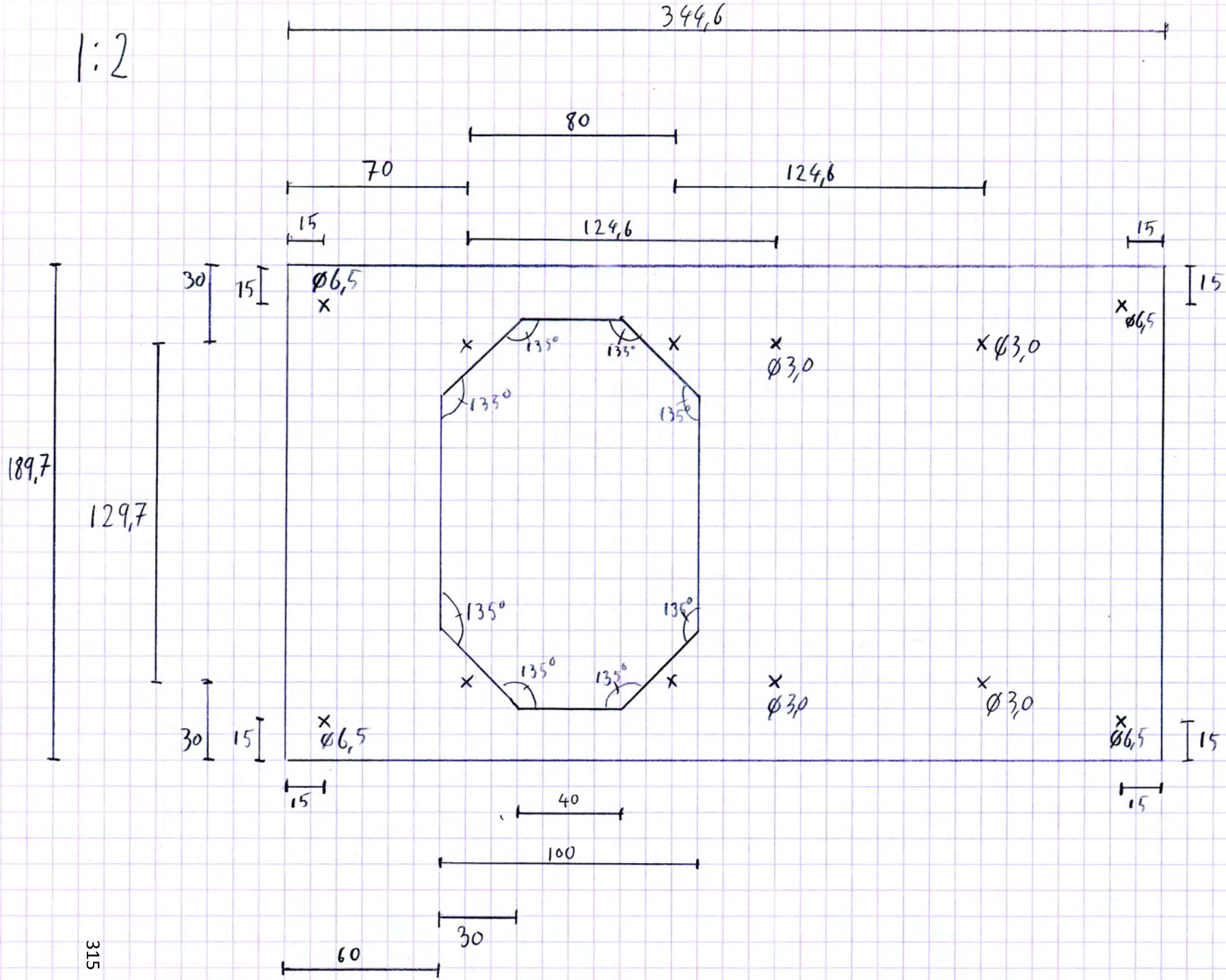
344,6
80
70
124,6
15
124,6
15
30
15
Ø6,5
15
Ø6,5
135°
135°
135°
135°
Ø3,0
Ø3,0
189,7
129,7
135°
135°
135°
135°
30
15
Ø6,5
Ø3,0
Ø3,0
Ø6,5
15
15
15
40
100
30
60

1 : 2

version 2

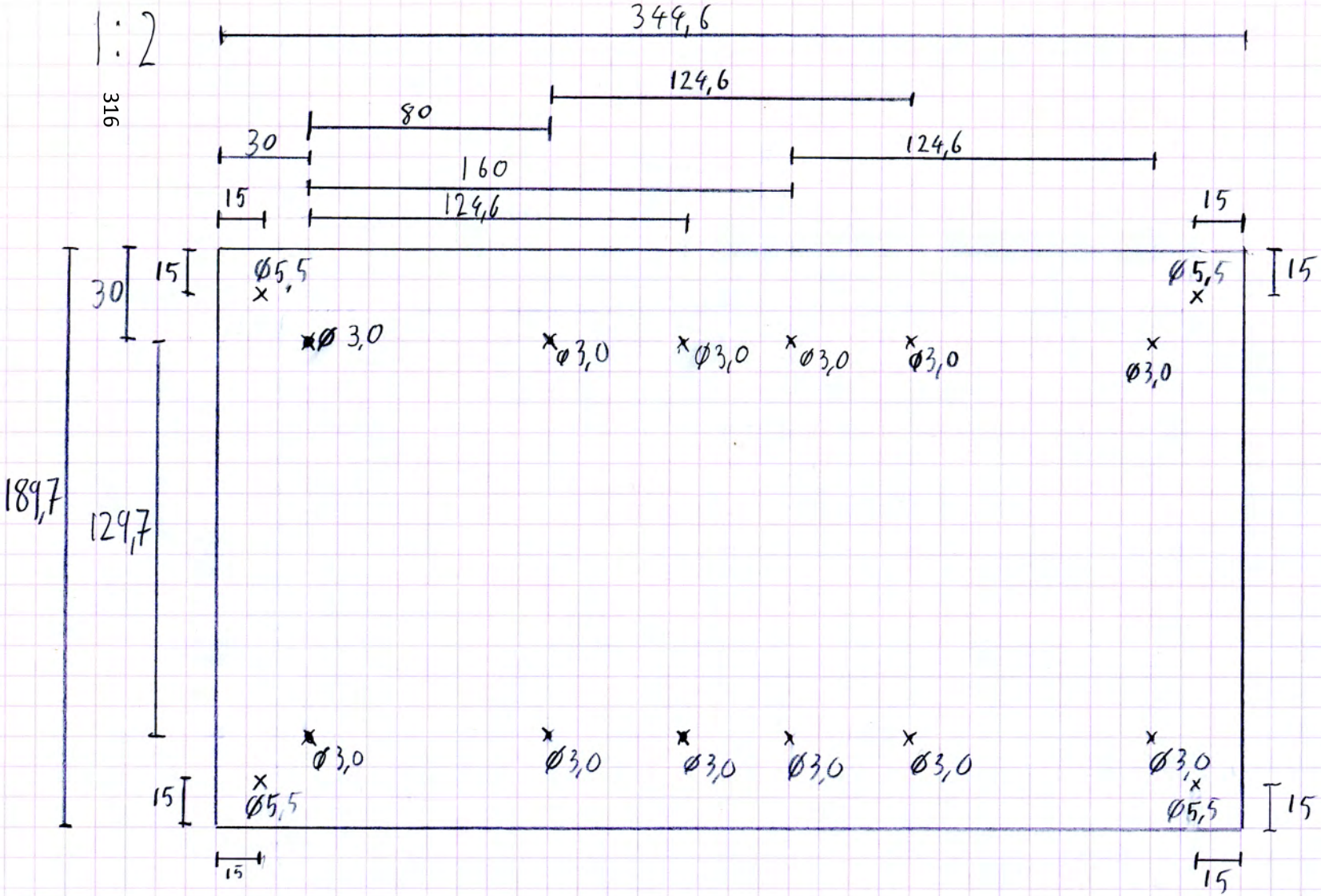
349,6
124,6
80
30
124,6
160
15
124,6
15
30
15
Ø5,5
Ø3,0
15
189,7
129,7
15
15
15

1:1

version 2

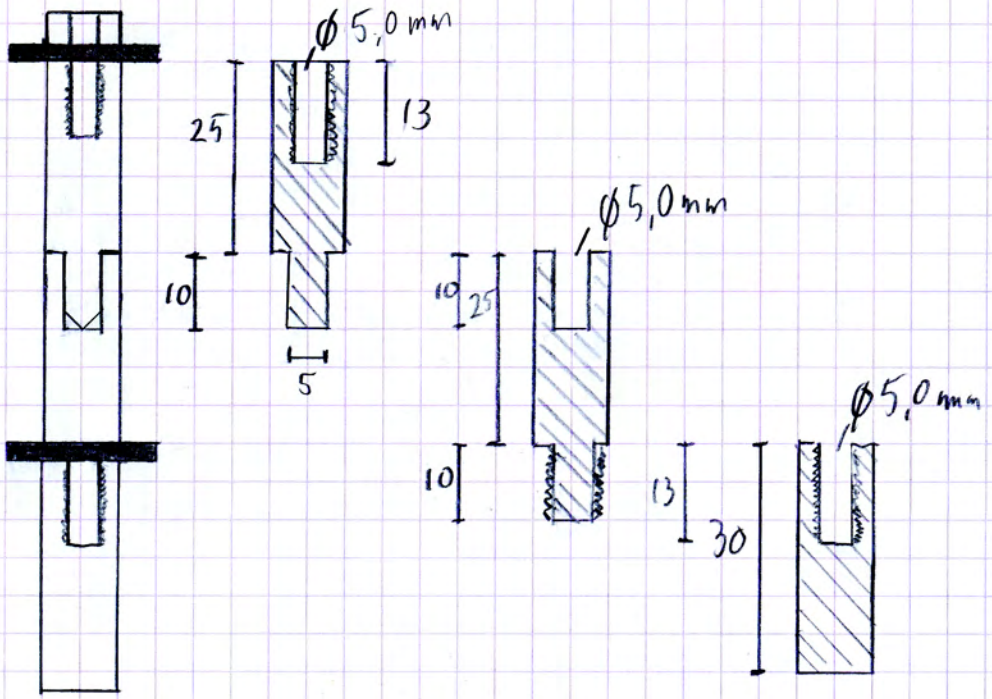

Appendix M

Cal1PE.C:

```
#include "TMultiGraph.h"
#include "TFile.h"
#include "TTree.h"
#include "TBrowser.h"
#include "TH2.h"
#include "TRandom.h"
#include "TMath.h"
#include <iostream>
#include <fstream>
#include "TStyle.h"
#include "TText.h"
#include <iomanip>
#include <stdio.h>
#include "TSystem.h"



Double_t fit1pe(Double_t *x, Double_t *par)
{

  Double_t result1=0.;

  for (Int_t i=0;i<15;i++)
    {

      Double_t fac=1;
         if(i<1)
        {fac=1;}
      else{
 for (Int_t var=1;var<i+1;var++)
        {
          fac *= var;
        }}

      Double_t P = (TMath::Exp((-1.)*par[0])*par[0]**i)/(fac);
      Double_t G1 =
1./((TMath::Sqrt(2.*TMath::Pi())*(TMath::Sqrt((i*par[3]**2+par[2]**2)))) ;
      Double_t G2 = TMath::Exp( ( (-1.) * (x[0] - par[5] - i*(par[1]))**2
)/(2.*(i*par[3]**2+par[2]**2)));

      result1 += P * G1 * G2;
    }

 Double_t result = result1;
 result *= par[4];
  return result;
 // return  result2;
}



Double_t peFct(Double_t *x, Double_t *param)
{
  Double_t result = 0.;
  Double_t fact = 1;
  for (Int_t var=1;var<param[6]+1;var++)
    fact *= var;

      Double_t P = (TMath::Exp((-1.) * param[0]) * param[0]**param[6])/fact;
      Double_t G1 =
1./((TMath::Sqrt(2.*TMath::Pi())*(TMath::Sqrt((param[6]*param[3]**2+param[2]**2))))
) ;
      Double_t G2 = TMath::Exp( ( (-1.) * (x[0] - param[5] -
param[6]*(param[1]))**2 )/(2.*(param[6]*param[3]**2+param[2]**2)));
```

Appendix M

```
result += P * G1 * G2;
 result *= param[4];
return result;
}


void Cal1PE(int Runnr, int PMTnr, int index)
{
  //Create, fill and display raw data
  TString directory3 = ;
 directory3+= "Run_";
 directory3+= Runnr;
 // gSystem->MakeDirectory(directory);
directory3+= "/";
 directory3+= PMTnr;
 directory3+= "/";
TFile *file = new TFile(directory3+"ped_1pe.root");
  TH1I *pedestal;
  char str[2];
  sprintf(str,"%d",index);
  pedestal = (TH1I*) gDirectory->Get(str);
  pedestal->GetYaxis()->SetTitle("Number of events");
  pedestal->GetXaxis()->SetTitle("Charge signal (ADC counts)");



   TF1* gaussPE;

  TCanvas *pedestalDisp = new TCanvas("cavas","pedestal - 1pe",200,60,700,700);
   pedestalDisp->SetLogy();
  pedestalDisp->cd();
  pedestalDisp->SetFillColor(0);
  pedestalDisp->SetFrameFillColor(0);
  pedestal->Draw();



  //Evaluate 1pe characteristics
  cout << "Pedestal " << index << endl;
  Double_t pedX, pedX2,singleX,pedRMS,pX,pRMS,pConstant;
    pedX2 = pedestal->GetMaximumBin();

    //bad data: All at max:
 if(pedX2>390){
     pedX2=390;}

    //  Float_t MinFitInt = pedX2*10-700;
    //     Float_t MaxFitInt = pedX2*10+700;


    if (pedX2<250){
     Float_t MinFitInt = pedX2*10-25;
     Float_t MaxFitInt = pedX2*10+70;
}
else {
     Float_t MinFitInt = pedX2*10-10;
     Float_t MaxFitInt = pedX2*10+10;
     }

    //  Float_t MinFitInt = 1100;
    //  Float_t MaxFitInt = 1200;

 ofstream filepedX2;            //SJ
 filepedX2.open ("d:/pedX2.dat", ios::app);   //SJ
  filepedX2 << pedX2;   //SJ
  filepedX2<<"\n";   //SJ
  filepedX2.close();
```

Appendix M

```
  TF1* G1 = new TF1("G1","gaus",MinFitInt,MaxFitInt);
  G1->SetLineColor(3);
  G1->SetLineWidth(1);
  G1->SetParameter(1,pedX2);
  pedestal->Fit(G1,"R");
    pedX = G1->GetParameter(1);
    pedRMS = G1->GetParameter(2);
          if(pedRMS<2){
TF1* G1 = new TF1("G1","gaus",pedX2*10-150,pedX2*10+120);
  G1->SetLineColor(3);
  G1->SetLineWidth(1);
  G1->SetParameter(1,pedX2);
  pedestal->Fit(G1,"R");
    pedX = G1->GetParameter(1);
    pedRMS = G1->GetParameter(2);
    }


TF1* G2 = new TF1("G2","gaus",pedX2*10+10,pedX2*10+1000);
  G2->SetLineColor(4);
  G2->SetLineWidth(1);
   pedestal->Fit(G2,"R");
     pX = G2->GetParameter(1);
    pRMS = G2->GetParameter(2);
pConstant = G2->GetParameter(0);
 if(pX-pedX<pRMS/2){TF1* G2 = new TF1("G2","gaus",pedX2*10+100,pedX2*10+1500);
  G2->SetLineColor(4);
  G2->SetLineWidth(1);
   pedestal->Fit(G2,"R");
     pX = G2->GetParameter(1);
    pRMS = G2->GetParameter(2);
pConstant = G2->GetParameter(0);
}


 if(pedX>800){
   if(90>pX-pedX){
    pX = pedX+160;
    pRMS = 110;
    pConstant = 150;}}
 else{if(30>pX-pedX){
     pX = pedX+70;
    pRMS = 101;
    pConstant = 150;}}

       if(pConstant>300){pConstant = 300;}
       if(pConstant<30){pConstant = 30;}


       //    if(pRMS<200){pRMS = 200;}


    //no data:
if(pedRMS<0.001){pedX = 0.001;
    pedRMS = 0.001;
     pX = 0.01;
    pRMS = 0.01;
}
//dead PMF
 if(pedX>3000){pedX = 0.001;
    pedRMS = 0.001;
     pX = 0.01;
    pRMS = 0.01;
}

  Float_t MaxFit =  pedX-100;
```

Appendix M

```
  TF1* fct3    = new TF1("fct3",fit1pe,MaxFit,5000,6);
  fct3->SetParLimits(0,0,10);
  fct3->SetParLimits(1,0,10000000);
  fct3->SetParLimits(3,0,10000000);
  // fct3->SetParLimits(4,0,1000000000);

  Float_t sum = 0;
  Int_t sum_start =MaxFit/10+20;
  for (Int_t isum=sum_start;isum<=400;isum++){
    sum += pedestal->GetBinContent(isum);
    // return sum;
     }

  //  fct3->SetParameter(0,.02);
  //  Double_t start_fct3p0 = pConstant**1.35/7800;
  //   if start_fct3p0>0.11){start_fct3p0 = 0.09;}
//if start_fct3p0<0.005){start_fct3p0 = 0.005;}
//  fct3->SetParameter(0,start_fct3p0);
  fct3->SetParameter(0,sum/95000);
  fct3->SetParameter(1,pX-0.95*pedX+45);
  // if(pedX<pX) {fct3->SetParameter(1,pX+5000)}
  // if (pedX>2000)fct3->SetParameter(1,pedX);{}
  fct3->FixParameter(2,pedRMS);
  fct3->SetParameter(3,1.95*pRMS+45);
  // fct3->SetParameter(4,pRMS*1700);
 fct3->SetParameter(4,99999);
  fct3->FixParameter(5,pedX);
  //  if(pedX>2000) { fct3->FixParameter(5,pedX-2000);}
  fct3->SetLineColor(4);


  // fct3->SetLineColor(4);

  fct3->SetParName(0,"Mu");
  fct3->SetParName(1,"1pe mean");
  fct3->SetParName(2,"ped RMS");
  fct3->SetParName(3,"1pe RMS");
  fct3->SetParName(4,"Norm");
  fct3->SetParName(5,"ped mean");


  pedestal->Fit(fct3,"R+") ;
   gStyle->SetOptStat("");
   gStyle->SetOptStat(0000000000);
   gStyle->SetOptFit(0000);


//Print of mu vaules on plot

pt = new TPaveText(1.0,1.0,0.58,0.81, "NDC"); // NDC sets coords
                                              // relative to pad dimensions
pt->SetFillColor(0); // text is black on white
pt->SetTextSize(0.04);
pt->SetTextAlign(12);
text = pt->AddText("#chi^{2} / NDF");
text = pt->AddText("#mu");
//text = pt->AddText("#mu_{CT}");
pt->Draw();       //to draw your text object

pt2 = new TPaveText(1.0,1.0,0.741,0.812, "NDC"); // NDC sets coords
pt2->SetFillColor(0);
pt2->SetLineColor(0); // text is black on white
pt2->SetTextSize(0.04);
pt2->SetTextAlign(12);
char buf0[10];
 sprintf(buf0, "= %.0f", fct3->GetChisquare());
 text = pt2->AddText(buf0);
char buf[10];
```

```
sprintf(buf, "= %.2f", fct3->GetParameter(0));
 text = pt2->AddText(buf);
 /*char buf2[10];
sprintf(buf2, "= %.2f", fct3->GetParameter(6));
text = pt2->AddText(buf2);*/
 // text = pt->AddText("#pm ");
   pt2->Draw();       //to draw your text object


pt3 = new TPaveText(1.0,1.0,0.865,0.812, "NDC"); // NDC sets coords
pt3->SetFillColor(0);
pt3->SetLineColor(0); // text is black on white
pt3->SetTextSize(0.04);
pt3->SetTextAlign(12);
 text = pt3->AddText("/ ");
 text = pt3->AddText("#pm ");
 // text = pt3->AddText("#pm ");
pt3->Draw();       //to draw your text object

pt4 = new TPaveText(1.0,1.0,0.9,0.812, "NDC"); // NDC sets coords
pt4->SetFillColor(0);
pt4->SetLineColor(0); // text is black on white
pt4->SetTextSize(0.04);
pt4->SetTextAlign(12);
char buf5[10];
sprintf(buf5, "%.0f", fct3->GetNDF());
 text = pt4->AddText(buf5);
char buf3[10];
sprintf(buf3, "%.2f", fct3->GetParError(0));
 text = pt4->AddText(buf3);
 /*char buf4[10];
sprintf(buf4, "%.2f", fct3->GetParError(6));
text = pt4->AddText(buf4);*/
 // text = pt->AddText("#pm ");
   pt4->Draw();       //to draw your text object


    for (Int_t ii=1;ii<15;ii++)
    {
      TF1 *fit = new TF1("Npe",peFct,MaxFit,5000,9);
      //TF1 *fit = new TF1("Npe",peFct,MinFitInt,5000,9);
      //TF1 *fit = new TF1("Npe",peFct,MaxFit,300,7);
      fit->FixParameter(0,fct3->GetParameter(0));
      fit->FixParameter(1,fct3->GetParameter(1));
      //fit->SetParameter(2,fct3->GetParameter(2));
      fit->FixParameter(3,fct3->GetParameter(3));
      fit->SetParameter(4,fct3->GetParameter(4));
      fit->FixParameter(5,fct3->GetParameter(5));
      fit->FixParameter(7,fct3->GetParameter(6));
      // fit->FixParameter(8,fct3->GetParameter(7));
      fit->FixParameter(6,ii);
      // fit->SetLineColor(ii);
      if(10>ii){ fit->SetLineColor(ii);}
      else{fit->SetLineColor(ii+31);}
      fit->SetLineWidth(1);
      fit->DrawCopy("same");
    }

       pedestal->SetMaximum(pedestal->GetMaximum()+500);
        pedestal->SetAxisRange(0,4000);
//Calculating gain factor
        Int_t w1pe=250;
        Double_t fct3p1 = fct3->GetParameter(1);
        if(fct3p1<1){fct3p1=1;} //for bad data
        Int_t gainfactor= w1pe/fct3p1*16;
if(gainfactor<1){gainfactor=16;}//bad analog channel
if(gainfactor>63){gainfactor=16;}//bad analog channel
```

Appendix M

```
//File saving

TString directory = ;
 directory+= "Run_";
 directory+= Runnr;
 // gSystem->MakeDirectory(directory);
directory+= "/";
 directory+= PMTnr;
 directory+= "/";
 // gSystem->MakeDirectory(directory);
 /**
Double_t pemean=1;
 pemean = fct3->GetParameter(1) -  fct3->GetParameter(5);

 ofstream myfile;            //SJ
 myfile.open ( directory+ "1pemean.dat", ios::app);   //SJ
  myfile << pemean;   //SJ
  myfile<<"\n";   //SJ
  myfile.close();
 */

 ofstream myfile2;            //SJ
  myfile2.open ( directory+ "index.dat", ios::app);   //SJ
  myfile2 << index+1;   //SJ
  myfile2<<"\n";   //SJ
  myfile2.close();

 ofstream myfile3;            //SJ
  myfile3.open ( directory+ "Mu.dat", ios::app);   //SJ
  myfile3 << fct3->GetParameter(0);   //SJ
  myfile3<<"\n";   //SJ
  myfile3.close();

 ofstream myfile4;            //SJ
  myfile4.open ( directory+ "1pe mean.dat", ios::app);   //SJ
  myfile4 << fct3->GetParameter(1);   //SJ
  myfile4<<"\n";   //SJ
  myfile4.close();

 ofstream peMeanError;            //SJ
 peMeanError.open ( directory+ "1pe mean Error.dat", ios::app);   //SJ
 peMeanError << fct3->GetParError(1);   //SJ
 peMeanError<<"\n";   //SJ
 peMeanError.close();

 ofstream myfile5;            //SJ
  myfile5.open ( directory+ "1pe RMS.dat", ios::app);   //SJ
  myfile5 << fct3->GetParameter(3);   //SJ
  myfile5<<"\n";   //SJ
  myfile5.close();

 ofstream peRMSError;            //SJ
  peRMSError.open ( directory+ "1pe RMS Error.dat", ios::app);   //SJ
  peRMSError << fct3->GetParError(3);   //SJ
  peRMSError<<"\n";   //SJ
  peRMSError.close();

 ofstream myfile6;            //SJ
  myfile6.open ( directory+ "Norm.dat", ios::app);   //SJ
  myfile6 << fct3->GetParameter(4);   //SJ
  myfile6<<"\n";   //SJ
  myfile6.close();

 ofstream myfile7;            //SJ
  myfile7.open ( directory+ "ped mean.dat", ios::app);   //SJ
  myfile7 << fct3->GetParameter(5);   //SJ
  myfile7<<"\n";   //SJ
  myfile7.close();
```

Appendix M

```
ofstream myfile8;            //SJ
  myfile8.open ( directory+ "ped RMS.dat", ios::app);   //SJ
  myfile8 << fct3->GetParameter(2);   //SJ
  myfile8<<"\n";   //SJ
  myfile8.close();

ofstream myfile10;            //SJ
  myfile10.open ( directory+ "Mu Error.dat", ios::app);   //SJ
  myfile10 << fct3->GetParError(0);   //SJ
  myfile10<<"\n";   //SJ
  myfile10.close();

ofstream myfile11;            //SJ
  myfile11.open ( directory+ "pedX.dat", ios::app);   //SJ
  myfile11 << pedX2;   //SJ
  myfile11<<"\n";   //SJ
  myfile11.close();

ofstream fileGainfactor;            //SJ
  fileGainfactor.open ( directory+ "gainfactor.txt", ios::app);   //SJ
  fileGainfactor << gainfactor;   //SJ
  fileGainfactor<<"\n";   //SJ
  fileGainfactor.close();
  /*
ofstream sumfile;            //SJ
  sumfile.open ( directory+ "sum.dat", ios::app);   //SJ
  sumfile << sum;   //SJ
  sumfile<<"\n";   //SJ
  sumfile.close();
  */
//Dead channels
  if(fct3->GetParameter(1)/(fct3->GetParameter(3))<0.8)
          {
 ofstream fileDeadChannels;            //SJ
  fileDeadChannels.open ( directory+ "DeadChannels.dat", ios::app);   //SJ
  fileDeadChannels << index+1;   //SJ
  fileDeadChannels<<"\n";   //SJ
  fileDeadChannels.close();
          }
        if(fct3->GetParameter(1)/(fct3->GetParameter(3))>3)
          {
 ofstream fileDeadChannels;            //SJ
  fileDeadChannels.open ( directory+ "DeadChannels.dat", ios::app);   //SJ
  fileDeadChannels << index+1;   //SJ
  fileDeadChannels<<"\n";   //SJ
  fileDeadChannels.close();
          }
if(fct3->GetParameter(1)/(fct3->GetParameter(3))>0.8)
          {
if(fct3->GetParameter(1)/(fct3->GetParameter(3))<3)
          {
if(fct3->GetParameter(0)<0.00001)
  {
 ofstream fileDeadChannels;            //SJ
  fileDeadChannels.open ( directory+ "DeadChannels.dat", ios::app);   //SJ
  fileDeadChannels << index+1;   //SJ
  fileDeadChannels<<"\n";   //SJ
  fileDeadChannels.close();
  }}}

if(fct3->GetParameter(1)/(fct3->GetParameter(3))>0.8)
          {
if(fct3->GetParameter(1)/(fct3->GetParameter(3))<3)
          {
if(fct3->GetParameter(0)>0.00001)
  {
if(fct3->GetParameter(1)<40)
```

Appendix M

```
  {
 ofstream fileDeadChannels;            //SJ
  fileDeadChannels.open ( directory+ "DeadChannels.dat", ios::app);   //SJ
  fileDeadChannels << index+1;   //SJ
  fileDeadChannels<<"\n";   //SJ
  fileDeadChannels.close();
  }}}}

 directory+= "ROOT/";
  gSystem->MakeDirectory(directory);
 directory+= index+1;
pedestalDisp->SaveAs(directory+ ".root");

        TString directory2 = ;
 directory2+= "Run_";
 directory2+= Runnr;
 // gSystem->MakeDirectory(directory);
directory2+= "/";
 directory2+= PMTnr;
 directory2+= "/";
 // gSystem->MakeDirectory(directory);

 directory2+= "GIF/";
  gSystem->MakeDirectory(directory2);
 directory2+= index+1;
pedestalDisp->SaveAs(directory2+ ".gif");



}
gROOT->reset();
```

Appendix N

readCOSMICS.C:

```
#include <iostream.h>
#include <fstream.h>
#include <iomanip>
#include <stdio.h>
#include "TSystem.h"


#include "readCOSMICS.h"

using namespace std;

// We define a structure holding one run context
typedef struct pmf_record
{
         unsigned char gain_array[NUMCHAMD];
         short dac0;
         int trig_source;
         int q_acqmode;
}PMFRecord, *PMFRecordPtr;

// Global variable
PMFRecord pmfr;

/*******************************************************/
int histCOSMICS(int run_num)
/*******************************************************/
{


for (int kapt_id=1; kapt_id<6; kapt_id++)
{

for (int pmf_id=1; pmf_id<6; pmf_id++)
{

int pmf_NUMB =  (kapt_id-1)*5+pmf_id;

TString directory = "ROOTFILE/";
directory+= "Run_";
directory+= run_num;
gSystem->MakeDirectory(directory);
directory+= "/";
directory+= pmf_NUMB;
gSystem->MakeDirectory(directory);

TString rootfile_name;
rootfile_name = directory + "/ped_1pe.root";

cout << "Run nÃ‚Â°" << run_num << ", kapton cable nÃ‚Â°" << kapt_id << " and pmf
nÃ‚Â° " << pmf_NUMB << endl;
cout << "Output filename: " << rootfile_name << endl;

//Opening root file where histogram and tree will be stored

TFile *tFileOut = new TFile(rootfile_name,"RECREATE");

TH1I *ADCAll[NUMCHAMD];
//Creating histograms
for (unsigned int cha=0;cha<NUMCHAMD;cha++)
         {
         TString histname= "";
         histname+=cha;
         TString histitle="ADC channel ";
         histitle+= cha+1;
         ADCAll[cha]= new TH1I(histname,histitle,400,0,4000);
```

```
        }

readMapping(MarocToPMArray);

ifstream fbin_dig;
ifstream fbin_ana;

int i,chan_i,chan_j;

char array_dig[64];
short array_ana[64];

char binfile_name[128];

//Opening digital and analog binary files
sprintf(binfile_name,"LUMI_PMF%1d/Data/Dig_R%04d_pmf%02d.bin",kapt_id,run_num,pmf_N
UMB);
fbin_dig.open(binfile_name,ios::binary);

sprintf(binfile_name,"LUMI_PMF%1d/Data/Ana_R%04d_pmf%02d.bin",kapt_id,
run_num,pmf_NUMB);
fbin_ana.open(binfile_name,ios::binary);

if(fbin_dig && fbin_ana)
        {
         long type = 1, nbytes, step, cnt;
         unsigned long evtnum, time, val1, val2;
         char ext[4] = "", *ptr;
         short val;

        // Then, we have to know the file size in bytes
         fbin_dig.seekg (0, ios::end);
         nbytes = fbin_dig.tellg();
         fbin_dig.seekg (0, ios::beg);

         if( nbytes == 0)
                {
                fbin_dig.close();
                cout << "The digital file size is zero.\n Try another file,
please." << endl;
                }


         fbin_ana.seekg (0, ios::end);
         nbytes = fbin_ana.tellg();
         fbin_ana.seekg (0, ios::beg);

         if( nbytes == 0)
                {
                fbin_ana.close();
                printf("The analog file size is zero.\n Try another file,
please.");
                }

         // From the raw binary file we recover the number of event, the threshold
and the gains
         Event_count = int(ReadHeader( run_num, pmf_id-1));

         while(!fbin_dig.eof() && !fbin_ana.eof())
                {
                //reading digital binary file
                fbin_dig.read((char*)&evtnum, sizeof(long));// event number
                fbin_dig.read((char*)&time, sizeof(long));   // time tag
                fbin_dig.read((char*)&val2, sizeof(long));   // first part of the
64 trigger hits
                fbin_dig.read((char*)&val1, sizeof(long));// second part

                Event=int(evtnum);
```

Appendix N

```
                    Time=25.*float(time)/1000.;

                    // Array preparation
                    for(i = 0; i < 32; i++)
                            {
                            array_dig[MarocToPMArray[i]-1] = (char) val1 & 0x00000001;
                            val1>>=1;
                            }
                    for(; i < 64; i++)
                            {
                            array_dig[MarocToPMArray[i]-1] =  (char) val2 &
0x00000001;
                            val2>>=1;
                            }

                    //reading analog binary file
                    fbin_ana.read((char*)&evtnum, sizeof(long));// event number
                    fbin_ana.read((char*)&time, sizeof(long));// time tag

                    for(i = 0; i < 64; i++)
                            {
                            fbin_ana.read((char*)&val,sizeof(short));

                            if(val & 0x8000)
                                    val = -1;
                            array_ana[MarocToPMArray[i]-1] = val;
                            }

                    // Fill array for the tree and fill histograms
                    for(i = 1; i < 65; i++)
                            {
                            if (int(fmod(double(i),double(8)))>0)
                                    {
                                    chan_i=int(i/8)+1;
                                    chan_j=9-int(fmod(double(i),double(8)));
                                    }
                            else
                                    {
                                    chan_i=int(i/8);
                                    chan_j=1;
                                    }

                            if (array_dig[i-1]==0) AllHits[i-1]=false;
                            else
                                    {
                                    AllHits[i-1]=true;
                                    }

                            AllADC[i-1]=int(array_ana[i-1]);
                            ADCAll[i-1]->Fill(AllADC[i-1]);

                            }

                    if(evtnum ==  Event_count)
                            break;
                    }
            }
            else
                    {
                    cout << "Binary file not found or faulty, try another one " <<
endl;
                    }
            fbin_dig.close();
            fbin_ana.close();

tFileOut->Write();
tFileOut->Close();
```

```
delete tFileOut;

} //end of loop over pmf
} //end of lopp over kapton
return 0;

}

/* ========================================================================== */
void readMapping(int MarocToPMArray[NUMCHAMD])
/* ========================================================================== */
{
int Maroc_chan;
ifstream mapping;
mapping.open("MAROC_to_MAPMT.dat");
for (int i=0;i<64;i++)
        {
        mapping >> Maroc_chan >> MarocToPMArray[i];
        }
mapping.close();
}

/* ========================================================================== */
long ReadHeader(int run_num, int pmf_id)
/* ========================================================================== */
{

 ifstream fbin;
 char filename[128];
 long i, evt_max, evt_cnt, pattern;
 int elapsed, lumi_id = pmf_id/5; // the LUMI_PMF id (0 to 4)  is computed from the
pmf id (1 to 25)

// We specify the raw binary file from which we want to get the context back
// Its name is made up of the run number and the LUMI_PMF id
 sprintf(filename,"LUMI_PMF%1d/Data/Raw_R%04d_L%1d.bin",lumi_id+1,run_num,
lumi_id+1);

 fbin.open(filename,ios::binary);
        if(!fbin)
                {
                cout << "Binary file not found" << endl;
                }
        else
                {
                pmf_id %= 5; // we get the "local" (within the LUMI_PMF) pmf id (0
- 4)

                fbin.read((char*)&pattern, sizeof(long));
                fbin.read((char*)&i, sizeof(long));
                fbin.read((char*)&evt_max, sizeof(long));
                fbin.read((char*)&elapsed, sizeof(long));
                fbin.read((char*)&evt_cnt, sizeof(long));

                Event_count = int(evt_cnt);

                for(i = 0; i<5; i++)
                        {
                        fbin.read((char*)&pmfr, sizeof(PMFRecord)); // yes

                        if( i == pmf_id) // Is it the requested slot ?
                                break;            // Ok we'are done (
                        }

                        // now our PMFrecord has been read so we can print into
the file the parameters

                        Thres=int(pmfr.dac0);
```

```
                        for(i =0; i < 64; i++)
                                {
                                Gain[i]=int(pmfr.gain_array[i]);
                                }
                }
                fbin.close();

        return evt_cnt; // things were fine so let's return the event count
}
```

readCOSMICS.h:

```
//INCLUDES

// Standard libraries

#include <fstream.h>

#include <iostream>

#include <stdlib.h>

#include <cmath>

// TDAQ release

// Root

#include "TFile.h"

#include "TTree.h"

#include "TH1I.h"

#include "TH2I.h"

#include <string.h>

//// File I/O (found in /usr/include/ )

//#include <unistd.h>

//#include <sys/types.h>

//#include <sys/stat.h>

//#include <fcntl.h>



//CONSTANTS


#include "constants.h"


//GLOBAL VARIABLES


int MarocToPMArray[NUMCHAMD];
int Event_count, Event;
short Thres;
```

Appendix N

```
int Gain[NUMCHAMD];
float Time;
int AllADC[NUMCHAMD];
bool AllHits[NUMCHAMD];


//Histogram declearation

TH2I *ADCmap;
TH2I *HITSAll;


TTree *ALFA_tree;


//FUNCTIONS

//read mapping between cable and pmt

void readMapping(int mapping[NUMCHAMD]);

//read header to know the run settings
long ReadHeader(int run_num, int pmf_id);

//main

int histCOSMICS(int run_num);
```

Appendix O

AllCH.C:

```
#include "cosmic.C"

void AllCH(int Runnr, int PMTnr)
{
  for (Int_t index=0;index<64;index++)
 {
 cosmic(Runnr,PMTnr,index);
  }
}
```

Run1.C:

```
#include "AllCH.C"

void Run1(int Runnr)
{
 AllCH(Runnr,1);
 AllCH(Runnr,2);
 AllCH(Runnr,3);
 AllCH(Runnr,4);
 AllCH(Runnr,5);
 AllCH(Runnr,6);
}
```

Run2.C:

```
#include "AllCH.C"

void Run2(int Runnr)
{
 AllCH(Runnr,7);
 AllCH(Runnr,8);
 AllCH(Runnr,9);
 AllCH(Runnr,10);
 AllCH(Runnr,11);
 AllCH(Runnr,12);
}
```

Run3.C:

```
#include "AllCH.C"

void Run3(int Runnr)
{
 AllCH(Runnr,13);
 AllCH(Runnr,14);
 AllCH(Runnr,15);
 AllCH(Runnr,16);
 AllCH(Runnr,17);
 AllCH(Runnr,18);
}
```

Run4.C:

```
#include "AllCH.C"

void Run4(int Runnr)
{
 AllCH(Runnr,19);
 AllCH(Runnr,21);
 AllCH(Runnr,22);
 AllCH(Runnr,24);
 AllCH(Runnr,25);
}
```

Appendix P

cosmic.C (5 Orsay board version):

```
#include "TMultiGraph.h"
#include "TFile.h"
#include "TTree.h"
#include "TBrowser.h"
#include "TH2.h"
#include "TRandom.h"
#include "TMath.h"
#include <iostream>
#include <fstream>
#include "TStyle.h"
#include "TText.h"
#include <iomanip>
#include <stdio.h>
#include "TSystem.h"

Double_t fit1pe(Double_t *x, Double_t *par)
{

  Double_t result1=0.;

  for (Int_t i=1;i<15;i++)
    {

      Double_t fac=1;
         if(i<1)
        {fac=1;}
      else{
 for (Int_t var=1;var<i+1;var++)
        {
          fac *= var;
        }}

      Double_t P = (TMath::Exp((-1.)*par[0])*par[0]**i)/(fac);
      Double_t G1 =
1./((TMath::Sqrt(2.*TMath::Pi())*(TMath::Sqrt((i*par[3]**2+par[2]**2))))) ;
      Double_t G2 = TMath::Exp( ( (-1.) * (x[0] - par[5] - i*(par[1]))**2
)/(2.*(i*par[3]**2+par[2]**2)));

      result1 += P * G1 * G2;
    }
  // result1 *= par[4];
 // return result;

 Double_t result2=0.;
  for (Int_t iiii=1;iiii<5;iiii++)
    {

      Double_t fac2=1;
         if(iiii<1)
        {fac2=1;}
      else{
 for (Int_t var=1;var<iiii+1;var++)
        {
          fac2 *= var;
        }}
      Double_t Pct = (TMath::Exp((-1.)*par[6])*par[6]**iiii)/(fac2);
      Double_t G1ct =
1./((TMath::Sqrt(2.*TMath::Pi())*(TMath::Sqrt((iiii*par[3]**2+par[2]**2))))) ;
      Double_t G2ct = TMath::Exp( ( (-1.) * (x[0] - par[5] - iiii*(par[1]))**2
)/(2.*(iiii*par[3]**2+par[2]**2)));

      result2 += Pct * G1ct * G2ct;
    }
  // result2 *= par[7];
 Double_t result = result1 + result2;
```

```
 result *= par[4];
  return result;
 // return  result2;
}


Double_t peFct(Double_t *x, Double_t *param)
{
  Double_t result = 0.;
  Double_t fact = 1;
  for (Int_t var=1;var<param[6]+1;var++)
    fact *= var;

      Double_t P = (TMath::Exp((-1.) * param[0]) * param[0]**param[6])/fact;
      Double_t G1 =
1./((TMath::Sqrt(2.*TMath::Pi())*(TMath::Sqrt((param[6]*param[3]**2+param[2]**2))))
) ;
      Double_t G2 = TMath::Exp( ( (-1.) * (x[0] - param[5] -
param[6]*(param[1]))**2 )/(2.*(param[6]*param[3]**2+param[2]**2)));

result += P * G1 * G2;
 result *= param[4];
return result;
}
Double_t peFctCT(Double_t *x, Double_t *param)
{
Double_t result2=0.;
 Double_t fact = 1;
  for (Int_t var=1;var<param[6]+1;var++)
    fact *= var;

      Double_t Pct = (TMath::Exp((-1.)*param[7])*param[7]**param[6])/(fact);
      Double_t G1ct =
1./((TMath::Sqrt(2.*TMath::Pi())*(TMath::Sqrt((param[6]*param[3]**2+param[2]**2))))
) ;
      Double_t G2ct = TMath::Exp( ( (-1.) * (x[0] - param[5] -
param[6]*(param[1]))**2 )/(2.*(param[6]*param[3]**2+param[2]**2)));

      result2 += Pct * G1ct * G2ct;

 result2 *= param[4];
 return result2;
}

void cosmic(int Runnr, int PMTnr, int index)
{
  //Create, fill and display raw data
  TString directory3 = ;
 directory3+= "Run_";
 directory3+= Runnr;
 // gSystem->MakeDirectory(directory);
directory3+= "/";
 directory3+= PMTnr;
 directory3+= "/";
TFile *file = new TFile(directory3+"ped_1pe.root");
  TH1I *pedestal;
  char str[2];
  sprintf(str,"%d",index);
  pedestal = (TH1I*) gDirectory->Get(str);
  pedestal->GetYaxis()->SetTitle("Number of events");
  pedestal->GetXaxis()->SetTitle("Charge signal (ADC counts)");



   TF1* gaussPE;

  TCanvas *pedestalDisp = new TCanvas("cavas","pedestal - 1pe",200,60,700,700);
   pedestalDisp->SetLogy();
```

```
  pedestalDisp->cd();
  pedestalDisp->SetFillColor(0);
  pedestalDisp->SetFrameFillColor(0);
  pedestal->Draw();



  //Evaluate 1pe characteristics
  cout << "Pedestal " << index << endl;
  Double_t pedX, pedX2,singleX,pedRMS,pX,pRMS,pConstant;
    pedX2 = pedestal->GetMaximumBin();

    //  Float_t MinFitInt = pedX2*10-700;
    //     Float_t MaxFitInt = pedX2*10+700;


    if (pedX2<250){
     Float_t MinFitInt = pedX2*10-90;
     Float_t MaxFitInt = pedX2*10+75;
}
else {
     Float_t MinFitInt = pedX2*10-10;
     Float_t MaxFitInt = pedX2*10+10;
     }

    //  Float_t MinFitInt = 1100;
    //  Float_t MaxFitInt = 1200;

 ofstream filepedX2;            //SJ
 filepedX2.open ("d:/pedX2.dat", ios::app);   //SJ
  filepedX2 << pedX2;   //SJ
  filepedX2<<"\n";   //SJ
  filepedX2.close();


  /*  TF1* G1 = new TF1("G1","gaus",MinFitInt,MaxFitInt);
  G1->SetLineColor(3);
  G1->SetLineWidth(1);
  G1->SetParameter(1,pedX2);
  pedestal->Fit(G1,"R");
    pedX = G1->GetParameter(1);
    pedRMS = G1->GetParameter(2);
          if(pedRMS<1){
TF1* G1 = new TF1("G1","gaus",pedX2*10-150,pedX2*10+120);
  G1->SetLineColor(3);
  G1->SetLineWidth(1);
  G1->SetParameter(1,pedX2);
  pedestal->Fit(G1,"R");
    pedX = G1->GetParameter(1);
    pedRMS = G1->GetParameter(2);
    }


TF1* G2 = new TF1("G2","gaus",pedX2*10+50,pedX2*10+1000);
  G2->SetLineColor(4);
  G2->SetLineWidth(1);
   pedestal->Fit(G2,"R");
     pX = G2->GetParameter(1);
    pRMS = G2->GetParameter(2);
pConstant = G2->GetParameter(0);
 if(pX-pedX<pRMS/1.5){TF1* G2 = new TF1("G2","gaus",pedX2*10+100,pedX2*10+1500);
  G2->SetLineColor(4);
  G2->SetLineWidth(1);
   pedestal->Fit(G2,"R");
     pX = G2->GetParameter(1);
    pRMS = G2->GetParameter(2);
pConstant = G2->GetParameter(0);
}
```

```
   */

  if(pedX>800){
    if(90>pX-pedX){
     pX = pedX+160;
     pRMS = 110;
     pConstant = 150;}}
  else{if(30>pX-pedX){
      pX = pedX+70;
     pRMS = 101;
     pConstant = 150;}}

        if(pConstant>300){pConstant = 300;}
        if(pConstant<30){pConstant = 30;}


        //    if(pRMS<200){pRMS = 200;}


     //no data:
 if(pedRMS<0.001){pedX = 0.001;
     pedRMS = 0.001;
      pX = 0.01;
     pRMS = 0.01;
 }
 //dead PMF
  if(pedX>3000){pedX = 0.001;
     pedRMS = 0.001;
      pX = 0.01;
     pRMS = 0.01;
 }

   //read Fit calibration files.
 TString directoryRead = ;
  directoryRead+= "Run_";
  directoryRead+= Runnr;
  // gSystem->MakeDirectory(directory);
 directoryRead+= "/";
  directoryRead+= PMTnr;
  directoryRead+= "/";
  // gSystem->MakeDirectory(directory);
    ifstream in1pemean; //Declare the stream variable
    Double_t buffer1pemean;
    in1pemean.open( directoryRead+ "1pe mean.cal"); //Open the file.
    for(int iii = 0; iii < index+1; iii++){
    in1pemean>>buffer1pemean;}  //Read the number.
    in1pemean.close();//Close the file.

    ifstream in1peRMS; //Declare the stream variable
    Double_t buffer1peRMS;
    in1peRMS.open( directoryRead+ "1pe RMS.cal");   //Open the file.
    for(int iii = 0; iii < index+1; iii++){
    in1peRMS>>buffer1peRMS;} //Read the number.
    in1peRMS.close(); //Close the file.

    ifstream inpedmean; //Declare the stream variable
    Double_t bufferpedmean;
    inpedmean.open( directoryRead+ "ped mean.cal");   //Open the file.
    for(int iii = 0; iii < index+1; iii++){
    inpedmean>>bufferpedmean;} //Read the number.
    inpedmean.close(); //Close the file.

    ifstream inpedRMS; //Declare the stream variable
    Double_t bufferpedRMS;
    inpedRMS.open( directoryRead+ "ped RMS.cal");   //Open the file.
    for(int iii = 0; iii < index+1; iii++){
    inpedRMS>>bufferpedRMS;} //Read the number.
    inpedRMS.close(); //Close the file.
```

Appendix P

```
  Float_t MaxFit =  bufferpedmean+15;

  TF1* fct3    = new TF1("fct3",fit1pe,MaxFit,5000,7);
  fct3->SetParLimits(0,0,10);
  fct3->SetParLimits(1,0,10000000);
  fct3->SetParLimits(3,0,10000000);
  // fct3->SetParLimits(4,0,1000000000);




   /*
  //  fct3->SetParameter(0,.02);
  Double_t start_fct3p0 = pConstant**1.35/7800;
    if start_fct3p0>0.11){start_fct3p0 = 0.09;}
//if start_fct3p0<0.005){start_fct3p0 = 0.005;}
  fct3->SetParameter(0,start_fct3p0);
  fct3->SetParameter(1,pX-0.95*pedX);
  // if(pedX<pX) {fct3->SetParameter(1,pX+5000)}
  // if (pedX>2000)fct3->SetParameter(1,pedX);{}
  fct3->FixParameter(2,pedRMS);
  fct3->SetParameter(3,1.95*pRMS+45);
  // fct3->SetParameter(4,pRMS*1700);
 fct3->SetParameter(4,99991);
  fct3->FixParameter(5,pedX);
  //  if(pedX>2000) { fct3->FixParameter(5,pedX-2000);}
  fct3->SetLineColor(4);
   */

   fct3->SetParameter(0,4);
   fct3->FixParameter(1,buffer1pemean);
   fct3->FixParameter(2,bufferpedRMS);
   fct3->FixParameter(3,buffer1peRMS);
   fct3->SetParameter(4,9000);
   fct3->FixParameter(5,bufferpedmean);
   fct3->SetParameter(6,1.1);
   fct3->SetLineColor(4);

  // fct3->SetLineColor(4);

  fct3->SetParName(0,"Mu");
  fct3->SetParName(1,"1pe mean");
  fct3->SetParName(2,"ped RMS");
  fct3->SetParName(3,"1pe RMS");
  fct3->SetParName(4,"Norm");
  fct3->SetParName(5,"ped mean");
 fct3->SetParName(6,"Mu CT");


  pedestal->Fit(fct3,"R+") ;
   gStyle->SetOptStat("");
   gStyle->SetOptStat(0000000000);
   gStyle->SetOptFit(0000);


//Print of mu vaules on plot

pt = new TPaveText(1.0,1.0,0.58,0.81, "NDC"); // NDC sets coords
                                              // relative to pad dimensions
pt->SetFillColor(0); // text is black on white
pt->SetTextSize(0.04);
pt->SetTextAlign(12);
text = pt->AddText("#chi^{2} / NDF");
text = pt->AddText("#mu");
text = pt->AddText("#mu_{CT}");
pt->Draw();       //to draw your text object
```

```
pt2 = new TPaveText(1.0,1.0,0.741,0.812, "NDC"); // NDC sets coords
pt2->SetFillColor(0);
pt2->SetLineColor(0); // text is black on white
pt2->SetTextSize(0.04);
pt2->SetTextAlign(12);
char buf0[10];
 sprintf(buf0, "= %.0f", fct3->GetChisquare());
 text = pt2->AddText(buf0);
char buf[10];
sprintf(buf, "= %.2f", fct3->GetParameter(0));
 text = pt2->AddText(buf);
 char buf2[10];
sprintf(buf2, "= %.2f", fct3->GetParameter(6));
text = pt2->AddText(buf2);
 // text = pt->AddText("#pm ");
   pt2->Draw();       //to draw your text object


pt3 = new TPaveText(1.0,1.0,0.865,0.812, "NDC"); // NDC sets coords
pt3->SetFillColor(0);
pt3->SetLineColor(0); // text is black on white
pt3->SetTextSize(0.04);
pt3->SetTextAlign(12);
 text = pt3->AddText("/ ");
 text = pt3->AddText("#pm ");
 text = pt3->AddText("#pm ");
pt3->Draw();       //to draw your text object

pt4 = new TPaveText(1.0,1.0,0.9,0.812, "NDC"); // NDC sets coords
pt4->SetFillColor(0);
pt4->SetLineColor(0); // text is black on white
pt4->SetTextSize(0.04);
pt4->SetTextAlign(12);
char buf5[10];
sprintf(buf5, "%.0f", fct3->GetNDF());
 text = pt4->AddText(buf5);
char buf3[10];
sprintf(buf3, "%.2f", fct3->GetParError(0));
 text = pt4->AddText(buf3);
 char buf4[10];
sprintf(buf4, "%.2f", fct3->GetParError(6));
text = pt4->AddText(buf4);
 // text = pt->AddText("#pm ");
   pt4->Draw();       //to draw your text object


    for (Int_t ii=1;ii<15;ii++)
    {
      TF1 *fit = new TF1("Npe",peFct,MaxFit,5000,9);
      //TF1 *fit = new TF1("Npe",peFct,MinFitInt,5000,9);
      //TF1 *fit = new TF1("Npe",peFct,MaxFit,300,7);
      fit->FixParameter(0,fct3->GetParameter(0));
      fit->FixParameter(1,fct3->GetParameter(1));
      //fit->SetParameter(2,fct3->GetParameter(2));
      fit->FixParameter(3,fct3->GetParameter(3));
      fit->SetParameter(4,fct3->GetParameter(4));
      fit->FixParameter(5,fct3->GetParameter(5));
      fit->FixParameter(7,fct3->GetParameter(6));
      // fit->FixParameter(8,fct3->GetParameter(7));
      fit->FixParameter(6,ii);
      // fit->SetLineColor(ii);
      if(10>ii){ fit->SetLineColor(ii);}
      else{fit->SetLineColor(ii+31);}
      fit->SetLineWidth(1);
      fit->DrawCopy("same");
    }
```

Appendix P

```
for (Int_t ii=1;ii<5;ii++)
    {
      TF1 *fit2 = new TF1("Npe",peFctCT,MaxFit,5000,9);
      //TF1 *fit = new TF1("Npe",peFct,MaxFit,300,7);
      fit2->FixParameter(0,fct3->GetParameter(0));
      fit2->FixParameter(1,fct3->GetParameter(1));
      //fit->SetParameter(2,fct3->GetParameter(2));
      fit2->FixParameter(3,fct3->GetParameter(3));
      fit2->SetParameter(4,fct3->GetParameter(4));
      fit2->FixParameter(5,fct3->GetParameter(5));
      fit2->FixParameter(7,fct3->GetParameter(6));
      // fit2->FixParameter(8,fct3->GetParameter(7));
      fit2->FixParameter(6,ii);
      fit2->SetLineColor(ii);
      fit2->SetLineStyle(2);

      fit2->SetLineWidth(1);
      fit2->DrawCopy("same");
    }

        pedestal->SetMaximum(pedestal->GetMaximum()+500);
        pedestal->SetAxisRange(0,4000);
        /*
//Calculating gain factor
        Int_t w1pe=250;
        Double_t fct3p1 = fct3->GetParameter(1);
        if(fct3p1<1){fct3p1=1;} //for bad data
        Int_t gainfactor= w1pe/fct3p1*16;
if(gainfactor<1){gainfactor=16;}//bad analog channel
if(gainfactor>63){gainfactor=16;}//bad analog channel
        */

//File saving

TString directory = ;
 directory+= "Run_";
 directory+= Runnr;
 // gSystem->MakeDirectory(directory);
directory+= "/";
 directory+= PMTnr;
 directory+= "/";
 // gSystem->MakeDirectory(directory);
 /**
Double_t pemean=1;
 pemean = fct3->GetParameter(1) -  fct3->GetParameter(5);

 ofstream myfile;            //SJ
 myfile.open ( directory+ "1pemean.dat", ios::app);   //SJ
  myfile << pemean;   //SJ
  myfile<<"\n";   //SJ
  myfile.close();
 */

 ofstream myfile2;            //SJ
  myfile2.open ( directory+ "index.dat", ios::app);   //SJ
  myfile2 << index+1;   //SJ
  myfile2<<"\n";   //SJ
  myfile2.close();

 ofstream myfile3;            //SJ
  myfile3.open ( directory+ "Mu.dat", ios::app);   //SJ
  myfile3 << fct3->GetParameter(0);   //SJ
  myfile3<<"\n";   //SJ
  myfile3.close();

 ofstream myfile4;            //SJ
  myfile4.open ( directory+ "1pe mean.dat", ios::app);   //SJ
  myfile4 << fct3->GetParameter(1);   //SJ
```

```
  myfile4<<"\n";   //SJ
  myfile4.close();

 ofstream peMeanError;            //SJ
 peMeanError.open ( directory+ "1pe mean Error.dat", ios::app);   //SJ
 peMeanError << fct3->GetParError(1);   //SJ
 peMeanError<<"\n";   //SJ
 peMeanError.close();

 ofstream myfile5;            //SJ
  myfile5.open ( directory+ "1pe RMS.dat", ios::app);   //SJ
  myfile5 << fct3->GetParameter(3);   //SJ
  myfile5<<"\n";   //SJ
  myfile5.close();

 ofstream peRMSError;            //SJ
  peRMSError.open ( directory+ "1pe RMS Error.dat", ios::app);   //SJ
  peRMSError << fct3->GetParError(3);   //SJ
  peRMSError<<"\n";   //SJ
  peRMSError.close();

 ofstream myfile6;            //SJ
  myfile6.open ( directory+ "Norm.dat", ios::app);   //SJ
  myfile6 << fct3->GetParameter(4);   //SJ
  myfile6<<"\n";   //SJ
  myfile6.close();

 ofstream myfile7;            //SJ
  myfile7.open ( directory+ "ped mean.dat", ios::app);   //SJ
  myfile7 << fct3->GetParameter(5);   //SJ
  myfile7<<"\n";   //SJ
  myfile7.close();

ofstream myfile8;            //SJ
  myfile8.open ( directory+ "ped RMS.dat", ios::app);   //SJ
  myfile8 << fct3->GetParameter(2);   //SJ
  myfile8<<"\n";   //SJ
  myfile8.close();


ofstream myfile10;            //SJ
  myfile10.open ( directory+ "Mu Error.dat", ios::app);   //SJ
  myfile10 << fct3->GetParError(0);   //SJ
  myfile10<<"\n";   //SJ
  myfile10.close();

ofstream myfileMuCT;            //SJ
  myfileMuCT.open ( directory+ "Mu ct.dat", ios::app);   //SJ
  myfileMuCT << fct3->GetParameter(6);   //SJ
  myfileMuCT<<"\n";   //SJ
  myfileMuCT.close();

ofstream myfileMuCTErr;            //SJ
  myfileMuCTErr.open ( directory+ "Mu ct Error.dat", ios::app);   //SJ
  myfileMuCTErr << fct3->GetParError(6);   //SJ
  myfileMuCTErr<<"\n";   //SJ
  myfileMuCTErr.close();

ofstream myfile11;            //SJ
  myfile11.open ( directory+ "pedX.dat", ios::app);   //SJ
  myfile11 << pedX2;   //SJ
  myfile11<<"\n";   //SJ
  myfile11.close();
  /*
ofstream fileGainfactor;            //SJ
  fileGainfactor.open ( directory+ "gainfactor.txt", ios::app);   //SJ
  fileGainfactor << gainfactor;   //SJ
  fileGainfactor<<"\n";   //SJ
```

Appendix P

```
  fileGainfactor.close();
  */
//Dead channels
  if(fct3->GetParameter(1)/(fct3->GetParameter(3))<0.8)
          {
 ofstream fileDeadChannels;            //SJ
  fileDeadChannels.open ( directory+ "DeadChannels.dat", ios::app);   //SJ
  fileDeadChannels << index+1;   //SJ
  fileDeadChannels<<"\n";   //SJ
  fileDeadChannels.close();
          }
        if(fct3->GetParameter(1)/(fct3->GetParameter(3))>3)
          {
 ofstream fileDeadChannels;            //SJ
  fileDeadChannels.open ( directory+ "DeadChannels.dat", ios::app);   //SJ
  fileDeadChannels << index+1;   //SJ
  fileDeadChannels<<"\n";   //SJ
  fileDeadChannels.close();
          }
if(fct3->GetParameter(1)/(fct3->GetParameter(3))>0.8)
          {
if(fct3->GetParameter(1)/(fct3->GetParameter(3))<3)
          {
if(fct3->GetParameter(0)<0.00001)
  {
 ofstream fileDeadChannels;            //SJ
  fileDeadChannels.open ( directory+ "DeadChannels.dat", ios::app);   //SJ
  fileDeadChannels << index+1;   //SJ
  fileDeadChannels<<"\n";   //SJ
  fileDeadChannels.close();
  }}}

if(fct3->GetParameter(1)/(fct3->GetParameter(3))>0.8)
          {
if(fct3->GetParameter(1)/(fct3->GetParameter(3))<3)
          {
if(fct3->GetParameter(0)>0.00001)
  {
if(fct3->GetParameter(1)<40)
  {
 ofstream fileDeadChannels;            //SJ
  fileDeadChannels.open ( directory+ "DeadChannels.dat", ios::app);   //SJ
  fileDeadChannels << index+1;   //SJ
  fileDeadChannels<<"\n";   //SJ
  fileDeadChannels.close();
  }}}}

 directory+= "ROOT/";
  gSystem->MakeDirectory(directory);
 directory+= index+1;
pedestalDisp->SaveAs(directory+ ".root");

        TString directory2 = ;
 directory2+= "Run_";
 directory2+= Runnr;
 // gSystem->MakeDirectory(directory);
directory2+= "/";
 directory2+= PMTnr;
 directory2+= "/";
 // gSystem->MakeDirectory(directory);

 directory2+= "GIF/";
  gSystem->MakeDirectory(directory2);
 directory2+= index+1;
pedestalDisp->SaveAs(directory2+ ".gif");

}
gROOT->reset();
```

Appendix Q

Data4.C:

```
#include "TMultiGraph.h"
#include "TFile.h"
#include "TTree.h"
#include "TBrowser.h"
#include "TH2.h"
#include "TRandom.h"
#include "TMath.h"
#include <iostream>
#include <fstream>
#include "TStyle.h"
#include "TText.h"
#include <iomanip>
#include <stdio.h>
#include "TSystem.h"

void Data4(int Runnr)
{ for (Int_t PMTnr=1;PMTnr<26;PMTnr++)

{ for (Int_t index=1;index<65;index++)
    {
TString directoryRead = ;
 directoryRead+= "Run_";
 directoryRead+= Runnr;
 directoryRead+= "/";
 directoryRead+= PMTnr;
 directoryRead+= "/";

ifstream inMu; //Declare the stream variable
   Double_t bufferMu;
   inMu.open( directoryRead+ "Mu.dat"); //Open the file.
   for(int iii = 0; iii < index; iii++){
   inMu>>bufferMu;}  //Read the number.
   inMu.close();//Close the file.

ifstream inMuErr; //Declare the stream variable
   Double_t bufferMuErr;
   inMuErr.open( directoryRead+ "Mu Error.dat"); //Open the file.
   for(int iii = 0; iii < index; iii++){
   inMuErr>>bufferMuErr;}  //Read the number.
   inMuErr.close();//Close the file.

ifstream inMuCT; //Declare the stream variable
   Double_t bufferMuCT;
   inMuCT.open( directoryRead+ "Mu ct.dat"); //Open the file.
   for(int iii = 0; iii < index; iii++){
   inMuCT>>bufferMuCT;}  //Read the number.
   inMuCT.close();//Close the file.

ifstream inMuCTErr; //Declare the stream variable
   Double_t bufferMuCTErr;
   inMuCTErr.open( directoryRead+ "Mu ct Error.dat"); //Open the file.
   for(int iii = 0; iii < index; iii++){
   inMuCTErr>>bufferMuCTErr;}  //Read the number.
   inMuCTErr.close();//Close the file.

TString directoryWrite = ;
 directoryWrite= "Run_";
 directoryWrite+= Runnr;
 directoryWrite+= "/";
 directoryWrite+= PMTnr;
 directoryWrite+= "/";

 ofstream outData4;            //SJ
  outData4.open ( directoryWrite+ "Data4.dat", ios::app);   //SJ
  outData4 << bufferMu ;   //SJ
```

Appendix Q

```
outData4<<"\t";
outData4 << bufferMuErr ;
outData4<<"\t";
outData4 << bufferMuCT ;
outData4<<"\t";
outData4 << bufferMuCTErr ;
outData4<<"\n";   //SJ
outData4.close();


  }}}
```

Light yield in ALFA1

2 weeks of cosmic

DAQ by 5 Orsay test boards

1-12-2009

Sune Jakobsen, Sune.Jakobsen@CERN.ch

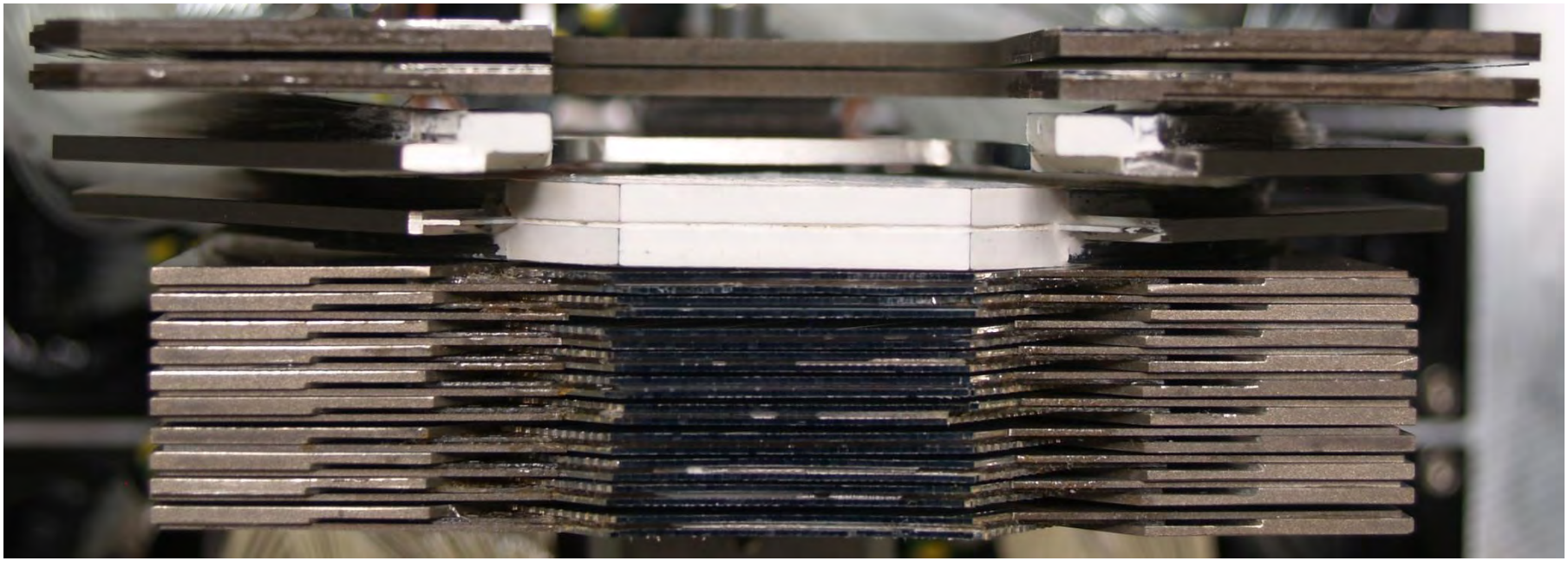

Fitting method:
First the MAPMT is calibrated using very low intensity LED light. The position of the 1 photo electron is fund by fitting:

$$f(x) = N \cdot \left(\sum_{i=0}^{n} \left[\frac{e^{-\mu} \cdot \mu^{i}}{i!} \cdot \frac{1}{\sqrt{2\pi}\sqrt{i \cdot \sigma_{1PE}{}^{2} + \sigma_{ped}{}^{2}}} \cdot e^{\frac{-(x - Q_{ped} - i \cdot Q_{1PE})^{2}}{2 \cdot (i \cdot \sigma_{1PE}{}^{2} + \sigma_{ped}{}^{2})}} \right] \right.$$

N	Normalizationfactor	Q_{1PE}	Charge of the 1 photoelectron
i	Number of photoelectrons	σ_{ped}	Charge deviation of the pedestal
n	Maximum number of photoelectrons	σ_{1PE}	Charge deviation of the 1 photoelectron
Q_{ped}	Charge of the pedestal	μ	Main light yield

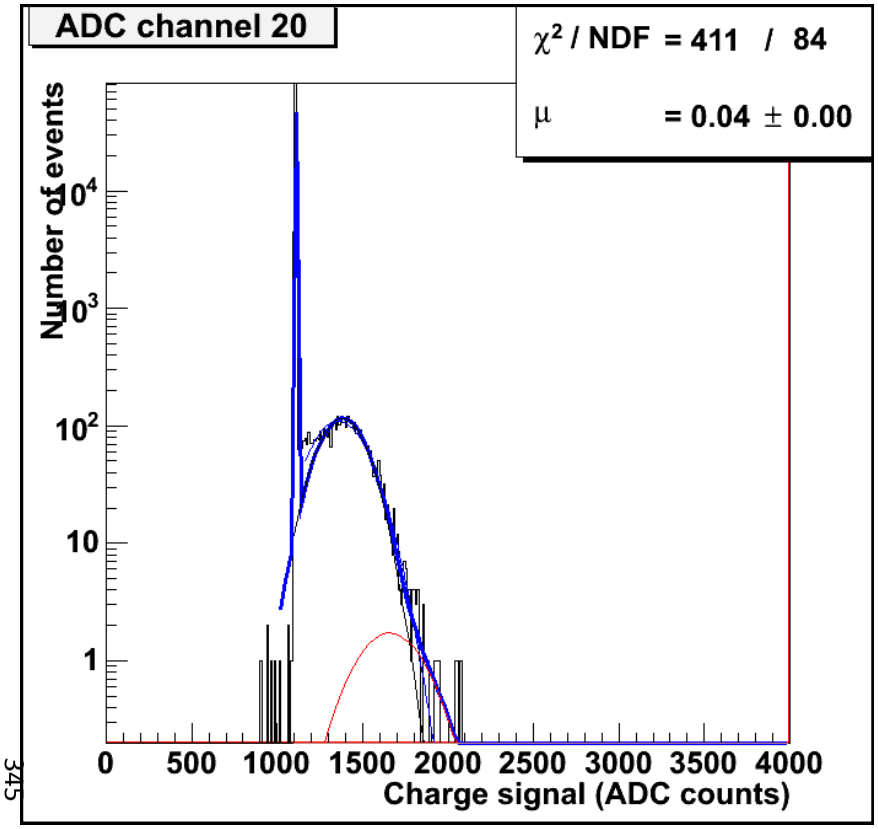

Most parameters (marked with red) are then locked to the calibration value. Data from the cosmic measurements are fitted with:

$$f(x) = N \cdot \left(\sum_{i=1}^{n} \left[\frac{e^{-\mu} \cdot \mu^{i}}{i!} \cdot \frac{1}{\sqrt{2\pi}\sqrt{i \cdot \sigma_{1PE}{}^{2} + \sigma_{ped}{}^{2}}} \cdot e^{\frac{-(x - Q_{ped} - i \cdot Q_{1PE})^{2}}{2 \cdot (i \cdot \sigma_{1PE}{}^{2} + \sigma_{ped}{}^{2})}} \right] \right.$$
$$\left. + \sum_{i=1}^{n} \left[\frac{e^{-\mu_{CT}} \cdot \mu_{CT}{}^{i}}{i!} \cdot \frac{1}{\sqrt{2\pi}\sqrt{i \cdot \sigma_{1PE}{}^{2} + \sigma_{ped}{}^{2}}} \cdot e^{\frac{-(x - Q_{ped} - i \cdot Q_{1PE})^{2}}{2 \cdot (i \cdot \sigma_{1PE}{}^{2} + \sigma_{ped}{}^{2})}} \right] \right)$$

μ_{CT} Crosstalk light yield

The second sum is included to described crosstalk.

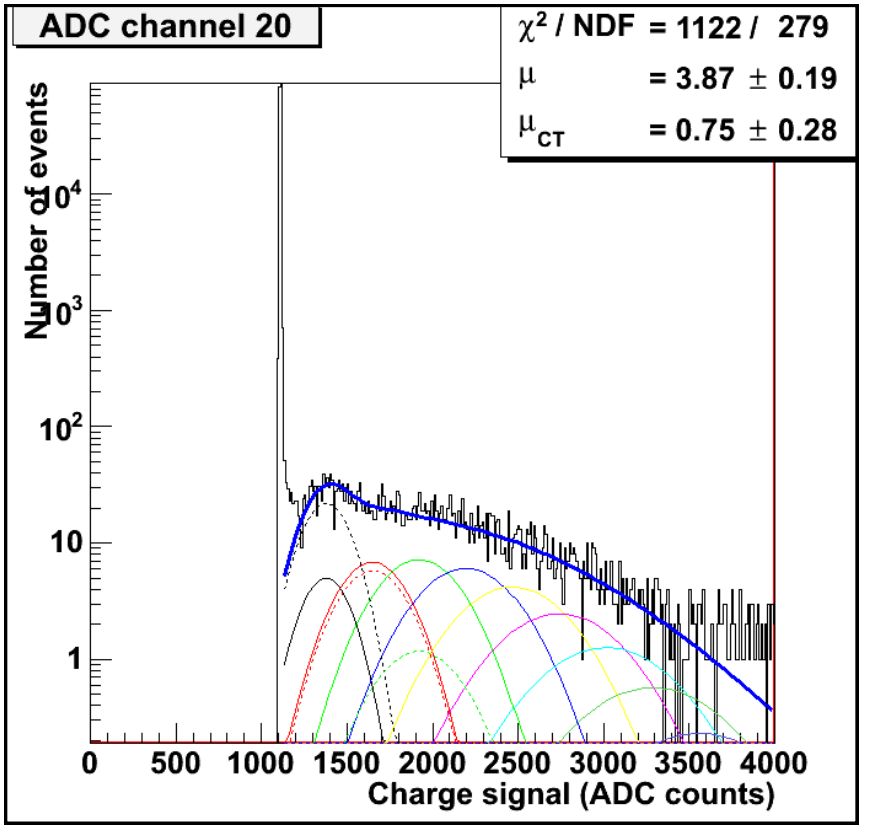

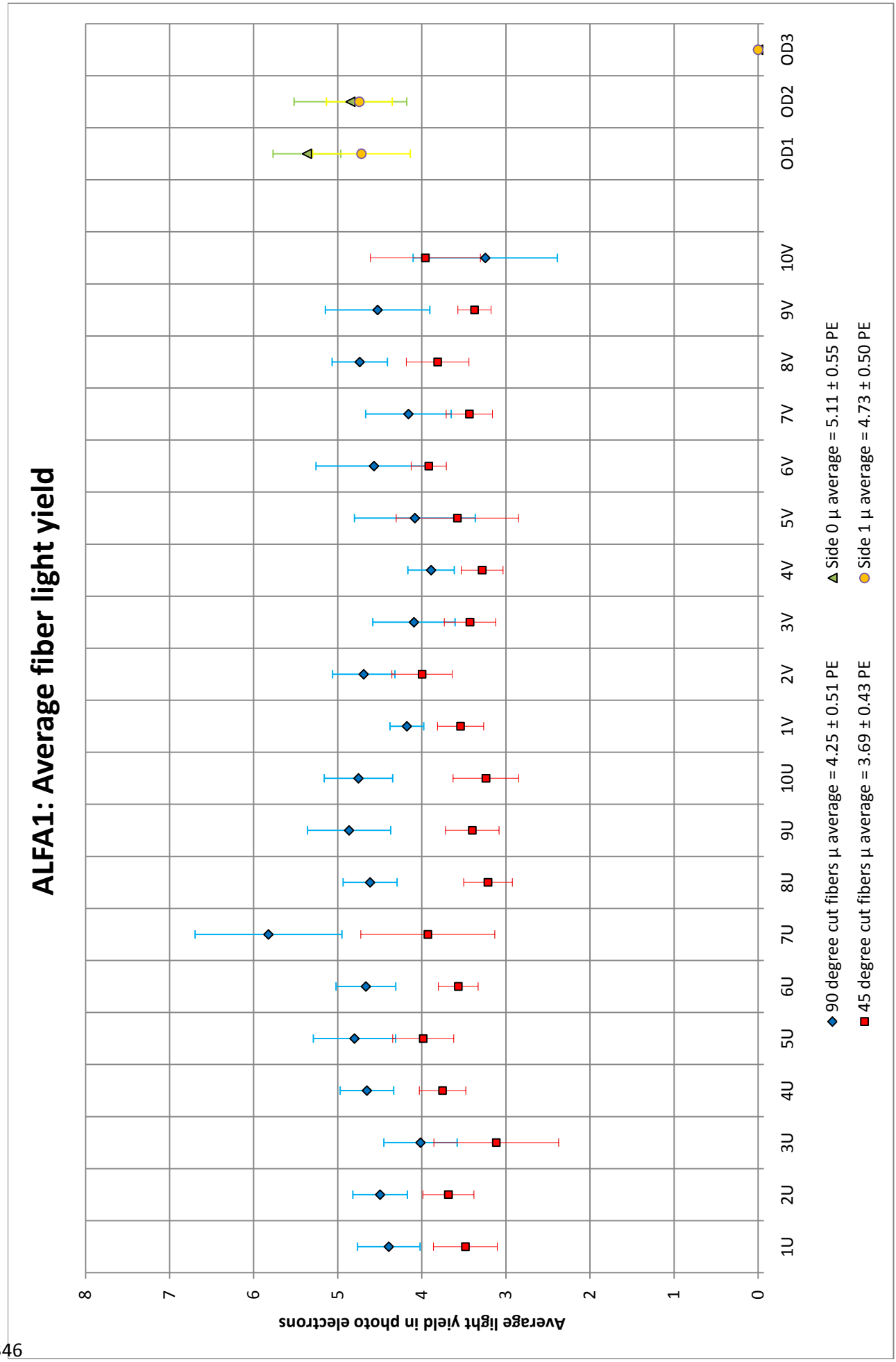
ALFA1: Average fiber light yield
Average light yield in photo electrons
0
1
2
3
4
5
6
7
8
1U
2U
3U
4U
5U
6U
7U
8U
9U
10U
1V
2V
3V
4V
5V
6V
7V
8V
9V
10V
OD1
OD2
OD3
90 degree cut fibers μ average = 4.25 ± 0.51 PE
45 degree cut fibers μ average = 3.69 ± 0.43 PE
Side 0 μ average = 5.11 ± 0.55 PE
Side 1 μ average = 4.73 ± 0.50 PE

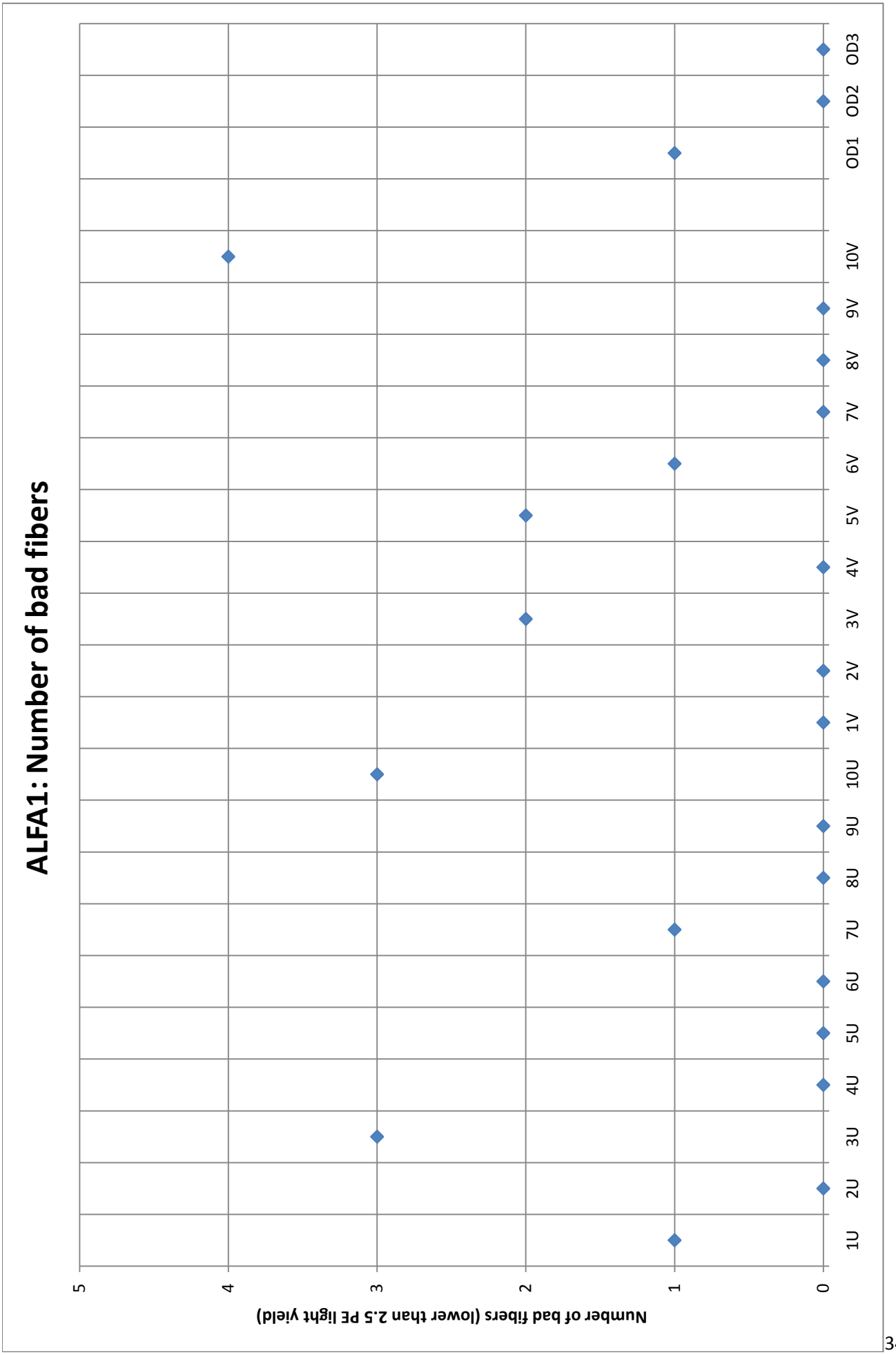
ALFA1: Number of bad fibers
Number of bad fibers (lower than 2.5 PE light yield)
0
1
2
3
4
5
1U
2U
3U
4U
5U
6U
7U
8U
9U
10U
1V
2V
3V
4V
5V
6V
7V
8V
9V
10V
OD1
OD2
OD3

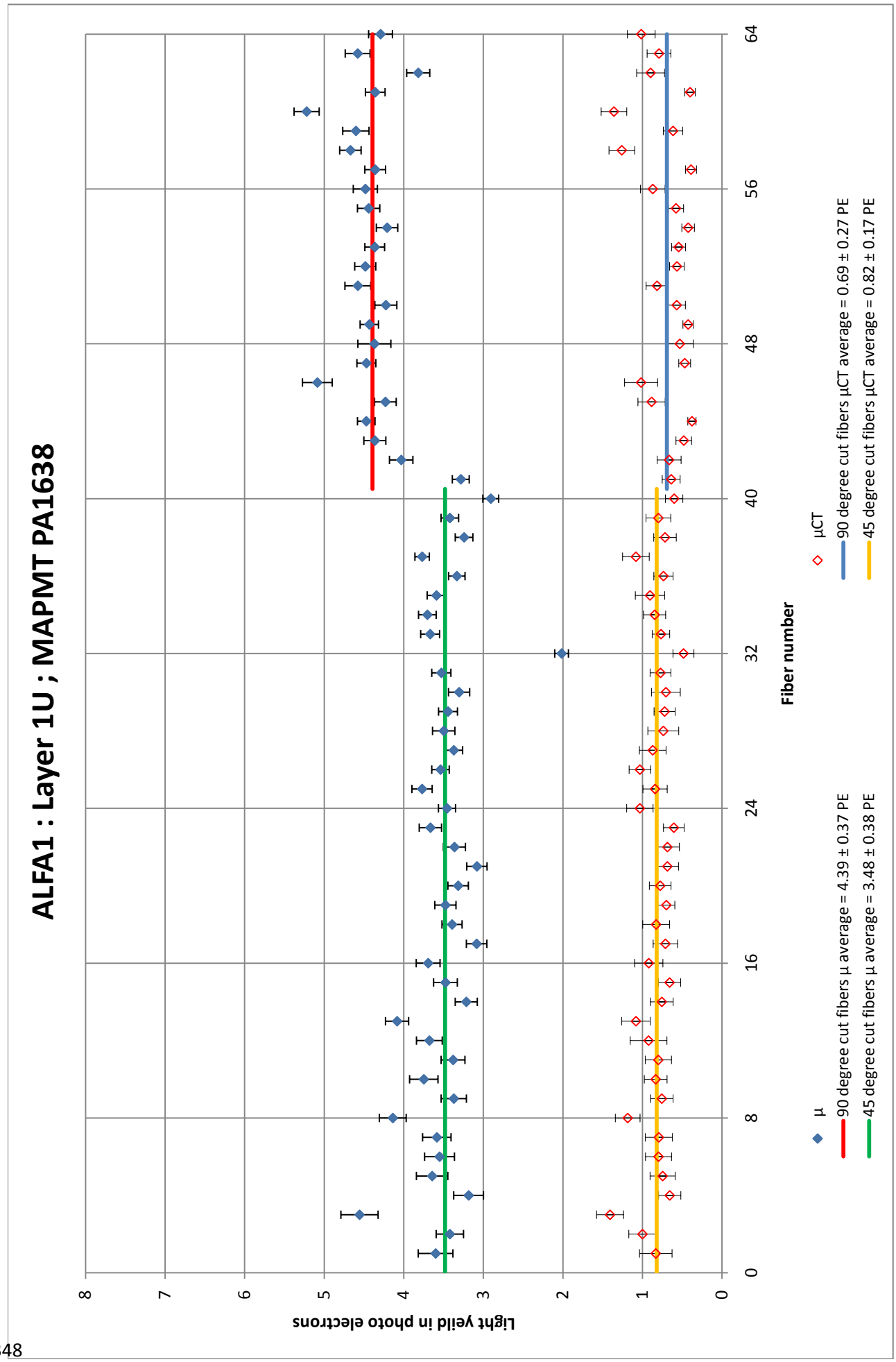
ALFA1 : Layer 1U ; MAPMT PA1638
Light yeild in photo electrons
Fiber number
0
1
2
3
4
5
6
7
8
0
8
16
24
32
40
48
56
64
μ
μCT
90 degree cut fibers μ average = 4.39 ± 0.37 PE
45 degree cut fibers μ average = 3.48 ± 0.38 PE
90 degree cut fibers μCT average = 0.69 ± 0.27 PE
45 degree cut fibers μCT average = 0.82 ± 0.17 PE

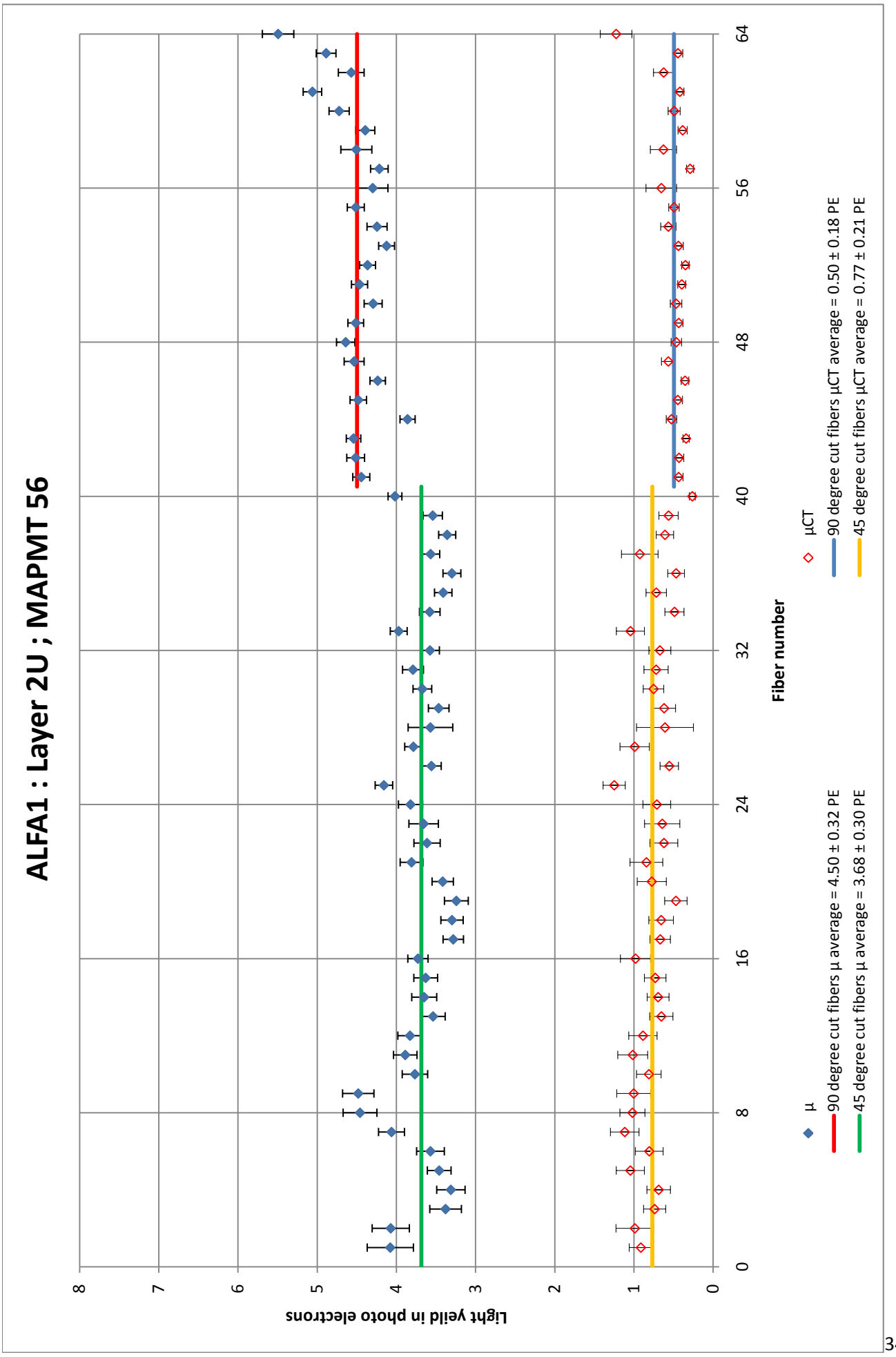
ALFA1 : Layer 2U ; MAPMT 56
Light yeild in photo electrons
Fiber number
0
1
2
3
4
5
6
7
8
0
8
16
24
32
40
48
56
64
μ
μCT
90 degree cut fibers μ average = 4.50 ± 0.32 PE
90 degree cut fibers μCT average = 0.50 ± 0.18 PE
45 degree cut fibers μ average = 3.68 ± 0.30 PE
45 degree cut fibers μCT average = 0.77 ± 0.21 PE

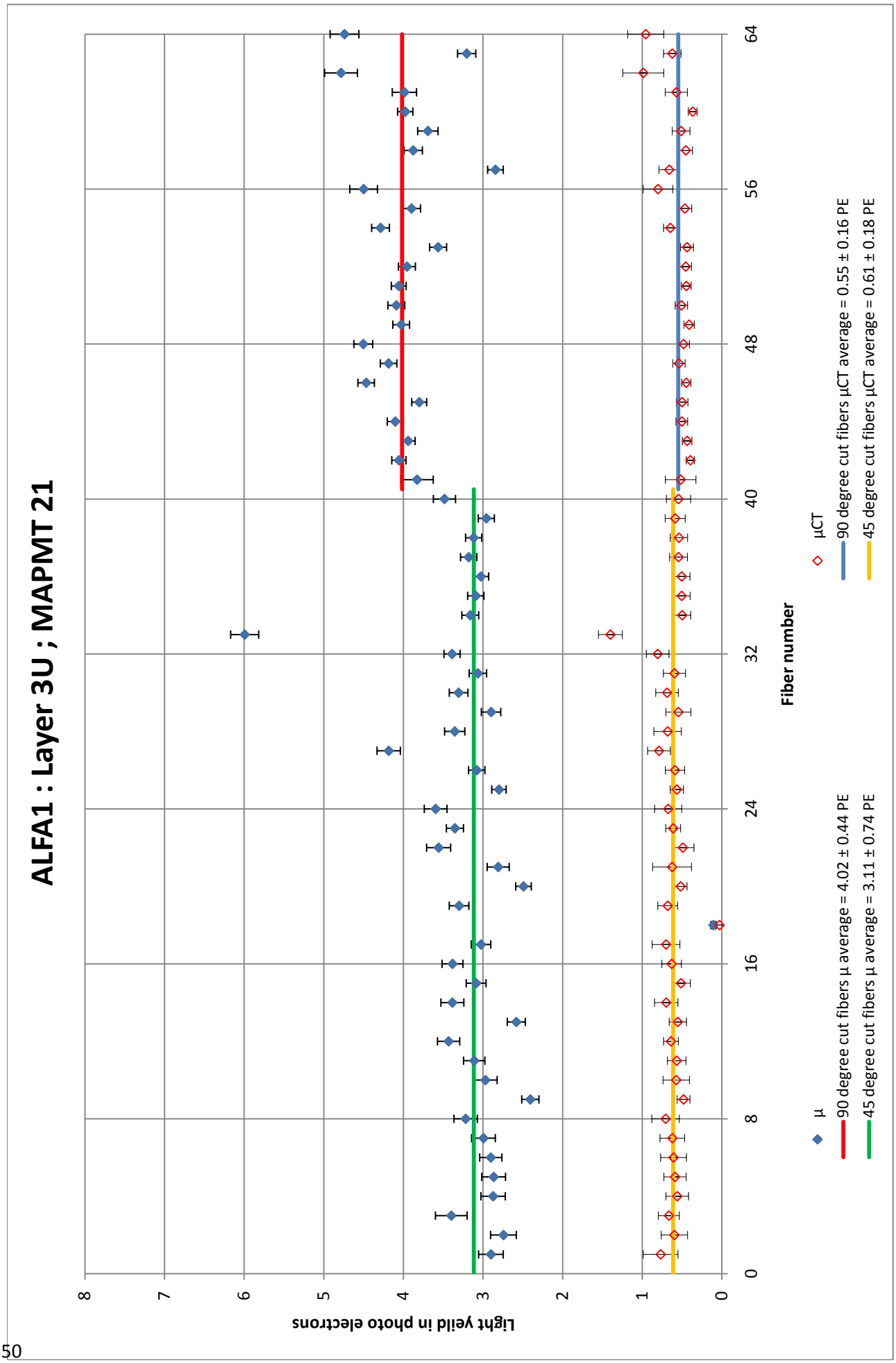
ALFA1 : Layer 3U ; MAPMT 21
Light yeild in photo electrons
Fiber number
0
1
2
3
4
5
6
7
8
0
8
16
24
32
40
48
56
64
μ
μCT
90 degree cut fibers μ average = 4.02 ± 0.44 PE
90 degree cut fibers μCT average = 0.55 ± 0.16 PE
45 degree cut fibers μ average = 3.11 ± 0.74 PE
45 degree cut fibers μCT average = 0.61 ± 0.18 PE

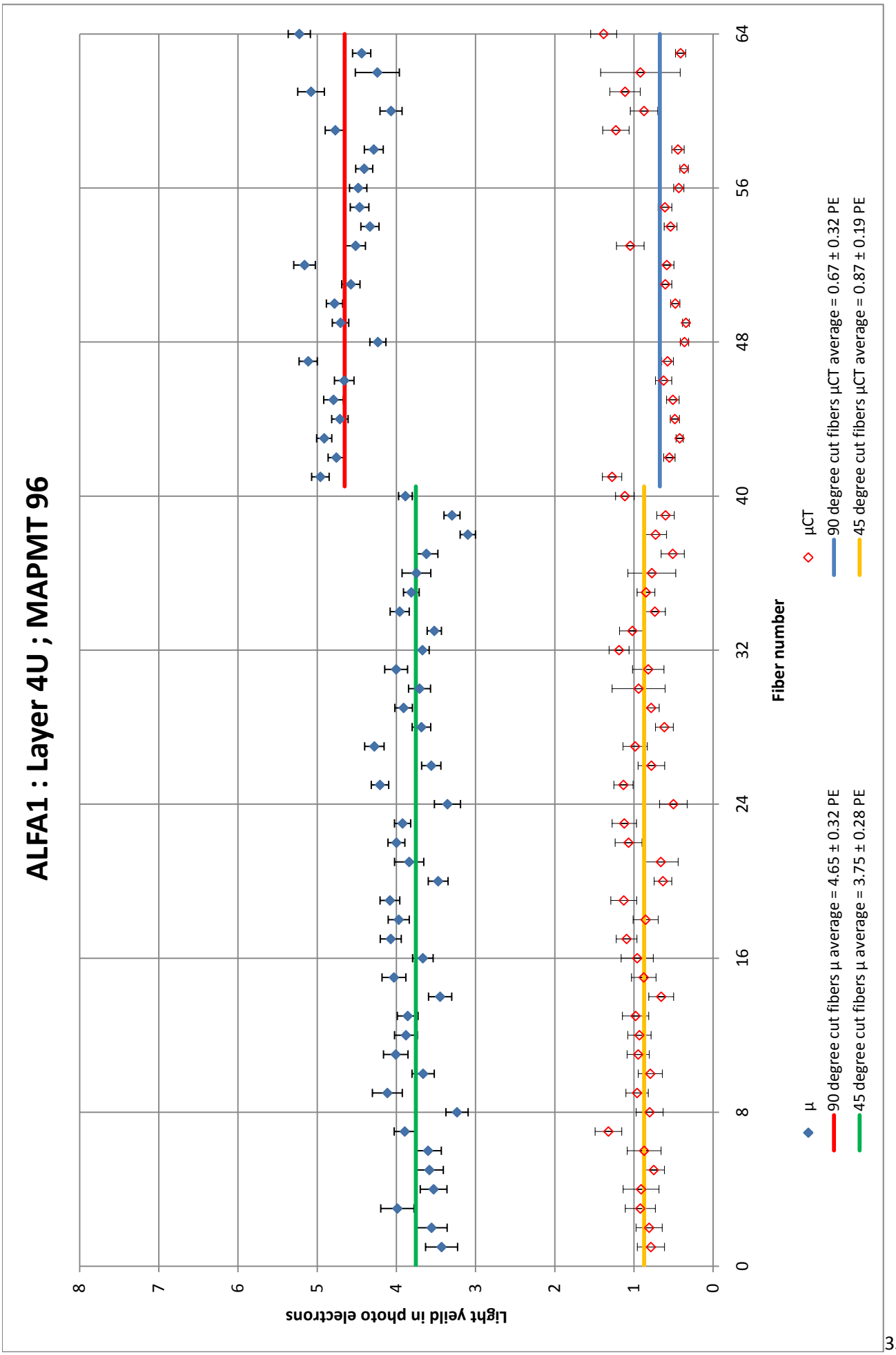
ALFA1 : Layer 4U ; MAPMT 96
Light yeild in photo electrons
Fiber number
μ
μCT
90 degree cut fibers μ average = 4.65 ± 0.32 PE
45 degree cut fibers μ average = 3.75 ± 0.28 PE
90 degree cut fibers μCT average = 0.67 ± 0.32 PE
45 degree cut fibers μCT average = 0.87 ± 0.19 PE

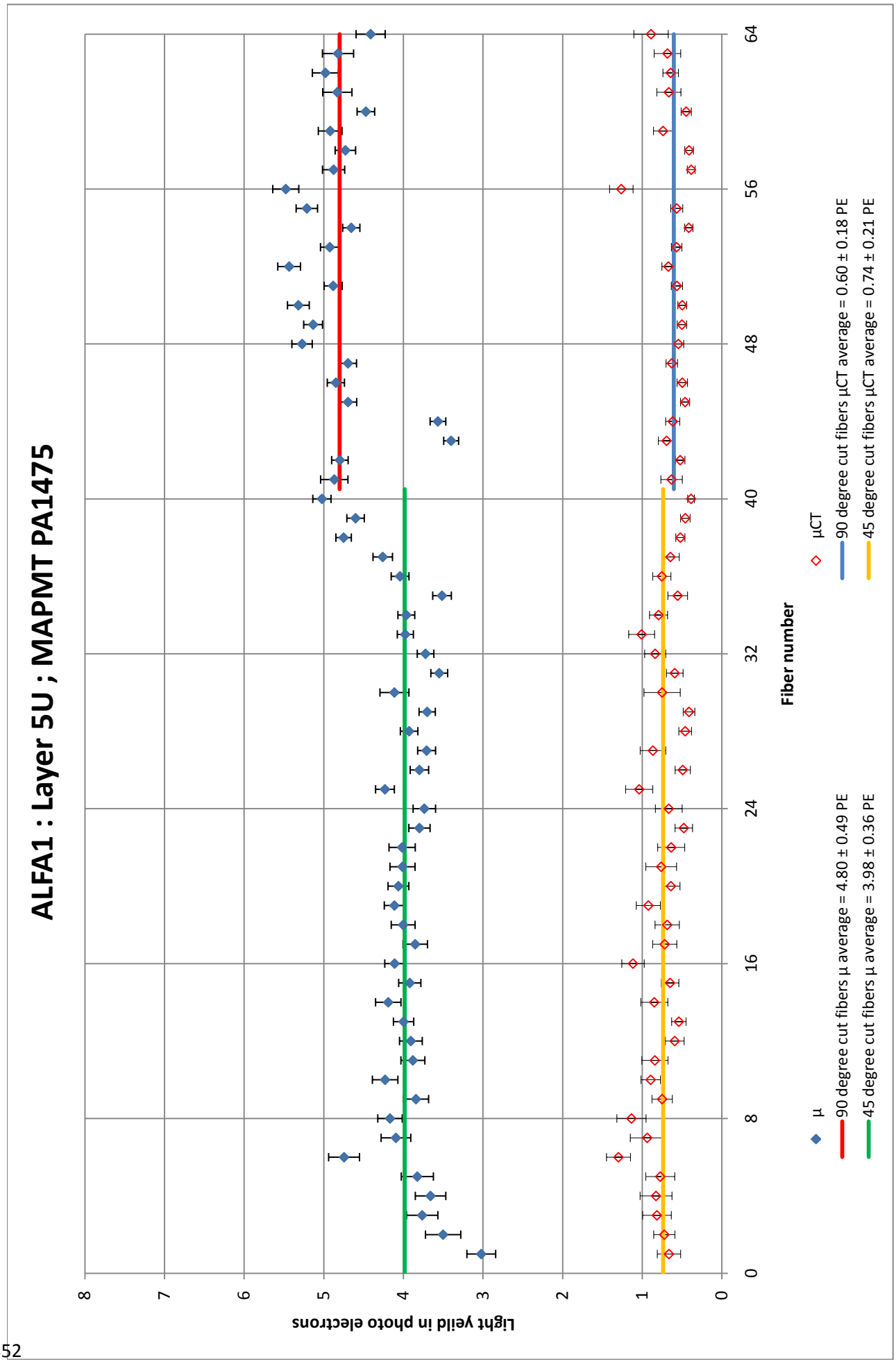
ALFA1 : Layer 5U ; MAPMT PA1475
Light yeild in photo electrons
Fiber number
μ
μCT
90 degree cut fibers μ average = 4.80 ± 0.49 PE
45 degree cut fibers μ average = 3.98 ± 0.36 PE
90 degree cut fibers μCT average = 0.60 ± 0.18 PE
45 degree cut fibers μCT average = 0.74 ± 0.21 PE

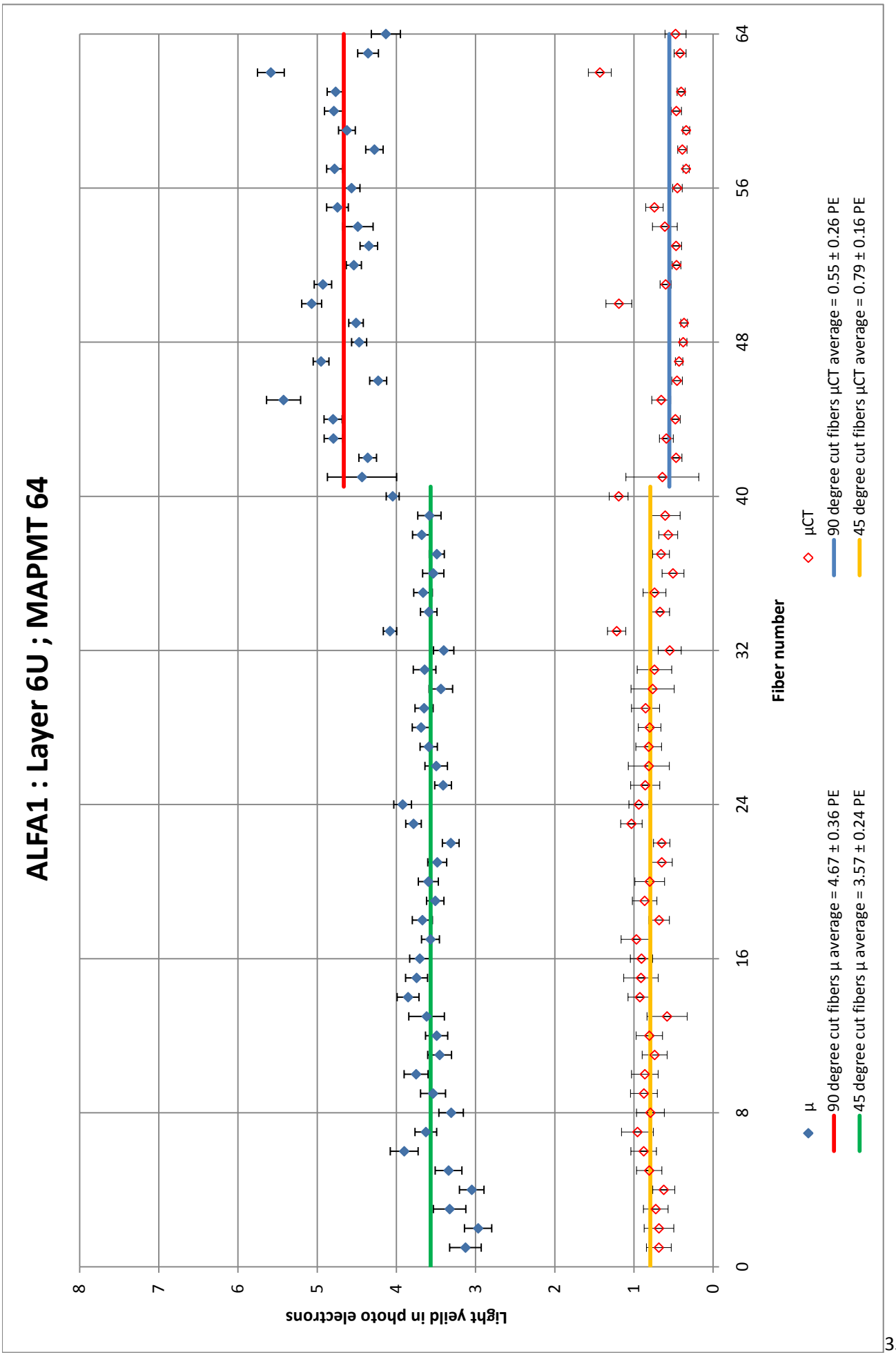
ALFA1 : Layer 6U ; MAPMT 64
Light yeild in photo electrons
Fiber number
0
1
2
3
4
5
6
7
8
0
8
16
24
32
40
48
56
64
μ
μCT
90 degree cut fibers μ average = 4.67 ± 0.36 PE
90 degree cut fibers μCT average = 0.55 ± 0.26 PE
45 degree cut fibers μ average = 3.57 ± 0.24 PE
45 degree cut fibers μCT average = 0.79 ± 0.16 PE

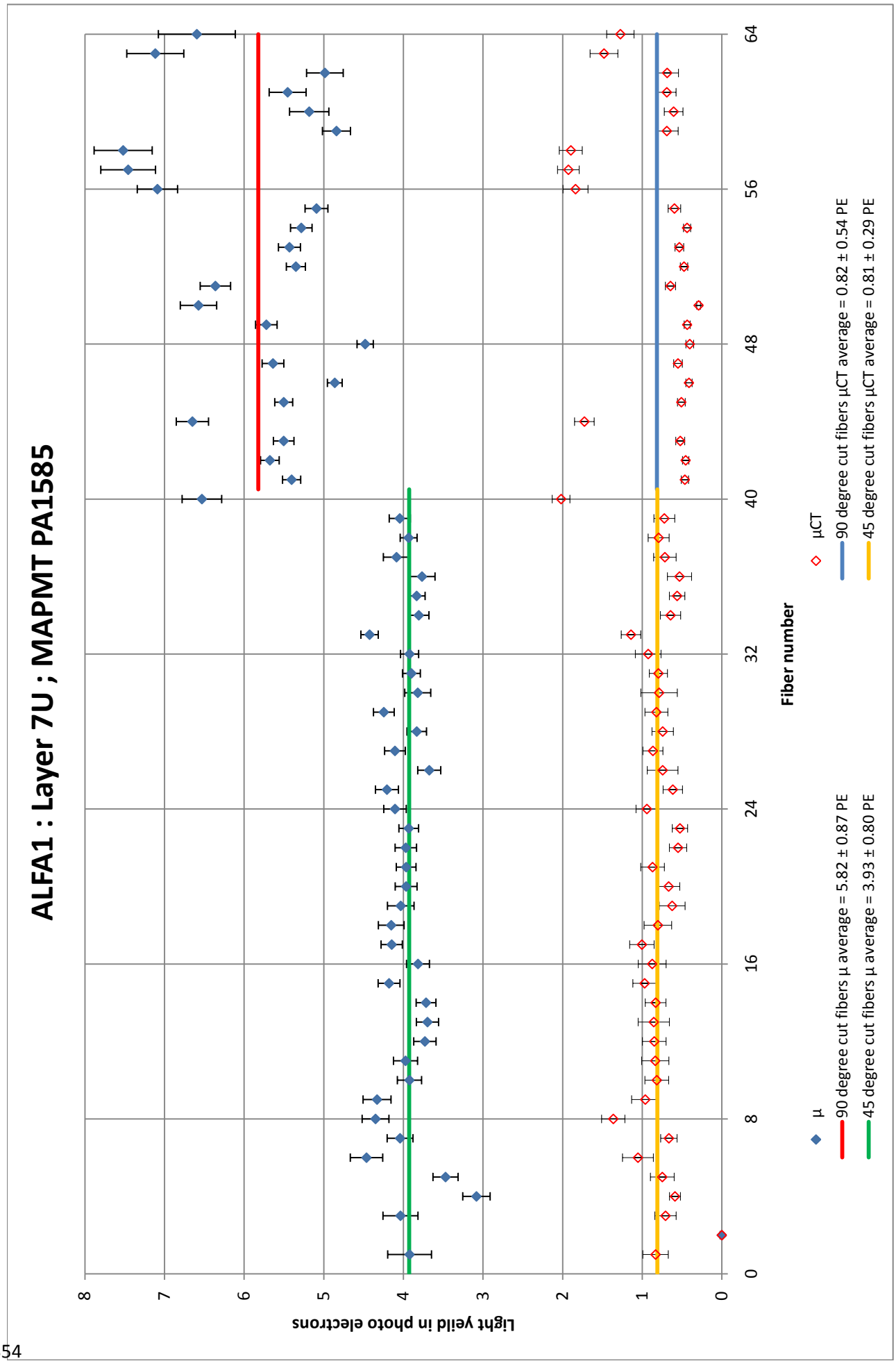
ALFA1 : Layer 7U ; MAPMT PA1585
Light yeild in photo electrons
Fiber number
0
1
2
3
4
5
6
7
8
0
8
16
24
32
40
48
56
64
μ
μCT
90 degree cut fibers μ average = 5.82 ± 0.87 PE
45 degree cut fibers μ average = 3.93 ± 0.80 PE
90 degree cut fibers μCT average = 0.82 ± 0.54 PE
45 degree cut fibers μCT average = 0.81 ± 0.29 PE

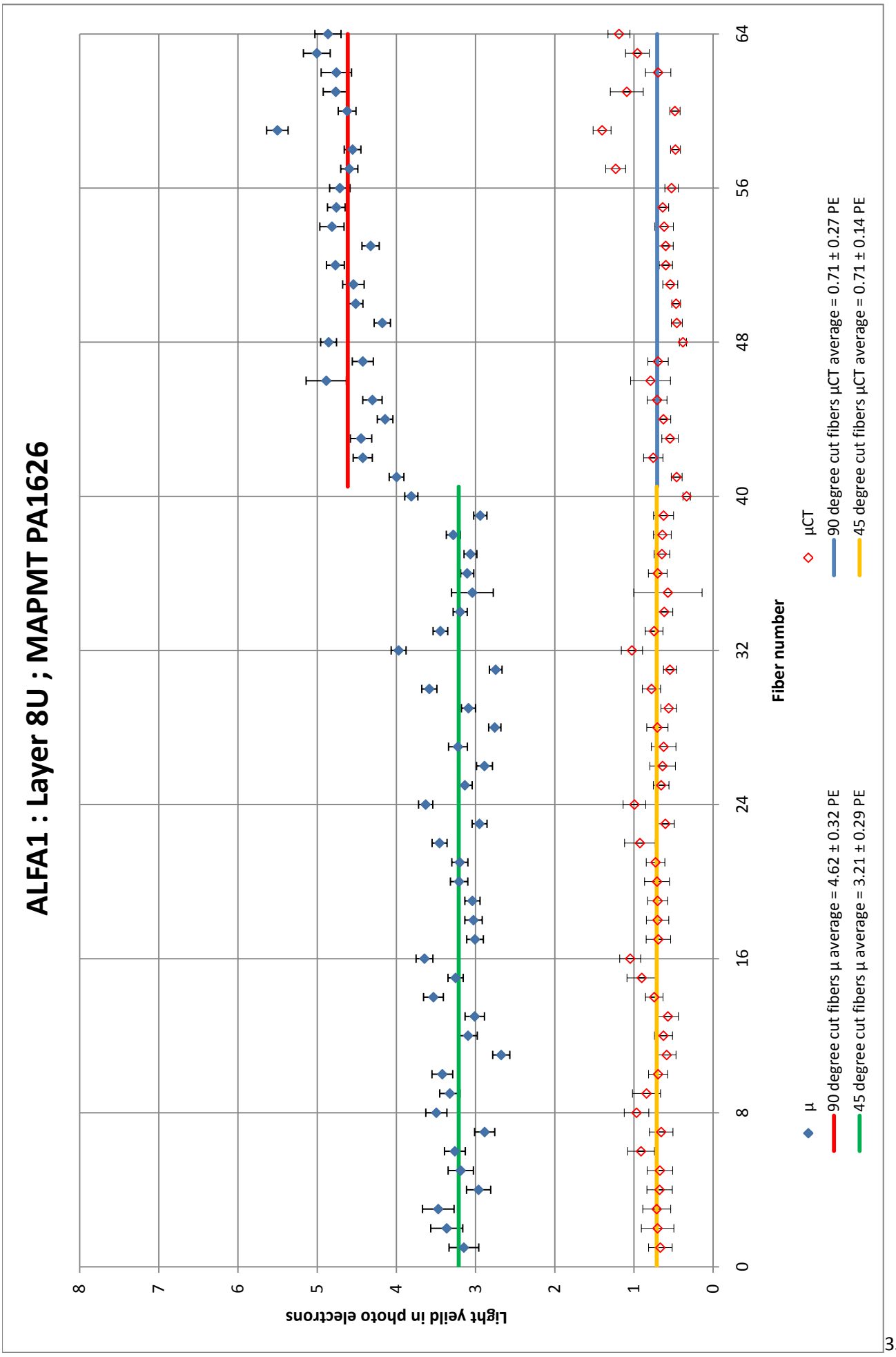
ALFA1 : Layer 8U ; MAPMT PA1626
Light yeild in photo electrons
Fiber number
0
1
2
3
4
5
6
7
8
0
8
16
24
32
40
48
56
64
μ
μCT
90 degree cut fibers μ average = 4.62 ± 0.32 PE
90 degree cut fibers μCT average = 0.71 ± 0.27 PE
45 degree cut fibers μ average = 3.21 ± 0.29 PE
45 degree cut fibers μCT average = 0.71 ± 0.14 PE

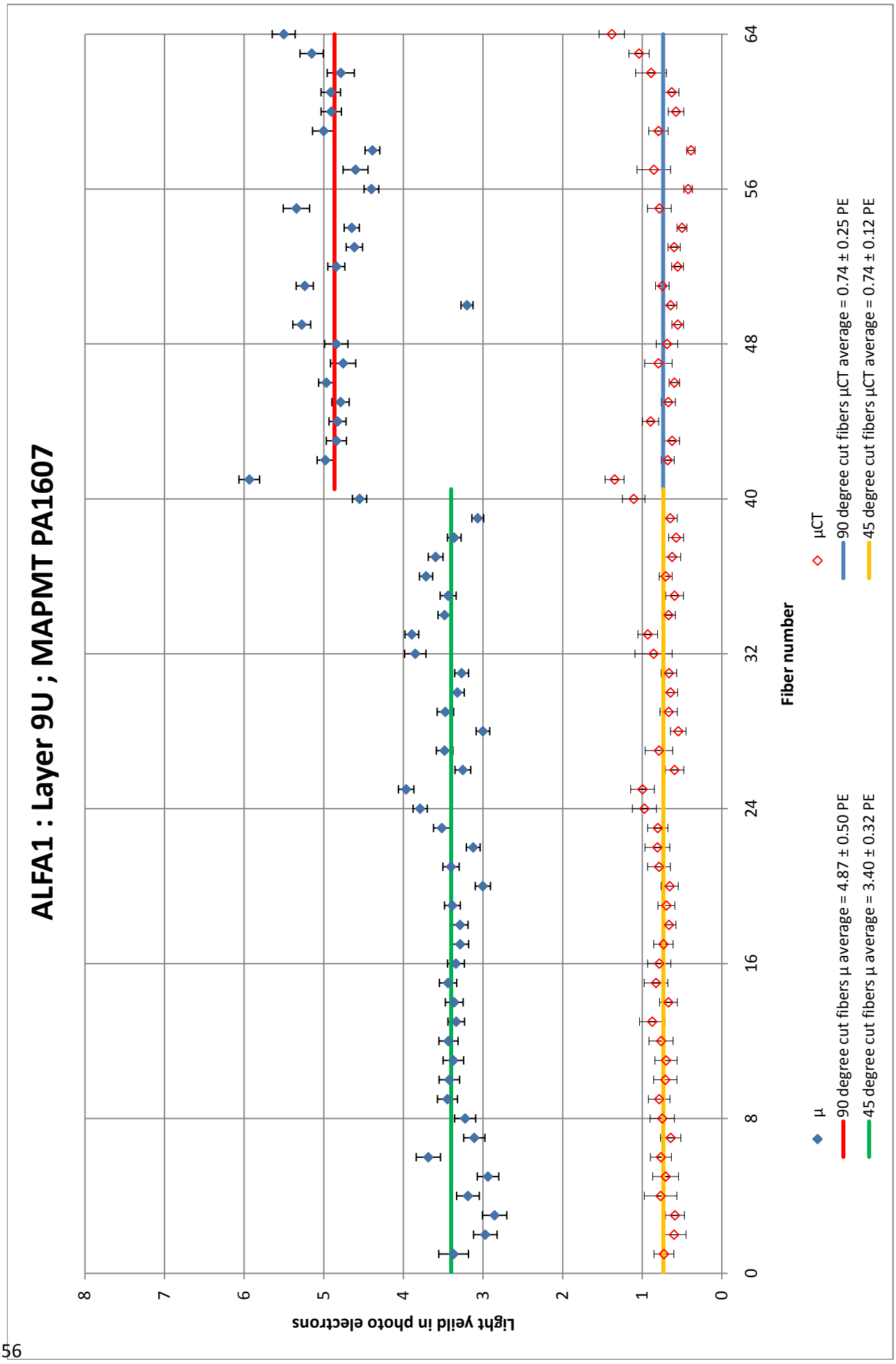
ALFA1 : Layer 9U ; MAPMT PA1607
Light yeild in photo electrons
Fiber number
0
1
2
3
4
5
6
7
8
0
8
16
24
32
40
48
56
64
μ
μCT
90 degree cut fibers μ average = 4.87 ± 0.50 PE
45 degree cut fibers μ average = 3.40 ± 0.32 PE
90 degree cut fibers μCT average = 0.74 ± 0.25 PE
45 degree cut fibers μCT average = 0.74 ± 0.12 PE

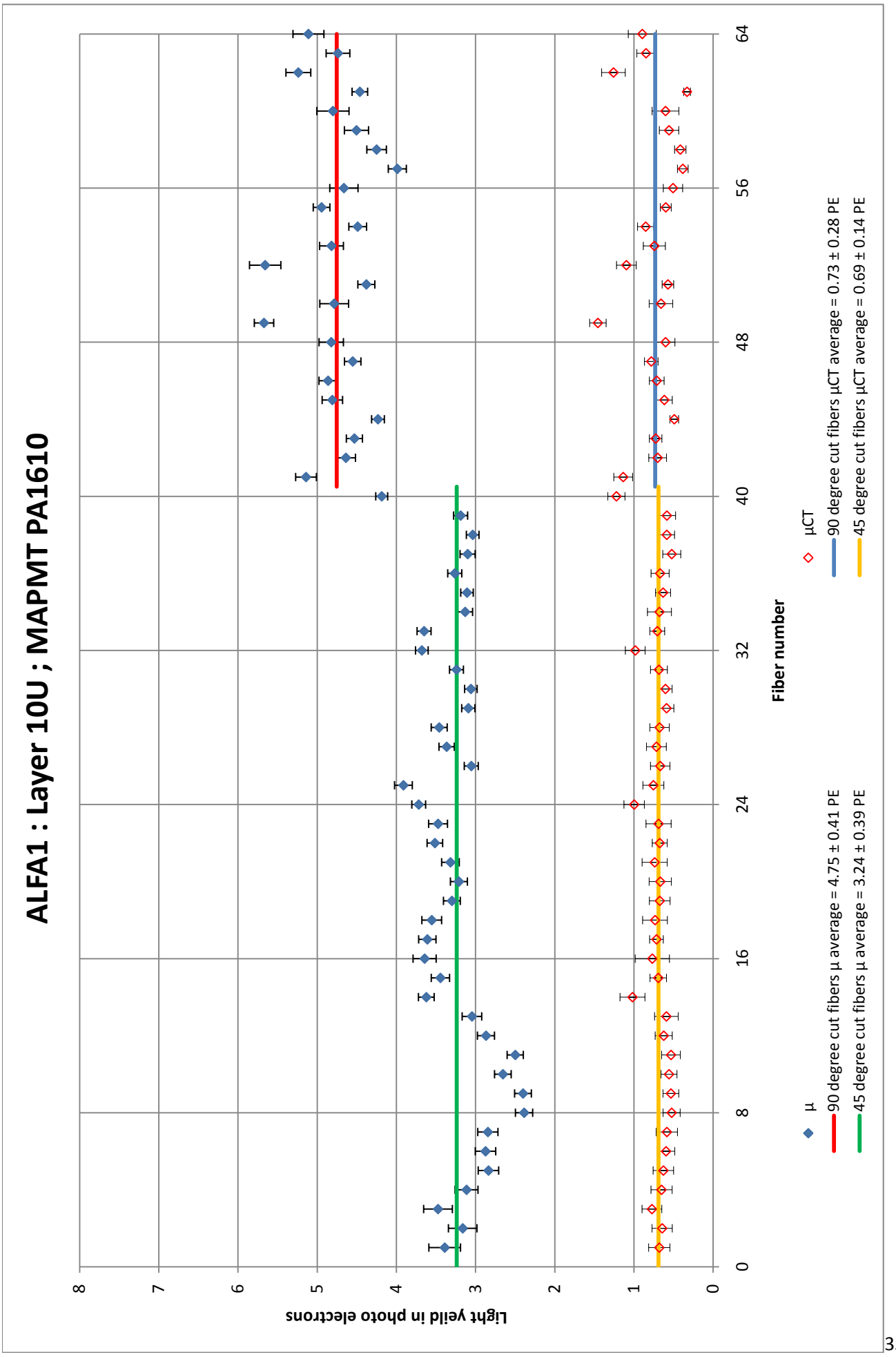
ALFA1 : Layer 10U ; MAPMT PA1610
Light yeild in photo electrons
Fiber number
0
1
2
3
4
5
6
7
8
0
8
16
24
32
40
48
56
64
μ
90 degree cut fibers μ average = 4.75 ± 0.41 PE
45 degree cut fibers μ average = 3.24 ± 0.39 PE
μCT
90 degree cut fibers μCT average = 0.73 ± 0.28 PE
45 degree cut fibers μCT average = 0.69 ± 0.14 PE

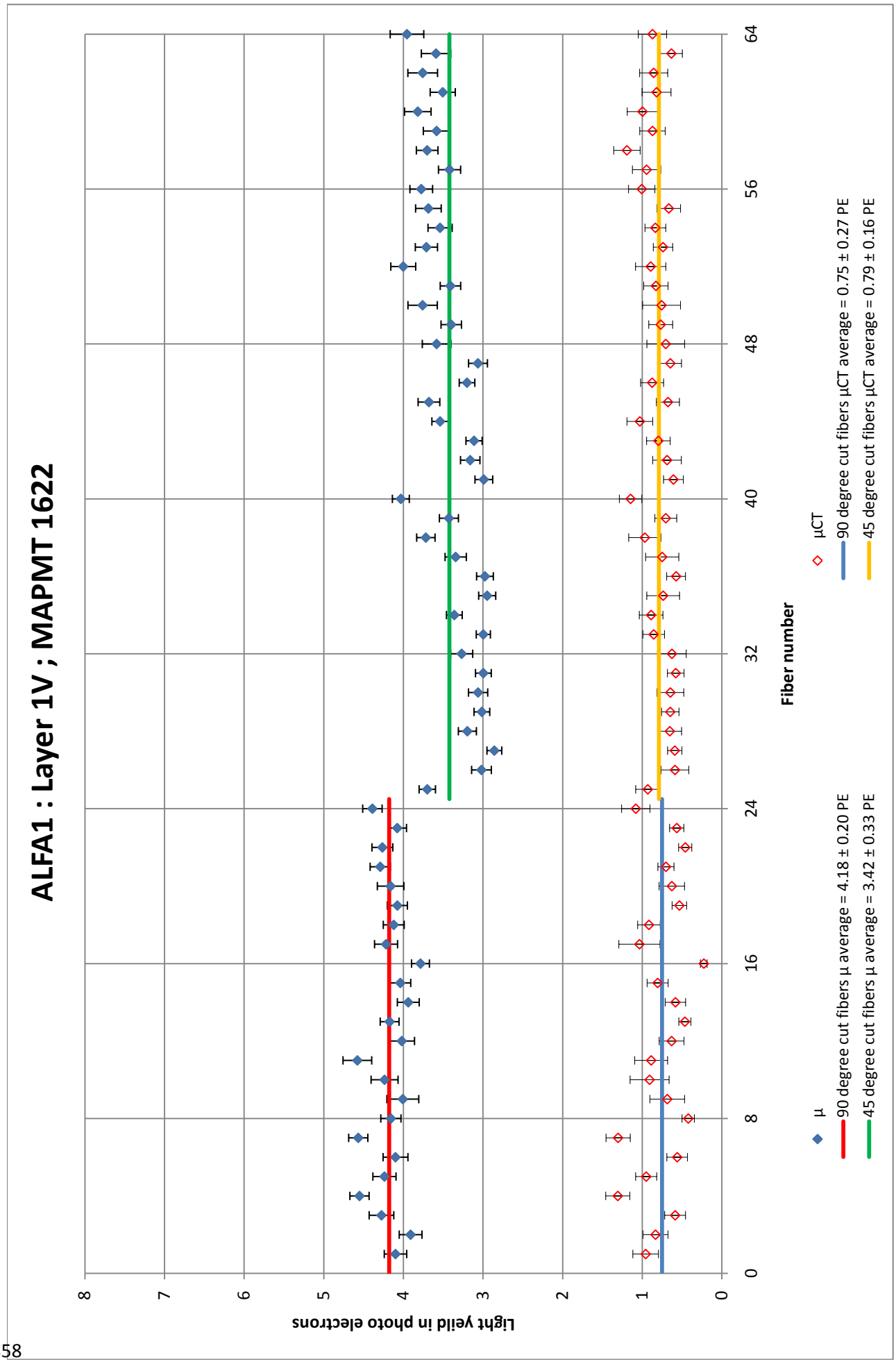
ALFA1 : Layer 1V ; MAPMT 1622
Light yeild in photo electrons
Fiber number
0
1
2
3
4
5
6
7
8
0
8
16
24
32
40
48
56
64
μ
μCT
90 degree cut fibers μ average = 4.18 ± 0.20 PE
90 degree cut fibers μCT average = 0.75 ± 0.27 PE
45 degree cut fibers μ average = 3.42 ± 0.33 PE
45 degree cut fibers μCT average = 0.79 ± 0.16 PE

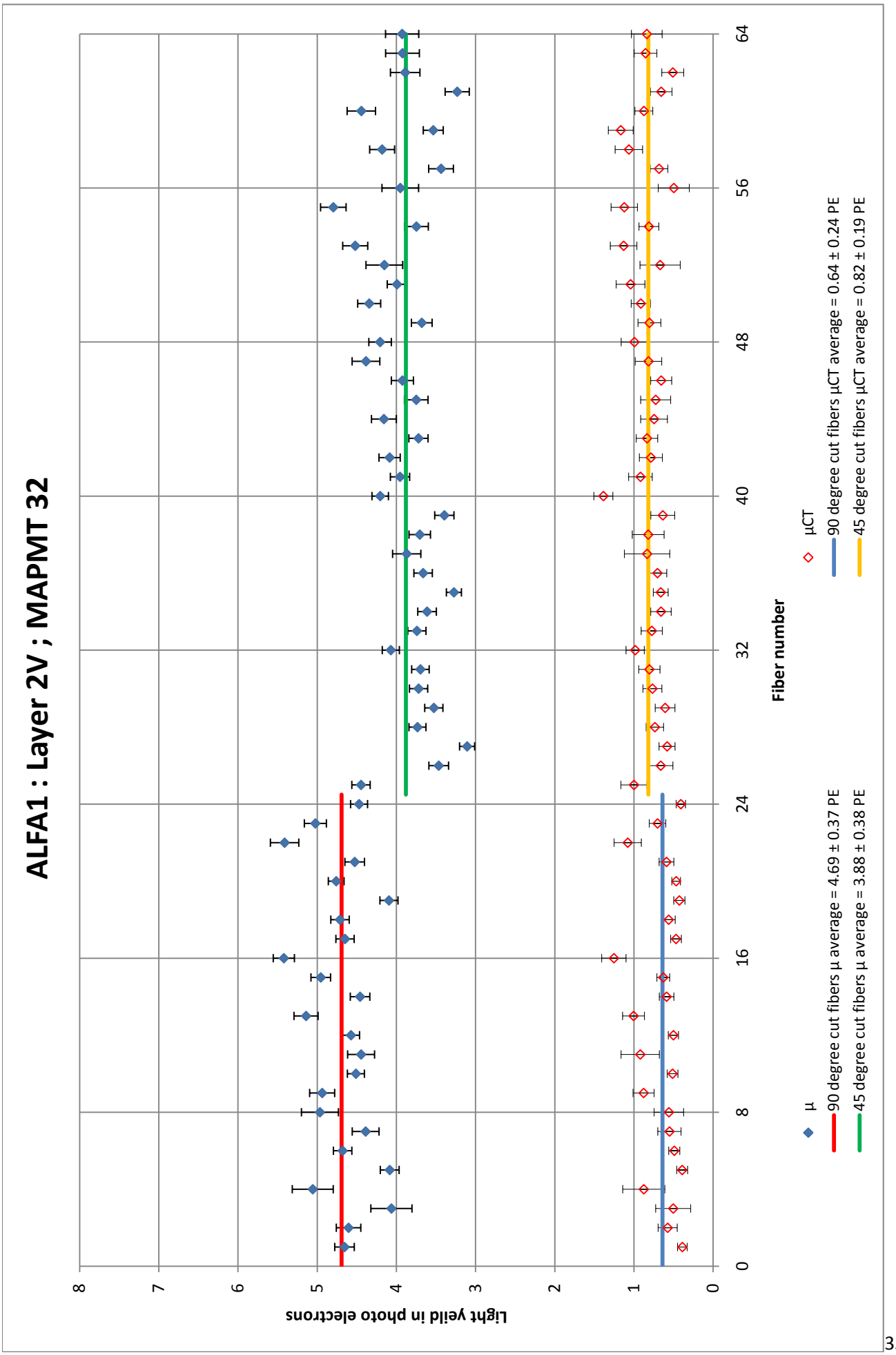
ALFA1 : Layer 2V ; MAPMT 32
Light yeild in photo electrons
Fiber number
0
1
2
3
4
5
6
7
8
0
8
16
24
32
40
48
56
64
μ
μCT
90 degree cut fibers μ average = 4.69 ± 0.37 PE
45 degree cut fibers μ average = 3.88 ± 0.38 PE
90 degree cut fibers μCT average = 0.64 ± 0.24 PE
45 degree cut fibers μCT average = 0.82 ± 0.19 PE

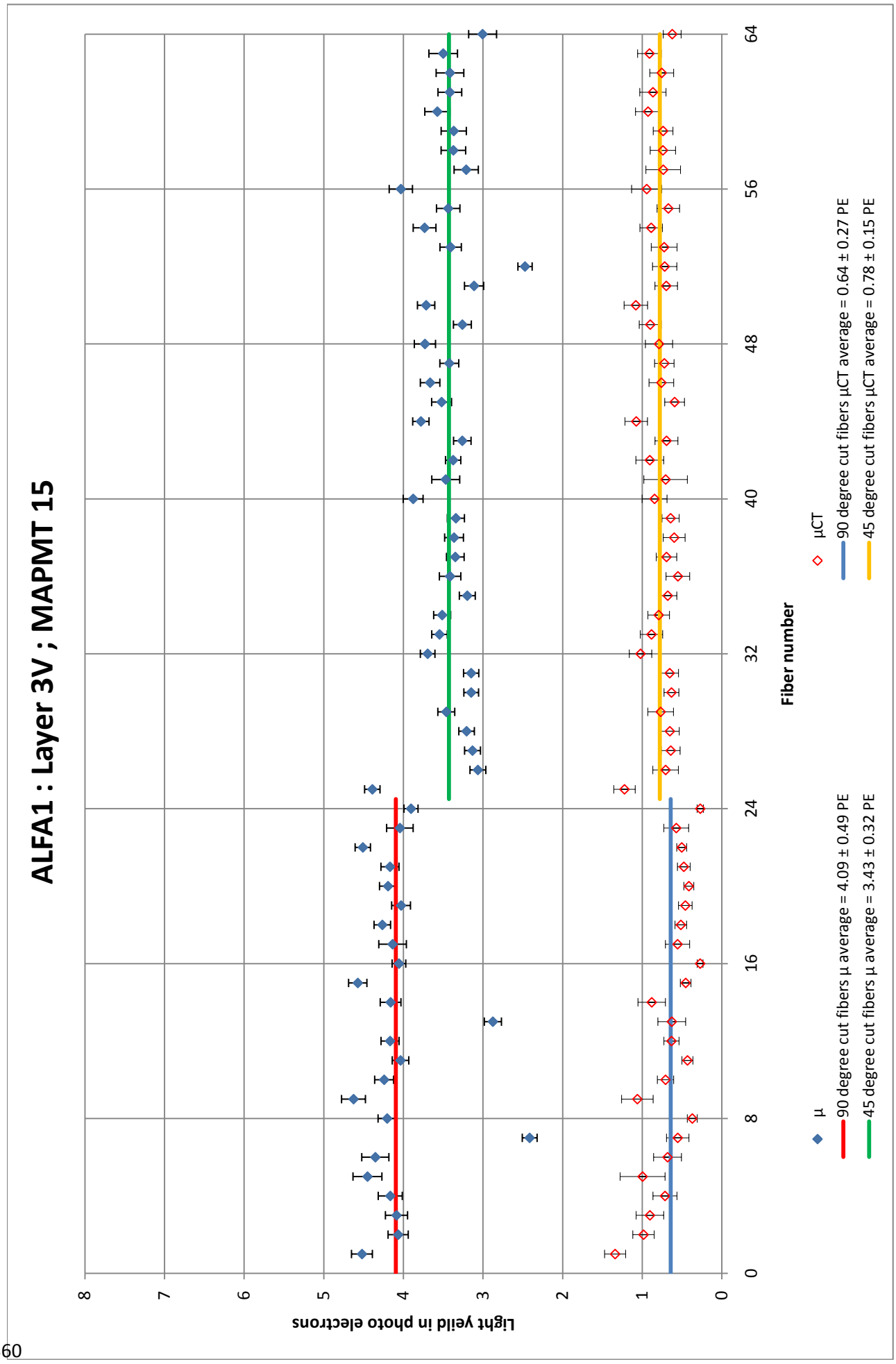
ALFA1 : Layer 3V ; MAPMT 15
Light yeild in photo electrons
Fiber number
0
1
2
3
4
5
6
7
8
0
8
16
24
32
40
48
56
64
μ
90 degree cut fibers μ average = 4.09 ± 0.49 PE
45 degree cut fibers μ average = 3.43 ± 0.32 PE
μCT
90 degree cut fibers μCT average = 0.64 ± 0.27 PE
45 degree cut fibers μCT average = 0.78 ± 0.15 PE

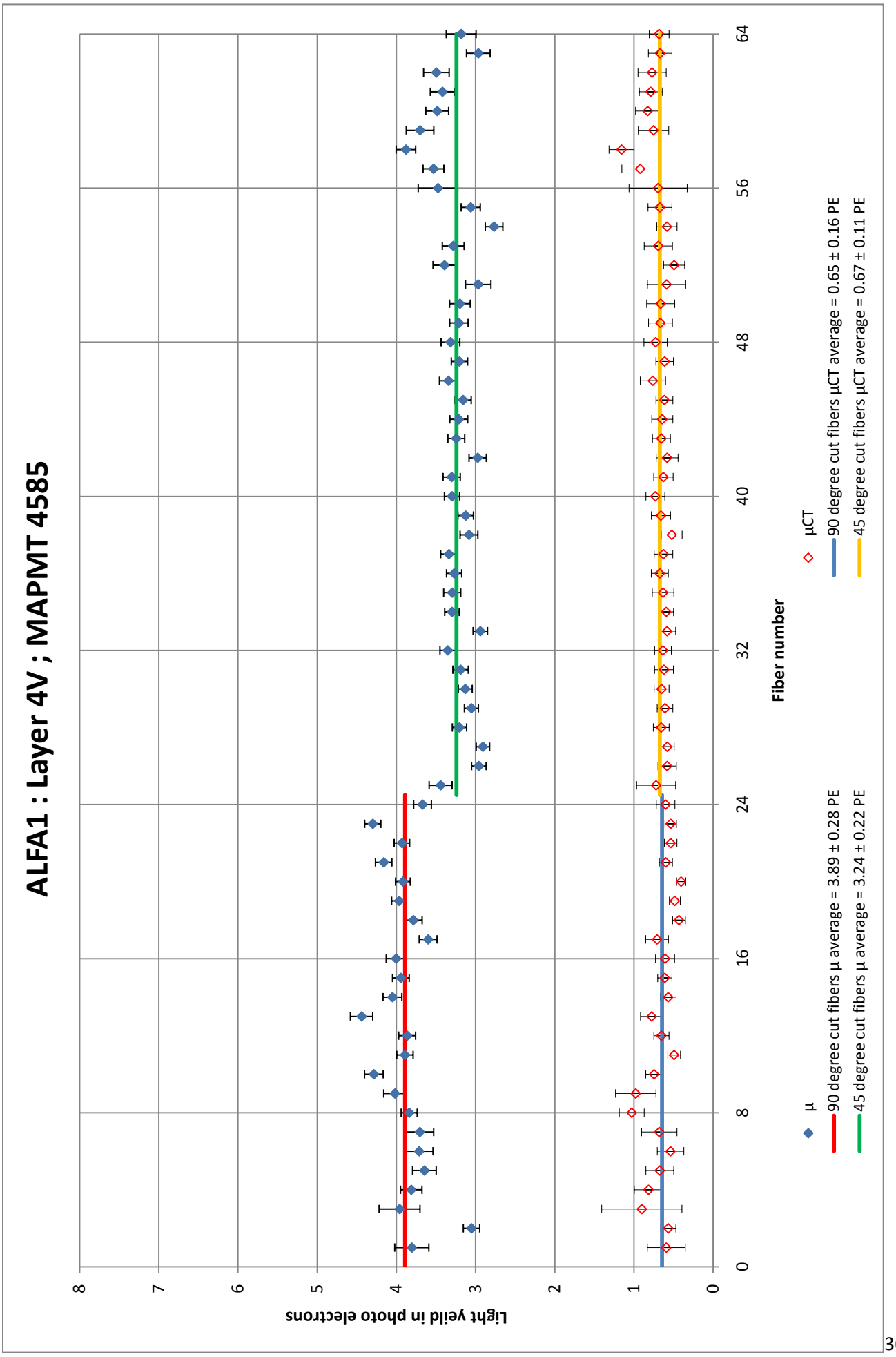
ALFA1 : Layer 4V ; MAPMT 4585
Light yeild in photo electrons
Fiber number
0
1
2
3
4
5
6
7
8
0
8
16
24
32
40
48
56
64
μ
90 degree cut fibers μ average = 3.89 ± 0.28 PE
45 degree cut fibers μ average = 3.24 ± 0.22 PE
μCT
90 degree cut fibers μCT average = 0.65 ± 0.16 PE
45 degree cut fibers μCT average = 0.67 ± 0.11 PE

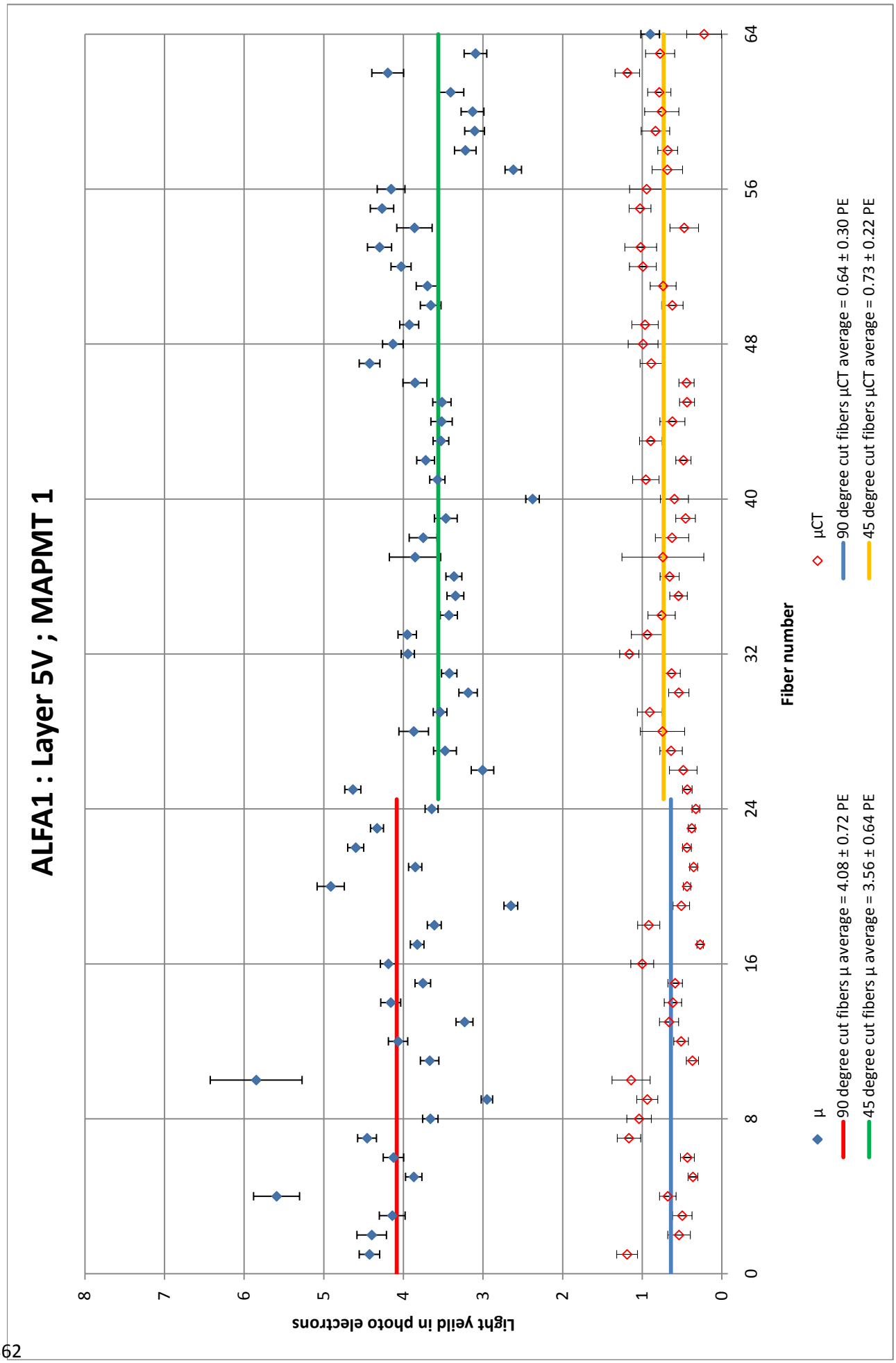
ALFA1 : Layer 5V ; MAPMT 1
Light yeild in photo electrons
Fiber number
0
1
2
3
4
5
6
7
8
0
8
16
24
32
40
48
56
64
μ
μCT
90 degree cut fibers μ average = 4.08 ± 0.72 PE
45 degree cut fibers μ average = 3.56 ± 0.64 PE
90 degree cut fibers μCT average = 0.64 ± 0.30 PE
45 degree cut fibers μCT average = 0.73 ± 0.22 PE

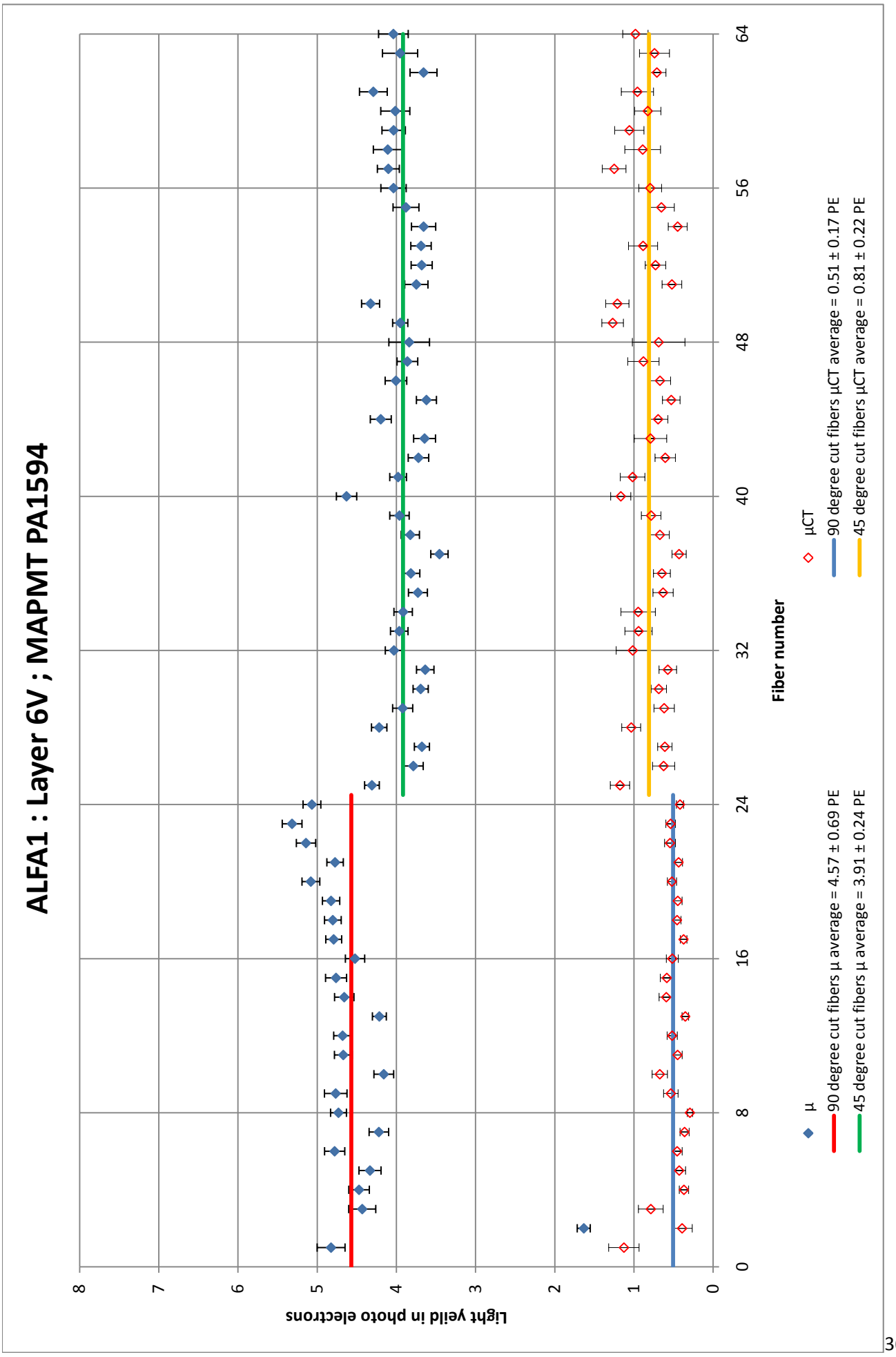
ALFA1 : Layer 6V ; MAPMT PA1594
Light yeild in photo electrons
Fiber number
μ
μCT
90 degree cut fibers μ average = 4.57 ± 0.69 PE
45 degree cut fibers μ average = 3.91 ± 0.24 PE
90 degree cut fibers μCT average = 0.51 ± 0.17 PE
45 degree cut fibers μCT average = 0.81 ± 0.22 PE

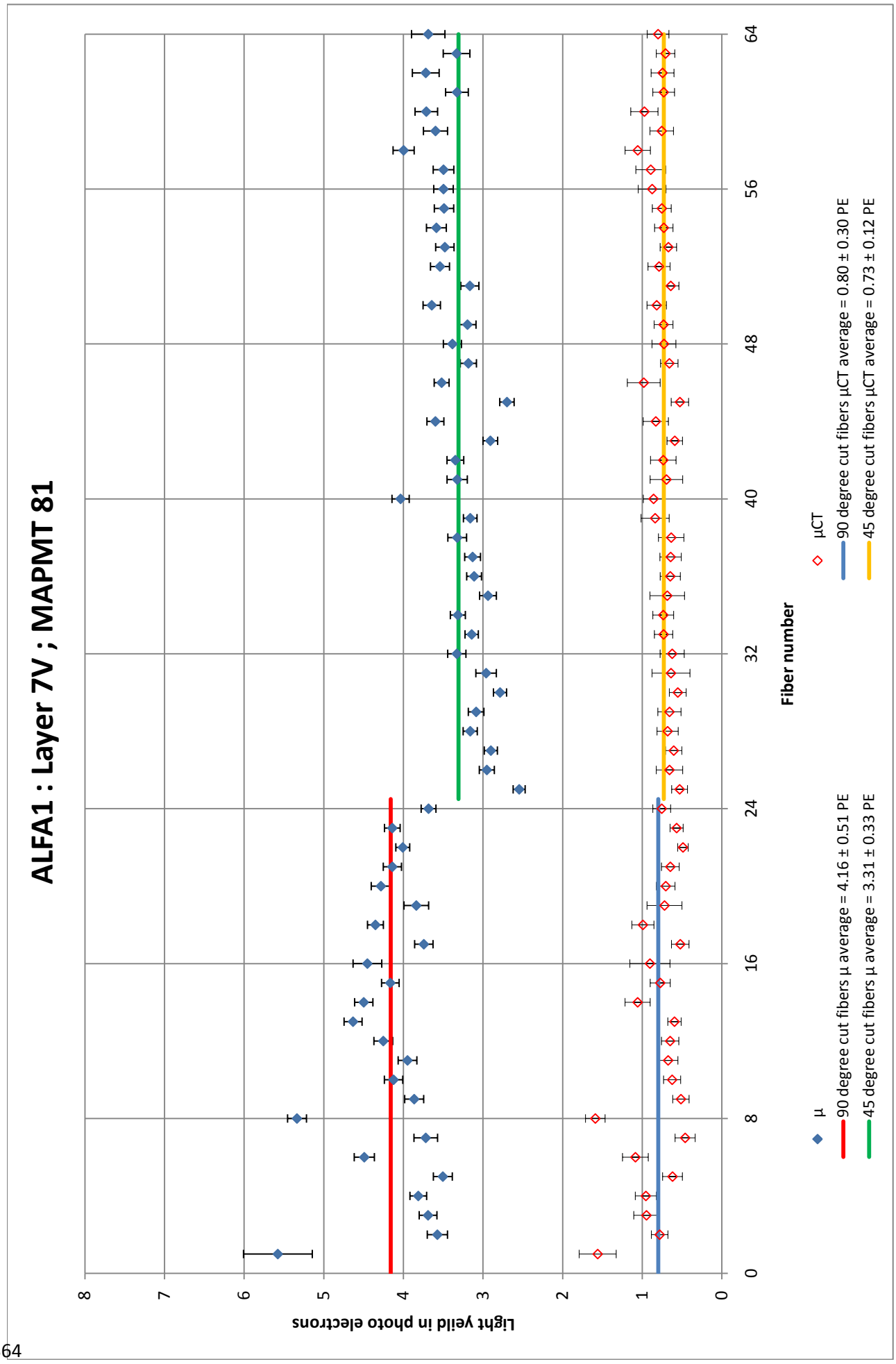
ALFA1 : Layer 7V ; MAPMT 81
Light yeild in photo electrons
Fiber number
0
1
2
3
4
5
6
7
8
0
8
16
24
32
40
48
56
64
μ
μCT
90 degree cut fibers μ average = 4.16 ± 0.51 PE
45 degree cut fibers μ average = 3.31 ± 0.33 PE
90 degree cut fibers μCT average = 0.80 ± 0.30 PE
45 degree cut fibers μCT average = 0.73 ± 0.12 PE

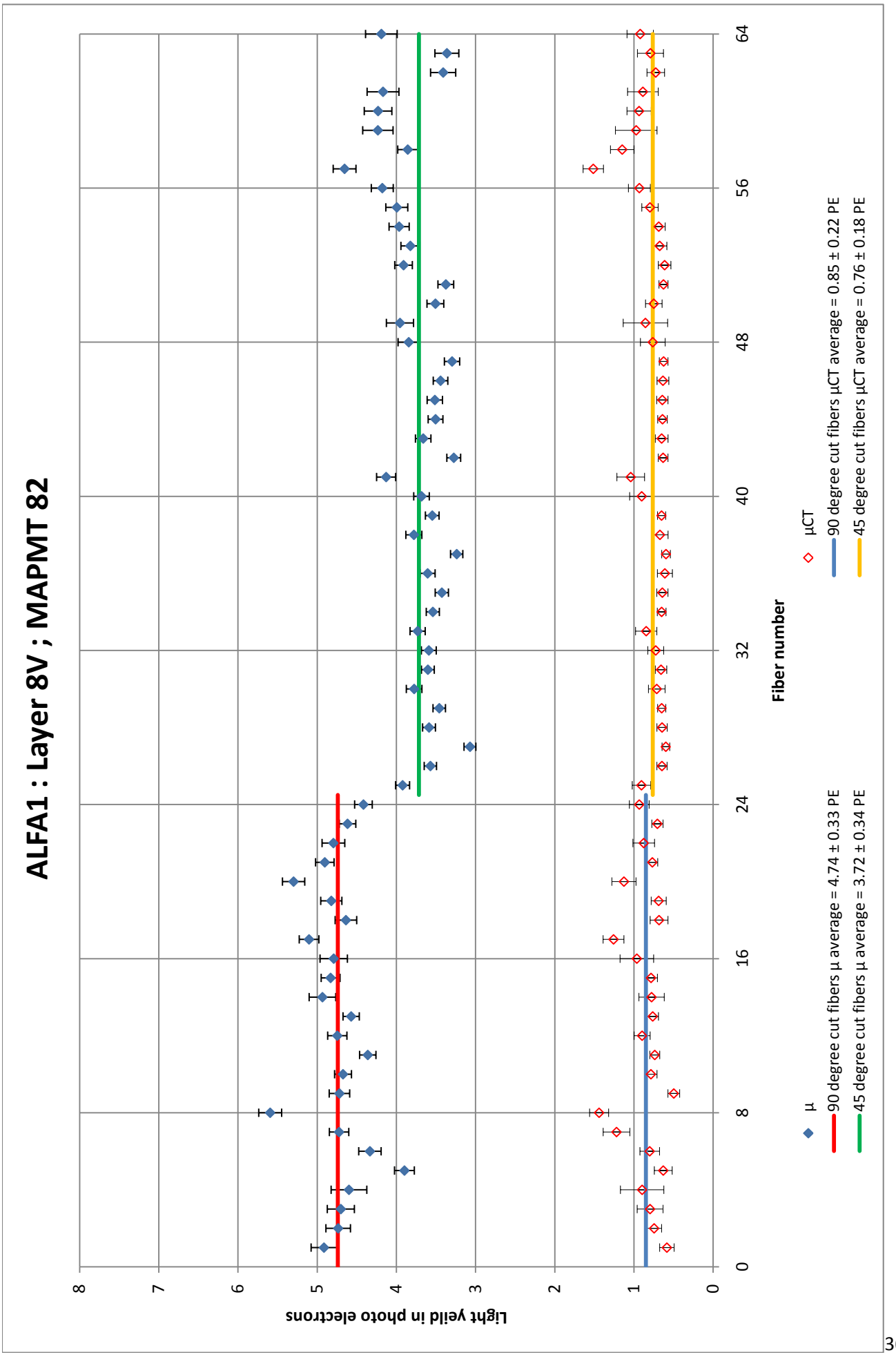
ALFA1 : Layer 8V ; MAPMT 82
Light yeild in photo electrons
Fiber number
μ
μCT
90 degree cut fibers μ average = 4.74 ± 0.33 PE
45 degree cut fibers μ average = 3.72 ± 0.34 PE
90 degree cut fibers μCT average = 0.85 ± 0.22 PE
45 degree cut fibers μCT average = 0.76 ± 0.18 PE

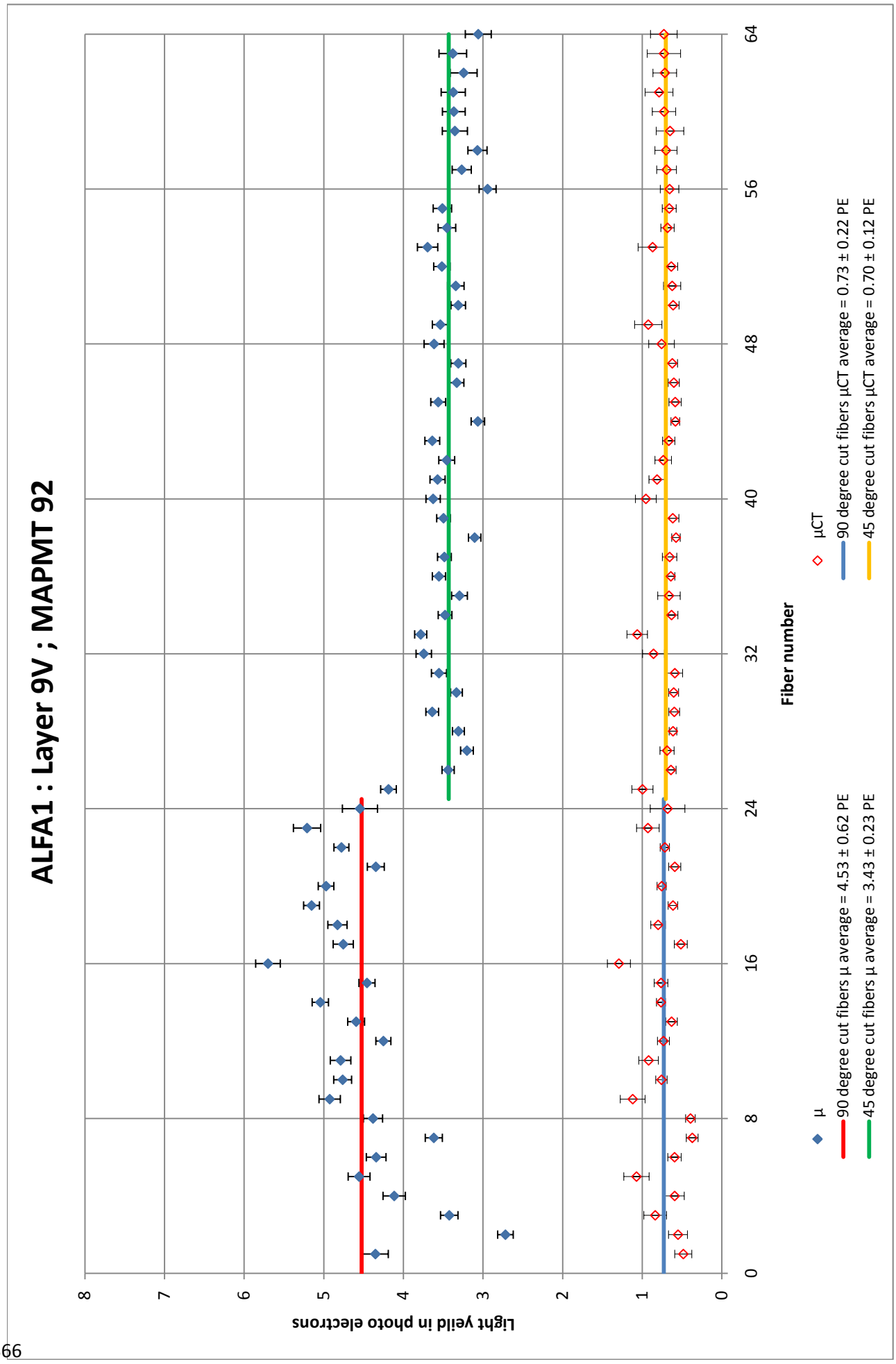
ALFA1 : Layer 9V ; MAPMT 92
Light yeild in photo electrons
Fiber number
0
1
2
3
4
5
6
7
8
0
8
16
24
32
40
48
56
64
μ
μCT
90 degree cut fibers μ average = 4.53 ± 0.62 PE
45 degree cut fibers μ average = 3.43 ± 0.23 PE
90 degree cut fibers μCT average = 0.73 ± 0.22 PE
45 degree cut fibers μCT average = 0.70 ± 0.12 PE

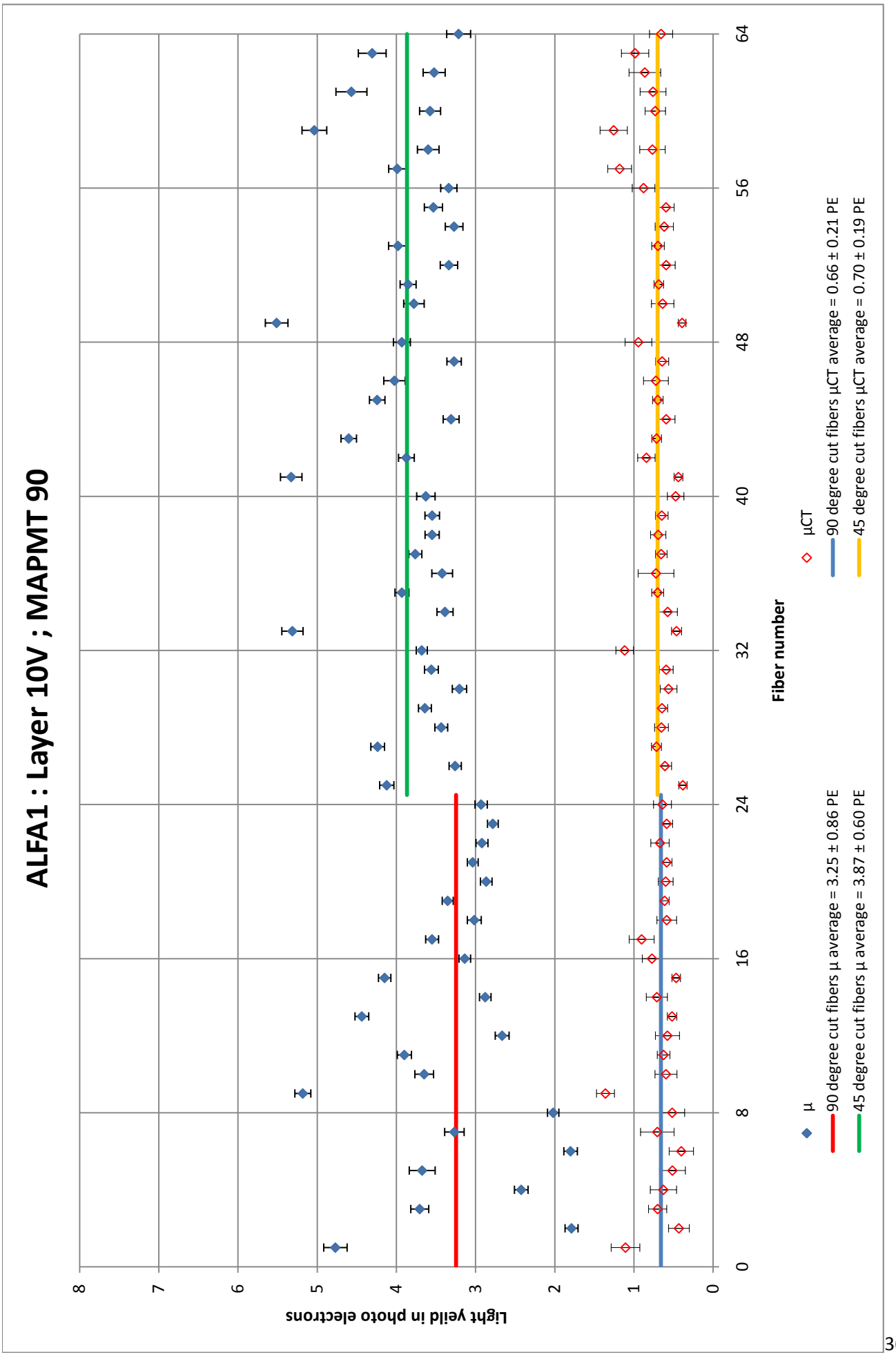
ALFA1 : Layer 10V ; MAPMT 90
Light yeild in photo electrons
Fiber number
0
1
2
3
4
5
6
7
8
0
8
16
24
32
40
48
56
64
μ
90 degree cut fibers μ average = 3.25 ± 0.86 PE
45 degree cut fibers μ average = 3.87 ± 0.60 PE
μCT
90 degree cut fibers μCT average = 0.66 ± 0.21 PE
45 degree cut fibers μCT average = 0.70 ± 0.19 PE

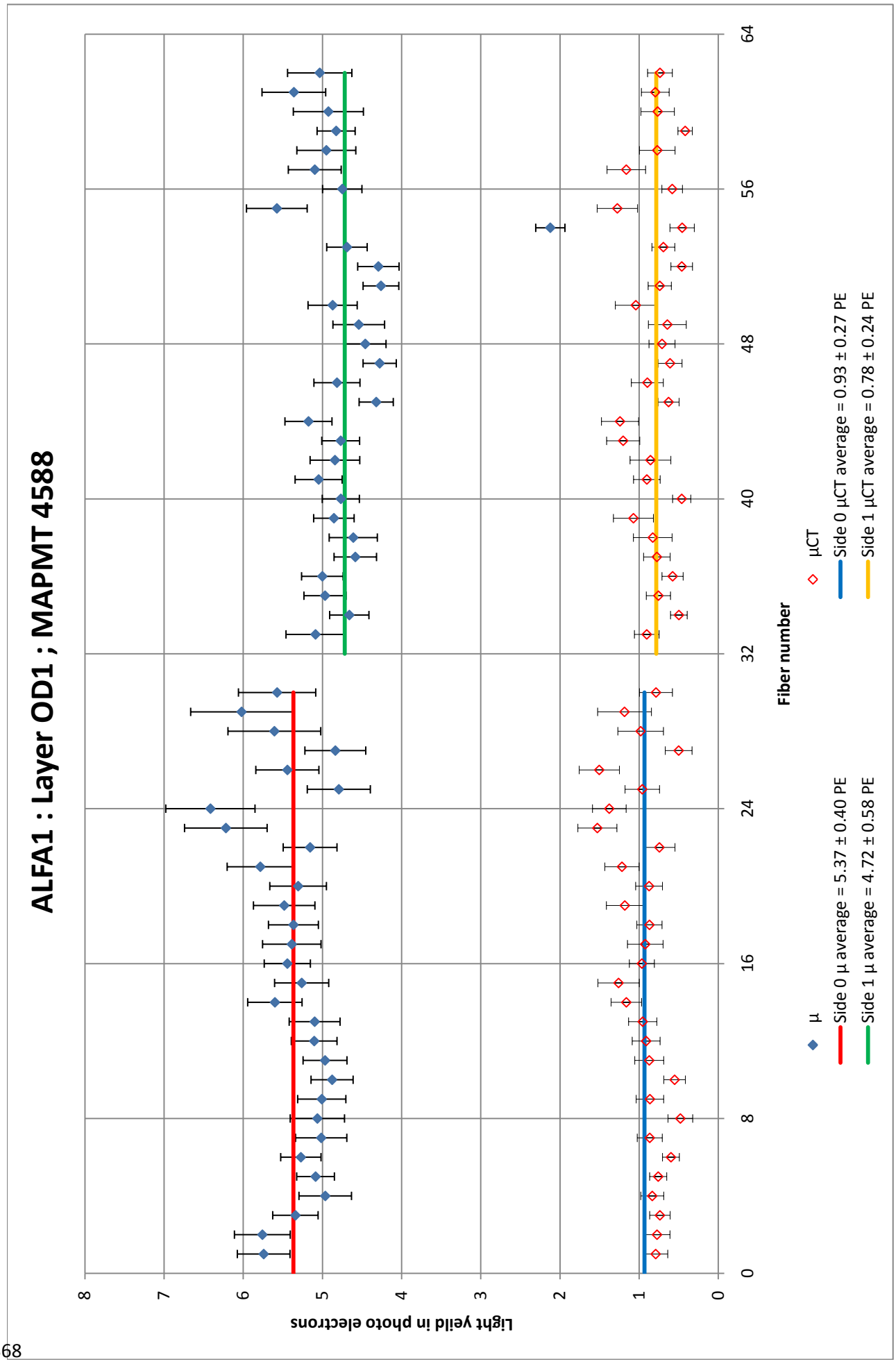
ALFA1 : Layer OD1 ; MAPMT 4588
Light yeild in photo electrons
Fiber number
0
1
2
3
4
5
6
7
8
0
8
16
24
32
40
48
56
64
μ
μCT
Side 0 μ average = 5.37 ± 0.40 PE
Side 1 μ average = 4.72 ± 0.58 PE
Side 0 μCT average = 0.93 ± 0.27 PE
Side 1 μCT average = 0.78 ± 0.24 PE

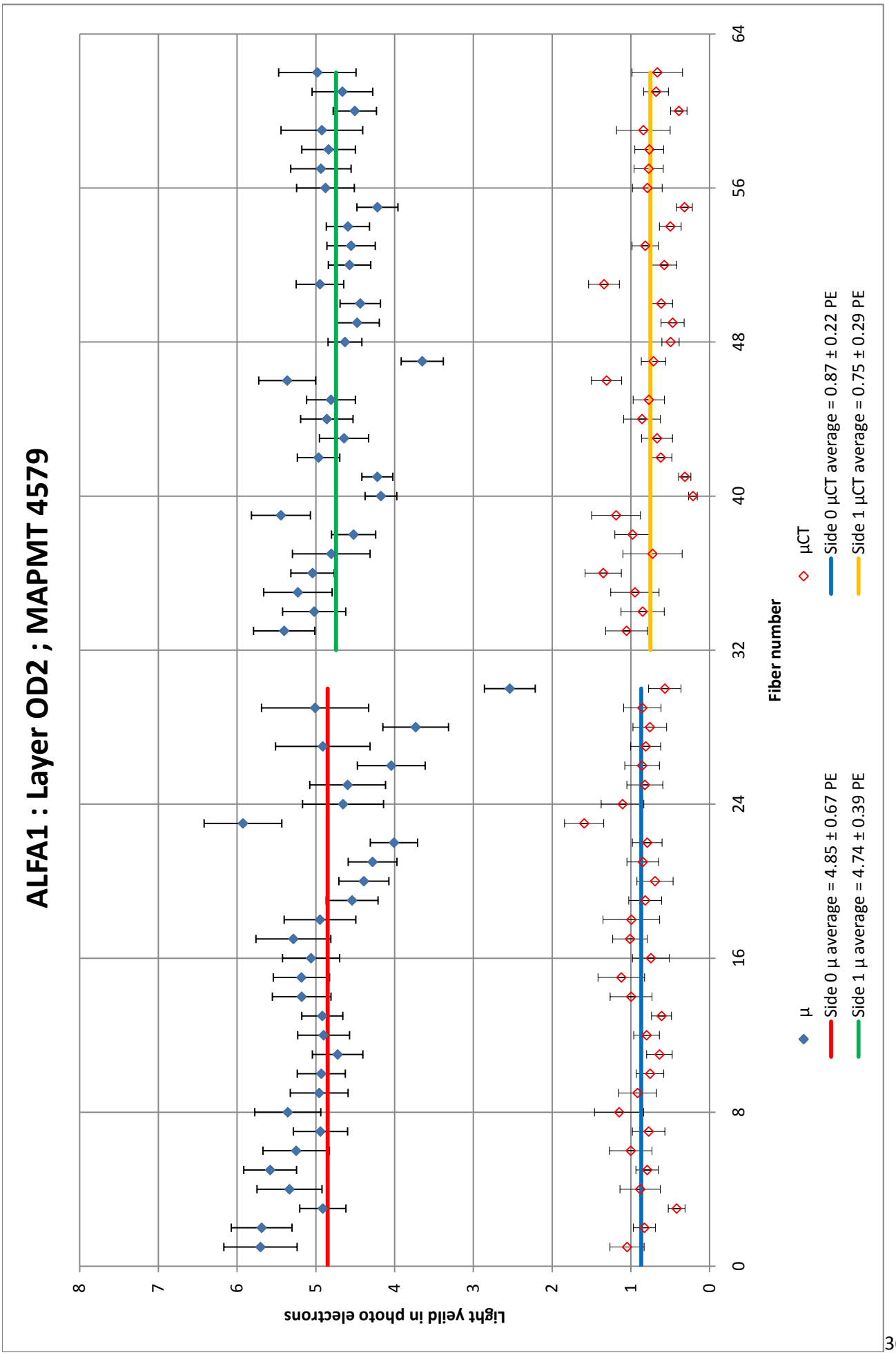
ALFA1 : Layer OD2 ; MAPMT 4579
Light yeild in photo electrons
Fiber number
μ
μCT
Side 0 μ average = 4.85 ± 0.67 PE
Side 1 μ average = 4.74 ± 0.39 PE
Side 0 μCT average = 0.87 ± 0.22 PE
Side 1 μCT average = 0.75 ± 0.29 PE

Appendix S

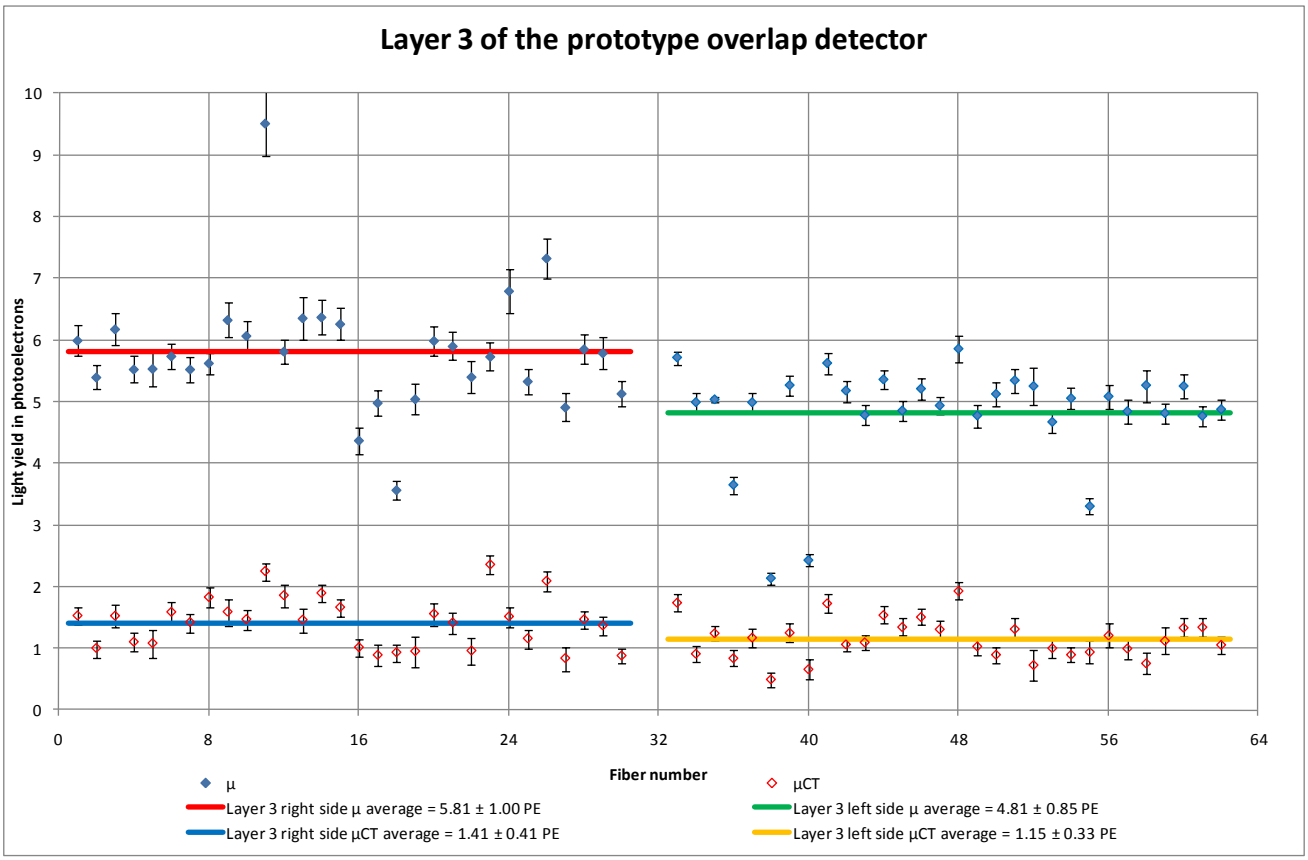

Light yield in each fiber of layer 3 in the prototype overlap detector. The very high light yield in fiber number 11 is artificial because of a range overflow.

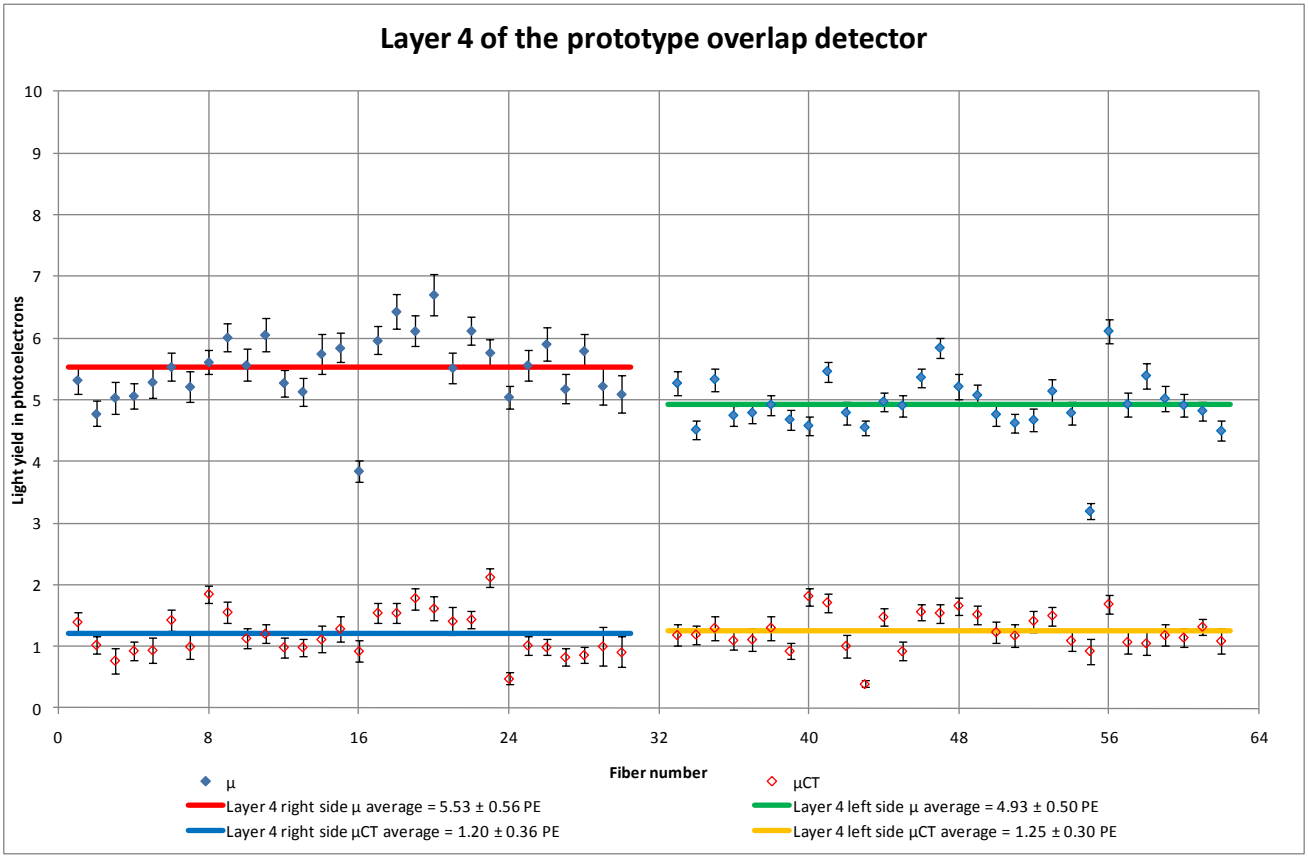

Light yield in each fiber of layer 4 in the prototype overlap detector

ALFA1

(former Set3)

MAPMT
PMF
Layer

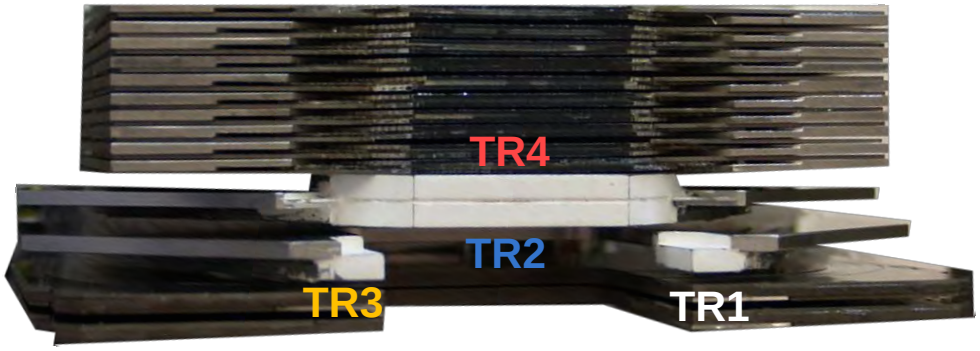

1-5
6-10
TR

HV cable 6
HV cable 5
HV cable 1

Appendix T

ALFA2

(former Set2)

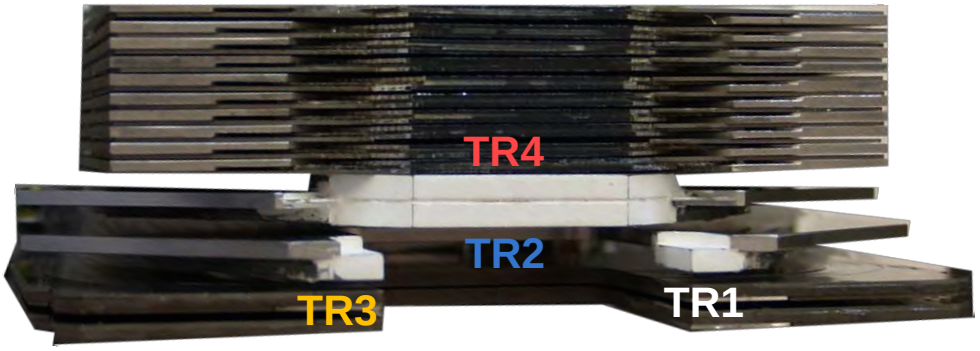

HV cable 8 — TR

HV cable 4 — 6-10

HV cable 3 — 1-5

KA0271 3U 23 | PA1639 2U 22 | PA1588 1U 21 | PA1591 3V 20 | PA4485 2V 19 — Kapton 5

PA1644 5U 18 | PA1521 4U 17 | PA1632 1V 16 | KA0270 5V 15 | PA1648 4V 14 — Kapton 4

PA1589 7U 13 | PA0948 6U 12 | PA1548 7V 11 | PA1633 6V 10 — Kapton 3

KA0272 9U 9 | PA1530 8U 8 | PA1583 10U 7 | PA1617 9V 6 | PA1631 8V 5 — Kapton 2

TR2 TR3 TR1 TR4

PA4477 OD1 4 | PA4488 OD2 3 | PA1616 OD3 2 | PA1624 10V 1 — Kapton 1

372

MAPMT PMF Layer

DataCal.C:

```
#include "TMultiGraph.h"
#include "TFile.h"
#include "TTree.h"
#include "TBrowser.h"
#include "TH2.h"
#include "TRandom.h"
#include "TMath.h"
#include <iostream>
#include <fstream>
#include "TStyle.h"
#include "TText.h"
#include <iomanip>
#include <stdio.h>
#include "TSystem.h"


void DataCal(int Runnr, int PMTnr)

{ for (Int_t index=1;index<65;index++)
    {
TString directoryRead = ;
 directoryRead+= "Run_";
 directoryRead+= Runnr;
 directoryRead+= "/";
 directoryRead+= PMTnr;
 directoryRead+= "/";

ifstream in1PE; //Declare the stream variable
   Double_t buffer1PE;
   in1PE.open( directoryRead+ "1pe mean.dat"); //Open the file.
   for(int iii = 0; iii < index; iii++){
   in1PE>>buffer1PE;}  //Read the number.
   in1PE.close();//Close the file.

ifstream in1PEErr; //Declare the stream variable
   Double_t buffer1PEErr;
   in1PEErr.open( directoryRead+ "1pe mean Error.dat"); //Open the file.
   for(int iii = 0; iii < index; iii++){
   in1PEErr>>buffer1PEErr;}  //Read the number.
   in1PEErr.close();//Close the file.

ifstream in1PERMS; //Declare the stream variable
   Double_t buffer1PERMS;
   in1PERMS.open( directoryRead+ "1pe RMS.dat"); //Open the file.
   for(int iii = 0; iii < index; iii++){
   in1PERMS>>buffer1PERMS;}  //Read the number.
   in1PERMS.close();//Close the file.


ifstream in1PERMSErr; //Declare the stream variable
   Double_t buffer1PERMSErr;
   in1PERMSErr.open( directoryRead+ "1pe RMS Error.dat"); //Open the file.
   for(int iii = 0; iii < index; iii++){
   in1PERMSErr>>buffer1PERMSErr;}  //Read the number.
   in1PERMSErr.close();//Close the file.

TString directoryWrite = ;
 directoryWrite= "Run_";
 directoryWrite+= Runnr;
 directoryWrite+= "/";

 ofstream outData4;            //SJ
  outData4.open ( directoryWrite+ "DataCal.dat", ios::app);   //SJ
  outData4 << buffer1PE ;   //SJ
  outData4<<"\t";
  outData4 << buffer1PEErr ;
```

```
  outData4<<"\t";
  outData4 << buffer1PERMS ;
  outData4<<"\t";
  outData4 << buffer1PERMSErr ;
  outData4<<"\n";   //SJ
  outData4.close();

    }}
```

DataCalAll.C:

```
#include "DataCal.C"

void DataCalAll(int Runnr)
{
  DataCal(Runnr, 16);
  DataCal(Runnr, 17);
  DataCal(Runnr, 18);
  DataCal(Runnr, 19);
  DataCal(Runnr, 6);
  DataCal(Runnr, 7);
  DataCal(Runnr, 8);
  DataCal(Runnr, 9);
  DataCal(Runnr, 10);
  DataCal(Runnr, 21);
  DataCal(Runnr, 22);
  DataCal(Runnr, 24);
  DataCal(Runnr, 25);
  DataCal(Runnr, 1);
  DataCal(Runnr, 2);
  DataCal(Runnr, 3);
  DataCal(Runnr, 4);
  DataCal(Runnr, 5);
  DataCal(Runnr, 11);
  DataCal(Runnr, 12);
  DataCal(Runnr, 13);
  DataCal(Runnr, 14);
  DataCal(Runnr, 15);
}
```

SplitGainFactors.C:

```
#include "TMultiGraph.h"
#include "TFile.h"
#include "TTree.h"
#include "TBrowser.h"
#include "TH2.h"
#include "TRandom.h"
#include "TMath.h"
#include <iostream>
#include <fstream>
#include "TStyle.h"
#include "TText.h"
#include <iomanip>
#include <stdio.h>
#include "TSystem.h"

void SplitGainFactors()
{
 //Make directory
TString directoryWrite = ;
 directoryWrite= "GainFactors";
 directoryWrite+= "/";
 gSystem->MakeDirectory(directoryWrite);

for (Int_t index=1;index<1473;index++)
    {
```

```
  //Read
ifstream inGF; //Declare the stream variable
   Double_t bufferGF;
   inGF.open("GFAll.dat"); //Open the file.
   for(int iii = 0; iii < index; iii++){
   inGF>>bufferGF;}  //Read the number.
   inGF.close();//Close the file.


  //Write
 if (index>=0 && index <= 64)
            {
 ofstream outGF;
  outGF.open ( directoryWrite+ "16.txt", ios::app);
  outGF << bufferGF ;
  outGF<<"\n";
  outGF.close();
            }
 if (index>=65 && index <= 128)
            {
 ofstream outGF;
  outGF.open ( directoryWrite+ "17.txt", ios::app);
  outGF << bufferGF ;
  outGF<<"\n";
  outGF.close();
            }
 if (index>=129 && index <= 192)
            {
 ofstream outGF;
  outGF.open ( directoryWrite+ "18.txt", ios::app);
  outGF << bufferGF ;
  outGF<<"\n";
  outGF.close();
            }
 if (index>=193 && index <= 256)
            {
 ofstream outGF;
  outGF.open ( directoryWrite+ "19.txt", ios::app);
  outGF << bufferGF ;
  outGF<<"\n";
  outGF.close();
            }
 if (index>=257 && index <= 320)
            {
 ofstream outGF;
  outGF.open ( directoryWrite+ "6.txt", ios::app);
  outGF << bufferGF ;
  outGF<<"\n";
  outGF.close();
            }
 if (index>=321 && index <= 384)
            {
 ofstream outGF;
  outGF.open ( directoryWrite+ "7.txt", ios::app);
  outGF << bufferGF ;
  outGF<<"\n";
  outGF.close();
            }
 if (index>=385 && index <=448 )
            {
 ofstream outGF;
  outGF.open ( directoryWrite+ "8.txt", ios::app);
  outGF << bufferGF ;
  outGF<<"\n";
  outGF.close();
            }
 if (index>=449 && index <= 512)
            {
```

```
ofstream outGF;
 outGF.open ( directoryWrite+ "9.txt", ios::app);
 outGF << bufferGF ;
 outGF<<"\n";
 outGF.close();
            }
if (index>=513 && index <= 576)
            {
ofstream outGF;
 outGF.open ( directoryWrite+ "10.txt", ios::app);
 outGF << bufferGF ;
 outGF<<"\n";
 outGF.close();
            }
if (index>=577 && index <= 640)
            {
ofstream outGF;
 outGF.open ( directoryWrite+ "21.txt", ios::app);
 outGF << bufferGF ;
 outGF<<"\n";
 outGF.close();
            }
if (index>=641 && index <=704 )
            {
ofstream outGF;
 outGF.open ( directoryWrite+ "22.txt", ios::app);
 outGF << bufferGF ;
 outGF<<"\n";
 outGF.close();
            }
if (index>=705 && index <= 768)
            {
ofstream outGF;
 outGF.open ( directoryWrite+ "24.txt", ios::app);
 outGF << bufferGF ;
 outGF<<"\n";
 outGF.close();
            }
if (index>=769 && index <= 832)
            {
ofstream outGF;
 outGF.open ( directoryWrite+ "25.txt", ios::app);
 outGF << bufferGF ;
 outGF<<"\n";
 outGF.close();
            }
if (index>=833 && index <= 896)
            {
ofstream outGF;
 outGF.open ( directoryWrite+ "1.txt", ios::app);
 outGF << bufferGF ;
 outGF<<"\n";
 outGF.close();
            }
if (index>=897 && index <= 960)
            {
ofstream outGF;
 outGF.open ( directoryWrite+ "2.txt", ios::app);
 outGF << bufferGF ;
 outGF<<"\n";
 outGF.close();
            }
if (index>=961 && index <= 1024)
            {
ofstream outGF;
 outGF.open ( directoryWrite+ "3.txt", ios::app);
 outGF << bufferGF ;
 outGF<<"\n";
```

```
 outGF.close();
            }
if (index>=1025 && index <= 1088)
            {
ofstream outGF;
 outGF.open ( directoryWrite+ "4.txt", ios::app);
 outGF << bufferGF ;
 outGF<<"\n";
 outGF.close();
            }
if (index>=1089 && index <= 1152)
            {
ofstream outGF;
 outGF.open ( directoryWrite+ "5.txt", ios::app);
 outGF << bufferGF ;
 outGF<<"\n";
 outGF.close();
            }
if (index>=1153 && index <= 1216)
            {
ofstream outGF;
 outGF.open ( directoryWrite+ "11.txt", ios::app);
 outGF << bufferGF ;
 outGF<<"\n";
 outGF.close();
            }
if (index>=1217 && index <= 1280)
            {
ofstream outGF;
 outGF.open ( directoryWrite+ "12.txt", ios::app);
 outGF << bufferGF ;
 outGF<<"\n";
 outGF.close();
            }
if (index>=1281 && index <= 1344)
            {
ofstream outGF;
 outGF.open ( directoryWrite+ "13.txt", ios::app);
 outGF << bufferGF ;
 outGF<<"\n";
 outGF.close();
            }
if (index>=1345 && index <= 1408)
            {
ofstream outGF;
 outGF.open ( directoryWrite+ "14.txt", ios::app);
 outGF << bufferGF ;
 outGF<<"\n";
 outGF.close();
            }
if (index>=1409 && index <= 1472)
            {
ofstream outGF;
 outGF.open ( directoryWrite+ "15.txt", ios::app);
 outGF << bufferGF ;
 outGF<<"\n";
 outGF.close();
            }

   }}
```

CalibrationFiles.C:

```
#include "TMultiGraph.h"
#include "TFile.h"
#include "TTree.h"
#include "TBrowser.h"
#include "TH2.h"
```

```
#include "TRandom.h"
#include "TMath.h"
#include <iostream>
#include <fstream>
#include "TStyle.h"
#include "TText.h"
#include <iomanip>
#include <stdio.h>
#include "TSystem.h"


void CalibrationFiles(int Runnr)
{ for (Int_t PMTnr=1;PMTnr<26;PMTnr++)

{ for (Int_t index=1;index<65;index++)
    {
TString directoryRead = ;
 directoryRead+= "Run_";
 directoryRead+= Runnr;
 directoryRead+= "/";
 directoryRead+= PMTnr;
 directoryRead+= "/";

ifstream in1PE; //Declare the stream variable
   Double_t buffer1PE;
   in1PE.open( directoryRead+ "1pe mean.dat"); //Open the file.
   for(int iii = 0; iii < index; iii++){
   in1PE>>buffer1PE;}  //Read the number.
   in1PE.close();//Close the file.

ifstream in1PERMS; //Declare the stream variable
   Double_t buffer1PERMS;
   in1PERMS.open( directoryRead+ "1pe RMS.dat"); //Open the file.
   for(int iii = 0; iii < index; iii++){
   in1PERMS>>buffer1PERMS;}  //Read the number.
   in1PERMS.close();//Close the file.

ifstream inpedmean; //Declare the stream variable
   Double_t bufferped;
   inpedmean.open( directoryRead+ "ped mean.dat"); //Open the file.
   for(int iii = 0; iii < index; iii++){
   inpedmean>>bufferped;}  //Read the number.
   inpedmean.close();//Close the file.

ifstream inpedRMS; //Declare the stream variable
   Double_t bufferpedRMS;
   inpedRMS.open( directoryRead+ "ped RMS.dat"); //Open the file.
   for(int iii = 0; iii < index; iii++){
   inpedRMS>>bufferpedRMS;}  //Read the number.
   inpedRMS.close();//Close the file.

TString directoryWrite = ;
 directoryWrite= "Calibration";
directoryWrite+= "/";
gSystem->MakeDirectory(directoryWrite);

 directoryWrite+= PMTnr;
 directoryWrite+= "/";

 gSystem->MakeDirectory(directoryWrite);


 ofstream out1pemean;
  out1pemean.open ( directoryWrite+ "1pe mean.cal", ios::app);
  out1pemean << buffer1PE ;
  out1pemean<<"\n";
  out1pemean.close();
```

```
ofstream out1peRMS;
 out1peRMS.open ( directoryWrite+ "1pe RMS.cal", ios::app);
 out1peRMS << buffer1PERMS ;
 out1peRMS<<"\n";
 out1peRMS.close();

ofstream outpedmean;
 outpedmean.open ( directoryWrite+ "ped mean.cal", ios::app);
 outpedmean << bufferped ;
 outpedmean<<"\n";
 outpedmean.close();

ofstream outpedRMS;
 outpedRMS.open ( directoryWrite+ "ped RMS.cal", ios::app);
 outpedRMS << bufferpedRMS ;
 outpedRMS<<"\n";
 outpedRMS.close();

   }}}
```

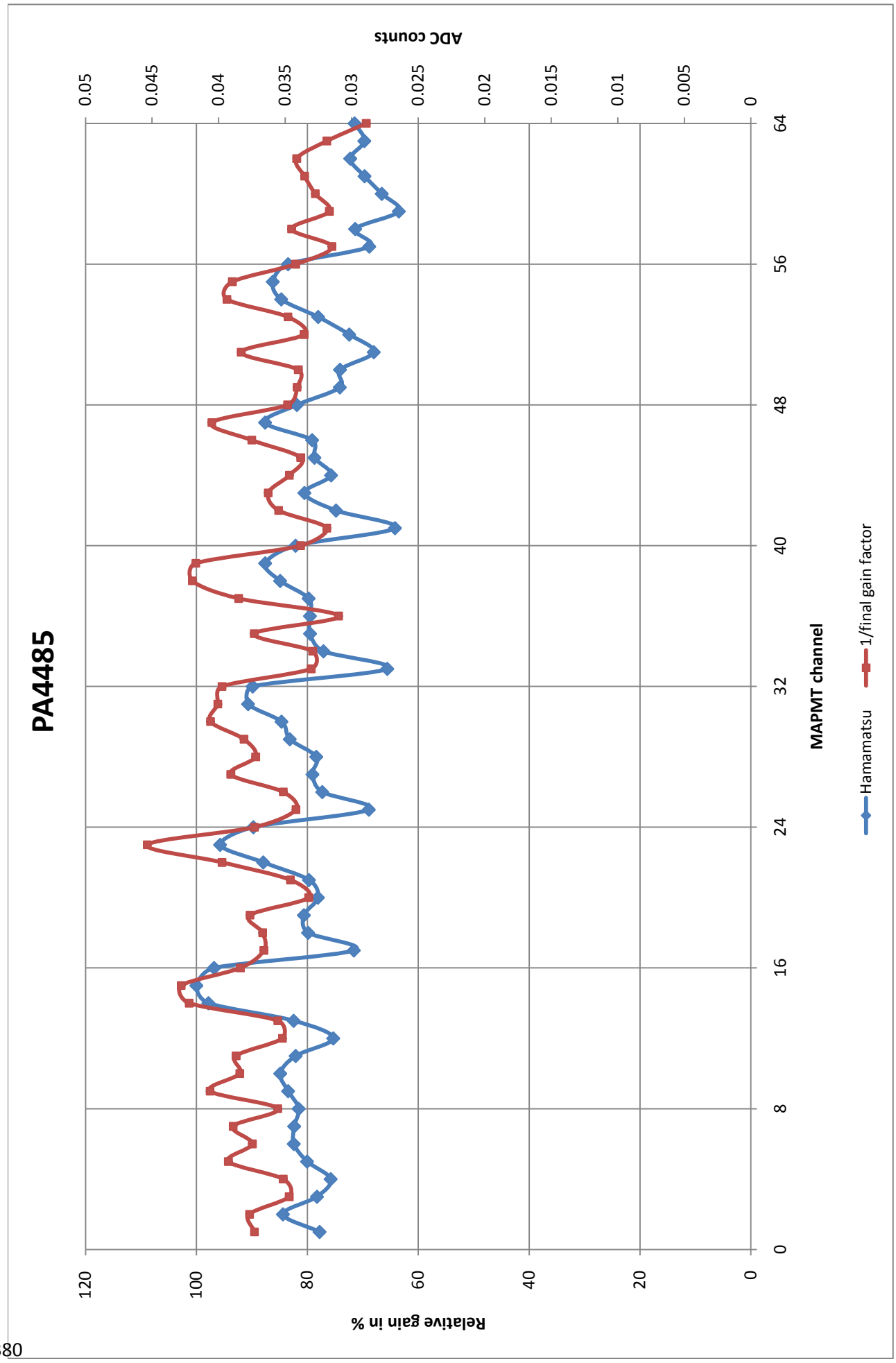
PA4485
Relative gain in %
ADC counts
MAPMT channel
Hamamatsu
1/final gain factor
120
100
80
60
40
20
0
0.05
0.045
0.04
0.035
0.03
0.025
0.02
0.015
0.01
0.005
0
0
8
16
24
32
40
48
56
64

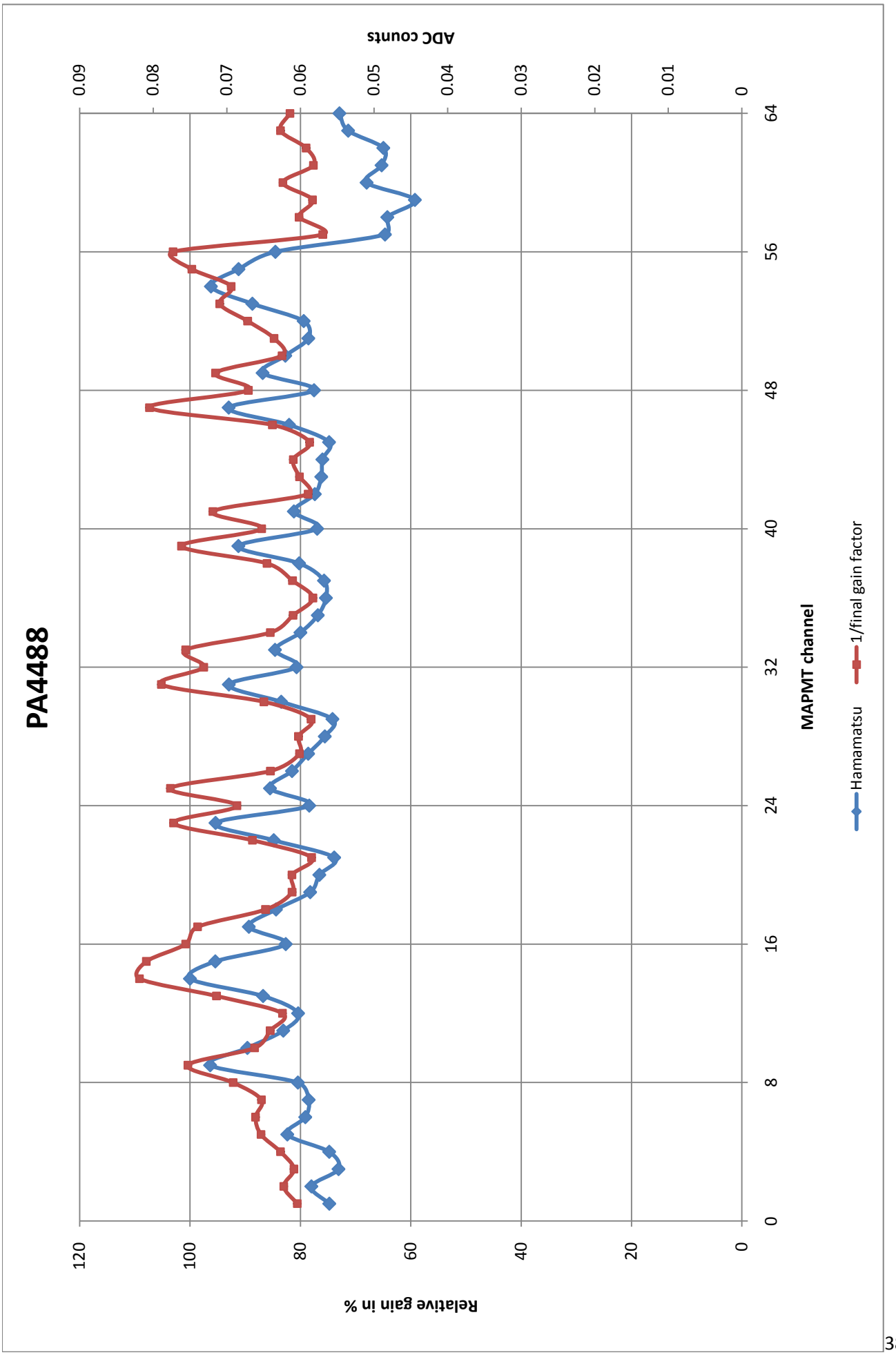
PA4488
Relative gain in %
ADC counts
MAPMT channel
Hamamatsu
1/final gain factor
120
100
80
60
40
20
0
0.09
0.08
0.07
0.06
0.05
0.04
0.03
0.02
0.01
0
8
16
24
32
40
48
56
64

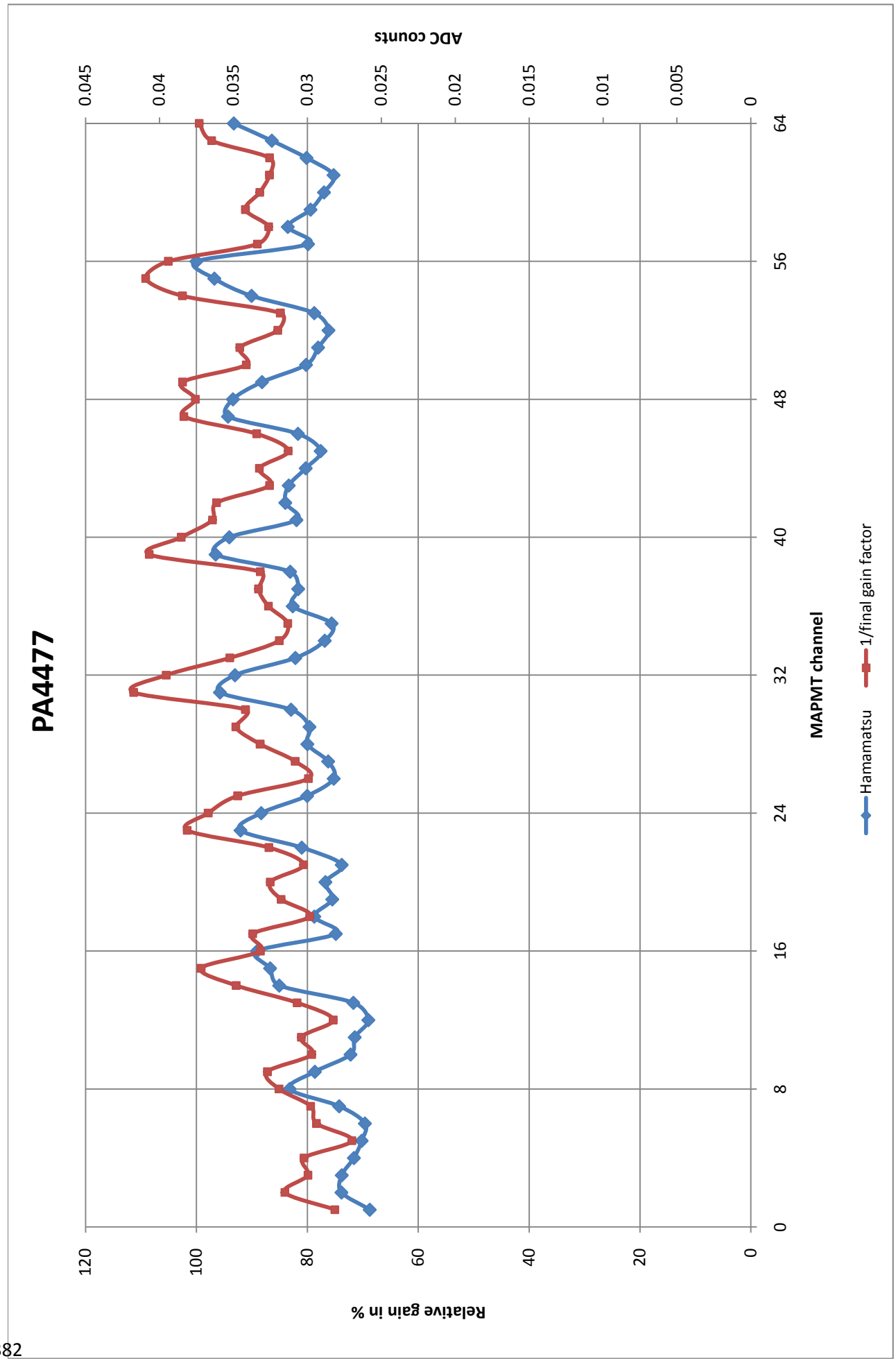
PA4477
Relative gain in %
ADC counts
MAPMT channel
Hamamatsu
1/final gain factor
0
20
40
60
80
100
120
0
0.005
0.01
0.015
0.02
0.025
0.03
0.035
0.04
0.045
0
8
16
24
32
40
48
56
64

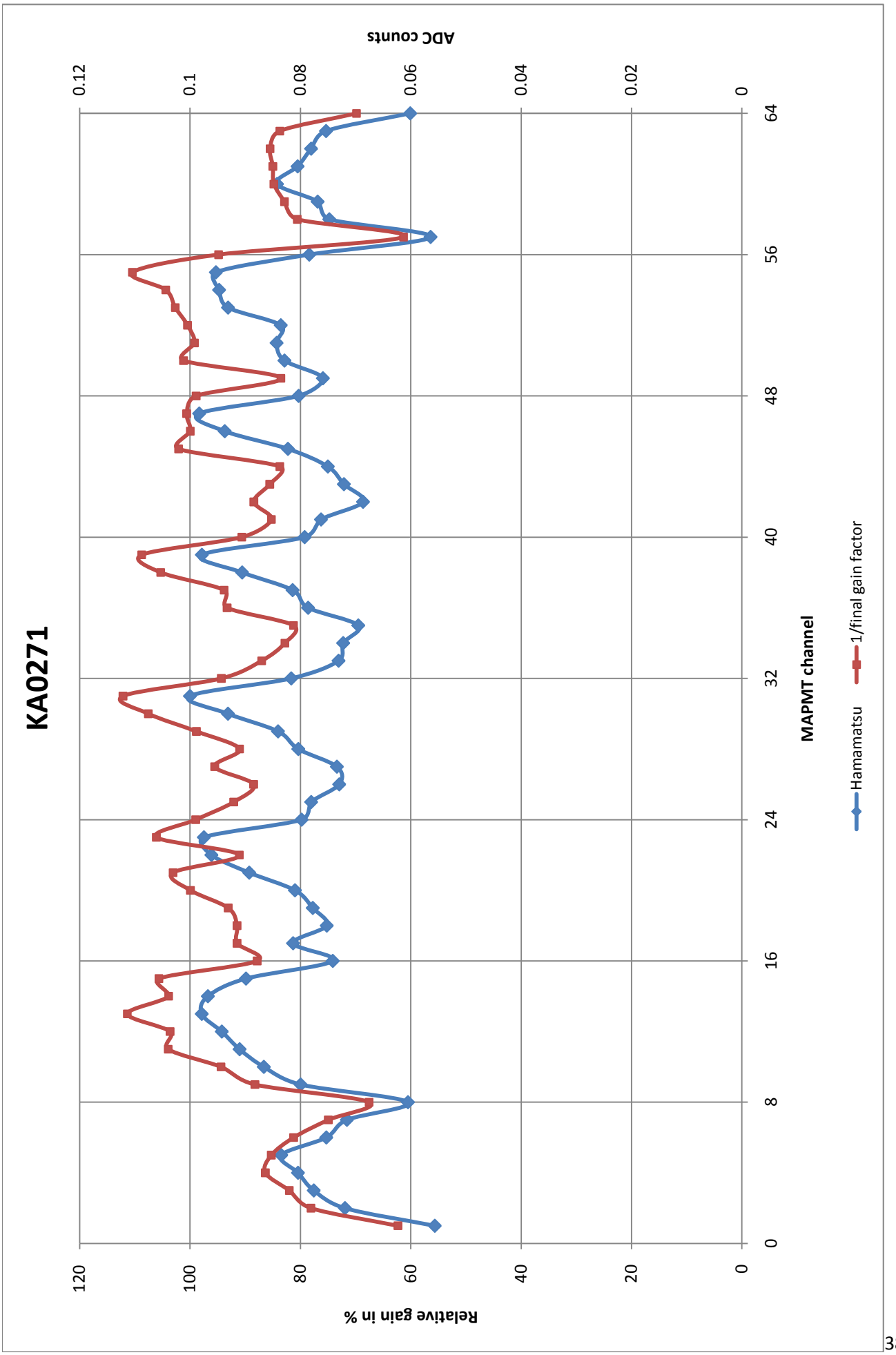
KA0271
Relative gain in %
ADC counts
MAPMT channel
Hamamatsu
1/final gain factor
120
100
80
60
40
20
0
0.12
0.1
0.08
0.06
0.04
0.02
0
0
8
16
24
32
40
48
56
64

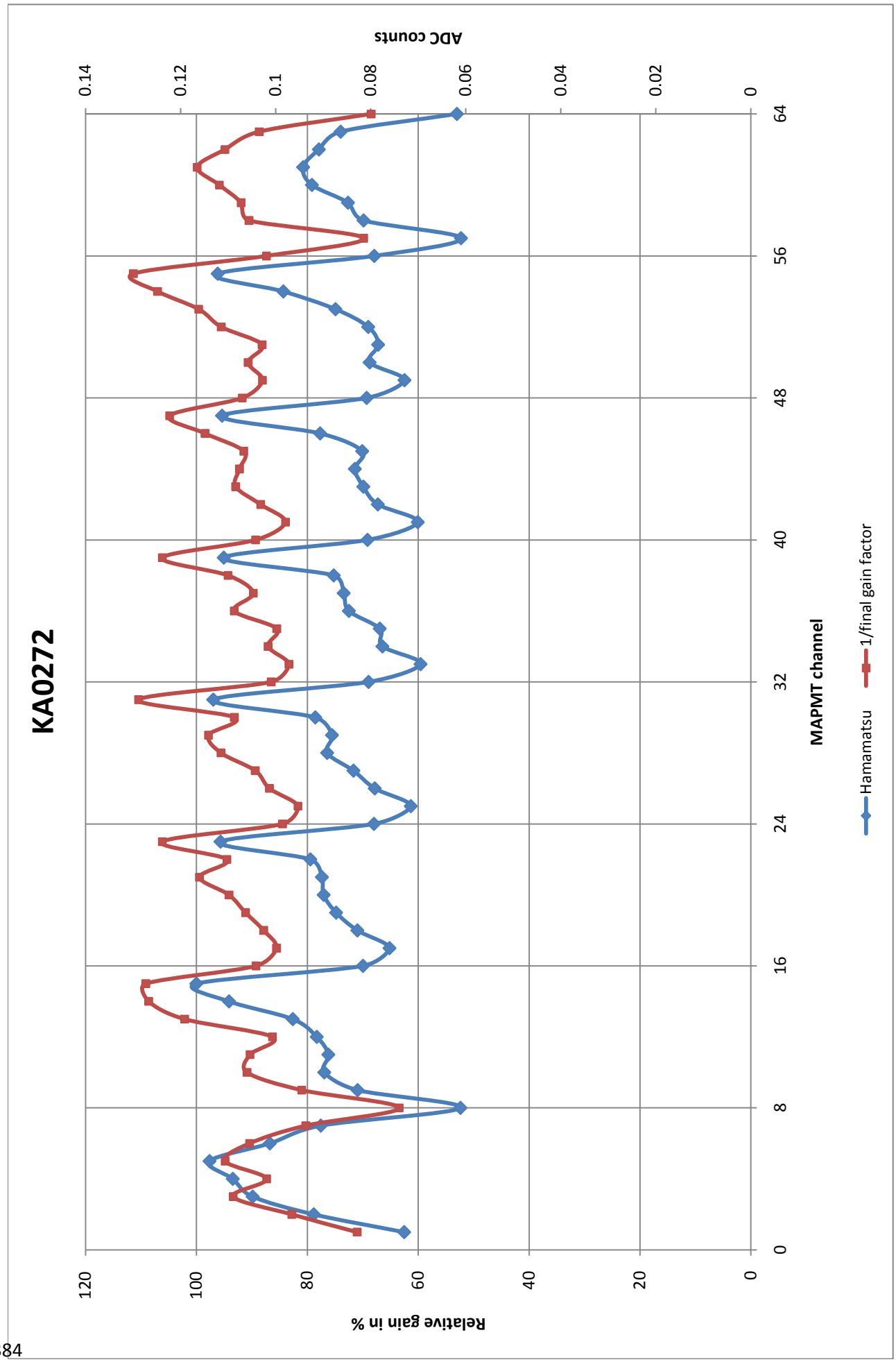
KA0272
Relative gain in %
ADC counts
MAPMT channel
Hamamatsu
1/final gain factor
120
100
80
60
40
20
0
0.14
0.12
0.1
0.08
0.06
0.04
0.02
0
0
8
16
24
32
40
48
56
64

Appendix X

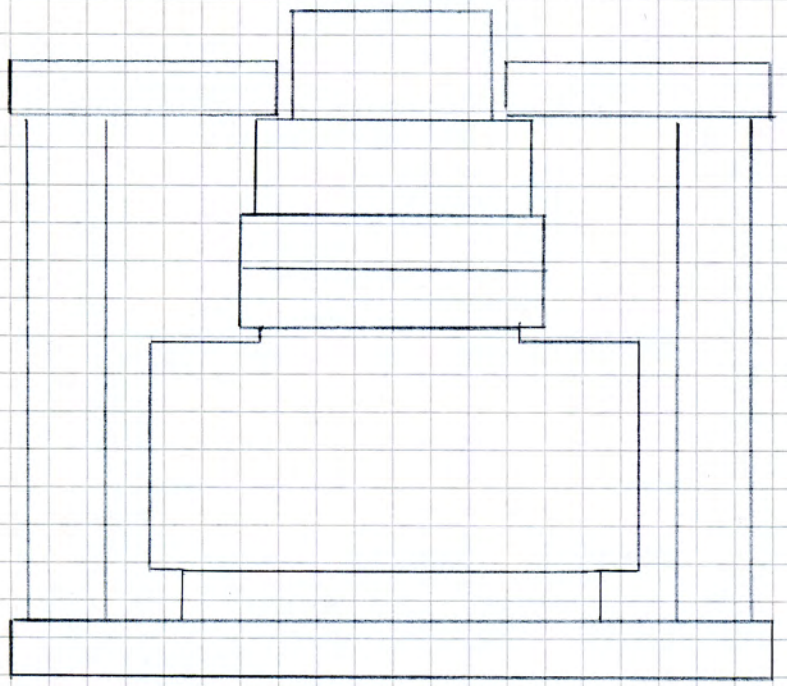

+ M4
⊗ Ø3,3
× Ø4,4

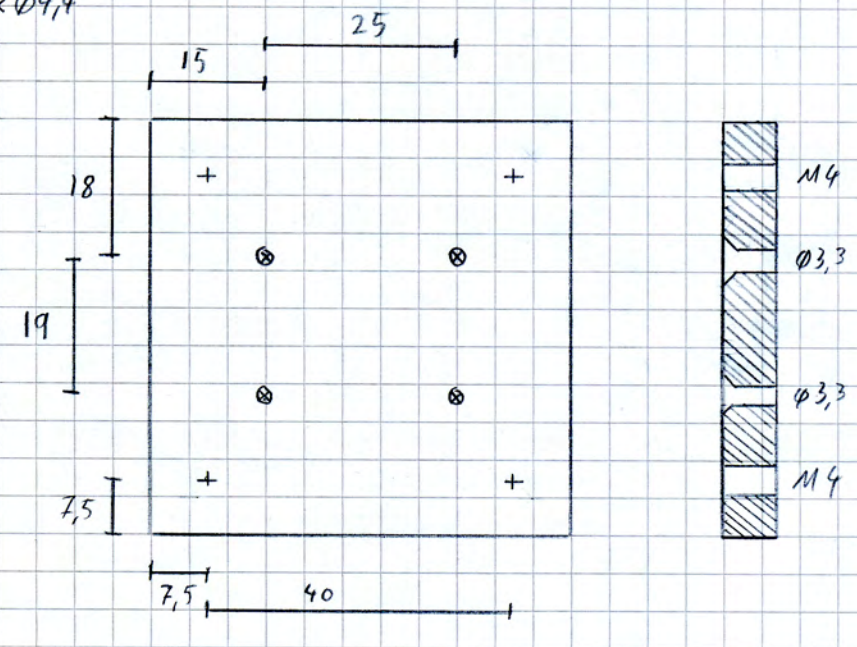

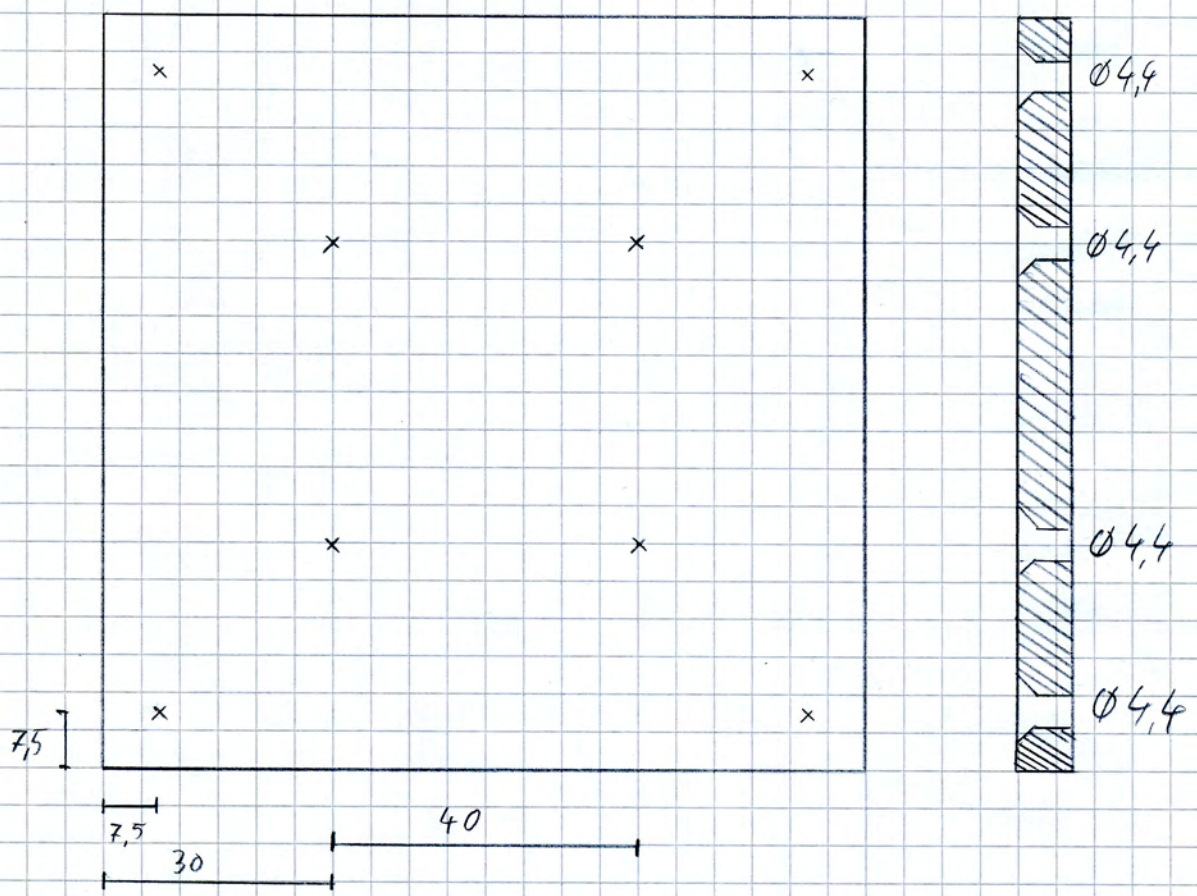

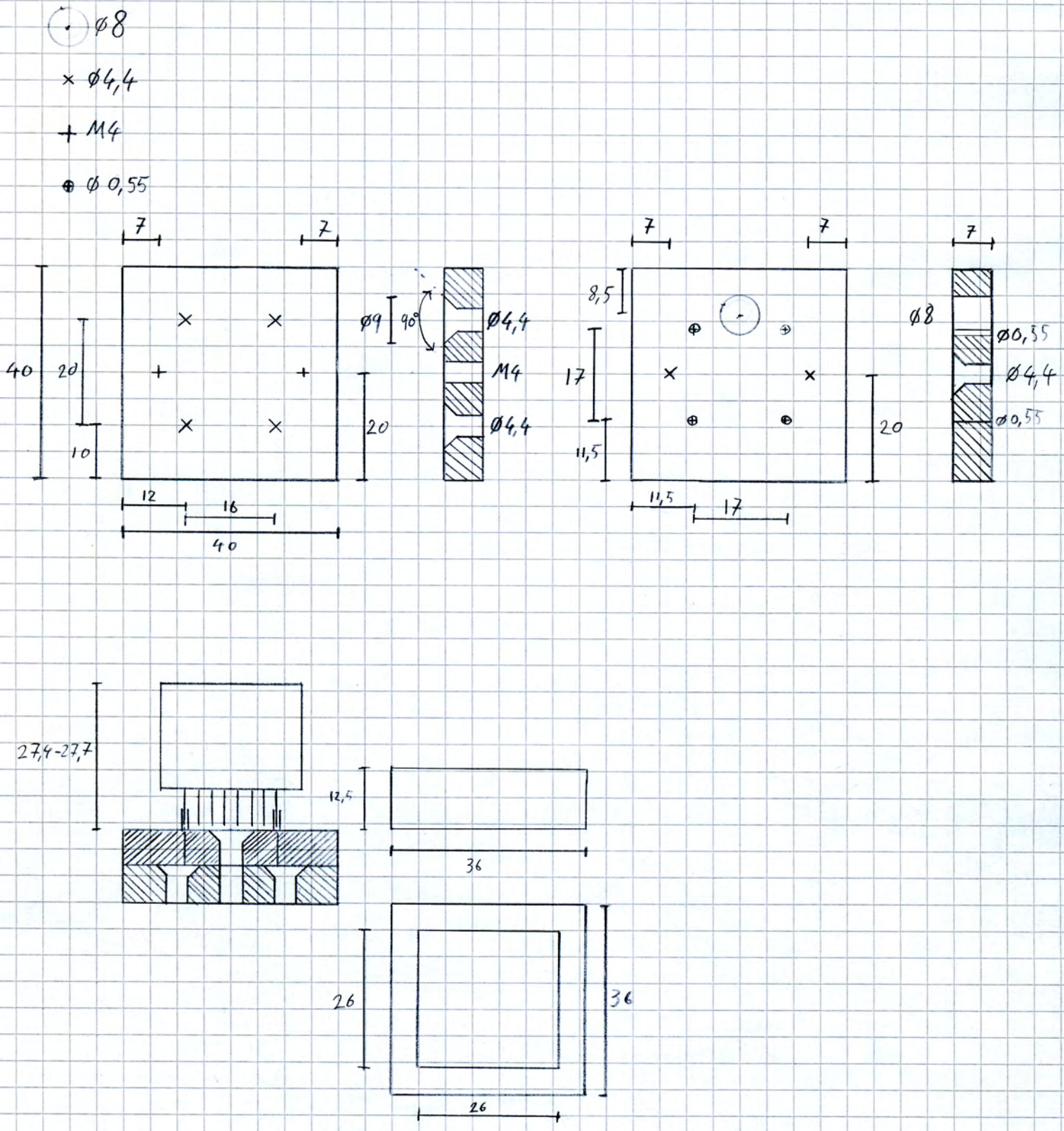
ø8
× ø4,4
+ M4
⊕ ø 0,55
7
7
40
20
10
12
16
40
ø9
90°
ø4,4
M4
ø4,4
20
7
7
8,5
17
11,5
11,5
17
20
7
ø8
ø0,55
ø4,4
ø0,55
27,4-27,7
12,5
36
26
36
26

Appendix X

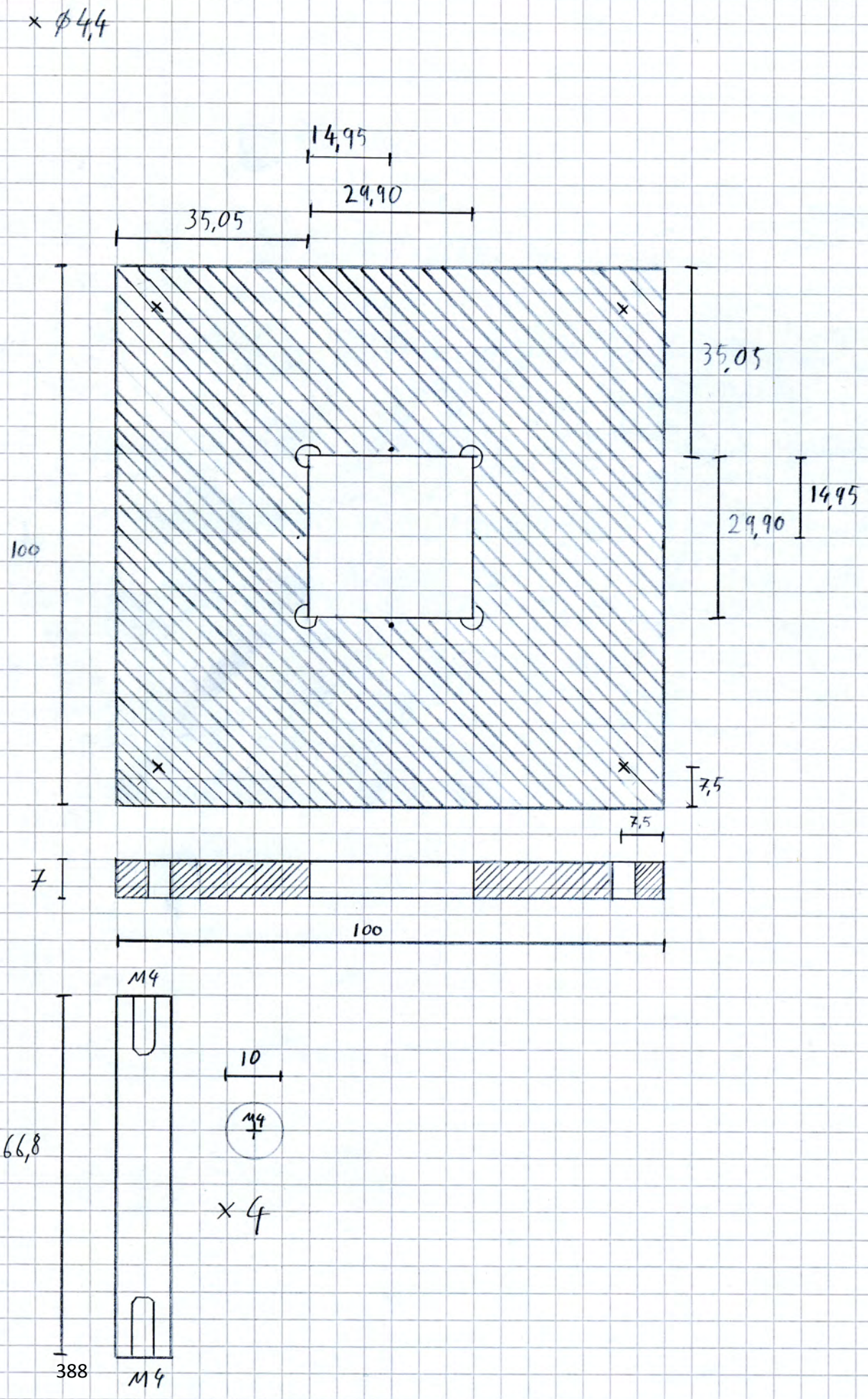
× ϕ4,4
14,95
29,90
35,05
35,05
14,95
29,90
100
7,5
7,5
7
100
M4
10
M4
66,8
× 4
388
M4

Appendix X

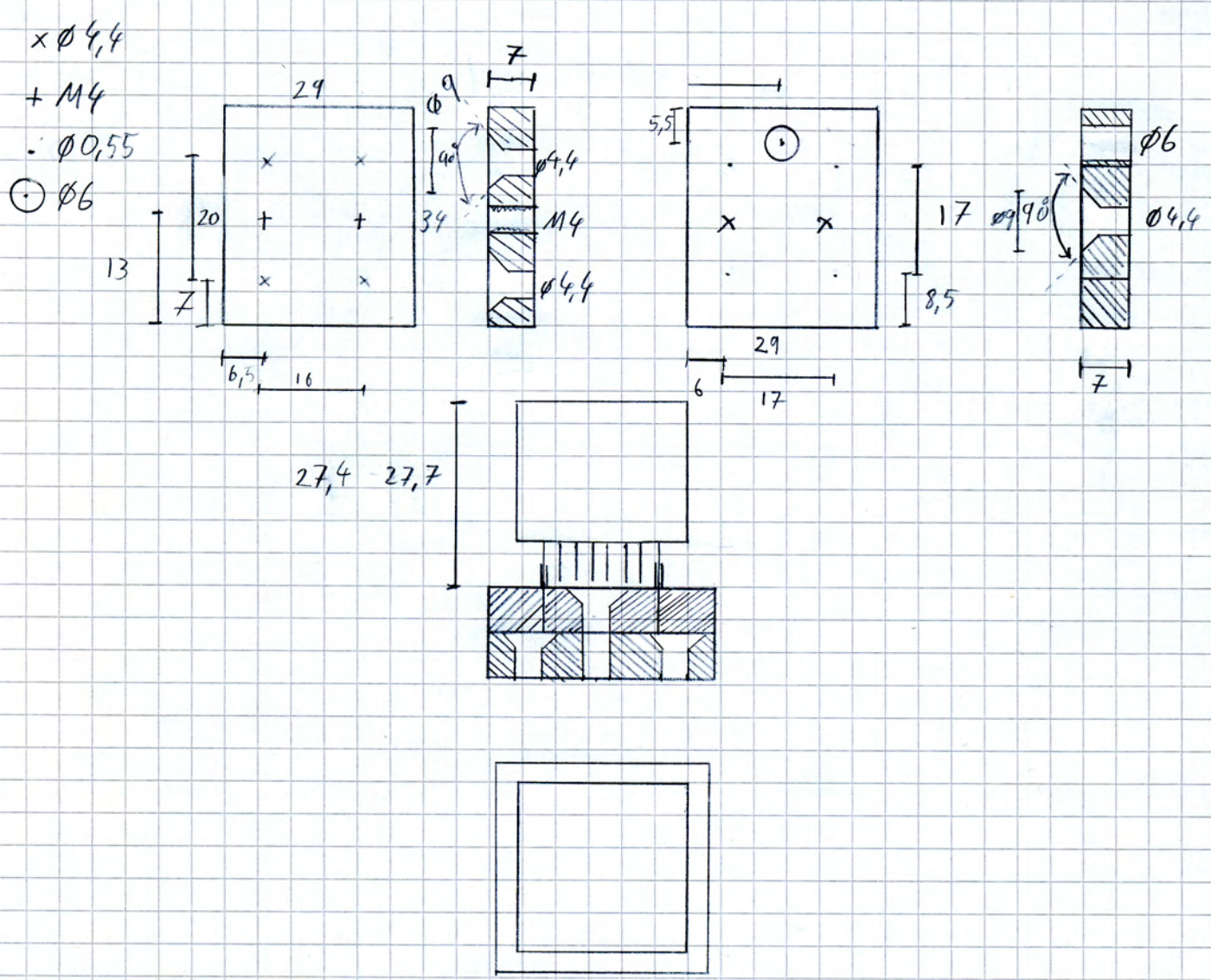
× Ø4,4
+ M4
· Ø0,55
⊙ Ø6
29
7
Ø
9
40°
Ø4,4
M4
Ø4,4
20
34
13
7
6,5
16
5,5
17
8,5
29
6
17
Ø6
Ø9
90°
Ø4,4
7
27,4
27,7

10:1 Appendix X Shims for MAPMT

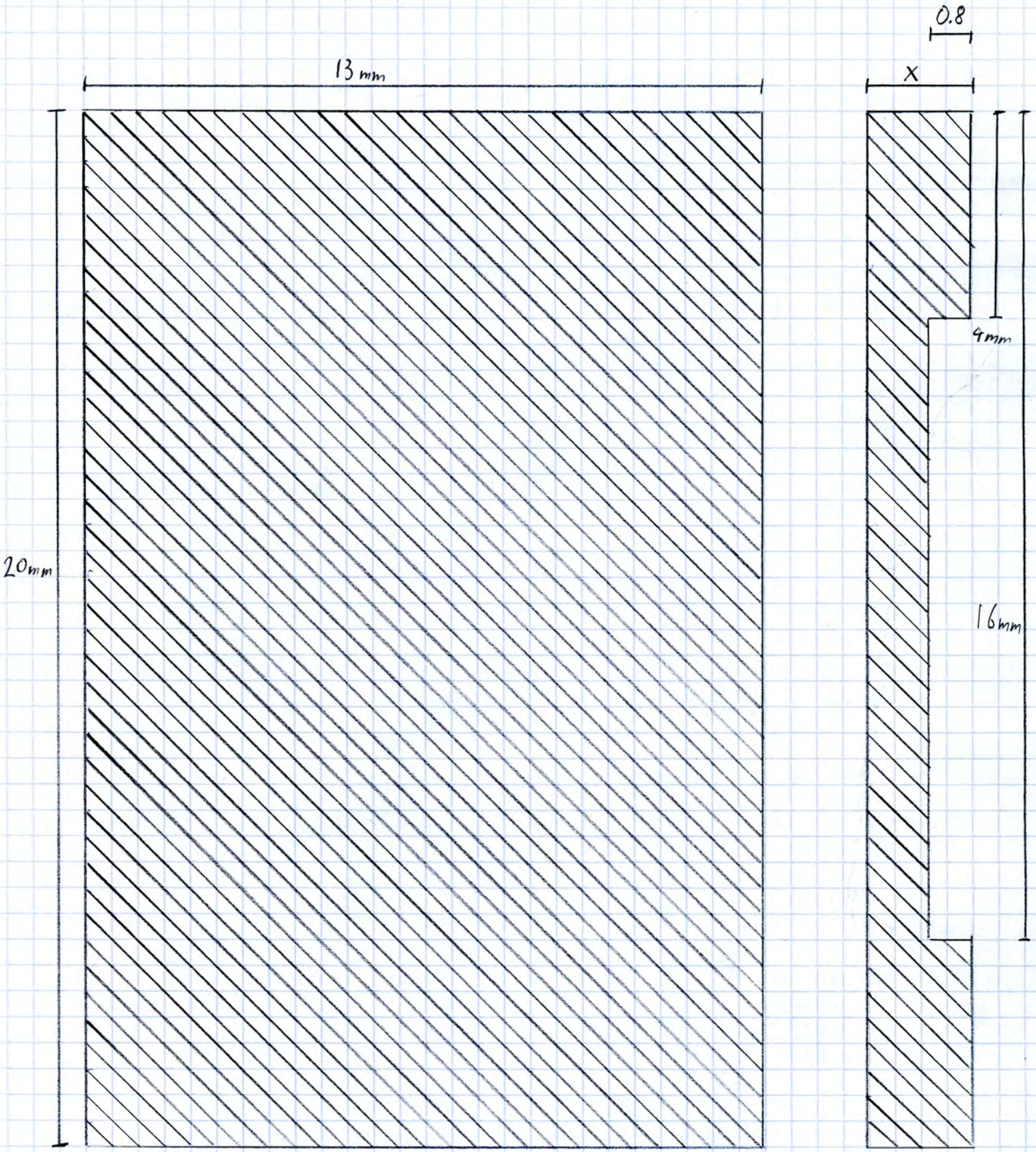

x =	1.5	1.6	1.7	1.8	1.9	2.0	2.1	2.2	2.3	2.4	2.5	2.6	2.7	2.8	2.9
	1.55	1.65	1.75	1.85	1.95	2.05	2.15	2.25	2.35	2.45	2.55	2.65	2.75	2.85	

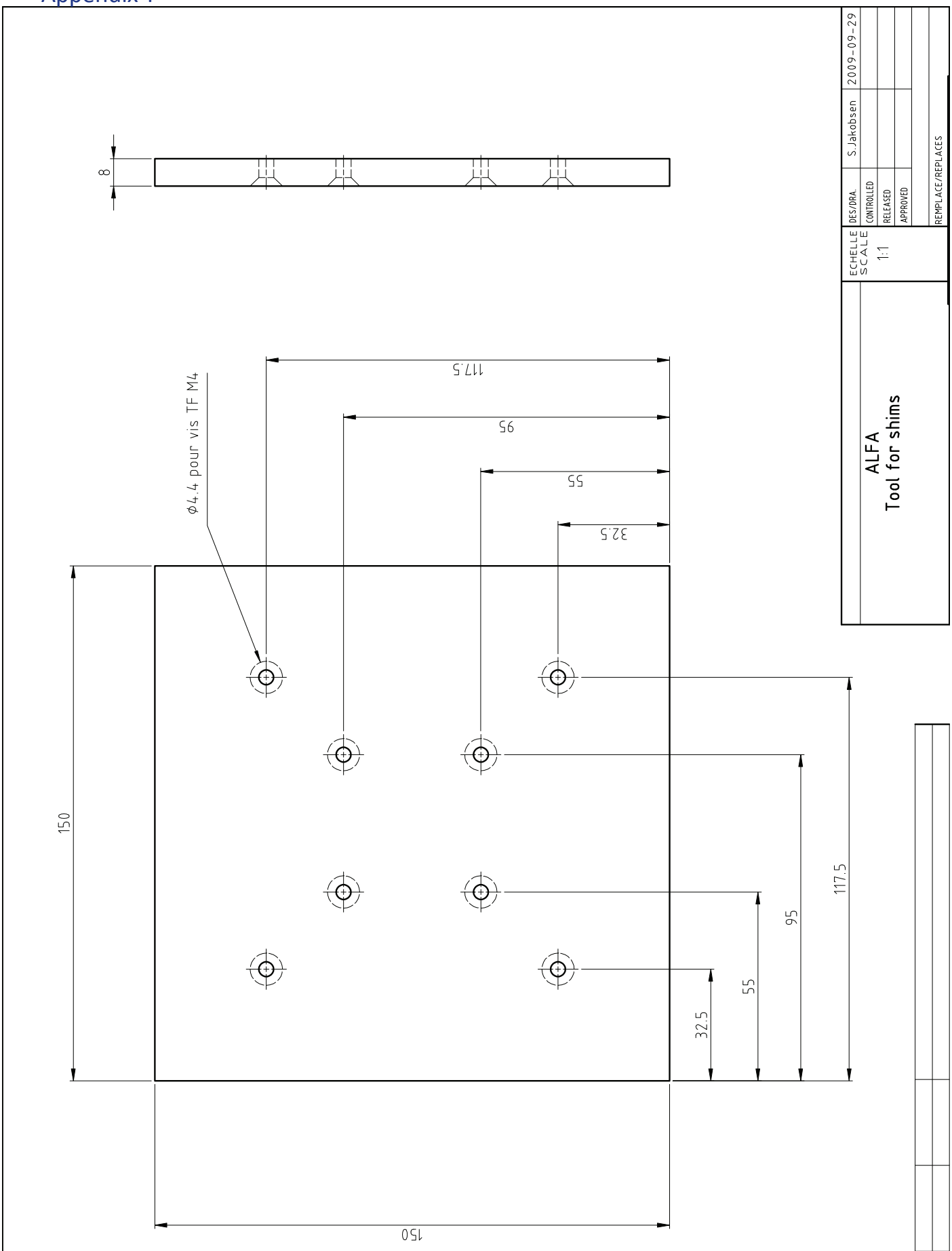
8
117.5
95
55
32.5
Ø4.4 pour vis TF M4
150
150
117.5
95
55
32.5
ALFA
Tool for shims
ECHELLE
SCALE
1:1
DES/DRA.
S.Jakobsen
2009-09-29
CONTROLLED
RELEASED
APPROVED
REMPLACE/REPLACES

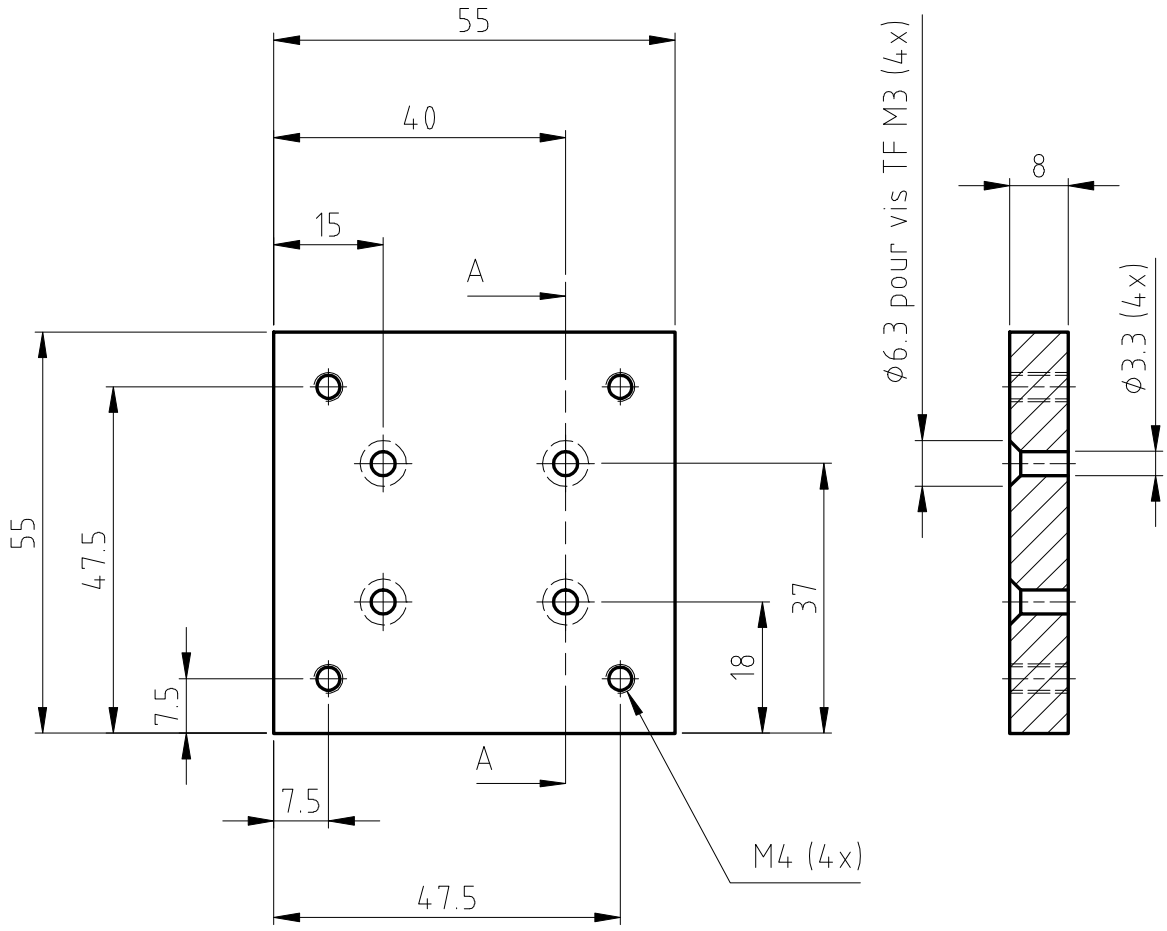

Alloy Anticorodal AW-6082

General tolerances ISO 2768 fH

Ra 1.6

ALFA Tool for shims Base plate 2	ECHELLE SCALE 1:1	DES/DRA.	A. BRAEM	2009-09-29
		CONTROLLED		
		RELEASED		
		APPROVED		
		REMPLACE/REPLACES		

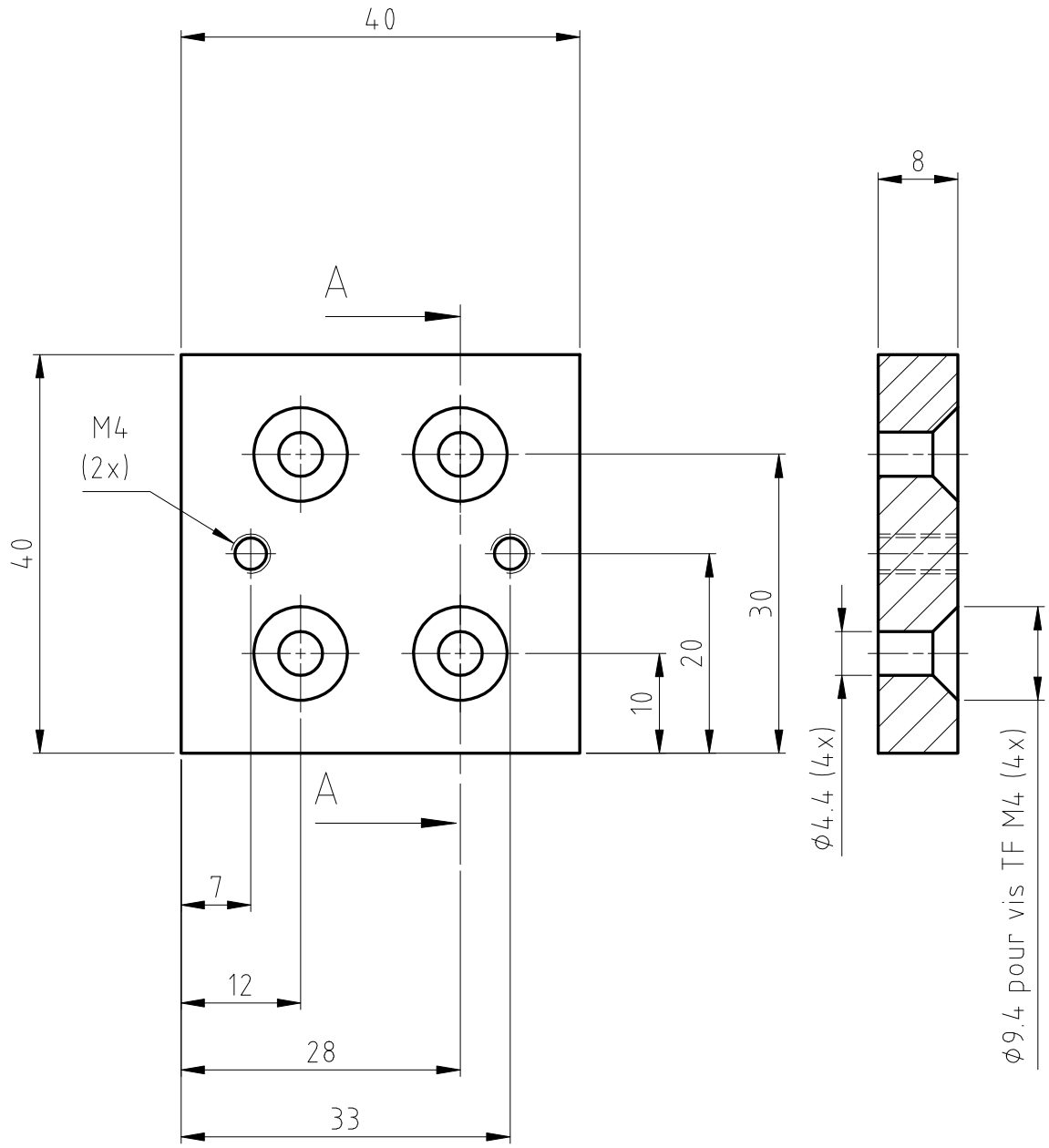

Alloy Anticorodal AW-6082

Ra 1.6

General tolerances ISO 2768 fH

ALFA Tool for shims PM support 1	ECHELLE SCALE 1.5:1	DES/DRA.	A. BRAEM	2009-09-29
		CONTROLLED		
		RELEASED		
		APPROVED		
		REMPLACE/REPLACES		

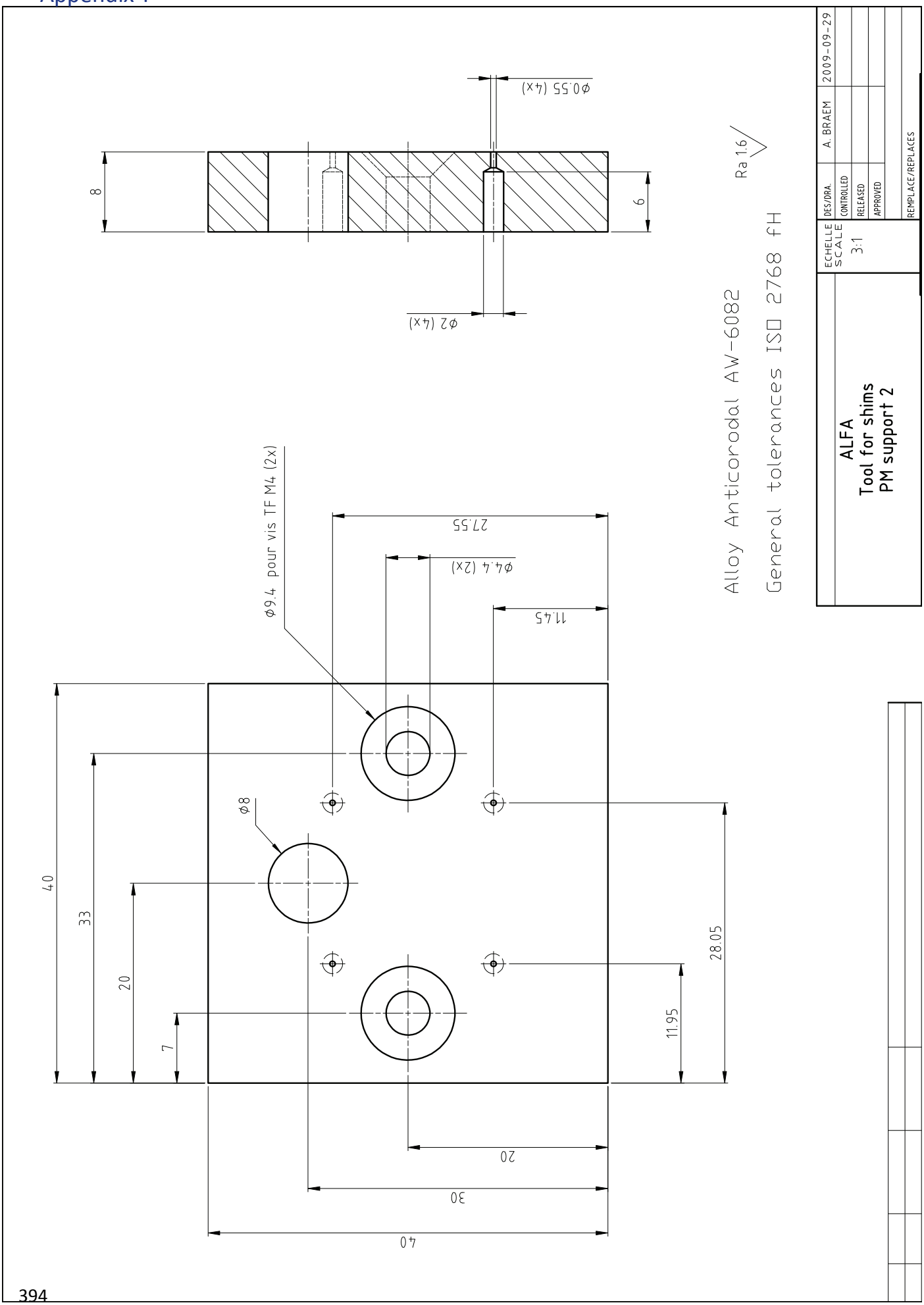
ALFA
Tool for shims
PM support 2
ECHELLE SCALE 3:1
DES/DRA. A. BRAEM 2009-09-29
CONTROLLED
RELEASED
APPROVED
REMPLACE/REPLACES
Alloy Anticorodal AW-6082
General tolerances ISO 2768 fH
Ra 1.6
ϕ0.55 (4x)
ϕ2 (4x)
8
6
ϕ9.4 pour vis TF M4 (2x)
27.55
ϕ4.4 (2x)
11.45
ϕ8
40
33
20
7
28.05
11.95
20
30
40

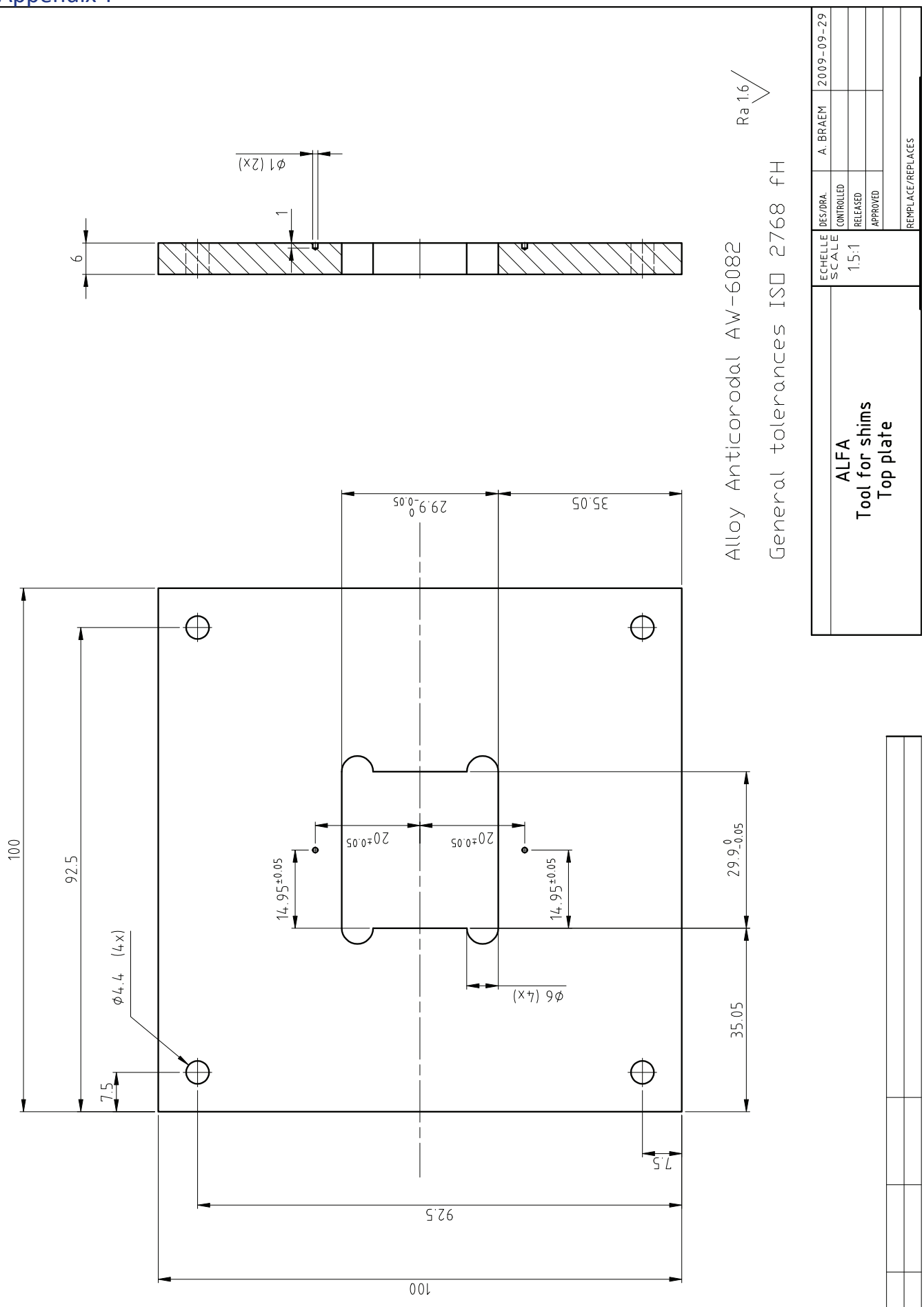
Ø1 (2x)
1
6
Ra 1.6
Alloy Anticorodal AW-6082
General tolerances ISO 2768 fH
29.9 0 -0.05
35.05
100
92.5
Ø4.4 (4x)
7.5
20±0.05
20±0.05
14.95±0.05
14.95±0.05
29.9 0 -0.05
Ø6 (4x)
35.05
7.5
92.5
100
ECHELLE SCALE 1:1
DES/DRA. A. BRAEM 2009-09-29
CONTROLLED
RELEASED
APPROVED
REMPLACE/REPLACES
ALFA
Tool for shims
Top plate

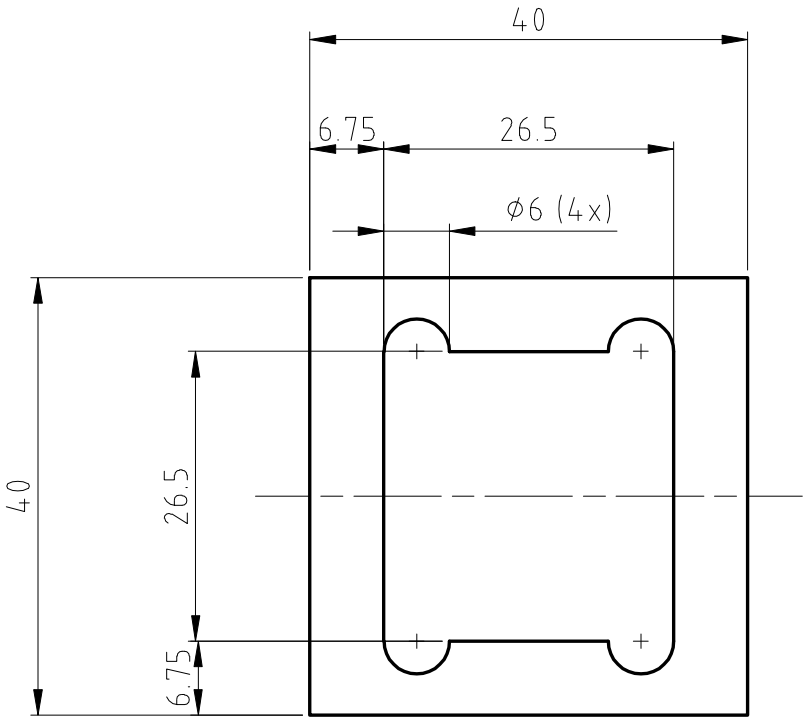

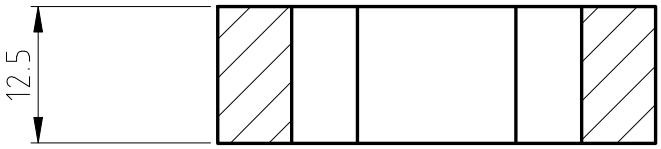

Alloy Anticorodal AW-6082

Ra 1.6

General tolerances ISO 2768 fH

ALFA Tool for shims Frame	ECHELLE SCALE 1.5:1	DES/DRA.	A. BRAEM	2009-09-29
		CONTROLLED		
		RELEASED		
		APPROVED		
		REMPLACE/REPLACES		

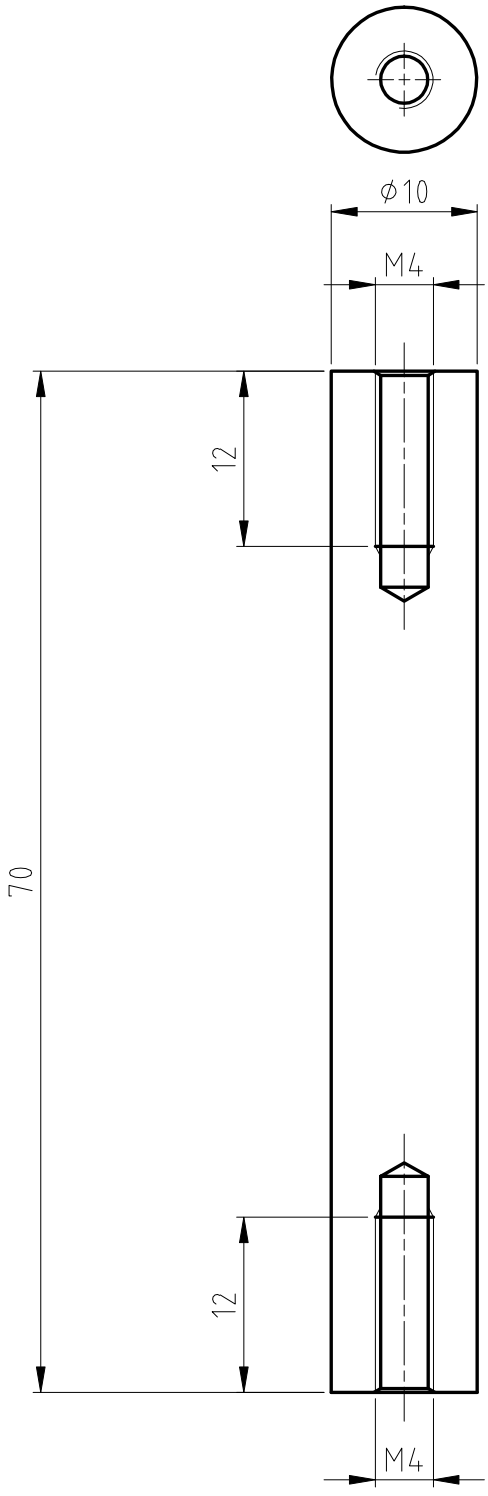

Alloy Anticorodal
AW-6082
General tolerances
ISO 2768 fH

Ra 1.6

ALFA Tool for shims Spacer	ECHELLE SCALE 2:1	DES/DRA.	A. BRAEM	2009-09-29
		CONTROLLED		
		RELEASED		
		APPROVED		
		REMPLACE/REPLACES		

1:1

398

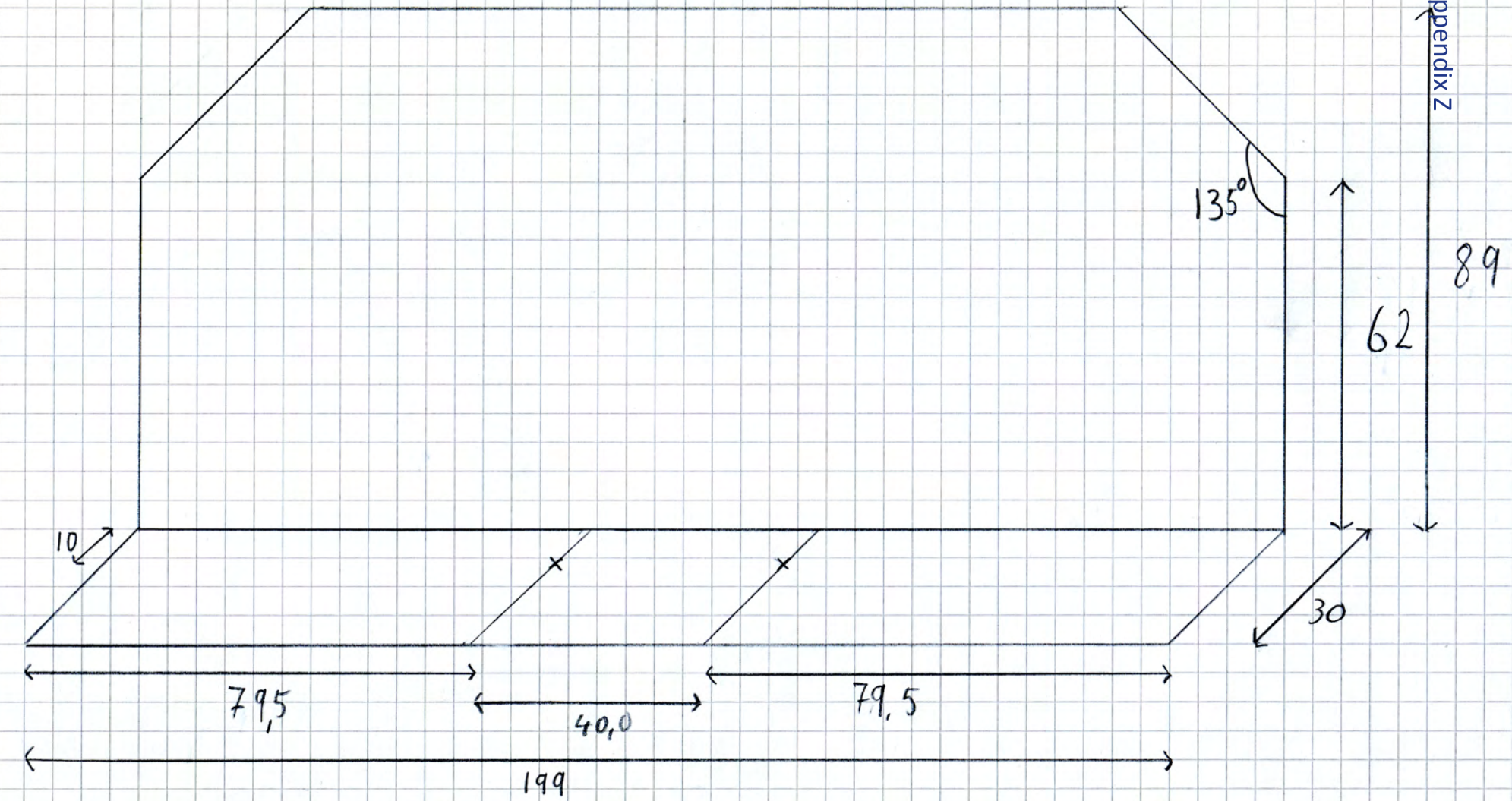

Appendix Z

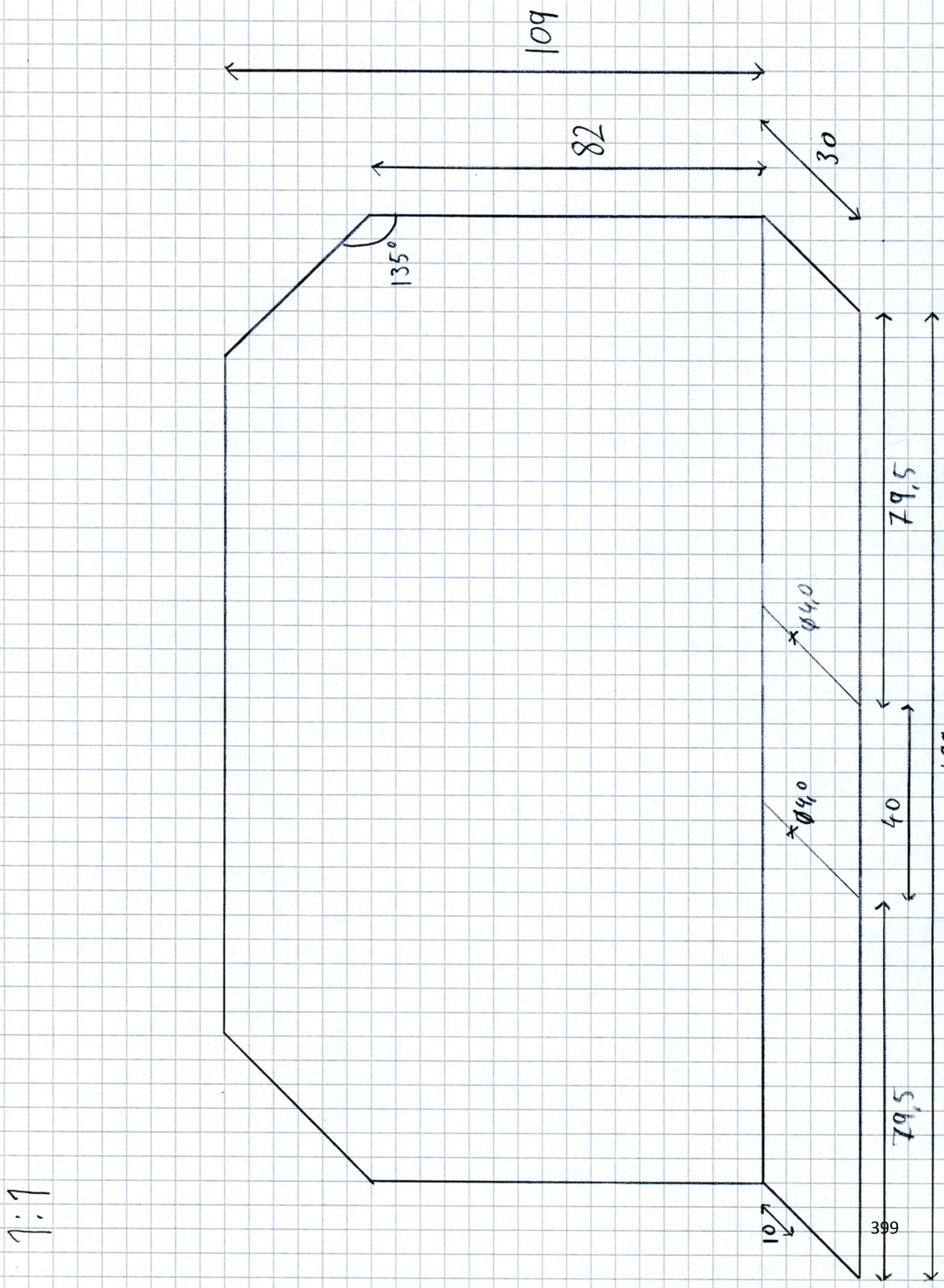

Appendix Z